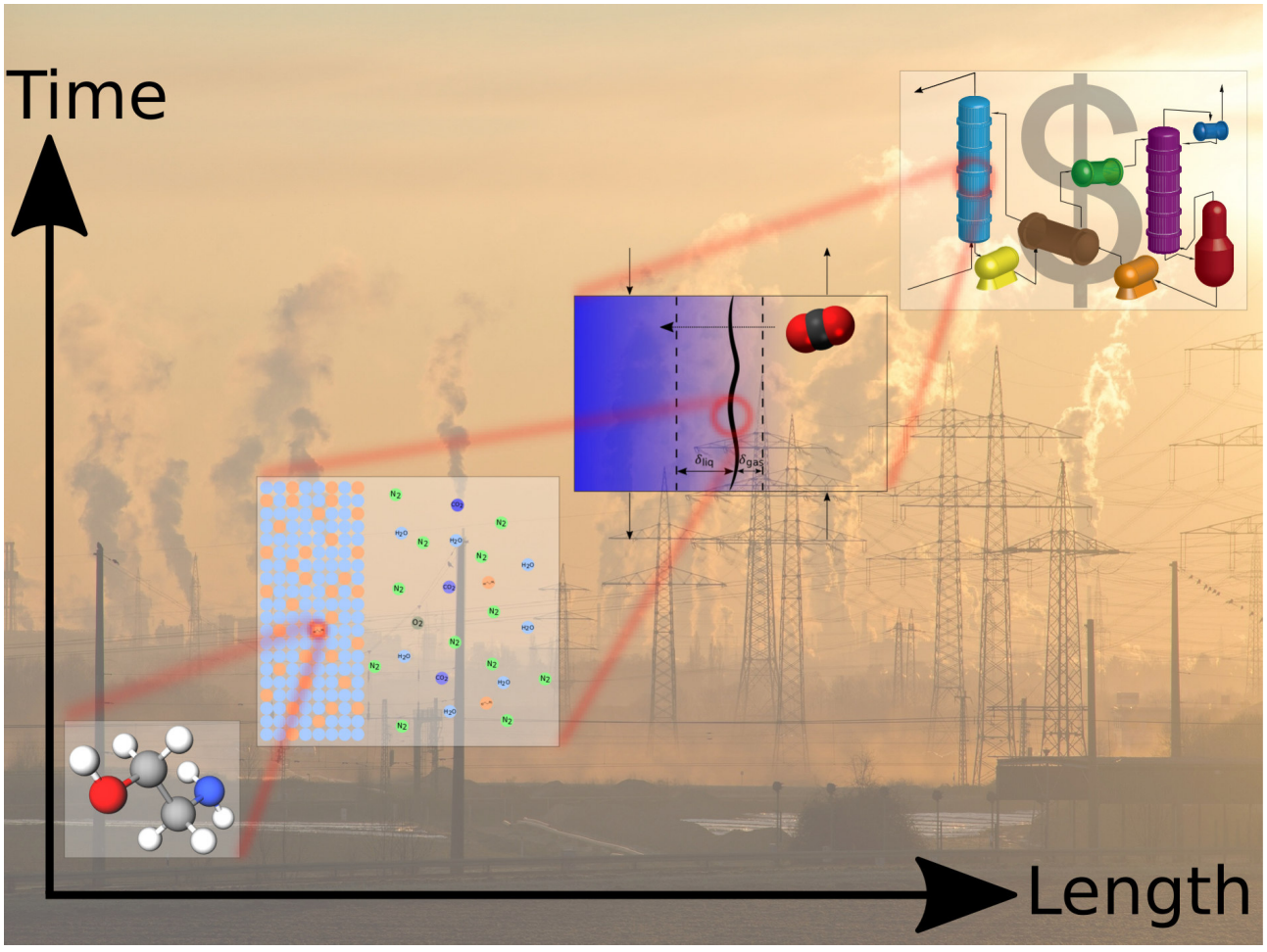
Imperial College London

A Framework for the Techno-Economic Screening of Absorption-based CO_2 Capture.



Patrick Christian Brandl

Centre for Environmental Policy
Imperial College of Science, Technology and Medicine

London, June 2024

This dissertation is submitted in part fulfilment of the requirements for the degree of *Doctor of Philosophy* and the *Diploma of Imperial College*.

Abstract

Capturing and storing CO_2 (Carbon Capture and Storage, CCS) is integral to the mitigation of climate change, and the transition to a net-zero emissions world. The large-scale deployment of CCS is slower than required, which is widely attributed to its high cost. Significant cost savings are expected to be delivered through developing new solvents, yet is not clear if the thousands of newly proposed materials will significantly reduce the capture cost. In this thesis, a framework for the techno-economic screening of absorption-based capture systems (SQUASH) is presented. The tool combines thermodynamic models with cost-optimal equipment sizing, enabling the computational fast, high-throughput, techno-economic short-cut screening of solvents with embedded error quantification. Its database contains 464 candidate solvents, yet only 18% could be successfully screened due to a substantial lack of data.

SQUASH was applied to examine the relationships between operating conditions, utility cost, amine chemical class, thermo-physical properties including their error, process performance, and capture cost. Poly-amines were identified as the most promising class. This work demonstrates that differences of $\$2/t_{CO_2}$ in mean capture cost between solvents can be differentiated with statistical significant confidence within the tool. The differences in capture costs between the solvents reduce with increasing CO_2 concentration, and the average relative difference in capture cost between two adjacently ranked solvents is only 1.1% at CO_2 concentrations found in cement or steel plants. This means that the solvent selection for industrial applications might become less dependent on the techno-economic performance. Alternative solvents and blends of aqueous amines explore the same thermo-physical property space already investigated by aqueous amines for decades. The theoretical achievable room for cost savings deliverable by solvent R&D over the current benchmark CESAR1 is limited to 29%. Further cost savings can only be realised by creating synergies with modifications to the process.

Declaration of Originality

Supervisors: Prof. Niall Mac Dowell, Prof. Jason Hallett, and Dr Mai Bui.

I hereby declare that except where specific reference is made to the work of others, the contents of this dissertation are original and have not been submitted in whole or in part for consideration for any other degree or qualification in this, or any other university. This dissertation is my own work and contains nothing which is the outcome of work done in collaboration with others, except as specified in the text.

Patrick Brandl

Copyright Declaration

©The copyright of this thesis rests with the author. Unless otherwise indicated, its contents are licensed under a Creative Commons Attribution-Non Commercial 4.0 International Licence (CC BY-NC). Under this licence, you may copy and redistribute the material in any medium or format. You may also create and distribute modified versions of the work. This is on the condition that: you credit the author and do not use it, or any derivative works, for a commercial purpose. When reusing or sharing this work, ensure you make the licence terms clear to others by naming the licence and linking to the licence text. Where a work has been adapted, you should indicate that the work has been changed and describe those changes. Please seek permission from the copyright holder for uses of this work that are not included in this licence or permitted under UK Copyright Law.

If any presented material is re-used from any publication then the source is referenced and permission was granted by their copy-right holders where applicable (see electronic supporting material). In addition, all text, figures, and tables were re-drawn for this thesis.

Patrick Brandl

"Thermodynamik ist ein übles Fach!"
Peter Brandl

Acknowledgments

I would like to thank the Centre For Environmental Policy and Department of Chemical Engineering at Imperial College London for the hosting me during my studies, and gratefully acknowledge the financial support by the EPSRC, UKCCSRC, Canada's Oil Sands Innovation Alliance (COSIA), CO2 Capture Project (CCP), and the Petroleum Institute as well as the Imperial College Library and British Library for providing access to the only remaining public copies of the early papers cited in this thesis.

I would also like to thank Professors Niall Mac Dowell and Jason Hallett for providing me with the opportunity to pursue this thesis under their supervision. Thank you for the years of insight and expertise on low-carbon technologies. I would also like to thank the many people who have provided great contributions to the work in this thesis and who I have collaborated with, including the Clean Fossil and Bioenergy Group researchers for all their valuable input during group meetings and discussions. In particular, many thanks to Dr Mai Bui and Dr Renato Cabral for our fruitful and often endless discussions around thermodynamic and economic modelling. Heartfelt thanks to my colleagues Dylan, Chris, Courtnae, Sara, Dan, Hermann, Nathan, and Caroline for making every day better than the previous one. Move Imperial provided me with a platform to balance academic rigour with performance sport and charity work to complete a personal development that otherwise I would not have achieved. Heartfelt thanks to the Imperial Squash Club and the Squad for being a second family.

This thesis is dedicated to my family who went through hardship and loss while I devoted much of my life to my academic journey. My family has always been a rock on which I could lean and a shield behind which I could stand. They remind me that good things will happen if one stays positive and never gives up.

Glossary

For solvent abbreviations please see Table B.1.

Abbreviation	Explanation
α	Significance level for statistical tests
$\beta_{\mathrm{B,j}}$	Cost factor for unit j
$\beta_{\mathrm{m,j}}$	Material factor for unit j
$\beta_{\mathrm{t,j}}$	Cost factor for unit j
χ^2	Chi-squared test
$\Delta\Theta_{\mathrm{Min}}$	Minimum working capacity
$\Delta\Theta_{\mathrm{Work}}$	Working capacity, difference between rich and lean loading
ΔH	Change in enthalpy
ΔH_{Abs}	Total heat of absorption
ΔH_{Vap}	Heat of vapourisation
ΔH_{Diss}	Heat of dissolution
ΔH_{Reac}	Heat of reaction
$\Delta H^o_{\mathrm{Reac}}$	Standard enthalpy of reaction
Δp	Pressure drop
ΔS	Change in entropy over reaction
ΔT_{LM}	Logarithmic mean temperature difference
ϵ	Void fraction packing
η	Viscosity
η_{Fac}	Herning and Zipperer approximated factor used in Wilke's method
γ	Darcy friction factor
λ	Thermal conductivity
μ	Mean (average) value of a data family
ω	Efficiency
ϕ	Association factor

ψ	Factor used to adjust variables for sensitivty studies
$\Re$	Universal gas constant
ρ	Density
σ	Surface tension
Θ	Loading
Θ_{Lean}	Lean loading of solvent entering absorber
$\Theta_{\text{Lean}}^{\text{Opt}}$	Optimal lean loading at capture cost minimum
Θ_{Rich}	Rich loading of solvent leaving absorber
ς	Effective roughness height
ζ	Time dependant variable in gPROMS
A	Area
AACE	American Association of Cost Engineering
AARD	Absolute average relative deviation
AAS	Amino acid salts
ACTL	Alberta Carbon Trunk Line
AGPU	Acid gas pick up
ALAMO	Automated learning of algebraic models
aMDEA	Activated MDEA
ANOVA	Analysis of variance
APBS	Amine-promoted buffer salts
APH	Air preheater
AV^i	Atomic diffusion volume of compound i
BECCS	Bioenergy with carbon capture and storage
BOL	Binding organic liquids
BOO	Build, own, operate
c	Concentration
C_{j}	Cost of j
C_{Shell}	Shell contant
$c_{\text{V,SF}}$	Standard gas superficial velocity

c_p	Isobaric heat capacity
CAMD	Computer aided molecular design
CAPEX	Capital expenditure
CapRat	Capture rate
CAS	Chemical abstracts service of the American Chemical Society
CCS	Carbon capture and storage
CCU	Carbon capture and utilisation
CDR	Carbon dioxide removal
CEPCI	Chemical engineering plant cost index
CESAR1	13 wt% PZ + 27 wt% AMP blend
$CI_{95\%,L}$	Lower 95% confidence interval
$CI_{95\%,U}$	Upper 95% confidence interval
COP	United Nations Climate Change Conferences
COSMO-RS	COnductor like Screening MOdel for Real Solvents
CP	Variable in GPDC pressure drop approach
CRF	Capital recovery factor
CSIRO	Commonwealth Scientific and Industrial Research Organisation
CW	Cooling water
D^i	Diffusivity coefficient of compound i
D_{P}	Diameter of packing
D_j	Diameter of equipment j
DAC(CS)	Direct air capture (with carbon storage)
DES	Deep eutectic solvents
df	Degree of freedom
df'	Degree of freedom corrected by Welch-Satterthwaite
df_d	Degree of freedom denominator
df_n	Degree of freedom numerator
DFT	Density functional theory
DGD	Solvent degradation rate

DIPPR	Design Institute for Physical Properties
DOE	US Department of Energy
E	Enhancement factor
e	Thickness
E_{A}	Activation energy
E_{Elec}	Mayr's electrophilicity parameter
E_{Inf}	Infinite enhancement factor
EOR	Enhanced oil recovery
EPC	Engineering, procurement and construction
EPRI	Electric Power Research Institute
ESP	Electrostatic precipitators
ETS	Emissions trading scheme
EU ETS	European Union Emissions Trading System
f	Fugacity
F	Statistical metric in ANOVA
$F^{\star}$	Corrected F-ratio in Brown-Forsythe's ANOVA
F^{i}	Mass flow rate of compound i
$f_{\mathrm{cb,c}}$	Two-phase correction factor
F_{Lang}	Lang factor
$f_{\mathrm{nb,s}}$	Nucleate boiling suppression factor
f_{Fit}	Fitting function
f_{Flood}	Flood factor
F_{LV}	Weighted flow rate ratio
F_{i}	Mass flow rate of compound i
FDG	Flue gas desulfurisation
FFED	Front-end engineering design
Fr	Froude's number
FT-IR	Fourier-transform infrared spectroscopy
G	Gibbs free energy

g	Gravitational constant
GGR	Greenhouse gas removal
GHG	Greenhouse gas
GPDC	Generalised pressure-drop correlation
gPROMS	PROcess modelling system software
GSA	Global sensitivity analysis as implemented in gPROMS ModelBuilder
H	Enthalpy
h	Heat transfer coefficient
h_{Ops}	Operating hours per year
Ha	Hatta number
He	Henry's law constant
HEX	Heat exchanger
HSD	Honestly significant difference
hu	Hold-up
IEA	International Energy Agency
IEAGHG	IEA Greenhouse Gas R&D Programme
IF	Interface
IGCC	Integrated gasification combined cycle
IIASA	International Institute for Applied Systems Analysis
IL	Ionic Liquid
IN_F	Installation factor
InChI	International chemical identifier
IPCC	Intergovernmental Panel on Climate Change
IR	Interest rate
ITC	Investment tax credit
IUPAC	International Union of Pure and Applied Chemistry
J^i	Molar flux of compound i
$j_{\mathrm{f,Shell}}$	Shell friction factor
j_{Shell}	Shell side factor in Kern's method

K	Equilibrium constant
k^i	Mass transfer coefficient of compound i
$\log k_{\text{Mayr}}$	Mayr's nucleophilicity factor
k_2	Second order reaction rate constant
KEPCO	Korea Electric Power Corporation
KPI	Key performance indicator
l	Length
L/G	Liquid to gas ratio
L_i	Liquid molar flow rate of stream i
LCA	Lifecycle assessment
LCFS	Low carbon fuel standard
LMTD	Logarithmic mean temperature approach
LNG	Liquefied natural gas
M	Molarity
m	Molality
MAE	Mean absolute error
MHEX	Main heat exchanger
MHIENG	Mitsubishi Heavy Industries Engineering
MNDO	Modified neglect of diatomic overlap
MO	Molecular orbital method
MQ	Mean square
MSE	Mean squared error
Mtpa	Mega ton per annum
MW^i	Molecular weight of compoind i
N	Number of data points
n^i	Moles of compound i
n_{Ann}	Annuity period
N_{Nuc}	Mayr's solvent dependant nucleophilicity parameter
n_j	Sample size of population j

NAS	Non-aqueous solvent
NETL	National Energy Technology Laboratory
NETs	Negative emissions technologies
NG	Natural gas
NGCC	Natural gas combined cycle
Nm_j	Number of equipment j
NMR	Nuclear magnetic resonance
NRTL	Non-random two-liquid model
Nu	Nusselt number
OPEX	Operating expenditure
$\mathbf{OPEX}_{\mathrm{Fix}}$	Fixed operating expenditure
$\mathbf{OPEX}_{\mathrm{Steam}}$	Steam operating expenditure (Variable OPEX)
$\mathbf{OPEX}_{\mathrm{Var}}$	Variable operating expenditure
p	Pressure
p**-value**	Value for statistical analysis
p^i	Partial pressure of compound i
P_{Elec}	Total electrical power demand
p^i_{Vap}	Vapour pressure of compound i
P_j	Power of unit j
PH	Pump head
$\mathbf{pK}_{\mathrm{a}}$	Acid dissociation constant
PNNL	Pacific Northwest National Laboratory
ppm	Parts per million
Pr	Prandtl number
PTC	Production tax credit
PV	Photovoltaic
Q	Heat
q	Corrected p-value adjusted for running multiple tests
Q_{Abs}	Desorption of CO_2 contribution to specific reboiler duty

Q_{Lat}	Latent heat contribution to specific reboiler duty
Q_{Reb}	Specific reboiler duty
Q_{Sens}	Sensible heat contribution to specific reboiler duty
q_s	Corrected p-value for Tukey's HSD
QS	Square sum
QSPR	Quantitative structure property relationships
R&D	Research and development
R^2	Pearson's correlation index
R2	Coefficient of determination
RCP	Representative concentration pathway
Re	Reynold's number
RIL	Reversible ionic liquids
RITE	Research Institute of Innovative Technology for the Earth
$RMSE$	Root mean square error
S	Entropy
s	Standard deviation
s_{Nuc}	Mayr's solvent and nucleophile specific sensitivity parameter
SAFT	Statistical associating fluid theory
Sc	Schmidt number
SCR	Selective catalytic reduction
SE	Standard error of sum of means
SMILES	Simplified molecular-input line-entry system
SQUASH	Name of screening model
SS	Stainless steel
SSP	Shared socioeconomic pathways
T	Temperature
t	Metric in t-test
$t^\star$	Critical t-value
TAC	Total annualised cost

TCM	Technology Centre Mongstad
Tukey HSD	Tukey's honestly significant difference post-hoc test
u	Velocity
U	Overall heat transfer coefficient
UKCCSRC	UK Carbon Capture and Storage Research Centre
UNIQUAC	Universal quasichemical
V_i	Gaseous molar flow rate of stream i
VLE	Vapour liquid equilibrium
Vol	Absolute volume
VPSA	Vacuum pressure swing adsorption
W	Corrected F-ratio in Welch's ANOVA
w_i	Weight fraction of compound i
W_j	Weight of equipment j
WACC	Weighted average cost of capital
We	Weber's number
x	Random variable
x^i	Mole fraction of compound i in liquid phase
$x^{\text{Opt}}_{\text{Amine}}$	Optimal mole fraction of amine
X_{tt}	Lockhart-Martinelli two-phase flow parameter
$\bar{x}$	Individual mean value
y^i	Mole fraction of compound i in gaseous phase
y_{CO_2}	CO_2 concentration (mol) in flue gas
z	Stoichiometric factor
z_{Test}	z-score for statistical analysis
ZEP	Zero emissions platform
ZT	Column height

List of Figures

2.1 Adding a hydroxyl group at β-position of unhindered amines does not always reduce the absorption capacity due to adverse interactions between steric -, and electronic effects, and intra-molecular bonding. 18

2.2 Overview of screening studies by type (experimental vs modelling), number of amines screened, and level of detail: thermo-physical properties (molecule symbol), capture process KPIs *e.g.,* reboiler duty (process symbol), and techno-economics ($ symbol). SQUASH (this study) is the first fully optimised techno-economic screening of a large candidate pool. Details about screening studies in appendix. 22

3.1 Decision tree analysing if a new molecule should be added to the database, merged with an existing entry, or rejected. 39

3.2 Overview of the Excel database for candidates. 40

3.3 Decision tree for fitting data. 42

3.4 Semi-empirical VLE fit (solid lines) and available literature data points (dots) for 30 wt% *aq.* MEA at multiple temperatures (colour bar) ranging from 25°C (blue) to 125°C (red). The limit corresponds to the lowest possible partial pressure (99.5% capture rate from $y_{CO_2} = 1\text{mol\%}$ at $p_{\text{Abs}} = 115\,\text{kPa}$). 47

3.5 Semi-empirical VLE fit (solid lines) and available literature data points (dots) for 30 wt% *aq.* PZ at multiple temperatures (colour bar) ranging from 25°C (blue) to 125°C (red). The limit corresponds to the lowest possible partial pressure (99.5% capture rate from $y_{CO_2} = 1\text{mol\%}$ at $p_{\text{Abs}} = 115\,\text{kPa}$). 48

3.6 Semi-empirical VLE fit (solid lines) and available literature data points (dots) for CESAR1 (13wt% PZ + 27wt% AMP blend) at multiple temperatures (colour bar) ranging from 25°C (blue) to 125°C (red). The limit corresponds to the lowest possible partial pressure (99.5% capture rate from $y_{CO_2} = 1\text{mol\%}$ at $p_{Abs} = 115\,\text{kPa}$). 49

3.7 Shares of amines in database broken down by number of alkalinity (number of N-atoms: Mono, Di, Tri, or poly ≥ 4) and chemical class (number of C-atoms bonded directly to the N-atom) for mono-amines. 94% of candidates contain one or two alkalinities per molecule. 52

3.8 Molar mass 464 candidates with an average of 131 g/mol. Solid lines show the normal distribution curve for amines, carboxylic acids, and amino acids. 53

3.9 Comparing thermo-physical properties of unloaded solvents at 40°C and 30 wt% as a factor of MEA. The axes for heat of absorption, viscosity, and heat capacity are inverted. The logarithm of the reaction rate is selected due to the orders of magnitude in differences between candidates. Density is mass based (kg/m^3), the VLE is based per alkalinity mol_{CO_2}/mol_{Alk}, and all other properties are molar based. Cost reductions relative to MEA are towards the outside (values > 1), and cost increases relative to MEA are towards the center (values < 1). 54

3.10 Comparing thermo-physical properties averaged by chemical class. Cost reductions relative to MEA are highlighted in green (values > 1), and cost increases are highlighted in red (values < 1). 55

3.11 The gPROMS model is wrapped with an Excel interface to allow users interacting with the tool without learning the coding-syntax of the software. The Global System Analysis cannot be used with Excel. 56

3.12 Process flow diagram which considers an archetypal post-combustion CO_2 capture plant comprising an absorber-stripper configuration. The dashed line shows the system boundary, where upstream and downstream processes are omitted for a solvent screening study. 57

3.13 Impact of capture rate and flue gas composition on limiting maximum lean loading that leads to saturation at top of the absorber at 40°C. Lean loading has to be smaller than the limit to achieve a specified capture rate. 62

3.14 One-at-a-time sensitivity analysis: Impact of varying the assumed prices/costs of amine, packing, steam, shell material (steel), and water on the capture cost. Baseline: 30 wt% MEA, flue gas CO_2 concentration $y_{CO_2} = 4$ mol% (gas-power), 90% capture rate. 98

3.15 Impact of lean loading on L/G ratio, specific reboiler duty, and capture cost at constant flue gas flow rate, y_{CO_2}= 4 mol%, and 90% capture rate for MEA. Optimal lean loading leads to minimum capture cost which is close to the minimum reboiler duty. 100

3.16 Impact of lean loading on L/G ratio, reboiler duty, and capture cost at constant flue gas flow rate, y_{CO_2}= 12 mol%, and 90% capture rate. Optimal lean loading leads to minimum capture cost which is close to the minimum reboiler duty. . . 100

3.17 The impact of changing composition (weight fraction at bottom, mole fraction at top) of MEA on capture cost (blue line, left scale) and specific reboiler duty (red symbols, right scale). Optimal weight fraction around 50 wt% leads to minimum cost. 101

3.18 Using the cold end temperature difference $\Delta T_{\mathrm{ColdEnd}}$ (top row) or the LMTD (bottom row) to describe the temperature approach in the main heat exchanger return the same results. The impact on rich solvent outlet temperature T_{RichSol} (left column), specific reboiler duty (middle column), and capture cost TAC in $\$/t_{CO_2}$ (right column) are shown over a range of lean loadings. Solvent is 30 wt% MEA, capture rate is 90%, and flue gas CO_2 concentration is 12 mol%. 103

3.19 Comparing the heat duty breakdown with Oexmann's work and Kothandaraman's rate-based model for MEA for a coal-fired flue gas and similar operating conditions. 106

4.1 Workflow of deriving the statistical significance for the solvent ranking. Step 1: Gathering data in the literature, Step 2: Calculating the mean error and standard deviation. Step 3: Calculating the mean capture cost and its standard deviation by propagating the errors in gPROMS using the global system analysis. Step 4: Testing the capture cost mean and its standard deviation for statistical significance in Prism. 109

4.2 Overview of collected studies reporting errors for liquid densities of capture solvents. Mean error, standard deviation, sample size and 95% confidence interval are calculated for the full set and a subset. 111

4.3 Screenshot of the input interface of gPROMS's Global System Analysis. Shown is an example of factors for thermo-physical properties, and sample size $n = 200$. 113

4.4 Output of the Global System Analysis with mean capture cost and its standard deviation as well as minimum and maximum values observed during the run. . . 114

4.5 Example of output of the GSA of the model for two solvents: Solvent A has a capture cost mean of $\$100/t_{CO_2}$ and solvent B of $\$115/t_{CO_2}$. The standard deviation of solvent A is $\$5.56/t_{CO_2}$ and solvent B is $\$8.89/t_{CO_2}$. Both solvents' normal distribution of the capture cost is shown on the right axis. 118

4.6 Input of Prism with the mean capture cost, standard deviation and sample size of solvents A-G. Each row is a t-test between a pair of solvents with already tested combinations (AvB = BvA) and same solvent combinations (AvA) omitted. 122

4.7 Output of running multiple t-tests for solvents A-G. The first column indicates the first solvent of the comparison with the remaining solvent of the pair being the preceeding one in the alphabet, *e.g.,* the first row represents the t-test of solvent A and B. Yes/No indicates wheter the p-value is below the significance level of 5% leading to rejecting the null hypothesis. 123

4.8 Input of Prism with the mean capture cost, standard deviation and sample size of solvents A-G . Three columns each represent the input for one solvent. Also shown is selecting non-homogeneity of variance (left), mean of every solvent (middle), and Games-Howell with family-wide 95% confidence interval (right). . 125

4.9 Output of running an ordinary one-way ANOVA with Tukey's HSD post-hoc test for solvents A-G. 127

4.10 Output of running Welch's and Brown-Forsythe's ANOVA analysis with Games-Howell post-hoc test for solvents A-G 128

4.11 Impact of number of samples n used in Monte-Carlo calculation within the Global System Analysis in gPROMS. Default $n = 200$. $n > 50$ required for Games-Howell post-hoc test. 131

4.12 Impact of changing flue gas CO_2 composition (y_{CO_2} = 2mol% to y_{CO_2} = 30mol%) on capture cost for five aqueous amine solvents utilised at their optimal concentration and operating conditions. The coloured area correspond to the 95% confidence interval and the mean capture cost is shown as a line. 137

5.1 Screened solvents ranked by their capture cost for a gas-power flue gas $y_{CO_2} = 4$ mol%. Each solvent is utilised at their individual optimal operating conditions and concentration in their individually optimally sized plant while capturing the same amount of CO_2. 95% confidence intervals shown as error bars. 140

5.2 Results for Welch's ANOVA followed by Games-Howell post-hoc test for the top 20 solvents. Yes = null hypothesis is rejected, *i.e.,* solvents are not equal. No = failed to reject, *i.e.,* there is no evidence to support that they are equal. 141

5.3 Example of some solvents sorted into ranks with statistical significance. 141

5.4 Capture cost breakdown for a typical gas-power flue gas $y_{CO_2} = 4$ mol% normalised to 100% for each solvent. See Fig. 5.1 for absolute values. Best performing solvents are dominated by steam cost, and most poor performers dominated by absorber cost. 142

5.5 Impact of changing the basis for screening between optimised concentration (solvent-specific), constant mole fraction ($x_{Amine} = 11$ mol% for all solvents), or mass fraction ($w_{Amine} = 30$ kg%). The operating conditions and equipment sizes vary between the cases even for the same solvent. 144

5.6 Impact of flue gas CO_2 composition ($y_{CO_2} = 2$ mol% to $y_{CO_2} = 30$ mol%) on capture cost. Chemical classes shown as colour. Typical applications are referenced with their flue gas compositions as vertical dotted lines. 145

5.7 Impact of changing flue gas composition $y_{CO_2} = 4$ mol% (top), $y_{CO_2} = 12$ mol% (middle), and $y_{CO_2} = 20$ mol% (bottom) on capture cost and ranking. Many poly-amines (yellow, all amines with more than one alkalinity) rank best and many tertiary amines (blue) rank worst indicating a trend in chemical class. Readers are directed to the interactive animation available online. 147

5.8 Venn diagram showing the top ten (left) and bottom ten (right) ranked solvents at y_{CO_2} = 4 mol% (orange) and y_{CO_2} = 30 mol% (blue). Seven out of ten candidate solvents stay in the top/bottom ten over a wide range of flue gas composition covering all meaningful applications. 148

5.9 Impact of lean loading Θ_{Lean} on specific reboiler duty Q_{Reb} (red-dashed, right axis) and capture cost (left axis) at constant flue gas flow rate, y_{CO_2}= 4 mol%, and 90% capture rate for MEA for three steam prices \$20/t_{Steam} (black, solid line), \$40/t_{Steam} (blue, dash-dot line), and \$200/t_{Steam} (green, dash-dot-dot line). Cost optimal lean loading moves towards the minimum specific reboiler duty for higher steam prices. 149

5.10 Solvents ranked by their capture cost for y_{CO_2} = 4 mol% at constant flue gas flow rate, 90% capture rate, and \$40/t_{Steam}. Each solvent is utilised at their individual optimal operating conditions and concentration in their individually optimally sized plant while capturing the same amount of CO_2. The specific reboiler duty is shown as colour. 150

5.11 Solvents ranked by their capture cost for y_{CO_2} = 4 mol% at constant flue gas flow rate, 90% capture rate, and \$200/t_{Steam}. Each solvent is utilised at their individual optimal operating conditions and concentration in their individually optimally sized plant while capturing the same amount of CO_2. The specific reboiler duty is shown as colour. 150

5.12 Chemical structures of the top and bottom ten ranked solvents at y_{CO_2} = 4 mol%. Noticeably many poly-amines feature in the top ten, and tertiary amines in the bottom ten, respectively. 152

5.13 Ranking of solvents at y_{CO_2} = 4 mol% with working capacity (symbol size), specific reboiler duty (blue low, red high), and chemical class (symbol). Trends in all three KPIs observable. 153

5.14 Ranking of solvents with molar mass (symbol size), pK_a (colour; blue low, red high), and chemical class (symbol shape). Trend in pK_a observable. 155

5.15 Capture cost over amine's molar mass, and optimised amine concentration $x^{\text{Opt}}_{\text{Amine}}$ (colour). No clear trend observable. 157

5.16 Linking equilibrium loading Θ_{Equi} (symbol size) for $y_{CO_2} = 4$ mol%, reaction rate constant k_2 (colour), and heat of absorption ΔH_{Abs} at (40°C) to capture cost. Normal distribution curves in heat of absorption and capture cost shown outside the axes. Visual trend in kinetics and equilibrium loading observable. 158

5.17 Breakdown of specific reboiler duty Q_{Reb} into absorption Q_{Abs}, latent Q_{Lat}, and sensible Q_{Sens} duties. Solvents sorted by negative heat of absorption ΔH_{Abs} and indicated by colour (blue low, red high). Clear trend between heat of absorption and Q_{Abs} but not overall duty. 159

5.18 Comparing five poor performing solvents (TEDA, DPAB, NMM, TEA, TIPA) with a high performer (bis-APA). 160

6.1 *One-way* sensitivity analysis: Impact of changing thermo-physical properties on capture cost for flue gas CO_2 concentration 4 mol% (left) and 12 mol% (right). The width of each one dimensional sensitivity corresponds to the property's range of aqueous amines as found in the database. Decreasing viscosity, heat capacity, surface tension, Henry's coefficient, and heat of absorption as well as increasing density, loading (VLE), thermal conductivity, and reaction rate will lead to reduced capture cost. 166

6.2 Water content (white) of screened amines at optimised amine concentration expressed as mole fraction (grey). Solvents are ranked by capture cost from left to right. Most solvents contain more than 50% water. 169

6.3 Impact of activating 30 wt% TEDA (circle) and 30 wt% TEA (star) by blending with 5 mol% PZ on capture cost (colour scale; blue = low cost, red = high cost). Blending improves reaction rate constant k_2 and rich loading Θ_{Rich} for a gas-power flue gas y_{CO_2} = 4mol%. Values correspond to 40°C. MEA (white dashed lines) added as reference. 170

6.4 Impact of activating 30 wt% TEDA and 30 wt% TEA by blending with 5 mol% PZ on capture cost. Significant cost reduction in CAPEX achieved, but the activated amines fail to outperform 30 wt% MEA. 171

6.5 Comparing thermo-physical properties of various unloaded solvents at 40°C as a factor of 30 wt% (aq) MEA. A cost reduction relative to MEA is highlighted in green with values larger than parity. Note the inverse scale for heat of absorption, viscosity, surface tension, and heat capacity. 175

6.6 Deriving the ideal solvent starting from MEA by optimising the solvent properties and its impact on capture cost (colour bar, left scale) and specific reboiler duty (red, right scale) at y_{CO_2}= 4 mol% and 90% capture rate. 176

6.7 Capture cost of screened amines, CESAR1 (performance benchmark), the Gibbs-Helmholtz solvent, and the ideal solvent for flue gas CO_2 concentrations between y_{CO_2} = 2mol% and y_{CO_2}= 30 mol%. Tax credit US §45Q and EU ETS prices added for reference. The available potential for cost reductions through solvent improvement is highlighted in blue (based on the current performance benchmark CESAR1). 178

A.1 Impact of flue gas flowrate and CO_2 concentrations on capture cost (TAC) with common flue gas sources at a capture rate of 90%. Black lines indicate annual captured CO_2 at 1 Mtpa_{CO_2} and 0.1 Mtpa_{CO_2} being the minimal threshold to be eligible for the §45Q tax credit. Solvent is 30 wt% MEA. 323

B.1 Overview of the different means. 401

B.2 Impact of different averaging methods on the active absorber packing height for five solvents as a function of CO_2 flue gas concentration. Packing height calculated by KPIs at top (ZT_{Top}, red line), bottom (ZT_{Btm}, orange line), logarithmic average as presented in Eqn. B.1 (ZT_{LogMean}, black line), and logarithmic mean driving force as presented in Eqn. B.2 (ZT_{Mean}, purple dashed line). 402

B.3 Design philosophy of SQUASH with clear focus to prioritise the multi-scale and high-throughput screening of a large database of candidate solvents requiring flexibility in thermodynamic and process modelling at short computational times. 405

B.4 Example of the relationships and interactions between operating input parameter, thermo-physical solvent properties, key performance indicators (KPIs), and cost for the absorber. 406

B.5 Comparing simplified linear temperature profiles inside the main heat exchanger for two lean loadings and two flue gas CO_2 concentrations. Solvent is 30 wt% MEA and capture rate is 90%. Hot end temperature difference is not a function of CO_2 concentration but only of lean loading (and solvent). 406

B.6 Hot and cold end temperature differences as a function of lean loading for flue gas CO_2 concentration of 4 mol% (left) and 12 mol% (right) at constant 20 K temperature approach. Solvent is 30 wt% MEA and capture rate is 90%. 408

B.7 Impact of lean loading and temperature approach on rich solvent outlet temperature T_{RichSol} (left column), specific reboiler duty (middle column), and capture cost TAC in $\$/\mathrm{ton}_{\mathrm{CO_2}}$ (right column) for flue gas CO_2 concentrations of 12 mol% (top row) and 4 mol% (bottom row). Solvent is 30 wt% MEA and capture rate is 90%. Same trends are observed as already discussed in main body. 409

B.8 Equilibrium loading trends of screened amines over flue gas composition at a pressure of 110 kPa and 40°C. Poly-amines (orange) contain more than one alkalinity per amine resulting on average in much higher capacity. Data from SQUASH database. 409

D.1 Weight limitation as a function of diameter and height for the absorber. Above the line multiple units are required. Typical range highlighted with colour. . . . 416

D.2 Capital Recovery Factor CRF as estimated by $CRF = \frac{i \cdot (1+i)^n}{(1+i)^n - 1}$ with interest rate i and annuity period n. Common CRF values highlighted at 4% and 11% (grey) as well as US Fed's base rate at 0.25% (white dashed vertical line). 424

D.3 Breakdown of specific reboiler duty Q_{Reb} into absorption Q_{Abs}, latent Q_{Lat}, and sensible Q_{Sens} duties. Solvents sorted by increasing capture cost from left to right. Negative ΔH_{Abs} is indicated by colour (blue low, red high). Clear trend between heat of absorption and Q_{Abs} but not overall duty. 424

D.4 Deriving the ideal solvent starting from MEA by optimising the solvent properties and its impact on capture cost (colour bar, left scale) and specific reboiler duty (red, right scale) at y_{CO_2} = 4mol% and 90% capture rate. 426

D.5 Deriving the ideal solvent starting from MEA by optimising the solvent properties and its impact on capture cost (colour bar, left scale) and specific reboiler duty (red, right scale) at y_{CO_2}= 12mol% and 90% capture rate. 427

D.6 Deriving the ideal solvent starting from MEA by optimising the solvent properties and its impact on capture cost (colour bar, left scale) and specific reboiler duty (red, right scale) at y_{CO_2}= 12mol% and 95% capture rate. 427

List of Tables

2.1 Summary of equilibrium reactions of amines. All occur in liquid phase with exception of the phase-transition / absorption step of CO_2. Carbamic acid $R_1R_2CO_2H$ ($R_1R_2NH_2^+CO_2^-$ in its zwitterion form) is acidic enough and hydrolyses to carbamate. Reaction pathways for a poly-amine are shown via a generic example with two non-identical secondary alkalinities with alkyl chains indicated as R_1, R_2, R_3. $R_1NH_2^+R_2NCO_2^-R_3$ and $R_1NCO_2^-R_2NH_2^+R_3$ are stable zwitterions. Kinetics of instantaneous protonations are not observable. . . . 12

2.2 General principle: Trends of adding electron donating or withdrawing substituents in α, β, or γ-positions to the nitrogen on loading and kinetics. * Adding steric hindrance reduces the reaction rate of primary and secondary amines relative to their unhindered counterparts, and increase the loading. Indicated below is only the direct comparison of substituents introducing similar steric hindrance at the same α-position. Intra-molecular bonding might reverse these trends. . . 17

3.1 Overview of which properties can be found in well known databases, and a recommended method for closing a potential data gap. 43

3.2 Examples of semi-empirical VLE models linking partial pressure p_{CO_2} and equilibrium loading Θ. $A - G$ are parameter to be fitted. 46

3.3 Overview of methods used to calculate thermo-physical properties of mixtures. . 51

3.4 Default approach to equipment design including type, sizing limits, sizing method, and material selection. SS = stainless steel. 58

3.5 Summary of default operating conditions. Temperature approach in main heat exchanger is optimised. 59

3.6 Correlations used in the screening tool with their reported uncertainty expressed as average absolute relative deviation (AARD). 60

3.7 List of key thermodynamic assumptions. 67

3.8 Details of random packing used in absorber and stripper. 68

3.9 Details of structured packing Mellapak 2X. 69

3.10 Summary of key economic parameters taken from with IEAGHG. 91

3.11 Validation of this work against Technology Centre Mongstad 2014 baseline data. 104

4.1 Mean error, standard deviation, lower $CI_{95\%,L}$ and upper $CI_{95\%,U}$ 95% confidence intervals and sample size (number of methods) for collected studies of thermophysical properties by means of predicting (Pred), measuring (Exp), or combined (total). 112

4.2 Comparing Solvents A-G with their mean capture cost, standard deviation, standard error and lower $CI_{95\%,L}$ as well as upper 95% $CI_{95\%,U}$ confidence interval. . 121

4.3 Comparing Solvents A-G with their p-values as tested with multiple two-sample, two-tailed t-tests. If p-value $< 0.05 = \alpha$ then null hypothesis is rejected. 121

4.4 Comparing the results of running multiple two-sample, two-tailed t-tests, one-way ANOVA with Tukey's HSD post-hoc, and Welch's ANOVA with Games-Howell post-hoc for solvents A-G (see Tab. 4.2). Yes = null hypothesis rejected *i.e.,* solvents rank not equally. No = fail to reject null hypothesis $\neq$ solvents rank same (no statistical evidence). Only the test on the right is valid. Type I errors are underlinedand type II errors double underlined. 129

4.5 Examples of selecting an approach to the error input into the GSA including advantages and disadvantages. 131

4.6 Capture cost means and standard deviations (StdDev) for five solvents at their individual optimal operating conditions for $y_{CO_2} = 4$ mol% with either using the full (Full) dataset of errors, just experimental methods (Exp), or just predictions (Pred). 133

4.7 Results of running Welch's ANOVA followed by Games-Howell post-hoc test for the input. There is no statistical evidence to suggest that the results are not equal. 133

4.8 Statistical test input (capture cost mean and standard deviation StdDev) and result of Welch's ANOVA for comparing five solvents with random and structured packings. 134

4.9 Mean capture cost, standard deviation, sample size and the corresponding lower $CI_{95\%,L}$ and upper $CI_{95\%,U}$ confidence interval for five solvents at their individual optimal operating conditions for $y_{CO_2} = 4$ mol%. 136

4.10 Mean capture cost, standard deviation, sample size and the corresponding lower $CI_{95\%,L}$ and upper $CI_{95\%,U}$ confidence interval for five solvents at their individual optimal operating conditions for $y_{CO_2} = 12$ mol%. 136

4.11 Result of Welch's ANOVA with Games-Howell post-hoc test for solvents at varying y_{CO_2}. Yes = null hypothesis is rejected, *i.e.,* solvents are not equal with statistical significance. 137

6.1 Weight-, mole-fractions, molality, and molar mass of amine and solution (solute + solvent). CESAR1 and a preferred embodiment of CANSOLV are added as current performance benchmarks. 168

6.2 Upper and lower bounds of property optimisation with the reference liquid given in brackets. Properties of unloaded 30 wt% *aq.* MEA and pure water added for reference. All values at 40°C. Surface tension values are measured against saturation temperature. 173

A.1 List of experimental and modelling screening studies sorted by number of amines and categorised by approach (experimental vs modelling) and KPIs. Other KPIs include *e.g.,* transport properties, absorption rate, pK_a, or degradation. Short-cut modelling indicated with brackets. 309

B.1 List of candidate amines with IUPAC name, abbreviation as used in this thesis, chemical class, CAS number, molecular sum formula, molar mass, and PubChem ID. Some amines do not have a CAS number or abbreviation assigned. 326

B.2 List of candidate amino acids with IUPAC name, abbreviation as used in this thesis, CAS number, molecular sum formula, and molar mass. 376

B.3 List of candidate carboxylic acids with IUPAC name, abbreviation as used in this thesis, CAS number, molecular sum formula, and molar mass. 378

B.4 Liquid density coefficients of pure amines. 380

B.5 VLE coefficients for semi-empirical correlation. 381

B.6 Henry's coefficients. 384

B.7 Liquid heat capacity coefficients of pure amines. 387

B.8 Vapour pressure coefficients of pure amines for Antoine equation. 389

B.9 Liquid thermal conductivity coefficients of pure amines. 390

B.10 Surface tension coefficients of pure amines. 392

B.11 Liquid Viscosity coefficients of pure amines. 393

B.12 Heat of vapourisation coefficients of pure amines. 395

B.13 Pre-exponential factor, activation energy in J/mol, and stoichiometric coefficient. 396

B.14 Total heat of absorption ΔH_{Abs} in kJ/mol, molar volume at normal boiling point V_{Mol} in cm^3/mol, and atomic diffusion volume AV. 398

B.15 Limiting regimes for analytically derived expressions for the enhancement factor E. Only valid for a second order (one in CO_2 and one in Amine) irreversible reaction
$CO_2 + z$ Amine $\rightarrow$ P, assuming $c_{CO_2} = 0$. Hatta number Ha $= \frac{\sqrt{k_2 D_{CO_2} c_B}}{z k_L}$. Additionally, Wellek *et al.,* correlation listed. 404

B.16 Weight-, mole-fractions, molality, and molar mass of amine and solvent of screened amines at constant mole-fraction. 405

B.17 References for solvent data and their uncertainties. * indicates that referenced data was extrapolated. Heat of absorption includes heat of dissolving CO_2 and heat of reaction (equals overall heat of absorption). 407

B.18 Further amine data including references. 408

C.1 List of screened CO_2 capture amines. 411

D.1 Combined expanded relative uncertainty of measuring (indicated by $\star$) and predicting thermo-physical properties of aqueous amine solvents. Values are rounded and expressed as Average absolute relative deviation (AARD). 416

D.2 Comparing calculated (SQUASH) and measured (Exp.) thermo-physical properties of aqueous MEA, DEA, MDEA, AMP, and PZ containing 30 wt% amine at 40 °C and 110 kPa. RD = relative deviation. Note, measured values are reported without their error, and this comparison is no validation. 425

D.3 Comparing the capture cost calculated by either a process simulation or the Global System Analysis for five solvents at their individual optimal operating conditions for $y_{CO_2} = 4$ mol%. 426

D.4 Excerpt of dimensionless numbers describing the ideal solvent at the top of the absorber for 90% capture and y_{CO_2}= 10 mol%. 428

Contents

Abstract **i**

Declaration of Originality **ii**

Copyright Declaration **iii**

Acknowledgments **v**

Glossary **vi**

List of Figures **xv**

List of Tables **xxvii**

1 Introduction **1**

1.1 Aim & Scope 2

1.2 Objectives 2

1.3 Thesis Outline 3

2 Scientific Background **5**

2.1 Carbon Capture and Storage (CCS) 5

2.1.1 The Value of CCS for a Net-Zero Emissions World 5

2.1.2 Technology Landscape 7

2.2 Thermodynamic Fundamentals of Absorption-based Carbon Capture 9

2.3 Finding Better Solvents 16

2.3.1 Structure-Property Relationships 16

2.3.2 Solvent Screening 19

2.3.3 Screening Tools 27

2.4 Uncertainty of CCS Process Modelling 30

2.4.1 Statistical Background 30

2.4.2 Methods for Determining Uncertainty 33

2.4.3 Previous Works 36

2.5 Research Gap 37

3 Screening Tool **38**

3.1 Objectives 38

3.2 Solvent Database 38

3.2.1 Procedure 38

3.2.2 Equations 45

3.2.3 Thermo-physical Property Space 51

3.3 Model Formulation 55

3.3.1 Framework and Flowsheet 55

3.3.2 Process Modelling 57

3.3.3 Cost Models 90

3.4 Optimising Operating Conditions 99

3.5 Model Comparison 103

3.6 Conclusions . . . 107

4 Error of *in-silico* Solvent Screening 109

4.1 Objectives . . . 109

4.2 From Input Uncertainty to Capture Cost Error . . . 110

4.3 Inferential Statistical Analysis . . . 116

4.4 Impact of Modelling Approach on Ranking . . . 130

4.5 Ranking Aqueous Amines under Uncertainty . . . 135

4.6 Conclusions . . . 137

5 Techno-economic Screening of CO_2 Capture Solvents 139

5.1 Objectives . . . 139

5.2 Ranking Aqueous Amines . . . 139

5.3 Impact of Flue Gas Composition . . . 145

5.4 Impact of Steam Cost . . . 148

5.5 The Relationship between Amine Class, Properties, and Capture Cost . . . 151

5.6 Conclusions . . . 161

6 The Limit of Solvent R&D 164

6.1 Objectives . . . 164

6.2 Impact of Thermo-Physical Properties . . . 164

6.3 Water Content . . . 167

6.4 Blending as Cost-effective Optimisation . . . 169

6.5 Developing an Ideal Solvent . . . 172

6.6 How good will Solvents ever be? . . . 178

6.7 Conclusions . . . 181

7 Conclusions and Outlook **182**

7.1 Conclusions . . . 182

7.2 Outlook . . . 184

Bibliography **186**

A Additional Scientific Background **295**

A.1 Net-zero World . . . 295

A.2 Commercial Amine-based Capture Solvents . . . 297

A.3 Other Capture Solvents . . . 305

A.3.1 Chilled Ammonia . . . 305

A.3.2 Physical Solvents . . . 305

A.3.3 Phase-Change Solvents . . . 306

A.3.4 Ionic Liquids . . . 306

A.3.5 Deep Eutectic Solvents . . . 307

A.3.6 Amino Acids . . . 307

A.4 List of Screening Studies . . . 308

A.5 More Structure Property Relationships . . . 319

A.6 Effect of Plant Scale . . . 323

A.7 Distributions 324

B Supporting Information for SQUASH 325

B.1 Database 325

B.1.1 Solvent Candidates: Amines 325

B.1.2 Solvent Candidates: Amino Acids 376

B.1.3 Solvent Candidates: Carboxylic Acids 378

B.2 Database Parameter 380

B.3 Impact of Logarithmic Mean 400

B.4 Enhancement Factor 403

B.5 Additional Figures and Tables 405

C Lower Limit of Heat of Absorption 410

D Additional Figures and Tables 416

1. Introduction

Carbon capture and storage (CCS) is integral to the affordable and scalable mitigation of climate change [1–4] and limiting warming to well below 2°C as agreed in Paris in 2016 [5–8]. The most mature technology is flue gas scrubbing which separates the CO_2 contained within a gaseous stream via absorption into a liquid. Significant cost reductions are widely expected to be delivered by developing new solvents. Thousands of materials have been proposed in recent years alone [9], often based on a handful of thermo-physical properties such as heat of absorption or kinetics [10]. There is therefore a need to better understand how developing new solvents helps achieve capture cost reductions while separating it from process modifications.

Solvent screening is an attractive method to fast-track promising solvent candidates. Previous screening work has been comparing solvents' absorption capacity, pK_a, and heat of absorption at constant weight fraction, partial pressure, or temperature often leading to single data-points per solvent. *In-silico* techno-economic modelling studies utilising rigorous models require considerable computational effort and are restricted in the number of potential solvents. Hence, it is challenging to quickly and accurately screen a large number of solvents. While plenty of literature is available, there is no openly accessible database for solvent data yet, which is challenging from a practical viewpoint. Whilst amine-based post-combustion capture technology is used to illustrate the approach, the framework can be applied to other absorption solvents. Similar approaches have been recently carried out for solid sorbents [11–19].

Over the course of 120 years, chemical solvents moved from aqueous single amine solvents to formulated blends that are currently setting the performance benchmarks for CO_2 capture from low pressure flue-gases. While the operational experience grew and commercial projects went on-stream, the fundamental thermodynamic and process elements have remained similar and the same physical property space has been repeatedly explored for over a century. Solvent development evidently still focusses on improving VLE, kinetics, and heat of absorption even 50 years after deploying the first commercial sterically hindered blends with inhibitors. There-

fore, there is the need to quantify the theoretical available room for improvement for solvent R&D and validate if further solvent improvements can drastically reduce the capture cost. This sets realistic expectations regarding solvent R&D and clarifies if delaying the widespread deployment of current aqueous amine capture technologies would be justified.

1.1 Aim & Scope

This work explores the techno-economic performance of absorption-based CO_2 capture by screening aqueous amine solvents and quantifying economic limits in solvent R&D. It focusses on improvements derived solely from advances in thermo-physical properties, which are less represented in comparison to improvements in process topology or intensification. The aim of this work is create insight into the thermo-physical property space of CO_2 capture solvents. The scope is to create a database of more than 100 solvent candidates and to develop a techno-economic tool allowing a high number of solvents to be screened within seconds and rank them with statistical significance. The key aims are 1) identifying if there is a cost-optimum amine chemical class for absorption-based post-combustion CO_2 capture, 2) determining which key characteristic should be targeted, and 3) quantifying how far solvent R&D can further reduce the capture cost over current benchmarks.

1.2 Objectives

1. Examining past and current solvents (open access and proprietary), and providing insight into the rationale behind deploying aqueous amines for the past decades.

2. Creating a database of at least 100 candidate molecules for CO_2 capture with their already existing thermo-physical properties and associated errors. The database should be readable for a screening model and easily accessible for users. The aim is to set a starting point for a collaborative and open resource.

3. Developing a tool that is able to screen solvents within seconds at their individual optimal techno-economical performance and equipment sizes, and rank them based on their capture cost for a range flue gas compositions.

4. Identifying potential sources of error and testing the differences in mean capture costs for statistical significance.

5. Discussing the relationships between amine chemical class, thermo-physical properties, process performance, and capture cost.

6. Analysing the bottlenecks of current absorption-based CO_2 capture, and quantifying the available room of capture cost reductions solely achievable by future solvent R&D.

1.3 Thesis Outline

The structure of the thesis is as follows:

- **Chapter 2: Scientific Background** provides the scientific background of absorption-based CO_2 capture. It gives an overview of the approaches taken in the literature to find better solvents, and explores trends between molecular characteristics and techno-economic performance.

- **Chapter 3: Screening Tool** details the methodology for the developed multi-scale screening tool and database.

- **Chapter 4: Error of *in-silico* Solvent Screening** quantifies the screening tool's error caused by errors in thermo-physical properties, and tests differences in mean capture cost between solvents for statistical significance by comparing multiple inferential analysis approaches.

- **Chapter 5: Techno-Economic Screening of CO_2 Capture Solvents** ranks candidate solvents based on their capture cost and explores the impact of amine concentration, steam costs, and flue gas CO_2 concentration on the ranking and cost breakdown.

- **Chapter 6: The Limit of Solvent R&D** characterises alternative chemistries such as amino acids (precipitating and non-precipitating), water-lean binding organic liquids, phase change solvents, and amine-free carboxylic acid salts. The role of developing new

solvents is assessed by limiting possible capture cost reductions solely achievable by future solvent R&D.

- **Chapter 7: Conclusions and Outlook** draws the main conclusions and suggests further areas of study.
- **Appendix** provides additional scientific background, supporting information for the screening model, additional figures and tables.

2. Scientific Background

2.1 Carbon Capture and Storage (CCS)

2.1.1 The Value of CCS for a Net-Zero Emissions World

Mitigating climate change is one of the biggest challenges for humanity in the 21st century [1–5, 5, 20]. Limiting warming of the atmosphere to well below 2°C was internationally agreed during United Nations Climate Change Conferences (COP) in Paris in 2016 and Glasgow in 2021 [6, 8]. Although considerable local reductions of carbon emissions from fossil fuel combustion and industrial processes were achieved through improvements in efficiency and reduction, the world appears not on track [21] to limit warming to well below 2°C above pre-industrial levels, as agreed in Paris [22–24].

The historic low prices of fossil fuel energy in the past decades was partly subsidised by unpriced CO_2 emissions, continuing a dependency on fossil fuels at the expense of the environment [22, 23, 25, 26]. The Intergovernmental Panel on Climate Change (IPCC) and International Energy Agency (IEA) provide more details on emission sources, trends, mitigation measures, and shared socio-economic pathways (SSP) (formerly known as representative concentration pathways, RCP) [20, 22, 27]. In summary, in order to meet the Paris climate goal, the cumulative net-emissions must become negative in 2055-2075, depending on the pathway (see section A.1 in the appendix for more context).

Carbon capture and storage (CCS) is a suite of technologies and is integral to the affordable, reliable, equitable, and scalable mitigation of climate change [7]. While the individual technologies and applications vary in purpose and value to the system [28], they all share the common principle of capturing and storing CO_2. The CO_2 emissions are captured from point sources *e.g.* power plants and industry, or from the atmosphere, which is also known as direct air CCS (DACCS) [29–39].

In CCS, separated carbon dioxide is treated and transported to a storage site via pipelines, ships, or trucks depending on location, volume, and distance. It can be stored in natural terrestrial systems (forests, biochar), oceans (fertilisation, deep-ocean injection), or engineered solutions. Such engineered solutions contain enhanced weathering of rocks (grinding and dispersal of silicates), or injecting the CO_2 into suitable subsurface rock formations [40]. Injected CO_2 is securely trapped and gradually dissolves into formation waters in depleted oil and gas reservoirs or saline aquifers. It also chemically reacts within basalts or forms hydrates in deep sea-bed sediments [40].

The duration for which separated CO_2 is locked away classifies a system into either long-time ($>$ 100 000 years) or temporary ($<$ 1 000 years) storage [40]. Temporary storage includes utilising CO_2 (CCU) by chemically or physically binding it in a value-added product such as polymers, concrete or chemicals. The lifetime of these products is short in comparison to the time-scales required to impact the balance of the natural carbon cycle [40, 41], yet they could play an important role in a circular economy [5, 42].

CCS as a tool for mitigating climate change was first proposed by Marchetti from IIASA in 1977 [43–45] when he described collecting, transporting, and disposing CO_2 as a geo-engineering operation. Marchetti considered capturing CO_2 from gas streams, including exhaust from coal-, gas-, and oil-fired power plants, and industrial processes such as steam methane reforming. Steinberg *et al.* built upon the work at IIASA, and explored various applications for CO_2 capture processes, including industrial processes, *e.g.* hydrogen production [46], power generation [47, 48, 48–50], and even direct air capture, until the early 1980s when interest in separation from power plant flue gases took over [51–61]. Interestingly, much of the research in the 1970s kept close to the standard/archetypal absorber-stripper configuration already known from the 1930s.

Large scale deployment of CCS has materialised to around 80 facilities over the last decades, of which less than half ($<$ 30) are still in operation in 2021 [62, 63]. There are around 30 leading companies offering capture technology with some having decades worth of experience in developing new solvents [64, 65]. The rate of deployment must accelerate by a factor of

100 to meet climate goals, which is a daunting task given the track-record of CCS [63], and requires effective policy measures [62]. Critics argue that meeting short-term climate targets by 2030 is possible without CCS by expanding renewables, increasing energy efficiency, and closing coal-power. Additionally, public perception of CCS is mixed to negative [66–70] requiring active communication and community engagement to increase the acceptance of CCS [71, 72]. Deploying CCS on the scale required seems unlikely to happen without a framework of coordinated policies [73] that help overcome the perceived cost of CCS.

The debate about CCS is far from settled, with major projects being cancelled (Compostilla in Spain, Texas Clean Energy Project in USA, and Peterhead, White Rose, Longannet, Kingsnorth, and Don Valley projects all in UK), delayed (Gorgon CCS project in Australia, and Lake Charles in USA), failed (Kemper County in USA), or simply being "mothballed" (Petra Nova in USA, and Schwarze Pumpe in Germany) [62, 70, 74, 75, 75, 76]. Some of these projects suffered from setbacks due to technology, reliability, finance. and business model problems, resulting in them being listed as examples for the paradigm that "CCS does not work" [62]. The decision to "mothball" Petra Nova draws a likeness to the early 1980s when the collapse in oil price led to the widespread closure of capture units [77]. The next section reviews some CCS context focussing on the role of absorption-based CO_2 capture. The US Department of Energy has set a target of reducing the capture cost to $\$40/t_{CO_2}$ by 2025, and less than $\$30/t_{CO_2}$ by 2035 [78]. Commentators are anticipating that reaching these targets will require "step-changes", "breakthroughs", or "silver bullets" [79] over current costs.

2.1.2 Technology Landscape

Capture technologies have historically been classified into pre-combustion, post-combustion, and oxyfuel applications based on the separation concept and stream position. The key difference is that either the fuel is shifted into hydrogen and CO_2 is separated before any combustion occurs, or, CO_2 is separated and purified from an acidic gas stream that resulted from the processing of fossil fuels. Burning a fuel in oxygen-enriched environment creates a nearly pure CO_2 stream requiring little further separation. Pre-combustion and oxyfuel processes can not easily be retro-fitted to existing plants.

Many factors such as CO_2 partial pressure, flue gas composition, or process constraints are fundamental in selecting an appropriate capture process *e.g.,* absorption, adsorption, membrane, or cryogenic systems. An overview of the vast technology landscape is presented in [7, 80–87] and reviews on absorption systems are presented in [19, 84, 88–95].

The most mature technology (based on commercial readiness) is known as flue gas scrubbing and separates CO_2 contained within a gaseous stream via absorption into a solvent [81, 96–100]. One differs between physical solvents, in which CO_2 is dissolved, and chemical solvents, in which the CO_2 chemically reacts with a solute after it is physically absorbed into the liquid. The term "solvent" conventionally refers to the whole liquid phase.

Bottoms [101] and Allen and Michalske [102] independently from each other filed for US patents in October 1930 claiming the process of using aqueous (alkanol)amines to separate carbon dioxide out of a gas mixture. At that point alkanolamines, which were discovered in Germany mid-19th century [103, 104], became more available. Amongst the patented molecules are the widely known monoethanolamine (MEA), diethanolamine (DEA), triethanolamine (TEA). Despite MEA not setting performance standards any more, it manifested itself as literature benchmark due to its easily and openly accessible data. The vast majority of literature on CCS selected MEA as capture solvent (see Tab. 3.7 to 3.13 in [7]).

The feasibility of capture technologies *e.g.,* MEA scrubbing, seawater absorption, potassium carbonate scrubbing, refrigeration (cryogenic), and molecular sieves at varying capture rates at sources has been analysed since the 1970s [43, 45, 105–109]. Assuming a 90% capture rate has become ubiquitous [7, 110, 111] in both academia and policy and dates back to these early studies. In no case is a 90% capture rate optimal or represents a hard border [112–114].

Second generation solvents are aqueous blends of amines which are currently commercially utilised. CESAR1 (blend of 2-amino-2-methyl-1-propanol AMP and Piperazine PZ) is assumed to be the current open-source performance benchmark [115]. It is less known that the first patent for a capture solvent dates back over 120 years, and that the AMP+PZ blend is already utilised for nearly half a century. An overview of the historic development and commercial solvents is given in the appendix A.2.

2.2 Thermodynamic Fundamentals of Absorption-based Carbon Capture

The key chemical difference between the amines used for CO_2 capture is their direct or indirect reaction pathway with CO_2. The sum reactions are given in the following simplified overall reaction equations:

Carbamate-route	$2\ R_1R_2NH + CO_2 \rightleftharpoons R_1R_2NCO_2^- + R_1R_2NH_2^+$
Bicarbonate-route	$R_1R_2R_3N + CO_2 + H_2O \rightleftharpoons HCO_3^- + R_1R_2R_3NH^+$
Blends	$R_1R_2NH + R_1R_2R_3N + CO_2 \rightleftharpoons R_1R_2NCO_2^- + R_1R_2R_3NH^+$
Poly-amines	$R_1NR_2NR_3 + CO_2 \rightleftharpoons R_1NH^+R_2NCO_2^-R_3$

In summary, primary (*e.g.*, MEA) and secondary (*e.g.*, DEA) amines, that are free from steric hindrance around the nitrogen, form carbamic acid, which is widely assumed to be acidic enough to undergo hydrolysis and form carbamate and a proton [116]. The required acidity is assumed to be $pK_a < 7$ [117, 118] with the pK_a of MEA's carbamte estimated to be $pK_a = 7.55$ [119, 120]. The amino nitrogen is a nucleophile (Lewis base) during the initial reaction and donates its lone electron pair to an electrophile (Lewis acid) such as CO_2 or HCO_3. The released proton reacts with a base *e.g.* another amine molecule (weak base). Tertiary amines (*e.g.* methyldiethanolamine MDEA) react only indirectly with CO_2 in the presence of water to form bicarbonate and protonated tertiary amine by acting as Brønsted-base and/ or base-catalyst [121–124]. The formation of carbamate / deprotonation of carbamic acid is undesirable as such, as it will protonate a free amine that will not be able to react with CO_2 any more. Therefore, the theoretical limiting equilibrium ratio of CO_2 to alkalinity is 1:2 for primary and secondary, and 1:1 for tertiary amines [124, 125]. Regardless of the pathway, the absorption depends on unprotonated bases acting as proton acceptors often described via Lewis acid-base reactions [126, 127] but the Brønsted basicity and Lewis basicity are largely uncorrelated [128].

The carbamate of sterically hindered amines (*e.g.* 2-amino-2-methyl-1-propanol AMP) is unstable and the equilibrium is shifted towards the zwitterion intermediate from which bicarbonate is formed [129–133]. The carbamate hydrolysis frees up the AMP molecule, which can react

with another CO_2 molecule, leading to a reaction with a 1:1 CO_2 to alkalinity ratio. Hence, the limiting equilibrium ratio for sterically hindered amines is higher than 1:2 and depends on the degree of hydrolysis [132]. In reality, both pathways contribute to the absorption depending on the amine's basicity. The CO_2 to alkalinity ratio will vary between zero and one assuming that the equilibrium is shifted by a constant supply of CO_2 [134]. These trends are reversed when the temperature is increased because the reactions are exothermic (lower physical solubility plays a less important role in reactive systems of interest [134]). The equilibrium loading does not equal to the aforementioned equilibrium ratio, because the loading describes the whole liquid phase (*i.e.* solute and solvent) which is additionally influenced by physical absorption (more important at high pressures).

The carbamate stability cannot be described by a single direct or indirect (molecular) characteristic [127, 135, 136]. This indicates that the complex superposition of molecular orientation, intra-molecular bonding, pH, pK_a, concentration, solvation effects, electronic -, and steric-considerations (field - and resonance effects [137]) need to be analysed to fully understand and predict the performance of hindered amines. The reaction rate decreases compared to the unhindered counterparts due to the steric hindrance, but is partially compensated by an increase in effective amine concentration (freed amine increases concentration of amines that can react with CO_2 compared to carbamate forming counterparts).

Multiple competing reactions occur in amine mixtures (blends) depending on each alkalinity's relative basicity and carbamate stability (*e.g.,* $R_1R_2R_3N$ is a stronger base than R_1R_2NH) [138]. Poly-amines (*e.g.* PZ, aminoethyl ethanolamine (AEEA), diethylenetriamine (DETA), or tetraethylenepentamine (TEPA), see Tab. B.1 for abbreviations) have more than one alkalinity per molecule (number of N-atoms > 1) [139]. They offer the opportunity to combine the different reaction pathways. The inherent stoichiometric advantage of combining reacting and proton accepting (intra-molecular proton transfer) roles in one molecule leads to an increased CO_2 to amine ratio for carbamate forming alkalinities, *e.g.* 1:1 for a simple di-amine with two non-tertiary alkalinities like piperazine (PZ). Adding functionality to a molecule does not linearly increase its absorption capacity and reaction kinetics due to side-reactions, steric, and electronic considerations, and also increases viscosity or heat of absorption [140, 141].

Alternative chemistries, *e.g.* CO_2BOLs, also yield a limiting equilibrium ratio of CO_2 to solute of 1:2 when one alcohol and one base react with one carbon dioxide molecule, and 1:1 if the alcohol and base functionalities are linked in one molecule.

Accurately predicting reaction rates is crucial for designing the absorber and stripper columns. Kinetic data can be measured using laboratory-scale wetted wall columns, stopped-flow apparatus, stirred cell reactors, wetted sphere absorbers, laminar jet absorbers, or string of disc contactors. A review of these experimental setups can be found in [83, 142]. Translating reaction mechanisms and measured data into widely applicable kinetic models for CO_2 capture is not a straight-forward task [83].

The CO_2-chemistry in water is well known and summarised in Tab. 2.1. The two protonation equilibria are instantaneous and kinetically not observable. The autoprotolysis is added for completeness. The CO_2-aqueous amine chemistry is more complex, and two fundamentally different pathways exist: 1. The reactive carbamate route, 2. The non-reactive base-catalysed bicarbonate / hydration route.

There are three competing mechanisms describing the reactions between CO_2 and primary and secondary amines after the phase-transition / absorption into the liquid phase: 1. Zwitterionic carbamate route, 2. Termolecular reaction, 3. Direct reaction to carbamic acid followed by deprotonation [127]. The most prominent mechanism was originally proposed by Caplow [117], and involves the formation of a zwitterionic form of the carbamate
$CO_{2(aq)} + R_1R_2NH \rightleftharpoons R_1R_2NH_2{}^+CO_2{}^-$ followed by a slow proton exchange reaction with a base (another free amine) $R_1R_2NH_2{}^+CO_2{}^- + R_1R_2NH \rightleftharpoons R_1R_2NHCO_2{}^- + R_1R_2NH_2{}^+$. Termolecular reactions do not happen at scale [119, 120]. However, termolecular mechanism [143–145] and also variable order reactions are able to empirically describe the interactions. The third mechanism was found to be insufficient to describe the carbamate kinetics in basic aqueous solutions [119, 120, 146].

The reaction between H_2CO_3 and amine is impacted by the solution's pH value. Unprotonated amines require a solution with a high pH which shifts the equilibrium away from carbonic acid to bicarbonate and carbonate. Puxty and Maeder [147] observed that while aqueous

Table 2.1: Summary of equilibrium reactions of amines. All occur in liquid phase with exception of the phase-transition / absorption step of CO_2. Carbamic acid $R_1R_2CO_2H$ ($R_1R_2NH_2^+CO_2^-$ in its zwitterion form) is acidic enough and hydrolyses to carbamate. Reaction pathways for a poly-amine are shown via a generic example with two non-identical secondary alkalinities with alkyl chains indicated as R_1, R_2, R_3. $R_1NH_2^+R_2NCO_2^-R_3$ and $R_1NCO_2^-R_2NH_2^+R_3$ are stable zwitterions. Kinetics of instantaneous protonations are not observable.

Reaction pathway	Equations
Autoprotolysis	$H_2O \rightleftharpoons OH^- + H^+$
CO_2 and water reactions	$CO_{2(g)} \rightleftharpoons CO_{2(aq)}$
	$CO_{2(aq)} + H_2O \rightleftharpoons H_2CO_3$
	$CO_{2(aq)} + OH^- \rightleftharpoons HCO_3^-$
	$CO_3^{2-} + H^+ \rightleftharpoons HCO_3^-$
	$HCO_3^- + H^+ \rightleftharpoons H_2CO_3$
Carbamate route	$CO_{2(aq)} + R_1R_2NH \rightleftharpoons R_1R_2NH_2^+CO_2^-$
	$R_1R_2NH_2^+CO_2^- \rightleftharpoons H^+ + R_1R_2NHCO_2^-$
	$R_1R_2NH + H^+ \rightleftharpoons R_1R_2NH_2^+$
	$H_2CO_3 + R_1R_2NH \rightleftharpoons R_1R_2NCO_2H + H_2O$
	$HCO_3^- + R_1R_2NH \rightleftharpoons R_1R_2NCO_2^- + H_2O$
Bicarbonate route	$CO_{2(aq)} + H_2O \rightleftharpoons HCO_3^- + H^+$
	$R_1R_2R_3N + H^+ \rightleftharpoons R_1R_2R_3NH^+$
Poly-amines, two sec. alk.	$CO_{2(aq)} + R_1NHR_2NHR_3 \rightleftharpoons R_1NHR_2NCO_2^-R_3 + H^+$
	$CO_{2(aq)} + R_1NHR_2NHR_3 \rightleftharpoons R_1NCO_2^-R_2NHR_3 + H^+$
	$CO_{2(aq)} + R_1NHR_2NCO_2^-R_3 \rightleftharpoons R_1NCO_2^-R_2NCO_2^-R_3 + H^+$
	$CO_{2(aq)} + R_1NCO_2^-R_2NHR_3 \rightleftharpoons R_1NCO_2^-R_2NCO_2^-R_3 + H^+$
	$R_1NHR_2NHR_3 + H^+ \rightleftharpoons R_1NH_2^+R_2NHR_3$
	$R_1NHR_2NHR_3 + H^+ \rightleftharpoons R_1NHR_2NH_2^+R_3$
	$R_1NH_2^+R_2NHR_3 + H^+ \rightleftharpoons R_1NH_2^+R_2NH_2^+R_3$
	$R_1NHR_2NH_2^+R_3 + H^+ \rightleftharpoons R_1NH_2^+R_2NH_2^+R_3$
	$R_1NHR_2NCO_2^-R_3 + H^+ \rightleftharpoons R_1NH_2^+R_2NCO_2^-R_3$
	$R_1NCO_2^-R_2NHR_3 + H^+ \rightleftharpoons R_1NCO_2^-R_2NH_2^+R_3$

amine systems are well known, their standard reactions are not sufficient to explain the reverse reaction of a carbamate solution at equilibrium, or reversing the equilibrium by adding acids. It

is necessary to at least include the reaction between bicarbonate and amine forming carbamate and water. The carbamate route is in general faster than the carbonate route.

The reaction $CO_{2(aq)}+OH^- \rightleftharpoons HCO_3^-$ is in presence of a tertiary amine of little importance due to the other competing anions HCO_3^- and CO_3^{2-} [123, 127, 148]. Side reactions are too slow or deemed unreactive and neglected [120]. This includes nucleophilic attacks from an amine nitrogen on carbonate CO_3^{2-}, protonated amines acting as nucleophiles, and reactions of the alcohol group of alkanolamines with carbonic acid to form dicarbamate or esters. Graphical summaries can be found in [149]. A commanding review on the modelling of aqueous amines for CO_2 capture can be found in [127].

Water is highly polar and able to form hydrogen bonds which might interact with the amine-CO_2 chemistry. Its role is contested with Han and Armstrong [150] observing no interactions, Arstad *et al.,* [151] attributing water a catalytic role during the formation of carbamic acid, da Silva and Svendsen [145, 152] finding water to stabilise the carbamate, and Perinu *et al.,* [153] explaining reduced electron density at the nitrogen with the solvent effect of water's lone pair of electrons. Water slows down nucleophilic reactions (SN2 especially) by H-bonding to the nucleophile, thus, water affects the reactions of carbamate forming amines, because it impacts the amine's nucleophillic attack on the CO_2 (*i.e.* its Lewis base strength).

Despite the overall kinetics being well known, there is some uncertainty behind the reaction order, exact form of zwitterion species, and no consensus has been reached on how important individual reactions actually are especially at changing conditions regarding concentration, pH, and pK_a [142, 154–157]. The reaction order can not be determined solely by the reaction equations, but by experiments or molecular dynamics [155]. The absorption reaction order for primary and secondary amines is between 2 and 3 for most conditions and is often reduced to a pseudo-first order reaction [142]. There is uncertainty behind the validity of adopting *a-priori* a pseudo-first order reaction which might lead to breaking the underlying thermodynamic conditions when the amine is utilised at low concentrations or slower-than expected kinetics [158]. For example, measuring the kinetics with stopped-flow setups requires low concentrations (< 0.2M) [142]. Therefore, there cannot be a guarantee that all solvents can always be described

with a pseudo-first order absorption reaction, and, that this assumption holds true over the whole range that could be analysed, *e.g.,* candidate amines with very low solubility.

Thermodynamic models describing the vapour liquid equilibrium (VLE) can be broadly classified in: 1. Non-rigorous / empirical models, 2. Rigorous excess Gibbs energy models (*e.g.,* Pitzer, e-NRTL, UNIQUAC, Austgen-model [159, 160]), and 3. Equation of state models (*e.g.,* SAFT) [81, 91, 94, 127, 161–163]. Well known examples are the models of Kent-Eisenberg [164] (non-rigorous), Chen-Evans [165] (rigorous), and Deshmukh-Mather [166] (rigorous). Rayer *et al.,* [167] reviewed the rigorous models in more detail, and other contributions [91, 161, 168, 169] compiled lists of available thermodynamic models. Afkhamipour *et al.*, [170] analysed the impact of parameters on the equilibrium loading for four tertiary amines (1DMA2P, DEA2P, DEEA, DEAB) and ranked in statistically significant order CO_2 partial pressure > amine concentration > temperature. They developed a framework to compare the prediction accuracy of Kent-Eisenberg, modified Kent-Eisenberg, and Deshmukh-Mather models, and found AARDs of less than 3.6% with the Deshmukh-Mather model.

The total heat of absorption can be measured or calculated. Experiments measure the total enthalpy change caused by physical dissolution $CO_{2(g)} \rightleftharpoons CO_{2(aq)}$, total reaction heat, and any excess heats [134, 171]. It is not possible to separately measure the individual contributions in a reactive system. The term (total) heat of absorption refers to the macroscopic measured enthalpy change, thus, the sum of all contributions. Versteeg *et al.,* [124] estimated the heat of dissolution to be constant -17 kJ/mol_{CO_2} and McCann *et al.,* estimated, using the N_2O analogy, -15 kJ/mol_{CO_2} for MEA, -13 kJ/mol_{CO_2} for DEA, -17 kJ/mol_{CO_2} for MDEA, and -16 kJ/mol_{CO_2} for AMP [134, 171]. The heat of every individual reaction (see Tab. 2.1) adds to the total reaction heat. McCann *et al.,* [171] found the protonation of amine to be the dominating contribution for both carbamate and bicarbonate routes with it being about three times the value of the physical dissolution heat. However, there is some uncertainty behind the values of each reaction, as it is not always possible to attribute a measured heat to a specific reaction, and if they always add up without excess enthalpies [171]. The error of measured heats of absorption is attributed to experimental apparatus, procedure and conditions, and in general smaller than calculated values. Most experiments measure the integral heat of absorption which

is not identical to the differential heat of absorption [172].

Heats of absorption can be estimated based on the VLE via the Gibbs-Helmholtz equation 2.1, or via the individual equilibrium constants K_{Eq} and the van't Hoff equation 2.3. The well known expression in Eqn. 2.2 can be derived from the Gibbs-Helmholtz or Clausius-Clapeyron equations when assuming that speciation and the activity constant ratio are constant over temperature and any excess enthalpy equals zero [173].

$$\left(\frac{\delta(G/T)}{\delta T}\right)_{p_{\mathrm{Tot}}} = -\frac{H}{T^2} \equiv \left(\frac{\delta(G/T)}{\delta(1/T)}\right)_{p_{\mathrm{Tot}},n} = H \tag{2.1}$$

$$\Delta H_{\mathrm{Abs}} = R \cdot \left(\frac{\delta \ln f_{\mathrm{CO_2}}}{\delta(1/T)}\right)_{\Theta,p_{\mathrm{Tot}}} \tag{2.2}$$

$$\left(\frac{d \ln K_{\mathrm{Eq}}}{dT}\right)_{p_{\mathrm{Tot}},n} = \frac{\Delta_{\mathrm{Reac}} H^{\emptyset}}{RT^2} \equiv \left(\frac{d \ln K_{\mathrm{Eq}}}{d1/T}\right)_{p_{\mathrm{Tot}},n} = -\frac{\Delta_{\mathrm{Reac}} H^{\emptyset}}{R} \tag{2.3}$$

The fugacity $f_{\mathrm{CO_2}}$ can be simplified assumed to be equal to the partial pressure $p_{\mathrm{CO_2}}$ at little additional error, because the experimental error in measuring the VLE already propagates to 20-30% error in the heat of absorption [172, 174–177]. The uncertainty using the van't Hoff approach is reported as 2-30% [171]. Differential heats of absorption are not a function of the temperature if calculated by the Gibbs-Helmholtz approach. This is also the case for VLE correlations containing the temperature only in its first-order.

Textbooks and Mathias *et al.,* [172] present the thermoydnamic rigorous derivation of the commonly used expression in Eqn. 2.2. Equation 2.2 is sometimes presented in a modified way *e.g.,* multiplied by (-1) to yield positive values for ΔH_{Abs}, without the underlying assumptions (constant total pressure and apparent moles), or the partial derivatives replaced by total derivatives. The equilibrium constant is only a function of temperature (at constant total pressure), thus the total derivative d instead of the commonly used partial derivative δ is correct for the van't Hoff equation 2.3.

2.3 Finding Better Solvents

2.3.1 Structure-Property Relationships

This section discusses structure-property relationships which are tested if they translate to chemical class-capture cost relationships. Whilst amine-based post-combustion capture technology is used to illustrate the screening approach, the framework can be applied to other absorption systems.

Structure-activity relationships date back to the nineteenth century [178] and are established ways to link observable effects and properties to molecular characteristics [179]. There is an abundance of studies linking molecular structures, intermediates, and reaction products to few selected thermo-physical properties such as pK_a, reaction rate, absorption capacity, and heat of reaction. Methods such as NMR, qualitative molecular orbital arguments, initio continuum modelling, density functional theory DFT modified neglect of diatomic overlap calculations, molecular dynamics, and infra-red FT-IR were used to quantify the impact of substituents on the amine-CO_2 interactions and carbamate stability [127, 180–186]. These effects differ between hindered and un-hindered amines, and despite numerous attempts to date, no consensus has been reached on how to best describe them. This is due to the adverse interactions of steric -, and electronic effects, and intra-molecular bonding that highly depends on the respective molecule.

The general principle presented in Tab. 2.2 is the result of reviewing over 100 studies reporting structure-property relationships, and it describes the impact of electron donating and withdrawing substituents of similar size and position on the loading and reaction rate of primary, secondary and tertiary amines. These are only indications as intra-molecular bonding and the proximity of functional groups trade-off and might reverse the trends.

The example in Fig. 2.1 illustrates how nuanced these effects are: According to the general principle, one would expect the CO_2 absorption capacity to be reduced when a hydroxyl group is added at the β-position of un-hindered amines (*e.g.,* NEED and DAP). However, adding a

Table 2.2: General principle: Trends of adding electron donating or withdrawing substituents in α, β, or γ-positions to the nitrogen on loading and kinetics. * Adding steric hindrance reduces the reaction rate of primary and secondary amines relative to their unhindered counterparts, and increase the loading. Indicated below is only the direct comparison of substituents introducing similar steric hindrance at the same α-position. Intra-molecular bonding might reverse these trends.

Substituent	**Example**	**Primary/Secondary**		**Tertiary**
		Un-hindered	Hindered*	
e^- donating	$-CH_3$, $-CH_2CH_3$	loading ↑, rate ↑	loading ↓, rate ↑	loading ↑, rate ↑
e^- withdrawing	$-OH$	loading ↓, rate ↓	loading ↑, rate ↓	loading ↓, rate ↓

hydroxyl group to NEED increases its capacity while adding the same group at the same position (β-position between the two alkalinities) of DAP decreases the capacity [187]. This is due to the electron withdrawing effect of the hydroxyl group weakening both alkalinities in DA2P while AEEA could form a ring-structure via intra-molecular bonding. This example highlights the difficulties that need to be overcome to successfully derive a widely valid structure-performance relationship that does not require analysing the molecular 3D configuration. No consensus has been found to date if amine structure-property relationships translate into meaningful cost reductions, and as shown, these relationships become less pronounced with increasing complexity of the molecular structure due to the adverse interactions of more functional groups in close proximity to each other.

A range of methods (NMR, qualitative molecular orbital arguments, initio continuum modelling, density functional theory DFT modified neglect of diatomic overlap calculations, molecular dynamics, and infra-red FT-IR) were used to quantify the impact of substituents on the amine-CO_2 interactions and carbamate stability [127, 152, 180–186, 188]. These effects differ between hindered and un-hindered amines, and despite numerous attempts to date, no consensus has been reached on how to describe them. Hook [182] reports that amines with α-substitutions tend to precipitate more than non-hindered counterparts due to the rapid formation of bicarbonate.

Oexmann and Kather [174] showed that focusing solely on the heat of absorption without considering the whole process is inadequate to assess solvents. They use rigorous thermodynamic

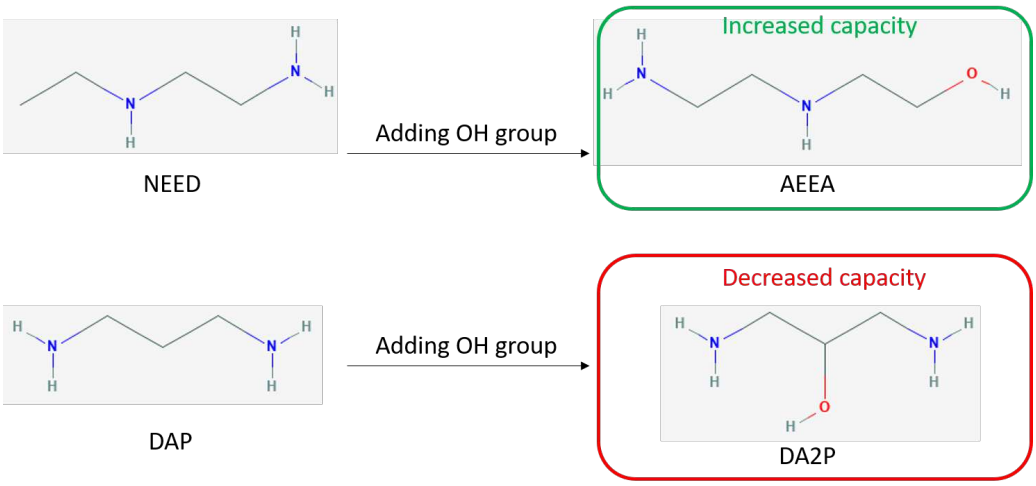


Figure 2.1: Adding a hydroxyl group at β-position of unhindered amines does not always reduce the absorption capacity due to adverse interactions between steric -, and electronic effects, and intra-molecular bonding.

modelling of a post-combustion capture plant integrated into a coal power plant to show that operating conditions such as stripper pressure, cyclic capacity, and operating temperatures need to be included when assessing solvents. They find that amines with high heats of absorption, *e.g.,* even higher than MEA, benefit from a temperature swing between absorber and stripper, *i.e.,* an increase in stripper pressure and temperature reduce water vapour at the stripper's head, thus, less reboiler duty is required. Vice versa, amines with low heats of absorption profit from vacuum stripping at lower temperatures. Those recommendations come at the dispense of other factors such as solvent degradation (at higher temperatures), or more work for compressing CO_2 (from vacuum pressures). They conclude that those effects must be included in an overall optimisation, which depends on the flue gas source (coal power in Oexmann and Kather's case) and the quality of steam available. Defining a system boundary for any screening study might be biased to some degree, and require balancing the capture unit's integration with the flexibility for capture applications.

Mathias *et al.* [9, 172, 189–191] applied thermodynamic principles to highlight the link between heat of absorption and the VLE as described by the Gibbs-Helmholtz equation. They found a "best thermodynamic solvent" by creating an artificial solvent following a "Goldilocks" [192] approach by systemically varying the CO_2 capacity and corresponding heat of absorption in an Aspen Plus model. They assumed a coal power flue gas, constant flowsheet topology,

constant kinetics, and kept the lean loading constant although the eight artificial solvents vary in their VLE. The artificial solvent resembled tertiary or hindered amines and was derived by modifying the enthalpy and amine cation's Gibbs energy of formation at infinite dilution in water. Mathias *et al.* define the optimal thermodynamic range for the heat of absorption to be between -60 kJ/mol$_{CO_2}$ and -70 kJ/mol$_{CO_2}$ accounting for the trade-off between equilibrium loading and heat of absorption. They also suggest using the Gibbs-Helmholtz equation as a tool to check for thermodynamic consistent data having identified discrepancies between VLE and calorimetric data in the literature.

The research group at UT Austin [193] quantified the effect of changing the heat of absorption for a generic solvent (using a similar approach to Mathias *et al.,*) on three stripper configurations: 1. Simple stripper, 2. Multi-pressure stripper, 3. Vacuum stripper. They found that the optimal heat of absorption depends on the stripper configuration with vacuum strippers being preferred for solvents with $-\Delta H_{\text{Abs}} < 88$ kJ/mol$_{CO_2}$ and multi-pressure strippers for $-\Delta H_{\text{Abs}} > 88kJ/mol_{CO_2}$. In another study by the same research group, Lin and Rochelle [194] identified the optimal negative heat of absorption to be in the range 70 - 120 kJ/mol$_{CO_2}$ for the advanced flash stripper. Kim and Lee [195] found the optimal negative heat of absorption to be in the range 60 - 80 kJ/mol$_{CO_2}$ for a simple stripper. Therefore, no consensus on an optimal heat of absorption has been found yet. Further relationships are discussed in the appendix A.5.

2.3.2 Solvent Screening

Scoring and ranking molecules according to their performance by using a computer model is generally referred to as *in-silico* screening. The term dates back to when computing power increased to offer an alternative to experiments such as high-throughput screening and is an established method in the pharmaceutical sector [196].

Cost reductions are widely expected to be delivered by developing new capture solvents, and screening is a promising approach to fast-track candidate solvents. The available approaches are experimental screening [197–199], computer aided molecular design (CAMD) [200–210] using SAFT [211–216], data envelopment analysis [217], machine learning [179], artificial intelligence

[218], heuristic blending [219], and process modelling [115, 220]. There is no favourite method because each approach has individual advantages and disadvantages that will be discussed in the following paragraphs.

Both experimental and *in-silico* screening use key performance indicators (KPIs) to rank solvents with experimental approaches measuring data of fewer solvents at higher accuracy, effort, and cost compared to *in-silico* approaches. *In-silico* screening is widely considered cheaper and faster, allowing more solvents to be screened at the same time. Selecting KPIs suitable for screening is non-trivial [161, 221, 222] and may involve first order aspects such as absorption capacity, heat of absorption, and kinetics, or, second order aspects such as degradation, volatility, or corrosion [90]. Some KPIs are less suitable than others, *e.g.,* comparing mass transfer rates between studies should include all conditions such as interfacial areas and bubble sizes/-forms. Not all stakeholders target the same KPIs and the selected approaches (experimental vs *in-silico*) will provide insight into KPIs and produce different rankings, *e.g.,* experimental screening setups will not be able to report capture cost.

Rapid experimental screening avoids time-consuming equilibrium measurements by injecting acidic gas in a solvent sample inside a gas-liquid contact chamber under heavy mixing. The inlet and outlet concentrations are measured and the absorption rate is the key result. While such setups are widely known, previously published screening studies differ in procedure (*e.g.*, injection time, volume, measurement) and conditions (*e.g.*, amine concentration, partial pressure) making it difficult to conclusively compare the studies. VLE data generated by fast/rapid screening are due to their nature lower than equilibrium measurements. Bernhardsen and Knuutila [198] give an overview of the setups used by groups from RITE in Japan [223], Masdar Institue in United Arab Emirates [197, 224], University of Twente in Netherlands [225], NTNU in Norway [226–228], CSIRO in Australia [229], and Korea Institute of Energy Research [230–232]. Missing are the setups at UT Austin in USA [233], University of Illinois in USA [234], Hunan University in China [235, 236], and University of Regina in Canada [237–239]. Some discrepancies and inconsistencies in previous screening approaches *e.g.,* loadings measured by rapid screening setups larger than their corresponding equilibrium value, are discussed by Bernhardsen and Knuutila [198]. The advantages and disadvantages of experimental techniques used

for measuring absorption kinetics are reviewed in [91] and [83].

According to a search on Scopus [240], around 2000 studies containing the keywords *CO_2 capture*, *solvent*, and *techno-economic* have been published in the last ten years. Missing so far is a comprehensive overview of studies comparing amines via experimental or modelling approaches targeting KPIs on molecular, process, or techno-economic level which helps minimising repetitive work and focus on the key issues. Figure 2.2 summarises 115 studies on a quantitative level only, and highlights this work's contribution in presenting a full techno-economic analysis for a large number of amines (see Tab. A.1 for list of studies). For readability purposes, studies reporting fewer than three solvents including many site-specific techno-economic modelling studies are omitted. The vast majority of literature reports experimental screening approaches targeting thermo-physical properties (indicated by the molecule symbol). Far fewer studies report KPIs associated with the process *e.g.,* reboiler duties (indicated by the process symbol), and six studies compare solvents on a full techno-economic basis (indicated by the $ symbol). This contribution reports a short-cut, optimised techno-economic screening of CO_2 capture solvents for a large pool of candidates at the techno-economic level.

Selected approaches and studies with their key assumptions and conclusions are discussed over the next paragraphs to provide a qualitative assessment. One of the first ever screening of amines for CO_2 capture was performed by Bottoms preceding his patent in 1930 [101, 241]. He experimentally tested primary, secondary, and tertiary as well as linear and cyclic amines, alkanolamines, alkylamines, hydrazines, poly-amines, amino acids, and heterocyclic nitrogen bases. He listed some amines as particularly suitable of which all but the hydrazines were screened as part of this work. Interestingly, Bottoms [101, 241] completely ignored kinetics but discussed degradation and identified heat stable salts as a potential problem. He compared the amines to aqueous alkali solutions, which were the benchmark at that time.

77 years later, Bernhardsen and Knuutila [198] conducted the yet largest screening with 132 single aqueous amine solvents. The solvents are compared at 30 wt% amine, constant partial pressure, and 40℃. The KPIs of interest were absorption capacity, cyclic capacity, and pK_a. No single amine was found to be superior in both absorption and cyclic capacity yet many amines

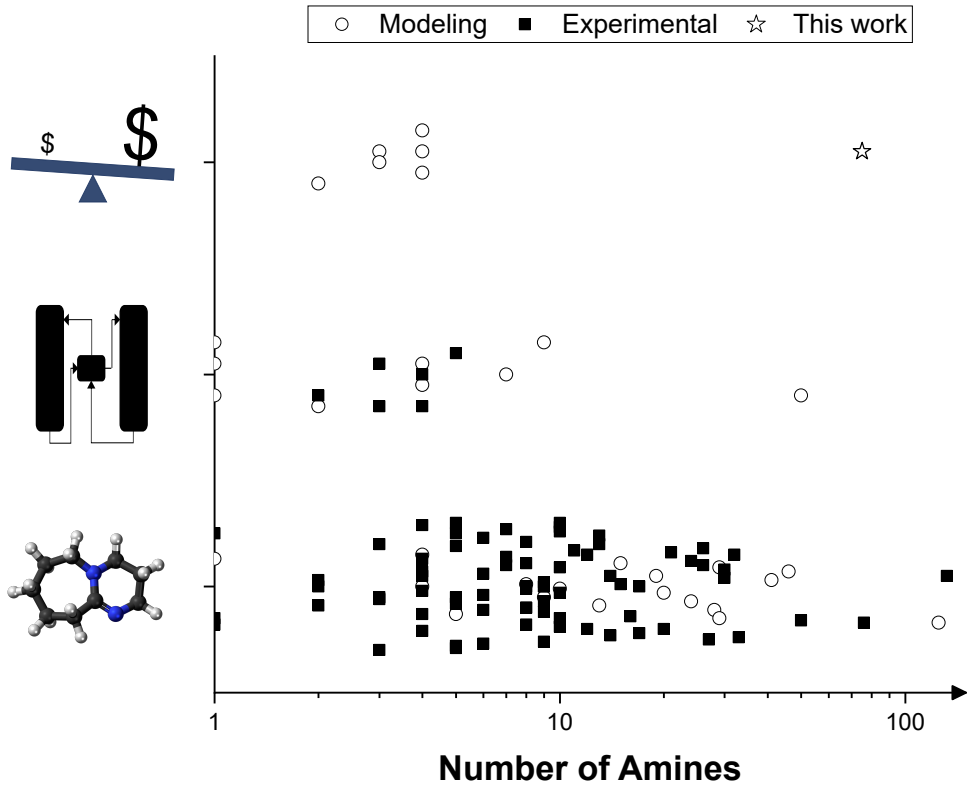


Figure 2.2: Overview of screening studies by type (experimental vs modelling), number of amines screened, and level of detail: thermo-physical properties (molecule symbol), capture process KPIs *e.g.,* reboiler duty (process symbol), and techno-economics ($ symbol). SQUASH (this study) is the first fully optimised techno-economic screening of a large candidate pool. Details about screening studies in appendix.

outperformed MEA. Bougie and Iliuta [133] reviewed properties (density, viscosity, vapour pressure, heat capacity, heat of absorption, diffusivity, absorption capacity and kinetics) of 13 sterically hindered amines and their binary and ternary blends without drawing a comparison to MEA.

Porcheron *et al.* [242, 243] screened 50 mono-amines at 30 wt% utilised in an archetypal absorber-stripper process by measuring absorption isotherms at 40°C. They built a phenomenological short-cut model that uses a limited set of lab-scale measurements (isotherms) to predict the required reboiler duty. An artificial solvent with a cyclic capacity of 1 mol/mol and a molar mass of 130 g/mol yielded a specific reboiler duty of 2.8 MJ/kg_{CO_2} in their model. Porcheron *et al.* suggest to utilise statistical learning modelling and quantitative structure property relationships (QSPR) where solvents would be considered structured data [242, 243]. Such an approach requires a large database, which is currently not readily available. Most data is spread

throughout the literature and differences in approach and inconsistencies make it a non-trivial task.

Robinson *et al.,* [244] and Conway *et al.*, [245] analysed structural derivatives of piperidine with similarity to piperazine by selectively adding carbon chains, hydroxyl groups, and alkalinities, around the cyclic ring parent structure. They measured cyclic capacity via FT-IR [244] and 13 C NMR spectroscopy [245] at y_{CO_2}=15 mol% and 40℃ and 90℃. Nearly all candidates outperformed MEA in cyclic capacity but their underlying assumptions in the presented short-cut estimation of the reboiler duties deem the results rather relative than absolute. In a follow up study by the same authors [246], they systematically designed di- and tri-amines and found eight candidates with more than 200% higher cyclic capacity (per alkalinity) than PZ. A similar study by Muchan *et al.,* [141] analysed the impact of adding amine functionalities from one (MEA) to five (TEPA) alkalinities and found that equilibrium loadings and absorption rates increased non-linearly but regeneration energy decreased with an increasing number of amine groups.

In another study by the same authors, [247], Conway *et al.,* modelled the impact of blending 2.5M MEA with an equimolar artificial amine resembling a sterically hindered or tertiary amine by modifying equilibrium constants and heat of absorption. In a further study [248] they mixed 14 blends containing MEA, AMP, DEEA and DMEA and quantified the impact of mixing ratios and overall amine concentrations on the capacity and mass transfer rate at 40℃. They found that mass transfer rates were slower compared to MEA and the absorption capacity was similar to MEA. However, the blends' cyclic capacity was much higher than MEA's, and they concluded that 3M MEA + 3M AMP was the optimal compromise.

Puxty *et al.,* [229] experimentally screened 76 amines at 30 wt% for absorption capacity. They used the alkalinity normalised loading mol_{CO_2}/mol_{Alk} for a comparison of amines that either have one or multiple alkalinities. They found seven amines to have higher than expected absorption capacities and ultimately were unable to explain the performance solely with the reaction pathways. In another study [249], they screened 68 co-solvents to reduce the higher-than-expected vapour pressure of promising BZA based solvents. They kept the concentrations

constant at 30 wt% BZA + 30 wt% co-solvent with the remainder being water, and the temperature at 40℃. In even another recent study, Puxty *et al.,* [250] examined the potential of utilising aromatic amines that have not been considered widely due to their assumed low solubility in water [251] and toxicity [252]. They limited the selection to molecules with separated amino group and aromatic functionalities, *e.g.,* BZA, which are less prone to possible degradation reactions due to their delocalised electron systems. The rationale is that the rigid aromatic structure leads to a smaller entropy and enthalpy change during the amino protonation, thus reducing the regenerative heat requirement. They analysed ten aromatic amines and measured two candidates in a pilot plant finding mass transfer rates in the range of MEA.

El Hadri *et al.,* [197] screened 30 amines at 30 wt% and 40℃ for absorption capacity and heat of absorption as well as kinetics for a sub-selection of amines. They identified six amines (five tertiary, one secondary) with lower heats of absorption at higher equilibrium loadings than MEA. El Hadri *et al.,* propose the use of tertiary amines due to their low heat of absorption and high loading. Another study by the same research group [253] suggest to abandon further research activity on MDEA, 1DMA2P, 2DMA2P and 3DMA2P due to low absorption capacities and recommends a blend of EAE or MAE with TMPDA.

A research group based at the Khalifa University, Abu Dhabi focuses on molecular modelling approaches, in particular soft-SAFT [254], for screening absorbents (aqueous amines [255, 256], non-aqueous hybrid amines [257–259], deep eutectic solvents [260, 261], ionic liquids [262]) and adsorbents [263]. These assessments use Kim *et al.,*'s short-cut model [264] to estimate the energy requirement and the cyclic capacity by assuming non-optimised fixed operating conditions for the absorber and reboiler. The associated chemical absorption processes (DES and ILs are physical solvents capturing at pressures > 1000 kPa [261]) were not evaluated due to the lack of mass transfer rates and kinetics.

Yamada *et al.*, [265, 266] used ^{13}C NMR analysis to differentiate between the structural isomers AP, PAE, and IPAE in regards to the reaction mechanisms and absorption capacity. They used density functional theory with dielectric continuum solvation models to analyse the impact of alkyl and alcohol chain lengths in alkanolamines. Their results show that the alcohol length

affects the absorption capacity by forming intra-molecular hydrogen bonds and the alkyl chain length had only minor impact.

Ye *at al.,* [234] screened phase-change ternary blends containing an absorption promoter (24 primary or secondary mono- and poly-amines) and regeneration promoter (tertiary amines, DMCA and DEEA). They found blends with linear absorption promoter to show better performance than their cyclic or secondary isomer counterparts. The tested poly-amines did not greatly increase the equilibrium loading presumably due to solubility and kinetic limitations. They identified poly-amines with three to four alkalinities and four to six carbon atoms to show the best performance at minimal operational concerns (solid precipitates, high viscosity, and high volatility). In particular, they claim TETA + DEEA to be the most desirable blend. These results were confirmed by other tests [232]. Yu *et al.,* [267] used molecular dynamics to find the optimal synergy in multi-amine blends between MEA, DEA, MDEA, TEA, AMP. They limited the analysis to diffusivity and mass transfer KPIs and found the synergy in ternary amine systems to be superior compared to quaternary and quintuple mixtures.

Limleamthong *et al.,* [217, 268] used data envelopment analysis and created a non-parametric analytical tool that simultaneously assesses the LCA (cradle to gate ignoring operations of capture plant), and performance of 125 aliphatic, acyclic amines. Their model uses correlations to predict the KPIs and no capture plant is designed. They interpreted the screening as a multi-criteria decision-making problem [269] and found that no single pareto optimal amine exists based on their KPIs (vapour pressure, viscosity, capacity, surface tension, toxicity), with vapour pressure being the most critical property. Interestingly, 36% of the 125 solvents were identified as insufficient for CO_2 capture.

A chemoinformatics study [179] developed quantitative structure-property relationships (QSPR) by building a database, assigning molecular descriptors/fingerprints, and correlating data via neural networks. They identified 41 mostly tertiary candidate solvents of which 25 amines had a dataset containing only absorption capacity, absorption rate, and heat of absorption. Interestingly, they rejected a sub-sample size of six candidate solvents as insufficient data and found 41 candidates being too few. While this study is more advanced in terms of machine-learning

and data-visualisation compared to other studies, it crucially misses to include chemical information such as steric hindrance in their approach, thus, brute forced relationships with low predictability. Popescu *et al.*, [270] created a surrogate model based on collected equilibrium loading and heat of absorption data for nine amines and seven blends. Most of their surrogate model data shows huge discrepancies to this work's database, in particular, they list the heat of absorption for MEA as -28 kJ/mol_{CO_2} which is inconsistent with the reported loadings and the Gibbs-Helmholtz equation. As a consequence, they find MEA to be the best performing solvent, even outperforming PZ, although they calculated a L/G ratio of 16 mol/mol for MEA, which is ten times higher than measured in pilot plants [271]. Both studies [179, 270] exemplify the need for a database and chemical information necessary to correctly interpret data and structure-performance relationships.

Two other chemoinformatics studies [186, 272] successfully developed QSPRs via machine learning. Momeni and Riahi [272] used only four molecular descriptors for linear amines free of steric hindrance. Rozanska *et al.,* [186] successfully trained the algorithm on 177 solvents with an extended list of group descriptors, and limiting their solvent selection on one chemical class. They used computationally demanding molecular dynamics with classical force fields to predict the Gibbs free energies and solvation energies [273] which enabled them to accurately predict the reaction rate of 24 tertiary amines. Rozanska *et al.,* found that only explicit molecular dynamics simulations are able to accurately predict kinetics based on the molecular structure, because only that method captures the amine disrupting the solvation cells. These solvation effects and small changes in molecular structure have considerable impact on the reaction rate, but so far implicit solvation models and cheminformatics-based QSPR relationships failed to capture them. Their model is only valid if the rate determining step is limited by the activation barrier of $CO_2 + OH^- \rightleftharpoons HCO_3^-$ and the educts' concentration. Ultimately, this approach is constrained by the need for experimental data, fixed chemical class (tertiary amines), and computational effort.

Further screening studies including studies focussing on practical elements such as degradation [274], volatility [275], or corrosion are listed in the appendix Tab. A.1 with number of amines screened, methods, KPIs, are further details. The main observations drawn from the literature

review is that the studies with the most amines [197, 198, 229, 242, 243] screened them at constant 30% weight fraction without providing evidence behind that assumption, and limited the scope to selected thermo-physical properties. The insight generated is helpful, but not sufficient to rule out specific chemical classes.

2.3.3 Screening Tools

This section discusses first the available process models and topologies deployed in previous screening studies, and then thermodynamic approaches for modelling heat and mass transfer. The aim is to identify the needs and preferred models for a screening model that could be used in this work.

Process Modelling Comparing and identifying a superior simulation tool is a non-trivial task as each model was develop for a specific purpose [276]. Luo *et al.,* [276] compared six commercial simulators (Aspen Rad Frac, Protreat, Promax, Aspen Rate Sep., CHEMASIM from BASF, and CO2SIM from SINTEF/NTNU) with sixteen datasets from pilot plants utilising 30 wt% MEA. Overall performance matched reasonable well, however, reboiler duties were less accurately predicted. The Octavius FP7 project [277] compared six simulators (three in-house tools CO2SIM, CAPCO2, and IFP Energies Nouvelles's model as well as three Aspen tools) again utilising 30 wt% MEA and found that predicted thermo-physical properties varied by 5-10% (AARD). All tools are rate-based but differ in modelling context, numerical approach, and thermodynamic models. Both studies [276, 277] were able match the results of the tools with pilot plant data by fine-tuning the software. This in turn led to over-fitting, and poorer accuracy outside the benchmark of MEA. The resulting expected accuracy in KPIs such as capture rate, flooding, reboiler duty, or solvent flow rate is ± 10%. In both studies [276, 277], the temperature profiles and reboiler temperature scattered more than ± 10%.

The HiPerCap project [278] screened and assessed post-combustion technologies (absorption, membrane, adsorbent) utilised in archetypal process topologies and battery limits similar to this work. The project compared four solvents: Enzyme catalysed PRLD and DMMEA, precipitating alanine and taurine, and two strong bicarbonate forming solvents. No system outperformed

CESAR1 and all absorption systems ranked closely to each other.

Agbonghae *et al.*, [279] minimised the capture cost of an archetypal capture unit utilising 30 wt% MEA by optimising equipment size, solvent circulation rate, and lean loading. They modelled four commercial sized power plants (400 MW_e and 450 MW_e NGCC as well as 673 MW_e and 827 MW_e coal-power) and found the optimal L/G ratio (kg/kg) to be 0.96 for NGCC and 2.8 for coal.

Asprion *et al.,* [280, 281] developed a toolbox INES as an interface between experiments and process development that integrates and combines different approaches and tools. It is a platform that involves the full workflow of a process developer including data selection and reconciliation, model validation, sensitivity analysis, optimization, design of experiments, and operations with a focus on industrial needs for BASF. It is based on BASF's in-house tool CHEMASIM and provides interfaces to other software such as Excel, plant information management systems *e.g.,* Info-Plus.21 (ASPEN) or PI (OSIsoft). The INES toolbox is a process design tool and appears not suitable for rapid screening [280]. Applying frameworks such as INES for screening through an often incomplete database will cause problems in consistency and computational effort [280, 281]. A combination of two approaches appears favourable: First, an initial screening identifies the most interesting candidate molecules, followed by the INES toolbox accurately designing the process for industrial needs.

Other noteworthy tools are the Carbon Capture Simulation Initiative (CCSI)'s capture model presented in [282–286], UT Austin's Pheonix model [287], the iCCS3 tool developed by SINTEF [288, 289], and Raksajati's model [290, 291]. They all include rigorous thermodynamic models requiring considerable computational effort making them less practical for screening solvents. The main observation is that screening studies use an archetypal process topology, and include some optimisation regarding equipment size and operating conditions *e.g.,* lean loading.

Model Selection There is a risk of introducing systematic errors by selecting different approaches between candidates. The aim of this section is to identify preferred approaches which should be used to model the capture plant for a diverse candidate pool. Various methods

have been reviewed in [162, 163, 292–297], and individual aspects are discussed over the next paragraphs.

Razi *et al.,*'s [292] review on the absorber's hydrodynamic design found large uncertainties when applying correlations at scales required for CCS outside their verified validity range. They compared eleven hydrodynamics correlations (pressure drop, flooding point) and 17 mass transfer and interfacial area correlations by modelling an absorber with structured packings utilising MEA at fixed operating conditions. They further validated ten mass transfer and interfacial area correlations (Bravo *et al.* (1985) [298], Bravo *et al.* (1992) [299], Billet and Schultes [300, 301], Rocha *et al.* [302], Brunazzi *et al.* [303, 304], Gualito *et al.* [305], Xu *at al.* [306], Tsai *et al.* [307], Hanley and Chen [308], Zakeri [309]) and three kinetic models (Versteeg [124], Phoenix [287, 310, 311], and AspenPlus/Hikita *et al.,* [312, 313]) describing MEA utilised in the CESAR pilot plant absorber at the DONG Esbjerg facility (400MW_e coal-power) [293]. They found discrepancies between simulated and measured results with a wide spread between the correlations due to the high number of involved parameter, various underlying assumptions, and application ranges. Razi *et al.,* [293] conclude that any rigorous model requires a kinetic model as well as correlations for mass transfer and interfacial area preferably developed for a specific solvent which has been validated against plant data. This guidance is not practical for a screening model.

Putta *et al.* [294] followed up on Razi *et al.,*'s work and found that the kinetic model selection affects the rate of absorption more than the mass transfer model selection. Changing the correlation for the Henry's coefficient introduced the largest discrepancies. They compared four thermodynamic models (Putta *et al.*'s e-NRTL model [314], Aronu *et al.*'s extended UNIQUAC model [315], Hessen *et al.*'s refined e-NRTL model [316], and Aspen Plus's e-NRTL-RK model [312]) and six kinetic models (Hikita *et al.* [313, 317], Versteeg *et al.* [123], Aboudheir *et al.* [154], Aspen Plus [312], Luo *et al.* [318], Putta *et al.* [314]) and again found no superior model. They compared nine models for the Henry's law coefficient, and eight models for the CO_2 diffusivity recommending that N_2O-analogy based predictions are superior over Stokes-Einstein correlations [314]. Putta *et al.* strongly advise against a "pick n' mix" approach by blending methods presented in the open literature and implemented in commercial process

simulators *e.g.,* mixing an open literature kinetic model and a physio-chemical thermodynamic model from a commercial tool. Comparing individual thermodynamic parameters entangled with a specific method or correlation (*e.g.,* velocities inside a column) need to be seen in the wider context of the overall absorber design [314]. This also applies to experimental screening reporting the mass transfer rate which depends on the interfacial area that will differ from set-up to set-up [198].

Amirkhosrow *et al.* [319] compared four mass transfer correlations and 15 kinetic correlations (second order and termolecular) and additionally analysed the impact of discretizing the liquid film. They confirmed that developing an accurate absorber model is viable without discretizing the liquid film for the case of MEA. Afkhamipour and Mofarahi [320] present a comprehensive list of mass transfer studies for a range of solvents (MEA, DEA, MDEA, AMP, PZ, 1DMA2P, DETA, DEEA) in randomly packed columns, and highlight that most correlations are only valid for a specific combination of solvent and packing. Such empirical correlations enable short-cut modelling without calculating enhancement factors but are highly limited. The main observation is that a variety of process modelling approaches are available, however, no general recommendation for specific heat and mass transfer models has given in the literature that would cover the candidate pool.

2.4 Uncertainty of CCS Process Modelling

2.4.1 Statistical Background

Distributions Any output calculated under uncertainty can be described through a probability function, *e.g.,* standard, normal or Gaussian. A normal distribution is characterised by uni-modal, bell-shaped, and symmetrically distributed values with variable mean and standard deviation. The mean, mode, and median values are equal. The mean μ indicates its location and the deviation σ indicates its spread [321]. A normal distribution is described with the

following equation with x indicating a random variable, *e.g.,* capture cost.

$$f(x) = \frac{1}{\sigma\sqrt{2\pi}} \cdot e^{-\frac{1}{2}\left(\frac{x-\mu}{\sigma}\right)^2} \tag{2.4}$$

The standard deviation σ can be calculated by the individual values x_i, the mean of the population μ, and the population size N. If a finite amount of samples n is analysed, then $N = n-1$ [321].

$$\sigma = \sqrt{\frac{\sum (x_i - \mu)^2}{N}} \tag{2.5}$$

In case of a sample data set, the standard deviation s is calculated by $s = \sqrt{\frac{\sum_{i=1}^{n}(x_i-\bar{x})^2}{n-1}}$. The notation $x \sim \mathcal{N}(\mu, \sigma^2)$ means that the variable X follows a normal distribution with a mean of μ and a variance of σ^2.

A standard distribution is a special case of a normal distribution with the mean being zero and the standard deviation equal to one. Any normal distribution can be transferred into a standard distribution by calculating the z-score from the data points x. The mean of the z-scores is zero and its standard deviation is one. Any normal distribution is a modified (stretched or squeezed) standard distribution. Approximately 68% of data points fall within one standard deviation of the mean, approximately 95% of data points fall within two standard deviations of the mean, and approximately 99.7% of data points fall within three standard deviations of the mean [321]. The central limit theorem says that any sample's mean will be normally distributed if the sample size is large enough, regardless of the actual distribution (*e.g.,* Poisson, binomial, see A.7 in the appendix). By convention, the central limit theorem applies if $N > 30$ and the population has finite variance [322].

A confidence interval CI can be calculated by

$$CI = \bar{x} \pm z\frac{s}{\sqrt{n}} \text{ and } CI_{95\%} = \bar{x} \pm 1.96\frac{s}{\sqrt{n}} \tag{2.6}$$

with the sample mean $\bar{x}$, confidence level z, sample standard deviation s (σ is the population's standard deviation), and the sample size N. A 95% confidence level means that 95% of all

samples will be expected to be within a confidence interval of ±1.96 standard errors $\frac{s}{\sqrt{N}}$ of the sample mean, *i.e.,* $z = 1.96$ [321]. The 95% confidence interval is used for data fitting, and to describe the calculated capture cost mean. For the latter it means that running the model with any combination of individual contributing errors for one solvent at otherwise unchanged operating conditions for 100 times will results in 95 mean capture costs falling in that range [321]. For data fitting it means that 95% of all data points are expected to be within ±1.96 standard errors of the value calculated by a fitted function.

Statistical Indices The ability to accurately predict a value x_i^{Pred} through a function based on a number N of data points with value x_i^{Data} and mean value $\bar{x}^{\text{Data}} = \frac{1}{N}\sum_{i=0}^{N-1} x_i^{\text{Data}}$ can be described through the following well known statistical indices [321].

- Coefficient of determination $R2 = 1 - \frac{\sum_{i=0}^{N-1}(x_i^{\text{Data}} - x_i^{\text{Pred}})^2}{\sum_{i=1}^{N}(x_i^{\text{Data}} - \bar{x}^{\text{Data}})^2}$
- Mean squared error $\text{MSE} = \frac{\sum_{i=0}^{N-1}(x_i^{\text{Data}} - x_i^{\text{Pred}})^2}{N}$,
- Root mean square error $\text{RMSE} = \sqrt{\frac{\sum_{i=0}^{N-1}(x_i^{\text{Data}} - x_i^{\text{Pred}})^2}{N}}$,
- Mean absolute error $\text{MAE} = \frac{1}{N}\sum_{i=0}^{N-1} |x_i^{\text{Data}} - x_i^{\text{Pred}}|$, and
- Average absolute relative deviation $\text{AARD} = \frac{100\%}{N}\sum_{i=0}^{N-1} |\frac{x_i^{\text{Data}} - x_i^{\text{Pred}}}{x_i^{\text{Data}}}|$

The coefficient of determination R2 is an indication for goodness of fit, and represents the variance in the independent input data x_i^{Data}. R2's range is limited to $(-\infty, 1]$ with R2 = 1 being the best fit. R2 describes how well any sample is going to be predicted by the function and shall not be mistaken with Pearson's correlation index R_{Pearson}. R_{Pearson} is a statistical index that quantifies the strength and direction of a linear function between two variables and is limited to $[-1, 1]$. $R_{\text{Pearson}} \approx 0$ indicates no linear relationship, $R_{\text{Pearson}} \approx 1$ a strong positive linear relationship, and $R_{\text{Pearson}} \approx -1$ a strong negative linear relationship. It is meaningless for non-linear relationships [321].

Both mean square error MSE and root mean square error RSME are limited to $[0, \infty)$ with the best score being zero. They are often used to quantify the accuracy of *e.g.,* a regression

model, and measure the difference between the predicted values and the actual values. The mean absolute error MAE is also used to quantify the accuracy of models by averaging the absolute differences between x_i^{Data} and x_i^{Pred} and its range is $[0, \infty)$. MSE, RMSE, and MAE depend on the scale of x_i. In contrast, the average absolute relative deviation AARD (or mean absolute percentage error), enables comparing the accuracy of different methods or functions independent of the scale of x_i by normalising the deviation. AARD ranges from $[0\%, \infty)$ with low values indicating higher accuracy, *i.e,* AARD $= 0$ is a perfect fit [321].

2.4.2 Methods for Determining Uncertainty

Process modelling is an established tool for predicting techno-economic performances [81]. Uncertainty analysis in process modelling is equally established [323–332], yet only a handful of studies [290, 333, 334] combined both fields and tried to quantify the error in calculated CO_2 capture performance and cost. The main challenge is describing errors that are propagating through models in a mathematically sound and computationally effective way. Some tools simply do not allow for such tasks by hiding the underlying models from the user.

Important terms are uncertainty, variability, and bias [335, 336]. Uncertainty describes the deviation between an assumed, calculated, or measured value and its real value. Sometimes it is not possible to know the real value, and one can only get very close to it *e.g.,* measuring the temperature of an object. Variability can be quantified and describes the range of potential values *e.g.,* the temperatures of an object before and after it is heated up, or the price of goods. Bias describes the impact of making certain assumptions and decisions that favour one outcome over others. Some biases are illogical, *e.g.,* modellers concluding their model must be accurate if some performance indices match experimental pilot data. Other biases are combined, *e.g.,* shifting capital into operating costs (or vice versa) when the corresponding cost of capital or cost of consumables are dominating. Six categories of uncertainties have been identified in the literature [337], and not all of them are quantifiable:

1. *Contextual* uncertainty, describing the impact of decisions on system boundary/battery limits.

2. *Model* uncertainty, describing the impact of (*e.g.,* thermodynamic) models used to describe processes.

3. *Parameter* uncertainty, describing the impact of assuming specific parameter, *e.g.,* price of steam or amines.

4. *Input* uncertainty, describing the impact of the quality of data fed into the model, *e.g.,* accuracy of thermo-physical properties measured.

5. *Methodological* uncertainty, describing the impact of using a specific method, *e.g., in-silico* screening versus experimental screening.

6. *Epistemic* uncertainty, describing impact of the state of knowledge base, *e.g.,* well-established versus contested reliability.

CO_2 capture solvents date back over a century [101], thus, one can assume a well-established knowledge base for screening aqueous amines. Methodological uncertainty was discussed in section 2.3.2. Contextual uncertainty is often a source of discrepancies between techno-economic assessments, *e.g.*, omitting upstream and downstream units of the capture unit which are outside the boundary layer. The remaining three categories of uncertainties (model, parameter, and input) can be determined by the following methods [191, 335, 337–339]: 1. Sensitivity analysis , 2. Validation, 3. Model comparison, 4. Multiple model simulation, 5. Bayesian networks, 6. Scenario analysis, 7. Error propagation, 8. Monte-Carlo analysis, 9. Polynomial chaos expansion, 10. Pedigree analysis.

Varying a variable within a range (classic one-at-a-time sensitivity analysis) is the most common and simplest method of quantifying any uncertainty, but it ignores interactions between variables, thus, it is not a suitable method of describing any actual errors [335]. Its main purpose is evaluating the impact of variables and identifying the variables with the highest sensitivity. Some modelling platforms do not offer built-in sensitivity features, and users rely on factors or manipulating underlying coefficients. The input range for a sensitivity analysis is often randomly selected *e.g.*, $\pm 50\%$, and some variables are not subject to variability because

they are the result of complex non-linear calculations *e.g.,* mass transfer rate [335]. Sensitivities quantify the variability of input parameter *e.g.*, price of steam, on the capture cost. Some studies [340] varied thermo-physical properties by ± 50% regardless of the range observed in solvents. Educated guesses informed by the available data range return more meaningful results and are known as one-way sensitivity analysis. This work selected one-way sensitivities to analyse the impact of thermo-physical properties and one-at-a-time sensitivities for prices of consumables. During a validation the output data of a model is compared to real world data. Such approach will only quantify the relative difference between the model's KPIs and reality and not the uncertainty in the model's KPIs. Validating against real world data is critical and essential to prove the goodness of the tool in matching reality. The purpose of this work is to relatively rank candidate solvents. Data for some pilot plants and solvents is available, thus, only a limited validation is possible.

Propagation- and probabilistic methods quantify errors by propagating levels of uncertainty through a model [341]. They differ in the way how errors propagate: Full Gaussian error propagation is often numerically and practically too challenging for a complicated network of equations. Probabilistic methods, *e.g.,* Monte-Carlo analysis, determine the error by repeated random sampling. In a Monte-Carlo analysis probability density functions of uncertainties (fitted to the actual uncertainties of the variables) are propagated through a model in many runs [326]. The same happens during a polynomial chaos expansion but is simultaneously combined with a sensitivity analysis. Probabilistic methods return information about how likely an outcome is, and are more suited to determine variability [335, 337]. Poorly compiled probability density functions will yield weak results, and might create a false sense of certainty [335].

Pedigree analysis is a qualitative method in which experts judge the confidence in data and knowledge, thus, it is biased and subjective [337]. Subjectivity can be reduced with pedigree matrices and set quality criteria after which the experts are rating (sub)models and data [342]. Increasing the number of experts might average out any outliers, however, qualified experts in CO_2 capture modelling are a finite source. When the experts' judgements are propagated through a model then this method becomes semi-quantitative. This method identifies model

weaknesses *e.g.,* any input KPIs that rank low in the quality criteria (*i.e.,* low confidence) and simultaneously have considerable impact on the output KPI.

2.4.3 Previous Works

Previous works [343, 344] linked experimental uncertainties with perturbation schemes for liquid phase fugacity coefficients for pure components and mixtures. The perturbation of thermodynamic models is replicated by introducing uncertainties in the directly associated physical properties and implemented in Aspen and BASF's in-house tool CHEMASIM [343, 344]. In the case of negligible Poynting correction, Burger *et al.,* [344] derived an analytical expression for the pertubation factor of the vapour pressure using equation of states, allowing a physical interpretation. They applied it to the VLE of CO_2 in methanol as calculated by the Soave-Redlich-Kwong equation. It is unlikely that analytical expressions for the error of a higher order KPI such as specific reboiler duty or capture cost can be derived. Mathias and coworkers [190, 191, 334, 345, 346] focused in particular on the uncertainty associated with the VLE of systems and its impact on the process design.

Uncertainties in solvent based CO_2 capture simulations have been reported for MEA [337, 347], AMP [191, 334], CESAR1 [333], and adsorbents [348, 349]. However, they are based on sensitivity/pedigree analysis rather than propagations, and did not quantify errors. The difference between two capital cost estimates for the same system (CESAR1) was 110% [333] although both studies claim a $\pm$ 30% accuracy.

Quality (costing) guidelines from the USA [350] or EU [351] and the field's leading bodies IEGHG and ZEP (Zero Emissions Platform) [352], only recommend simple one dimensional sensitivity analysis instead of sound uncertainty quantifications, thus, providing unsatisfactory guidance. This void was partially filled by Van der Spek *et al.,* [335], yet it remains to be seen if practitioners adopt the more complicated approaches. An overview of available software for uncertainty and sensitivity analysis is presented in [335].

It is not clear, if the uncertainties in thermo-physical properties prevent a statistical significant screening with a short-cut model. The capture cost error is directly correlated to the

underlying uncertainty in the thermo-physical property data, thermodynamic correlations, and costing equations that propagate through the equation network. In this work, background and foreground uncertainties are discussed, input uncertainty propagated, and differences between mean capture cost tested on statistical significance.

2.5 Research Gap

A rapid screening approach is attractive due to its speed and simplicity. There is the need for a database and screening model that relatively ranks candidate amine solvents based on differences in their thermo-physical properties. It should be able to propagate input errors, and test the relative differences on statistical significance. The tool should sit between detailed rigorous models that require more computational effort, and equilibrium models that lack equipment sizing. It should reflect the most important KPIs, and include economic optimisation. It would be useful to have a tool that allows data input by non-engineers.

3. Screening Tool

3.1 Objectives

This chapter presents the solvent database and model formulation of the screening tool SQUASH (**S**creening and **QU**antitative **A**ssessment of **S**olvents **H**euristics). The objective is to create a database containing at least 100 candidates, and develop a short-cut model that can rank the candidates within seconds by screening under uncertainty. Only solvents with already existing full datasets are to be screened, and at least one amine representing each primary-, secondary-, tertiary-, or poly-amines with two-, three-, or four alkalinities. The model should be made accessible through a graphic user interface allowing importing input data and exporting results. Some material from this chapter has been published in [112].

3.2 Solvent Database

3.2.1 Procedure

Candidate Selection The database contains information regarding the chemical class, structure, abbreviations, alternative names, IUPAC nomenclature, CAS number, InChI, SMILES, PubChem CID, molecular formula, Reaxys ID, molar mass, standard state, boiling as well as melting temperatures at atmospheric pressure. All data entries underwent a standard protocol to account for wrongly annotated solvents, structural discrepancies (*i.e.,* compounds with non-matching structure and other characteristics), and structural duplicates (*i.e.,* identical compounds). Figure 3.1 summarises the work flow.

It is intended to screen only solvents, thus, it is required to filter for candidate molecules. The required filter criteria in order of sequence are listed below:

1. Matching CAS number, molecular weight, and molecular structure ensuring proper identification of the molecule.

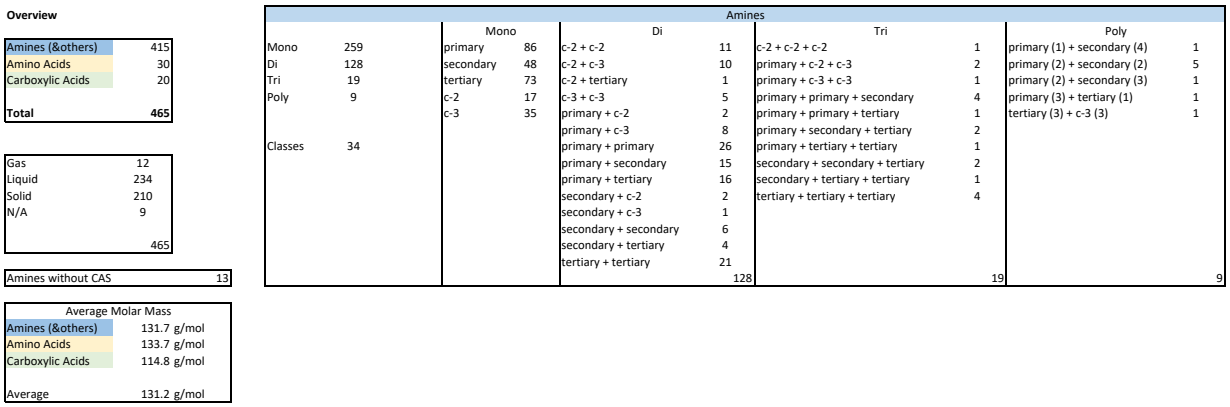


Figure 3.1: Decision tree analysing if a new molecule should be added to the database, merged with an existing entry, or rejected.

2. Boiling point $> 20°C$ eliminating gases at standard conditions (1 atm and 20 °C). Gases are unfit for the modelled capture process.
3. If a molecule is solid at standard conditions, then its solubility in water has to exceed at least 1 mol%.

The requirements on phase, boiling point and solubility will eliminate molecules that cannot be modelled with the process topology selected, *e.g.*, solid adsorbents which should be utilised in a pressure swing system. The solubility limit corresponds to the commonly found lower end of molarities for commercial aqueous amines [353]. It corresponds to a molality of $\approx 0.5 \frac{\text{mol}_{\text{Solute}}}{\text{kg}_{\text{H}_2\text{O}}}$. Molarity M is given in $\frac{\text{mol}_{\text{Solute}}}{\text{L}_{\text{Solution}}}$ and molality m in $\frac{\text{mol}_{\text{Solute}}}{\text{kg}_{\text{H}_2\text{O}}}$. The requirements do not exclude poor choices, *e.g.*, candidates with low boiling points, causing solvent evaporation. These candidates could theoretically be screened, and will likely return high capture cost. Setting further thresh-

olds indicative of high-performing solvents *e.g.*, heat of absorption, could eliminate candidates which is not in the interest of this work. Information about possible multiphase behaviour was entered into the database, although the archetypal process topology is not capable of extracting the maximum performance of multi-phase solvents. The molecules were then entered into an Excel database sorted by their chemical class. Figure 3.2 shows the summary of that Excel file.



Overview

Amines (&others)	415
Amino Acids	30
Carboxylic Acids	20
Total	**465**

Gas	12
Liquid	234
Solid	210
N/A	9
	465

Amines without CAS	13

Average Molar Mass	
Amines (&others)	131.7 g/mol
Amino Acids	133.7 g/mol
Carboxylic Acids	114.8 g/mol
Average	131.2 g/mol

Amines									
		Mono		Di		Tri		Poly	
Mono	259	primary	86	c-2 + c-2	11	c-2 + c-2 + c-2	1	primary (1) + secondary (4)	1
Di	128	secondary	48	c-2 + c-3	10	primary + c-2 + c-3	2	primary (2) + secondary (2)	5
Tri	19	tertiary	73	c-2 + tertiary	1	primary + c-3 + c-3	1	primary (2) + secondary (3)	1
Poly	9	c-2	17	c-3 + c-3	5	primary + primary + secondary	4	primary (3) + tertiary (1)	1
		c-3	35	primary + c-2	2	primary + primary + tertiary	1	tertiary (3) + c-3 (3)	1
				primary + c-3	8	primary + secondary + tertiary	2		
Classes	34			primary + primary	26	primary + tertiary + tertiary	1		
				primary + secondary	15	secondary + secondary + tertiary	2		
				primary + tertiary	16	secondary + tertiary + tertiary	1		
				secondary + c-2	2	tertiary + tertiary + tertiary	4		
				secondary + c-3	1				
				secondary + secondary	6				
				secondary + tertiary	4				
				tertiary + tertiary	21				
					128		19		9

Figure 3.2: Overview of the Excel database for candidates.

464 candidates with a focus on amines were identified (see chapter B.1 in the appendix). The candidate pool is more than ten times larger than [179] which found 41 solvents not being enough for machine learning based approaches. It is also 3.5 times larger than the most comprehensive screening so far [198]. About 45% of all candidates are solid at standard conditions.

Thirteen amines in the database have no CAS number assigned, which is widely seen as the gold standard of chemical identification. This points out the need for a standard protocol for proposing candidate molecules. It is common practice to refer to the amines by an abbreviation. However, these vary between sources, and based on experience, approximately 10% of the literature referred to the same compound by different names and/or abbreviations. In some cases, chemical structure and other identifiers did not match to the same molecule, or chemical names were not possible to find. The database contains alternative names and abbreviations that were used in the literature for the same chemical structure to help identifying molecules. Each collected data point is linked with the source and molecule making tracking the data easier.

Fitting The decision matrix of fitting data points to pre-determined functions f_{Fit} is shown in Fig. 3.3. Plotting and reviewing data before any fitting found common pitfalls to be wrong units, or swapped parameter in the literature. This step helped cleaning the data of wrong input, by comparing data series from studies using AARD > 50% as threshold, but is not used to eliminate any outliers or studies.

All data fitting was performed in Origin [354] using the iterative, non-linear curve fitting function with the orthogonal distance regression with a convergence of 1^{-12} based on the χ^2 value [355]. This method minimises the reduced χ^2_v value which is obtained by dividing the residual sum of squares by the degrees of freedom. The convergence value does not describe the quality of the fit and is only used to stop iterating if the orthogonal distance from the data to the fit between two successive iterations is less than 1^{-12}. The initialisation parameter for the fitting were varied and the impact on χ^2_v observed. Reduced χ^2_v and the adjusted coefficient of determination R2 were used to describe the goodness of fit [356]. χ^2_v is calculated using the number of data points n, degree of freedom df (number data points - number parameters), difference between data point and calculated value $y - f$, and the standard deviation s [357]:

$$\chi^2_v = \frac{1}{n - df} \sum_{i=1}^{n} \frac{(y_i - f_i)^2}{s_i^2} \tag{3.1}$$

Values $\chi^2_v >> 1$ indicate a poor fit, $\chi^2_v \approx 1$ indicates a good fit, and values $\chi^2_v < 1$ indicate an over-fit as likely the error variance is overestimated [357]. The target functions for all thermo-physical properties except the VLE were taken from DIPPR [358] with a maximum of three fitting parameter to limit over-fitting [321]. If χ^2_v could be improved (AARD >50%) by excluding whole series of data then the series in question would be investigated. If there was no clear evidence *e.g.*, two data series with AARD > 50%, then both series were kept. Overall good fits $\chi^2_v \approx 1$ and $R2 \approx 1$ were obtained for the solvents screened in this work. Some candidates were rejected based on poor fits due to large discrepancies in the data with AARD > 50%. The last step of the procedure shown in Fig, 3.3 is a quality check. This means the fitted parameter were implemented in gPROMS, the model run for a stability check, and the calculated properties compared with solvent data if available.

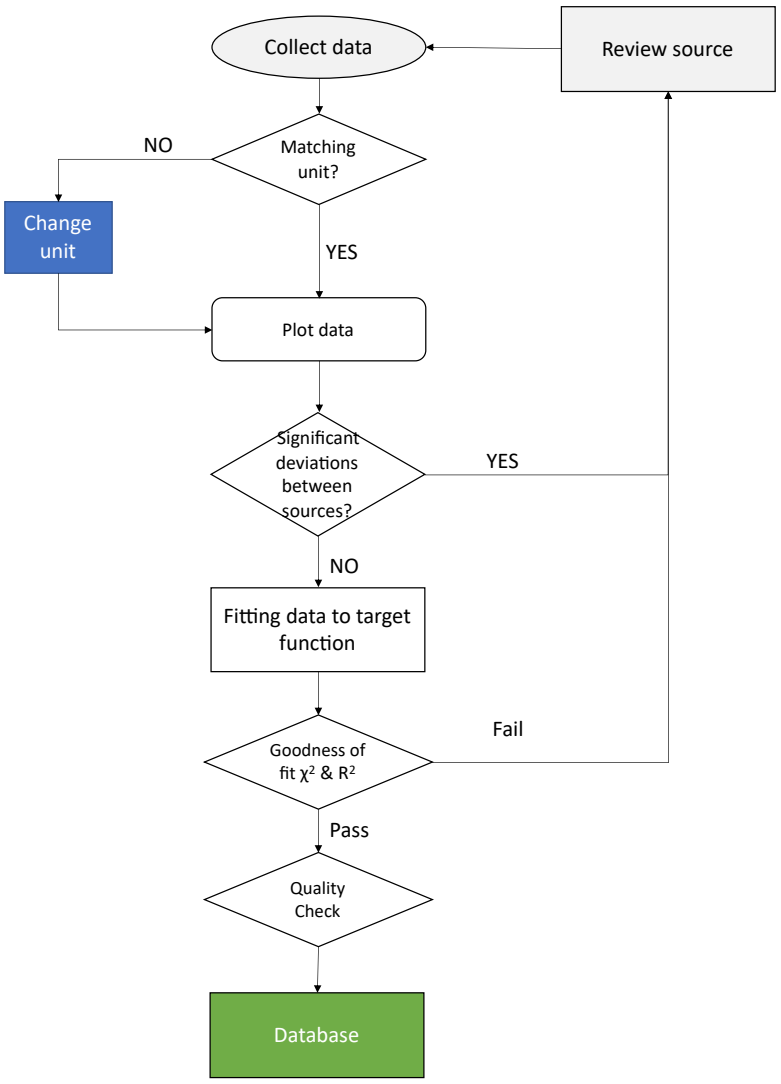


Figure 3.3: Decision tree for fitting data.

Table 3.1 provides an overview of which thermo-physical properties can be found in well known databases. DIPPR [358] and Yaw's critical properties [359] provide a best fit correlation for transport properties using both experimentally measured and predicted data. Reaxys is a search tool for chemical structures, linking data to published studies. Landolt-Börnstein provides an extensive database of published data-points for viscosity and vapour pressure. If correlations for pure properties were available in the existing databases then no fitting was required. The open literature *e.g.*, papers, provided most data points for VLE, kinetics, and heat of absorption. The references are listed with every data point in the database. VLE data collections are available in [91, 133, 167, 198, 270, 360–362]. The lack of any standard in reporting solvent data causes gaps and accessibility issues that ultimately limit the knowledge transfer [363, 364]. Manually collecting and verifying data was a time consuming task. For example, the database contains

263 entries for heat of absorption, and 191 entries for the reaction rate constant. The equations used to calculate the thermo-physical properties require a minimum number of data points to determine the coefficients. The minimum requirements are six VLE points at relevant partial pressures (ideally 0.001 kPa to 100 kPa), and temperatures (ideally 20°C to 140°C) due to the use of six coefficients. A pressure and temperature range is required to determine the VLE across the absorber and the regeneration section. A minimum of two reaction rate constants at different temperatures are required to determine the pre-exponential factor and activation energy used in the Arrhenius equation [365].

Table 3.1: Overview of which properties can be found in well known databases, and a recommended method for closing a potential data gap.

Property	**DIPPR 801**	**Yaw's**	**Reaxys**	**Landolt-Börnstein**	**Gap-filling method**
Density	✓	✓	✓		[366–368]
Viscosity	✓			✓	[369]
Heat capacity	✓	✓			[370]
Surface tension		✓			[371]
Thermal conductivity	✓	✓	✓		[372]
Heat of Vapourisation	✓	✓			[373]
Vapour pressure	✓	✓		✓	[374]
Molar Volume	✓	✓			[367]
Henry's coefficient	✓				[375–377]
VLE					
Kinetics					pK_a correlation [123, 378–381]
Heat of absorption					Gibbs-Helmholtz / van't Hoff [172]

Data Gaps Only 18% (74 amines out of 415 amines) were able to be screened, because these are the only ones with already complete sets of data. Missing VLE data is the most prominent data-gap for the remaining candidates. The number of solvents with a complete dataset is in the range of previous studies that focus on only a selection of the required data, *e.g.,* Bernhardsen and Knuutila [198] experimentally screened 132 amines, and Puxty *et al.,* [229] screened 76 amines. 6% of the candidates were rejected due to inconsistencies and discrepancies in the

reported data, identified by AARD>50% between data series.

The number of candidate molecules could be increased by closing data gaps, *e.g.*, 17 candidate molecules are missing only kinetic data preventing them from being screened (relative increase of 23% compared to the 73 candidates). Despite the pool of unscreened candidates, all chemical classes are represented, and it is deemed unnecessary to introduce a different systematic approach to increase the number of candidates ready for screening.

The literature was systematically researched, and it is likely that some datasets were overlooked despite best efforts. There is no easily accessible database for VLE and kinetics for CO_2 capture solvents, and data was often digitally extracted from figures. Implementing a standard protocol for reporting solvent data and uploading the data into an open-access database similar to recent suggestions for solid materials would improve research and accessibility.

This work successfully screened 73 candidate amines, which have a full dataset and do not require any method to close data gaps. Some recommended methods to close data gaps are listed in Tab. 3.1. These use quantitative structure-activity relationships [382] and are linked to the candidate molecule's structure. Predicting properties such as density or viscosity is established, but it is much more difficult to accurately predict the VLE, heat of absorption, and kinetics [382].

Missing reaction rate constants can be estimated by pK_a correlations which are constrained to specific molecular structures and steric hindrance. Seven pK_a correlations (four for primary and secondary, and three for tertiary) were identified. This work found only one correlation valid for sterically hindered primary amines [381], which unfortunately returns unreasonable values when compared with reference values from other research groups. It is difficult to express steric hindrance as a function of pK_a, and the potential impact is considerable because the reaction rate of these amines differ up to a factor of 100.

Missing heat of absorption data could be estimated using VLE data and the Gibbs-Helmholtz Eqn. 2.2. The fugacity f is assumed to be equal to the partial pressure as the compressibility factor of air (similar to flue gases) at 20°C is approximately one [383]. Multiple studies [172,

174–177] found the AARD of that method to be 20-30%. Differential heats of absorption are not a function of the temperature if calculated by the Gibbs-Helmholtz equation. Other short-cut simulations use a constant ΔH_{Abs} value, which is averaged over the relevant loading ranges and temperature, *i.e.,* assuming the same value in absorber and stripper regardless of temperature and loading [14, 113, 114, 384–388]. Most experiments measure the integral heat of absorption which is related to the differential heat of absorption but not identical [172]. Therefore, Eqn. 2.1 is only an approximation.

Statistical associating fluid theory equations of state (SAFT) [211, 212] is a statistical mechanical method to predict the interactions between molecules in a system and is based on Wertheims first-order thermodynamic perturbation theory [213–216]. Many versions exist [389–391] *e.g.* PC-SAFT [392], soft-SAFT [254], SAFT-VR [393]. The group interactions needed for more complicated amines for SAFT-γ-Mie became available recently [394]. SAFT and this model can be combined [395].

Data for thermal conductivity for the blend of amine and water proved particularly scarce, because this work found only four studies [396–399]. This limited the ability to compare calculated thermal conductivities of the solvent with reference values.

3.2.2 Equations

VLE Numerous semi-empirical VLE models have been published with data fitted to a specific dataset of solvent, concentration, temperature, loading, and pressure. A thorough review of VLE models is presented in [127, 162, 163]. Some examples of empirical correlations are summarised in Tab. 3.2. The semi-empirical VLE correlation used in this work was derived by comparing with other semi-empirical models (see Tab. 3.2). Park *et al.,* [400] developed a semi-empirical model containing multiple equations and equilibrium constants. The correlation used in [112, 395, 401] is identical to Xu and Rochelle's VLE model [402]. It suffered from numeric instabilities due to the even ordered polynomials. Those could be avoided by adequate initialisation. The final version used in this work runs more robust and proved easier to fit to VLE data. The correlation parameter are listed in the appendix B.2.

Table 3.2: Examples of semi-empirical VLE models linking partial pressure p_{CO_2} and equilibrium loading Θ. $A-G$ are parameter to be fitted.

Model	Equation	Comment
Gabrielsen et al., [403]	$p_{CO_2} = K_{CO_2} x_{CO_2} \cdot \frac{x^0_{Amine}\Theta}{(x^0_{Amine}(1-n\Theta))^n}$ $\ln K_{CO_2} = A + \frac{B}{T} + C x^0_{Amine}\Theta + D\sqrt{x^0_{Amine}\Theta}$	x^0_{Amine} = initial concentration of amine, n=1 for MDEA, n=2 for MEA and DEA, K_{CO_2} = combined Henrys law and chemical equilibrium constant.
Xu and Rochelle [402]	$\ln p_{CO_2} = A + \frac{B}{T} + C\Theta + D\Theta^2 + E\frac{\Theta}{T} + F\frac{\Theta^2}{T}$	Simple polynomial function
Brúder *et al.,* [226]	$\ln p_{CO_2} = A\ln\Theta + k_1 + \frac{B}{1+k_2+\exp(-k_3\ln\Theta)}$	k_1, k_2, k_3 are functions of temperature.
Goto *et al.,* [404]	$p_{CO_2} = K \cdot \frac{(1-n)^{1-n} n^n \Theta^2 {x^0_{Amine}}^2}{\{[1-(2-n)\Theta]x^0_{Amine}\}^{2-n}}$ $K = A\exp\left(-\frac{B}{RT}\right)$	x^0_{Amine} = initial concentration of amine, $0 < n < 1$, K = overall equilibrium constant, combined carbamate and bicarbonate routes into one semi-empirical equation.
Oexmann [405]	$\ln p_{CO_2} = A + \frac{B}{T} + C\Theta + D\frac{\Theta}{T} + E\Theta^2 + F\frac{\Theta^2}{T} + G\Theta^3 + H\frac{\Theta^3}{T} + G\Theta^4$	
SQUASH as published in [112, 395, 401]	$\ln p_{CO_2} = A + \frac{B}{T} + C\Theta + D\frac{\Theta}{T} + E\Theta^2 + F\frac{\Theta^2}{T}$	Identical with Xu and Rochelle [402]
This work	$\ln p_{CO_2} = A\ln\Theta + B\ln(1/T) + \frac{C}{1+\exp\left(\frac{D}{T}+E\right)} + F$	Numerically more robust and easier to fit than previous SQUASH version.

VLE data ranging from 20°C up to 160°C and pressures from p_{CO_2}= 0.001 kPa up to 1000 kPa were fitted using orthogonal distance regression. The lowest expected partial pressure is derived from y_{CO_2} = 1 mol%, capture rate 99.5%, p_{abs} = 115 kPa, and assuming a 10 kPa pressure drop [406]. Examples of the semi-empirical VLE correlation (solid lines) can be seen in Fig. 3.4 (MEA), Fig. 3.5 (PZ), and Fig. 3.6 (CESAR1). The dotted line in Fig. 3.4 represents a correlation only valid for 313 K (isothermal).

Henry's Law Coefficients Data for Henry's law coefficients was fitted to Penttila *et al.,*'s [407] correlation based on the N_2O analogy [375, 408–410]. It uses the factors He_{A12}, He_{B12}, He_{C12}, $He_{N_2O,A}$, and $He_{N_2O,A}$. CO_2 has a higher solubility than N_2O in water, *i.e.*, the Henry's coefficient of N_2O in the solvent $He^{N_2O}_{Mix}$ is always higher than $He^{CO_2}_{Mix}$.

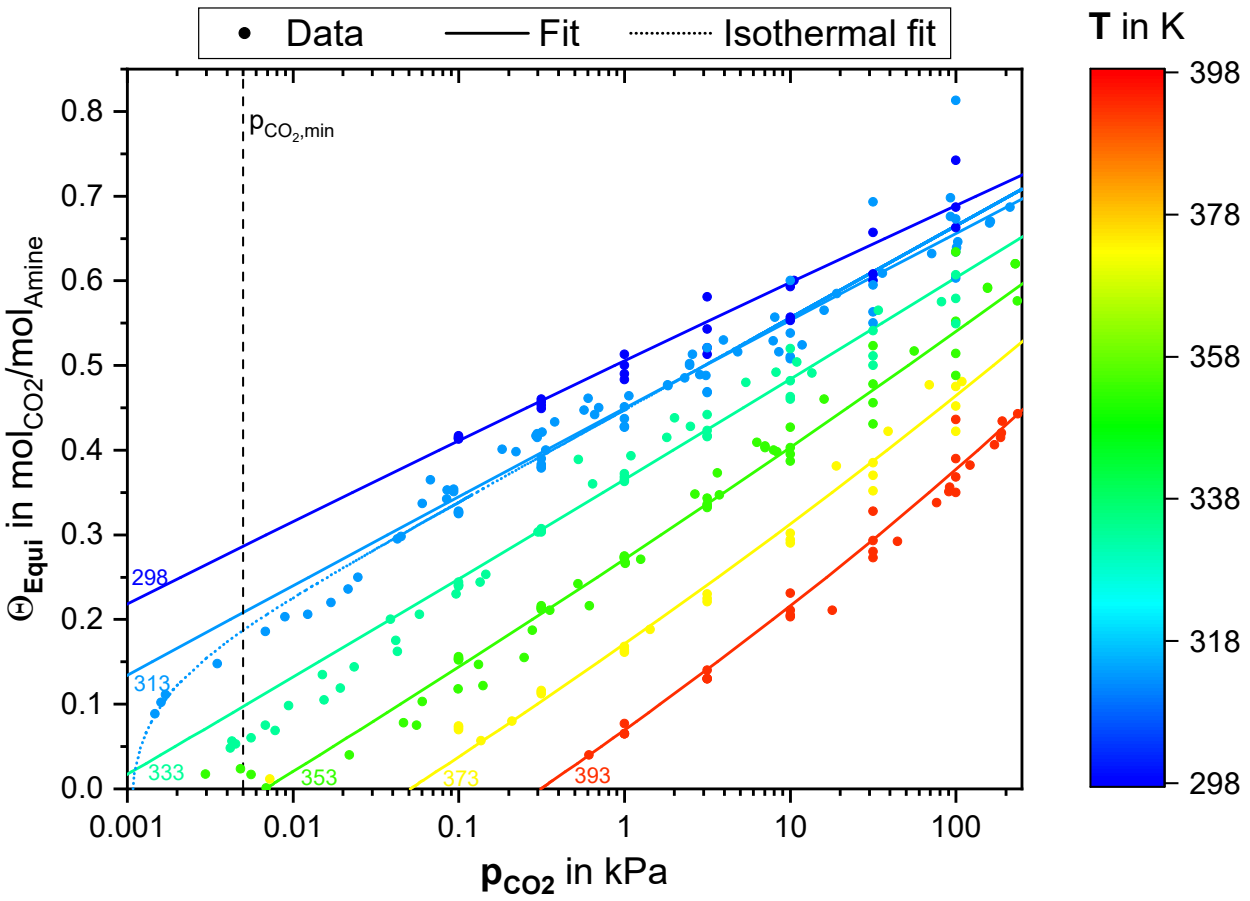


Figure 3.4: Semi-empirical VLE fit (solid lines) and available literature data points (dots) for 30 wt% *aq.* MEA at multiple temperatures (colour bar) ranging from 25°C (blue) to 125°C (red). The limit corresponds to the lowest possible partial pressure (99.5% capture rate from $y_{CO_2} = 1\text{mol\%}$ at $p_{Abs} = 115\,\text{kPa}$).

$$
\begin{aligned}
\mathrm{He}_{\mathrm{H_2O}}^{\mathrm{CO_2}} &= \exp\left(145.369 - \frac{8172.355}{T} - 19.303 \cdot \ln T\right) \\
\mathrm{He}_{\mathrm{H_2O}}^{\mathrm{N_2O}} &= \exp\left(158.245 - \frac{9048.596}{T} - 20.860 \cdot \ln T - 0.00252 \cdot T\right) \\
\mathrm{He}_{\mathrm{Amine}}^{\mathrm{N_2O}} &= \mathrm{He}_{\mathrm{N_2O,A}} + \mathrm{He}_{\mathrm{N_2O,B}} \cdot T \\
\mathrm{He}_{\mathrm{Mix}}^{\mathrm{N_2O}} &= \mathrm{He}_{\mathrm{Amine}}^{\mathrm{N_2O}} \cdot x^{\mathrm{Amine}} + \mathrm{He}_{\mathrm{H_2O}}^{\mathrm{N_2O}} \cdot x^{\mathrm{H_2O}} + \\
&\qquad \mathrm{He}_{\mathrm{A12}} \cdot (x^{\mathrm{Amine}} \cdot x^{\mathrm{H_2O}})^2 \cdot (1 - T/\mathrm{He}_{\mathrm{B12}}) \cdot \exp(-\mathrm{He}_{\mathrm{C12}} \cdot x^{\mathrm{Amine}}) \\
\mathrm{He}_{\mathrm{Mix}}^{\mathrm{CO_2}} &= \mathrm{He}_{\mathrm{Mix}}^{\mathrm{N_2O}} \frac{\mathrm{He}_{\mathrm{H_2O}}^{\mathrm{CO_2}}}{\mathrm{He}_{\mathrm{H_2O}}^{\mathrm{N_2O}}}
\end{aligned}
\tag{3.2}
$$

Kinetics The reaction rate constant k_2 is calculated by the Arrhenius [365] equation using the pre-exponential factor $k_{2,\mathrm{PreExp}}$, activation energy E_A and universal gas constant $\Re$.

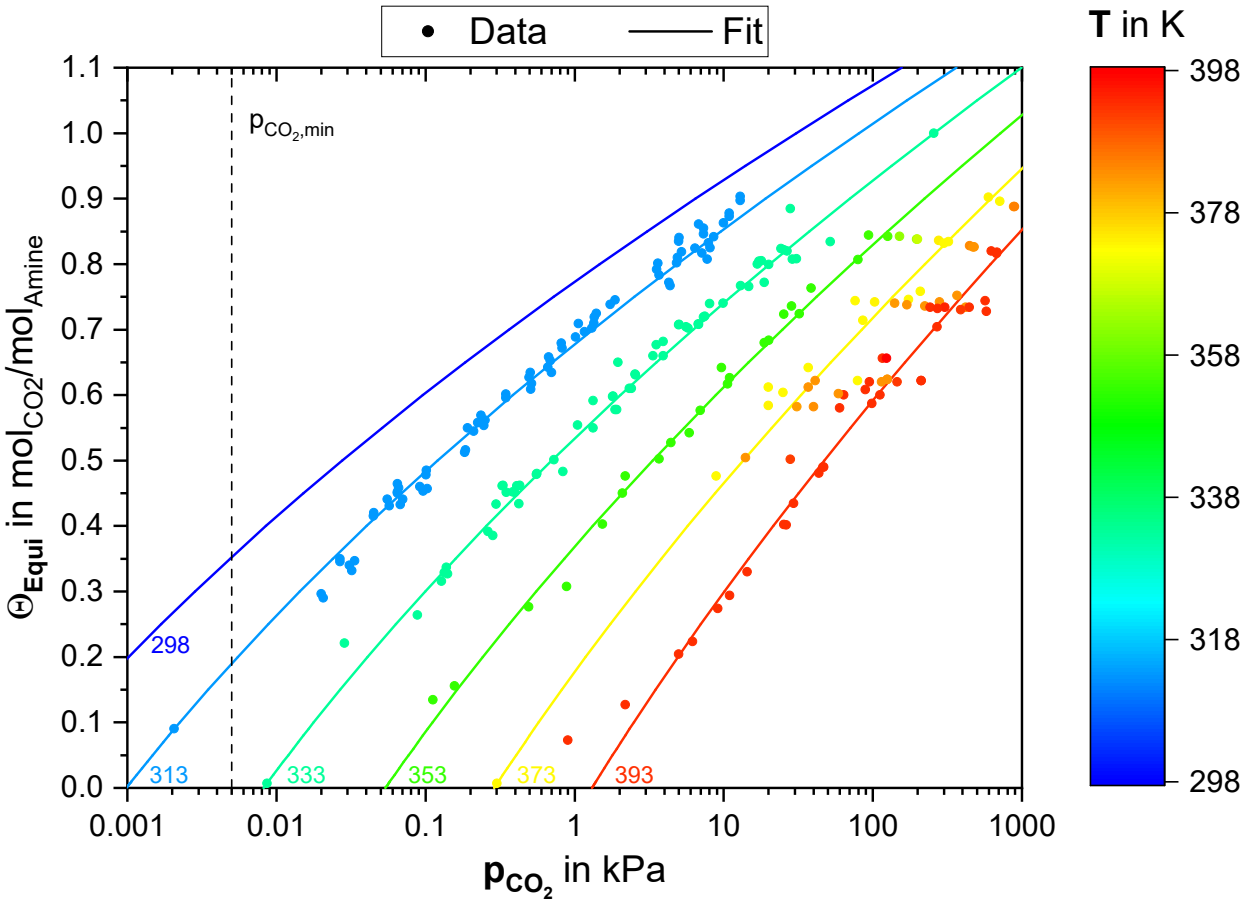


Figure 3.5: Semi-empirical VLE fit (solid lines) and available literature data points (dots) for 30 wt% *aq.* PZ at multiple temperatures (colour bar) ranging from 25°C (blue) to 125°C (red). The limit corresponds to the lowest possible partial pressure (99.5% capture rate from $y_{CO_2} = 1\text{mol\%}$ at $p_{Abs} = 115\,\text{kPa}$).

$$k_2 = k_{2,\text{PreExp}} \cdot \exp\left(\frac{-E_A}{\Re \cdot T}\right) \tag{3.3}$$

Transport Properties The following equations are used to describe the amine's pure properties in the gas V and liquid L phase as a function of the temperature T and coefficients $A-F$ using DIPPR's equations [358]. Listed below are heat capacity c_P, density ρ, viscosity η, thermal conductivity λ, surface tension σ, vapour pressure p_{Vap}, and heat of vapourisation ΔH_{Vap}. Some of these properties are not considered transport properties, however, for reading purposes are listed together [411]. The gas phase density is calculated using the ideal gas law [411]. The vapour pressure is described using Antoine's and Buck's equations [411].

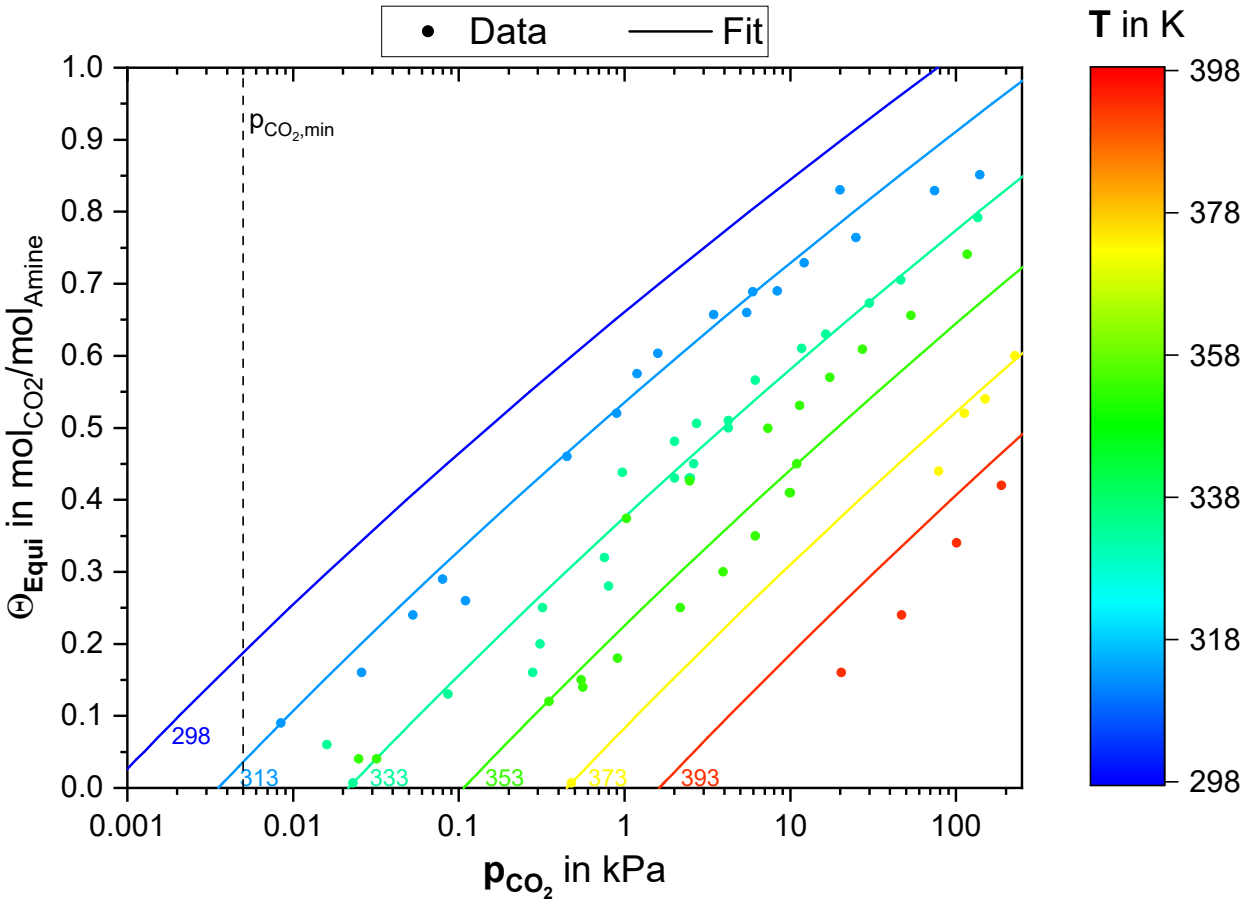


Figure 3.6: Semi-empirical VLE fit (solid lines) and available literature data points (dots) for CESAR1 (13wt% PZ + 27wt% AMP blend) at multiple temperatures (colour bar) ranging from 25°C (blue) to 125°C (red). The limit corresponds to the lowest possible partial pressure (99.5% capture rate from $y_{CO_2} = 1\text{mol}\%$ at $p_{Abs} = 115\,\text{kPa}$).

$$
\begin{aligned}
c_{\mathrm{P,L}} &= A_{c_{\mathrm{P,L}}} \cdot + B_{c_{\mathrm{P,L}}} \cdot T + C_{c_{\mathrm{P,L}}} \cdot T^2 \\
c_{\mathrm{P,V}} &= A_{c_{\mathrm{P,V}}} \cdot + B_{c_{\mathrm{P,V}}} \cdot T + C_{c_{\mathrm{P,V}}} \cdot T^2 \\
C\rho_{\mathrm{L}} &= A_{\rho_{\mathrm{L}}} + B_{\rho_{\mathrm{L}}} \cdot T + C_{\rho_{\mathrm{L}}} \cdot T^2 \\
\rho_{\mathrm{V}} &= \frac{p \cdot MW^i}{\Re \cdot T} \\
\eta_{\mathrm{L}} &= \exp\left(A_{\eta_{\mathrm{L}}} + \frac{B_{\eta_{\mathrm{L}}}}{T} + C_{\eta_{\mathrm{L}}} \ln T\right) \\
\eta_{\mathrm{V}} &= A_{\eta_{\mathrm{V}}} + B_{\eta_{\mathrm{V}}} \cdot T \\
\lambda_{\mathrm{L}} &= A_{\lambda_{\mathrm{L}}} + B_{\lambda_{\mathrm{L}}} \cdot T + C_{\lambda_{\mathrm{L}}} \cdot T^2 \\
\lambda_{\mathrm{V}} &= A_{\lambda_{\mathrm{L}}} + B_{\lambda_{\mathrm{L}}} \cdot T \\
\sigma &= A_{\sigma_{\mathrm{L}}} + B_{\sigma_{\mathrm{L}}} \cdot T + C_{\sigma_{\mathrm{L}}} \cdot T^2 \\
p_{\mathrm{Vap}} &= \exp\left(A_{p_{\mathrm{Vap}}} + \frac{B_{p_{\mathrm{Vap}}}}{C_{p_{\mathrm{Vap}}} \cdot T}\right) \\
\Delta H_{\mathrm{Vap}} &= A_{\Delta H_{\mathrm{Vap}}} + B_{\Delta H_{\mathrm{Vap}}} \cdot T + C_{\Delta H_{\mathrm{Vap}}} \cdot T^2
\end{aligned}
\tag{3.4}
$$

Mixtures Thermo-physical properties of mixtures in gas and liquid phase are estimated via mixing rules (summarised in Tab. 3.3) using the pure properties (see Eqn. 3.4) at temperature T. Heat capacity $c_{\mathrm{P,Mixture}}$ and liquid density ρ_{Solvent} are calculated using the mole weighted average [411]. Gas phase density ρ_{V} is determined by the ideal gas law. Gas phase viscosity η_{V} is uses Wilke's method with the Herning and Zipperer approximation for the factor η_{Fac} [411, 412]. Liquid phase viscosity η_{Solvent} is calculated using a mole weighted average with a correction for the amine as systems containing water often exhibit a maximum or a minimum [411]. Thermal conductivity $\lambda_{\mathrm{Mixture}}$ of a mixture is calculated using the mass weighted average [411]. Surface tension σ_{L} is determined by Asprion's modified physical mixing rule using the fitting factor f_σ [371].

$$
\begin{aligned}
c_{\mathrm{P,Mixture}} &= \sum_{i}^{n} x^i \cdot c_{\mathrm{P}}^i \\
\rho_{\mathrm{Solvent}} &= \sum_{i}^{n} x^i \cdot \rho^i \\
\rho_{\mathrm{V}} &= \frac{p \cdot MW^i}{\Re \cdot T} \\
\eta_{\mathrm{Solvent}} &= \sum_{i \neq \mathrm{Amine}}^{n} x^i \cdot \eta^i + x^{\mathrm{Amine}} \cdot \eta^{\mathrm{Amine}} \cdot 14.24 (\eta^{\mathrm{Amine}})^{-0.9} \\
\eta_{\mathrm{V}} &= \sum_{i}^{n} \frac{y^i \cdot \eta^i}{\sum_{j=1}^{n} y^j \eta_{\mathrm{Fac},ij}} = \sum_{i}^{n} \frac{y^i \cdot \eta^i}{\sum_{i=j}^{n} y^j \sqrt{\frac{MW^j}{MW^i}}} \\
\lambda_{\mathrm{Mixture}} &= \sum_{i}^{n} w^i \cdot \lambda^i \\
\sigma_{\mathrm{L}} &= \sigma^{i=1} + \sum_{i \geq 2}^{n} \frac{f_\sigma x^i}{1 + \sum_{j \geq 2}^{n} (f_\sigma - 1)\, x^j} \left(\sigma^i - \sigma^{i-1}\right)
\end{aligned}
\tag{3.5}
$$

The non-ideality of the liquid phase of CO_2-loaded solvents is well known [90, 413, 414] and describing these effects with mixing rules is challenging. Calculating the surface tension of aqueous solvents is difficult and multiple approaches were compared [371, 415]. The impact of the input error of thermo-physical properties on the relative solvent ranking will be analysed in the next chapter.

Table 3.3: Overview of methods used to calculate thermo-physical properties of mixtures [411].

Property	Gas	Liquid
Heat Capacity	Linear mole weighted average [411]	Linear mole weighted average [411]
Viscosity	Method of Wilke with Herning and Zipperer approximation [411, 412]	Modified linear mole weighted average with power law correction [411]
Density	Ideal gas law [411]	Linear mole weighted average [411]
Thermal Conductivity	Linear mass weighted average [411]	Linear mass weighted average [411]
Surface Tension	Modified physical mixing rule by Asprion [371]	

3.2.3 Thermo-physical Property Space

Figure 3.7 shows the candidates broken down by number of alkalinity (number of N-atoms per amine), and the shares of chemical classes within mono-amines.

Common examples for the classes are MEA for primary, DEA for secondary, MDEA for tertiary, pyridine for c-2 (cyclic-secondary), piperidinoethanol for c-3 (cyclic-tertiary), PZ for di-amines, Barton's base for tri-amines, triethylenetetramine (TETA) for four alkalinities, and tetraethylenepentamine (TEPA) for five alkalinities. Sterically hindered-amines, *e.g.,* AMP, are not classified as an independent class, because the impact of hindrance is not binary. Aromatic-amines, *e.g.,* BZA, also already classify under the previously listed classes.

The vast majority (94%) of candidates contain one or two alkalinities. Primary amines represent the most common chemical sub-class with 63% share. About 51% of all candidates are primary, secondary, or tertiary amines reflecting the focus on those classes over the past 90 years. Poly-amines contain more than one alkalinity per molecule, and could theoretically absorb on average more CO_2 than mono-amines at the same partial pressure. However, this depends on various factors such as steric hindrance, and there are examples of mono-amines with higher equilibrium loadings than poly-amines [198, 242].

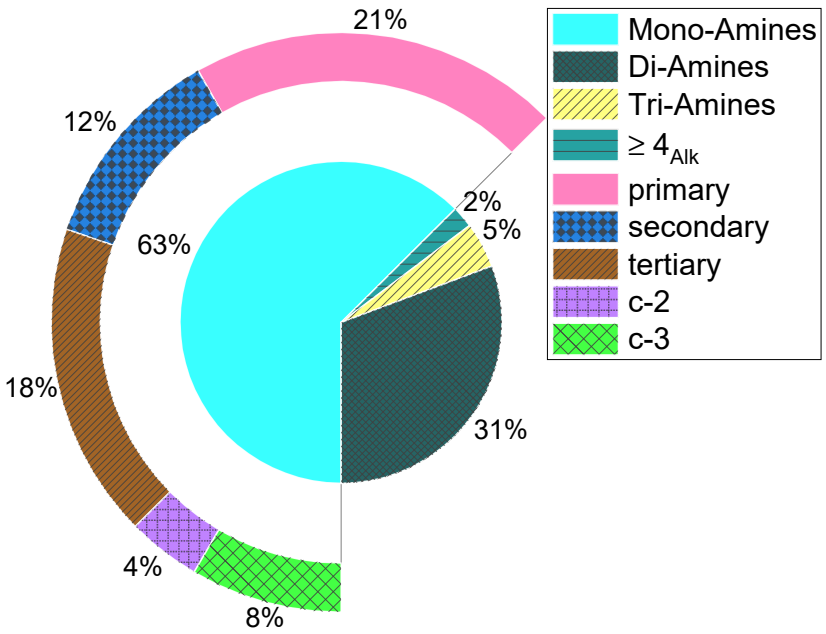


Figure 3.7: Shares of amines in database broken down by number of alkalinity (number of N-atoms: Mono, Di, Tri, or poly ≥ 4) and chemical class (number of C-atoms bonded directly to the N-atom) for mono-amines. 94% of candidates contain one or two alkalinities per molecule.

Figure 3.8 shows the molar mass of the candidates with their normal distribution curves for amines, carboxylic acids, and amino acids. The average molar mass is 131 g/mol, which is more than twice the value of MEA. Only 12 molecules were identified with a lighter molar mass than MEA, which include *e.g.,* ethylenediamine (EDA), isopropylamine (IPA), or acetic acid. Bernhardsen and Knuutila [198] found an average molar mass of 100 g/mol which is lighter than the average identified in this work. The heaviest amine analysed in the literature is poly(ethylenimine) with an estimated molar mass of over 10 000 g/mol [416], which is in the order of zeolithe 13X (its molar mass is 13.4 kg/mol). The candidates' molar mass impacts heat and mass transport, and might correlate with capture cost.

Figure 3.9 shows the normalised thermo-physical properties of unloaded solvents at 30 wt% against MEA as a spider diagram. Such diagram is helpful to visualise the thermo-physical property space described by the key properties displayed as axes. Each solvent is represented by a coloured line forming an octagon. Each dimension is normalised relative to MEA to help displaying the differences between individual solvents. Favourable properties (based on the individual trends, see [340]) leading to cheaper capture cost are found towards the outside of the graph, *i.e.*, large area inside the octagon. Unfavourable properties are found towards the center,

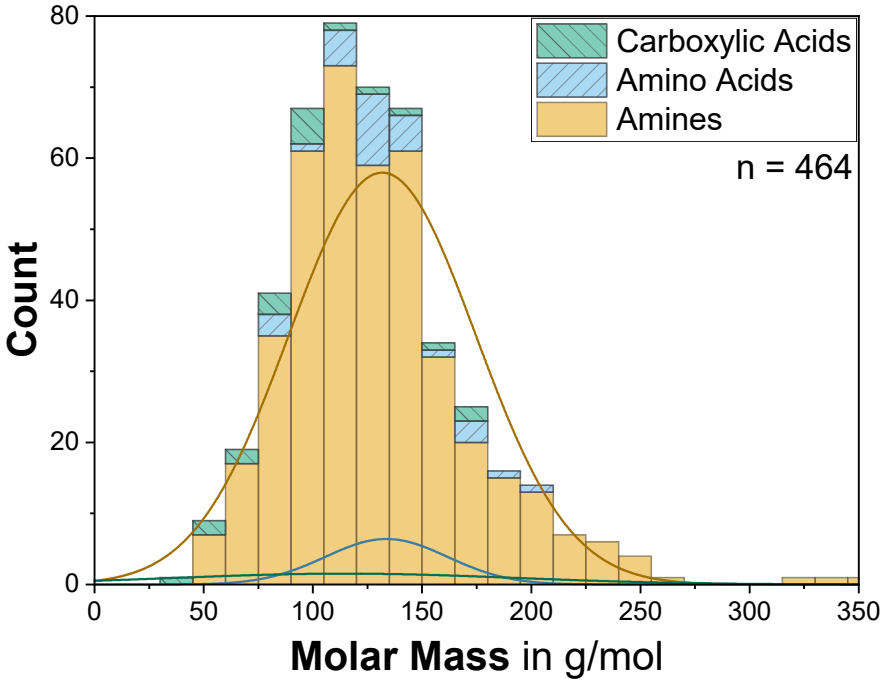


Figure 3.8: Molar mass 464 candidates with an average of 131 g/mol. Solid lines show the normal distribution curve for amines, carboxylic acids, and amino acids.

i.e., small area inside the octagon. The axis for viscosity, heat capacity, and surface tension are inverted, because low property values are favourable [340]. The reaction rate constant for candidates differ by multiple orders of magnitude. In order to show the relative differences, the logarithm of the reaction rate constants are shown relative to MEA. All properties except density and VLE are molar-based and the temperature is 40°C.

Values < 1 represent a capture cost increase relative to MEA, and values > 1 represent a capture cost reduction relative to MEA. For example, higher density leads to reduced volume flow rate inside the capture plant, thus, to lower capture cost. A solvent with higher density and otherwise identical properties compared to MEA will have a relative value > 1 just for the density axis, and values $= 1$ for all other properties. The area for the octagon would be larger compared to MEA. The properties of an ideal solvent would be towards the outside of the graph forming the largest possible octagon area.

All aqueous solvents have similar thermal conductivity, heat capacity, density, and surface tension with normalised differences of less than 10%. It is unlikely that these properties are the main cause for the differences in amines' techno-economic performance. The difference in

viscosity ranges from 1 to 2.1 on the normalised scale. The normalised difference in logarithmic reaction rate constant range from zero to 1.2, indicating that most candidates react slower than MEA per alkalinity. Despite the deceptive range in this plot, the absolute differences in the reaction rates are the largest for out of all properties. The VLE and heat of absorption show the largest spread in the plot ranging from zero to 3 and 2.5 respectively, indicating that some solvents have either higher or lower equilibrium loadings per alkalinity compared to MEA.

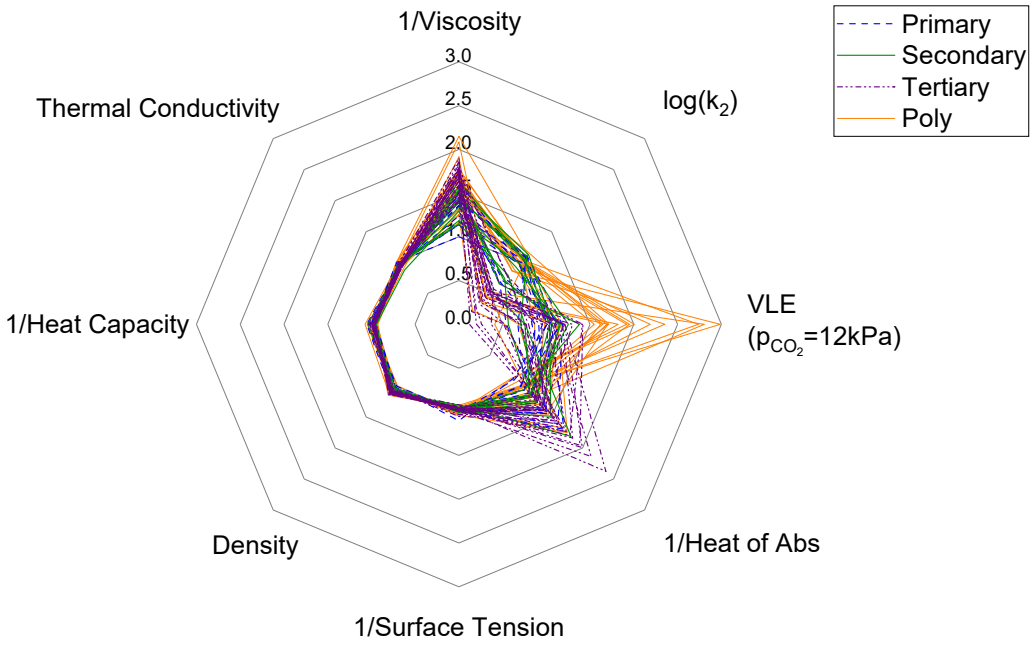


Figure 3.9: Comparing thermo-physical properties of unloaded solvents at 40°C and 30 wt% as a factor of MEA. The axes for heat of absorption, viscosity, and heat capacity are inverted. The logarithm of the reaction rate is selected due to the orders of magnitude in differences between candidates. Density is mass based (kg/m^3), the VLE is based per alkalinity mol_{CO_2}/mol_{Alk}, and all other properties are molar based. Cost reductions relative to MEA are towards the outside (values > 1), and cost increases relative to MEA are towards the center (values < 1).

Figure 3.10 shows the properties of the solvents averaged by chemical class. Primary (blue dashed line) and secondary (green solid line) amines differ on average less than 5% in surface tension, density, heat capacity, and thermal conductivity. Tertiary amines (dash-dotted purple line) average the lowest heat of absorption, lowest equilibrium loading, slowest reaction rate constant, and lowest viscosity. Poly-amines have the highest equilibrium loading, yet the difference to the other classes in heat of absorption is not as large. Poly-amines and tertiary amines have on average the lowest viscosities. The biggest differences between the chemical classes are observed in viscosity, kinetics, VLE, and heat of absorption. The trends shown in Fig. 3.10 are

based on averages and comparing it with the individual trends in Fig. 3.9 indicates that there will be some outliers within each chemical class.

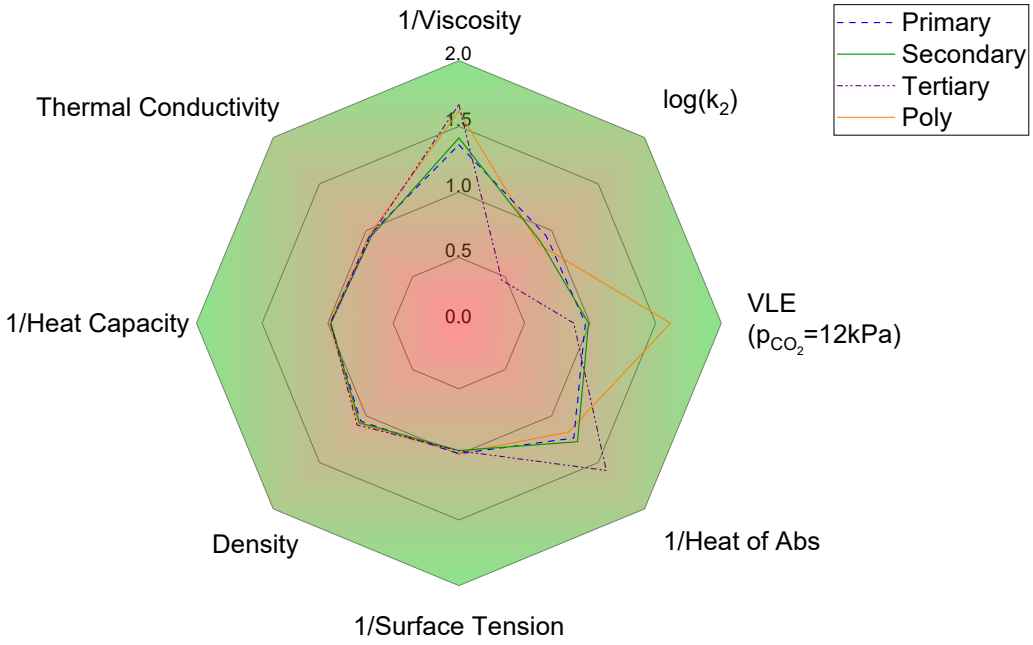


Figure 3.10: Comparing thermo-physical properties averaged by chemical class. Cost reductions relative to MEA are highlighted in green (values > 1), and cost increases are highlighted in red (values < 1).

3.3 Model Formulation

3.3.1 Framework and Flowsheet

Figure 3.11 shows the flow of data in and out of the screening model implemented in gPROMS Modelbuilder [417] with an Excel interface. Selecting a widely known interface is thought to increase the pool of potential users for the model without the need to own the software, or, knowing the gPROMS specific programming language.

Figure 3.12 shows the archetypal capture process in which all solvents are utilised. The direct contact cooler cools down warm flue gas emitted by a source and removes excess water as well as some impurities. The blower increases its pressure such that there is enough positive pressure difference to the atmosphere to drive the cleaned flue gas through the stack. The CO_2 is separated from the flue gas in the absorber column by the capture solvent, in which it either chemically reacts or physically dissolves. The water wash and demister ensure that amine

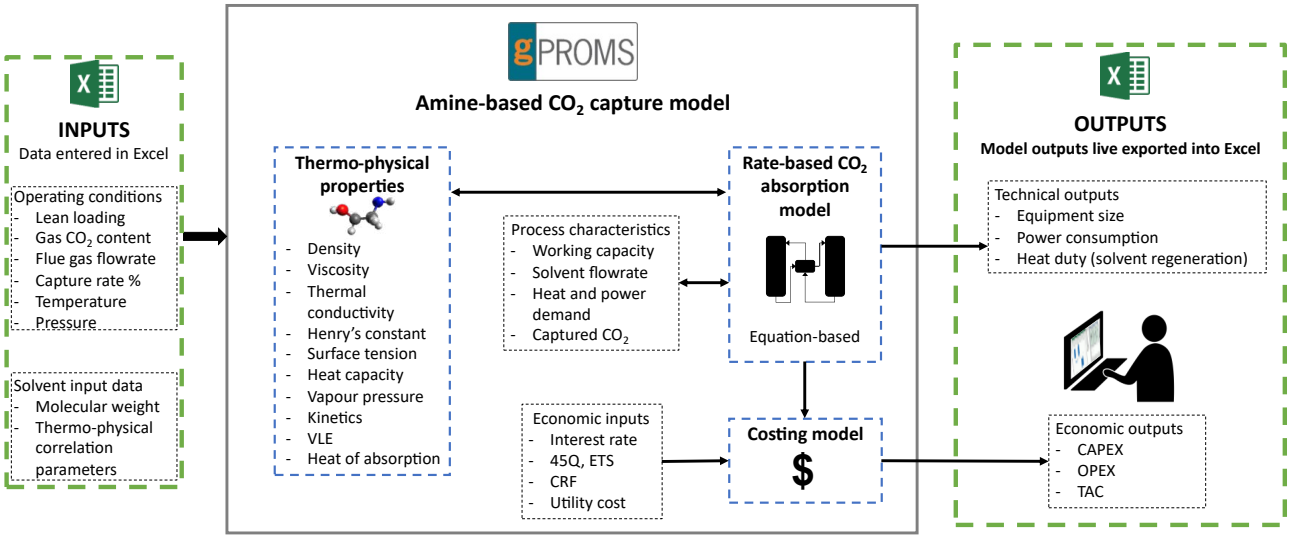


Figure 3.11: The gPROMS model is wrapped with an Excel interface to allow users interacting with the tool without learning the coding-syntax of the software. The Global System Analysis cannot be used with Excel.

emission limits are met and solvent losses minimised, before the cleaned flue gas is released into the atmosphere. The CO_2 rich solvent leaves the absorber and is pumped with a rich-solvent pump through the main heat exchanger to the top of the stripper column.

In the regeneration section, the rich solvent is heated and partially evaporated inside the steam-fed reboiler, and CO_2 is released from the solvent into the stripper's steam. The condenser removes a majority of the water contained in the CO_2-enriched gas leaving the stripper, and feeds it back to the solvent cycle to keep the water balance. This reflux could effectively act as a water-wash at the top of the stripping column. The captured CO_2 is dried and compressed depending on the downstream chain, *e.g.,* ultimately be fed into a pipeline and sent for storage. The hot lean solvent leaving the reboiler heats up the cold rich solvent inside the main heat exchanger, which is important for the overall thermal efficiency of the process. The solvent is further cooled down inside a lean solvent cooler to the specified solvent inlet temperature. The lean solvent pump overcomes the pressure losses of the main heat exchanger, lean solvent cooler, and height difference to the absorber inlet.

The upstream and downstream scope is assumed to be independent from the solvent choice and, therefore, omitted from the scope. Integrated capture plants offer some advantages (see [418–420], however, this work assumes the capture plant to operate independently of the flue

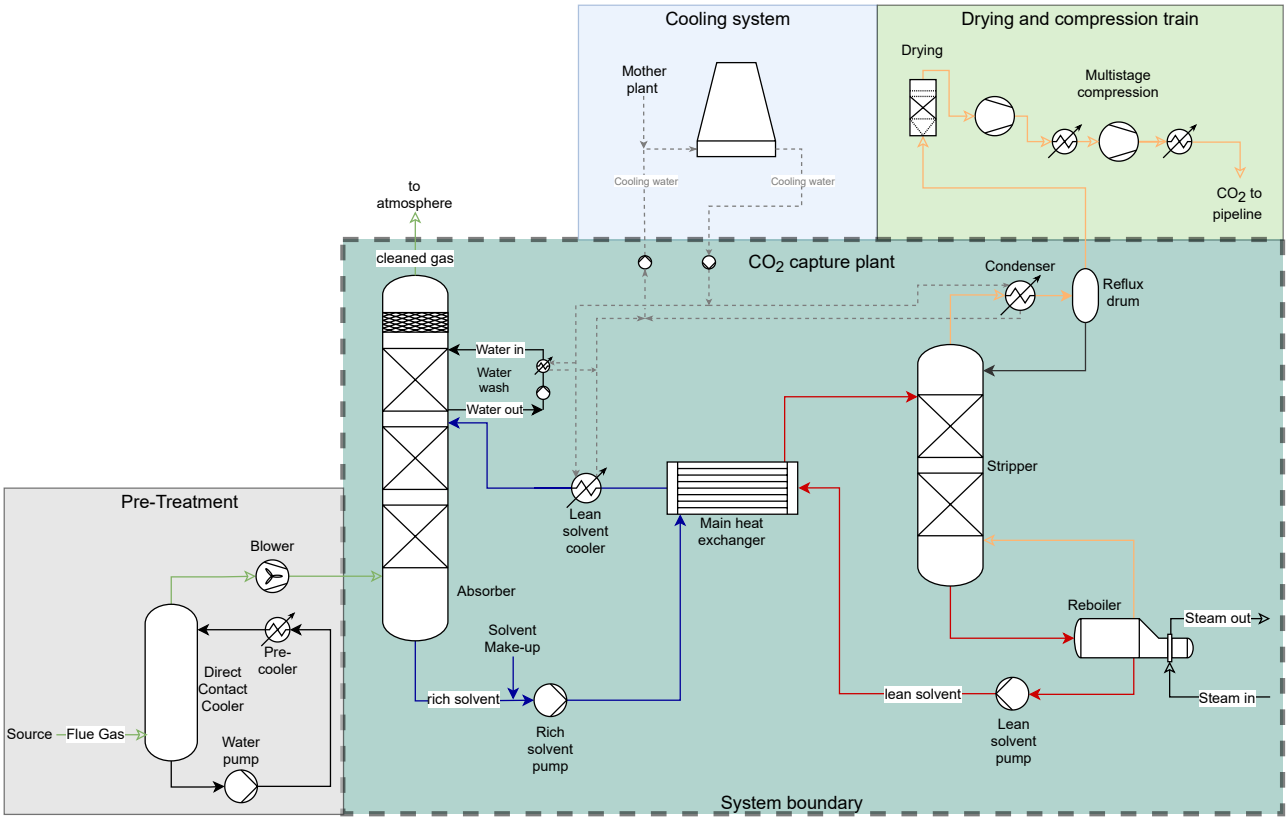


Figure 3.12: Process flow diagram which considers an archetypal post-combustion CO_2 capture plant comprising an absorber-stripper configuration. The dashed line shows the system boundary, where upstream and downstream processes are omitted for a solvent screening study.

gas source. Utilities such as steam, cooling water, and power are assumed to be available and their costs are included.

3.3.2 Process Modelling

The approach for this work is summarised in Tab. 3.4 (equipment design), Tab. 3.5 (default operating conditions), and Tab. 3.6 (correlations). The approach is described in detail over the following sections separated into process modelling (unit by unit) and costing approach.

Columns

Both columns were modelled using a short-cut, one-stage approach based a logarithmic mean driving force. It is expected to be more accurate than equilibrium models, however, it does not discretize over the column height, thus, neglects to account for the temperature profile over the

Table 3.4: Default approach to equipment design including type, sizing limits, sizing method, and material selection. SS = stainless steel.

Equipment	Type	Limit	Method	Material
Absorber	Packed or structured column	$<$ 980000 lbs	single stage short-cut	SS304
Stripper	Packed or structured column	$<$ 980000 lbs	single stage short-cut	SS304
Main heat exchanger	Horizontal shell and tube	$<$ 12000 ft^2	Tube: Nusselt correlations [421] Shell: Kern's method [422]	SS316
Lean solvent cooler	Horizontal shell and tube	$<$ 12000 ft^2	Tube: Nusselt correlations [421] Shell: Kern's method [422]	SS316
Reboiler	Vertical shell and tube	$<$ 12000 ft^2	Tube: Chen's corrected method [423–425] Shell: $h_{\text{Steam}} = 8\ \frac{\text{kW}}{\text{m}^2\ \text{K}}$	SS316
Condenser	Horizontal shell and tube	$<$ 12000 ft^2	Tube: Nusselt correlations [421] Shell: Kern's method [422]	SS316
Pump	Centrifugal pump	$<$ 3500 gpm	Haaland's method [426]	SS304

column. This method is not suitable for process design, however, it is expected to be sufficient to model a relative cost impact caused by the thermo-physical properties of the solvent.

The mass balance is calculated by summing the molar flow rates of vapour at the inlet V_{In}, liquid at the inlet L_{In}, vapour at the outlet V_{Out} and liquid at the outlet L_{Out} multiplied with their respective mole fractions of compounds i in the liquid x^i and vapour phase y^i. All x^i and y^i sum to one as shown in Eqn. 3.6, however, they are not all active to avoid over-determining

Table 3.5: Summary of default operating conditions. Temperature approach in main heat exchanger is optimised.

Parameter	Value
Absorber operating pressure	115 kPa_a
Absorber solvent inlet temperature	40 ℃
Approach to equilibrium	90%
Flooding factor	70%
Flue gas flow rate	default 17.7 kmol/s $\approx$ 500 kg/s at $y_{CO_2} = 4$mol%
CO_2 fraction in flue gas	2-30 mol%
Flue gas temperature after pre-treatment	40℃
Capture rate	90% or 95%
CO_2 purity	95% (wet)
Reboiler pressure	159 kPa
Steam	147 ℃ and 250 kPa_a
Main heat exchanger temperature approach	20℃ (LMTD) (optimisation parameter)
Minimum working capacity	0.005 mol_{CO_2}/mol_{Amine}

the system, *e.g.,* y^i_{In} is already set by the flue gas composition.

$$\begin{aligned} V_{\text{In}} \cdot y^i_{\text{In}} + L_{\text{In}} \cdot x^i_{\text{In}} &= V_{\text{Out}} \cdot y^i_{\text{Out}} + L_{\text{Out}} \cdot x^i_{\text{Out}} \\ \sum_i x^i &= 1 \\ \sum_i y^i &= 1 \end{aligned} \tag{3.6}$$

The flue gas composition always contains $y^{H_2O}_{\text{In}} = 6$ mol%, $y^{O_2}_{\text{In}} = 5$ mol%, with the balance being $y^{N_2}_{\text{In}} = 1 - y^{H_2O}_{\text{In}} - y^{O_2}_{\text{In}} - y^{CO_2}_{\text{In}}$. The molar flow rate of flue gas is kept constant at 17.7 kmol/s. The CO_2 concentration $y^{CO_2}_{\text{In}}$ is an input parameter and varied between 2 mol% to 30 mol%. The solvent selection will impact the absorber's pressure drop which might cause the flue gas pressure at the absorber inlet to be not sufficient. The maximum irrigated pressure drop in the absorber is assumed to be 100 mbar [406], thus, the inlet pressure is set to 115 kPa.

Table 3.6: Correlations used in the screening tool with their reported uncertainty expressed as average absolute relative deviation (AARD).

Correlation	Reference	AARD
Reaction rate constant	Arrhenius equation [365, 427]	<4.75%
Effective surface area	Onda *et al.* (random packing) [428]	20.0%
	Shi and Mersmann [429] and Rocha *et al.,*'s [302] (structured packing)	%
Mass transfer coefficient	Onda *et al.* (random packing) [428, 430, 431]	20.0% (liquid)
	Shi and Mersmann [429] and Rocha *et al.,*'s [302] (structured packing)	
Enhancement factor	Wellek *et al.* [432]	1.2%
Henry's coefficient	N_2O analogy [407, 408, 433]	NaN
Gas phase diffusivities	Fuller *et al.* [434–437]	4.0%
Liquid phase diffusivities	Wilke and Chang [438] (Binary)	7.8%
	Takahashi *et al.* [411, 438, 439](CO_2)	4.0%
	Wilke and Chang as modified by Perkins and Geankoplis [411, 440, 441](other)	5.9%
Pressure drop and holdup	Billet and Schultes [301, 442] (random packing)	9.1%
	GDPC [443, 444] (structured packing)	8.7%
Single phase heat transfer coefficient	Nusselt corelations [421, 445]	NaN
Multiphase heat transfer coefficient	Chen's method with Lockhart–Martinelli correction [421]	NaN
Darcy friction factor	Haaland approximation of Colebrook–White equation [426]	3-5%

The loading Θ is defined as CO_2 mole fraction x^{CO_2} divided by amine mole fraction x^{Amine}. The lean loading Θ_{Lean} refers to the solvent at absorber inlet, the rich loading Θ_{Rich} to the solvent at absorber outlet, the working capacity $\Delta\Theta_{Work}$ to the difference between rich and lean loading, and the equilibrium loading $\Theta_{Equi}\left(p_{CO_2}, T\right)$ to the equilibrium at temperature T and partial

pressure $p_{\mathrm{CO_2}}$.

$$\begin{aligned}
\Theta &= \frac{x^{\mathrm{CO_2}}}{x^{\mathrm{Amine}}} \\
\Theta_{\mathrm{Equi,}}\left(T, p_{\mathrm{CO_2}}\right) = \ln p_{\mathrm{CO_2}} &= A_{\mathrm{VLE}} \ln \Theta + B_{\mathrm{VLE}} \ln\left(1/T\right) + \frac{C_{\mathrm{VLE}}}{1+\exp\left(\frac{D_{\mathrm{VLE}}}{T}+E_{\mathrm{VLE}}\right)} + F_{\mathrm{VLE}} \\
\Theta_{\mathrm{Rich}} &= 90\% \cdot \Theta_{\mathrm{Equi}}\left(T_{\mathrm{Abs,Btm}}, p_{\mathrm{CO_2,In}}\right) \\
\Delta\Theta_{\mathrm{Work}} &= \Theta_{\mathrm{Rich}} - \Theta_{\mathrm{Lean}} \\
\Delta\Theta_{\mathrm{Min}} &= \Theta_{\mathrm{Equi}}\left(p_{\mathrm{CO_2}}^{\mathrm{Top}}, T^{\mathrm{Top}}\right) - \Theta_{\mathrm{Lean,Max}}
\end{aligned} \tag{3.7}$$

The equilibrium loading is given through a semi empirical correlation based on the database using the factors A_{VLE}-F_{VLE}. The rich loading is calculated using a 90% approach to equilibrium loading at the conditions at the inlet of the absorber [14]. The temperature $T_{\mathrm{Abs,Btm}}$ is determined through the enthalpy balance. The partial pressure $p_{\mathrm{CO_2,In}} = p_{\mathrm{V,In}} \cdot y_{\mathrm{In}}^{\mathrm{CO_2}}$ is set by the flue gas pressure and composition. The working capacity $\Delta\Theta_{\mathrm{Work}}$ ultimately determines the required solvent flow rate for a given capture rate, flue gas composition, and flue gas flow rate. The cost-optimal lean loading $\Theta_{\mathrm{Lean}}^{\mathrm{Opt}}$ is the result of optimising the operating conditions to achieve minimum capture cost.

The minimum working capacity $\Delta\Theta_{\mathrm{Min}}$, also known as minimum acid gas pick up AGPU, is defined as the working capacity just before the solvent pinches at the top of the absorber. The driving force for the mass transfer would be close to zero, because the absorbed CO_2 in the solvent would be close to equilibrium with the remaining partial pressure in the gas phase. The back pressure (partial pressure caused by CO_2 in solvent) cannot be higher than the remaining partial pressure in the flue gas, thus, guaranteeing a minimum driving force for mass transfer into the solvent. The lean solvent is "overstripped" [405] beyond its corresponding maximum lean loading $\Theta_{\mathrm{Lean,Max}}$ by setting $\Delta\Theta_{\mathrm{Min}}$. This prevents excessive column heights. To illustrate this point, Fig. 3.13 shows the maximum lean loading as a function of the capture rate assuming a constant 5 kPa pressure drop for 30 wt% MEA and a range of flue gas CO_2 concentrations. Higher capture rates reduce the operating window of lean loadings with a sharp drop at capture rates larger than 97%. The trend is caused by solvent's VLE, and the studied

amines show similar trends. Not all of them have sufficiently high $\Theta_{\mathrm{Lean,Max}}$ to achieve capture rates well above 90%. The impact of capture rate on process performance and cost is discussed in [44, 77, 114, 384, 385, 388, 446–469], with some evaluating techno-economic performance using capture rates as high as 99% [114, 388, 467–469].

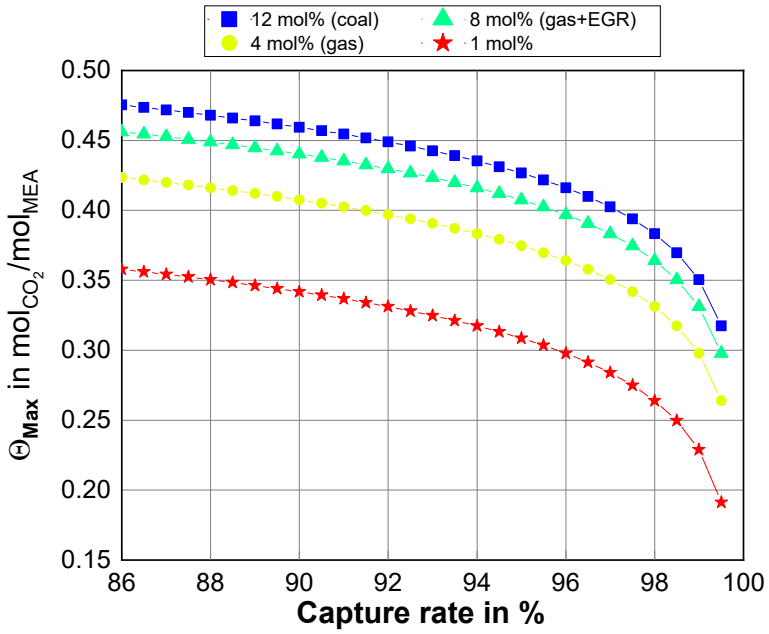


Figure 3.13: Impact of capture rate and flue gas composition on limiting maximum lean loading that leads to saturation at top of the absorber at 40°C. Lean loading has to be smaller than the limit to achieve a specified capture rate.

The molar flow rate of absorbed CO_2 $n_{\mathrm{Abs}}^{\mathrm{CO_2}}$ is calculated by multiplying the capture rate CapRat with the molar flow rate of CO_2 in the flue gas.

$$n_{\mathrm{Abs}}^{\mathrm{CO_2}} = \mathrm{CapRat} \cdot V_{\mathrm{In}} \cdot y_{\mathrm{In}}^{\mathrm{CO_2}} \tag{3.8}$$

The equilibrium constant of compound i, K^i, is calculated as the ratio between gas phase and liquid phase mole fraction. Henry's law is used for nitrogen and oxygen. Water and amine are calculated by Raoult's law assuming ideality (partial pressure p^i equals mole fraction of i

multiplied with vapour pressure of pure compound p^{β}_{Vap}).

$$\begin{aligned} K^{i} &= \frac{y^{i}_{\mathrm{Out}}}{x^{i}_{\mathrm{Out}}} \\ K^{\mathrm{N_2}} &= \mathrm{He}^{\mathrm{N_2}} \\ K^{\mathrm{O_2}} &= \mathrm{He}^{\mathrm{O_2}} \\ K^{\mathrm{H_2O}} &= \frac{p^{\mathrm{H_2O}}_{\mathrm{Vap}}}{p_{\mathrm{Col}}} \\ K^{\mathrm{Amine}} &= \frac{p^{\mathrm{Amine}}_{\mathrm{Vap}}}{p_{\mathrm{Col}}} \end{aligned} \tag{3.9}$$

The concentration of CO_2 at the gas-liquid interface (IF) $c^{\mathrm{CO_2}}_{\mathrm{IF}}$ is calculated assuming physical absorption, thus, applying Henry's law. This further assumes ideal gas and liquid, and that no reaction occurs in the interface. For example, $c^{\mathrm{CO_2}}_{\mathrm{IF}}$ at the top of the active absorber packing could be calculated using the Henry's coefficient of CO_2 in the solvent $c^{\mathrm{CO_2}}_{\mathrm{IF}} = \frac{y^{\mathrm{CO_2}}_{\mathrm{Out}} \cdot (p_{\mathrm{Abs}} - \Delta p_{\mathrm{Irr}})}{\mathrm{He}^{\mathrm{CO_2}}_{\mathrm{Mix}}}$.

The columns are assumed to be adiabatic [470, 471] and the strict enthalpy balance uses the molar flow rates, heat capacity c_{p}, temperature at the inlet and outlet and phase change contributions. Heat is transferred through the exothermic absorption of CO_2 described through the total heat of absorption ΔH_{Abs} multiplied with $n^{\mathrm{CO_2}}_{\mathrm{Abs}}$, and the endothermic vapourisation of water with $\Delta H^{\mathrm{H_2O}}_{\mathrm{Vap}}$ multiplied with the difference of molar flow rate of H_2O between the inlet and outlet.

$$\begin{aligned} V_{\mathrm{Out}} c_{\mathrm{p,V,Out}} T_{\mathrm{V,Out}} + L_{\mathrm{Out}} c_{\mathrm{p,L,Out}} T_{\mathrm{L,Out}} = V_{\mathrm{In}} c_{\mathrm{p,V,In}} T_{\mathrm{V,In}} + L_{\mathrm{In}} c_{\mathrm{p,L,In}} T_{\mathrm{L,In}} \\ + \Delta H^{\mathrm{H_2O}}_{\mathrm{Vap}} n^{\mathrm{H_2O}}_{\mathrm{Vap}} + n^{\mathrm{CO_2}}_{\mathrm{Abs}} \cdot \Delta H_{\mathrm{Abs}} \end{aligned} \tag{3.10}$$

The enthalpy balance implemented in the model estimates the enthalpy change of the solvent ΔH_{L} and vapour ΔH_{V} using averaged flow rates and heat capacity for increased numeric stability.

$$\begin{aligned} \Delta H_{\mathrm{L}} &= \Delta H_{\mathrm{V}} + \Delta H^{\mathrm{H_2O}}_{\mathrm{Vap}} \cdot \left(V_{\mathrm{Out}} y^{\mathrm{H_2O}}_{\mathrm{Out}} - V_{\mathrm{In}} y^{\mathrm{H_2O}}_{\mathrm{In}} \right) + n^{\mathrm{CO_2}}_{\mathrm{Abs}} \cdot \Delta H_{\mathrm{Abs}} \\ \Delta H_{\mathrm{L}} &= 0.5 \cdot \left(L_{\mathrm{In}} c_{\mathrm{p,L,In}} + L_{\mathrm{Out}} c_{\mathrm{p,L,Out}} \right) \left(T_{\mathrm{L,In}} - T_{\mathrm{L,Out}} \right) \\ \Delta H_{\mathrm{V}} &= 0.5 \cdot \left(V_{\mathrm{In}} c_{\mathrm{p,V,In}} + V_{\mathrm{Out}} c_{\mathrm{p,V,Out}} \right) \left(T_{\mathrm{V,In}} - T_{\mathrm{V,Out}} \right) \end{aligned} \tag{3.11}$$

ΔH_{Abs} is assumed to be independent of the temperature, and $\Delta H_{\mathrm{Vap}}^{\mathrm{H_2O}}$ is calculated at the logarithmic mean temperature between inlet and outlet.

The equation linking $n_{\mathrm{Abs}}^{\mathrm{CO_2}}$ to the mass transfer area and column size uses the liquid side mass transfer coefficient k_{L}, enhancement factor E, concentration of CO_2 at the interface $c_{\mathrm{IF}}^{\mathrm{CO_2}}$, effective (wet) packing specific packing area, a_{wet}, cross sectional area $A_{\mathrm{Col,CS}}$, and height of packing ZT_{Pack}.

$$n_{\mathrm{Abs}}^{\mathrm{CO_2}} = k_{\mathrm{L}} \cdot E \cdot c_{\mathrm{IF}}^{\mathrm{CO_2}} \cdot a_{\mathrm{wet}} \cdot A_{\mathrm{Col,CS}} \cdot ZT_{\mathrm{Pack}} \tag{3.12}$$

The enhancement factor is calculated through the Wellek *et al.,* [432] correlation using the Hatta [472] number Ha and infinite enhancement E_{Inf} assuming an irreversible reaction [473–475].

$$\begin{aligned} E &= 1 + \frac{1}{\left[(E_{\mathrm{Inf}} - 1)^{-1.35} + \left(\frac{\mathrm{Ha}}{\tanh \mathrm{Ha}} - 1\right)^{-1.35}\right]^{1/1.35}} \\ E_{\mathrm{Inf}} &= 1 + \frac{D_{\mathrm{L}}^{\mathrm{Amine}} \cdot c_{\mathrm{Bulk}}^{\mathrm{Amine}}}{z \cdot D_{\mathrm{CO_2,L}} \cdot c_{\mathrm{IF}}^{\mathrm{CO_2}}} \\ \mathrm{Ha} &= \frac{\sqrt{k_2 \cdot D^{\mathrm{CO_2}} \cdot c_{\mathrm{B}}^{\mathrm{Amine}}}}{z \cdot k_{\mathrm{L}}} \end{aligned} \tag{3.13}$$

The Hatta number Ha uses the second order reaction rate constant k_2, diffusivity coefficient of CO_2 in solvent $D_{\mathrm{CO_2,L}}$, concentration of amine in the bulk phase $c_{\mathrm{B}}^{\mathrm{Amine}}$, stoichiometric factor z, and liquid side mass transfer coefficient k_{L}. It depends on the reaction order and describes the ratio of maximum amount of consumed compound in the liquid film to the maximum amount of transferred compound if no chemical reaction occurs and the bulk concentration is zero. Ha indicates where the reaction pane is located (either in bulk, in film, or at interface). The reaction pane moves closer to the interface with faster kinetics. The infinite enhancement factor E_{Inf} assumes the transport of amine to the reaction pane (= interface) is the rate determining step. It is calculated using the diffusivity coefficient of amine in solvent $D_{\mathrm{L}}^{\mathrm{Amine}}$, and the concentration of amine in the bulk $c_{\mathrm{Bulk}}^{\mathrm{Amine}}$ which is assumed to be constant. The stoichiometric factor z depends on the reaction and equals two for carbamate forming mono-amines and equal one for bicarbonate forming mono-amines.

A pseudo-first order is often assumed a-prior [14, 340, 476], which would require, amongst other

conditions, a ratio of $\frac{c^{\text{Amine}}}{c^{\text{CO}_2}} > 15$ [432]. There is no guarantee that all solvents in the database meet all the assumptions behind a specific reaction regime, which is why the Wellek approach was chosen. Other approaches are discussed in the appendix B.4.

The reaction rate constant k_2 is calculated by the Arrhenius [365] equation using the pre exponential factor $k_{2,\text{PreExp}}$, activation energy E_A and universal gas constant $\Re$.

$$k_2 = k_{2,\text{PreExp}} \cdot \exp\left(\frac{-E_\text{A}}{\Re \cdot T}\right) \tag{3.14}$$

The approach for calculating the mass transfer follows the two film theory, assuming that the non-reactive equilibrium at the interface can be described with Henry's law. The overall mass transfer coefficient based on the liquid side $k_{\text{Tot,L}}$ is calculated using the mass transfer coefficient in the gas phase k_V and liquid side k_L as well as the Henry's coefficient He^{CO_2}. Both k_V and k_L are calculated depending on the packing type. Random packings were modelled with Onda *et al.,* [428, 430, 431] correlations. Structured packings were modelled using Shi and Mersmann [429] and Rocha *et al.,*'s [302] approach.

$$\frac{1}{k_{\text{Tot,L}}} = \frac{k_\text{V}}{\text{He}^{\text{CO}_2}} + \frac{1}{k_\text{L}} \tag{3.15}$$

Gas phase diffusivity coefficients D^i_V are calculated with the Fuller *et al.* [434–437] approach as described in [411] using the molar weight of the vapour phase MW_V. The atomic diffusion volume is calculated using data provided in [411] which only requires the number of atoms per molecule. As reference, the atomic diffusion volumes for a couple of interesting gases are $AV^{\text{Air}} = 19.7$, $AV^{\text{CO}_2} = 26.9$, and $AV^{\text{Flue Gas}} = 18.4$ (assuming $y_{\text{CO}_2} = 12$ mol%).

$$D^i_\text{V} = \frac{0.00143 \cdot T_\text{V}^{1.75}}{p_\text{Col} \cdot MW_\text{V}^{0.5} \cdot \left[(AV^i)^{1/3} + (AV_\text{V})^{1/3}\right]^2} \tag{3.16}$$

The liquid phase diffusivity coefficient of CO_2 is calculated using the Takahashi *et al.* [411, 438, 439] model. It requires the molar volume V^i_Mol, molar volume of the solvent $V_{\text{Mol,L}}$, and the binary diffusion coefficient of CO_2 in pure i $D_i^{\text{CO}_2}$. The molar volume of CO_2 at normal boiling

point is calculated with Maloka's correlation [477] which proved more accurate compared to [478, 479].

$$D_{\mathrm{L}}^{\mathrm{CO_2}} = \left(\frac{\eta_{\mathrm{L}}}{V_{\mathrm{Mol}}^{i}}\right)^{-1/3} \cdot \sum_{\substack{i=1 \\ i\neq \mathrm{CO_2}}}^{n} x_i \cdot D_{\mathrm{i}}^{\mathrm{CO_2}} \cdot \left(\frac{\eta_{\mathrm{i}}}{V_{\mathrm{Mol}}^{i}}\right)^{1/3} \tag{3.17}$$

The binary liquid phase diffusivity coefficient at infinite dilution $D_{\mathrm{i}}^{\mathrm{CO_2}}$ (*i.e.,* CO_2 in pure water, and CO_2 in pure amine) is calculated with the Wilke and Chang equation [438] using the association factor ϕ, and the molar volume at normal boiling point V_{Mol}^{i}.

$$D_{\mathrm{i}}^{\mathrm{CO_2}} = 7.4 \cdot 10^{-8} \cdot \frac{(\phi \cdot MW^{\mathrm{i}})^{1/2} \cdot T_{\mathrm{L}}}{\eta_{\mathrm{i}} \cdot (V_{\mathrm{Mol}}^{i})^{0.6}} \tag{3.18}$$

ϕ is assumed to be 2.6 for water [438] and 2.26 for all amines [480].

The liquid phase diffusivity coefficient of the other components (*e.g.,* amine in solvent) are calculated with the Wilke and Chang equation as modified by Perkins and Geankoplis [411, 440].

$$D_{\mathrm{L}}^{\mathrm{Amine}} = \frac{1}{\eta_{\mathrm{L}}^{0.8}} \cdot \sum_{\substack{j=1 \\ j\neq i}}^{n} x_j D_{\mathrm{j}}^{\mathrm{Amine}} \cdot \eta_{\mathrm{j}}^{0.8} \tag{3.19}$$

Calculated diffusivity coefficients were compared to [478, 480, 481] and showed good agreement with AARD $< 7\%$. Miyabe and Isogai [481] demonstrated that the modified Wilke-Chang equation can be applied to predict the molecular diffusivity of polar solutes in apolar and polar solvents with 71 systems showing a mean square deviation of less than 19%.

The superficial gas velocity $u_{\mathrm{V,sf}}$ is based on total cross-sectional area and is calculated by using the column diameter and a flood factor $f_{\mathrm{Flood}} = 70\%$ [482].

$$D_{\mathrm{Col}} = \sqrt{\frac{4 \cdot F_{\mathrm{V}}}{\frac{\pi \cdot \rho_{\mathrm{V}} \cdot u_{\mathrm{V,sf}}}{f_{\mathrm{Flood}}}}} \tag{3.20}$$

All assumptions of the approach are listed for clarity in Tab. 3.7 [483–488]. The two key assumptions are that all CO_2 molecules absorbed into the liquid react in the film and that the amine concentration does not deplete. The model could handle both mass transfer (diffusion) and reaction controlled scenarios, however, it is likely that the conditions inside the absorber

and stripper lead to mass transfer limited scenarios [489–491]. Lu *et al.,* [491] determined the transition between diffusion controlled and reaction controlled regime for fast reactions, but failed to do so for slow reactions. Slow reacting solvents are kinetically limited and the concentration of amine becomes an important factor [492]. Hace [493] analysed the concentration profiles for absorption systems at varying Hatta numbers for minimum and maximum mass transfer conditions. According to their results, film thickness calculated by the two film theory agreed well with the Danckwerts model [494, 495]. Even in the cases Ha < 4 (MDEA), the CO_2 concentration in the liquid phase reduced to zero within 10 μm (maximum mass transfer case) and 100 μm (minimum mass transfer). Therefore, it is reasonable to assume that no free CO_2 is present in the bulk liquid even for the slowest reacting solvents [491, 493].

Table 3.7: List of key thermodynamic assumptions.

1. Film theory holds true
2. Equilibrium at interface can be described with Henry's law
3. Reaction product does not accumulate at interface
4. Reactions are irreversible (equilibrium shifted to either absorption or desorption)
5. No free CO_2 in bulk liquid
6. (Free) amines do not deplete (diffusion of amine to interface never becomes rate determining)

The approaches for k_{L}, a_{wet}, and the pressure drop depend on the type of packing which will be discussed in the next paragraphs.

Random Packing Plastic Pall rings were selected as random packing (see Tab. 3.8). The effective (wet) packing area a_{eff} and liquid side mass transfer coefficient k_{L} are calculated via Onda *et al.,* [428, 430, 431] correlations using the dry specific packing area a_{P}, critical surface tension of the packing σ_{P}, surface tension of the solvent σ_{L}, diameter of the packing D_{P},

Table 3.8: Details of random packing Pall rings. Values from [496].

Feature	Value
Type	Random
Make	Pall rings
Material	Plastic
Nominal diameter	25 mm
Specific area of packing	225 m^2/m^3
Packing factor	55 ft^{-1}
Void fraction	0.887
Critical surface tension	33 mN/m
Packing constant P (for Billet-Schultes correlation)	0.865
Packing constant H (for Billet-Schultes correlation)	0.528
Packing constant S (for Billet-Schultes correlation)	2.696
Packing constant (for Onda correlation)	5.23

gravity g, Reynold's Re, Weber's We, Froude's Fr, and Schmidt's number Sc.

$$
\begin{aligned}
a_{\text{eff}} &= a_{\text{P}} \cdot \left[1 - \exp\left(-1.45 \cdot \left(\frac{\sigma_{\text{P}}}{\sigma_{\text{L}}}\right)^{0.75} \cdot \text{Re}_{\text{L}}^{0.1} \cdot \text{Fr}_{\text{L}}^{-0.05} \cdot \text{We}_{\text{L}}^{0.2}\right)\right] \\
\text{Re}_{\text{L}} &= \frac{\rho_{\text{L}} \cdot u_{\text{L,sf}}}{\eta_{\text{L}} \cdot a_{\text{P}}} \\
\text{We}_{\text{L}} &= \frac{\rho_{\text{L}} \cdot u_{\text{L,sf}}^2}{\sigma_{\text{L}} \cdot a_{\text{P}}} \\
\text{Sc}_{\text{L}} &= \frac{\eta_{\text{L}}}{\rho_{\text{L}} \cdot D_{\text{L}}^{\text{CO}_2}} \\
\text{Fr}_{\text{L}} &= \frac{a_{\text{P}} \cdot u_{\text{L,sf}}^2}{g} \\
k_{\text{L}} &= 0.0051 \cdot \frac{\text{Re}_{\text{L}}^{2/3} \cdot (a_{\text{P}} \cdot D_{\text{P}})^{0.4}}{} \cdot \left(\frac{\rho_{\text{L}}}{\eta_{\text{L}} \cdot g}\right)^{-1/3}
\end{aligned}
\tag{3.21}
$$

The diameter of the column is estimated using a 70% flooding approach, following packing vendors' recommendation of operating sufficiently below the flooding limit. The pressure drop

is calculated using the Billet and Schultes method [442, 497].

Table 3.9: Details of structured packing Mellapak 2X [498].

Feature	Value
Type	Structured
Make	Sulzer Mellapak 2X
Material	Stainless steel [499]
Specific area of packing a_p	205 m^2/m^3 [500]
Packing factor	23 ft^{-1} [500]
Void fraction ϵ	0.98 [500]
Base width (B)	0.03022 m [500]
Crimp height (h)	0.0143 m [500]
Corrugation angle θ_{Pack}	60°[500]
Surface enhancement factor F_{SE}	0.350 [302]
Packing cost	\$1758/ft^3 [444]

Structured Packing Mellapak 2X [498] was selected and Tab. 3.9 summarises the characteristics. Structured packings require a different approach to calculating the mass transfer coefficient, velocities, and pressure drop. The additional equations follow the approach of Shi and Mersmann [429] and Rocha *et al.,* [302]. The effective specific packing area a_{eff} is calculated using the dry specific packing area a_{P}, packing factor F_{P}, hydraulic diameter $S_{\mathrm{Pack}} = 4 \cdot \frac{\epsilon_{\mathrm{Pack}}}{a_{\mathrm{P}}}$, hold-up hu_{L}, Reynold's number Re, Weber's number We, Froude's number Fr, and the super-

ficial velocity of the liquid in an empty tower $u_{\mathrm{L,s}}$ [302, 429, 501].

$$
\begin{aligned}
\frac{a_{\mathrm{eff}}}{a_p} &= F_{SE}\frac{29.12\left(\mathrm{We_L Fr_L}\right)^{0.15} S_{\mathrm{Pack}}^{0.359}}{\mathrm{Re_L^{0.2}}\epsilon^{0.6}\left(1-0.93\cos\gamma\right)\left(\sin\theta_{\mathrm{Pack}}\right)^{0.3}} \\
\text{If } \sigma_{\mathrm{L}} &< 0.055\ \frac{\mathrm{N}}{\mathrm{m}}: \quad \cos\gamma = 0.9 \\
\text{If } \sigma_{\mathrm{L}} &\geq 0.055\ \frac{\mathrm{N}}{\mathrm{m}}: \quad \cos\gamma = 5.211\cdot 10^{-16.835\cdot\sigma_{\mathrm{L}}} \\
u_{\mathrm{V,SF}} &= \frac{u_{\mathrm{L,s}}}{\epsilon_{\mathrm{Pack}}\cdot hu_{\mathrm{L}}\cdot\sin\theta_{\mathrm{Pack}}} \\
\mathrm{Re_L} &= \frac{\rho_{\mathrm{L}}\cdot S_{\mathrm{Pack}}\cdot u_{\mathrm{L,s}}}{\eta_{\mathrm{L}}} \\
\mathrm{We_L} &= \frac{u_{\mathrm{L,s}}\cdot\rho_{\mathrm{L}}\cdot S_{\mathrm{Pack}}}{1} \\
\mathrm{Fr_L} &= \frac{u_{\mathrm{L,s}}^2}{g\cdot S_{\mathrm{Pack}}}
\end{aligned}
\tag{3.22}
$$

The γ-function depends on the surface tension. For reference, the average surface tension of aqueous amines is $0.05\ \frac{\mathrm{N}}{\mathrm{m}}$ and varies between $0.01-0.08\ \frac{\mathrm{N}}{\mathrm{m}}$. The numeric stability declined in comparison to the random packing, because the γ-function returns either 0.9 for $\sigma_{\mathrm{L}} = 0.0549$ or 0.75 for $\sigma_{\mathrm{L}} = 0.0550$.

Equation 3.12 is valid for both random and structured packings in which a_{wet} is either calculated by Eqn. 3.21 or by Eqn. 3.22. The liquid mass transfer coefficient k_{L} is calculated using the side dimension of corrugation S [302].

$$
k_{\mathrm{L}} = 2\cdot\left(\frac{D_{\mathrm{CO_2},L}\cdot C_{\mathrm{Pack,E}}\cdot u_{\mathrm{L}}}{\pi\cdot S}\right)^{0.5} \tag{3.23}
$$

The irrigated pressure drop p_{Irr} is calculated by the GPDC approach [499] using the superficial gas velocity $u_{\mathrm{V,SF}}$, standard gas superficial velocity $c_{\mathrm{V,SF}}$, packing factor F_{P}, mass flow rate of liquid F_{L} and gas F_{V}, and weighted flow rate ratio F_{LV}. This approach is valid for $0.005 \leq$

$\frac{F_\mathrm{L}}{F_\mathrm{V}} \leq 5$ and $0.25\ \frac{\mathrm{in}_{\mathrm{H_2O}}}{ft} \leq \Delta p_\mathrm{Irr} \leq 1.5\ \frac{\mathrm{in}_{\mathrm{H_2O}}}{ft}$ [14].

$$
\begin{aligned}
CP &= C_\mathrm{SF} F_\mathrm{p}^{0.5} \frac{\eta_\mathrm{L}}{\rho_\mathrm{L}}^{0.05} \\
c_\mathrm{V,SF} &= u_\mathrm{V,SF} \left(\frac{\rho_V}{\rho_L - \rho_V} \right)^{0.5} \\
F_\mathrm{LV} &= \frac{F_\mathrm{L}}{F_\mathrm{V}} \cdot \left(\frac{\rho_G}{\rho_L} \right)^{0.5} \\
CP &= \frac{3.8617 \cdot \left(\frac{\Delta p_\mathrm{Irr}}{Z T_\mathrm{Col}} \right)^{0.6609}}{\left[1 + 6.3763 \left(\Delta P / Z T \right)^{(0.6609/0.7206)} \cdot F_\mathrm{LV}^{0.2898} \right]^{0.7206}} \\
&\quad \cdot \left[1 - \exp\left(-0.9093 \cdot F_\mathrm{LV}^{-0.6819} \right) \right]
\end{aligned}
\tag{3.24}
$$

The flooding point is calculated as $\Delta p^\mathrm{Flood} = 0.12 \cdot F_p^{0.7}$. Assuming 70% flooding is within the optimal range identified by [444]. The results for the pressure drop and effective packing area were compared with [444, 500, 502] and showed good agreement. Zakeri *et al.,* [500] found the error in their experimental setup for the dry pressure drop to be $2-3\%$ and the wet pressure drop to be $2-4\%$.

Using structured packings would yield superior performance compared to random packing, however, the selected correlations have smaller validity range compared to the ones available for random packings [302, 429, 430]. Random packings were chosen for both absorber and stripper columns, because the model prioritises a wider validity range over lower absolute capture cost. It will be analysed if the packing selection impacts the relative ranking between solvents.

Mechanical Design The L/G ratio is calculated on a mole basis L/G_Mol and mass basis L/G_Mass with V_In being the flue gas molar flow rate entering the absorber and the liquid molar flow rate of solvent L_In entering the absorber.

$$
\begin{aligned}
L/G_\mathrm{Mol} &= \frac{L_\mathrm{In}}{V_\mathrm{In}} \\
L/G_\mathrm{Mass} &= \frac{F_L}{F_V}
\end{aligned}
\tag{3.25}
$$

The design of the column follows the approach in [503]. The column's shell thickness e_Col is cal-

culated using the minimum thickness $e_{\text{Col,Min}}$, highest pressure inside the column $p_{\text{Col}} = 0.3\ \frac{\text{N}}{\text{mm}^2}$, inside diameter $D_{\text{Col,In}}$, design stress $p_{\text{Col,Des}} = 145 \frac{\text{N}}{\text{mm}^2}$ (304 stainless steel at 100°C) and corrosion allowance $e_{\text{Corr}} = 2$ mm. The outside diameter $D_{\text{Col,Out}}$ is calculated by adding the wall thickness twice e_{Col}.

$$\begin{aligned} e_{\text{Col,Min}} &= \frac{p_{\text{Col}} \cdot D_{\text{Col,In}}}{2 \cdot p_{\text{Col,Des}} - p_{\text{Col}}} \\ e_{\text{Col}} &= e_{\text{Col,Min}} + e_{\text{Corr}} \\ D_{\text{Col,Out}} &= D_{\text{Col,In}} + 2 \cdot e_{\text{Col}} \end{aligned} \tag{3.26}$$

For example, if $D_{\text{Col,I}} = 12$ m then the column's shell thickness is $e_{\text{Col}} \approx 14.4$ mm.

The shell's weight W_{Col} is calculated assuming domed ends and uniform wall thickness [503]. The equation returns the weight in Newton, and the costing correlations require pounds.

$$W_{\text{Col}} = 240 \cdot 1.15 \cdot D_{\text{Col,Out}} \cdot (ZT_{\text{Col}} + 0.8 \cdot D_{\text{Col,Out}} m) \cdot e_{\text{Col}} \tag{3.27}$$

The design is limited in the shell weight 4250 lbs $< W_{\text{Col,lbs}} <$ 980000 lbs. If the upper limit is exceeded, then the flue gas stream is separated equally into a number of columns $Nm_{\text{Col}} = \frac{W_{\text{Col,lbs}}}{980000\ \text{lbs}}$.

In addition, a limit on the absorber diameter was set to 18 m to prevent unrealistic column designs by increasing the number of absorbers and splitting the flue gas stream equally. Solvent from multiple absorber units would be mixed before the main heat exchanger and sent to a shared stripper. Diameters for the absorber reported in the literature range between 10-18 m at comparable conditions [14, 113, 114, 384–388]. Canepa and Wang [387] analysed the impact of installing multiple units on the absorber diameter for MEA and found the diameter for one absorber to be $\approx$ 18.5 m, and for three units $\approx$ 11 m. An NETL study from 2007 [504] limits the column diameter to $<$ 40 ft (12.2 m), due to structural integrity concerns [387], however, the original study does not provide evidence for the 40 ft limitation. A short-cut equation [505] for distillation columns returns absorber diameter between 11-16 m for the range studied in this work.

Figure D.1 in the appendix shows the relationship from Eqn. 3.27 plotted as a function of

height and diameter. For reference, the absorber designed for the 0.4 $\text{Mtpa}_{\text{CO}_2}$ capture plant at Heidelberg Material's cement plant in Brevik is 50 m tall and weighs 202 tons without the stack. The typical range identified in the literature is highlighted in colour.

The solvent volume inside the active packing $Vol_{\text{S,Col}}$ is estimated by assuming half of the available volume is filled with solvent [506].

$$Vol_{\text{S,Col}} = \frac{Vol_{\text{P}} \cdot \epsilon_{\text{P}}}{2} \tag{3.28}$$

Post-Treatment The port-treatment section consists of a water wash column, demister, heat exchanger, and pump. Its practical purpose is ensuring amine emission limits are met and amine losses minimised, before the cleaned flue gas is released into the atmosphere. The emission limit is assumed to be 1 $\text{ppm}_{\text{Amine}}$, derived from the environmental permit for the capture plants in Brevik and Klemetsrud (project Longship as part of the Northern Lights value chain) [507]. Size and water consumption in the water wash are determined by the flue gas flow rate, amine volatility, and potential degradation products.

Most amine would be lost through the water-wash (approximately 55% for MEA) and oxidative degradation (approximately 25% for MEA) whereas emissions to air are only accounting for the smallest contribution to the overall amine loss (approximately 3% for MEA) [508]. AMP is one of the most volatile amines and sets a practical benchmark for water-wash systems [509–513].

Rigorously modelling the water wash column is not required for the purpose of initially screening solvents and this is left for other studies [65, 275, 514–517]. The pressure drop of the water wash column and demister are relevant to the design of the absorber. The capital and operating expenditure contribute to the total capture cost. The water-wash column is assumed to sit on top of the active absorber packing inside the absorber tower. It uses the same packing, same column diameter, and its height is set to $ZT_{\text{WW}} = 4$ m using literature reference values [275, 514, 518, 519] [509–513].

The required water flow rate is calculated by a fixed L/G ratio $L/G = 2$ kg/kg. It is assumed that the amine concentration at the top of the water wash equals 1 ppm with the difference

between inlet and outlet being completely absorbed into the water. The cleaned flue gas leaves in thermal equilibrium with the water wash inlet. The irrigated pressure drop of the water wash column is calculated with the same approach as the absorber, depending on the packing type.

The approach to the cooling water temperature inside the water wash cooler is 10 K, resulting in the water entering the water wash column at $T_{\mathrm{WW,In}} = 313$ K. The demister height is set to $ZT_{\mathrm{DM}} = 0.5$ m. The total absorber height is calculated as the sum of column, water wash, and demister $ZT_{\mathrm{Abs}} = ZT_{\mathrm{Col}} + ZT_{\mathrm{DM}} + ZT_{\mathrm{WW}}$.

Multi-Stage Modelling The short-cut modelling can be expanded to include multi-stage modelling by calculating a number of theoretical stages, each using the short-cut approach. The number of theoretical stages is a model parameter and optimised [281, 405, 520, 521]. Modelling the absorber through a multi-stage approach will increase the accuracy as it takes the profile over the column height into account. This is important in particular for the temperature and pressure drop profiles. The modelling approach impacts the required mass transfer area *i.e.,* column height and solvent flow rate. Most CO_2 is absorbed in the bottom third of the column [444] which should lead to an increase of the solvent's temperature compared to the short-cut approach which calculates an average temperature. The difference in solvent's temperature at the absorber bottom will impact the equilibrium loading, leading to lower values compared to the short cut approach at same $p_{\mathrm{CO_2}}$.

It is expected that the short-cut model will deviate the most at conditions when the mass transfer driving force at the top of the absorber is low, *e.g.,* at low CO_2 concentration in the flue gas and high capture rates. This is because the absorber is calculated as a single stage using the logarithmic mean driving force. It is partially resolved by implementing the minimum working capacity and limiting the capture rate. The model will also deviate most for solvents with highly exothermic reactions, by overestimating the solvent's working capacity at the same lean loading.

The computational effort in deploying a multi-stage model increased such that it appeared

prohibitively high and was in contrast to the purpose of the model. The time to converge increased to 5-10 minutes per solvent and operating condition. The decision was made to prioritise quick convergence.

Heat Exchangers

The process uses three single-phase heat exchangers (main heat exchanger, lean solvent cooler, and water wash cooler), as well as two two-phase change heat exchangers (reboiler and condenser). All exchangers, except the reboiler, are modelled as horizontal shell and tube units. The reboiler is modelled as a vertical thermosyphon. They share the following design equations and differ in the heat transfer coefficient correlations.

Each heat exchanger's heat flux Q_{Hex} is calculated by the product of required heat transfer area A_{Hex}, overall heat transfer coefficient U_{Hex}, and the logarithmic mean temperature difference ΔT_{LM} [506].

$$Q_{\text{Hex}} = U_{\text{Hex}} \cdot A_{\text{Hex}} \cdot \Delta T_{LM} \tag{3.29}$$

The logarithmic mean temperature difference ΔT_{LM} was estimated using Paterson's [522] approach for increased numeric stability. It uses the geometric ΔT_{GM} and arithmetic mean ΔT_{AM} at the hot end $T_{\text{h,In}} - T_{\text{c,Out}}$ and cold end $T_{\text{h,Out}} - T_{\text{c,In}}$.

$$\begin{aligned}
\Delta T_{LM} &= \frac{(T_{\text{h,In}} - T_{\text{c,Out}}) - (T_{\text{h,Out}} - T_{\text{c,In}})}{\ln \frac{T_{\text{h,In}} - T_{\text{c,Out}}}{T_{\text{h,Out}} - T_{\text{c,In}}}} \\
\Delta T_{LM} &\approx \frac{2}{3} \cdot \Delta T_{GM} + \frac{1}{3} \cdot \Delta T_{AM} \\
\Delta T_{GM} &= \sqrt{(T_{\text{h,In}} - T_{\text{c,Out}}) \cdot (T_{\text{h,Out}} - T_{\text{c,In}})} \\
\Delta T_{AM} &= \frac{(T_{\text{h,In}} - T_{\text{c,Out}}) + (T_{\text{h,Out}} - T_{\text{c,In}})}{2}
\end{aligned} \tag{3.30}$$

The maximum heat transfer area is limited to 1200 ft^2. The number of required exchangers Nm_{Hex} equals one if $A_{\text{Hex}} \leq 1200$ ft^2. If $A_{\text{Hex}} > 1200$ ft^2 then the total flow is separated equally into $Nm_{\text{Hex}} = \lceil \frac{A_{\text{Hex,sft}}}{1200} \rceil$ exchangers (rounded up to nearest full integer).

Single-Phase The overall heat transfer coefficient based on the outside area U uses the heat transfer coefficient inside the hot tube h_{h}, the heat transfer coefficient outside the tube in the colder shell h_{c}, the heat transfer resistance due to fouling expressed as heat transfer coefficient $h_{\mathrm{Foul}} = 6000\ \frac{\mathrm{W}}{\mathrm{m^2\ K}}$, the tube thickness $\frac{D_{\mathrm{Tub,Out}} - D_{\mathrm{Tub,In}}}{2} = 2.11$ mm (BWG14), and thermal conductivity of the tube material $\lambda_{\mathrm{Wall}} = 50\ \frac{\mathrm{W}}{\mathrm{m\ K}}$ [506].

$$\frac{1}{U} = \frac{1}{h_{\mathrm{c}}} + \frac{1}{h_{\mathrm{Foul}}} + \frac{D_{\mathrm{Tub,Out}} \cdot \ln \frac{D_{\mathrm{Tub,Out}}}{D_{\mathrm{Tub,In}}}}{2 \cdot \lambda_{\mathrm{Wall}}} + \frac{D_{\mathrm{Tub,Out}}}{D_{\mathrm{Tub,In}}} \cdot \frac{1}{h_{\mathrm{Foul}}} + \frac{D_{\mathrm{Tub,Out}}}{D_{\mathrm{Tub,In}}} \cdot \frac{1}{h_{\mathrm{h}}} \tag{3.31}$$

The design assumes a staggered and triangular configuration using the number of passes $Nm_{\mathrm{Pass}} = 4$, number of baffles $Nm_{\mathrm{Baf}} = 3$, number of tubes Nm_{Tub}, diameter of the bundle D_{Bun}, diameter of the shell D_{Shell}, equivalent diameter D_{Eq}, length of tube $l_{\mathrm{Tub}} = 48$ ft, pitch length l_{Pit}, shell length l_{Shell}, and clearance of 10% [506].

$$\begin{aligned} l_{\mathrm{Pit}} &= 1.25 \cdot D_{\mathrm{Tub,Out}} \\ D_{\mathrm{Bun}} &= D_{\mathrm{Tub,Out}} \cdot (Nm_{\mathrm{Tub}}/0.175)^{1/2.285} \\ D_{\mathrm{Shell}} &= 1.1 \cdot D_{\mathrm{Bun}} \\ D_{\mathrm{Eq}} &= 1.10 \cdot \frac{l_{\mathrm{Pit}}^2 - 0.917 \cdot D_{\mathrm{Tub,Out}}^2}{D_{\mathrm{Tub,Out}}} \end{aligned} \tag{3.32}$$

The volume inside the tubes Vol_{Tub} and shell Vol_{Shell} is calculated using the cross section area of the shell A_{Shell}, and of the tubes A_{Tub} [506].

$$\begin{aligned} A_{\mathrm{Tub}} &= \frac{\pi}{4} \cdot D_{\mathrm{Tub,In}}^2 \cdot \frac{Nm_{\mathrm{Tub}}}{Nm_{\mathrm{Pass}}} \\ A_{\mathrm{Shell}} &= (l_{\mathrm{Pit}} - D_{\mathrm{Tub,Out}}) \cdot \frac{l_{\mathrm{Tub}} \cdot D_{\mathrm{Shell}}}{l_{\mathrm{Pit}} \cdot Nm_{\mathrm{Baf}}} \\ A_{\mathrm{Hex}} &= \pi \cdot D_{\mathrm{Tub,Out}} \cdot l_{\mathrm{Tub}} \cdot Nm_{\mathrm{Tub}} \\ Vol_{\mathrm{Tub}} &= l_{\mathrm{Tub}} \cdot A_{\mathrm{Tub}} \cdot Nm_{\mathrm{Pass}} \\ Vol_{\mathrm{Shell}} &= \left(A_{\mathrm{Shell}} - \frac{\pi}{4} \cdot D_{\mathrm{Tub,Out}}^2 \cdot Nm_{\mathrm{Tub}} \cdot Nm_{\mathrm{Pass}} \right) \cdot l_{\mathrm{Tub}} \end{aligned} \tag{3.33}$$

Mass balances are calculated as $F_{\mathrm{h,In}} = F_{\mathrm{h,Out}}$ and $F_{\mathrm{c,In}} = F_{\mathrm{c,Out}}$ as well as $x_{\mathrm{h,In}}^i = x_{\mathrm{h,Out}}^i$ and $x_{\mathrm{c,In}}^i = x_{\mathrm{c,Out}}^i$ (no change in composition for each compound i). Each heat exchanger's

heat flux Q_{Hex} equals the difference between the enthalpy flows between inlets and outlets (in absence of sensible heat).

$$\begin{aligned} Q_{\mathrm{Hex}} &= L_{\mathrm{h,In}} \cdot c_{\mathrm{p,h,In}} \cdot T_{\mathrm{h,In}} - L_{\mathrm{h,Out}} \cdot c_{\mathrm{p,h,Out}} \cdot T_{\mathrm{h,Out}} \\ &= L_{\mathrm{c,Out}} \cdot c_{\mathrm{p,c,Out}} \cdot T_{\mathrm{c,Out}} - L_{\mathrm{c,In}} \cdot c_{\mathrm{p,c,In}} \cdot T_{\mathrm{c,In}} \end{aligned} \tag{3.34}$$

The heat transfer coefficients depend on the Reynold's number (laminar or turbulent flow regime) and are calculated through Nusselt Nu correlations using the Prandtl Pr and Reynold's Re number.

$$\begin{aligned} \mathrm{Re}_{\mathrm{Tub}} &= \frac{u_{\mathrm{h}} \cdot D_{\mathrm{Tub,In}} \cdot \rho_{\mathrm{h}}}{\eta_{\mathrm{h}}} \\ \mathrm{Re}_{\mathrm{Shell}} &= \frac{u_{\mathrm{c}} \cdot D_{\mathrm{Eq}} \cdot \rho_{\mathrm{c}}}{\eta_{\mathrm{c}}} \\ \mathrm{Pr}_{\mathrm{Tub}} &= \frac{c_{\mathrm{p,h}} \cdot \eta_{\mathrm{h}}}{\lambda_{\mathrm{h}}} \\ \mathrm{Pr}_{\mathrm{Shell}} &= \frac{c_{\mathrm{p,c}} \cdot \eta_{\mathrm{c}}}{\lambda_{\mathrm{c}}} \\ \mathrm{Nu}_{\mathrm{Tub}} &= \frac{h_{\mathrm{h}} \cdot D_{\mathrm{Tub,In}}}{\lambda_{\mathrm{h}}} \\ \mathrm{Nu}_{\mathrm{Shell}} &= \frac{h_{\mathrm{c}} \cdot D_{\mathrm{Eq}}}{\lambda_{\mathrm{c}}} \end{aligned} \tag{3.35}$$

The thermo-physical properties c_{p}, λ, ρ, and η change between inlet and outlet. The properties for Eqn. 3.35 are calculated using the logarithmic mean temperature for the cold $T_{LM,c}$ and hot stream $T_{LM,h}$. The temperature at the tube's wall T_{Wall} is calculated using the mean shell-side bulk temperature $T_{LM,c}$, the mean tube-side bulk temperature $T_{LM,h}$, and h_{h} [506].

$$\begin{aligned} T_{LM,c} &= \frac{T_{\mathrm{c,Out}} - T_{\mathrm{c,In}}}{\ln(T_{\mathrm{c,Out}}/T_{\mathrm{c,In}})} \\ T_{LM,h} &= \frac{T_{\mathrm{h,In}} - T_{\mathrm{h,Out}}}{\ln(T_{\mathrm{h,In}}/T_{\mathrm{h,Out}})} \\ T_{\mathrm{Wall}} &= \frac{U}{h_{\mathrm{h}}} \cdot (T_{LM,c} - T_{LM,h}) + T_{LM,h} \end{aligned} \tag{3.36}$$

The liquid velocities u_c and u_h are calculated using the mass flow rate F and cross sectional area.

$$\begin{aligned} u_c &= \frac{F_c}{A_{\mathrm{Shell}} \cdot \rho_{\mathrm{c}}} \\ u_h &= \frac{F_h}{A_{\mathrm{Tub}} \cdot \rho_{\mathrm{h}}} \end{aligned} \tag{3.37}$$

The threshold between laminar and turbulent flow inside the tube is set at Re = 2500 assuming that the unpredictable transition region between the regimes is modelled as laminar flow. The Nusselt correlations for laminar $\mathrm{Nu}'_{\mathrm{Tub,l}}$ and turbulent flow $\mathrm{Nu}_{\mathrm{Tub,t}}$ use the viscosity at wall temperature $\eta_{\mathrm{h,W}}$ and a constant C_{Tub} (0.021 for gases, 0.023 for non-viscous liquids, 0.027 for viscous liquids defined as ten times more viscous than water) [506]. However, $\mathrm{Nu}_{\mathrm{Tub,l}}$ cannot be less than 3.5 regardless of the correlation result $\mathrm{Nu}'_{\mathrm{Tub,l}}$ [506].

$$\begin{aligned}
\text{If Re} > 2500 \text{ then } \mathrm{Nu}_{\mathrm{Tub,t}} &= C_{\mathrm{Tub}} \cdot \mathrm{Re}_{\mathrm{Tub}}^{0.8} \cdot \mathrm{Pr}_{\mathrm{Tub}}^{0.33} \cdot \left(\frac{\eta_{\mathrm{h}}}{\eta_{\mathrm{h,W}}}\right)^{0.14} \\
\text{If Re} \leq 2500 \text{ then } \mathrm{Nu}'_{\mathrm{Tub,\,l}} &= 1.86 \cdot (\mathrm{Re}_{\mathrm{Tub}}\ \mathrm{Pr}_{\mathrm{Tub}})^{0.33} \cdot \left(\frac{D_{\mathrm{Eq}}}{l_{\mathrm{Tub}}}\right)^{0.33} \cdot \left(\frac{\eta_{\mathrm{h}}}{\eta_{\mathrm{h,W}}}\right)^{0.14} \\
\mathrm{Nu}_{\mathrm{Tub,l}} &= \max\left(3.5, \mathrm{Nu}'_{\mathrm{Tub,l}}\right)
\end{aligned} \tag{3.38}$$

Kern's method [422] is used to estimate the heat transfer coefficient in the shell h_{c} through a Nusselt $\mathrm{Nu}_{\mathrm{Shell}}$ correlation using the shell side factor j_{Shell} [506].

$$\begin{aligned}
\mathrm{Nu}_{\mathrm{Shell}} &= j_{\mathrm{Shell}} \cdot \mathrm{Re}_{\mathrm{Shell}} \cdot \mathrm{Pr}_{\mathrm{Shell}}^{1/3} \cdot \left(\frac{\eta_{\mathrm{c}}}{\eta_{\mathrm{c,W}}}\right)^{0.14} \\
j_{\mathrm{Shell}} &= 10^{[-0.4714 \cdot \log \mathrm{Re}_{\mathrm{Shell}} - 0.4305]}
\end{aligned} \tag{3.39}$$

The pressure drops in the tube ΔP_{Tub} and in the shell $\Delta P_{\mathrm{Shell}}$ are calculated by Frank's approach [523], using the tube friction factor $j_{\mathrm{f,Tub}}$, shell friction factor $j_{\mathrm{f,Shell}}$ (same expression as Eqn. 3.53, digitised from [506]), and a constant C_{Shell} (0.25 for Re < 2500, else 0.14) [506].

$$\begin{aligned}
\Delta P_{\mathrm{Tub}} &= N m_{\mathrm{Pass}} \left[8 j_{\mathrm{f,Tub}} \frac{l_{\mathrm{Tub}}}{D_{\mathrm{Tub,In}}} \left(\frac{\eta_{\mathrm{c}}}{\eta_{\mathrm{c,W}}}\right)^{-C_{\mathrm{Shell}}} + 2.5\right] \frac{\rho_{\mathrm{h}} u_{\mathrm{h}}^2}{2} \\
\Delta P_{\mathrm{Shell}} &= 8 j_{\mathrm{f,Shell}} \frac{D_{\mathrm{Shell}}}{D_{\mathrm{Eq}}} (N m_{\mathrm{Baf}} + 1) \frac{\rho_{\mathrm{c}} u_{\mathrm{c}}^2}{2} \left(\frac{\eta_{\mathrm{c}}}{\eta_{\mathrm{c,W}}}\right)^{-0.14}
\end{aligned} \tag{3.40}$$

The main heat exchanger is modelled assuming single-phases only. ΔT_{LM} of the main heat exchanger is an operating parameter which is optimised for minimum capture cost. It is limited by either a minimum temperature approach of 1 K assumed to be achievable in manufacturing [506], or by suppressing any potential two-phase flow occurring at either end. The latter set in most cases the limit, if the optimisation minimised ΔT_{LM}.

Two-Phase Both two-phase heat exchangers are fed with the gaseous stream to the shell and the liquid stream to the tubes, *i.e.,* the condenser is fed with cooling water to the tubes, and the wet-CO_2 rich vapour stream to the shell. The reboiler is fed with the regenerated solvent to the tubes, and steam to the shell. It is assumed only vapour enters the process side of the condenser, and only liquid enters the process side of the reboiler. The single-phase equations use h to indicate the (hot) stream inside the tubes and c to indicate the (cold) stream in the shell. Some of these equations remain valid for two-phase exchangers by replacing h with tube and c with shell. The design follows the principles of the single flow heat exchangers assuming a single pass triangular configuration. Listed below are only equations that differ to the single-phase flow.

The number of passes $Nm_{\mathrm{Pass}} = 1$, number of baffles $Nm_{\mathrm{Baf}} = 1$, clearance of 70 mm, condenser's length of tube $l_{\mathrm{Tub,Cond}} = 16$ ft, reboiler's length of tube $l_{\mathrm{Tub,Reb}} = 24$ ft, thickness 3.05 mm (BWG11), as well as the equations for the diameter of the bundle D_{Bun} and condenser's shell $D_{\mathrm{Shell,Cond}}$ changed compared to the single-phase exchanger [506].

$$\begin{aligned} Nm_{\mathrm{Pass}} &= 1 \\ Nm_{\mathrm{Baf}} &= 1 \\ l_{\mathrm{Tub,Cond}} &= 16 \text{ ft} \\ l_{\mathrm{Tub,Reb}} &= 24 \text{ ft} \\ D_{\mathrm{Bun}} &= D_{\mathrm{Tub,Out}} \cdot \left(\frac{Nm_{\mathrm{Tub}}}{0.319} \right)^{1/2.142} \\ D_{\mathrm{Shell,Cond}} &= D_{\mathrm{Bun}} + 70 \text{ mm} \end{aligned} \tag{3.41}$$

The overall heat transfer coefficient based on the outside area U is calculated with Eqn. 3.31 in which h_{c} is replaced to h_{Steam} for the reboiler and h_{V} for the condenser, as well as h_{h} replaced to h_{fb} (forced boiling) for the reboiler and h_{CW} (cooling water, see Eqn. 3.38) for the condenser [506].

$$\begin{aligned} h_{\mathrm{Steam}} &= 8000 \ \frac{\mathrm{W}}{\mathrm{m}^2 \ \mathrm{K}} \\ h_{\mathrm{V}} &= 0.95 \cdot \lambda_{\mathrm{L}} \left[\frac{\rho_L (\rho_L - \rho_V) g}{\eta_{\mathrm{L}} \frac{F_{\mathrm{L}}}{l_{\mathrm{Tub}}}} \right]^{1/3} \end{aligned} \tag{3.42}$$

The film coefficient for condensing steam h_{Steam} could be calculated, however, according to [506] it will not be a limiting factor, thus, assuming $h_{\text{Steam}} = 8000\ \frac{\text{W}}{\text{m}^2\ \text{K}}$ to reduce computational effort. The mean condensation film coefficient around horizontal tubes h_{V} is calculated using Kern's method, assuming that the condensate L (water) is of low viscosity to ignore the correction for the number of tube rows [422]. The properties are calculated at the logarithmic mean temperature between T_{Wall} and T_{Cond} (see Eqn. 3.36).

The forced boiling heat transfer coefficient h_{fb} is estimated with Chen's model [423], which sums the corrected convective $f_{\text{cb,c}} \cdot h_{\text{cb}}$ and corrected nucleate boiling $f_{\text{nb,s}} \cdot h_{\text{nb}}$ heat transfer coefficients. The convective coefficient h_{cb} is calculated using Eqn. 3.38 and corrected using the Lockhart-Martinelli two-phase flow parameter X_{tt} and weight fraction of vapour w_V [424]. The nucleate boiling coefficient h_{nb} is calculated with the Forster and Zuber correlation [425].

$$
\begin{aligned}
h_{\text{fb}} &= f_{\text{cb,c}} \cdot h_{\text{cb}} + f_{\text{nb,s}} \cdot h_{\text{nb}} \\
h_{\text{nb}} &= f_s \cdot 0.00122 \cdot \left[\frac{\lambda_{\text{L}}^{0.79} \cdot c_{\text{p,L}}^{0.45} \cdot \rho_L^{0.49}}{\sigma_{\text{L}}^{0.5} \cdot \eta_{\text{L}}^{0.29} \cdot \left(Q_{\text{Lat}} F_{\text{V}}\right)^{0.24} \cdot \rho_V^{0.24}} \right] \left(T_{\text{Wall}} - T_{\text{Sat}}\right)^{0.24} \left(p_{\text{Vap},T_{\text{Wall}}} - p_{\text{Vap},T_{\text{Sat}}}\right)^{0.75} \\
\frac{1}{X_{tt}} &= \left(\frac{w_V}{1 - w_V}\right)^{0.9} \left(\frac{\rho_V}{\rho_L}\right)^{0.5} \left(\frac{\eta_V}{\eta_L}\right)^{0.1}
\end{aligned}
\tag{3.43}
$$

The two-phase correction factor $f_{\text{cb,c}}$ and nucleate boiling suppression factor $f_{\text{nb,s}}$ are calculated after digitising the figures in [506] with $\beta^1_{f_{\text{nb,s}}} = -0.218$ and $\beta^2_{f_{\text{nb,s}}} = 2.915$.

$$
\begin{aligned}
\text{If } \log\frac{1}{X_{tt}} < 1\text{:} \quad & f_{\text{cb,c}} = 10^{\left(0.1862 \cdot \left(\log \frac{1}{X_{tt}}\right)^2 + 0.63 \cdot \log \frac{1}{X_{tt}} + 0.4427\right)} \\
\text{If } \log\frac{1}{X_{tt}} \geq 1\text{:} \quad & f_{\text{cb,c}} = 10^{\left(0.7143 \cdot \log \frac{1}{X_{tt}} + 0.4117\right)} \\
\text{If } \text{Re}_L f_c^{1.25} \leq 10000\text{:} \quad & f_{\text{nb,s}} = 0.9 \\
\text{If } 10000 < \text{Re}_L f_c^{1.25} < 429500\text{:} \quad & f_{\text{nb,s}} = \beta^1_{f_{\text{nb,s}}} \cdot \ln\left(\text{Re}_L f_c^{1.25}\right) + \beta^2_{f_{\text{nb,s}}} \\
\text{If } \text{Re}_L f_c^{1.25} \geq 429500\text{:} \quad & f_{\text{nb,s}} = 0.05
\end{aligned}
\tag{3.44}
$$

Mass balances for cooling water and steam side remain unchanged. The mass balances in the

condenser shell and reboiler tubes differ.

$$\begin{aligned} \text{Shell, Con: } V_{\text{In}} \cdot y^i_{\text{In}} &= V_{\text{Out}} \cdot y^i_{\text{Out}} + L_{\text{Out}} \cdot x^i_{\text{Out}} \\ \text{Tub, Reb: } L_{\text{In}} \cdot x^i_{\text{In}} &= V_{\text{Out}} \cdot y^i_{\text{Out}} + L_{\text{Out}} \cdot x^i_{\text{Out}} \end{aligned} \tag{3.45}$$

The minimum T_{Cond} is determined by a 10 K approach to $T_{\text{CW,Out}}$ resulting in 313 K if the cooling water is available at 298 K and its increase is set to 5 K. This condenser temperature is sufficient to provide a 95% purity of CO_2 in the vapour stream leaving the condenser towards the system boundary [524].

The required heat to cool down the CO_2-rich vapour and create the condensate inside the shell $Q_{\text{Cond,Shell}}$ is calculated as sum of sensible and latent heat $Q^{\text{Sens}}_{\text{Cond}} + Q^{\text{Lat}}_{\text{Cond}}$. The heat contribution of absorbing small amounts of CO_2 into the condensate is neglected, but should be considered if the regeneration is operated at elevated pressures due to higher amounts of absorbed CO_2. The amount of absorbed CO_2 in the reflux to the stripper column is calculated with Henry's law.

$$\begin{aligned} Q_{\text{Cond,Shell}} &= Q^{\text{Sens}}_{\text{Cond}} + Q^{\text{Lat}}_{\text{Cond}} \\ &= V_{\text{Cond,In}} \cdot c_{p,\text{Cond,In}} \cdot (T_{\text{V,In}} - T_{\text{Cond}}) + L_{\text{Cond}} \sum_i x^i \Delta H^i_{\text{Vap}} \end{aligned} \tag{3.46}$$

The heat capacity of the vapour entering the condenser $c_{p,\text{Cond,In}}$ is assumed to be constant between $T_{\text{V,In}}$ and T_{Cond}.

Regeneration

Reboiler: Process side The reboiler duty in real plants can be measured by the steam supply side which includes all heat losses and inefficiencies. In this work, the reboiler duty Q_{Reb} is determined by an energy balance around the reboiler (Reb), stripper (Str), and condenser (Cond). It can be broken down into three contributions, Q_{Sens}, Q_{Latent}, and Q_{Abs} assuming adiabatic equipment.

1. Sensible heat Q_{Sens}, which is required to heat up the rich solvent to stripping temperature.

2. Latent heat Q_{Latent}, which is required to create the stripping steam and is dispatched as

cooling load in the condenser.

3. Total heat of absorption Q_{Abs} which is required to release the CO_2 [405]. Q_{Abs} includes the dominating contributions of reaction heats (protonation and carbamate formation if applicable) and dissolution [134]. Versteeg *et al.,* [124] estimated the heat of dissolution to be constant -17 $\mathrm{kJ/mol_{CO_2}}$.
$\Delta H_{\mathrm{Abs}} = \Delta H_{\mathrm{Diss}} + \Delta H_{\mathrm{Reac}}$ and $\Delta H_{\mathrm{Reac}} = \Delta H^{o}_{\mathrm{Reac}} + \int_{T^o}^{T} c_{\mathrm{p}} d\bar{T}$. The total heat of absorption refers to the macroscopic measured enthalpy change and thus the sum of all contributions. It is not possible to independently measure heats of reaction and heats of dissolution in a reactive system.

The reboiler duty Q_{Reb} is calculated as sum of the three contributions.

$$Q_{\mathrm{Reb}} = Q_{\mathrm{Abs}} + Q_{\mathrm{Lat}} + Q_{\mathrm{Sens}} \tag{3.47}$$

The contribution due to the desorption reaction is calculated as product of released CO_2 and total heat of desorption.

$$Q_{\mathrm{Abs}} = y^{\mathrm{CO_2}}_{\mathrm{Cond,out}} \cdot V_{\mathrm{Cond,out}} \cdot \Delta H_{\mathrm{Des}} \tag{3.48}$$

It is assumed that $\Delta H_{\mathrm{Des}} = -\Delta H_{\mathrm{Abs}}$. Kim *et al.* [525] quantified for MEA the difference between $\Delta H_{\mathrm{Abs,\ 40^\circ}} - \Delta H_{\mathrm{Abs,\ 120^\circ}} \approx 13 \frac{\mathrm{kJ}}{\mathrm{mol_{CO_2}}}$ (15%). However, they concluded that the temperature dependence could not be validated. In another study, Lu *et al.* [526] found the average difference for 15 amines between absorbing and regeneration conditions (not just limited to temperature) to be $\approx 14.7 \frac{\mathrm{kJ}}{\mathrm{mol_{CO_2}}}$ (21%). Both studies found $\Delta H_{\mathrm{Abs,\ 120^\circ}} < \Delta H_{\mathrm{Abs,\ 40^\circ}}$ ($|\Delta H_{\mathrm{Abs,\ 120^\circ}}| > |\Delta H_{\mathrm{Abs,\ 40^\circ}}|$), thus, the contribution of Q_{Abs} might be underestimated by neglecting a potential dependence on the temperature by 15-21% on average, if confirmed to be true. However, the deviations reported by Kim *et al.* are within the error range reported by Artanto *et al.* [527]. They found the error of measuring Q_{Reb} in their set-up to be $0.3 - 0.4 \frac{\mathrm{MJ}}{\mathrm{kg_{CO_2}}}$ and the error of Q_{Abs} to be $0.3 \frac{\mathrm{MJ}}{\mathrm{kg_{CO_2}}} \approx 13 \frac{\mathrm{kJ}}{\mathrm{mol_{CO_2}}}$. Furthermore, most screened solvents did not report sufficient data to correlate ΔH_{Abs} with the temperature.

The latent contribution Q_{Lat} is calculated by solving an energy balance around the condenser,

which includes cooling the inlet vapour stream from $T_{\mathrm{V,In}}$ down to the condenser temperature T_{Cond}, and condensing the liquid reflux $Q_{\mathrm{Cond}}^{\mathrm{Lat}}$ (see Eqn. 3.46).

$$Q_{\mathrm{Lat}} = Q_{\mathrm{Cond}}^{\mathrm{Sens}} + Q_{\mathrm{Cond}}^{\mathrm{Lat}} = V_{\mathrm{Cond,In}} \cdot c_{p,\mathrm{Cond,In}} \cdot (T_{\mathrm{V,In}} - T_{\mathrm{Cond}}) + L_{\mathrm{Cond}} \sum_i x^i \Delta H_{\mathrm{Vap}}^i \quad (3.49)$$

The sensible contribution Q_{Sens} is calculated by the required heat to warm up the rich solvent to the stripping temperature.

$$Q_{\mathrm{Sens}} = T_{\mathrm{L,Reb,Out}} \cdot c_{p,\mathrm{Reb,Out}} \cdot L_{\mathrm{Reb,Out}} - T_{\mathrm{L,Str,In}} \cdot c_{p,\mathrm{Str,In}} \cdot L_{\mathrm{Str,In}} \quad (3.50)$$

Equation 3.50 assumes that the stripper bottom temperature equals the reboiler temperature $T_{\mathrm{L,Reb,Out}}$, *i.e.,* the sole purpose of reboiler is evaporating water and creating stripping steam. Q_{Sens} is often, *e.g.,* [527], calculated by multiplying the solvent flow rate with its heat capacity and the temperature difference between lean solvent leaving the reboiler and the rich solvent entering the stripper $L_{\mathrm{Solvent}} \cdot c_p \cdot (T_{\mathrm{Reb,Out}} - T_{\mathrm{Str,In}})$. This assumes constant solvent flow rate and heat capacity. Instead, this work takes into account that the solvent flow rate and composition changes between stripper inlet and reboiler outlet by calculating the individual heat capacity c_p and flow rate L (see Eqn. 3.50). For example, the heat capacity at stripper inlet is 3.4% higher than at reboiler outlet for 30 wt% MEA at $\Theta_{\mathrm{Lean}} = 0.18$ $\mathrm{mol_{CO_2}/mol_{MEA}}$ and $\Theta_{\mathrm{Rich}} = 0.44$ $\mathrm{mol_{CO_2}/mol_{MEA}}$. The solvent flow rate at reboiler outlet is 3.5% smaller than at stripper inlet, due to the released CO_2. In that example, the increase in heat capacity and reduction of flow rate trade each other off, and the deviation to the previously mentioned approach for Q_{Sens} is 0.1%. It is not guaranteed that these changes trade each other off, as the change in heat capacity is dependent on temperature and lean loading, and the change in solvent flow rate on the working capacity.

The stripping steam flow rate is calculated by setting the reboiler pressure p_{Reb} and lean loading. The corresponding vapour composition is calculated as equilibrium over the lean solvent leaving the reboiler using the VLE for CO_2 and Raoult's law for other compounds at T_{Reb}. The condenser pressure $p_{\mathrm{Cond}} = p_{\mathrm{Reb}} - \Delta p_{\mathrm{Str}} > 105$ kPa_a is calculated by the reboiler

pressure and pressure drop inside the stripper column Δp_{Str}. If $\Delta p_{\mathrm{Stripper}}$ exceeds the minimum condenser pressure, then the reboiler pressure is increased until the condition is met. Pressure loss between reboiler outlet and stripper inlet is neglected.

Reboiler: Steam side The required steam flow rate F_{Steam} is calculated by solving the steam side of the reboiler. It includes cooling down super heated steam from T_{Steam} to T_{Vap}, condensing it completely, and sub-cooling it to $T_{\mathrm{Reb,C}}$. The heat capacities are calculated at the logarithmic mean temperature difference between the starting and end temperature using Eqn. 3.36.

$$Q_{\mathrm{Reb}} = F_{\mathrm{Steam}} \cdot \left[c_{\mathrm{p,\ Steam}} \cdot (T_{\mathrm{Steam}} - T_{\mathrm{Vap}}) + \Delta H_{\mathrm{Vap}} + c_{\mathrm{p,\ H_2O}} \cdot (T_{\mathrm{Vap}} - T_{\mathrm{Reb,C}}) + \right] \quad (3.51)$$

It is assumed steam at 250 kPa_a and 147°C is available [527], *i.e.*, the steam is super heated by 20K (saturation temperature of 127°C). ΔH_{Vap} and the heat capacities are calculated through correlations. As reference, the specific enthalpy of the super heated steam before sub-cooling is 2758 $\mathrm{kJ/kg_{H_2O}}$, with a contribution of $\Delta H_{\mathrm{Vap}} = 2181\ \mathrm{kJ/kg_{H_2O}}$. The default sub-cooling is $T_{\mathrm{Vap}} - T_{\mathrm{Reb,C}} = 5\mathrm{K}$ [506].

Pumps and Pipeline

Pressure losses due to pipeline friction Δp_f, equipment pressure loss Δp_{Unit}, and equipment height H_Z are compensated by pumps. The lean solvent pump drives the solvent through the main heat exchanger, lean solvent cooler, and to the top of the active absorber packing. The rich solvent pump drives the solvent through the main heat exchanger and to the top of the stripper. The water wash pump drives the water to the top of the water wash section. All pumps are calculated with a mass balance in which the inlet mass flow, composition, and temperature equals the out flowing stream. They are assumed to be centrifugal single stage pumps [528].

$$\begin{aligned} F_{\text{In}} &= F_{\text{Out}} \\ x^i_{\text{In}} &= x^i_{\text{Out}} \\ T_{\text{In}} &= T_{\text{Out}} \\ \Delta p &= p_{\text{L,Out}} - p_{\text{L,In}} \end{aligned} \tag{3.52}$$

The flow rate is converted into gallons per minute F_{gpm} required for the design calculations. The Darcy friction factor γ is calculated with Haaland's approximation of the Colebrook-White equation [426].

$$\frac{1}{\sqrt{\gamma}} = -1.8 \log \left[\left(\frac{\varsigma / D_{\text{in}}}{3.7} \right)^{1.11} + \frac{6.9}{\text{Re}} \right] \tag{3.53}$$

It uses the Reynold's number Re, pipe's inside diameter D_{in}, pipe's effective roughness height $\varsigma = 0.045$ mm, pipe length between units $L_{\text{Pipe}} = 30$ m, solvent's velocity u_L, and solvent mass flow rate F_S.

$$\begin{aligned} \text{Re} &= \frac{\rho_L u_L D_{\text{in}}}{\eta_L} \\ u_L &= \frac{4 F_S}{\pi D^2_{\text{in}} \rho_L} \end{aligned} \tag{3.54}$$

The required power demand P_{Pump} is calculated using the pump efficiency $\omega_{\text{Pump}} = 70\%$, and gravitational constant g.

$$\begin{aligned} P_{\text{Pump}} &= g H_{\text{z}} + \frac{\Delta p + \Delta p_f}{\rho_L} \cdot \frac{F_S}{\omega_{\text{Pump}}} \\ u_l &= \frac{4 \cdot F_S}{\pi D^2_{\text{in}} \cdot \rho_L} \\ \Delta p_f &= 4\gamma \cdot \frac{L_{\text{Pipe}}}{D_{\text{in}}} \rho_L u_L \\ PH &= \frac{\Delta p_f + \Delta p}{\rho \cdot g} + H_z \end{aligned} \tag{3.55}$$

The maximum flow rate per pump is limited to $F_{\text{gpm}} < 3500$ gpm, and the pump head PH is limited to < 200 ft [529]. The number of pumps Nm_{Pump} equals one if $F_{\text{gpm}} < 3500$ gmp. If $F_{\text{gpm}} > 3500$ gpm then the total flow is separated equally into $Nm_{\text{Pump}} = \lceil \frac{F_{\text{gpm}}}{3500} \rceil$ pumps (rounded up to nearest full integer).

Other KPIs

Annual Operating Hours The annual operating hours h_{Ops} are given by assuming that the plant is running for 335 days per year resulting in an availability of 91.8%.

$$h_{\text{Ops}} = 24 \cdot 335 = 8040\text{h/a} \tag{3.56}$$

Captured CO_2 The annual amount of captured CO_2 expressed as molar flow rate $n_{\text{Ann}}^{\text{CO}_2}$ or mass flow rate $m_{\text{Ann}}^{\text{CO}_2}$ is given by the CO_2 content leaving the condenser.

The capture rate CapRat is the ratio of $n_{\text{Ann}}^{\text{CO}_2}$ and the CO_2 contained in the flue gas $n_{\text{FG,Ann}}^{\text{CO}_2}$. The annual captured mass flow rate of CO_2 in million tonnes is annotated with $\text{Mtpa}_{\text{CO}_2}$.

$$\begin{aligned} n_{\text{Ann}}^{\text{CO}_2} &= h_{\text{Ops}} \cdot y_{\text{Cond,out}}^{\text{CO}_2} \cdot V_{\text{Cond,out}} \\ m_{\text{Ann}}^{\text{CO}_2} &= n_{\text{Ann}}^{\text{CO}_2} \cdot MW^{\text{CO}_2} \\ \text{CapRat} &= \frac{n_{\text{Ann}}^{\text{CO}_2}}{V_{\text{FG}}^{\text{CO}_2} \cdot h_{\text{Ops}}} \end{aligned} \tag{3.57}$$

Cooling Water The required mass flow rate of cooling water for the plant $m_{\text{Cooling}}^{\text{H}_2\text{O}}$ and total required cooling duty Q_{Cooling} is calculated by adding up the contributions from the lean solvent cooler, condenser, and water wash cooler. It assumes cooling water to be available at an average annual temperature of 298 K ($\approx$ 25℃) and its temperature to increase by 5 K, *i.e.*, $T_{\text{c,Out}} - T_{\text{c,In}} = 303\text{ K} - 298\text{ K} = 5\text{ K}$.

$$\begin{aligned} m_{\text{Cooling}}^{\text{H}_2\text{O}} &= (L_{\text{Cool,out}} + L_{\text{Cond,out}} + L_{\text{WW Cool,out}}) \cdot MW^{\text{H}_2\text{O}} \\ Q_{\text{Cooling}} &= Q_{\text{Cool}} + Q_{\text{Cond}} + Q_{\text{WWCool}} \end{aligned} \tag{3.58}$$

Power Demand The total power demand $P_{\text{Elec,Tot}}$ is given by adding the requirements of all pumps. The total power demand depends on the solvent flow rate and equipment height of the

absorber.

$$P_{\text{Elec,Tot}} = P_{\text{Pump,LeanSol}} + P_{\text{Pump,RichSol}} + P_{\text{Pump,WW}} + P_{\text{Pump,CW}} \tag{3.59}$$

Solvent Make-up Amine and water lost through the top of the absorber, post-treatment section, and CO_2 product stream (5% water) are added before the rich solvent pump. This assumes that lost and degraded amine is replaced, and the water is returned from the compression train. The degradation rate $DGD_{\text{Sol}} = 1.6\frac{\text{kg}_{\text{Amine}}}{\text{t}_{\text{CO}_2}}$ is assumed to include all amine losses.

Process Modifications

Process modifications and heat integration aim at increasing the efficiency of the capture plant by reducing the reboiler duty and solvent flow rate [530]. Examples for modifications are alternative contactors *e.g.*, membranes, intercooled or interheated absorber, split flow arrangements, interheated stripper, solvent recycle, split, or flash, alternative heat exchanger arrangements, overhead condenser bypass or compression, lean or rich vapour compression, multi-pressure stripper, multi-stage flash stripper, and many more [530–535].

Absorber inter-cooling refers to the method of withdrawing a slip-stream of the solvent from the temperature bulge within the absorber column, cooling it down via a solvent cooler, and re-injecting the solvent into the column [530]. The position of the solvent withdrawal should match with the maximum temperature inside the column, or else the inter-cooling is less effective [536]. Reducing the solvent's temperature towards the rich pinch should increase the rich loading and reduce the solvent flow rate at constant capture rate. The reduced solvent flow rate leads to a smaller sensible heat contribution inside the regeneration and a reduced overall specific reboiler duty. The temperature profile within the absorber would be flatter and not showing a distinct maximum any more [536]. The kinetics and diffusivities slow with decreasing temperature while the mass transfer driving force increases. These trends trade-off and could ultimately decrease or increase the required mass transfer area requiring solvent-specific optimisation [530]. Inter-cooled absorbers appear effective for amines with large heat of absorption.

Studies confirm that inter-cooled absorbers do not improve all solvents equally [530], *e.g.*, Knudsen *et al.,* [537] found no clear effect for MEA, and a 7% reduction in reboiler duty for CESAR1. Rezazadeh *et al.,* found that absorber inter-cooling for MEA is most effective at lean loadings >0.3 $\mathrm{mol_{CO_2}mol_{MEA}^{-1}}$, and that for lower lean loadings the inter-cooler would not be helpful.

Synergies between process modification and solvent are complicated due to the large number of possible combinations [530]. If this work included process modifications, then some solvents would benefit more than others. Trends in capture cost would not be purely driven by differences in thermo-physical properties any more, and disentangling the individual factors becomes highly complicated. Additionally, the computational effort would increase as many possible combinations per solvent would need to be calculated. Therefore, this work selected the archetypal process topology to focus on just the differences in the thermpo-physical property space.

Solution Strategy

The model is sequentially initialised and then converged to their full calculated values by using a time dependant variable ζ. The generic equation uses x_{Init} as the initialised value and x_{Calc} as the variable implemented in the model. The initialisation is set with $\zeta = 1$, and the model is converged by $\zeta \to 0$.

$$x = x_{\mathrm{Init}} \cdot \zeta + x_{\mathrm{Calc}} \cdot (1 - \zeta) \tag{3.60}$$

The columns were initialised with a fixed solvent outlet temperature $T_{\mathrm{Abs,L,Out}} = T_{\mathrm{L,Out}} + 20$ K and $T_{\mathrm{Str,L,Out}} = T_{\mathrm{V,In}} - 10$ K, simple mass balance for the liquid phase $L_{\mathrm{In}} \cdot x^i_{\mathrm{In}} = L_{\mathrm{Out}} \cdot x^i_{\mathrm{Out}}$, assigned values the mass transfer and pressure drop $\Delta p_{\mathrm{Irr}} = 2$ kPa. The assigned variables for the mass transfer were k_{V}, k_{L}, $\mathrm{Re_V}$, $\mathrm{Re_L}$, $\mathrm{Sc_V}$, $\mathrm{Sc_L}$, $\mathrm{Re_L^{IF}}$, $\mathrm{Fr_L}$, $\mathrm{We_L}$, $\mathrm{Sh_L}$, a_{wet}, and E. After a successful first initialisation, the equilibrium equations Eqn. 3.9, and mass balances Eqn. 3.6 are activated replacing the simple mass balance. Then, the solvent outlet temperature is calculated with Eqn. 3.11, and the mass transfer correlations are activated. Lastly, the pressure drop calculation replaces the assigned assumption.

The heat transfer inside the heat exchangers is initialised with assigned velocities, and heat transfer coefficients h_c and h_h. The reboiler is initialised by additionally assigning the Nusselt number inside the tubes $Nu_{Tub} = 150$ and calculating the stripping steam flow rate (boil up) F_{BoilUp} using the reboiler duty Q_{Reb} and heat of vaporisation at reboiler pressure $\Delta H_{Vap,reb}$, assuming that only water evaporates $F_{BoilUp} = \frac{Q_{Reb}}{\Delta H_{Vap,reb}}$. The condenser is additionally initialised with a simple material balance assuming the composition of the CO_2 product stream to be 5% H_2O and 95% CO_2 before activating the mass balance. The main heat exchanger is additionally initialised by setting the temperature difference at the hot end, before converging to the calculated temperature of the lean solvent coming from the reboiler and the optimised logarithmic mean temperature approach. Pumps are initialised assuming $\varsigma = 0.033$.

The individual units are connected by setting the outlet of one unit as inlet of another, *e.g.,* the rich solvent leaving the absorber equals the inlet of the rich solvent pump. The solvent loop is initialised with a lean loading of $\Theta^{Opt}_{Lean} = 0.3\ mol_{CO_2}/mol_{Amine}$. It is interrupted to allow for higher numeric stability. The loop breaker sits between the lean solvent cooler and the absorber inlet and is converged by solving $\Theta_{Lean} = 0.3\ mol_{CO_2}/mol_{Amine} \cdot \zeta + \Theta_{Lean,Input} \cdot (1 - \zeta)$. The maximum lean loading $\Theta_{Lean,Max}$ is an useful indication for setting an initial lean loading value and increases the numeric stability when running a sensitivity analysis. The convergence threshold of ζ was set to 10^{-5}.

Common problems were negative temperature differences and discontinuities when a new unit was added. Negative temperature differences in the main heat exchanger were solved by initialising the hot end temperature difference instead of the logarithmic mean temperature difference. Discontinuities in the absorber sizing leading to unrealistic high pressure drops were observed. Significant differences in the VLE caused this, and it was solved by initialising with a stable VLE followed by converging to the true VLE. A database of saved variable sets (successful process runs) proved practical. Typical computation times are seconds for each solvent. Multiple solvents can be screened in parallel, however, results of only one solvent can be exported to Excel at a time due to constraints within Excel.

3.3.3 Cost Models

Total Annualised Capture Cost

The costs are calculated using a factorial / bottom up methodology and split into capital expenditure ($CAPEX$) and operating expenditure ($OPEX$). The $CAPEX$ is calculated based on equipment size, number of units, solvent stock, and construction material (stainless steel, see Tab. 3.4). The $CAPEX$ is discounted using a capital recovery factor CRF, which depends on the interest rate IR (weighted average cost of capital WACC) and the annuity period n_{Ann}.

$$TAC = \frac{CRF \cdot CAPEX + OPEX}{m_{\mathrm{Ann}}^{\mathrm{CO_2}}} \tag{3.61}$$

The CRF is given by

$$CRF = \frac{IR(1+IR)^{n_{\mathrm{Ann}}}}{(1+IR)^{n_{\mathrm{Ann}}}-1} \tag{3.62}$$

An interest rate of 10% and an annuity period of 25 years have been assumed [538], resulting in $CRF \approx$ 11%. The impact of the CRF on the modelling is discussed in [112]. The sum of discounted $CAPEX$ and $OPEX$ describes the cost of capturing one tonne of CO_2 from flue gas with a specific CO_2 composition y_{CO_2}, and is known as total annualised costs TAC. The term "capture cost" always refers to the TAC. Key economic assumptions are listed in Tab. 3.10 and discussed in the following paragraphs.

CAPEX

The total $CAPEX$ is calculated by adding the solvent stock $CAPEX_{\mathrm{Solvent}}$ and the installed costs of all units $CAPEX_{\mathrm{Unit}}$ multiplied by a Lang factor $F_{\mathrm{Lang}} = 2.75 \cdot 1.45 = 3.9875$ [544]. The approach has been taken from [421, 542]. The following paragraphs explain the $CAPEX$ cost correlations for each unit and the one-time fill with solvent.

$$CAPEX = F_{\mathrm{Lang}} \cdot \sum CAPEX_{\mathrm{Unit}} + CAPEX_{\mathrm{Solvent}} \tag{3.63}$$

Table 3.10: Summary of key economic parameters assumed in this work taken from [538].

Parameter	**Value**
Interest rate	10%
Annuity period	25 years
Plant availability	335 days per year (91.8%)
Lang-factor	3.9875
Cost power	$\$44.7/\mathrm{MWh_{Elec}}$
Solvent degradation	$1.6\ \mathrm{kg_{Amine}}\ /\mathrm{t_{CO_2cap}}$
Cost amine	$\$1.1/\mathrm{kg_{Amine}}$ [539]
Cost de-mineralised water	$\$3.9/\mathrm{t_{H_2O}}$ [540]
Cost cooling water	$\$0.07/\mathrm{t_{H_2O}}$ [541]
Cost steam	$\$20.4/\mathrm{t_{Steam}}$ [540]
Cost plant operator	\$100 000/Operator [540]
Cost plastic Pall rings	$\$36.0/\mathrm{ft}^3$ [542]
Cost Mellapak 2X	$\$1758/\mathrm{ft}^3$ [542]
Operations & Maintenance	5% of $CAPEX$ [542]
CEPCI Oct 2020	595.9 [543]

Columns The $CAPEX$ of absorber, stripper, and water wash column $CAPEX_{\mathrm{Col}}$ has been calculated with the same approach [542]. It uses the number of columns Nm_{Col} if multiple columns are required, $CEPCI$ (with costing correlations base year 2003 adjusted to October 2020 pricing), cost contributions from the packing and internals $C_{\mathrm{Col,Pack}}$, tower shell $C_{\mathrm{Col,Shell}}$, and tower externals $C_{\mathrm{Col,Ext}}$ (*e.g.*, platform, ladders). The post-treatment section of the absorber was calculated separately.

$$\begin{aligned} CAPEX_{\mathrm{Col}} &= IN_F \cdot \frac{\mathrm{CEPCI}_{2020}}{\mathrm{CEPCI}_{2003}} \cdot Nm_{\mathrm{Col}} \cdot 1.218 \left(C_{\mathrm{Col,Shell}} + C_{\mathrm{Col,Pack}} + C_{\mathrm{Col,Ext}}\right) \\ C_{\mathrm{Col,Shell}} &= \beta_{\mathrm{m}} \cdot 1.218 \cdot \exp\left[6.629 + 0.1826 \cdot \ln W_{\mathrm{Col,lbs}} + 0.02297 \cdot \ln {W_{\mathrm{Col,lbs}}}^2\right] \\ C_{\mathrm{Col,Pack}} &= Vol_{\mathrm{Pack}} \cdot C_{\mathrm{Pack}} \\ C_{\mathrm{Col,Ext}} &= 300 \cdot D_{\mathrm{In,Col,ft}}^{0.7396} \cdot ZT_{\mathrm{Col,ft}}^{0.7068} \end{aligned} \tag{3.64}$$

Above equations use $IN_F = 1.9$ as the installation factor, $D_{\text{In,Col,ft}}$ as the inside diameter of the column in feet, $ZT_{\text{Col,ft}}$ as the height of the required packing in feet, $W_{\text{Col,lbs}}$ as the weight of the shell in pounds, $\beta_{\text{m}} = 1.7$ as the material factor (304 stainless steel, see Tab. 3.4), and the specific packing cost $C_{\text{Pack}} = \$36.0/\text{ft}^3$ (random Pall packing), or $C_{\text{Pack}} = \$1758/\text{ft}^3$ (Structured Mellapak 2X) [542]. The material factor β_{m} varies between 1.7 for carbon steel and 7.7 for titanium. 304 and 316 stainless steel are used for all equipment, *i.e.*, β_{m} is either 1.7 or 1.9.

Reboiler The CAPEX for the reboiler $CAPEX_{\text{Reb}}$ is calculated using the number of exchangers Nm_{Reb}, installation factor $IN_F = 1.9$, CEPCI (with costing correlations base year 2003 adjusted to October 2020 pricing), material factor $\beta_{\text{m}} = 1.9$ (316 stainless steel, see Tab. 3.4), and the heat transfer area per exchanger $A_{\text{Reb,sft}}$ in square feet [542].

$$
\begin{aligned}
CAPEX_{\text{Reb}} &= IN_F \cdot \frac{\text{CEPCI}_{2020}}{\text{CEPCI}_{2003}} \cdot Nm_{\text{Reb}} \cdot CAPEX_{\text{Reb,indiv}} \\
CAPEX_{\text{Reb,indiv}} &= 1.218 \cdot \beta_{\text{m}} \cdot \beta_{\text{B,Reb}} \cdot \beta_{\text{p,Reb}} \cdot \beta_{\text{d,Reb}} \\
\beta_{\text{B,Reb}} &= \exp\left(8.821 - 0.30863 \cdot \ln A_{\text{Reb,sqf}} + 0.0681 \cdot \ln {A_{\text{Reb,sqf}}}^2\right) \\
\beta_{\text{p,Reb}} &= 0.7771 + 0.04981 \cdot \ln A_{\text{Reb,sqf}} \\
\beta_{\text{d,Reb}} &= \exp\left(-0.9816 + 0.0830 \cdot \ln A_{\text{Reb,sqf}}\right)
\end{aligned}
\tag{3.65}
$$

Heat Exchangers The $CAPEX$ of the lean solvent cooler, main heat exchanger, condenser, and water wash cooler $CAPEX_{\text{Hex}}$ follows the approach in [542]. It uses the number of heat exchangers Nm_{Hex} if multiple units are required, installation factor $IN_F = 1.9$, $CEPCI$ (with costing correlations base year 2003 adjusted to October 2020 pricing), material factor $\beta_{\text{m}} = 1.9$ (316 stainless steel, see Tab. 3.4), and the heat transfer area per exchanger $A_{\text{Hex,sft}}$

in square feet. The equations match the vertical shell and tube exchanger (see Eqn. 3.65).

$$\begin{aligned} CAPEX_{\text{Hex}} &= IN_F \cdot \frac{\text{CEPCI}_{2020}}{\text{CEPCI}_{2003}} \cdot Nm_{\text{Hex}} \cdot CAPEX_{\text{Hex,indiv}} \\ CAPEX_{\text{Hex,indiv}} &= 1.218 \cdot \beta_{\text{m}} \cdot \beta_{\text{B,Hex}} \cdot \beta_{\text{p,Hex}} \cdot \beta_{\text{d,Hex}} \\ \beta_{\text{B,Hex}} &= \exp\left(8.821 - 0.30863 \cdot \ln A_{\text{Hex,sqf}} + 0.0681 \cdot \ln {A_{\text{Hex,sqf}}}^2\right) \\ \beta_{\text{p,Hex}} &= 0.7771 + 0.04981 \cdot \ln A_{\text{Hex,sqf}} \\ \beta_{\text{d,Hex}} &= \exp\left(-0.9816 + 0.0830 \cdot \ln A_{\text{Hex,sqf}}\right) \end{aligned} \tag{3.66}$$

Pumps The CAPEX for the lean solvent pump, rich solvent pump, water wash pump, and cooling water pump $CAPEX_{\text{Pump}}$ is calculated using the number of pumps Nm_{Pump}, the pump head in feet PH_{ft}, installation factor $IN_F = 2$, CEPCI (with costing correlations base year 2003 adjusted to October 2020 pricing), and shell material factor $\beta_{\text{m}} = 1.7$ (304 stainless steel, see Tab. 3.4) [542].

$$\begin{aligned} CAPEX_{\text{Pump}} &= IN_F \cdot \frac{\text{CEPCI}_{2020}}{\text{CEPCI}_{2003}} \cdot Nm_{\text{Pump}} \cdot CAPEX_{\text{Pump,indiv}} \\ CAPEX_{\text{Pump,indiv}} &= \beta_{\text{B}} \cdot \beta_{\text{m}} \cdot \beta_{\text{t}} \\ \beta_{\text{Pump}} &= \ln\left(F_{\text{gpm}} \cdot \sqrt{PH_{\text{ft}}}\right) \\ \beta_{\text{B,Pump}} &= 1.39 \cdot \exp\left(8.833 - 0.6019 \cdot \beta_{\text{Pump}} + 0.0519 \cdot \beta_{\text{Pump}}^2\right) \\ \beta_{\text{t,Pump}} &= \exp\left(5.1029 - 1.2217 \cdot \beta_{\text{Pump}} + 0.0771 \cdot \beta_{\text{Pump}}^2\right) \end{aligned} \tag{3.67}$$

Post-Treatment The $CAPEX$ of the post-treatment section $CAPEX_{\text{Post}}$ is calculated with the approach in [542, 545]. It sums the costs of the demister $CAPEX_{\text{WW,DM}}$ (calculated with approach from [545]), water wash cooler $CAPEX_{\text{WW,Cool}}$, water wash column $CAPEX_{\text{WW,Col}}$, and water wash pump $CAPEX_{\text{WW,Pump}}$. $CAPEX_{\text{WW,Col}}$ is estimated with Eqn. 3.64, $CAPEX_{\text{WW,Cool}}$ with Eqn. 3.66, and $CAPEX_{\text{WW,Pump}}$ with Eqn. 3.67. $CAPEX_{\text{WW,DM}}$ requires the installation factor $IN_F = 1.9$, inside diameter in feet $D_{\text{in,ft}}$, and height of the

demister ZT_{DM}.

$$\begin{aligned} CAPEX_{\mathrm{Post}} &= CAPEX_{\mathrm{WW,DM}} + CAPEX_{\mathrm{WW,Cool}} + CAPEX_{\mathrm{WW,Col}} + CAPEX_{\mathrm{WW,Pump}} \\ CAPEX_{\mathrm{WW,DM}} &= IN_F \cdot \frac{\mathrm{CEPCI}_{2020}}{\mathrm{CEPCI}_{2003}} \cdot 78.4 \cdot D_{\mathrm{in,ft}}^{1.66} \cdot \frac{ZT_{\mathrm{DM}}}{0.15} \end{aligned} \tag{3.68}$$

Solvent Fill-up The one-time solvent fill-up cost $CAPEX_{\mathrm{Solvent}}$ is calculated assuming that there is 1.45 more solvent in the total plant than in the equipment Vol_{Solvent} due to interconnecting pipes, storage tanks, and dead volumes [542]. The volumes consider only the liquid contributions of solvent, *i.e.*, cooling water or steam volumes are not considered. Solvent consists of de-mineralised water and amine with costs of $C_{\mathrm{Amine}} = \$1.1/\mathrm{kg}_{\mathrm{Amine}}$, and $C_{\mathrm{Demin,H_2O}} = \$3.91/t_{\mathrm{H_2O}}$.

$$\begin{aligned} CAPEX_{\mathrm{Solvent}} &= 1.45 \cdot \left(Vol_{\mathrm{Sol}} \rho_{\mathrm{Sol}} w_{\mathrm{Amine}} C_{\mathrm{Amine}} + Vol_{\mathrm{Sol}} \rho_{\mathrm{Sol}} w_{\mathrm{H_2O}} C_{\mathrm{Demin,H_2O}}\right) \\ Vol_{\mathrm{Sol}} &= Vol_{\mathrm{Sol}}^{\mathrm{Abs}} + Vol_{\mathrm{Sol}}^{\mathrm{Str}} + Vol_{\mathrm{Sol}}^{\mathrm{Reb}} + Vol_{\mathrm{Sol}}^{\mathrm{MHEX}} + Vol_{\mathrm{Sol}}^{\mathrm{Cool}} \end{aligned} \tag{3.69}$$

OPEX

The annual $OPEX$ is the sum of fixed $OPEX_{\mathrm{Fix}}$ and variable $OPEX_{\mathrm{Var}}$ expenditures.

$$OPEX = OPEX_{\mathrm{Fix}} + OPEX_{\mathrm{Var}} \tag{3.70}$$

Fixed OPEX $OPEX_{\mathrm{Fix}}$ includes operations and annual maintenance $OPEX_{\mathrm{O\&M}}$ as well as labour costs $OPEX_{\mathrm{Lab}}$.

$$OPEX_{\mathrm{Fix}} = OPEX_{\mathrm{Lab}} + OPEX_{\mathrm{O\&M}} \tag{3.71}$$

$OPEX_{\mathrm{Lab}}$ follows the approach in [546, 547] calculating the number of required operators Nm_{Ope} with Alkhayat and Gerrard's approach [548]. For this, the number of particulate processes $Nm_{\mathrm{ParPro}} = 0$ and non-particulate processes $Nm_{\mathrm{NonParPro}} = 7$ is used. Degradation

products such as heat stable salts are contained within a suspension, and the removal of those products involves pumping it into a truck. The non-particulate processes are the absorber, stripper, main heat exchanger, reboiler, condenser, lean solvent cooler, and pumps (collected), thus, $Nm_{\mathrm{NonParPro}} = 7$. Nm'_{Ope} is rounded up to the nearest half time equivalent Nm_{Ope}, *e.g.*, $Nm'_{\mathrm{Ope}} = 11.2 \rightarrow Nm_{\mathrm{Ope}} = 11.5$.

$$\begin{aligned} OPEX_{\mathrm{Lab}} &= C_{\mathrm{Ope}} \cdot Nm_{\mathrm{Ope}} \\ Nm'_{\mathrm{Ope}} &= 4 \cdot \sqrt{(6.29 + 31.7 \cdot Nm^2_{\mathrm{ParPro}} + 0.23 \cdot Nm_{\mathrm{NonParPro}})} \end{aligned} \tag{3.72}$$

$OPEX_{\mathrm{O\&M}}$ is calculated as a fixed fraction of total $CAPEX$ [542]. In reality $OPEX_{\mathrm{O\&M}}$ does not scale linearly with the $CAPEX$ but rather plant size, and complexity [542].

$$OPEX_{\mathrm{O\&M}} = 5\% \cdot CAPEX \tag{3.73}$$

Variable OPEX $OPEX_{\mathrm{Var}}$ includes steam $OPEX_{\mathrm{Steam}}$, electricity $OPEX_{\mathrm{Power}}$, cooling water $OPEX_{\mathrm{CW}}$, solvent make-up $OPEX_{\mathrm{Sol}}$ (accounting for all losses including degradation and losses through the stack), and EU ETS emission cost $OPEX_{\mathrm{ETS}}$, if activated. The default excludes any ETS costs due to residual emissions in the cleaned flue gas leaving the post-treatment section.

$$OPEX_{\mathrm{Var}} = OPEX_{\mathrm{Steam}} + OPEX_{\mathrm{Power}} + OPEX_{\mathrm{CW}} + OPEX_{\mathrm{Sol}} + (+OPEX_{\mathrm{ETS}}) \tag{3.74}$$

$OPEX_{\mathrm{Steam}}$ is calculated as the product of required steam flow rate F_{Steam}, annual operating hours h_{Ops}, and price of steam $C_{\mathrm{Steam}} = \$20.4/t_{\mathrm{Steam}}$. The impact of changing steam prices will be analysed.

$$OPEX_{\mathrm{Steam}} = F_{\mathrm{Steam}} \cdot h_{\mathrm{Ops}} \cdot C_{\mathrm{Steam}} \tag{3.75}$$

The steam costs are calculated by multiplying the mass flow rate of steam F_{Steam} with the specific price of steam C_{Steam}.

$$\mathrm{OPEX}_{\mathrm{Steam}} = F^{\mathrm{Steam}} \cdot C_{\mathrm{Steam}} \cdot OH \tag{3.76}$$

$OPEX_{\text{Power}}$ is calculated as the product of total electrical power demand P_{Elec} with the annual operating hours, and the price of power $C_{\text{Power}} = \$44.7/\text{MWh}_{\text{Elec}}$

$$OPEX_{\text{Power}} = P_{\text{Elec}} \cdot h_{\text{Ops}} \cdot C_{\text{Power}} \tag{3.77}$$

The power price of $\$44.7/\text{MWh}_{\text{Elec}}$ was calculated using a short run marginal cost model [549], and appears relatively low compared to market values in central Europe in 2022-2024 ($\approx \$80/\text{MWh}_{\text{Elec}}$). The impact of changing C_{Power} will be small, because $OPEX_{\text{Power}}$ contributed on average less than 3% to the $OPEX$.

The operational expense for cooling water $OPEX_{\text{CW}}$ is calculated as product between the total required cooling water flow rate F_{CW}, with the annual operating hours h_{Ops}, and the price of cooling water $C_{\text{CW}} = \$0.07/\text{t}_{\text{H}_2\text{O}}$.

$$OPEX_{\text{CW}} = P_{\text{Elec}} \cdot h_{\text{Ops}} \cdot C_{\text{CW}} \tag{3.78}$$

The solvent replacement cost is calculated using the degradation rate $DGD_{\text{Sol}} = 1.6\frac{\text{kg}_{\text{Amine}}}{\text{t}_{\text{CO}_2}}$, cost of amine $C_{\text{Amine}} = \$1.1/\text{kg}_{\text{Amine}}$, and annually captured CO_2 mass $m_{\text{Ann}}^{\text{CO}_2}$. As reference, a ten-times higher $DGD_{\text{Sol}} = 16\frac{\text{kg}_{\text{Amine}}}{\text{t}_{\text{CO}_2}}$ solvent replacement rate increases the total capture cost by 9.5% for baseline 30 wt% MEA.

$$OPEX_{\text{Sol}} = DGD_{\text{Sol}} \cdot m_{\text{Ann}}^{\text{CO}_2} \cdot C_{\text{Amine}} \tag{3.79}$$

The EU ETS costs are calculated by multiplying the EU ETS price C_{ETS} with the residual CO_2 emissions leaving at the top of the post-treatment section. The screening was run at $C_{\text{ETS}} = €0/t_{\text{CO}_2}$.

$$OPEX_{\text{ETS}} = y_{\text{Post,Out}}^{\text{CO}_2} \cdot V_{\text{Post,Out}} \cdot C_{\text{ETS}} \tag{3.80}$$

Exclusions and Impact of Cost of Consumables

Costs associated with start-up, turnarounds, dynamic operations, owner's cost (land, permitting, royalties, transaction, surveys, and studies), retro-fit, and integration, as well as spare parts are not included. Risk premiums are not included, and contingencies are already accounted for in the design and cost correlations [542, 542, 550, 551].

The capture costs presented in this work are indicative of the economic assumptions, time (October 2020), location (USA), and methods (short-cut modelling), and have to be compared within this work [335, 552–555]. A goal of the model is to screen all solvents without introducing an unquantified bias towards candidates. It is important to compare the relative ranking rather than the absolute capture cost.

Costs for consumables are volatile. Figure 3.14 shows a classical one-at-a-time sensitivity analysis of changing the prices of amine C_{Amine}, packing C_{Pack} (basis is random packing), steam C_{Steam}, shell material factor β_{m}, and water (C_{CW} and $C_{\text{Demin,H}_2\text{O}}$) on the capture cost. The baseline corresponds to 30 wt% MEA, and the prices listed in Tab. 3.10. The variation in steam cost have the highest impact followed by the packing cost, shell material, water, and finally amine cost. The trends are all linear as can be seen *e.g.,* from Eqn 3.75. This qualitative trend is in agreement with [333]. Halving steam cost (\$20.4/t_{Steam} to \$10.2/t_{Steam}) reduces the capture cost by 21% relative to the baseline of MEA.

Steam cost depend on the way it is produced, and there is a factor of ten between the cheapest and most expensive source [556, 557]. Roussanaly *et al.,* [556, 557] report total annualised costs of steam production and found \$6.7/t_{Steam} for excess heat from industrial core processes, \$12.7/t_{Steam} for low pressure steam out of a turbine, \$21.0/t_{Steam} for a coal combined heat and power plant, \$24.8/t_{Steam} for a natural gas boiler, and \$62/t_{Steam} for electric boilers (values adjusted for year and currency to this work). Their underlying prices for feedstock were €6/GJ_{NG}, €3/t_{Coal}, and €58/MWh. The annuity was 25 years at a capital discount rate of 8%. They found that doubling the natural gas price €3/GJ_{NG} to €6/GJ_{NG} increased the steam cost by a factor of 2.6 for a natural gas combined heat and power plant. Recently, the cost of

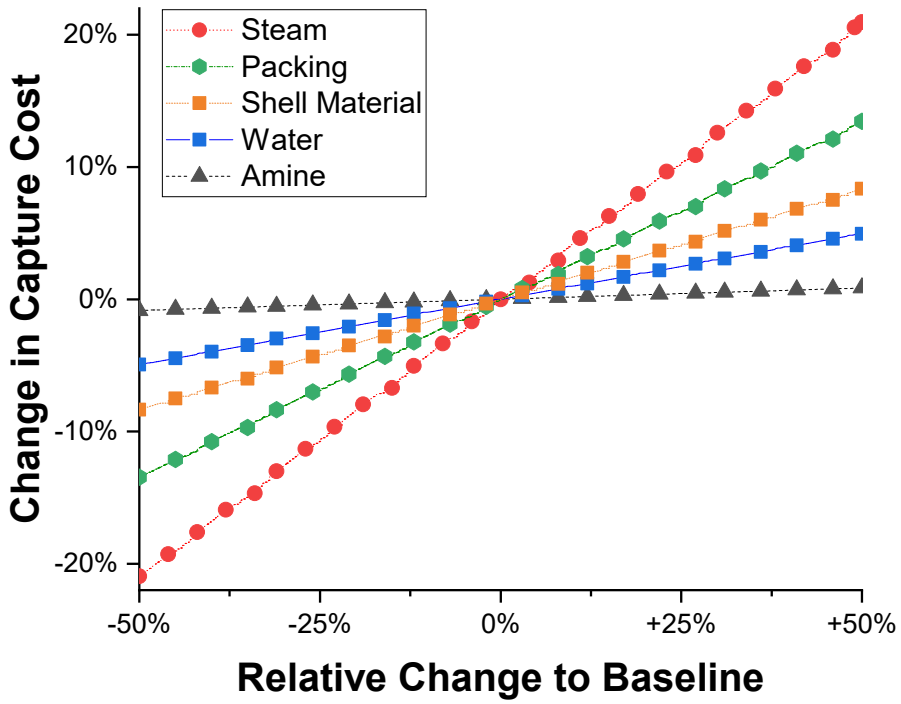


Figure 3.14: One-at-a-time sensitivity analysis: Impact of varying the assumed prices/costs of amine, packing, steam, shell material (steel), and water on the capture cost. Baseline: 30 wt% MEA, flue gas CO_2 concentration $y_{CO_2} = 4$ mol% (gas-power), 90% capture rate.

producing steam with natural gas has increased in central Europe due to a considerable price increase in natural gas. Given the apparent impact of steam cost on the capture cost, C_{Steam} will be included as a sensitivity for the solvent ranking.

The cost and production volumes of amines vary greatly with some speciality chemicals currently being produced at grams rather than tonnes, and costing in excess of $\$100/\text{kg}_{\text{Amine}}$. As reference, approximately 700 tons of MEA are required for a capture plant fitted to a 285 MW NGCC plant (500 kg/s flue gas) [558]. This work assumes constant amine prices of $\$1.1/\text{kg}_{\text{Amine}}$ (levels of MEA, DEA, TEA). Any amine that proves to be highly competitive would need to be produced on commodity levels. Other literature amine costs are $\$7.7/\text{kg}_{\text{PZ}}$, $\$10.2/\text{kg}_{\text{AMP}}$, $\$2.7/\text{kg}_{\text{MEA}}$ [559, 560]. MHI lists the cost of KS1 as $\$6.5/\text{kg}_{\text{KS1}}$ [333]. The cost of amines produced in large scale is relatively low, and the ± 50% variation in Fig. 3.14 does not cover costs of speciality amines.

3.4 Optimising Operating Conditions

The impact of operating conditions on the process has been discussed in other studies in depth [112, 282–285, 467, 468, 561, 562]. Based on these studies, this section focusses on the key parameter that must be optimised to achieve a relevant ranking. Optimising operating conditions will reduce the reboiler duty and capture cost as shown in [467, 468, 561, 563]. Optimising the operating parameter for minimum capture cost instead of only minimising reboiler duty allows to include the CAPEX-OPEX trade-offs into the optimisation. This is in particular important for changes in steam cost and flue gas CO_2 concentration. All solvents were individually optimised leading to minimum capture cost at constant capture rate. No generic correlation between operating conditions, minimum reboiler duty, and minimum capture costs was found, meaning each solvent differs in the operating conditions.

Lean Loading Figure 3.15 shows the impact of optimising the lean loading on the specific heat duty requirement and capture cost at constant flue gas composition ($y_{CO_2} = 4\text{mol}\%$) and 90% capture rate for 30 wt% *aq.* MEA. The left plot shows the specific reboiler duty (dashed line, left scale), rich loading (red symbols, right scale), and lean loading (grey symbols, right scale) over the liquid to gas ratio. The right plot shows the specific reboiler duty (red dashed, right scale) and the capture cost TAC (black, left scale) over the lean loading. The minimum specific reboiler duty is near 0.135 $\text{mol}_{CO_2}\text{mol}_{MEA}^{-1}$. The capture cost shows discontinuities due to the addition or removal of equipment. The minimum capture cost is near the minimum reboiler duty, but not identical and shifts to higher loadings with increasing CO_2 concentration in the flue gas (see Fig. 3.16). The trends agree well with the ones reported in [14] deploying a similar approach.

Amine Concentration Finding the optimal amine concentration is important for a relevant comparison. Freeman *et al.,* [564] showed that increasing the amine's concentration can lead to thermodynamic efficiency gains. However, van Krevelen *et al.,* [475] showed that the absorption rate only increases with the square root of amine concentration which makes increasing the

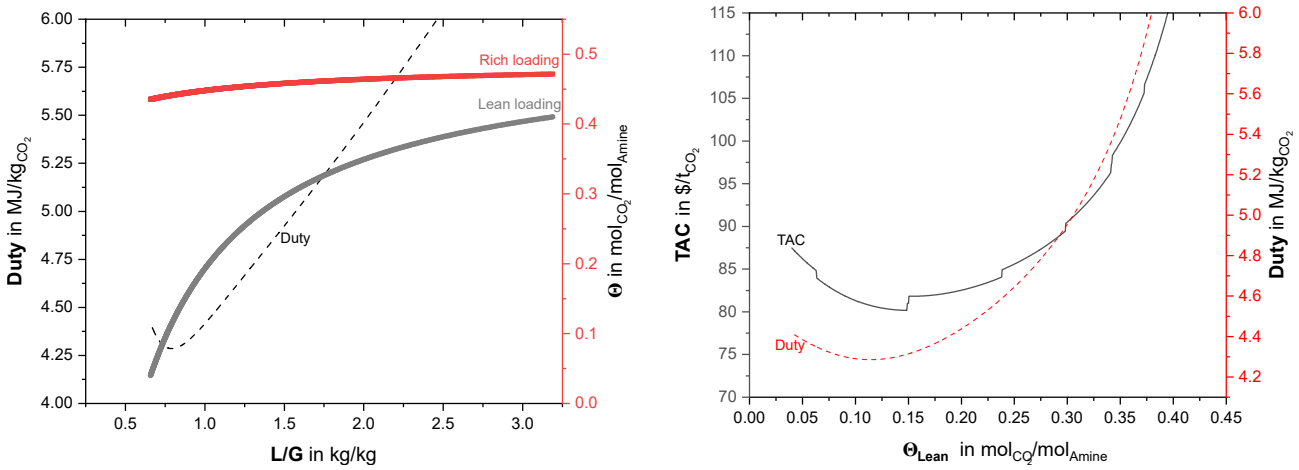


Figure 3.15: Impact of lean loading on L/G ratio, specific reboiler duty, and capture cost at constant flue gas flow rate, y_{CO_2}= 4 mol%, and 90% capture rate for MEA. Optimal lean loading leads to minimum capture cost which is close to the minimum reboiler duty.

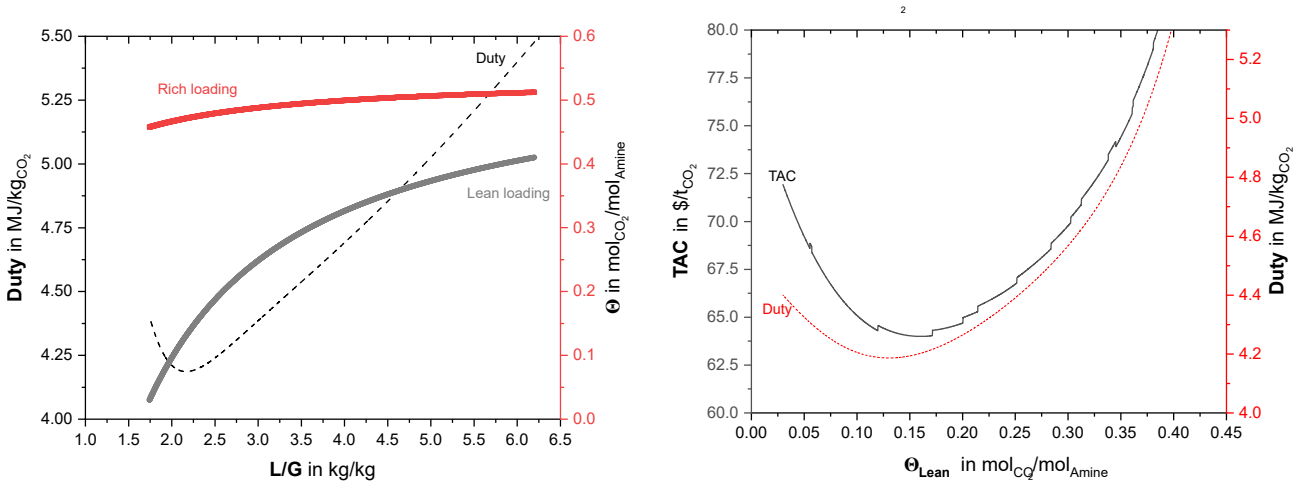


Figure 3.16: Impact of lean loading on L/G ratio, reboiler duty, and capture cost at constant flue gas flow rate, y_{CO_2}= 12 mol%, and 90% capture rate. Optimal lean loading leads to minimum capture cost which is close to the minimum reboiler duty.

amine concentration less effective. This can be directly seen in the equation for the molar flux J^{CO_2} assuming a fast pseudo-first order reaction [476].

$$J^{CO_2} = c_{IF}^{CO_2} \cdot \sqrt{c_{Bulk}^{Amine} \cdot k_2 \cdot D_L^{CO_2}} \tag{3.81}$$

Assuming 30 wt% for each solvent could favour lighter amines over heavier molecules, because a solvent with a lighter amine would contain more amine molecules. While increasing the amine concentration is limited by a potential limit on maximum solubility, it would require less total solvent to capture the same amount of CO_2 based on a simple mass balance. This comes

with the downside of less favourable properties, *e.g.,* increased viscosity which in turn reduces heat and mass transfer rates [565], and increased corrosion [566–568]. Corrosion rates tend to increase with increasing amine concentration, however, for AMP the opposite was found [512]. Therefore, there will be a trade-off between capital and operating expenses, which should show a minimum in capture cost.

Figure 3.17 highlights this trade-off for the case of MEA and a gas-power flue gas for which the optimal concentration leading to minimum cost is near 50 wt%. Such high concentration is widely assumed to be unrealistic due to foaming, corrosion, and degradation concerns [7]. However, Hartono *et al.,* [228] found the optimal concentration of 2PPE to be 50 wt% (12.2 mol%) and for 1-(2HE)PRLD to be 40 wt% (9.4 mol%) when they accounted for foaming, degradation, and viscosity. They found $w^{\text{Opt}}_{\text{2PPE}} = 43$ wt% and $w^{\text{Opt}}_{\text{1-(2HE)PRLD}} = 55$ wt% without accounting for foaming. A review [238] sets a concentration threshold at which amines are considered to be "concentrated" at 4-5 kmol/m^3 which is equal to 30 wt% MEA. Absorption capacity is conventionally reported in $\text{mol}_{\text{CO}_2}/\text{l}_{\text{Solvent}}$, $\text{mol}_{\text{CO}_2}/\text{mol}_{\text{Solvent}}$, or $\text{mol}_{\text{CO}_2}/\text{kg}_{\text{Solvent}}$ (solvent = whole liquid phase) which takes into account the loading $\text{mol}_{\text{CO}_2}/\text{mol}_{\text{Amine}}$ and the amine's concentration.

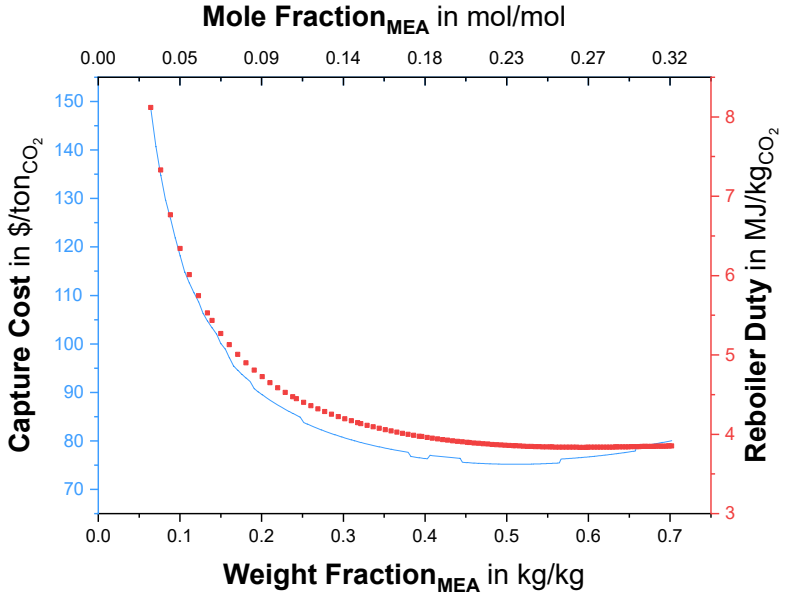


Figure 3.17: The impact of changing composition (weight fraction at bottom, mole fraction at top) of MEA on capture cost (blue line, left scale) and specific reboiler duty (red symbols, right scale). Optimal weight fraction around 50 wt% leads to minimum cost.

Main Heat Exchanger Temperature Approach The main heat exchanger's (MHEX) temperature approach is optimised for minimum total capture cost. This optimisation is a classic CAPEX-OPEX trade-off: Smaller driving temperature differences lead to a higher rich solvent outlet temperature which leads to lower sensitive heat requirements in the regeneration section at the cost of larger heat transfer areas. Limits are set by the minimum temperature approach achievable in design (assumed to be 1 K) and by avoiding two-phase flow inside the MHEX. The MHEX is designed with one degree of freedom, because the temperatures of the rich and lean solvent entering the MHEX are determined by other units, and one temperature (either rich solvent outlet or lean solvent outlet temperature) calculated through the energy balance.

Two methods of specifying the degree of freedom are: 1. Setting a temperature difference at the cold end $\Delta T_{\mathrm{ColdEnd}}$ (hot end also possible but less common), or 2. Setting a logarithmic mean driving temperature difference LMTD over the whole MHEX. There is no consensus on a preferred method, or optimal value with 20℃ widely assumed. Figure 3.18 shows that both methods are equally suitable to describe the temperature approach and yield the same results. The cases represent 30 wt% MEA, 90% capture rate, coal-power flue gas $y_{\mathrm{CO_2}}$= 12 mol% and show the $\Delta T_{\mathrm{ColdEnd}}$ method in the top row and the LMTD method in the bottom row. Both methods of describing the temperature approach are interchangeable. The temperature limit at which the solvent starts to boil is shown with a white dashed isotherm. The temperature represents the boiling point of the most volatile compound. There is a cost minimum between 15-25 K, and the default temperature approach is set to 20 K [115] (see Fig. B.7 for gas-power flue gas).

Pinching the streams at the hot end is favourable over pinching them at the cold end due to the higher exergy at elevated temperatures (see Fig. B.6). The hot end temperature difference depends on the lean loading and solvent flow rate (see Fig. B.5 for linear temperature profiles).

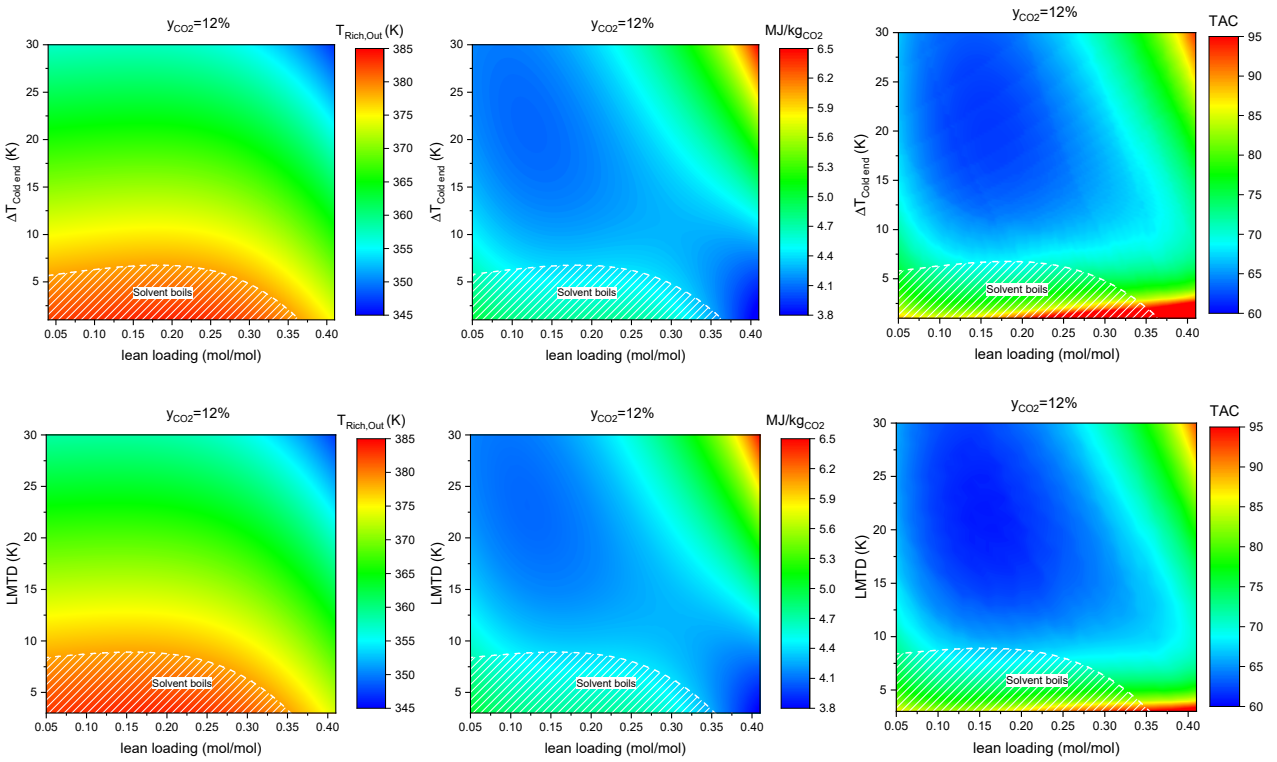


Figure 3.18: Using the cold end temperature difference $\Delta T_{\mathrm{ColdEnd}}$ (top row) or the LMTD (bottom row) to describe the temperature approach in the main heat exchanger return the same results. The impact on rich solvent outlet temperature T_{RichSol} (left column), specific reboiler duty (middle column), and capture cost TAC in $\$/t_{CO_2}$ (right column) are shown over a range of lean loadings. Solvent is 30 wt% MEA, capture rate is 90%, and flue gas CO_2 concentration is 12 mol%.

3.5 Model Comparison

The model aims to rank at least one candidate per chemical class within seconds by simultaneously solving a non-linear network of equations (see Fig. B.4) covering thermodynamics, operating conditions, equipment design, and costing. Earlier work [340] included an MEA based model which used a single-stage approach to modelling the absorber. That model was unfit for screening as it contained various restrictions: 1) It included Gabrielsen's [403] approach to VLE, which was initially also adopted in [14, 112] before being replaced [113] through other VLE approaches due to concerns over its accuracy. The previous hard coded VLE model was limited to three amines, and assumed equilibrium at the bottom of the absorber. 2) The expression for the enhancement factor was not valid and a wrong equation including a typo from [476] was implemented. 3) The implemented pressure drop model and mass transfer model

were not compatible. 4) Thermo-physical properties for MEA were hard-coded into the model. 5) The liquid phase diffusivity coefficient for CO_2 was calculated using the approach by Perkins and Geankoplis [440] which is not a recommended method [411]. 6) The model suffered from numeric instabilities.

The model is compared against TCM baseline data for MEA [271]. Table 3.11 summarises a comparison of available process parameter and equipment sizes at matching operating conditions against the 2014 baseline. Some model parameter (indicated by missing relative differences in Tab. 3.11) were set to match the TCM case as closely as possible. Missing TCM data is listed as NaN. Both datasets use random packing but their packing type is different.

Overall, good agreement was found with the exception of the absorber dimensions. The reboiler duty deviated 6% and the L/G ratio by 2%. The rich loading differs only 1.5% despite a temperature difference of 19% at the bottom of the absorber. The largest relative difference was found in the absorber's active packing height to diameter ratio. This work calculated a 26% narrower and 53% taller absorber. The active packing volume deviated by 8% compared to the 2014 baseline. The height of the TCM plant is shorter indicating a much faster mass transfer rate than calculated in this work.

The difference in the absorber's diameter and height could be explained by the single-stage short-cut model overestimating the column hight by over-weighting the low driving forces at the top of the absorber. The 5% difference in lean solvent flow rate and 9% lower void fraction also contribute to a smaller diameter in this work compared to TCM's data.

Table 3.11: Validation of this work against Technology Centre Mongstad 2014 baseline data [271].

KPI	Unit	TCM 2014 baseline	This work	Relative difference
References		[569–571]	This work	
Flue gas flow rate	kmol/s	0.55	0.55	
Flue gas flow rate	kg/s	16.0	16.0	

Continued on next page

Table 3.11 – *continued from previous page*

KPI	Unit	TCM 2014 baseline	This work	Relative difference
Flue gas flow rate	Sm^3/h	46970	46970	
y_{N_2}	mol/mol	78.6	79.5	1%
y_{CO_2}	mol/mol	3.6	3.6	
y_{H_2O}	mol/mol	2.5	2.5	
y_{O_2}	mol/mol	14.4	14.4	
y_{other}	mol/mol	0.9	0	NaN
$p_{Fluegas}$ (absorber inlet)	kPa	107.6	107.6	
$T_{Fluegas}$ (absorber inlet)	°C	25	25	
w_{MEA} (CO_2 free)	kg/kg	0.3	0.3	
Capture rate	%	93.5	93.5	
a_{Pack}	m^2/m^3	225	225	
Void fraction	-	0.97	0.887	-9%
$T_{Fluegas}$ (absorber outlet)	°C	38.1	36.5	-4%
$T_{Leansolvent}$ (absorber inlet)	°C	36.5	36.5	
$T_{Leansolvent}$ (reboiler outlet)	°C	122.3	119.1	-3%
$T_{Richsolvent}$ (absorber outlet)	°C	27.7	34.3	19%
$T_{Richsolvent}$ (stripper inlet)	°C	108.6	95.8	-13%
Θ_{Lean}	mol_{CO_2}/mol_{MEA}	0.23	0.23	
Θ_{Rich}	mol_{CO_2}/mol_{MEA}	0.48	0.47	-1.5%
$\Delta p_{Absorber}$	kPa	NaN	8.5	NaN
$\Delta p_{Absorber+Posttreatment}$	kPa	NaN	8.9	NaN
Solvent flow rate (lean)	kmol/s	NaN	0.62	NaN
Solvent flow rate (lean)	kg/s	15.3	14.6	-5%
L/G	kg/kg	NaN	0.91	NaN
L/G	mol/mol	NaN	1.12	NaN

Continued on next page

Table 3.11 – *continued from previous page*

KPI	Unit	TCM 2014 baseline	This work	Relative difference
L/G	kg/Sm^3	1.17	1.15	-2%
Specific reboiler duty	MJ/kg_{CO_2}	4.14	4.41	6%
Cooling duty	MW	NaN	1.8	NaN
CO_2 purity product	mol/mol	NaN	0.95	NaN
Absorber cross section area	m^2	7.1	3.84	-46%
Absorber packing height	m	24	51.4	53%
Absorber packing volume	m^3	170.4	185.4	8%
Stripper packing volume	m^3	10.6	14.1	24%
ΔT_{LMTD} (MHEX)	K	NaN	20	NaN
Heat transfer area (MHEX)	m^2	NaN	269.5	NaN
Emissions MEA	ppm	1	1	

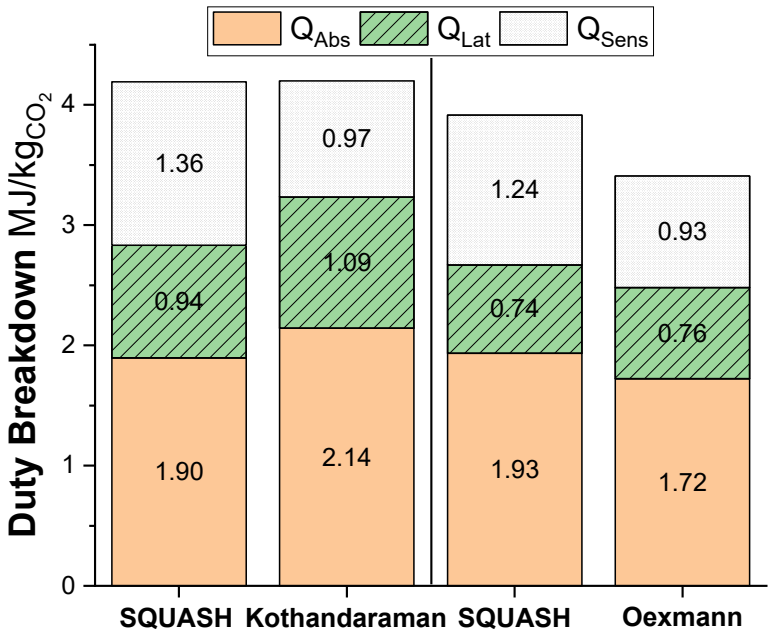


Figure 3.19: Comparing the heat duty breakdown with Oexmann's work [405] and Kothandaraman's rate-based model [572] for MEA for a coal-fired flue gas and similar operating conditions.

The specific reboiler duty breakdown (sensible heat, latent heat, and total heat of absorption) is compared with two other studies [405, 572] (see Fig. 3.19). This work agrees well with the work

by Oexmann *et al.* [405] and Kothandaraman [572] at their respective operating conditions. This work calculated a lower contribution of Q_{Abs} and Q_{Lat} and a higher contribution of Q_{Sens} in comparison to Kothandaraman's rate-based model. It returns a higher contribution of Q_{Abs} and Q_{Sens} in comparison to Oexmann's work [405]. The specific reboiler duty $Q_{\mathrm{Reb}} = Q_{\mathrm{Abs}} + Q_{\mathrm{Lat}} + Q_{\mathrm{Sens}}$ matches well between Kothandaraman's model and this work, and differs 15% to Oexmann *et al.*'s [405] model. The main deviation of this model appears to be the absorber dimensions with the tendency to overestimate its height.

3.6 Conclusions

The screening tool was developed together with a database of 464 candidate molecules. The database contains molecular characteristics *e.g.*, IUPAC nomenclature, CAS number, and molecular formula to ensure exact identification. A standard protocol enforced that only candidates deemed suitable, *i.e.*, with boiling point above 20°C, or solubility in water > 1 mol%, entered the database. Thermo-physical data was collected from established databases such as DIPPR [358], Yaw's critical properties [359], Reaxys, and Landolt-Börnstein (accessed through DIPPR [358]). Data for the VLE, Henry's law coefficients, heat of absorption, and kinetics was collected from the literature and fitted to pre-selected correlations.

94% of the candidates in the database contain one or two alkalinities per molecule. Primary amines represent the most common chemical sub-class with 63% share, and 51% of all candidates are primary, secondary, or tertiary amines. Only 18% (74 amines out of 415 amines) were able to be screened, because these are the only ones with already complete sets of data. Missing VLE data is the most prominent data-gap for the remaining candidates. 6% of the candidates were rejected due to inconsistencies and discrepancies in the reported data, identified by AARD>50% between data series. The number of candidate molecules could be increased by closing data gaps, *e.g.*, 17 candidate molecules are missing only kinetic data preventing them from being screened.

The relative differences between the solvents with full existing datasets are less than 10% for thermal conductivity, heat capacity, density, and surface tension. Hence, it is unlikely that these

properties are the main cause for the differences in the amines' techno-economic performance. In comparison, the range in normalised difference between the solvents and MEA in viscosity, reaction rate constant, equilibrium loading, and heat of absorption goes up to 300%.

A short-cut process model has been developed that converges within seconds, and is wrapped within an Excel interface. All solvents are used in the identical archetypal process topology. Process modifications, such as inter-cooled absorbers, or split-configurations, are excluded, because they would individually impact the trends in capture cost and solvents. The model deploys a single-stage description of the columns, and calculates heat and mass transfer rates to size equipment. The temperature approach in the main heat exchanger, lean loading, amine concentration, and equipment sizes are optimised for lowest capture cost. The calculated reboiler duty deviates 6% and the solvent flow rate 5% compared to TCM's 2014 baseline data for MEA. The model deviates 53% in absorber height and 46% in diameter, which is caused by the single-stage approach.

4. Error of *in-silico* Solvent Screening

4.1 Objectives

Errors in solvents' underlying thermo-physical properties cause an error in the calculated capture costs. It is of interest to find out if these errors could cause two solvents with different capture costs to be ranked equally, because the cost gap is not statistical significant enough. The aim of this section is to quantify such errors embedded in *in-silico* screening and in particular developing an approach to test the statistical significance of ranking screened solvents. The ultimate goal is quantifying confidence intervals and error bars for each screened solvent's capture cost and establishing whether solvents can be distinguished with statistical tests. For this, relevant sources of error are quantified and propagated through the screening model. The complete calculation process is summarised in Fig. 4.1.

This chapter starts with calculating the capture cost mean and its standard deviation from errors in thermo-physical properties. Then, the relevant statistical tests are discussed and used to determine the statistical significance of the calculated solvent ranking. Following this, key assumptions and design decisions made in the model are tested for impacting the ranking in a statistical significant way. Lastly, the whole calculation process and its relevance for the ranking is discussed for five exemplary solvents for a number of CO_2 concentrations.

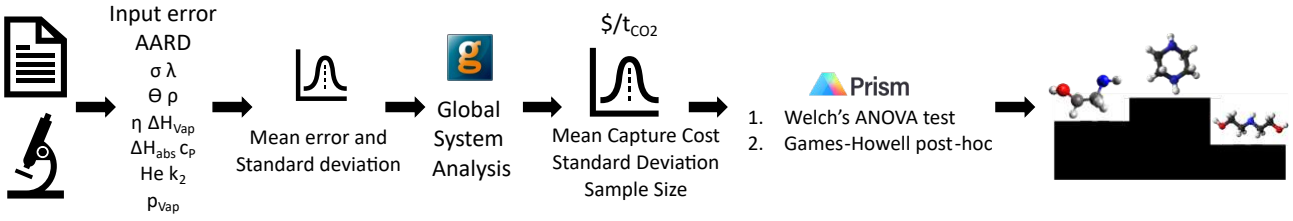


Figure 4.1: Workflow of deriving the statistical significance for the solvent ranking. Step 1: Gathering data in the literature, Step 2: Calculating the mean error and standard deviation. Step 3: Calculating the mean capture cost and its standard deviation by propagating the errors in gPROMS [417] using the global system analysis. Step 4: Testing the capture cost mean and its standard deviation for statistical significance in Prism [573].

4.2 From Input Uncertainty to Capture Cost Error

The work-flow starts with collecting errors of measuring or predicting thermo-physical properties reported in the literature focussing on CO_2 capture solvents. These errors describe the reliability of the methods deployed and are unique to the solvents and setup utilised. The uncertainty will differ within the same property between methods, setups, and approaches. For example, calculating the heat of absorption via the Gibbs-Helmholtz approach is about 30% [172] accurate, whereas Kim *et al.,* [176, 574, 575] measured it with only a 2% AARD uncertainty. As an example, Fig. 4.2 shows the collected studies for densities as entered into an Excel file. Shown are the individual studies reporting an error as absolute average relative deviation. If a study utilised multiple approaches, *e.g.,* different measurement methods, then these are listed separately for the same study (separate column entries). The studies reported data for multiple solvents at varying conditions (*e.g.,* concentration, pressure, temperature, loading). The mean error and its standard deviation as well as the corresponding sample size is shown on the right of Fig. 4.2. The lower $CI_{95\%,L}$ and upper $CI_{95\%,U}$ (noted as $CI_{95\%}$ High) 95% confidence intervals are calculated in three different ways, which will be further analysed: 1. using the full set, 2. using just experimental data (noted as *Exp only* in Fig. 4.2), or 3. using just computational methods (noted as *Pred only* in Fig. 4.2).

Table D.1 in the appendix summarises a collection of 150 studies reporting the combined expanded relative uncertainty of measuring or predicting thermo-physical properties of aqueous amine solvents. It is observed that, agnostic of method, predictions report on average larger errors than experimental measurements and the reported values vary up to 25% between studies. It is not the aim of this work to collect a complete list of studies and compare the individual methods. Instead, the aim is compiling a sample size sufficiently large enough to be representative of each property or method behind the thermo-physical properties for aqueous amine solvents. It will be investigated if, and to what degree, the differences in the data from the 150 data entries impacts the statistical significance of the ranking.

Table 4.1 lists the mean error, its standard deviation, and sample size (number of methods)

for the three approaches mentioned earlier, reflecting the combined data, just measured data, or just predicted data. This is the input for the GSA performed in gPROMS with the default approach using the total datasets listed in Tab. 4.1. Omitted from this table are molar mass and molar volume, which are assumed to be calculated without any error.

Density	Method	Average absolute relativedeviation (AARD)		
prediction	Schroeder	3.900%		
prediction	Le Bas (1915)	3.900%		
prediction	Tyn and Calus Method (1975)	2.800%		
prediction	Rackett 1970	4.090%	0.800%	
prediction	Yamada and Gunn (1973)	1.800%		
prediction	HBT Hankinson and Thomson (1979) + Thomson, et al. (1982)	2.560%		
prediction	Elbro, et al. (1991)	2.800%		
exp	Weiland et al 1998	3.436%		
exp	Han et al	3.959%		
exp	Jayarathna 2013	0.164%		
exp	Conception 2017	2.200%	0.700%	
exp	Rinker 1994	0.050%		
exp	Hsu 1997	0.050%		
exp	Tsend 1964	0.070%		
exp	Yang 2012	0.060%		
exp	Spasojevic 2013	1.050%		
exp	Zhao 2010	0.012%	0.319%	0.214%
exp	Chowdhury 2016	0.160%		
exp	Zhang 2015	0.002%		
exp	Marham 2002	0.070%		
exp	Zhang 1995	0.030%		
exp	Karunarathne 2020	0.120%	0.594%	

All	
Mean	1.33%
Standard deviatic	0.015
CI 95%Low	0.77%
CI95% High	1.89%
Sample size	27

PRED Only	
Mean	2.83%
Standard deviatic	0.011
CI 95%Low	2.09%
CI95% High	3.57%
Sample size	8

EXP ONLY	
Mean	0.24%
Standard deviatic	0.003
CI 95%Low	0.06%
CI95% High	0.42%
Sample size	19

Figure 4.2: Overview of collected studies reporting errors for liquid densities of capture solvents. Mean error, standard deviation, sample size and lower $CI_{95\%,L}$ and upper $CI_{95\%,U}$ (noted as $CI_{95\%}$ High) 95% confidence intervals are calculated for the full set or subsets (experimental or prediction). All studies for all properties are listed in Tab. D.1.

All properties average uncertainties less than 12% using the full datasets. Heat of vapourisation and density show the lowest mean errors with 1.3% and 1.4% respectively, which means, the confidence in the methods for calculating these properties is on average the highest. Viscosity and vapour pressure are the properties with the highest mean error (11.8% and 8%) indicating the lowest confidence. As reference, Mathias and Gilmartin [191, 334] found the uncertainty of calculating the liquid viscosity for aqueous AMP implemented in Aspen Plus to be about ±30%. Based on the compiled literature, accurately predicting viscosity (21.5% mean error) and heat of absorption (25% based off a single study) appears significantly harder compared to other properties, *e.g.,* density (2.8%), which is expressed through higher mean errors. The collected studies suggest that the differences in errors are caused by the method utilised and property but not by the solvents.

For some properties only few studies were identified, *e.g.,* predicting k_2, ΔH_{Vap}, He, or ΔH_{Abs}. The limited studies reporting about predictive methods for the reaction rate constant k_2 did

Table 4.1: Mean error, standard deviation, lower $CI_{95\%,L}$ and upper $CI_{95\%,U}$ 95% confidence intervals and sample size (number of methods) for collected studies of thermo-physical properties by means of predicting (Pred), measuring (Exp), or combined (total).

Property	Source	Mean	Standard deviation	$CI_{95\%,L}$	$CI_{95\%,U}$	Sample size
Density, ρ	Total	1.3 %	0.02	0.8 %	1.9 %	27
	Pred	2.8 %	0.01	2.1 %	3.6 %	19
	Exp	0.2 %	0.00	0.1 %	0.4 %	8
Viscosity, η	Total	12 %	0.11	8.0 %	16 %	34
	Pred	22 %	0.11	15 %	28 %	13
	Exp	5.7 %	0.06	3.4 %	8.1 %	21
Heat capacity, c_p	Total	3.1 %	0.02	1.8 %	4.4 %	13
	Pred	3.8 %	0.03	2.0 %	5.6 %	8
	Exp	2.0 %	0.03	-0.1 %	4.1 %	5
Thermal conductivity, λ	Total	4.3 %	0.03	2.3 %	6.3 %	11
	Pred	5.0 %	0.03	2.8 %	7.2 %	8
	Exp	1.4 %	0.01	0.4 %	2.3 %	2
Surface tension, σ	Total	3.1 %	0.05	1.6 %	4.6 %	36
	Pred	7.2 %	0.05	4.1 %	10 %	7
	Exp	1.3 %	0.03	0.2 %	2.3 %	25
Vapour pressure, p_{Vap}	Total	8.0 %	0.08	2.5 %	14 %	7
	Pred	8.8 %	0.09	1.2 %	16 %	5
	Exp	6.2 %	0.01	4.6 %	7.8 %	2
Heat of vapourisation, ΔH_{Vap}	Total	1.4 %	0.01	0.9 %	2.0 %	6
	Pred	2.3 %	0.00	2.3 %	2.3 %	1
	Exp	1.3 %	0.01	0.7 %	1.9 %	5
Henry's coefficient, He	Total	2.8 %	0.02	2.0 %	3.6 %	12
	Pred	6.9 %	0.00	6.9 %	6.9 %	1
	Exp	2.4 %	0.01	1.9 %	2.9 %	11
Rate constant, k_2	Total	4.8 %	0.03	2.8 %	6.7 %	11
	Pred	0.0 %	0.00	0.0 %	0.0 %	0
	Exp	4.8 %	0.03	2.8 %	6.7 %	11
VLE, Θ	Total	5.5 %	0.05	4.0 %	7.1 %	39
	Pred	15 %	0.05	10 %	19 %	6
	Exp	4.3 %	0.04	3.2 %	5.5 %	36
Total heat of absorption, ΔH_{Abs}	Total	4.7 %	0.06	1.8 %	7.6 %	15
	Pred	25 %	0.00	25 %	25 %	1
	Exp	3.2 %	0.02	2.3 %	4.1 %	14

not provide an error discussion, thus no entry is made at all. If only one study reported errors, then these values could be directly propagated through the model and calculating a mean error is unnecessary.

Other potential sources of error are *e.g.,* the thermodynamic correlations (see Tab. 3.6), sizing or costing equations. They are not changing between solvents and could be seen as a systematic error rather than an input error. Including these sources of error in the analysis will create little further insight. It is not required to include them if the capture costs calculated with the developed model will be ranked within the tool. Omitting *e.g.,* the costing correlations' errors leads to narrower confidence intervals, which should be taken into considerations when comparing with results outside this work.

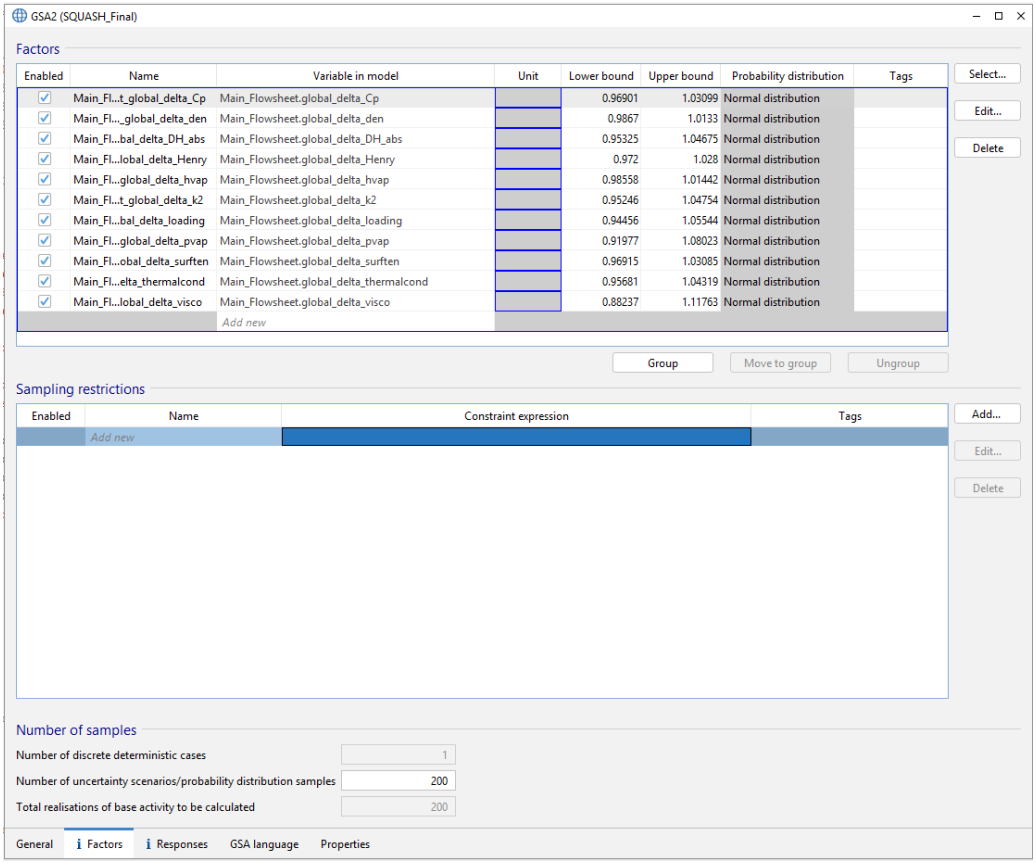


Figure 4.3: Screenshot of the input interface of gPROMS's Global System Analysis. Shown is an example of factors for thermo-physical properties, and sample size $n = 200$.

Step three of the work-flow uses the mean errors and standard deviations of the thermo-physical properties listed in Tab. 4.1 and propagate these through the model by using gPROM's Global System Analysis (GSA). The GSA calculates the mean capture costs and its standard deviation

Distribution Statistics

Variable	Units	Expected value	Std deviation	Minimum	Maximum
Main_Flowsheet_TAC	$/tonCO2	127.647	2.41851	122.741	135.333

Figure 4.4: Output of the Global System Analysis with mean capture cost and its standard deviation as well as minimum and maximum values observed during the run.

via a Monte-Carlo calculation. The Monte-Carlo method is the only built-in method to calculate uncertainties within gPROMS ModelBuilder V. 6.0.2. Instead of computing every possible combination of the inputs within their ranges, the Monte-Carlo method runs a number n of unique combinations calculating the mean and standard deviation of a result. It requires a range and a probability distribution function (options are uniform, discrete, normal, log-normal, multi-variant discrete and multivariate normal) per input variable. gPROMS was set to calculate the required random values through quasi-random (Sobol) sampling [576]. The procedure and settings remained constant for all simulations.

Figure 4.3 shows an example of GSA's input interface. The mean input errors can be propagated through the gPROMS model either one-by-one or all simultaneously by activating them in the factors tab. For ease of use, each thermo-physical property is multiplied with a factor ψ, *e.g.,* $\psi_{k_2} \cdot k_2$ with its default value being one. These factors are defined as a *variable* instead of a *parameter*, allowing gPROMS to vary it within the range and distribution given within the GSA entity. They can be used to adjust properties, execute sensitivity studies, and converge from one case to another if numeric instabilities occur. GSA's input factors include an upper and lower bound as well as distribution function (normally distributed). There are no correlated distributions in the factors, *i.e.,* the ψs are independent from each other.

The default upper and lower bounds correspond to the mean errors (see Tab. 4.1 and Tab. 3.6). The default approach uses constant input factors ψ for all solvents and the impact of using unique sets of input errors is analysed. It will be shown that using an individual combination of input mean error values for each solvent, despite being perceived as more accurate and spending more effort on it, does not actually change the statistical significance of the solvent ranking.

The number of uncertainty scenarios / probability distribution samples n represents how often

the Monte-Carlo calculation is run and should not be confused with the number of studies from which the input error data was taken. The number of samples n was set to 200 per factor group, which was the result of an optimisation. The sample size has to be sufficiently large such that the central limit theorem applies, expected to be true if $n >> 30$ [321, 577], but also small enough to optimise computational effort. Significantly increasing the Monte-Carlo sample size n increases the computational effort and the analysis ran for tens of minutes ($n = 1000$) instead of seconds ($n = 50$) or single minutes ($n = 200$). No upper sampling restrictions were set, however, a statistical test further requires $n > 50$.

The output response was set to the capture cost. The GSA's distribution statistics table with the capture cost mean and its standard deviation as well as minimum and maximum value observed during the GSA are shown in Fig. 4.4. One expects the Monte-Carlo calculated capture costs to be scattered around the mean depending on the range of the input error data. It is unlikely but possible that the Sobol sampling selects the upper and lower bounds of each error such that the capture cost reach the extreme upper and lower values. In reality, deviations will trade-off, and the minimum and maximum capture costs reported in GSA's output are not further processed. With this step finalised, the solvents can be ranked according to their mean capture costs. All error bars displayed in this work represent the 95% confidence interval as calculated by the capture cost mean and standard deviation of each solvent with Eqn. 2.6. The mean capture cost and its standard deviation are further processed outside gPROMS.

A minor mathematical observation is that the mean capture cost calculated by the GSA is unlikely to be exactly equal to the converged value of the process simulation for the same solvent at the same operating conditions. A process simulation run represents one case of the GSA in which all ψs are equal to one. Table D.3 shows the mean value from GSA for $n = 200$ and the converged process simulation for five solvents (MEA, DEA, MDEA, AMP, PZ) at their individual optimal operating conditions. The relative differences are less than 0.5% and on average 0.2%.

Unfortunately, the GSA has to be manually set, and the model prepared by defining variables for every error which is a disadvantage. It was an inconvenience that the GSA could not be included

in the schedule of the process entity with the ambition to automatically run it once optimising the operating parameter has finished. Using the GSA was limited to the screening only and not run for sensitivity studies. Long initialisation times caused problems which were solved by extensively using saved variable sets. No foreign process interface *e.g.,* Excel can be active while the GSA is running. This hinders automatically screening solvents while simultaneously quantifying the standard deviation. The described approach does not provide insights as to why certain observations are happening, *e.g.,* changes in viscosity leading to changes in heat and mass transfer for which sensitivity analysis are run instead.

The final step four of the procedure tests differences in calculated capture cost means for statistical significance in GraphPad Prism Version 9.5 [573]. Two independent statistical tests are run: First, a Welch's analysis of variance [356, 578, 579], and secondly a Games-Howell post-hoc test [580–582]. These tests establish the statistical significance, or lack of, the difference in capture cost between solvents. Only the capture cost means, standard deviations, and sample size are required input, eliminating the need to export and import all data points. The inferential statistical analysis executed during step four is explained in the next section.

4.3 Inferential Statistical Analysis

The field of statistical inference deals with analysing data with the intention to infer its underlying distribution of probability [583]. Testing hypotheses and deriving estimates by inferring properties assumed to be sampled from a larger population is an example of inferential statistical analysis. The aim of executing the following analysis is to determine if screened solvents' capture cost actually differ. This means more specifically, if the calculated capture cost distribution leads to statistically significant difference, thus, a clear ranking difference, or lack of. The test population represents every possible combination of errors propagating through the model for each solvent and impacting the capture cost as a numerical variable. Statistical tests build conclusions about a data population based on analysing only a sample (subset of the population) as it is not desirable to calculate every combination.

Hypothesis testing analyses if two samples are different by rejecting the null hypothesis. The

null hypothesis represents the case that two solvents rank equal and their actual mean capture cost are equal. The null-hypothesis can only be rejected if a test statistic, or p-value, is less than a critical value known as significance level α. The p-value is a statistical measurement indicating the probability of the observed results accepting the null hypothesis to be true, *i.e.,* low p-values represent cases which are unlikely to be observed if the null hypothesis is true. It can be interpreted as the strength of evidence against the null hypothesis. It does, however, not provide evidence in favour of the alternative hypothesis which is expressed as 'failing to reject'.

The significance level α can be freely set at the desired level of significance and represents the confidence in the results of the statistical test. Values < 0.01 represent strong statistical evidence against the null hypothesis and values > 0.1 are seen as weak evidence. This work assumes p-values < 0.05 as statistically significant taken from [584, 585]. If $p-\text{value} < 0.05$ then the null hypothesis (two solvents share same rank despite different capture cost) is rejected. At $\alpha = 5\%$ (equal to 95% confidence) it is 5% likely that solvents rank differently despite actually belonging to the same rank. In general, p-values could be an alternative addition to confidence levels for hypothesis testing. Type I errors happen when the null hypothesis is falsely rejected. Type II errors happen if the null hypothesis is falsely failed to reject, *i.e.,* null hypothesis was not rejected but should have been rejected.

Some common tests are z, t, F, χ^2, analysis of variance(ANOVA), and post-hoc tests. In the following paragraphs, the fundamentals of the tests are summarised and their applicability for screening discussed. The impact of selecting a specific test on the ranking and their calculation methods are demonstrated for a number of fictional solvents.

z-Test The area under any standard distribution described with the standard deviation s with an intersection x represents the probability of variables in that range with an overall mean of μ.

$$z_{\text{Test}} = \frac{x - \mu}{s} \tag{4.1}$$

The total sum or area under the standard distribution equals one. The z-score is linked to

a p-value representing the likelihood of values being observed above that z-score if the null hypothesis is true. z-score and corresponding p-value can be looked up in tables [321]. The z-score is a calculated to compare the means of two variables, where $p-\text{value} < \alpha$ means that a capture cost difference is less likely to have happened by chance. The z-test (or Gauß-test) is designed to reject or confirm a sample belonging to a specific population (one sample location test), however, it is less well designed to handle the cost distribution of two solvents [322].

Figure 4.5 shows every single calculated capture cost of the GSA for two fictional solvents. Solvent A has a calculated capture cost mean of $\$100/t_{CO_2}$ and solvent B of $\$115/t_{CO_2}$. The standard deviation of solvent A is $\$5.56/t_{CO_2}$ and solvent B is $\$8.89/t_{CO_2}$. The confidence interval (see Eqn. 2.6) is for solvent A $\$100/t_{CO_2} \pm 1.96 \cdot \frac{5.56}{\sqrt{200}} = \$100/t_{CO_2} \pm \$0.77/t_{CO_2}$ and for solvent B $\$115/t_{CO_2} \pm \$1.23/t_{CO_2}$. If the GSA is run many times then 95% of solvent's A calculated capture cost means would be between $\$99.2/t_{CO_2}$ and $\$100.8/t_{CO_2}$.

The z-score is $z = \frac{115-100}{5.56} = 2.70$, and by using the full z-score table [321], one finds the corresponding p-value to be $1 - 0.996535 = 0.0035$ which is much lower than 5%. Therefore, the null hypothesis is rejected and solvent B ranks not equal to solvent A. That means, the observed difference in capture cost mean between A and B is likely to be caused by their performance and thermo-physical properties.

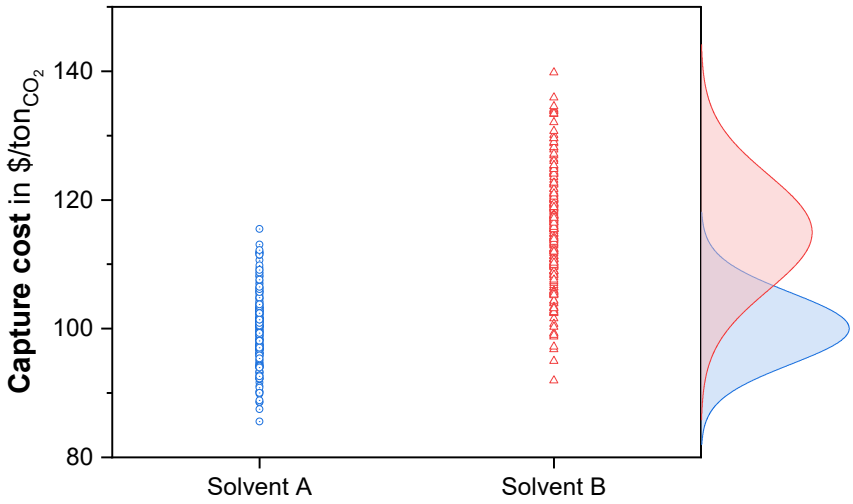


Figure 4.5: Example of output of the GSA for two fictional solvents: Solvent A has a capture cost mean of $\$100/t_{CO_2}$ and solvent B of $\$115/t_{CO_2}$. The standard deviation of solvent A is $\$5.56/t_{CO_2}$ and solvent B is $\$8.89/t_{CO_2}$. Both solvents' normal distribution of the capture cost are shown on the right axis.

χ^2-Test As with the z-test, the χ^2-test uses a table (or software) of critical values as threshold for statistical significance. The table supplies the right-tailed probabilities (for α) and left-tailed probabilities (for 1-α). The null hypothesis can be rejected if the calculated χ^2 is above the critical χ^2 as read from the table. For two-tailed tests the two critical values are found by looking for $1 - \alpha/2$ and $\alpha/2$ and the null hypothesis can be rejected if the calculated χ^2 is not between the two critical values. There are two χ^2-test variations: 1. Goodness of fit testing if the distribution of observations of a categorical variable is different from expectations.
2. Test of independence if two categorical variables are related. Pearson's χ^2 [586] assumes at least one categorical (non quantitative) variable, random samples, and minimum five observations per group. The formula for a random variable x is:

$$\chi^2 = \sum \frac{\left(x_{\text{observed}} - x_{\text{expected}}\right)^2}{x_{\text{expected}}} \tag{4.2}$$

A χ^2-test could be used to confirm if trends observed in *e.g.,* chemical classes are statistically significant. It is less suited to test quantitative differences in capture cost for multiple solvents expected not to belong to the same family.

t-Test A t-test compares two means of two populations of results. The t-score is linked to the p-value and critical values $t^\star$ can be found in a table or software. Required inputs are the degrees of freedom $df = N - 2$ with N being the total number of data points of both solvents $N = 2n$ and α. Two-tailed tests work for non-directional alternative hypothesis (*e.g.,* two solvents differ in capture cost), and one-tailed tests work for directional alternative hypothesis. The data between solvents is independent, *i.e.,* the error propagation for solvent A is not linked to the error of another solvent other than by chance. A two-tailed, dependent two-sample t-test with unequal variance appears suitable to compare two solvents and their capture cost means and deviations.

The widely known student's t-test requires normally distributed means of two populations with equal variance [587]. The lesser known [588] Welch's t-test [356, 578, 579] still assumes normally distributed means but unequal variance. Welch's t-score is calculated with the following formula

assuming normally distributed means / capture cost (guaranteed through input in the GSA and central limit theorem), non-paired and random samples (achieved through the solvents' input and quasi-random Sobol sampling), as well as unequal variance between the populations / solvents. $\bar{x}_i$ and $\bar{x}_j$ are the mean values, *e.g.,* the capture cost, and s_i and s_j the standard deviation of both samples [356].

$$t = \frac{\bar{x}_i - \bar{x}_j}{\sqrt{\frac{s_i^2}{n_i} + \frac{s_j^2}{n_j}}} \tag{4.3}$$

Welch's test differs from the student's t-test in the denominator, which is not based on the pooled variance estimate, and is more robust than an one-way analysis [356, 578, 579]. Large t-scores indicate more significant differences between two solvents, and if the corresponding $p < 5\% = \alpha$ then the null hypothesis is rejected *i.e.,* two solvents do not share the same rank.

The t-score for solvents A and B (see Fig. 4.5) is calculated by:

$$t = \frac{\bar{x}_A - \bar{x}_B}{\sqrt{\frac{s_A^2}{n_A} + \frac{s_B^2}{n_B}}} = \frac{100 - 115}{\sqrt{\frac{5.56^2}{200} + \frac{8.89^2}{200}}} = -20.3 \tag{4.4}$$

The critical value $t^\star = 1.967$ is found by looking at the table for two-tailed tests $\alpha = 0.05$ and $df = 398$. The corresponding p-value is $4.5 \exp -60 << 0.05$. Therefore, the null-hypothesis is rejected, meaning that solvent B has statistically significant not the same capture cost mean as solvent A.

Solvents C-G are added to the previously described solvents A and B (see Tab. 4.2). The number of unique t-test pairs is $\binom{n}{2} = \frac{n!}{2!(n-2)!}$ for n-solvents, *e.g.,* $\binom{7}{2} = \frac{7!}{2!(7-2)!} = 21$ tests for solvents A-G. Running multiple t-tests increases the likelihood of type I errors (null hypothesis is falsely rejected) [588, 589]. For solvents A-G, the probability of at least one $p-$value being less than 0.05 by chance is $1.00 - 0.95^{21} = 66\%$. The 73 screened solvents would require 2628 t-tests which will question the validity of the statistical approach, because the likelihood that the null hypothesis will be falsely rejected at least once by chance is $\approx$ 100% (almost certain).

Figure 4.6 and Fig. 4.7 show the input (mean capture cost, standard deviation and sample size) and output of Prism (Yes/No, p-value see Tab. 4.3) for running multiple t-tests for solvents A-G.

Table 4.2: Comparing Solvents A-G with their mean capture cost, standard deviation, standard error and lower $CI_{95\%,L}$ as well as upper 95% $CI_{95\%,U}$ confidence interval.

Item	Sol. A	Sol. B	Sol. C	Sol. D	Sol. E	Sol. F	Sol. G
Mean, $/t$_{CO_2}$	100.0	115.0	101.1	105.1	113.0	114.7	118.8
Standard deviation, $/t$_{CO_2}$	5.6	8.9	7.1	17.8	79.5	8.9	60.2
Standard error, $/t$_{CO_2}$	0.4	0.6	0.5	1.3	5.6	0.6	4.3
$CI_{95\%,L}$	99.3	113.8	100.1	102.6	102.0	113.4	110.4
$CI_{95\%,U}$	100.8	116.3	102.1	107.6	124.0	115.9	127.1

Table 4.3: Comparing Solvents A-G with their p-values as tested with multiple two-sample, two-tailed t-tests. If p-value $< 0.05 = \alpha$ then null hypothesis is rejected.

p-value	Sol. A	Sol. B	Sol. C	Sol. D	Sol. E	Sol. F	Sol. G
Solvent A	X	< 0.001	0.085	< 0.001	0.022	< 0.001	< 0.001
Solvent B		X	< 0.001	< 0.001	0.724	0.736	0.378
Solvent C			X	0.003	0.036	< 0.001	< 0.001
Solvent D				X	0.172	< 0.001	0.002
Solvent E					X	0.764	0.411
Solvent F						X	0.342
Solvent G							X

The p-values can be corrected for running multiple t-tests to q-values (shown in right column), *i.e.,* $q-\text{value} < \alpha$ is tested instead of $p-\text{value} < \alpha$ [590]. Despite corrections, it will be shown that an analysis of variance is more robust than multiple t-tests.

F-Test An F-test compares two variances, s_1^2 and s_2^2 of two normally-distributed populations 1 and 2. The null hypothesis is that both variances are equal.

$$F = \frac{s_2^2}{s_1^2} = \frac{\frac{1}{n_2-1}\sum_{i=1}^{n_2}(x_{2i}-\overline{x}_2)^2}{\frac{1}{n_1-1}\sum_{i=1}^{n_1}(x_{1i}-\overline{x}_1)^2} \tag{4.5}$$

F is always a positive number, and if both variances are equal then $F = 1$. The F-metric is used in multiple other statistical tests *e.g.,* analysis of variance.

Table format: Grouped		Group A Solvent 1			Group B Solvent 2		
		Mean	SD	N	Mean	SD	N
1	**Solvent B**	100.0	5.56	200	115.0	8.89	200
2	Solvent C	100.0	5.56	200	101.1	7.10	200
3	Solvent D	100.0	5.56	200	105.1	17.80	200
4	Solvent E	100.0	5.56	200	113.0	79.50	200
5	Solvent F	100.0	5.56	200	114.7	8.90	200
6	Solvent G	100.0	5.56	200	118.8	60.20	200
7	**Solvent C**	115.0	8.89	200	101.1	7.10	200
8	Solvent D	115.0	8.89	200	105.1	17.80	200
9	Solvent E	115.0	8.89	200	113.0	79.50	200
10	Solvent F	115.0	8.89	200	114.7	8.90	200
11	Solvent G	115.0	8.89	200	118.8	60.20	200
12	**Solvent D**	101.1	7.10	200	105.1	17.80	200
13	Solvent E	101.1	7.10	200	113.0	79.50	200
14	Solvent F	101.1	7.10	200	114.7	8.90	200
15	Solvent G	101.1	7.10	200	118.8	60.20	200
16	**Solvent E**	105.1	17.80	200	113.0	79.50	200
17	Solvent F	105.1	17.80	200	114.7	8.90	200
18	Solvent G	105.1	17.80	200	118.8	60.20	200
19	**Solvent F**	113.0	79.50	200	114.7	8.90	200
20	Solvent G	113.0	79.50	200	118.8	60.20	200
21	**Solvent G**	114.7	8.90	200	118.8	60.20	200

Figure 4.6: Input of Prism with the mean capture cost, standard deviation and sample size of solvents A-G (see Tab. 4.2). Each row is a t-test between a pair of solvents with already tested combinations (AvB = BvA) and same solvent combinations (AvA) omitted.

ANOVA An ANalysis Of VAriance, also known as ANOVA, tests if there are statistically significant differences in more than two groups. The ANOVA can bee seen as an extension of the independent t-test for more than two groups. It compares standard deviations by calculating the ratio of between-group (btw) to within-group (wi) variance and differs from a simple F-test that compares the variances of just two samples. The F-value is the mean square of each independent variable divided by the mean square of the residuals. Its null hypothesis is that all population / sample means are equal, *e.g.,* mean capture costs of all solvents are equal. The alternative hypothesis is that at least one group differs significantly from the overall mean. The independent variables are the solvents and the dependent variable the capture cost, *i.e.,* testing if the solvents have a statistical significant impact on the capture cost.

If the between-group and within-group variances are similar then their ratio will be close to one. High F-values represent smaller variances within groups than between groups, meaning higher

		Discovery?	P value	Mean of Solvent 1	Mean of Solvent 2	Difference	SE of difference	t ratio	df	q value
1	**Solvent B**	Yes	<0.000001	100.0	115.0	-15.00	0.7414	20.23	334.0	<0.000001
2	Solvent C	No	0.085341	100.0	101.1	-1.100	0.6377	1.725	376.4	0.057605
3	Solvent D	Yes	0.000142	100.0	105.1	-5.100	1.319	3.868	237.5	0.000149
4	Solvent E	Yes	0.022079	100.0	113.0	-13.00	5.635	2.307	200.9	0.017387
5	Solvent F	Yes	<0.000001	100.0	114.7	-14.70	0.7420	19.81	333.8	<0.000001
6	Solvent G	Yes	0.000018	100.0	118.8	-18.80	4.275	4.398	202.4	0.000024
7	**Solvent C**	Yes	<0.000001	115.0	101.1	13.90	0.8045	17.28	379.4	<0.000001
8	Solvent D	Yes	<0.000001	115.0	105.1	9.900	1.407	7.037	292.5	<0.000001
9	Solvent E	No	0.724024	115.0	113.0	2.000	5.657	0.3536	204.0	0.343834
10	Solvent F	No	0.736093	115.0	114.7	0.3000	0.8895	0.3373	398.0	0.343834
11	Solvent G	No	0.378195	115.0	118.8	-3.800	4.303	0.8831	207.7	0.210232
12	**Solvent D**	Yes	0.003446	101.1	105.1	-4.000	1.355	2.952	260.8	0.002961
13	Solvent E	Yes	0.036221	101.1	113.0	-11.90	5.644	2.108	202.2	0.026330
14	Solvent F	Yes	<0.000001	101.1	114.7	-13.60	0.8050	16.89	379.3	<0.000001
15	Solvent G	Yes	0.000053	101.1	118.8	-17.70	4.286	4.129	204.5	0.000063
16	**Solvent E**	No	0.171665	105.1	113.0	-7.900	5.761	1.371	218.9	0.108149
17	Solvent F	Yes	<0.000001	105.1	114.7	-9.600	1.407	6.822	292.6	<0.000001
18	Solvent G	Yes	0.002271	105.1	118.8	-13.70	4.439	3.086	233.5	0.002146
19	**Solvent F**	No	0.764077	113.0	114.7	-1.700	5.657	0.3005	204.0	0.343834
20	Solvent G	No	0.411299	113.0	118.8	-5.800	7.051	0.8225	370.7	0.215932
21	**Solvent G**	No	0.341793	114.7	118.8	-4.100	4.303	0.9528	207.7	0.201871

Figure 4.7: Output of running multiple t-tests for solvents A-G. The first column indicates the first solvent of the comparison with the remaining solvent of the pair being the preceeding one in the alphabet, *e.g.,* the first row represents the t-test of solvent A and B. Yes/No indicates wheter the p-value is below the significance level of 5% leading to rejecting the null hypothesis.

likelihood that the observed difference is real and not due to chance. Calculating an ANOVA by hand (see set of equations 4.6) is not practical. Required inputs are the solvents' mean μ_i, overall mean μ, square sum total QS_{Total}, square sum between QS_{btw} and within groups QS_{wi}, the variance ratio, and mean squares MQ, in order to calculate the F-value.

The significance level applies to the entire family of comparisons which makes it harder to reach significance and, therefore, reduces the chance of wrongly finding statistical significance that is entirely due to random sampling. The ANOVA was executed as single factorial without measurement repetition.

$$
\begin{aligned}
\mu &= \frac{\sum x}{N} \\
\mu_i &= \frac{\sum^{\text{Group}} x}{n^{\text{Group}}} \\
QS_{\text{Total}} &= \sum (x - \mu)^2 \\
QS_{\text{btw}} &= \sum^{\text{Groups}} n_i \left(\mu_i - \mu\right)^2 \\
QS_{\text{wi}} &= \sum^{Groups} \sum^{Group} (x_{mi} - \mu_i) \\
\text{ratio} &= \frac{QS_{\text{btw}}}{QS_{\text{Total}}} \\
MQ_{\text{btw}} &= \frac{QS_{\text{btw}}}{df_{btw}} \\
MQ_{\text{wi}} &= \frac{QS_{\text{wi}}}{df_{wi}} \\
F &= \frac{MQ_{\text{btw}}}{MQ_{\text{wi}}}
\end{aligned}
\tag{4.6}
$$

Both Welch's ANOVA and Brown-Forsythe ANOVA [591] are calculated with normally distributed data that violates the assumption of homogeneous variance by adjusting the calculations of F to W in Welch's ANOVA and to $F^\star$ in Brown-Forsythe's ANOVA and adjusting df reflecting the heterogeneity of within-group variances [592, 593].
W and $F^\star$ are identical to F of an ordinary one-way ANOVA if the sample size is equal for all groups. Otherwise, the p-value is calculated from W or $F^\star$ by the same algorithm as utilised to calculate p-value from F in Eqn. 4.6. The p-value can be interpreted in the same manner as in the analysis of variance table [322]. The degree of freedom for the numerator df_n is the same as for a regular one-way ANOVA, but the degree of freedom for the denominator df_d is different.

The Brown-Forsythe ANOVA tests for equality of means and is different to another test by Brown and Forsythe testing equality of variances [322]. Glantz *et. al.*, [322] recommend Welch's ANOVA over Brown-Forsythe's ANOVA unless the data is skewed (not the case in this work).

Figure 4.8 shows the input and output of running Welch's ANOVA in Prism. The solvents' mean capture cost, standard deviation and sample size are entered into one row as group. There is no evidence to support assuming equal variance a-priori, therefore, Welch's ANOVA is

selected (and Brown-Forsythe ANOVA automatically calculated with it). The family consists of the 21 tests for solvents A-G.

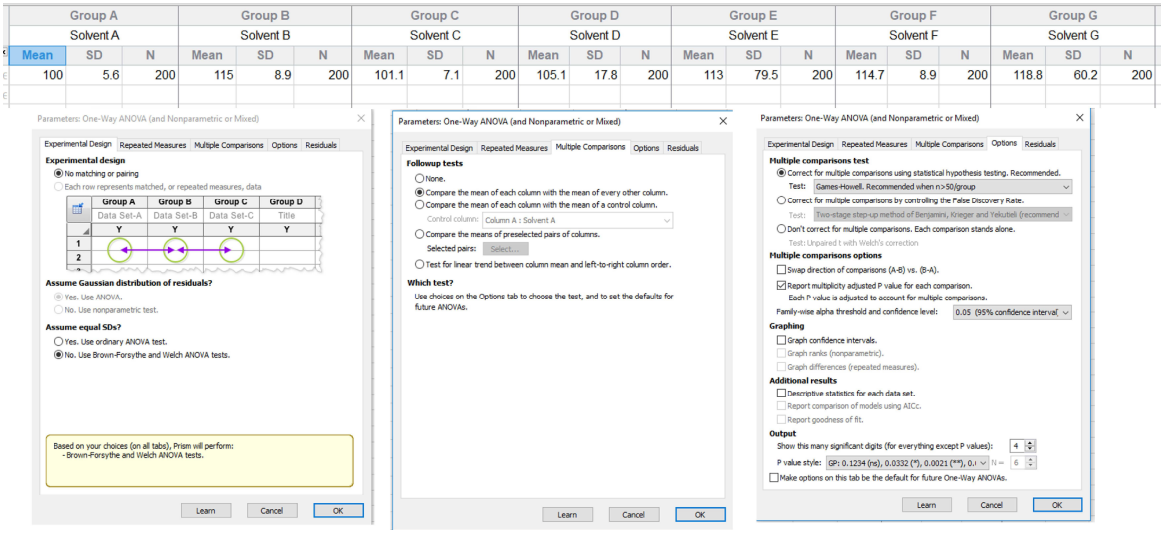


Figure 4.8: Input of Prism with the mean capture cost, standard deviation and sample size of solvents A-G (see Tab. 4.3). Three columns each represent the input for one solvent. Also shown is selecting non-homogeneity of variance (left), mean of every solvent (middle), and Games-Howell with family-wide 95% confidence interval (right).

Post-hoc Test An ANOVA itself provides only the information if there are significant differences between the population but not which pair is statistically significant different. Performing post-hoc tests such as Tukey's Honestly-Significant Difference (Tukey's HSD) [594] or Games-Howell [582] identifies which differences are significant, delivering the same result as repeatedly running a t-test at lower error [580, 581]. Both post-hoc tests compare every mean with every other mean. Prism actually computes the Tukey-Kramer test, which allows for the possibility of unequal sample sizes. This has no further impact because all solvents have the same sample size $n = 200$. The q-value for Tukey's HSD test is

$$q_s = \frac{\mu_i - \mu_j}{SE} \tag{4.7}$$

with the mean $\mu_i > \mu_j$ and SE being the standard error of the sum of the means. If q is larger than the critical value q_α obtained from the distribution, then two compared means are said to be significantly different at level α. Tukey's HSD assumes: 1. independent data within and among the groups, 2. normally distributed data, 3. equal within-group variance across the solvents (homogeneity of variance). As with the Brown-Forsythe ANOVA, there is no evidence to support assuming homogeneous variance a-priori [593, 595], therefore, Tukey's HSD is not valid to use. Instead, Games-Howell for large sample sizes ($n > 50$) for two groups i and j fulfilling just the first and second assumptions is deployed.

$$
\begin{aligned}
\mu_i - \mu_j &> q_{s,k,df'} \\
t &= \frac{\bar{\mu}_i - \bar{\mu}_j}{\sqrt{\frac{s_i^2}{n_i} + \frac{s_j^2}{n_j}}} \\
SE &= \sqrt{\frac{1}{2}\left(\frac{s_i^2}{n_i} + \frac{s_j^2}{n_j}\right)} \\
df' &= \frac{\left(\frac{s_i^2}{n_i} + \frac{s_j^2}{n_j}\right)^2}{\frac{\left(\frac{s_i^2}{n_i}\right)^2}{n_i - 1} + \frac{\left(\frac{s_j^2}{n_j}\right)^2}{n_j - 1}} \\
CI &= \mu_i - \mu_j \pm t\sqrt{\frac{1}{2}\left(\frac{s_i^2}{n_i} + \frac{s_j^2}{n_j}\right)}
\end{aligned}
\tag{4.8}
$$

Equation 4.8 uses the standard error SE, degrees of freedom using Welch's correction df' (calculated by Welch-Satterthwaite equation) [596, 597], the t-value from Welch's test (see Eqn. 4.3, and p-values calculated using Tukey's studentised range $q_{t*\sqrt{2},k,df}$.

Games-Howell tests often report looser confidence intervals compared to Tukey's tests if applied to groups fulfilling all three of Tukey's HSD's assumptions [595] (*i.e.,* additionally homogeneity of variances holds true).

Figure 4.9 shows the results an ordinary one-way ANOVA with Tukey's HSD post-hoc test in Prism. Figure 4.10 shows the results running Welch's and Brown-Forsythe's ANOVA analysis with Games-Howell post-hoc test in Prism.

ANOVA results | Multiple comparisons

Ordinary one-way ANOVA
Multiple comparisons

1	Number of families	1							
2	Number of comparisons per family	21							
3	Alpha	0.05							
4									
5	**Tukey's multiple comparisons test**	**Mean Diff.**	**95.00% CI of diff.**	**Below threshold?**	**Summary**	**Adjusted P Value**			
6	Solvent A vs. Solvent B	-15.00	-26.44 to -3.564	Yes	**	0.0022	A-B		
7	Solvent A vs. Solvent C	-1.100	-12.54 to 10.34	No	ns	>0.9999	A-C		
8	Solvent A vs. Solvent D	-5.100	-16.54 to 6.336	No	ns	0.8443	A-D		
9	Solvent A vs. Solvent E	-13.00	-24.44 to -1.564	Yes	*	0.0142	A-E		
10	Solvent A vs. Solvent F	-14.70	-26.14 to -3.264	Yes	**	0.0029	A-F		
11	Solvent A vs. Solvent G	-18.80	-30.24 to -7.364	Yes	****	<0.0001	A-G		
12	Solvent B vs. Solvent C	13.90	2.464 to 25.34	Yes	**	0.0063	B-C		
13	Solvent B vs. Solvent D	9.900	-1.536 to 21.34	No	ns	0.1406	B-D		
14	Solvent B vs. Solvent E	2.000	-9.436 to 13.44	No	ns	0.9986	B-E		
15	Solvent B vs. Solvent F	0.3000	-11.14 to 11.74	No	ns	>0.9999	B-F		
16	Solvent B vs. Solvent G	-3.800	-15.24 to 7.636	No	ns	0.9581	B-G		
17	Solvent C vs. Solvent D	-4.000	-15.44 to 7.436	No	ns	0.9465	C-D		
18	Solvent C vs. Solvent E	-11.90	-23.34 to -0.4637	Yes	*	0.0352	C-E		
19	Solvent C vs. Solvent F	-13.60	-25.04 to -2.164	Yes	**	0.0083	C-F		
20	Solvent C vs. Solvent G	-17.70	-29.14 to -6.264	Yes	***	0.0001	C-G		
21	Solvent D vs. Solvent E	-7.900	-19.34 to 3.536	No	ns	0.3900	D-E		
22	Solvent D vs. Solvent F	-9.600	-21.04 to 1.836	No	ns	0.1679	D-F		
23	Solvent D vs. Solvent G	-13.70	-25.14 to -2.264	Yes	**	0.0076	D-G		
24	Solvent E vs. Solvent F	-1.700	-13.14 to 9.736	No	ns	0.9995	E-F		
25	Solvent E vs. Solvent G	-5.800	-17.24 to 5.636	No	ns	0.7465	E-G		
26	Solvent F vs. Solvent G	-4.100	-15.54 to 7.336	No	ns	0.9399	F-G		
27									
28	**Test details**	**Mean 1**	**Mean 2**	**Mean Diff.**	**SE of diff.**	**n1**	**n2**	**q**	**DF**
29	Solvent A vs. Solvent B	100.0	115.0	-15.00	3.873	200	200	5.477	1393
30	Solvent A vs. Solvent C	100.0	101.1	-1.100	3.873	200	200	0.4016	1393
31	Solvent A vs. Solvent D	100.0	105.1	-5.100	3.873	200	200	1.862	1393
32	Solvent A vs. Solvent E	100.0	113.0	-13.00	3.873	200	200	4.747	1393
33	Solvent A vs. Solvent F	100.0	114.7	-14.70	3.873	200	200	5.367	1393
34	Solvent A vs. Solvent G	100.0	118.8	-18.80	3.873	200	200	6.864	1393
35	Solvent B vs. Solvent C	115.0	101.1	13.90	3.873	200	200	5.075	1393

Figure 4.9: Output of running an ordinary one-way ANOVA with Tukey's HSD post-hoc test for solvents A-G.

The p-values displayed in row 6 and 11 in Fig. 4.9 and Fig. 4.10 test the null hypothesis that the capture cost from solvents A-G are from a population with identical mean capture cost and represent the chance that random sampling returns the calculated costs. Small p-values mean that it is unlikely that the differences between solvents are due to random sampling. If $p-\text{value} < \alpha$ then the hypothesis that solvents A-G have an identical mean is rejected. If the null hypothesis is rejected then the test only confirms that at least one mean capture cost differs from the rest. Also shown in Fig. 4.9 and Fig. 4.10 are W, $F^{\star}$, df and a Yes/No indicator if the null hypothesis can be rejected for both tests.

The first column lists the pair that is being compared, followed by the difference in mean capture cost, 95% confidence interval of the mean capture cost difference, and a Yes/No indicator if the adjusted p-value in the second column from the right is below the significance level α. The 'Summary' column indicates the difference between the adjusted p-value and $\alpha = 0.05$ in a non-numerical way, *e.g.,* row 23 DvG in Fig. 4.10 shows that the corrected $p-\text{value} = 0.036$ is just below 0.05. A stricter significance limit of *e.g.,* $\alpha = 3\%$ would cause this test to fail to

ANOVA results | Multiple comparisons

Brown-Forsythe and Welch ANOVA tests
Multiple comparisons

1	Number of families	1							
2	Number of comparisons per family	21							
3	Alpha	0.05							
4									
5	**Games-Howell's multiple comparisons test**	**Mean Diff.**	**95.00% CI of diff.**	**Below threshold?**	**Summary**	**Adjusted P Value**			
6	Solvent A vs. Solvent B	-15.00	-17.21 to -12.79	Yes	****	<0.0001	A-B		
7	Solvent A vs. Solvent C	-1.100	2.995 to 0.7954	No	ns	0.6028	A C		
8	Solvent A vs. Solvent D	-5.100	-9.024 to -1.176	Yes	**	0.0027	A-D		
9	Solvent A vs. Solvent E	-13.00	-29.78 to 3.785	No	ns	0.2459	A-E		
10	Solvent A vs. Solvent F	-14.70	-16.91 to -12.49	Yes	****	<0.0001	A-F		
11	Solvent A vs. Solvent G	-18.80	-31.53 to -6.068	Yes	***	0.0004	A-G		
12	Solvent B vs. Solvent C	13.90	11.51 to 16.29	Yes	****	<0.0001	B-C		
13	Solvent B vs. Solvent D	9.900	5.722 to 14.08	Yes	****	<0.0001	B-D		
14	Solvent B vs. Solvent E	2.000	-14.85 to 18.85	No	ns	0.9998	B-E		
15	Solvent B vs. Solvent F	0.3000	-2.338 to 2.938	No	ns	0.9999	B-F		
16	Solvent B vs. Solvent G	-3.800	-16.61 to 9.012	No	ns	0.9748	B-G		
17	Solvent C vs. Solvent D	-4.000	-8.027 to 0.02665	No	ns	0.0528	C-D		
18	Solvent C vs. Solvent E	-11.90	-28.71 to 4.909	No	ns	0.3517	C-E		
19	Solvent C vs. Solvent F	-13.60	-15.99 to -11.21	Yes	****	<0.0001	C-F		
20	Solvent C vs. Solvent G	-17.70	-30.46 to -4.936	Yes	**	0.0010	C-G		
21	Solvent D vs. Solvent E	-7.900	-25.04 to 9.244	No	ns	0.8165	D-E		
22	Solvent D vs. Solvent F	-9.600	-13.78 to -5.422	Yes	****	<0.0001	D-F		
23	Solvent D vs. Solvent G	-13.70	-26.90 to -0.4975	Yes	*	0.0363	D-G		
24	Solvent E vs. Solvent F	-1.700	-18.55 to 15.15	No	ns	>0.9999	E-F		
25	Solvent E vs. Solvent G	-5.800	-26.70 to 15.10	No	ns	0.9826	E-G		
26	Solvent F vs. Solvent G	-4.100	-16.91 to 8.712	No	ns	0.9632	F-G		
27									
28	**Test details**	**Mean 1**	**Mean 2**	**Mean Diff.**	**SE of diff.**	**n1**	**n2**	**t**	**DF**
29	Solvent A vs. Solvent B	100.0	115.0	-15.00	0.7435	200	200	20.17	335.2
30	Solvent A vs. Solvent C	100.0	101.1	-1.100	0.6394	200	200	1.720	377.5
31	Solvent A vs. Solvent D	100.0	105.1	-5.100	1.319	200	200	3.865	238.0
32	Solvent A vs. Solvent E	100.0	113.0	-13.00	5.635	200	200	2.307	201.0
33	Solvent A vs. Solvent F	100.0	114.7	-14.70	0.7435	200	200	19.77	335.2
34	Solvent A vs. Solvent G	100.0	118.8	-18.80	4.275	200	200	4.397	202.4
35	Solvent B vs. Solvent C	115.0	101.1	13.90	0.8050	200	200	17.27	379.3

Figure 4.10: Output of running Welch's and Brown-Forsythe's ANOVA analysis with Games-Howell post-hoc test for solvents A-G

reject.

Table 4.4 summarises the results of running the three statistical test approaches on solvents A-G. Running multiple two-sample, two-tailed t-tests wrongly rejected the null hypothesis three times (A-E, C-D, C-E). The test resulted in statistical significance saying those three solvents are not equal, when in fact, there is no evidence to suggest this. That means three type I error occurred. The false discovery rate could be reduced by decreasing α, however, running a significant number of t-tests will always increase the likelihood of type I errors to occur.

The one-way ANOVA with Tukey's HSD post-hoc falsely rejects the null hypothesis for solvent pairs A-E and C-E (type I error) and falsely fails to reject for pairs A-D, B-D, and D-F (type II error). This is because the one-way ANOVA with Tukey's HSD post-hoc assumes equal variance for all solvents which is not the case (see Tab. 4.2). The difference in variance is larger for pairs A-E, C-E, A-D, and B-D. This example demonstrates that selecting an appropriate

statistical test matters for ranking solvents. The default method is a Welch's ANOVA with Games-Howell post-hoc test.

Table 4.4: Comparing the results of running multiple two-sample, two-tailed t-tests, one-way ANOVA with Tukey's HSD post-hoc, and Welch's ANOVA with Games-Howell post-hoc for solvents A-G (see Tab. 4.2). Yes = null hypothesis rejected *i.e.,* solvents rank not equally. No = fail to reject null hypothesis ≠ solvents rank same (no statistical evidence). Only the test on the right is valid. Type I errors are underlined and type II errors double underlined.

Comparison	Multiple t-test	One-way ANOVA + Tukey's HSD	Welch's ANOVA + Games-Howell
A-B	Yes	Yes	Yes
A-C	No	No	No
A-D	Yes	No	Yes
A-E	Yes	Yes	No
A-F	Yes	Yes	Yes
A-G	Yes	Yes	Yes
B-C	Yes	Yes	Yes
B-D	Yes	No	Yes
B-E	No	No	No
B-F	No	No	No
B-G	No	No	No
C-D	Yes	No	No
C-E	Yes	Yes	No
C-F	Yes	Yes	Yes
C-G	Yes	Yes	Yes
D-E	No	No	No
D-F	Yes	No	Yes
D-G	Yes	Yes	Yes
E-F	No	No	No
E-G	No	No	No
F-G	No	No	No

4.4 Impact of Modelling Approach on Ranking

This section discusses the impact of assumptions taken in the inferential analysis and thermodynamic modelling. They are the number of samples n used in the GSA's Monte-Carlo calculation, the selection of errors as input for the GSA, and lastly utilising random packings instead of structured packings.

The number of samples n used in the Monte-Carlo calculation within the GSA in gPROMS has to be larger than 50 due to the Games-Howell post-hoc test. There is no generic formula to determine the optimum number of samples. The number of samples was varied for five solvents (MEA, DEA, MDEA, AMP, PZ) at their individual optimal operating conditions for $y_{CO_2} = 4$ mol%. Figure 4.11 shows the mean capture cost over increasing number of samples n. The mean capture costs per solvent do not fluctuate much and the maximum relative difference is less than 0.1%. This is due to the already relatively large number of samples $n > 50$. The standard deviation reduced on average by less than 3% for the five solvents between $n = 50$ and $n = 800$. Wang *et. al.*, [598] demonstrate the variance of a mean over n is specific for the process modelled. True convergence for cases with high variance over n can be tested by using Richardson's method [599] in which n is continuously doubled. Increasing $n > 200$ does not further improve the inferential analysis in a statistical significant way.

The inferential analysis depends on the standard deviation of the capture cost which in turn depends on the error input of the thermo-physical properties into the GSA. In the following, approaches (see Tab. 4.5) are analysed and any potential impact on the inferential analysis discussed. The approaches differ in how specific they treat differences in the properties, methods deployed to derive the thermo-physical properties, and solvents. The default approach (total in Tab. 4.5) uses errors that are specific for each thermo-physical property and averaged over all studies regardless of the method deployed or aqueous amine solvent involved. This method will have the largest sample size and any outliers will be averaged out. Other approaches (Exp. and Pred. in Tab. 4.5) only differ by limiting the pool of studies by the category of method distinguishing only between experimentally or computationally derived thermo-physical

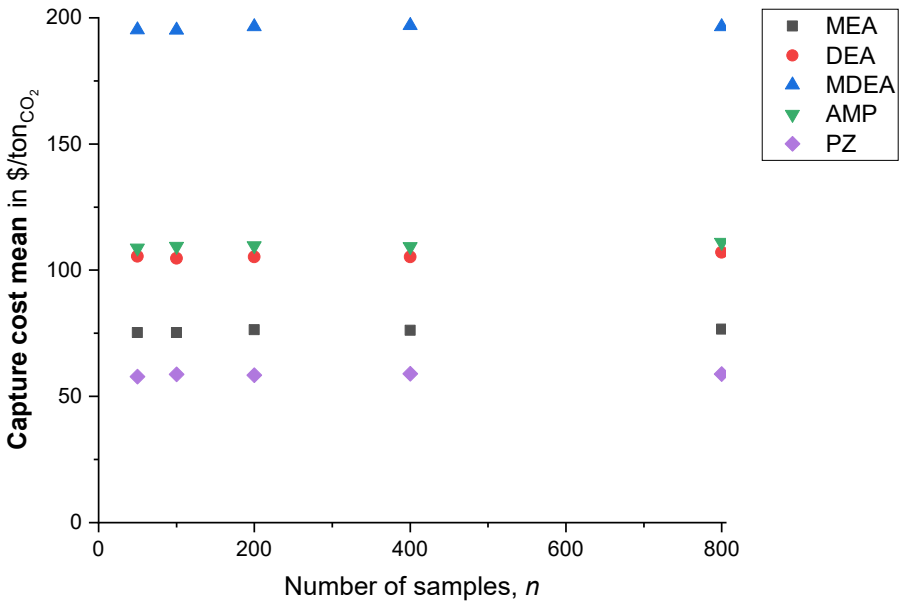


Figure 4.11: Impact of number of samples n used in Monte-Carlo calculation within the Global System Analysis in gPROMS. Default $n = 200$. $n > 50$ required for Games-Howell post-hoc test.

properties. These approaches use fewer studies thus are more prone to outliers. Using a solvent-unique set of errors requires all properties with their errors to be reported in the literature and restricts that method to those solvents only. An advantage is that the calculation process would be simplified as an error reported in the literature would be directly fed into the GSA. Using an uniform error regardless of property, solvent, or method loses any insight into the differences but requires minimal effort.

Table 4.5: Examples of selecting an approach to the error input into the GSA including advantages and disadvantages.

Option	Property	Method	Solvent	Advantage	Disadvantage
Total	Each property	All methods averaged	All solvents equal	Input data is based on larger sample size and potential outliers are identified.	
Exp	Each property	Just experimental methods averaged	All solvents equal	On average lowest error uncertainty	Based on smaller number of studies.
Pred	Each property	Just computational methods averaged	All solvents equal	Enables new compounds to be screened	Based on smaller number of studies
Unique	Each property	Unique from reference	Solvent unique	Direct connection between property method and capture cost error	Not possible to calculate if no error has been reported and outliers might go undetected
Uniform	All properties equal	All methods averaged over all properties	All solvents equal	Minimal effort	Difference between properties and methods is lost

The overall differences in error means and deviations appear small with a few exceptions (see Tab. 4.1). The collected studies suggest that differences in error are caused by the method and property but not by the solvents. The difference in error for ΔH_{Abs} using all samples (4.7%) versus using only predictions (25%) is close to 20%. The GSA would run the Monte-Carlo calculation in a much wider range resulting in larger standard deviations for the capture cost. This could lead to failing to reject the null hypothesis, thus, not being able to distinguish between solvents.

The null hypothesis is that the error selection does not impact the solvent ranking. That means the difference between the approaches is zero. For this, two Welch's ANOVA followed by Games-Howell post-hoc tests are run per solvent. Once between a solvent using the full (full) dataset and just experimental (exp). And another time between the same solvent using the full (full) dataset and just predicted data (pred). The output of the GSA (= required input for the inferential analysis) for five solvents (MEA, DEA, MDEA, AMP, PZ) at their individual optimal operating conditions for $y_{\mathrm{CO_2}} = 4$ mol% is shown in Tab. 4.6. As expected, all three approaches lead to nearly identical capture cost means for all solvents. The standard deviation using the experimental dataset is smallest for all solvents due to the input data (see Tab. 4.1) being almost half of the full data set.

Table 4.7 shows the results of the inferential analysis. All tests fail to reject, which means there is no evidence to support that the capture cost means calculated by the different approaches are not equal. There is no evidence to support that the different approaches (and potentially larger standard deviations) impact the outcome of the inferential analysis. Therefore, the default approach of using the maximum number of studies is valid. While desired for other applications, it appears not necessary to increase the accuracy / reduce the errors of thermophysical properties for the purpose of screening solvents within this work. This work found no impact on the inferential analysis even when the error input for the GSA was increased to 25% for every property. There is no evidence to suggest that the error ranges derived from the literature (or even far beyond) limit the screening. Therefore, methods predicting thermophysical properties with higher uncertainties could deliver a valuable insight as the ranking will still be statistically significant.

Table 4.6: Capture cost means and standard deviations (StdDev) for five solvents at their individual optimal operating conditions for $y_{CO_2} = 4$ mol% with either using the full (Full) dataset of errors, just experimental methods (Exp), or just predictions (Pred). See Tab. 4.1 for values.

Solvent	Full		Exp		Pred	
$/t$_{CO_2}$	Mean	StdDev	Mean	StdDev	Mean	StdDev
MEA	76.5	1.4	76.5	0.7	76.5	2.0
DEA	105	2.6	105	1.6	105	3.1
MDEA	196	10.0	196	6.4	196	14.7
AMP	110	2.7	110	1.7	110	4.6
PZ	58.4	1.6	58.6	0.9	57.4	4.7

Table 4.7: Results of running Welch's ANOVA followed by Games-Howell post-hoc test for the input listed in Tab. 4.6. There is no statistical evidence to suggest that the results are not equal.

Solvent 1	Solvent 2	Outcome
MEA_{Full}	MEA_{Exp}	Failed to reject
MEA_{Full}	MEA_{Pred}	Failed to reject
DEA_{Full}	DEA_{Exp}	Failed to reject
DEA_{Full}	DEA_{Pred}	Failed to reject
$MDEA_{Full}$	$MDEA_{Exp}$	Failed to reject
$MDEA_{Full}$	$MDEA_{Pred}$	Failed to reject
AMP_{Full}	AMP_{Exp}	Failed to reject
AMP_{Full}	AMP_{Pred}	Failed to reject
PZ_{Full}	PZ_{Exp}	Failed to reject
PZ_{Full}	PZ_{Pred}	Failed to reject

Two more comparisons were calculated for the five solvents and again found no statistical significant impact on the inferential analysis: 1) Using a unique (random) set of errors, *e.g.,* using specific values reported in the literature (see Tab. D.1), and 2) using the standard deviation calculated in the data fitting from Origin. For both methods, the mean errors differed to the default by $< 0.2\%$ and the standard deviation by $< 45\%$. All hypothesis tests failed to reject, again indicating that there is no sufficient evidence to suggest that they are not equal.

Structured packings are known for their cost effectiveness due to their improved heat and mass transfer efficiency and reduced pressure drop [298, 600]. They are more expensive compared to random packings [299, 601]. The impact of selecting a structured packing instead random packing is analysed by utilising Mellapak 2X (see Tab. 3.9) for five solvents for which the correlations are valid. Mellapak 2X was selected because it has been tested in columns with up to 15 m diameter [498]. The operating parameter have been optimised leading to differences in conditions between the packings. Welch's ANOVA followed by Games-Howell post-hoc test is run for the null hypothesis that there is no difference in capture costs between the packings.

Table 4.8: Statistical test input (capture cost mean and standard deviation StdDev) and result of Welch's ANOVA for comparing five solvents with random and structured packings.

Solvent	Random		Structured		Result
$\$/t_{CO_2}$	Mean	StdDev	Mean	StdDev	
MEA	77.8	2.4	77.1	2.2	Failed to reject
DEA	106.5	2.6	106.1	2.3	Failed to reject
MDEA	197.9	10.0	183.2	9.4	Rejected
AMP	111.2	2.7	109.6	2.7	Rejected
PZ	58.5	1.6	58.3	1.5	Failed to reject

All solvents' capture costs reduce by utilising the structured packing. The statistical tests failed to reject for MEA, DEA, and PZ. It rejected for MDEA and AMP, meaning that there is enough statistical evidence to suggest that the change in capture cost for MDEA and AMP is unlikely to have been observed by chance. This suggests that the packing selection does impact two out of the five solvents.

The main cost savings occurred in the absorber (stripper cost reduced only by $< 0.5\%$) because the wet packing area increased, the irrigated pressure drop decreased, and the superficial velocity also decreased. This leads to smaller required packing volume. The diameter shrinks (on average 17%) more than the height (average 2%). The optimal concentration and lean loading remained nearly constant suggesting that the packing selection strongly impacts the absorber column design. The solvent flowrate, as modelled, depends on the working capacity which is not directly affected by the packing.

The specific packing cost increased from \$1271/ft^3 to \$1758/ft^3 partially trading off the reduced size impact on the CAPEX. The absorber CAPEX decreased by 7% on average, and the stripper CAPEX reduced on average by 0.4%. The overall impact on the capture cost depends on the solvent. The absorber contributes for both MDEA and AMP more compared to MEA, DEA, and PZ. The absorber and stripper CAPEX contribution ranges from 5% for PZ, 9% for MEA, 15% for DEA, 21% for AMP and 36% for MDEA for the random packing. High-performing capture solvents are dominated by steam costs and the absorber contribution is relatively small. This trend is reversed for poorly performing solvents.

The results suggest that the packing selection has a statistically significant impact on poorly performing solvents. There is no evidence to suggest that the ranking for better performing solvents is impacted. The correlations used for the structured packing have smaller applicability compared to random packings. Random packings are the default, because of the ambition to screen through a wider thermo-physical property space. If, however, solvents of interest indicate larger absorber sizes, then structured packings will likely further improve the performance.

4.5 Ranking Aqueous Amines under Uncertainty

Table 4.9 and Tab. 4.10 summarise the mean, lower, and upper confidence interval, sample size and standard deviation for the five solvents at their individual optimal operating conditions for $y_{CO_2} = 4$ mol% and $y_{CO_2} = 12$ mol%. The 95% confidence intervals are calculated by adding or subtracting $\pm 1.96 \cdot \frac{s}{\sqrt{(200)}}$ from the mean capture cost (see Eqn. 2.6). The standard deviations differ between solvents and increase with increasing y_{CO_2}.

The confidence intervals appear relatively narrow, and are hard to see when plotted (see Fig. 4.12). This reflects an overall low impact of the uncertainty of the thermo-physical properties on the capture cost. The main reason is likely the limited error range (see Tab. 4.1) in combination with their direct impact as shown in [340] attributed to the process type. The values presented for the five solvents suggest that the error associated with thermo-physical properties does not prevent a statistical significant ranking.

Figure 4.12 shows the gap between solvents increasing and decreasing with some trends inter-

Table 4.9: Mean capture cost, standard deviation, sample size and the corresponding lower $CI_{95\%,L}$ and upper $CI_{95\%,U}$ confidence interval for five solvents at their individual optimal operating conditions for $y_{CO_2} = 4$ mol%.

$/t$_{CO_2}$	Mean	$CI_{95\%,L}$	$CI_{95\%,U}$	Standard deviation	Sample size
MEA	76.5	76.3	76.7	1.45	200
DEA	105.3	104.9	105.6	2.58	200
MDEA	196.5	195.1	197.9	10.0	200
AMP	109.7	109.3	110.1	2.70	200
PZ	58.4	58.2	58.7	1.63	200

Table 4.10: Mean capture cost, standard deviation, sample size and the corresponding lower $CI_{95\%,L}$ and upper $CI_{95\%,U}$ confidence interval for five solvents at their individual optimal operating conditions for $y_{CO_2} = 12$ mol%.

$/t$_{CO_2}$	Mean	$CI_{95\%,L}$	$CI_{95\%,U}$	Standard deviation	Sample size
MEA	60.6	60.3	60.9	2.19	200
DEA	75.5	75.1	75.8	2.35	200
MDEA	90.5	89.2	91.8	9.45	200
AMP	70.2	69.8	70.5	2.46	200
PZ	47.0	46.8	47.2	1.47	200

secting each other. The mean capture cost of MDEA and DEA as well as AMP and DEA are intersecting. Running a Welch's ANOVA with Games-Howell post-hoc test at various y_{CO_2} values will establish the statistical significance of the ranking. It is interesting to see at what point the statistical test indicates when MDEA and DEA or AMP and DEA cannot be differentiated any more. The results are listed in Tab. 4.11. The null hypothesis is rejected for nearly all combinations, meaning there is sufficient statistical evidence to suggest that the solvents are not equal. As expected, the test fails to reject DEA vs MDEA for $y_{CO_2} = 22.5$ mol% and $y_{CO_2} = 25$ mol%. The null hypothesis fails to reject $y_{CO_2} = 20$ mol% and $y_{CO_2} = 30$ mol%. This example suggests that small differences in the mean capture cost of $\approx$ $/t$_{CO_2}$ can already be differentiated with statistical significance.

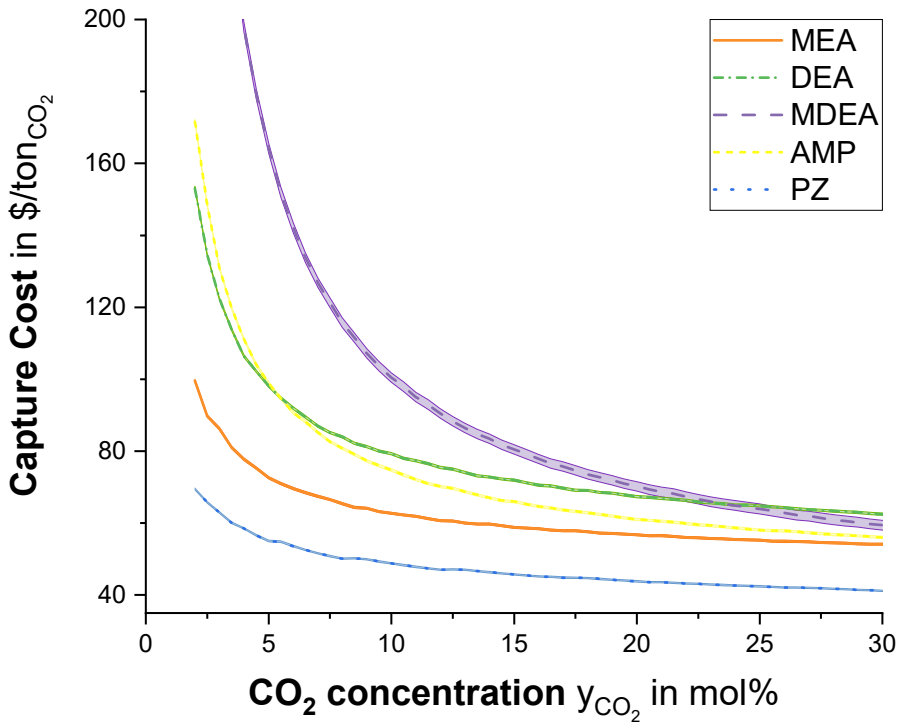


Figure 4.12: Impact of changing flue gas CO_2 composition (y_{CO_2} = 2mol% to y_{CO_2} = 30mol%) on capture cost for five aqueous amine solvents utilised at their optimal concentration and operating conditions. The coloured area correspond to the 95% confidence interval and the mean capture cost is shown as a line.

Table 4.11: Result of Welch's ANOVA with Games-Howell post-hoc test for solvents at varying y_{CO_2}. Yes = null hypothesis is rejected, *i.e.*, solvents are not equal with statistical significance.

y_{CO_2} =	5%	10%	15%	20%	22.5%	25%	30%
MEA vs. DEA	Yes	Yes	Yes	Yes	Yes	Yes	Yes
MEA vs. MDEA	Yes	Yes	Yes	Yes	Yes	Yes	Yes
MEA vs. AMP	Yes	Yes	Yes	Yes	Yes	Yes	Yes
MEA vs. PZ	Yes	Yes	Yes	Yes	Yes	Yes	Yes
DEA vs. MDEA	Yes	Yes	Yes	Yes	*No*	*No*	Yes
DEA vs. AMP	*No*	Yes	Yes	Yes	Yes	Yes	Yes
DEA vs. PZ	Yes	Yes	Yes	Yes	Yes	Yes	Yes
MDEA vs. AMP	Yes	Yes	Yes	Yes	Yes	Yes	Yes
MDEA vs. PZ	Yes	Yes	Yes	Yes	Yes	Yes	Yes
AMP vs. PZ	Yes	Yes	Yes	Yes	Yes	Yes	Yes

4.6 Conclusions

Ranking aqueous amines based on their techno-econonomic performance is highly desirable, however, it was not yet known if the uncertainty that propagates through such screening tools

prevents reaching statistically significant results. In this work, errors associated with therm-physical properties of CO_2 capture solvents were collected and mean errors with standard deviations calculated. These were then propagated through the model using a Monte-Carlo approach implemented in the Global System Analysis of gPROMS. The solvents' mean capture cost and standard deviations were finally used in statistical tests. Three hypothesis testing methods (Multiple *t*-testing, Welch's ANOVA with Tukey's post-hoc, Welch's ANOVA with Games-Howell post-hoc) have been compared with the only valid method to compare multiple solvents being Welch's analysis of variance followed by a Games-Howell post-hoc test. Various sensitivities such as the number of samples in the Monte-Carlo calculation, approach to selecting the input errors, or selecting a column packing were discussed. There is evidence to suggest that selecting random packings over structured ones leads to a statistical significant disadvantage for poorly performing solvents with large column sizes. The performance difference between those affected solvents and the ones of special interest is comfortably large. If, however, that difference becomes smaller, then a reassessment should take place. Being able to model more potential solvents is judged to outweigh the downside of disadvantaging poor performers. The presented approach is not exclusive to this work and could be applied to any *in-silico* screening.

In conclusion, screening solvents under uncertainty and obtaining statistically significant results is demonstrated. There is no statistical evidence to suggest that the differences in error means caused by thermo-physical properties impacts the solvent ranking. The results suggest that typical errors for solvents' input data do not cause statistical relevant concerns. Methods with higher uncertainty could, therefore, deliver valuable insights at statistically significant confidence. Most solvents (96%) calculated by the model can be accurately differentiated with statistical significance even at relatively low differences in mean capture cost of $\approx \$2/t_{CO_2}$.

5. Techno-economic Screening of CO_2 Capture Solvents

5.1 Objectives

The aim of this section is to rank candidate solvents based on their techno-economic performance. Trends in performance should be identified and linked to the capture cost. The impact of amine concentration, CO_2 concentration, and steam prices on the ranking will be investigated. Links between thermo-physical properties such as molar mass, or pK_a and process KPIs such as working capacity and specific reboiler duty are to be analysed.

5.2 Ranking Aqueous Amines

This section discusses the default ranking of the candidate solvents, its statistical significance, the cost breakdown, and any potential impact of screening at constant (arbitrarily) selected weight or mole fraction.

Default Ranking The candidate solvents are ranked based on increasing (mean) capture costs for a typical gas-power flue gas with $y_{CO_2} = 4$ mol% (see Fig. 5.1). The 95% confidence intervals for each solvent are shown as error bars. The mean capture cost for each solvent is written above each bar. The capture cost for each solvent represents the minimum for a solvent-specific plant utilising each amine at solvent-specific concentration and process conditions. All solvents are modelled to capture the same amount of CO_2. The capture cost range from \$47/t_{CO_2} to well above \$100/t_{CO_2}. About 60% of the screened solvents have capture costs between \$50-\$100/t_{CO_2}. About 40% of the candidate solvents could be omitted from future work assuming that a cost-difference factor of two or more between them and the best performing solvents is sufficient. This ranking demonstrates the concept that filtering solvents by their

overall techno-economic performance is possible.

The best performing candidates are *bis*-APA, AEPz, DETA, and EDA which have all fast kinetics and high CO_2 capacity. The poorest performing solvents are TEDA, TIPA, NMM, and TEA which are limited by slow kinetics and low CO_2 capacity.

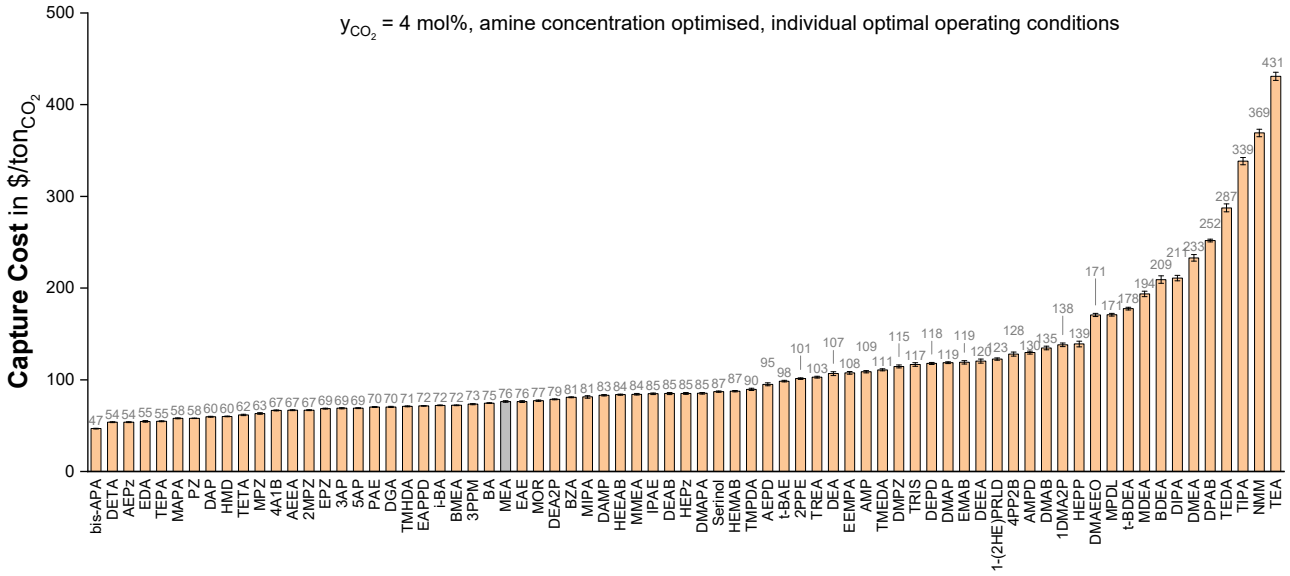


Figure 5.1: Screened solvents ranked by their capture cost for a gas-power flue gas y_{CO_2} = 4 mol%. Each solvent is utilised at their individual optimal operating conditions and concentration in their individually optimally sized plant while capturing the same amount of CO_2. 95% confidence intervals shown as error bars.

Statistical Significance The error bars represent the 95% confidence intervals caused by errors in the thermo-physical properties. The statistical significance test (Welch's ANOVA followed by Games-Howell post-hoc test) analysed all screened solvents at their optimal concentration and rejected the null hypothesis 2516 times. This means that for 2516 comparisons between two solvents the difference in capture cost being zero is unlikely to have been observed by chance, *i.e.,* the results suggest with statistical confidence that these pairs are not equal. The null hypothesis failed to reject 112 times (4% of all comparisons) meaning there is no statistical evidence to suggest that these pairs are not equal. Figure 5.2 shows the distribution of the failed rejections for the top 20 ranked solvents. The test rejects the null hypothesis for solvents ranked with a difference in capture cost of >5%, and fails only solvents ranked next to each other.

	bis-APA	DETA	AEPz	EDA	TEPA	MAPA	PZ	DAP	HMD	TETA	MPZ	4A1B	AEEA	2MPZ	EPZ	3AP	5AP	PAE	DGA	TMHDA
bis-APA	X	Yes	Yes	Yes	Yes	Yes	Yes	Yes	Yes	Yes	Yes	Yes	Yes	Yes	Yes	Yes	Yes	Yes	Yes	Yes
DETA		X	No	No	No	Yes	Yes	Yes	Yes	Yes	Yes	Yes	Yes	Yes	Yes	Yes	Yes	Yes	Yes	Yes
AEPz			X	No	No	Yes	Yes	Yes	Yes	Yes	Yes	Yes	Yes	Yes	Yes	Yes	Yes	Yes	Yes	Yes
EDA				X	No	Yes	Yes	Yes	Yes	Yes	Yes	Yes	Yes	Yes	Yes	Yes	Yes	Yes	Yes	Yes
TEPA					X	Yes	Yes	Yes	Yes	Yes	Yes	Yes	Yes	Yes	Yes	Yes	Yes	Yes	Yes	Yes
MAPA						X	No	Yes	Yes	Yes	Yes	Yes	Yes	Yes	Yes	Yes	Yes	Yes	Yes	Yes
PZ							X	Yes	Yes	Yes	Yes	Yes	Yes	Yes	Yes	Yes	Yes	Yes	Yes	Yes
DAP								X	No	Yes	Yes	Yes	Yes	Yes	Yes	Yes	Yes	Yes	Yes	Yes
HMD									X	Yes	Yes	Yes	Yes	Yes	Yes	Yes	Yes	Yes	Yes	Yes
TETA										X	No	Yes	Yes	Yes	Yes	Yes	Yes	Yes	Yes	Yes
MPZ											X	Yes	Yes	Yes	Yes	Yes	Yes	Yes	Yes	Yes
4A1B												X	No	No	Yes	Yes	Yes	Yes	Yes	Yes
AEEA													X	No	Yes	Yes	Yes	Yes	Yes	Yes
2MPZ														X	Yes	Yes	Yes	Yes	Yes	Yes
EPZ															X	No	No	Yes	Yes	Yes
3AP																X	No	No	No	Yes
5AP																	X	No	No	Yes
PAE																		X	No	No
DGA																			X	No
TMHDA																				X

Figure 5.2: Results for Welch's ANOVA followed by Games-Howell post-hoc test for the top 20 solvents. Yes = null hypothesis is rejected, *i.e.,* solvents are not equal. No = failed to reject, *i.e.,* there is no evidence to support that they are equal.

bis-APA ranks with statistical significance better than the next best solvents. The tests fail to reject for the second best solvent DETA with AEPz, EDA, and TEPA. This means DETA can be differentiated from *bis*-APA but not from AEPz, EDA, and TEPA, thus, multiple solvents rank second. The tests for AEPz, EDA, and TEPA also fail to reject, *i.e.,* four solvents cannot be distinguished from each other with statistical significance. MAPA is the next-best solvent that can be differentiated from the pool of solvents with statistical significance. Figure 5.3 shows the interpretation for the bottom end of the top 20 for EPZ, 3AP, 5AP, PAE, DGA, and TMHDA. Those solvents fail to reject the null hypothesis (see Fig. 5.2) leading to some solvent pairs not being able to be differentiated with statistical significance. The coloured areas represent a shared rank.

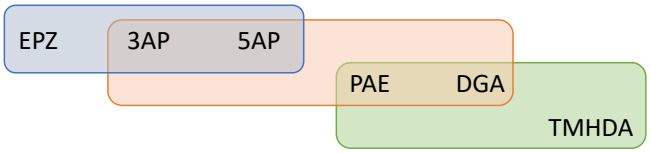


Figure 5.3: Example of some solvents sorted into ranks with statistical significance.

The ranking (see Fig. 5.1) demonstrates that the vast majority of solvents can be successfully ranked with statistical significance, although some solvents cannot be differentiated.

Cost Breakdown The breakdown of capital and operating costs for a gas-power flue gas $y_{CO_2} = 4$ mol% is shown in Fig. 5.4 (matching to the ranking previously presented in Fig. 5.1). Contributions to the CAPEX (coloured areas with a pattern) are broken down to the absorber, stripper, heat exchangers, and other. Contributions to the OPEX (coloured area without a pattern) are broken down to steam, maintenance, cooling, and other OPEX. All capture cost are normalised to 100%, *i.e.,* the same percentage of a poor performing solvent results in a higher $\$/t_{CO_2}$ value compared to a better performing solvent.

The capture costs are dominated by the operating expenditure, in particular by steam costs, for most solvents. The capture costs for the ten poorest performing solvents (except NMM) are dominated by capital expenditure (*i.e.,* sum of absorber, stripper, heat exchangers and other CAPEX in Fig. 5.4). Maintenance cost is a linear function of equipment size, thus scales with the CAPEX. The steam cost is the largest cost contribution for 54 solvents, which also have the lowest capture costs. The absorber cost dominates the remaining 19 solvents (towards the right in Fig. 5.4). This shows that low capture cost are a consequence of smaller equipment sizes which reduce capital expenditure. The focus should be on the dominating steam cost by *e.g.,* optimising process design or topology to further reduce costs of the better performing solvents. Measures aiming at further reducing the absorber size will not be most cost-effective for these solvents.

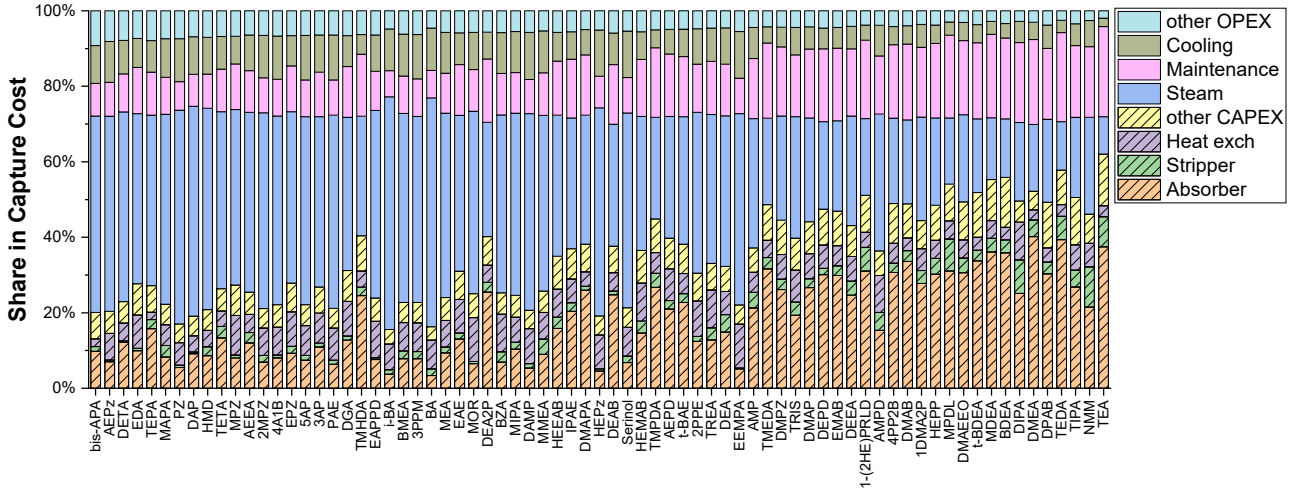


Figure 5.4: Capture cost breakdown for a typical gas-power flue gas $y_{CO_2} = 4$ mol% normalised to 100% for each solvent. See Fig. 5.1 for absolute values. Best performing solvents are dominated by steam cost, and most poor performers dominated by absorber cost.

Screening at Constant Concentration Previous screening studies assumed constant concentration of the amine. These include some of the most relevant screening studies so far with [187, 197, 223, 224, 229, 242, 245, 602–606] (see Tab. A.1 for full list). These studies either ubiquitously selected $w_{\text{Amine}} = 30$ wt%, or derived a constant concentration through a limited optimisation. The amine weight fraction is widely used as a measure for the concentration, because of its historic context and the fact that amines are bought by weight. A third of the screening studies presented in Fig. 2.2 used a constant weight fraction (especially $w_{\text{Amine}} = 30$ wt%) as a basis. Some studies [233, 607] imposed a limit on the amine concentration due to constraints caused by increased viscosity of the authors' preferred solvent. However, this limit might not be justified for other candidate solvents, therefore, systematically disadvantaging other candidate solvents. This questions if comparing amines at constant concentration matters for screening, because it might systematically impact the ranking.

There are multiple concentration-like metrics that could be used (see some examples below):

- Weight fraction w_{Amine} (amines are bought per weight)
- Mole fraction x_{Amine} (due to reaction stoichiometry)
- Alkalinity (number of amine groups per molecule)
- Nucleophilicity (reaction driving force, Lewis acid)
- Acid dissociation constant pK_a (reaction driving force, Brønsted acid)
- Volumetric flow rate of solvent (due to equipment design linked to the volumetric flow rate)

Some metrics are based on practical aspects such as weight or mole fraction, and others based on the chemistry or equipment sizing. They ultimately all describe the concentration of amine in the solvent. Screening solvents at constant concentration (regardless of the metric) will inevitably introduce a bias towards some amines, *e.g.,* favouring lighter or heavier amines.

Figure 5.5 shows the result of three screenings per solvent that differ in amine's concentration $w_{\text{Amine}} = 30$ wt% (pink), $x_{\text{Amine}} = 11$ mol% (blue), or individually optimised concentration (grey). The mole fraction $x_{\text{Amine}} = 11$ mol% was selected reflecting that 30 wt% MEA is approximately 11.2 mol%. The bars represent the capture cost for each solvent and are sorted

by increasing capture cost using the optimised concentration (grey). The logarithmic scale makes the differences between the approaches for well performing solvents appear larger.

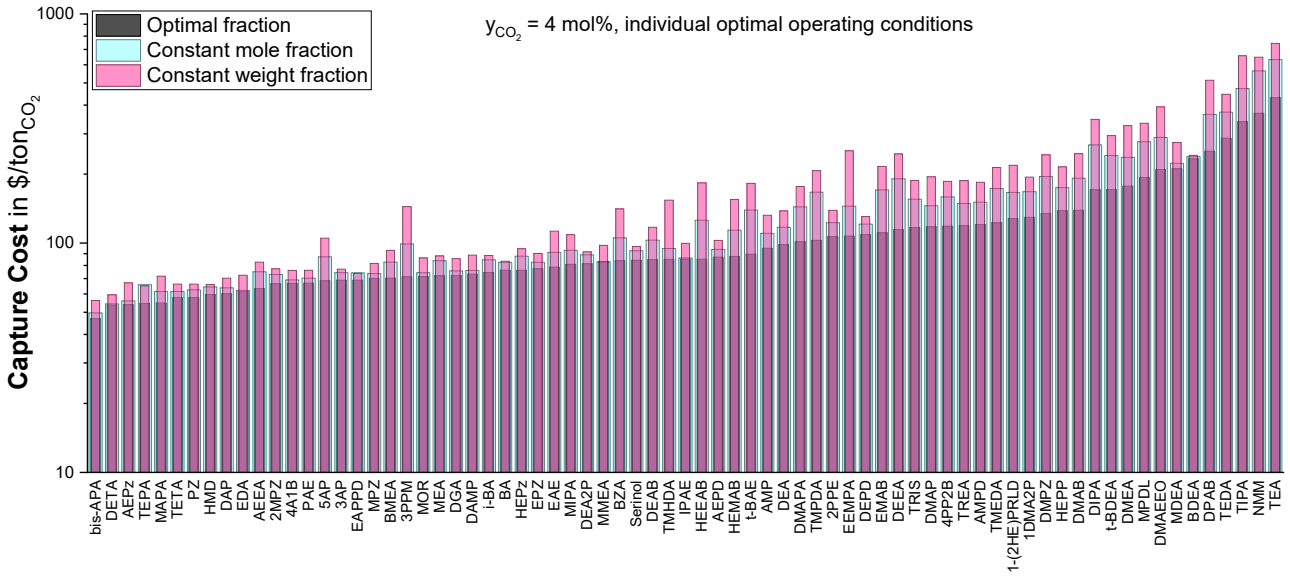


Figure 5.5: Impact of changing the basis for screening between optimised concentration (solvent-specific), constant mole fraction ($x_{\text{Amine}} = 11$ mol% for all solvents), or mass fraction ($w_{\text{Amine}} = 30$ kg%). The operating conditions and equipment sizes vary between the cases even for the same solvent.

Using a constant weight fraction (purple in Fig. 5.5) results in a different ranking compared to using a constant mole fraction (blue in Fig. 5.5) with all solvents returning higher capture costs. Screening solvents at a constant (arbitrarily set) mole fraction (or its equivalents molarity, or molality) does not provide the same ranking as the optimal fraction despite the chemical reaction with CO_2 being linked to the amine's stoichiometry. The capture cost differences per solvent between the approaches were tested on statistical significance. The null hypothesis was that the different approaches result in the same mean capture cost per solvent, *i.e.,* the differences do not matter. Welch's ANOVA followed by Games-Howell post-hoc tests were calculated as described in the previous chapter. All solvents except DMEA failed to reject the null hypothesis. There is statistical evidence to support that the different approaches lead to statistically significant impact on the capture cost. As the optimal concentration results in minimum capture costs for each solvent and is linked to the amine, screening studies should consider including amine concentration as an optimisation parameter. This work uses the cost-optimal concentration (grey in Fig. 5.5).

5.3 Impact of Flue Gas Composition

This section discusses the impact of the flue gas CO_2 concentration y_{CO_2} on the solvent ranking. Figure 5.6 shows the impact of flue gas CO_2 composition up to $y_{CO_2} = 30$ mol% on the capture cost for all screened solvents. Confidence intervals are removed for better readability. Typical CO_2 concentrations found in power and industry, *e.g.,* gas or coal-power, hydrogen, iron or steel are shown with dotted vertical lines. The chemical classes of the candidate amines are shown with the colour (primary = black, secondary = green, tertiary = blue, and poly = yellow).

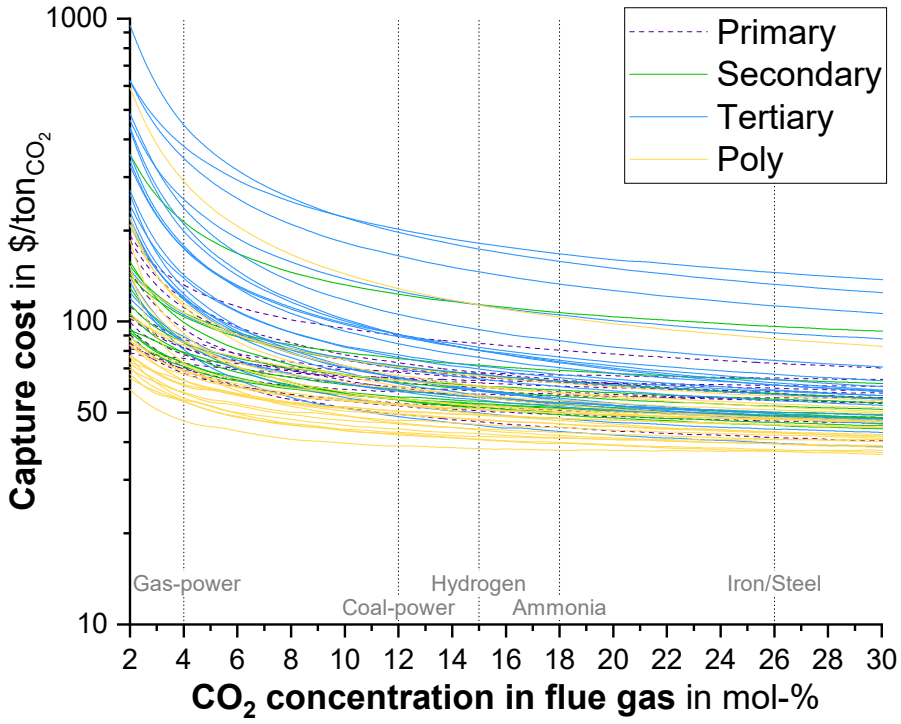


Figure 5.6: Impact of flue gas CO_2 composition ($y_{CO_2} = 2$ mol% to $y_{CO_2} = 30$ mol%) on capture cost. Chemical classes shown as colour. Typical applications are referenced with their flue gas compositions as vertical dotted lines.

The capture cost decreases non-linearly as y_{CO_2} increases. The change in capture cost is highest at $y_{CO_2} < 8$ mol% and flattens out for $y_{CO_2} > 20$ mol% for most solvents. The relative cost difference between the best performing solvents at $y_{CO_2} = 30$ mol% and $y_{CO_2} = 2$ mol% is approximately 33% $\left(\frac{\$53/t_{CO_2} - \$40/t_{CO_2}}{\$40/t_{CO_2}}\right)$. The same difference for the poor performing solvents is approximately 150% $\left(\frac{\$250/t_{CO_2} - \$100/t_{CO_2}}{\$100/t_{CO_2}}\right)$. The difference between the best and worst performing solvents is larger than the impact of the CO_2 concentration over the studied range.

Many poly amines are clustered towards lower capture costs while tertiary amines are clustered towards higher capture costs. The impact of y_{CO_2} on the capture cost is stronger for poorly performing solvents compared to the better performing ones. The solvents' ranking will change with CO_2 concentration (see in Fig. 5.7). Shown are three CO_2 concentrations $y_{CO_2} = 4$ mol% (top), $y_{CO_2} = 12$ mol% (middle), and $y_{CO_2} = 20$ mol% (bottom). The colour code for the chemical classes (see Fig. 5.6) is kept constant.

The differences in capture costs between the solvents reduce with increasing y_{CO_2}. The average relative difference in capture cost between two adjacent solvents is only 1.1% at $y_{CO_2} = 20$ mol%. This means that the solvent selection for industrial applications such as cement or steel might become less dependent on the predicted techno-economic performance. Figure 5.7 illustrates the change in solvent capture cost ranking for the chemical classes at varying flue gas CO_2 concentration. Many poly-amines (yellow) rank at low capture cost (towards the right), and many tertiary amines (blue) rank at higher-cost (towards the left), indicating a trend in chemical class. The reason for this cannot be pinned down to one single property but rather the combination of key properties.

Some solvents move up and down the ranking, but the ranking appears rather static. Seven out of ten solvents at the top and bottom of the overall ranking stay in a similar position over the full CO_2 concentration range. The Venn diagram Fig. 5.8 lists the solvents that remain in the top and bottom positions over the range of gas concentrations. Two CO_2 concentrations are shown with $y_{CO_2} = 4$ mol% (orange) and $y_{CO_2} = 30$ mol% (blue). DGA, TMHDA, and DEA2P are in the top ten solvents at high y_{CO_2} but suffer from higher capture cost increases with decreasing CO_2 concentration. This results in them not ranking inside the top ten at lower concentrations any more having been replaced by MPZ, HMD, and DAP respectively. Analogue to this, BA, DMAEEO, and AMPD suffered a smaller cost increase than their peers, resulting in BDEA, *t*-BDEA, and MDEA replacing them inside the bottom ten.

The results indicate that the CO_2 concentration has a significant impact on the capture cost. However, it has less impact on the ranking itself. The majority of solvents remain at their respective rank with few solvents moving up and down the order. This could allow reducing

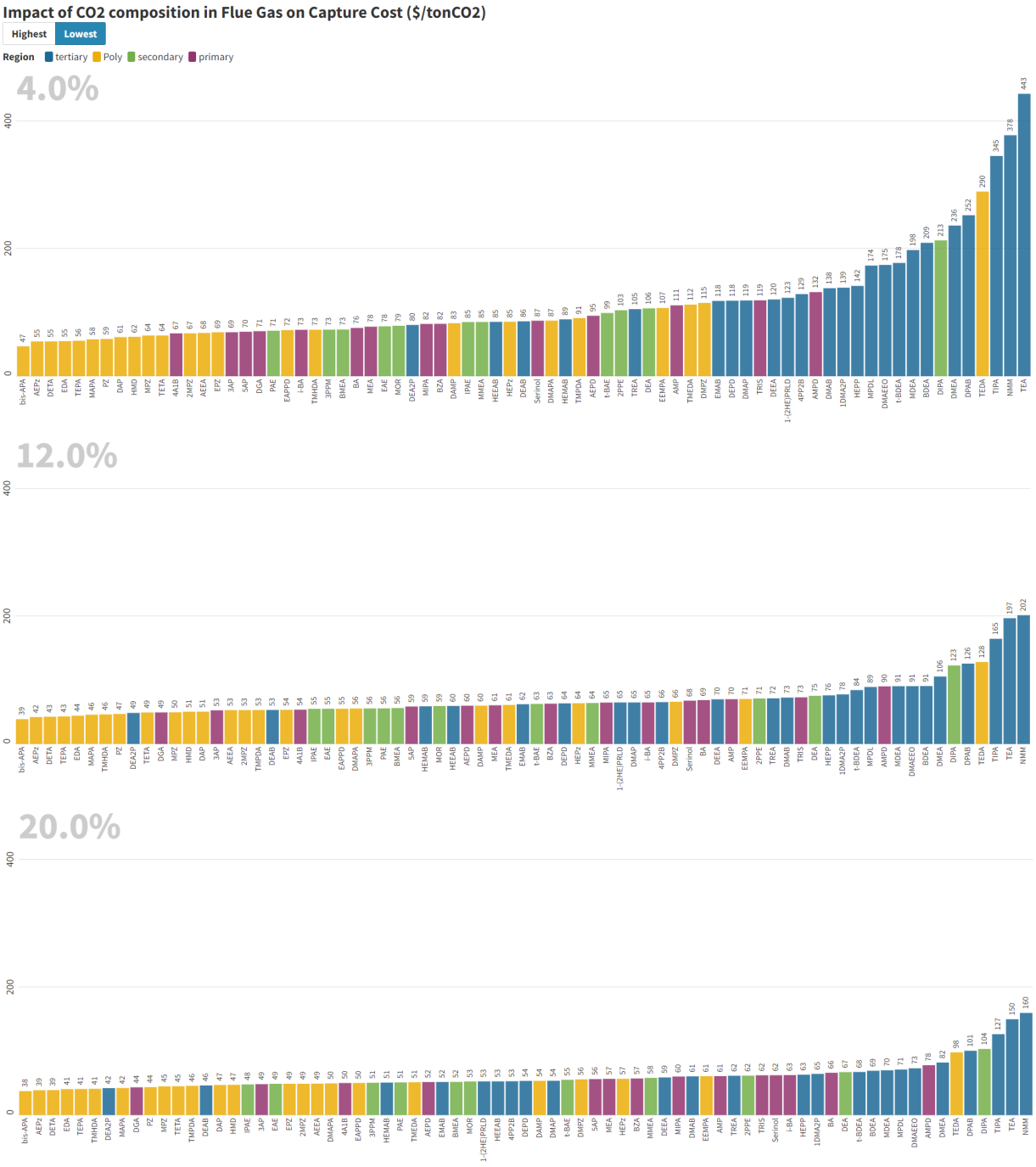


Figure 5.7: Impact of changing flue gas composition $y_{CO_2} = 4$ mol% (top), $y_{CO_2} = 12$ mol% (middle), and $y_{CO_2} = 20$ mol% (bottom) on capture cost and ranking. Many poly-amines (yellow, all amines with more than one alkalinity) rank best and many tertiary amines (blue) rank worst indicating a trend in chemical class. Readers are directed to the interactive animation available online [608].

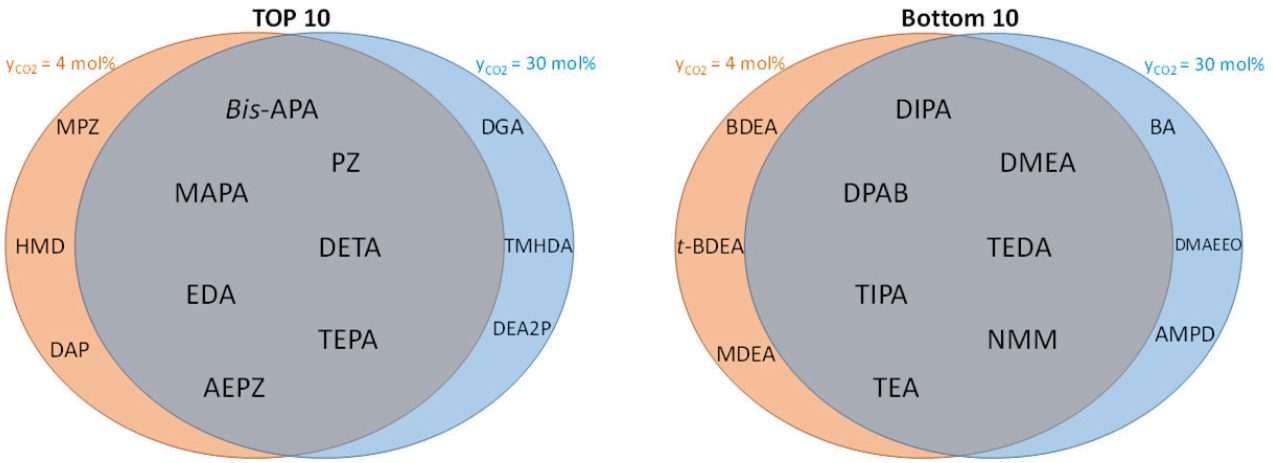


Figure 5.8: Venn diagram showing the top ten (left) and bottom ten (right) ranked solvents at $y_{CO_2} = 4$ mol% (orange) and $y_{CO_2} = 30$ mol% (blue). Seven out of ten candidate solvents stay in the top/bottom ten over a wide range of flue gas composition covering all meaningful applications.

efforts as it would not be required to test the full CO_2 concentration range. Further work could focus on a selection out of the group of well perming solvents *e.g.,* on stability, or corrosion.

5.4 Impact of Steam Cost

This section analyses the impact of steam costs C_{Steam} on the optimal operating conditions, capture cost, and ranking. Three steam costs representing double ($40.8/$t_{\text{Steam}}$) and ten-fold ($204/t_{Steam}) increases over the default steam costs ($20.4/$t_{\text{Steam}}$) have been modelled. For ease of reading the values have been annotated as $20/$t_{\text{Steam}}$, $40/$t_{\text{Steam}}$, and $200/$t_{\text{Steam}}$ in graphics and tables. Typical steam cost C_{Steam} were mentioned in chapter 3.3.3. Steam cost of $20/$t_{\text{Steam}}$ roughly correspond to the cost of a natural gas driven combined heat and power plant using $6/GJ$_{\text{NG}}$. The natural gas price in Europe [1] peaked mid-2022 to €^{2022}340/MWh$_{\text{NG}}$ = €^{2022}99.6/MMBTU ≈ $101/GJ$_{\text{NG}}$ but has recovered to < €50/MWh$_{\text{NG}}$.

Figure 5.9 shows the relationship between capture cost (left axis), lean loading Θ_{Lean}, and specific reboiler duty Q_{Reb} (red, right axis) for the three steam costs $20/$t_{\text{Steam}}$ (black), $40/$t_{\text{Steam}}$ (blue), and $200/$t_{\text{Steam}}$ (green) using 30 wt% MEA as an example.

The specific reboiler duty Q_{Reb} is not related to the steam price and remains unchanged. The

[1] EU Dutch Title Transfer Facility Virtual Trading Point

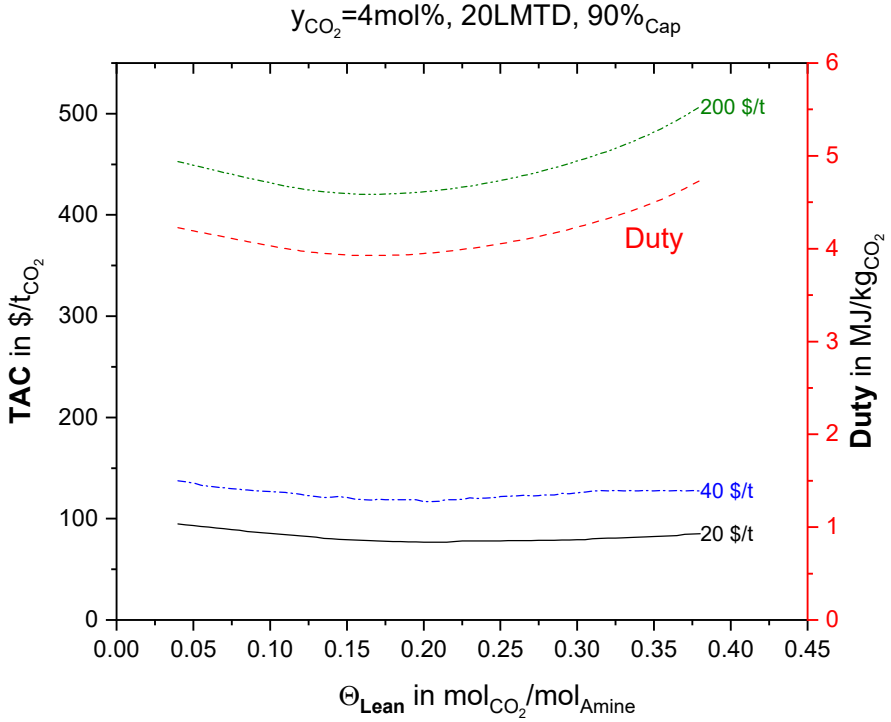


Figure 5.9: Impact of lean loading Θ_{Lean} on specific reboiler duty Q_{Reb} (red-dashed, right axis) and capture cost (left axis) at constant flue gas flow rate, y_{CO_2}= 4 mol%, and 90% capture rate for MEA for three steam prices \$20/t_{Steam} (black, solid line), \$40/t_{Steam} (blue, dash-dot line), and \$200/t_{Steam} (green, dash-dot-dot line). Cost optimal lean loading moves towards the minimum specific reboiler duty for higher steam prices.

capture cost increase with steam cost and the trend changes its shape to follow the reboiler duty profile. The cost optimal lean loading ($\Theta^{\text{Opt}}_{\text{Lean}}$ at capture cost minimum) at \$20/t_{Steam} is not identical with the reboiler minimum (Θ_{Lean} at specific reboiler duty minimum). It changes with increasing steam prices and moves closer to the minimum reboiler duty. The optimal lean loading $\Theta^{\text{Opt}}_{\text{Lean}}$ is close to 0.22 mol$_{CO_2}$/mol$_{\text{Amine}}$ for C_{Steam} = \$20/t_{Steam}. For \$40/t_{Steam} $\Theta^{\text{Opt}}_{\text{Lean}}$ is close to 0.20 mol$_{CO_2}$/mol$_{\text{Amine}}$, and for \$200/t_{Steam} $\Theta^{\text{Opt}}_{\text{Lean}}$ matches with the minimum specific reboiler duty at 0.18 mol$_{CO_2}$/mol$_{\text{Amine}}$. This is because the CAPEX-OPEX trade-off becomes increasingly dominated by the steam cost. At \$200/t_{Steam} the trade-off is completely dominated by the steam cost and causes all operating conditions to be optimised in order to minimise the specific reboiler duty. When steam costs are exceptionally high then the focus should be on reducing the reboiler duty because this will result in the highest cost savings.

The specific reboiler duty Q_{Reb} is a function of the heat contribution from absorption Q_{Abs}, latent Q_{Lat}, and sensible Q_{Sens} duties. Higher lean loadings lead to smaller working capacities

leading to higher solvent flow rates which in turn increases Q_{Sens}, creating a minimum in Q_{Reb}. Some solvents were dominated by Q_{Sens} suggesting that decreasing the solvent flow rate would reduce the overall specific reboiler duty.

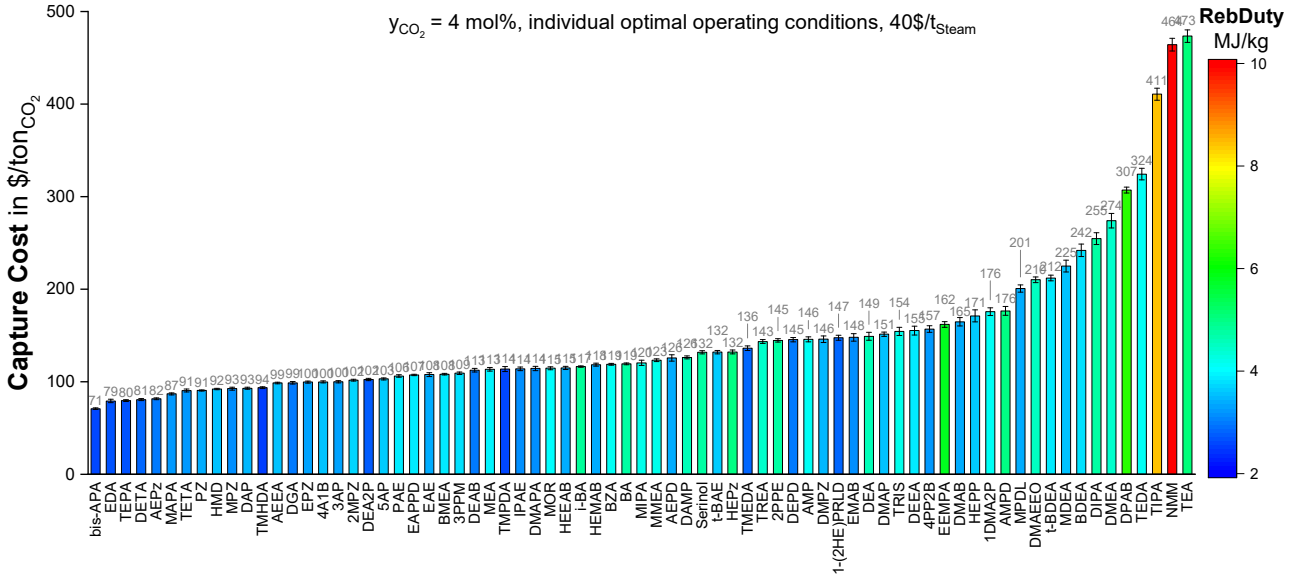


Figure 5.10: Solvents ranked by their capture cost for $y_{CO_2} = 4$ mol% at constant flue gas flow rate, 90% capture rate, and $\$40/t_{\text{Steam}}$. Each solvent is utilised at their individual optimal operating conditions and concentration in their individually optimally sized plant while capturing the same amount of CO_2. The specific reboiler duty is shown as colour.

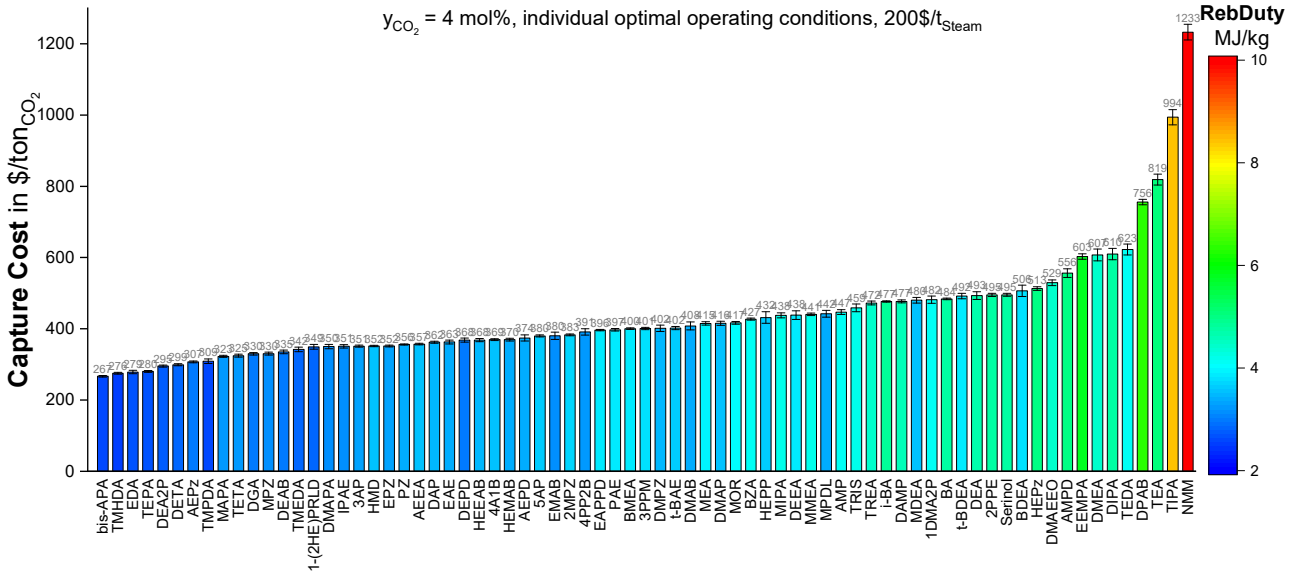


Figure 5.11: Solvents ranked by their capture cost for $y_{CO_2} = 4$ mol% at constant flue gas flow rate, 90% capture rate, and $\$200/t_{\text{Steam}}$. Each solvent is utilised at their individual optimal operating conditions and concentration in their individually optimally sized plant while capturing the same amount of CO_2. The specific reboiler duty is shown as colour.

Figure 5.10 and Fig. 5.11 show the ranking of the solvents utilised at their individual operating

conditions for the higher steam prices. The specific reboiler duty is indicated with the colour (blue = low duties; red = high duties). The differences in capture cost caused by the steam price for each individual solvent were tested for statistical significance using Welch's ANOVA followed by Games-Howell post-hoc test. The null hypothesis was rejected for each solvent (*e.g.,* comparing MEA's capture cost at $\$20/t_{\text{Steam}}$, $\$40/t_{\text{Steam}}$, and $\$200/t_{\text{Steam}}$) concluding that there is enough statistical evidence to suggest that the steam price statistically significantly impacts the capture cost. This is not surprising given that capture cost increased on average by 50% for $\$40/t_{\text{Steam}}$ and a factor of 4.8 for $\$200/\text{t}_{\text{Steam}}$.

Solvents with lower specific reboiler duties (blue) profit from increased steam prices compared to solvents with high specific reboiler duties, thus improve their relative ranking. The solvents rank at $\$200/t_{\text{Steam}}$ well aligned with their specific reboiler duty which is caused by the steam price assumption. The capture cost at $\$200/t_{\text{Steam}}$ appear prohibitively expensive. If steam prices are high and power prices remain low (*e.g.,* through high natural gas prices and high renewable power share), then electric boilers or steam free systems such as VPSAs should be analysed.

If steam is available for free, then $\Theta_{\text{Lean}}^{\text{Opt}}$ would be as low as possible to maximise the working capacity $\Delta\Theta_{\text{Work}} = \Theta_{\text{Rich}} - \Theta_{\text{Lean}} \approx \Theta_{\text{Rich}}$. The remaining capture cost would be dominated by the absorber CAPEX (see Fig. 5.4), thus, focus should be set on reducing equipment sizes as far as possible. Solvents with high specific reboiler duties (red in Fig. 5.10 and Fig. 5.11) would profit most and improve their ranking.

5.5 The Relationship between Amine Class, Properties, and Capture Cost

This section discusses the potential underlying trends in chemical structure, thermo-physical properties, chemical class, and capture cost. It is limited to typical gas-power CO_2 concentrations, however, the observations remain valid regardless of the CO_2 concentrations.

Chemical Structure The chemical structures of the best and worst solvents for a gas-power flue gas are shown in Fig. 5.12. Half of the top ten are di-amines and 80% are linear. Nine out of the bottom ten amines are tertiary mono-amines and 80% alkanolamines. No mono-amine or alkanolamine featured in the top ten and only one single amino group is tertiary.

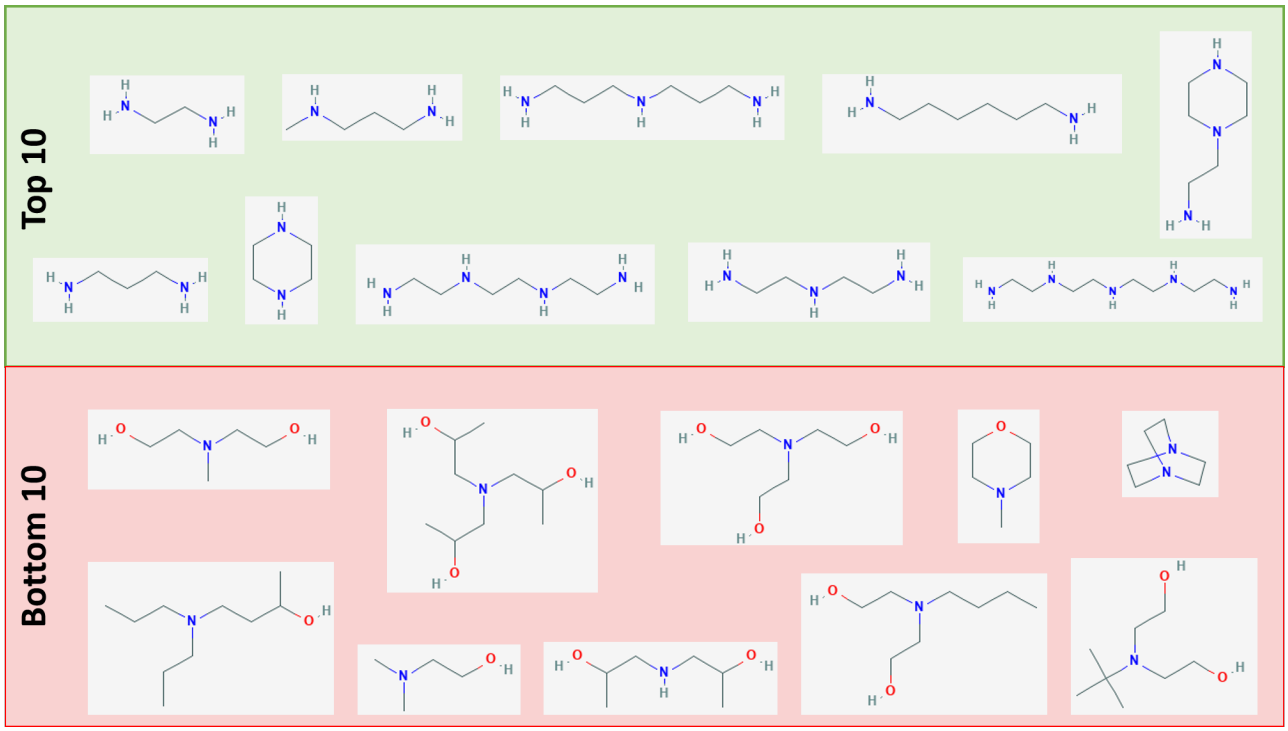


Figure 5.12: Chemical structures of the top and bottom ten ranked solvents at $y_{CO_2} = 4$ mol%. Noticeably many poly-amines feature in the top ten, and tertiary amines in the bottom ten, respectively.

Functional groups capable of protonating an alkalinity, *e.g.,* carboxylic groups protonating amino groups, reduce the amine's capacity, thus, lead to higher cost. Intra-molecular hydrogen bonding in particular from -OH groups at β- or γ- positions to the amine functionality impacts the performance as discussed in [135, 229, 266, 609–616]. Intra-molecular bonding might lead to ring structures (*e.g.,* DMEA, or AEEA), which reduces the amine's pK_a, destabilizes the carbamate formation, and ultimately shifts the absorption towards the bicarbonate route with higher absorption capacities [135, 229, 266, 609–616]. Such effects are captured in the VLE, but are not directly associated with the chemical class. It would be necessary to analyse each solvent's structure during absorption through *e.g.,* NMR or MO, to pin-point why each structure behaves in its way. However, what has been established is that specific chemical classes tend to show similar behaviour, leading to the cost ranking. Interestingly, the optimal

location of the C_2 - C_3 alkyl chains identified by researchers from CSIRO [187, 245, 617, 618] coincidences with the cost trends (see the number of carbon atoms between the alkalinities of the top performers in Fig. 5.12).

No alkanolamines rank in the top ten, and only one secondary alkanolamine in the bottom 10, so that further discussions about the role of intra-molecular hydrogen bonding are left for studies targeting these molecular structure - property relationships (see section 2.3.1). There is an observable trend between chemical class and capture cost favouring poly-amines. The following paragraphs expand on why and what thermo-physical properties might cause this preference in chemical class.

BZA is the only aromatic amine successfully screened out 20 candidates in the database, hence no conclusion can be drawn about this type of amine. Continuing work by Puxty *et al.*, [250] will potentially provide more candidate amines with complete datasets which will allow a more robust conclusion for that class of amine.

Working Capacity, Reboiler Duty, and Chemical Class Figure 5.13 shows the working capacity $\Delta\Theta_{\text{Work}}$ (symbol size), specific reboiler duty Q_{Reb} (colour), and chemical class (symbol shape) for the screened solvents in order of increasing capture cost.

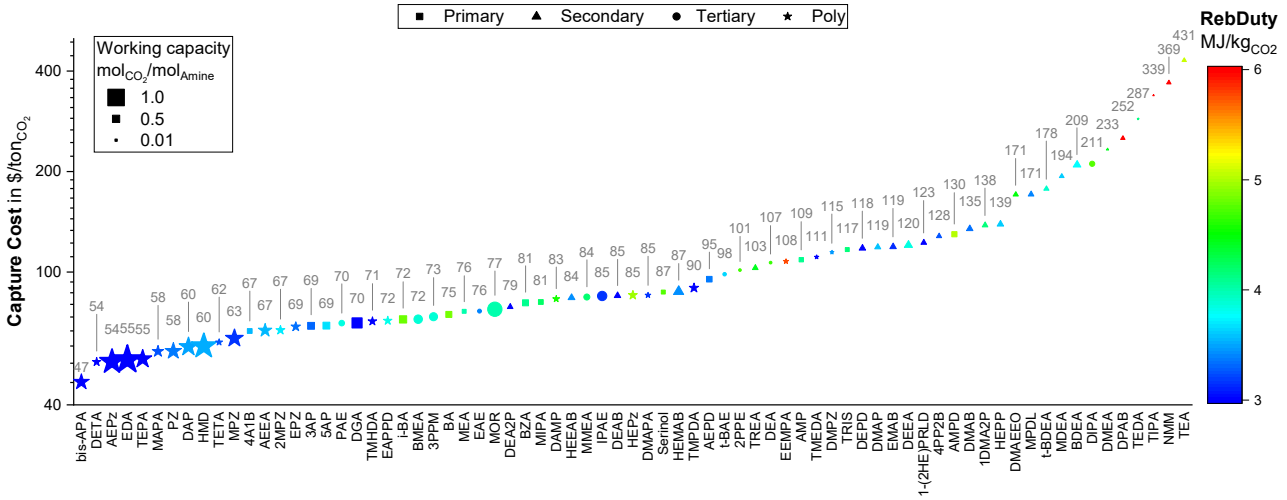


Figure 5.13: Ranking of solvents at $y_{CO_2} = 4$ mol% with working capacity (symbol size), specific reboiler duty (blue low, red high), and chemical class (symbol). Trends in all three KPIs observable.

The best performers are mainly poly-amines (star shape) shown with low specific reboiler duties

(blue) and large working capacities (larger symbol size), justifying continuing research on this particular amine class *e.g.,* [187, 606, 619]. Most tertiary amines show poor performance due to their high specific reboiler duties (red) and small working capacities (small symbols), thus they appear unfavourable for low pressure CO_2 capture. These trends are not exclusively strict, as shown by a couple of examples: 1) *bis*-APA's and DETA's working capacities are smaller than AEPZ's, EDA's or TEPA's working capacities but rank better. 2) DGA's specific reboiler duty is lower and its working capacity higher than solvents ranked next to DGA (PAE, or TMHDA). 3) EEMPA's reboiler duty is higher than the solvents next to it (DEA, or AMP).

High working capacities lead to in general smaller solvent flow rates, which in turn, reduce both capital and operating expenditures. Solvents with smaller specific reboiler duties require less steam, which in turn reduces the operating expenditure. The working capacity amongst the best performers varies, nevertheless, all best performers share low specific reboiler duties. The reboiler duty is a strong KPI for low capture cost, but it would not be suitable as a sole basis for ranking solvents, as shown by the scattering. This demonstrates that working capacity and reboiler duty are important KPIs but not sufficient on their own to reliable explain or predict the ranking.

pK_a and Molar Mass The relationship between capture cost and pK_a is illustrated in Fig. 5.14. The chemical class is shown as symbol shape, molar mass as symbol size, and pK_a as colour.

Many secondary (triangles) and tertiary amines (circles) have low pK_as (blue to green). Amines with high pK_a tend to perform better than solvents with low pK_a. This is observed by mainly yellow to green colours at low capture costs. High $pK_a > 10$ values can indicate faster kinetics, which can reduce equipment sizes, but are not directly correlated for all chemical classes. This observation is in agreement with other studies [126, 149, 229, 246]. Muchan *et al.,* [141] found that the pK_a of poly-amines could not accurately predict the reactivity (*i.e.,* no strong Brønsted relationship was observed), but noted that adding amine functionality reduced the overall pK_a. Puxty *et al.,* [229] observed that low pK_a alkalinities within a poly-amine are too weak bases to

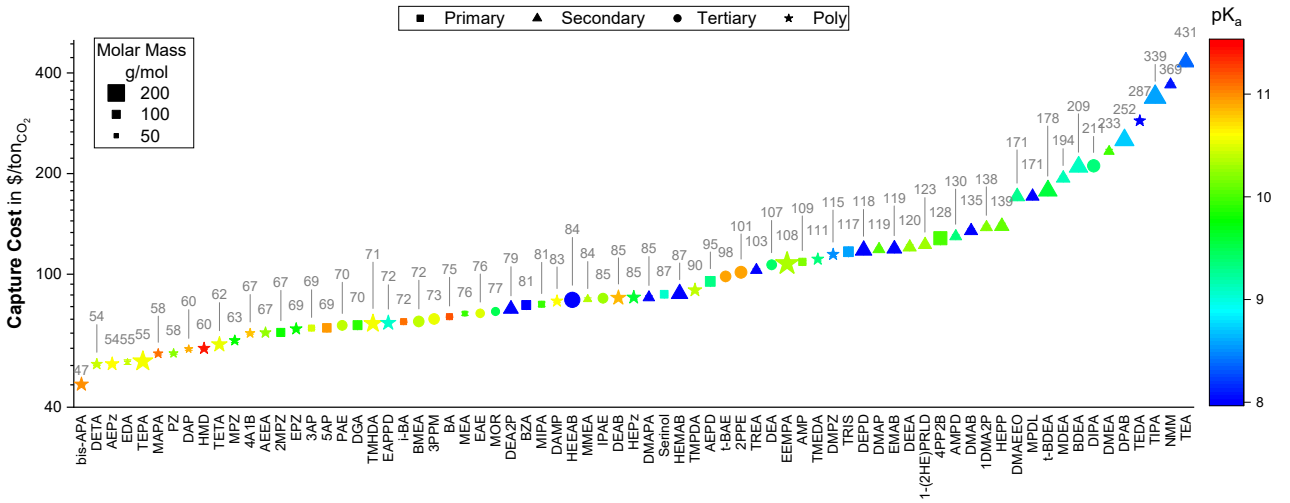


Figure 5.14: Ranking of solvents with molar mass (symbol size), pK_a (colour; blue low, red high), and chemical class (symbol shape). Trend in pK_a observable.

contribute to the absorption capacity. Hence, pK_a based predictions of kinetics or equilibrium loading are not reliable for poly-amines and provide only an indication.

Linking the amine's nucleophilicity to capture cost could describe multiple effects at once. Nucleophilicity of the amino group correlates with its basicity measured by the equilibrium with H^+ expressed through the pK_a [620]. Nucleophilicity is measured by the rate of reaction with the electrophile (CO_2) and depends on the reaction system. As long as the electrophile (CO_2) stays constant, one should theoretically be able to compare the nucleophilicities of amines. Strong nucleophiles react quickly with an electrophile, and weak nucleophiles react slowly with the same electrophile, depending on the steric hindrance. For example, *t*-butylamine is as basic as most primary amines but less nucleophillic because of steric hindrance. Tertiary amines tend to have higher nucleophilicities than secondary amines which again are more nucleophillic than primary amines.

There are quantitative approaches based on the reaction rate to determine nucleophilicity besides the pK_a of the conjugate acid. One well known approach was introduced by the Mayr group [621–623] calculating a nucleophilicity factor k_{Mayr} with published reactivity parameter s_{Nuc} (solvent and nucleophile specific sensitivity parameter), N_{Nuc} (solvent dependant nucle-

ophilicity parameter), and E_{Elec} (electrophilicity parameter).

$$\log k_{\mathrm{Mayr}} = s_{\mathrm{Nuc}} \cdot \frac{N_{\mathrm{Nuc}}}{E_{\mathrm{Elec}}} \tag{5.1}$$

Mayr's approach excludes steric effects and deviations by a factor of up to 100 should be expected, when both reaction partners are not listed in the database (20 entries in water). This unfortunately limits the usefulness of Mayr's approach to this work. Other work [620, 624, 625] also stayed short of quantitatively linking the molecular structure to the nucleophilicity. Therefore, it was not possible to quantitatively link the amines' nucleophilicty with the capture cost.

The cost of CO_2 capture has a strong relationship with pK_a, working capacity and reboiler duty, but none on their own correlate perfectly. These are important KPIs that need to be considered together when designing or selecting solvents for CO_2 capture, but further KPIs need to be included.

Figure 5.15 shows the molar mass and optimal concentration of amine (colour). There is no visual link between neither molar mass nor optimal mole fraction $x^{\mathrm{Opt}}_{\mathrm{Amine}}$ and capture cost. Some of the well performing solvents EDA (60 g/mol), *bis*-APA (131 g/mol), and TEPA (189 g/mol) cover nearly the whole range in molar mass. This is important because it allows scientists to freely design molecules without constraints on molecular size imposed by the capture process.

Kinetics and Heat of Absorption Working capacity, reboiler duty Q_{Reb}, and pK_a are ultimately linked to other thermo-physical properties, in particular equilibrium loading, heat of absorption, and kinetics. Figure 5.16 shows the heat of absorption ΔH_{Abs} and second order reaction rate constant k_2 as colour with fast reaction rates in red and slow reactions rates in blue (logarithmic scale). The symbol size corresponds to Θ_{Equi}. Figure 5.16 also shows the normal distribution curves for capture cost (on the right axis) and heat of absorption (on the top axis).

The colour shifts from top to down from blue to red, indicating that faster reacting solvents

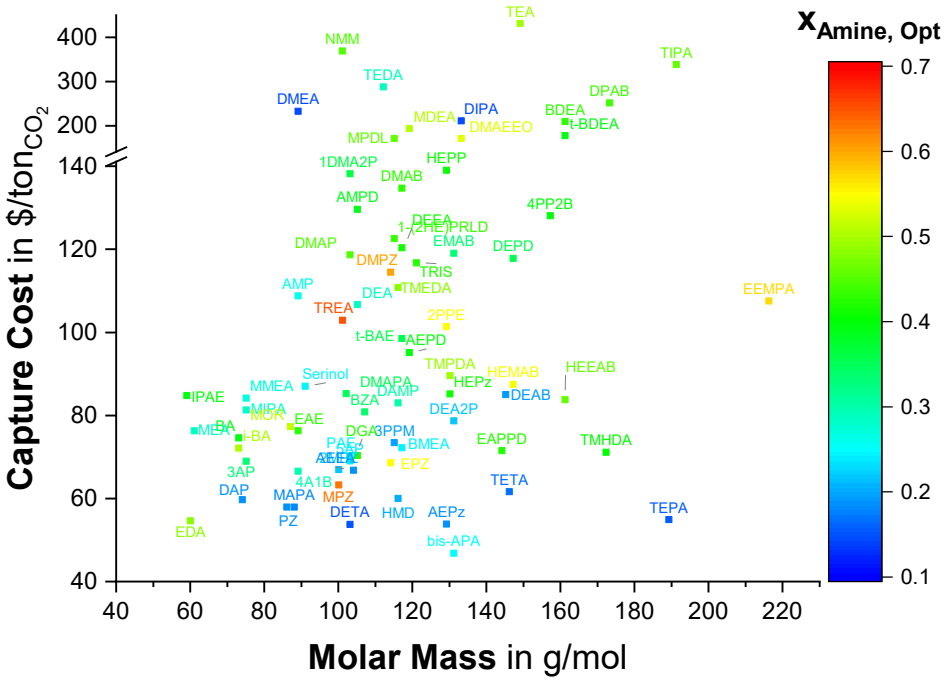


Figure 5.15: Capture cost over amine's molar mass, and optimised amine concentration $x_{\text{Amine}}^{\text{Opt}}$ (colour). No clear trend observable.

achieve lower capture cost. At the same time Θ_{Equi} increases with decreasing capture cost. Solvents with high equilibrium loading (larger symbol) and faster kinetics (red colour) lead to reduced capture cost. The aforementioned poly-amines react sufficiently fast and also have high working capacities (compare Fig. 5.13 with Fig. 5.16).

The solvents are scattered for ΔH_{Abs} indicating that no clear trend towards low heats is observable. There is a cluster of solvents (MAPA, AEPz, DETA, *bis*-APA, TEPA) between $65\frac{\text{kJ}}{\text{mol}_{\text{CO}_2}}$ and $85\frac{\text{kJ}}{\text{mol}_{\text{CO}_2}}$ which might be interpreted as a trend. Despite being counter-intuitive, a low negative heat of absorption does not guarantee low capture cost and low capture cost can be achieved with practically any heat of absorption, *e.g.,* ranging from EDA $49\frac{\text{kJ}}{\text{mol}_{\text{CO}_2}}$ to HMD 98 $\frac{\text{kJ}}{\text{mol}_{\text{CO}_2}}$.

Previous studies [9, 172, 189–191, 193–195] identified the "optimal" heat of absorption to be in a range that covers the whole scale of existing solvents, which makes these findings inconclusive. The "optimal" heat of absorption appears to depend on the analysed stripper configuration, adding to the complexity. This work's results indicate there is no clear trend towards low ΔH_{Abs} that could accurately predict the capture cost.

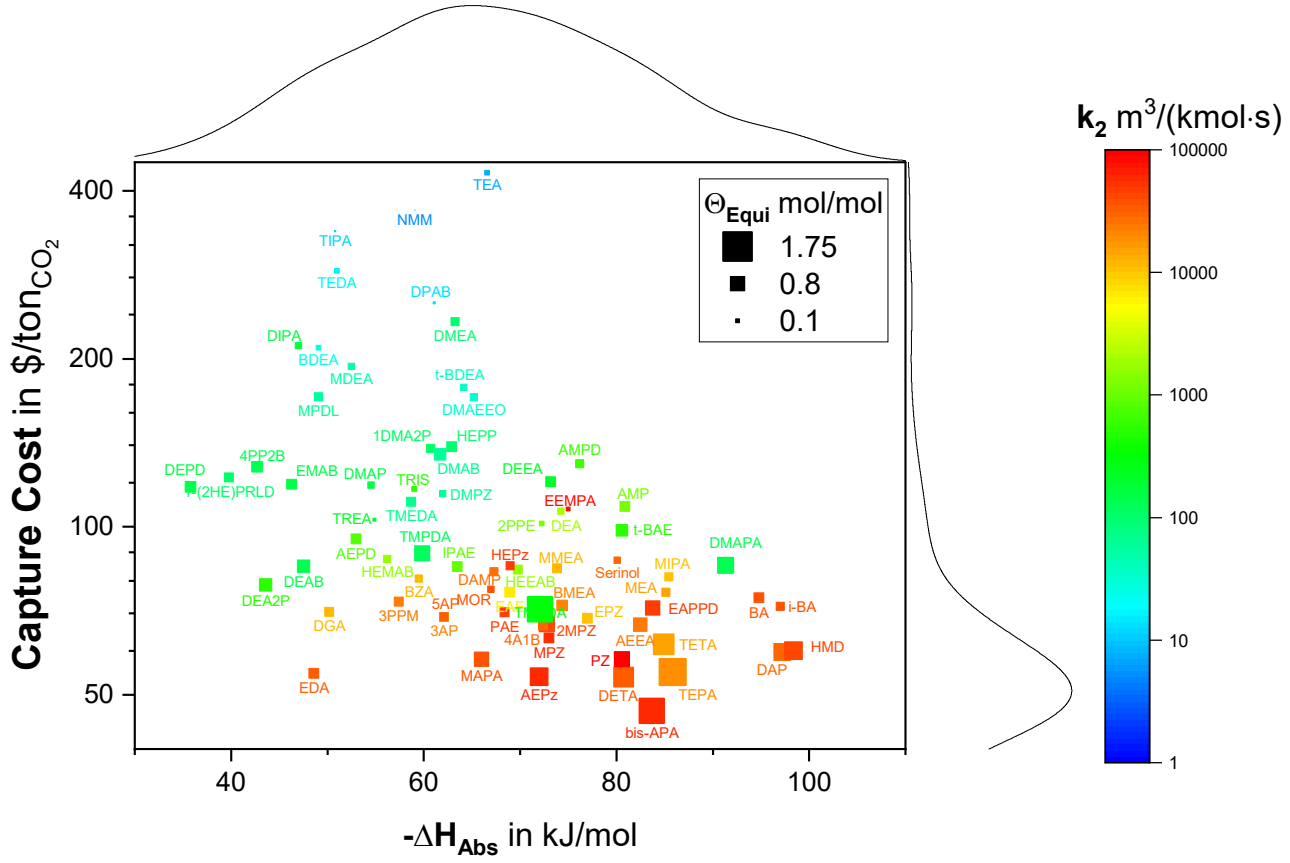


Figure 5.16: Linking equilibrium loading Θ_{Equi} (symbol size) for $y_{CO_2} = 4$ mol%, reaction rate constant k_2 (colour), and heat of absorption ΔH_{Abs} at (40°C) to capture cost. Normal distribution curves in heat of absorption and capture cost shown outside the axes. Visual trend in kinetics and equilibrium loading observable.

The heat of absorption ΔH_{Abs} impacts the reboiler duty Q_{Reb} regardless of heat integration, but does not solely determine Q_{Reb} as it is only one contribution. Figure 5.17 shows the contributions to Q_{Reb} for each solvent ranked by increasing ΔH_{Abs} with $-\Delta H_{\text{Abs}}$ shown as colour (blue = low, red = high). Many of the well performing solvents, *e.g.,* AEPz, DETA, *bis*-APA, or TEPA, have higher than average heat of absorption $\Delta H_{\text{Abs}} > 65 \frac{\text{kJ}}{\text{mol}_{CO_2}}$. The sum of the contributions Q_{Reb} is not correlated with ΔH_{Abs}. Q_{Abs} is directly correlated with the heat of absorption $-\Delta H_{\text{Abs}}$ multiplied by the net-CO_2 flow rate n^{CO_2}, which includes the different working capacities $\Delta\Theta_{\text{Work}}$.

The reboiler heat duty can be broken down into three contributions, Q_{Sens}, Q_{Latent}, and Q_{Abs} assuming adiabatic equipment. Figure 5.17 highlights the limitations of screening solvents using the heat of absorption as KPI *e.g.,* in [197]. The ranking ordered by increasing capture cost

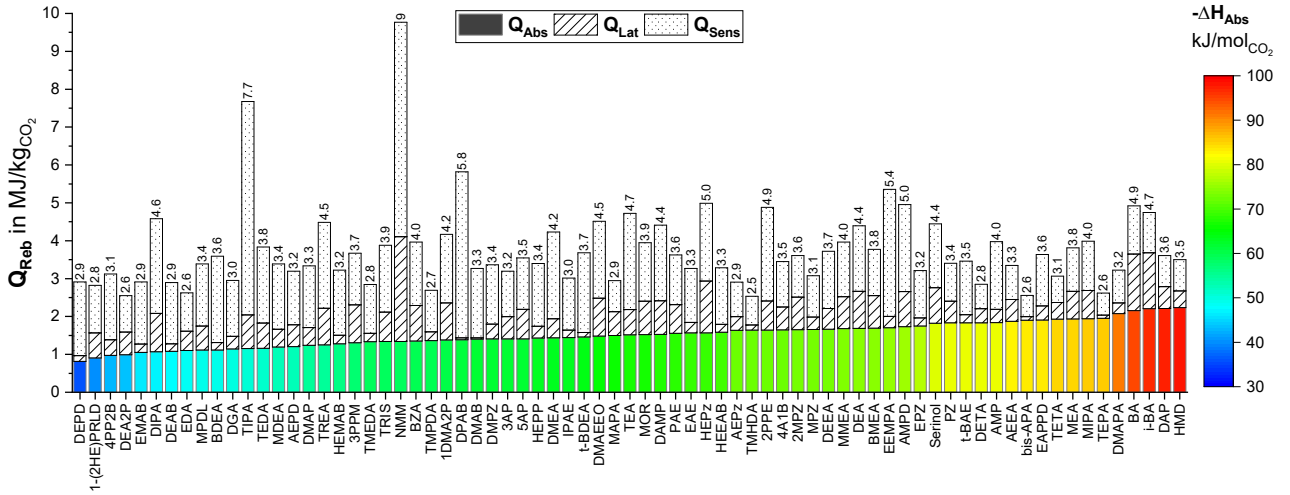


Figure 5.17: Breakdown of specific reboiler duty Q_{Reb} into absorption Q_{Abs}, latent Q_{Lat}, and sensible Q_{Sens} duties. Solvents sorted by negative heat of absorption ΔH_{Abs} and indicated by colour (blue low, red high). Clear trend between heat of absorption and Q_{Abs} but not overall duty.

is shown in Fig. D.3. A solvent with higher absolute heat of absorption could still result in lower overall reboiler duty when requiring less sensible $\mathrm{Q_{Sens}}$ and latent heat $\mathrm{Q_{Lat}}$, *e.g.,* DIPA vs HMD due to higher working capacities.

It is impossible to minimise solvent circulation rates and maximise cyclic capacities when both the protonation and carbamate reactions are simultaneously either strong or weak [626]. The Gibbs-Helmholtz equations describes that it is impossible to minimise the absolute heat of absorption while reducing the solvent circulation rate, meaning designers have to chose between either maximising cyclic capacities or minimising heat of absorption. These results agree with previous work based on MEA and fictional solvents [9, 174, 193, 194, 250] (see section 2.3.1).

Reducing the absolute heat of absorption is thermodynamically limited (see section C in the appendix). At the limit the reaction between amine and CO_2 would no longer be exergonic ($\Delta G < 0$, no reaction would occur) due to the reduction in overall entropy (ΔS) not being compensated by the reaction enthalpy ΔH_{Abs} any more.

Maximising the equilibrium loading is the alternative to minimising the heat of absorption. Adding CO_2-philic groups to a molecule increases its equilibrium loading and is not constrained by a strict thermodynamic limit. CO_2-philic groups tend to be polar and increase the entanglement/stiffness of the amine, in addition to the dipolar inter- and intra-molecular interactions.

This increases the CO_2-capacity, heat of absorption, and viscosity, but reduces the activation energy. This accelerates kinetics, because the activation energy E_A is inversely linked to the reaction rate constant as described by the Arrhenius equation $k_2 = k_{Pre} \cdot \exp\left(-\frac{E_A}{R \cdot T}\right)$. These changes partially trade each other off, and up until now it was not clear which properties to prioritise. According to the results of this work, favourable VLE characteristics at fast kinetics should be prioritised over low heats of absorption to achieve maximum cost reductions, agreeing with Oexmann and Mather's [174] and Kim and Lee's [195] theoretical work.

Solvent Comparison Figure 5.18 compares five poor performing solvents, (TEDA, DPBA, NMM, TEA and TIPA) with one of the best performing solvents, *bis*-APA. The spider diagram lists all thermo-physical properties with individual axes relative to each other. Data points close to the centre lead to higher capture cost, while data points towards the outside lead to lower capture cost.

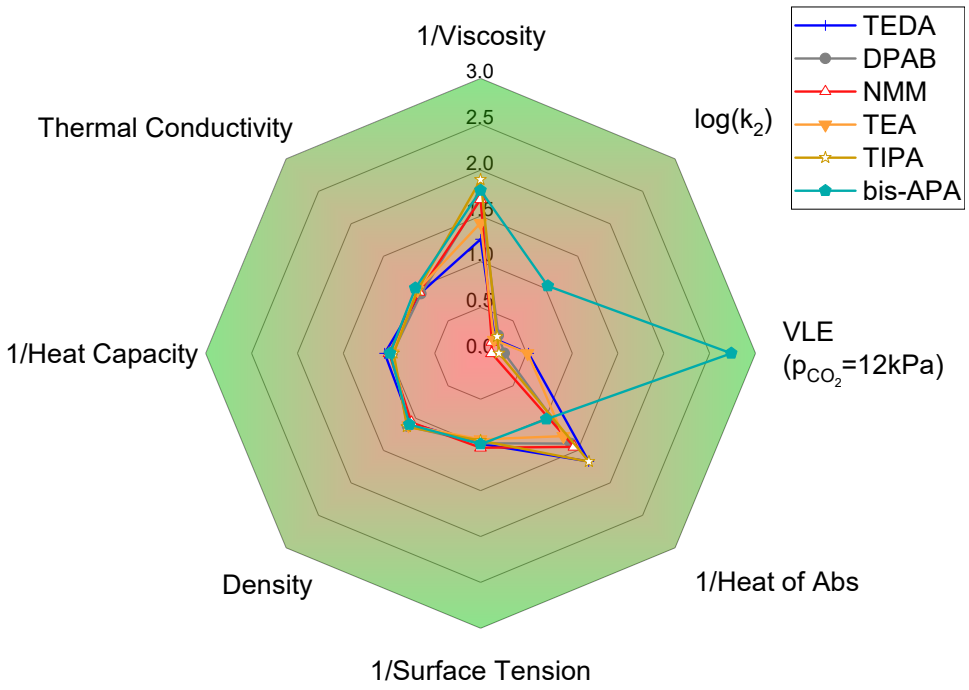


Figure 5.18: Comparing five poor performing solvents (TEDA, DPAB, NMM, TEA, TIPA) with a high performer (bis-APA). See Fig. 3.9 for explanation of scales.

The five poor performers all contain tertiary amino groups (TEDA being a di-amine and NMM a cyclic mono-amine), and have lower viscosity compared to MEA (indicated by values greater than one). TIPA is even less viscous than *bis*-APA at otherwise similar surface tension, density,

heat capacity, and thermal conductivity. The poor performers react an order of magnitude slower than *bis*-APA, which is in line with the tertiary amine chemical class. They have lower heats of absorption compared to *bis*-APA, which is in principle of advantage. However, all advantages of the poor performers are outweighed by having unfavourable VLE and kinetics. This provides examples for why selecting a capture solvent based only on low heat of absorption is misguided. Interestingly, *bis*-APA is comparable with MEA in terms of kinetics and heat of absorption. Thus, the cost improvements of *bis*-APA over MEA are attributed to its lower viscosity and much higher working capacity.

Cost reductions are attributed to a combination of thermo-physical properties, which are viscosity, kinetics, and VLE for aqueous amine solvents. Indicators of a well performing solvent are working capacities larger than 0.5 $\mathrm{mol_{CO_2}/mol_{Amine}}$, fast kinetics ($\mathrm{pK_a} > 10$), and viscosities smaller than 1.6 mPas. These properties happen to be commonly found in, but are not exclusive to, poly-amines. Heat of absorption is not to be prioritised over the previously listed properties. Spending less focus on surface tension, density, heat capacity, thermal conductivity, and molar mass will not adversely affect designing aqueous amine based capture solvents (compare with Fig. 3.9).

5.6 Conclusions

Overall, 73 amines out of the 464 candidate solvents were successfully screened. These solvents were ranked based on the minimum capture cost achieved in an optimised process, *i.e.* in terms of equipment size, amine concentration, and operating conditions. A techno-economic screening should optimise the amine concentration for minimum capture cost instead of assuming a constant concentration. The capture cost of the solvents ranged from $\$47/\mathrm{t_{CO_2}}$ to $\$430/\mathrm{t_{CO_2}}$, for a gas-power flue gas with 4 mol% CO_2 concentration.

Inferential analysis determines if there is enough statistical evidence to distinguish between solvents. This work identified Welch's ANOVA followed by a Games-Howell post-hoc test is a suitable and reliable method. It failed to reject the null hypothesis that the difference in mean capture cost between two solvents is zero in 4% of all comparisons. This means, there is no

statistical evidence to suggest that 4% of pairs are not equal. It demonstrates that the vast majority (96%) of solvents can be differentiated by their techno-economic performance with statistical significant confidence.

The price of steam impacts the capture cost, the operating parameter, and the ranking. If steam is available for free, then the optimal lean loading $\Theta_{\text{Lean}}^{\text{Opt}}$ is going to be as low as possible and the working capacity will be approximately equal to the rich loading. If steam prices are extremely high *e.g.,* $\$200/t_{\text{Steam}}$, then $\Theta_{\text{Lean}}^{\text{Opt}}$ is the result of minimising the reboiler duty. The capture cost would be prohibitively expensive, and the solvents would be ranked by reboiler duty, *i.e.,* the reboiler duty outweighs other aspects such as kinetics or VLE. The ranking is dominated by a selected set of thermo-physical properties at default steam cost of $\$20/t_{\text{Steam}}$.

Viscosity needs to be included in any solvent screening, because its impact is in the same order as VLE, heat of absorption, or kinetics. Less focus should be spent on thermal conductivity, heat capacity, density, and surface tension, because the differences between the screened solvents are small. The best performing solvents have lower capital expenditure compared to the worst performing solvents. The worst performing solvents are dominated by high absorber CAPEX cost. Steam cost can be addressed by further improving the efficiency of the capture unit through process intensification *e.g.* absorber intercooling, split configurations, mechanical lean vapour compression, or advanced flash stripper.

Most of the best performing solvents for a gas-power flue gas stayed top ranked across the 2-30 mol% CO_2 concentration range, reducing the complexity of the solvent selection. Links between chemical class and capture cost were identified or refuted by expressing the KPIs via the solvents' thermo-physical properties. The best performing solvents feature low reboiler duty, high working capacities > 0.5 $\text{mol}_{\text{CO}_2}/\text{mol}_{\text{Amine}}$, fast reaction rates high $\text{pK}_\text{a} > 10$, and viscosities < 1.6 mPas. Ultimately, the ranking is the result of the superposition of their thermo-physical properties, in particular the ones listed before. All of these happen to be found in linear poly-amines, yet there is no guarantee that designing a poly-amine will result in low capture cost. The alkalinities in most of best performing poly-amines are separated by C_2 - C_3 alkyl chains agreeing trends observed by others [187, 245, 617, 618], and supporting

further focussed research into these amines.

Tertiary amines perform poorly due to their relatively low working capacities and slow reaction rates. No trends between capture cost and the weight of the amine expressed as molar mass were observed, allowing to freely design new amines without a limit in molecular weight. Focussing on low total heat of absorption is misguided, as it is a combination of specific thermo-physical properties that lead to low capture cost.

The results indicate that at high flue gas CO_2 concentrations $y_{CO_2} = 30$ mol% many solvents will perform similar and solvent selection should consider practical elements, *e.g.,* degradation, toxicity, corrosion, but not exclusively thermodynamic-derived techno-economic performance. There is a pool of well performing solvents with an average relative difference in capture cost of less than 1.5%, despite *bis*-APA ranking best with statistic significance. If some candidates are ruled out due to practical issues, *e.g.* unusually high degradation, or limited supply, then there are other solvents at similar capture cost available.

6. The Limit of Solvent R&D

Material from this chapter has been published in [627].

6.1 Objectives

Absorption-based separation processes were introduced over 120 years ago, and thousands of new solvents have been proposed. While progress was achieved, solvent R&D has not yet delivered the level of cost reduction, which is widely desired. For much of the past 50 years, developing aqueous blends of amines was the focus of the scientific community, however, they ultimately fail to address the fundamental performance limiting issues despite outperforming benchmark technologies.

This chapter quantifies possible cost reductions by improving the solvent in terms of concentration, blending, and solvent R&D. The aim is to pin-point the bottlenecks of past and current absorption technology and set a thermo-physical property derived limit for solvent development. A thought-experiment that uses hypothetical solvents is presented to identify the limit of available cost reductions. The solvents considered in this work are the screened amine solvents (see chapter 5.2), CESAR1 (13 wt% PZ + 27 wt% AMP blend), which represents an up-to-date performance benchmark, amino acids (precipitating and non-precipitating), water-lean CO_2 binding organic liquids, phase change solvents, and amine-free carboxylic acid salts. The selection covers past, present, and future solvents and includes alternatives to amines with "new" chemistries that are currently researched. Important parameters such as the CO_2 composition in the flue gas ranging from 1-30 mol%, CO_2 capture rates of 90% and 95%, solute concentration, lean loading, and financial incentives are taken into account.

6.2 Impact of Thermo-Physical Properties

This section discusses the individual impact of thermo-physical properties on the capture cost, taking into account the range observed in the database. The relative impact of thermo-physical

properties has been already studied in the literature [10, 340, 628]. However, these studies ignored the available data range and just multiplied the individual properties with a random factor, *e.g.* ± 50% (creating an one-at-a-time sensitivity analysis). As a consequence, the impact of properties is exaggerated or understated.

Figure 6.1 shows an example of the true impact of the solvent's thermo-physical properties on the capture cost relative to 30 wt% MEA for y_{CO_2}= 4 mol% and y_{CO_2}= 12 mol% at 90% capture rate. Cost reductions are marked in green, and cost increases marked in red. The trends depend on the individual bottlenecks (see Fig. 6.3), and MEA is a representative benchmark as it shows average properties except for viscosity (see Fig. 3.9). The width of the trends corresponds to the maximum data-range identified in the database. Viscosity and the reaction rate constant span multiple orders of magnitude and their range is cut off at ±75%. The reaction rate has by far the largest range which is deceptively shrunken down due to the logarithmic scale in Fig. 3.9. The impact of density (turquoise), heat capacity (orange), and thermal conductivity (blue) can be barely seen due to their small ranges.

An increase in equilibrium loading, reaction rate, density, and thermal conductivity will lead to cost savings relative to MEA. A reduced Henry's coefficient, heat capacity, viscosity, surface tension, and heat of absorption will also lead to cost savings. Lower viscosity decreases heat and mass transport resistances due to thinner film layers. Higher thermal conductivity accelerates the heat transfer within the film layers. Lower Henry's coefficients increase the CO_2 concentration at the gas-liquid interface, increasing the driving force of mass transfer, and reducing the required mass transfer area. Higher density reduces the solvent's volume for the required molar solvent flow rate at constant capture rate. Lower surface tension increases the wet packing area, leading to smaller required heat and mass transfer areas. It impacts the stability of the liquid film in wetted wall and packed columns. The liquid film breaks up easier at lower surface tension and is stabilised at higher surface tensions [629]. Faster reaction rates reduce the required column heights until the mass transport becomes the limiting rate determining step. Higher equilibrium loading at constant partial pressure leads to a lower required (molar) solvent flow rate. Lower heat of absorption (at constant loading) will directly reduce the required heat demand for regeneration. The one-way sensitivity ignores the Gibbs-Helmholtz equation when

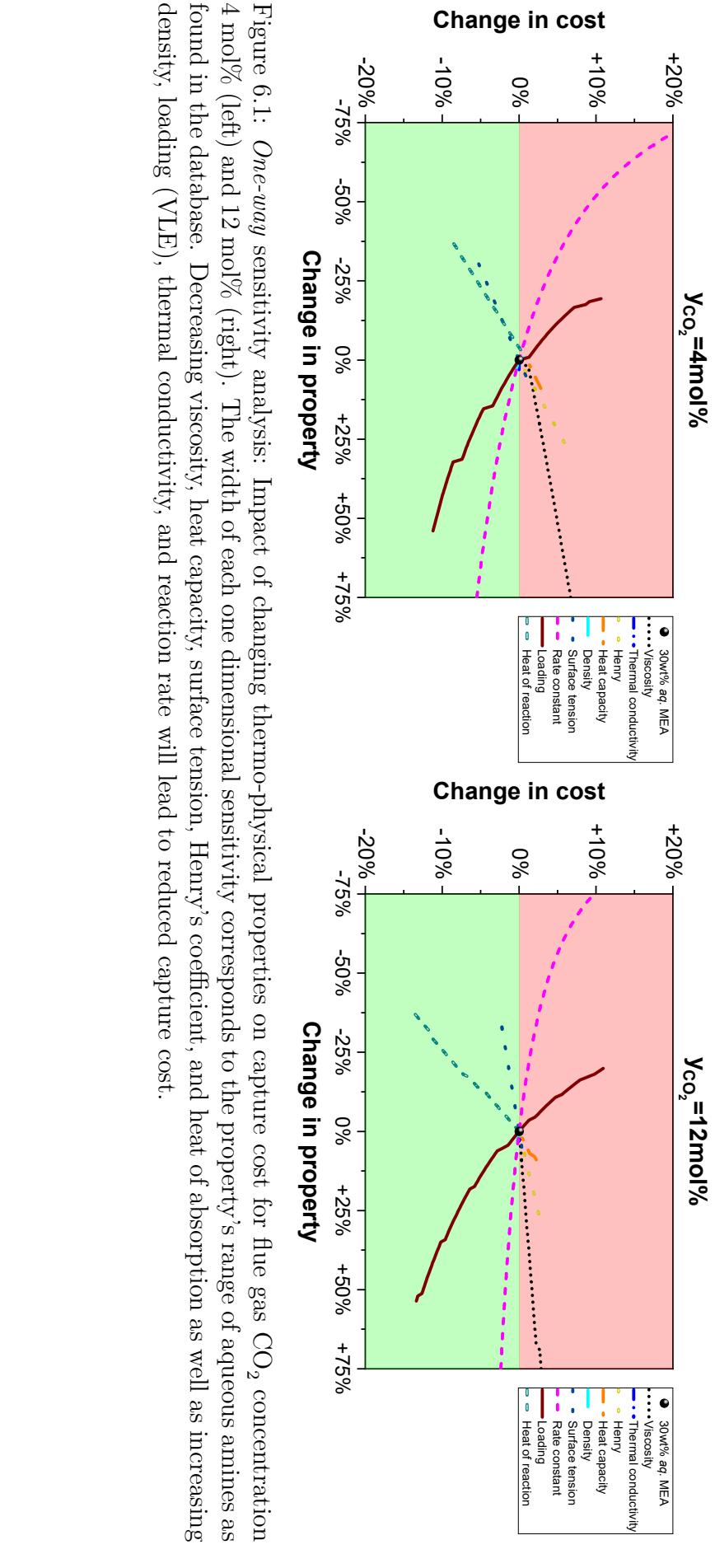


Figure 6.1: *One-way* sensitivity analysis: Impact of changing thermo-physical properties on capture cost for flue gas CO_2 concentration 4 mol% (left) and 12 mol% (right). The width of each one dimensional sensitivity corresponds to the property's range of aqueous amines as found in the database. Decreasing viscosity, heat capacity, surface tension, Henry's coefficient, and heat of absorption as well as increasing density, loading (VLE), thermal conductivity, and reaction rate will lead to reduced capture cost.

changing the VLE while keeping heat of absorption constant (and vice-versa). The results of this analysis were already implicitly implemented by inverting the scales in the spider diagrams, *e.g.,* Fig. 3.9. The CO_2 composition does not considerably influence the trends (compare left and right plots in Fig. 6.1).

6.3 Water Content

Most capture liquids developed over the past 120 years contain a solute (actively binding component, *e.g.,* amine) dissolved in a solvent (*e.g.,* water or alcohol). Section 6.3 deviates from the rest of the thesis by using solute and solvent according to their definitions, *i.e.,* "solvent" does not refer to the whole solution (= solute + solvent + others) as an inaccurate synonym. The solvent is not just a simple carrier, but contributes to some reaction routes *e.g.,* for tertiary amines, and offers a lower boiling point compared to most solutes *i.e.,* mostly solvent evaporates during the regeneration. Replacing water with organic solvents, *e.g.,* alcohols, could potentially reduce the specific reboiler duty, because some alcohols evaporate at lower temperatures compared to water while still providing the same functionality (−OH group) [630]. The solvent represents an intrinsic inefficiency, as it does not actively contribute to the capture task in most cases, thus, leading to higher flow rate, larger equipment, and higher reboiler duty through Q_{Sens}. Ideally, the absorption liquid should only contain as much solvent as required to provide enough stripping steam, thereby increasing the cyclic capacity. In reality, the solvent is often also used to tune overall thermo-physical properties such as viscosity and balance heats.

The point is that systems with high solvent shares are ineffective and have remained unchallenged over the past century besides recent trends to water-lean alternatives [192]. The widespread use of the weight fraction has partially hidden this issue, which is illustrated by six examples of representative aqueous amines in Tab. 6.1. Listed are the weight- and mole fraction, molality, and molar mass of amine as well as solution (total liquid).

A key observation, is that all solutions contain around 90 mol% water. The amine mole fraction varies between 6.1–12.0 mol% because of the amines' molar mass. The solutions' molar mass varies only by 6% (relative) between lightest (MEA) and heaviest (MDEA) for the single amine

Table 6.1: Weight-, mole-fractions, molality, and molar mass of amine and solution (solute + solvent). CESAR1 and a preferred embodiment of CANSOLV are added as current performance benchmarks.

Amine	Weight fraction	Mole fraction	Molality	Molar Mass in $\mathrm{kg\,kmol^{-1}}$	
	$w_{\mathrm{Amine}}\%$	$x_{\mathrm{Amine}}\%$	$\mathrm{mol_{Amine}/kg_{H_2O}}$	Amine	Solution
MEA	30	11.2	7.0	61.1	22.8
DEA	30	6.8	4.1	105	24.0
MDEA	30	6.1	3.6	119	24.2
AMP	30	8.0	4.8	89.1	23.7
PZ	30	8.2	5.0	86.1	23.6
CESAR1	40	12.0	7.1	-	26.4
CANSOLV	50	11.1	6.4	-	32.0

solvents. CESAR1 contains only 0.8 mol% more amine than 30 wt% MEA despite it deceptively containing 10 wt% more in weight fraction. This trend is also observed in commercial solvents, *e.g.,* in an aqueous blend of 30 wt% BHEPz, 15 wt% HEPz, and 5 wt% PZ, which is patented as a preferred embodiment by Shell Cansolv [515]. The total amine weight fraction is 50 wt% (matching the value reported in [631]), but the total effective amine mole fraction is only 11.1 mol% which is just less than 30 wt% MEA.

Figure 6.2 shows the amines at their optimal concentration expressed as mole fraction (see chapter 3.4). The solvents are ranked by increasing share of amine (grey). 85% of the screened aqueous amines consist of at least 50 mol% water, and average 36 mol% amine share over all candidates. These high amine concentrations are above levels currently deployed in commercial plants and topic of ongoing research [154, 632–635]. However, the results indicate that, even for these high concentrations, the majority of the liquid circulated within a capture plant is not actively contributing to the capture task. While increasing the solute concentration is favourable and reduces capture cost, it is not an exclusive means to circumvent the intrinsic inefficiencies of the conventional absorber-stripper process (*i.e.,* heating up and cooling down

mostly water), because of the concave cost trend (see chapter 3.4). Removing the penalty of high water contents present in most of the capture plant must be a central aim in achieving step change performance improvements. Simply replacing water with another non-CO_2 binding component that offsets *e.g.,* corrosion issues, will not be sufficient.

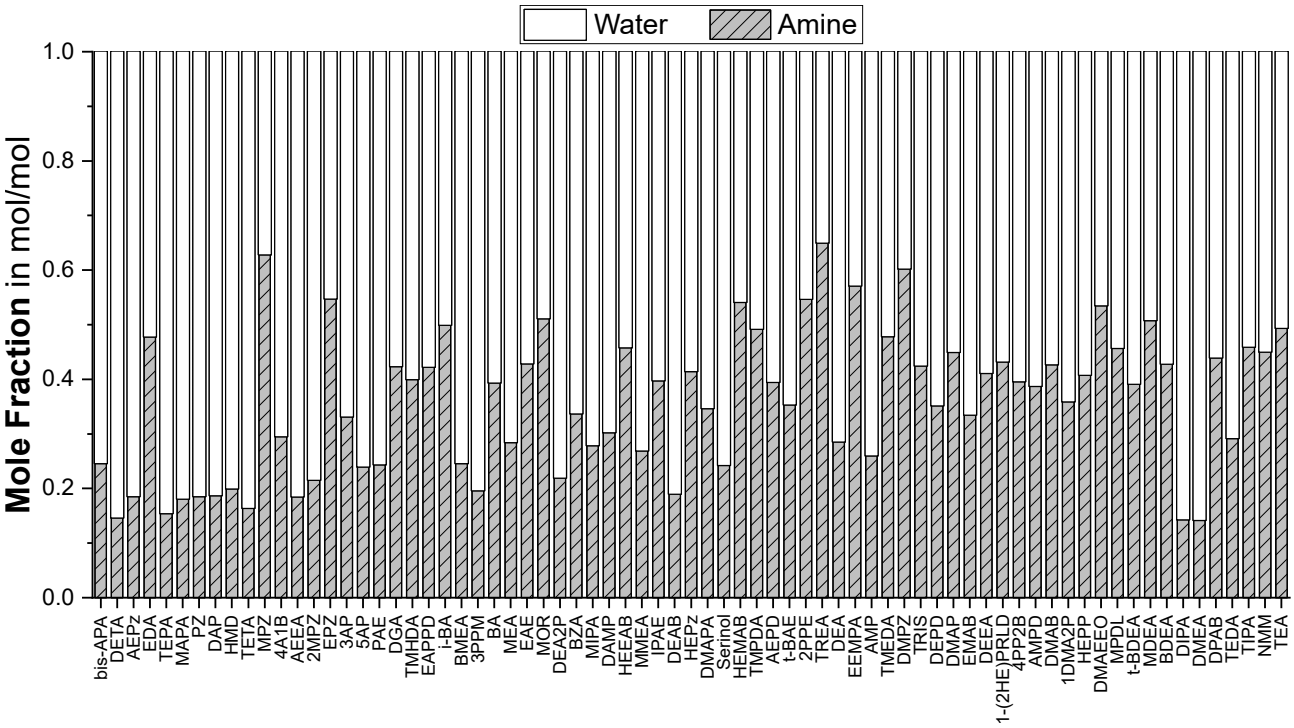


Figure 6.2: Water content (white) of screened amines at optimised amine concentration expressed as mole fraction (grey). Solvents are ranked by capture cost from left to right. Most solvents contain more than 50% water.

6.4 Blending as Cost-effective Optimisation

Blending is the dominating approach adopted during the past 50 years to improve the capture solvent's performance. This trend was started by activating tertiary amines (*e.g.,* aMDEA in 1977 [636]), and modern blends contain multiple components. The following analysis illustrates, how two poor performing tertiary amines, TEA and TEDA, can be improved by blending with another amine and quantifies where the cost reductions are generated. Figure 6.3 shows the impact of activating 30 wt% TEA (star) and 30 wt% TEDA (circle) with 5 mol% PZ on the rich loading, kinetics, and capture cost. The white dashed lines are reference lines for 30 wt% MEA's rich loading and reaction rate constant. The data points in Fig. 6.3 are based on 40°C. The colour indicating the capture cost corresponds to a two-dimensional sensitivity analysis based

on 30 wt% TEDA (circle).

The slopes of the contour lines (indicating constant capture cost) highlight that improving the kinetics of TEA and TEDA reduces the cost more than increasing the equilibrium loading. The cost-effectiveness of improving either VLE or the kinetics depends on the individual bottleneck. Increasing the equilibrium loading at slow reaction rate constants < 100 m^3/(kmol· s) has little effect. Further accelerating the kinetics of aTEA or aTEDA will yield less cost improvement compared to increasing their equilibrium loading. This might appear as an obvious observation, however, most blending studies are based on singled out thermo-physical properties and, crucially, not the overall pareto set of properties. A general quantifiable approach is missing and a simultaneous bottleneck analysis is often omitted.

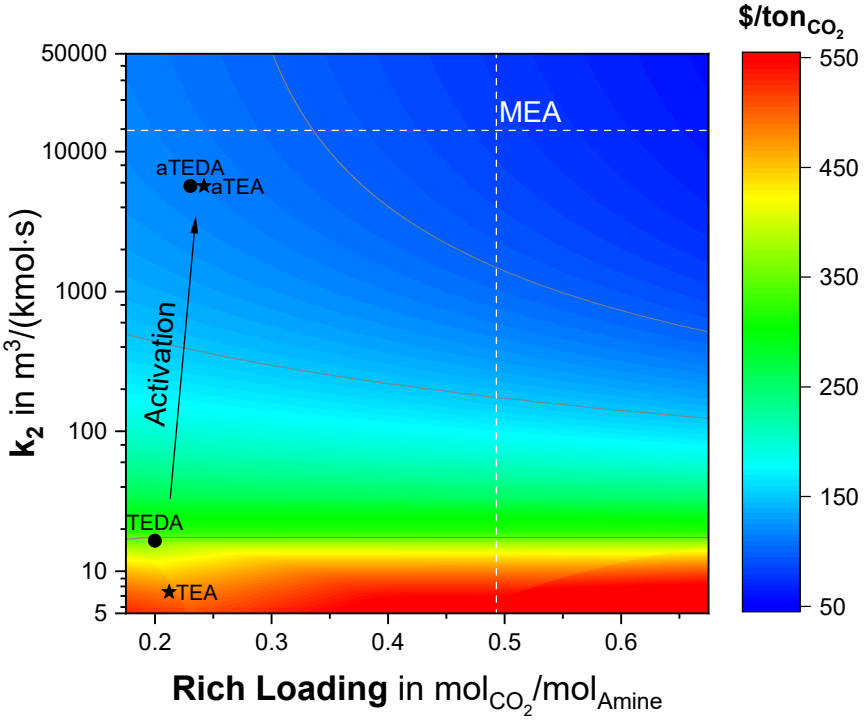


Figure 6.3: Impact of activating 30 wt% TEDA (circle) and 30 wt% TEA (star) by blending with 5 mol% PZ on capture cost (colour scale; blue = low cost, red = high cost). Blending improves reaction rate constant k_2 and rich loading Θ_{Rich} for a gas-power flue gas $y_{CO_2} = 4$mol%. Values correspond to 40°C. MEA (white dashed lines) added as reference.

Figure 6.4 shows the corresponding capture cost breakdowns. Contributions to the CAPEX (coloured areas with a pattern) are broken down to the absorber, stripper, heat exchangers, and other. Contributions to the OPEX (coloured area without a pattern) are broken down to steam, maintenance, cooling, and other OPEX. Activation leads to reductions in capital expenditure

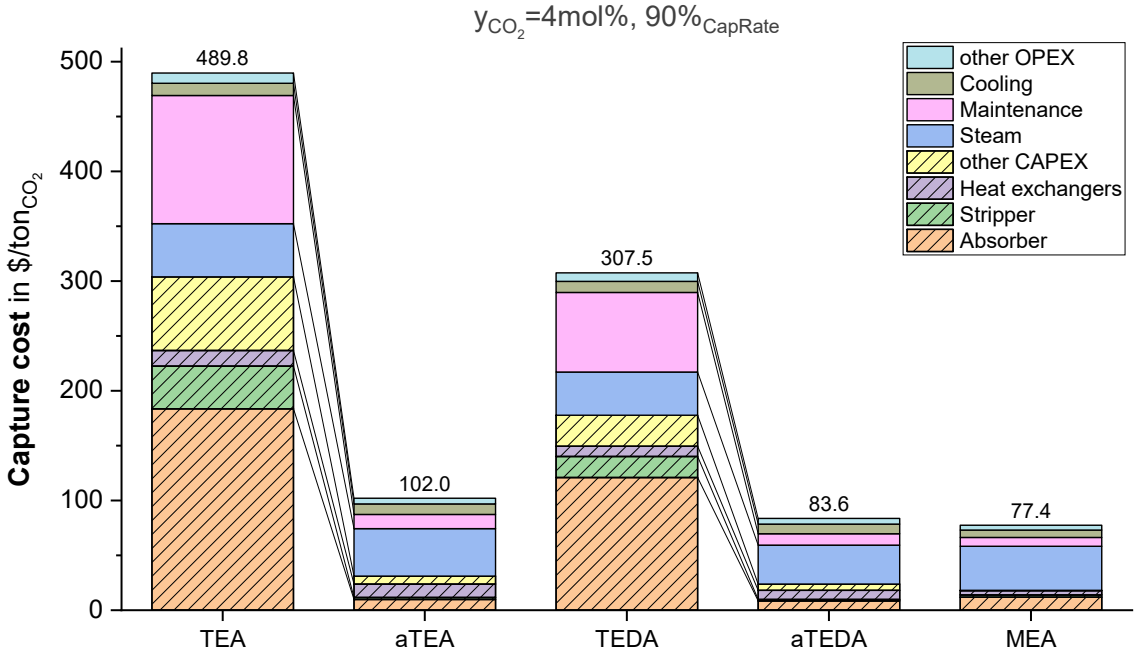


Figure 6.4: Impact of activating 30 wt% TEDA and 30 wt% TEA by blending with 5 mol% PZ on capture cost. Significant cost reduction in CAPEX achieved, but the activated amines fail to outperform 30 wt% MEA.

by reducing the absorber size for both TEA and TEDA. The operating expenditures (except maintenance cost), stay nearly constant.

The capture cost reduces by 80% for TEA and 73% for TEDA, which indicates that activating slow-reacting tertiary amines by blending with PZ is a highly effective method. However, these examples of activated solvents do not outperform MEA. Blending will be constrained by the bounds in each thermo-physical property.

Blending carbamate and carbonate forming amines is a popular way to combine fast kinetics and high capacity, however, blends containing multiple amines tend to have the volatility, toxicity and stability of the worst component in the formulation and its performance is not an arithmetic (linear) average between the single components [238, 637, 638]. Synergistic effects leading to cyclic capacities that exceed the values of the pure amines have not yet been observed and unfavourable concave patterns exist [127, 626]. Exceptions to this are Zhuang and Clements [639], who found a convex pattern, and *Shi et al.*, [640, 641] who reported a coordinative effect between MEA and DEA. Therefore, blending existing amines is unlikely to deliver a breakthrough in cost reduction as long as the underlying chemistry stays the same and will

primarily only reduce capital expenditure.

The alternative to blending is designing poly-amines with control over steric hindrance, chemical class type (primary, secondary, tertiary), and functionality, in order to combine the rapid reaction rate of primary and secondary amines as well as fast intra-molecular proton transfer to enhance bicarbonate formation.

6.5 Developing an Ideal Solvent

So far, research proposed ways *how* to improve solvents, but it is unknown *how far* solvent R&D can actually reduce the capture cost. The thermodynamic minimum work of separation sets an unachievable hard limit, because it is agnostic of any separation technology, ignores all heat and mass transfer inefficiencies, and assumes an ideal gas. Current solvents and processes tend to be compared between each other rather than with the minimum thermodynamic work. Other KPIs such as the specific reboiler duty are compared between solvents and processes. It would therefore be of interest to quantify a more realistic limit, that represents an ideal solvent (hypothetical construct), utilised in a real process with all the thermodynamic inefficiencies/losses due to heat and mass transfer. This ideal solvent will be derived in the following paragraphs, and it sets the performance limit on how good solvents will ever be.

The ideal solvent is a fictional solvent which has real thermo-physical properties that lead to minimum capture cost. It is the result of simultaneously optimising all solvent properties within certain boundaries that are "cherry-picked" to represent realistic physical limits. It embodies the concept of being able to individually optimise the solvent's thermo-physical properties, *i.e.,* creating an artificial solvent. Thus, there is no molecular structure or chemical class associated with it. The key insight that will be generated, is quantifying the impact on the capture cost if such ideal solvent existed, and not to actually derive a molecule that has those properties. From a thermodynamic point of view, it is a *real fluid* and differs to a mono-atomic ideal gas.

This approach differs to CAMD which solves for real molecules with boundaries set as wide as possible in order to not suppress any potential solutions. This model can optimise any single or all properties simultaneously without impacting other properties (no cross correlation).

However, the optimisation is constrained by links between individual properties, *e.g.,* VLE and heat of absorption as described by the Gibbs-Helmholtz equation. The best possible solvent that fulfils the Gibbs-Helmholtz equation is named the *Gibbs-Helmholtz solvent*, and the solvent resulting from dropping this constrain is named *ideal solvent*. The Gibbs-Helmholtz solvent is theoretically and physically achievable, and the ideal solvent represents an unachievable hypothetical construct.

There is no definition of what a realistic and physically achievable limit for thermo-physical properties is. In this work, the limits (see Tab. 6.2) are derived from the database. The properties of aqueous MEA and water at 40°C are added in Tab. 6.2 for reference. Each bound is derived from an experimentally measured pure liquid at 1 atm *e.g.,* water, or acetone. The approach is in general agnostic of the selection of the actual reference compound, because many liquids with similar values exist *e.g.,* see Fig. B.8.

Table 6.2: Upper and lower bounds of property optimisation with the reference liquid given in brackets. Properties of unloaded 30 wt% *aq.* MEA and pure water added for reference. All values at 40°C. Surface tension values are measured against saturation temperature.

Property	Unit	Lower bound	Upper bound	30 wt% MEA	Water
Surface tension	kg/s^2	0.03 (Acetone)	0.07 (Water)	0.06	0.07
Viscosity	mPa·s	0.67 (Water)	100 (CO_2BOLs)	1.61	0.67
Density	kg/m^3	685 (Octane)	1500 (Sulfuric acid)	1003	989
Heat capacity	J/(mol·K)	75.2 (Water)	776 (Trioctylamine)	88.3	75.2
Thermal conductivity	W/(m·K)	0.15 (Acetone)	0.63 (Water)	0.58	0.63
Reaction rate	$m^3/(kmol_{alk}·s)$	0 (Phy. abs.)	69800 (*aq.* KOH)	11800	–
Heat of absorption	kJ/mol_{CO_2}	36.7 (3–PM)	98.4 (HMD)	84.4	–
VLE ($p_{CO_2} = 15$kPa)	$\frac{mol_{CO_2}}{mol_{Amine}}$	0.39 (TEA)	1.96 (TEPA)	0.57	–

For example, mercury's liquid heat capacity (27.98 J/(mol·K) at 25°C) is an outlier in com-

parison to other liquids and would classify as an unrealistic bound. In contrast, water and trioctylamine set more realistic upper and lower limits, respectively [358, 642]. Binding organic liquids (BOLs) set the upper bound for viscosity, and physical absorption sets the lower limit for the reaction rate. The reaction of CO_2 in a potassium hydroxide solution (ion strength 3.0 kmol/m^3, 40°C [643]) sets the upper bound of a realistic reaction rate. Much faster reactions involving CO_2 are known, *e.g.,* photocatalytics, however they fail to meet the criteria of occurring in the liquid state, and being realistically achievable for an absorption-type system. 3-Piperidinemethanol (3-PM) and hexamethylenediamine (HMD) are well known amines with the lowest and highest heats of absorption [197, 644].

The optimisation unsurprisingly identifies the bounds as optimal, *i.e.,* lower bound for viscosity, heat capacity, and surface tension, and the upper bound for VLE, reaction rate, density, and thermal conductivity. The properties of the ideal solvent relative to the screened amines (see chapter 5.2) and alternative solvents are shown in Fig. 6.5 (see Fig. 3.9 for a full explanation of the spider diagrams). The alternative solvents and "new" chemistries are amino acids (potassium L-prolinate, ProK and potassium lysinate, LysK), phase-change solvents (DEEA + MAPA), amine-free carboxylic acid salts (potassium phenoxide, PhOK), or water-free CO_2BOLs (DBU in hexanol). The data for these solvents is taken from [188, 358, 630, 645–695].

The relative difference in density, heat capacity, and thermal conductivity is small to nearly undistinguishable for all existing solvents studied in this work. Surface tension and viscosity are spread more widely with a normalised range of 0.6-2.5 and 0.9-2.4 respectively. The largest relative differences are in heat of absorption, VLE, and reaction rate. The gap between the solvents and the ideal solvent indicates the maximum room for improvement, *i.e.,* only little improvement can be expected in heat capacity, thermal conductivity, and reaction rate. For example, piperazine reacts nearly as fast as the limit identified in this work. There appears to be large room for improvement in density, surface tension, viscosity, heat of absorption, and VLE. It is likely that future solvents will close the gap to *some* selected properties, but it is unlikely that any (water-based) solvent using chemical classes studied within this work will ever outperform *all* properties of the ideal solvent.

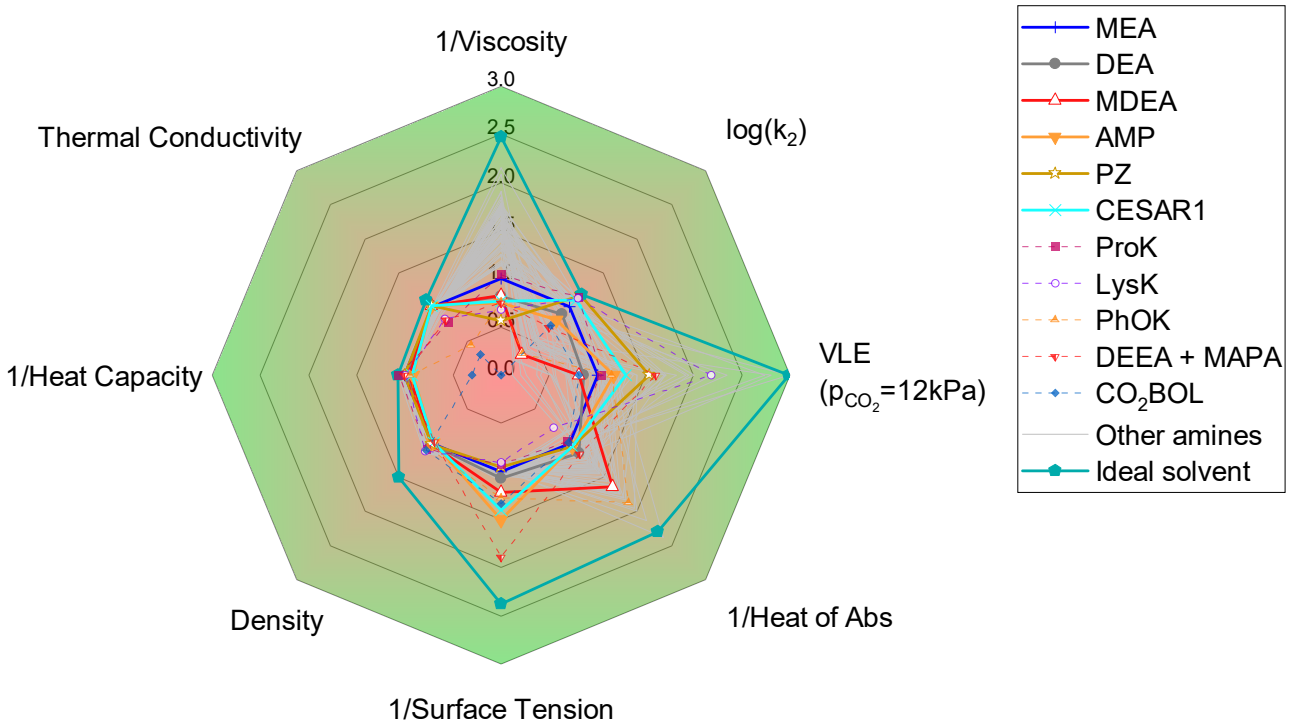


Figure 6.5: Comparing thermo-physical properties of various unloaded solvents at 40°C as a factor of 30 wt% (aq) MEA. A cost reduction relative to MEA is highlighted in green with values larger than parity. Note the inverse scale for heat of absorption, viscosity, surface tension, and heat capacity.

Figure 6.6 visualises a sequential step-by-step optimisation starting with MEA (first bar) and reaching the ideal solvent at the end (fifth bar) for y_{CO_2}= 4 mol% and 90% capture rate. The bars correspond to the capture cost (using the left scale) with the CAPEX shown with a pattern and the OPEX without a pattern. The red dots linked by a dashed line correspond to the specific reboiler duty (shown on right scale). The underlying process topology is an archetypal configuration and this does not represent the current state-of-the-art advanced processes. The order of the individual optimisation steps towards the ideal solvent are interchangeable, and for illustration reasons selected to be: 1. Transport properties including surface tension, 2. Kinetics, 3.Total heat of absorption, and 4. VLE. The dashed boxes refer to the Gibbs-Helmholtz solvent (second from right), and ideal solvent (right).

The first step towards ideality in Fig. 6.6 involves optimising viscosity, heat capacity, thermal conductivity, surface tension, and density (noted as transport properties). The individual impact can be seen in Fig. 6.1. The capture cost reduce by 18% to \$63.3/t_{CO_2} with the main savings coming from the absorber, stripper, and maintenance cost. Due to improved heat and

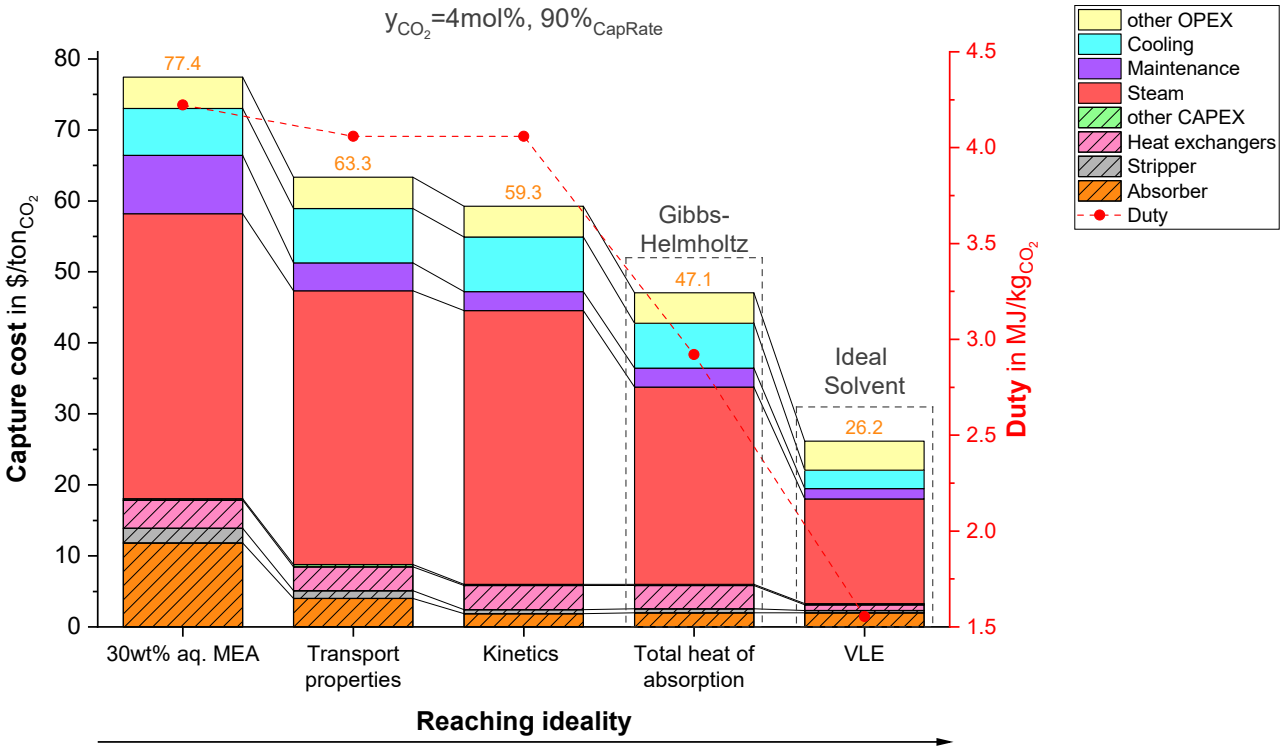


Figure 6.6: Deriving the ideal solvent starting from MEA by optimising the solvent properties and its impact on capture cost (colour bar, left scale) and specific reboiler duty (red, right scale) at y_{CO_2}= 4 mol% and 90% capture rate.

mass transfer the unit sizes shrink. The steam demand is reduced due to lower sensible heat Q_{Sens} contribution, leading to a reboiler duty of 4.06MJ/kg$_{CO_2}$ (4% less relative to MEA). The next step additionally includes the reaction rate (kinetics) together with the transport properties in the optimisation. The additional cost savings leading to \$59.3/t$_{CO_2}$ (23% relative to MEA) come predominantly from the columns. The reboiler duty practically stays constant, because the reaction rate does not impact neither the required solvent flow rate, nor the heat of absorption.

The next step additionally includes the heat of absorption in the optimisation together with the transport properties and kinetics. The capture cost shrink further down to \$47.1/t$_{CO_2}$ (39% less relative to MEA) and the reboiler duty to 2.92MJ/kg$_{CO_2}$ (31% less relative to MEA). The main saving comes from the steam cost, because the total heat of absorption is linked to Q_{Abs} which contributes to the reboiler duty (see Fig. 5.17). This solvent still fulfils all constrains including the Gibbs-Helmholtz equation, and is referred to as Gibbs-Helmholtz solvent. Two Gibbs-Helmholtz solvents are possible: One solvent minimises heat of absorption and calculates

the corresponding VLE (shown in Fig. 6.6). The other one maximises the VLE and calculates corresponding heat of absorption. The latter leads to lower capture cost (see chap. 5.5).

The last step includes the VLE (equilibrium loading) in the optimisation, in addition to the transport properties, kinetics, and heat of absorption. It results in the ideal solvent, which breaks the Gibbs-Helmholtz equation. The solvent flow rate and unit sizes are again reduced and the main cost savings result from decreased steam, cooling, and heat exchanger cost. The main heat exchanger's size remained rather constant in the previous steps, as its size depends on the solvent flow rate and temperature approach. Only the solvent flow rate can induce any changes in its size as the temperature approach is fixed between the steps (in order to optimise for minimum capture cost). The solvent flow rate is directly proportional to the sensible heat required for regenerating it. Therefore, the specific reboiler duty decreases to 1.55MJ/kg_{CO_2}, which is only 37% of what is estimated for MEA. The capture cost utilising the ideal solvent in an archetypal process capturing 90% of the CO_2 contained in a flue gas with y_{CO_2}= 4 mol% are \$26.2/t_{CO_2} (34% of MEA's capture cost).

The selected sequence presented in Fig. 6.6 matters only for the visualisation, and one should refer to Fig. 6.1 to quantify the impact of the individual properties. The trends stay qualitatively the same regardless of capture rate and flue gas CO_2 composition (see Fig. D.4, Fig. D.5, and Fig. D.6). For all cases, improving the solvent's properties yields a CAPEX reduction (as seen in Fig. 5.4). However, even the ideal solvent cannot completely overcome (although considerably reduce) the process intrinsic inefficiency expressed in the OPEX. Thus, additional process improvements are needed and solvent development on its own is not a silver bullet for capture cost reductions. Dimensionless numbers describing the ideal solvent are listed in Tab. D.4. These numbers can guide the path towards better solvents, although some are inevitably linked to operating conditions (*e.g.,* velocities), or design variables (*e.g.,* characteristic lengths), and only the full set describes the capture challenge.

6.6 How good will Solvents ever be?

This section discusses what lessons can be learned from the Gibbs-Helmholtz and ideal solvent for the deployment of CCS. Figure 6.7 shows the full techno-economic screening plotted over the CO_2 flue gas composition ranging from y_{CO_2} = 2mol% up to y_{CO_2} = 30mol% at 90% capture rate. The screened amines are shown in grey with well-known examples individually highlighted. The Gibbs-Helmholtz solvent (maximised VLE) shown in Fig. 6.7 differs from the one shown in Fig. 6.6 which has been minimising heat of absorption. The 2022 §45Q tax-credit (pink horizontal dashed line, \$85/t_{CO_2}) and EU ETS prices \$64/t_{CO_2} (October 2021) are added as reference.

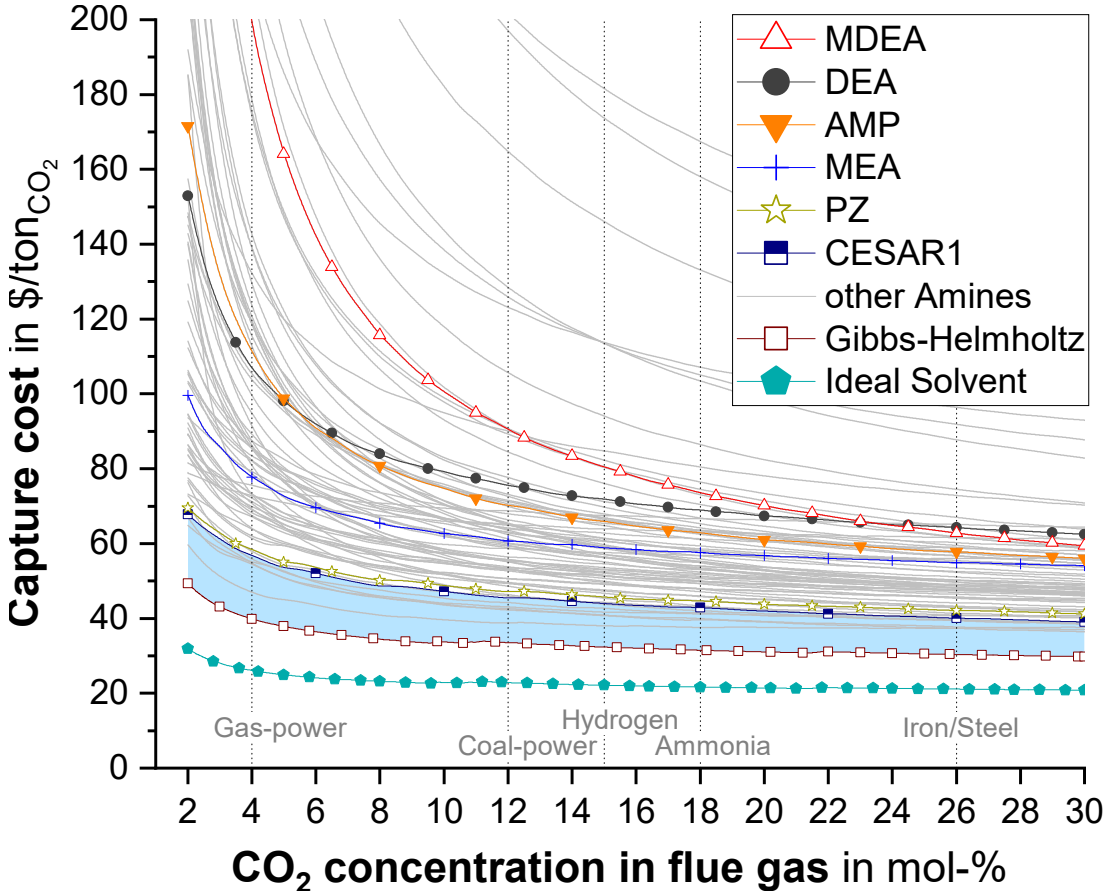


Figure 6.7: Capture cost of screened amines, CESAR1 (performance benchmark), the Gibbs-Helmholtz solvent, and the ideal solvent for flue gas CO_2 concentrations between y_{CO_2} = 2mol% and y_{CO_2}= 30 mol%. Tax credit US §45Q and EU ETS prices added for reference. The available potential for cost reductions through solvent improvement is highlighted in blue (based on the current performance benchmark CESAR1).

CESAR1 is setting the current open-literature performance benchmark, and the results agree it

being one of the best performing solvents. However, this work identified some poly-amines (grey lines) with lower capture cost, saving $\approx$ \$10/t_{CO_2} on average. The Gibbs-Helmholtz solvent outperforms all screened (existing) solvents and the cost saving over CESAR1 is $\approx$ \$17/t_{CO_2}. The difference in capture cost decreases with increasing y_{CO_2}.

The physically achievable room for improvement through solvent R&D is indicated by the gap between CESAR1 and the Gibbs-Helmholtz solvent (highlighted in blue). A 29% capture cost reduction over CESAR1 is physically possible, if one could find such solvent. Poly-amines appear to be the best available chemical class for this, and some examples (grey lines between CESAR1 and Gibbs-Helmholtz solvent) already explore the room for improvement.

If a solvent with the properties of the Gibbs-Helmholtz solvent is found, then the capture cost would break even with both §45Q tax-credit (\$50/t_{CO_2} until 2021, \$85/t_{CO_2} from 2022) and EU ETS prices for all CO_2 concentrations studied. Some solvents already break even with both EU ETS prices and §45Q tax-credit, and fewer solvents at CO_2 concentrations corresponding to gas-power. 2022's §45Q tax-credit level (higher than October 2021 EU ETS price), expands the number of viable solvents. Economic viability is assessed not just on annualised capture cost but on a business case including the full CCS value chain (*i.e.,* including cost for compression, transport, and storage) [7]. Capture cost tend to contribute the majority of the full value chain, and just breaking even with the subsidies indicates that there is still a gap in the business case.

Financial incentives for CCS exist with tax credits, *e.g.* 26 U.S. Code §45Q (Credit for carbon dioxide sequestration) in the USA, investment credits, *e.g.* 26 U.S. Code §48A (Qualifying advanced coal project credit) in the USA, Low Carbon Fuel Standard, *e.g.* LCFS in California, USA, or CO_2 prices *e.g.* the emissions trading scheme (ETS) in the EU. §48A offers an investment credit of up to 30% of the capital expenditure for advanced coal-based generation technologies (20% for IGCC). §45Q provides a tax credit of up to \$60/(t_{CO_2}) for CCU or EOR, and up to \$85/(t_{CO_2}) for permanent storage over 12 years and a minimum of 0.1 $Mtpa_{CO_2}$ (0.5 $Mtpa_{CO_2}$ for electricity generation). §45Q also provides up to \$130/(t_{CO_2}) for CDRs, which provide a different value to the system [29] but are linked to lower CO_2 concentration. It is the first scheme that links financial incentives to CO_2 concentration, and it might be worth

exploring to scale them to the mitigation potential expressed as size and concentration. This would consider the L-shaped cost curves shown by all solvents (see Fig. 6.7), regardless of their chemical class.

A long-term cost target of \$20/t_{CO_2} is unachievable through solvent R&D on its own. That target could only be barely met by breaking thermodynamics as shown with the ideal solvent. The relative difference between CESAR1 and the ideal solvent is 57% at y_{CO_2}= 30 mol% and 62% at y_{CO_2} = 1mol% meaning the capture cost will never be more than halved compared to CESAR1 within thr studies chemical classes, unless process improvements are introduced.

Future solvents will explore the area up to the Gibbs-Helmholtz solvent. This work sets a limit solely on solvent development and the capture cost do not represent a hard border (*i.e.,* only the solvent thermo-physical properties are limits). Improved process configurations (*e.g.,* advanced flash stripper), construction materials (*e.g.*, polymers or cement instead of steel, see [696]), or equipment (*e.g.,* 3D printed packings), will be able to further reduce the capture cost, although those changes are non-additive (see chapter 3.3.1).

Alternative pathways to reduce the cost associated with regeneration must be pursued to circumvent the intrinsic inefficiencies of the conventional closed-loop, thermo-swing absorber-stripper process. "New" and alternative solvents analysed in this work have similar thermo-physical properties but offer alternative paths forward by changing the chemistry, such that it enables using a fundamentally different process topology. Examples are anti-solvent regeneration, *e.g.,* polarity swing, reducing solvent circulation rates by removing inactive carriers, and minimising corrosion and degradation by avoiding aqueous amine environments [192, 567, 651, 697–707]. The central elements are to reduce the amount of solvent present in the regeneration, which should decrease the heat requirement, or completely avoid regeneration by a thermo-swing. It will be vital to exploit potential synergies between solvent and process including equipment intensification, which can compensate disadvantages of individual solvent systems, *e.g.* high viscosity of CO_2BOLs [192].

6.7 Conclusions

This work analysed the bottlenecks of solvent-based CO_2 capture. Increasing the concentration of the solute (*e.g.* amine) reduces the capture cost and partially addresses the intrinsic inefficiency of heating up and cooling down mostly water. However, it is not sufficient on its own due to the trends showing a distinctive minimum at $\approx$ 36 mol% on average. Replacing water with another non-CO_2 binding component as carrier, that offsets *e.g.* corrosion issues, will be helpful but not critical.

Despite the popularity and dominance of aqueous blends over the past 50 years, they will always be constrained by the bounds in each thermo-physical property of the pure amines and no excessive synergies have been observed. Without inducing a change in chemistry *e.g.* phase change by blending DEEA and MAPA, aqueous amine blends are unlikely to deliver a breakthrough in cost reductions.

A physically achievable Gibbs-Helmholtz solvent with optimal thermo-physical properties limits the room for cost savings available to future solvents. Improving all solvent properties yields a physically possible cost saving of up to 29% over CESAR1. Continuous solvent R&D outside the chemical classes analysed in this work might explore this room for improvement.

Reaching a long-term cost target of $\$20/t_{CO_2}$ is only possible by exploiting synergistic effects between solvent and process design, optimizing performance in conjunction with process intensification. Hence, developing new solvents without a fundamental change in the underlying process topology is not a silver bullet to solve the cost issues of CCS. Whilst R&D activity will obviously continue, with ambitious clean energy standards and enhanced CO_2 sequestration being discussed in the US and legislated "net zero" targets in the UK, EU, and China, allied with an EU ETS price in excess of $\$65/t_{CO_2}$, the immediate priority is to focus on deployment.

7. Conclusions and Outlook

7.1 Conclusions

Carbon capture and storage is integral to the mitigation of climate change, and the transition to a net-zero emissions world. Over the last 120 years, thousands of materials have been proposed for the capture of CO_2. In this work, a database and tool for the screening and quantitative assessment of solvents (SQUASH) was developed, enabling promising aqueous amine-based solvents to be relatively ranked.

In this work, 464 candidate solvents were identified, however, due to data gaps, only 73 could be successfully screened. This highlights the need for a standard protocol reporting solvent data and an easily accessible VLE and kinetics database. Focussing on aqueous amines, the solvents were expressed through their thermo-physical properties *i.e.,* molar mass, density, heat capacity, viscosity, thermal conductivity, surface tension, vapour pressure, heat of vapourisation, heat of reaction, VLE, Henry's coefficient, and kinetics. The amines were classified into primary, secondary, tertiary, and poly-amines. Trends between performance KPIs such as reboiler duty and capture cost were analysed.

It was not yet known if propagating errors in the underlying thermo-physical input data through a short-cut screening model prevents reaching statistically significant results. Errors of thermo-physical properties reported in the literature were collected, mean errors with standard deviations calculated, and then propagated through the model using a Monte-Carlo approach implemented in the Global System Analysis of gPROMS. A procedure to test the differences between solvents' mean capture cost for statistical significance was developed, and multiple inferential analysis methods compared. Welch's analysis of variance followed by a Games-Howell post-hoc test was identified as the preferred method. The results suggest that typical errors for solvents' input data do not cause statistical relevant concerns. Most solvents rank statistically significantly different due their individual thermo-physical properties and even relatively

low differences in mean capture cost of \$2/t_{CO_2} can be differentiated. Limited groups of two or three solvents each with similar capture costs cannot be differentiated, which accumulated to approximately 4% of all solvent comparisons. This work provides confidence in future solvent *in-silico* screening, in particular deploying methods with higher uncertainty, as they could deliver valuable insights at statistically significant confidence.

Screening CO_2 capture solvents should individually optimise the amine concentration, operating parameter such as lean loading, and equipment sizes. The historic focus on specific solvent properties, such as low heat of absorption, is not optimal, and the often neglected properties, viscosity and surface tension, proved equally important. The best performing solvents have lower capital expenditure compared to the worst performing solvents, which are dominated by large absorber cost. The remaining steam cost can be addressed by improving the efficiency of the capture unit through process intensification.

The ranking is influenced by the cost of steam required to regenerate the solvent. If steam prices are high *e.g.,* \$200/t_{Steam}, then the cost-optimal lean loading is the result of minimising the reboiler duty and solvents rank according to their reboiler duty. The ranking is more nuanced at moderate steam costs *e.g.,* \$20/t_{Steam} and dominated by a selected set of thermo-physical properties. The best performing solvents feature low reboiler duty, high working capacities > 0.5 $\text{mol}_{CO_2}/\text{mol}_{\text{Amine}}$, fast reaction rates $\text{pK}_\text{a} > 10$, and low viscosities < 1.6 mPas. Linear poly-amines with their alkalinities separated by C_2 - C_3 alkyl chains performed particularly well under all CO_2 concentrations analysed, supporting further research into these amines. The differences in capture cost between the solvents at high CO_2 concentrations found in cement or steel plants are relatively small (on average 1% between candidates). If practical issues such as high degradation, corrosion, or limited supply rule out a candidate, another solvent with similar capture cost might be available.

Despite the popularity and dominance of aqueous blends over the past 50 years, they will be constrained by the bounds in each thermo-physical property of the pure amines and no excessive synergies have been observed. Thus, new blends will re-explore the same thermo-physical property space. A physically achievable Gibbs-Helmholtz solvent with optimal thermo-physical

properties limits the room for cost savings available to future solvents within the studied classes. The theoretical achievable room for cost savings deliverable by solvent R&D over the current benchmark CESAR1 is limited to 29%. Alternative solvents and blends of aqueous amines explore the same thermo-physical property space already investigated by aqueous amines for decades.

Reaching widely anticipated capture cost reductions, *e.g.*, the long-term target of the US Department of Energy, is only possible by exploiting synergistic effects between solvent and process design, optimizing performance in conjunction with process intensification. Measures aiming at reducing the absorber's capital expenditure are less effective to further reduce the overall capture cost, because the best solvents are dominated by operating expenses. Developing new solvents without a fundamental change in the underlying process topology is not a silver bullet to solve the cost issues of CCS.

7.2 Outlook

The database was designed to be shared, and first research groups have accessed it with the intention of running their models with the collected data. This could enable more solvents to be screened. Establishing a machine-readable reporting template for solvent data (measured or predicted) is desirable. Such templates already exist for adsorbents, and is a necessary step to share the field's knowledge. Having continuously re-explored the same thermo-physical property space for the last century and still proposing solvents that require data to be manually extracted from manuscripts is not efficient.

It would be interesting to expand the work of Porcheron *et al.* [242, 243] by deriving QSPRs between chemical classes and capture cost by feeding the solvent database into their model. After having identified a group of promising solvents it is natural to investigate them further. Running more rigorous models *e.g.,* a multi-stage model with inter-coolers, or testing alternative stripper configurations, could confirm or reject the identified well-performing poly-amines. The model can be further improved by automatising the GSA and inferential analysis, and optimising the process topology at the same time.

Screening more solvents is unlikely to create new insights unless a focus is set on less represented chemical classes. Including other potential differentiators such as corrosion and toxicity might be helpful. The database and screening tool can be extended to include second order effects such as solvent-specific degradation and corrosion rates, toxicity, and amine prices. These topics are researched, *e.g.*, at the SaskPower Clean Energy Research Chair at the University of Regina in Canada. They are establishing links between solvent, flue gas composition, operating conditions, solvent degradation, and corrosion. If correlations become available, then they could be implemented in the model to individually optimise operating conditions, amine concentration, equipment material selection, and corrosion allowance.

Screening alternative chemistries in optimised topologies, *e.g.*, CO_2BOLs utilising anti-solvent regeneration, or phase-change solvents with split configurations, could complement the view on solvent based CO_2 capture. The ultimate goal is developing a super-structure optimisation tool with first examples being reported for CAMPD applications [708–711]. Such tools require sufficient solvent data published in the public domain, which is not yet the case for all new systems. Linking screening models with design tools such as INES [280] appears interesting from a commercial point of view by transparently embedding solvent selection into the process design. CAMD approaches [201–203, 207, 712] are restricted in the molecular design space and rely on some experimental data, in particular, for the reaction kinetics if applicable. This limitation might be overcome with *e.g.,* Rx-COSMO-CAMD approaches which predict kinetics based on transition-state theory and advanced quantum chemical methods [713, 714]. However, the computational effort is drastically increased over short-cut models (days versus seconds). Adding a superstructure optimisation for the process *i.e.,* creating a CAMPD model, would increase the computational effort due to the complexity and diversity of process intensification measures and the associated links between operating parameter and solvent performance [711]. This bottleneck could be solved by implementing reduced order models that result from quantum chemical methods, which is topic of ongoing research [186].

Bibliography

[1] S. Arrhenius, On the influence of carbonic acid in the air upon the temperature of the ground, The London, Edinburgh and Dublin philosophical magazine and journal of science 41 (251) (1896) 237–276.

[2] G. S. Callendar, The artificial production of carbon dioxide and its influence on temperature, Quarterly Journal of the Royal Meteorological Society 64 (275) (1938) 223–240. doi:10.1002/qj.49706427503.

[3] C. D. Keeling, R. B. Bacastow, A. E. Bainbridge, C. A. Ekdahl, P. R. Guenther, L. S. Waterman, J. F. S. Chin, Atmospheric carbon dioxide variations at Mauna Loa Observatory, Hawaii, Tellus 28 (6) (1976) 538–551. doi:10.1111/j.2153-3490.1976.tb00701.x.

[4] J. Cook, N. Oreskes, P. T. Doran, W. R. L. Anderegg, B. Verheggen, E. W. Maibach, J. S. Carlton, S. Lewandowsky, A. G. Skuce, S. A. Green, D. Nuccitelli, P. Jacobs, M. Richardson, B. Winkler, R. Painting, K. Rice, Consensus on consensus: A synthesis of consensus estimates on human-caused global warming, Environmental Research Letters 11 (4) (2016) 048002. doi:10.1088/1748-9326/11/4/048002.

[5] IPCC, Climate Change 2014: Mitigation of Climate Change: Contribution of Working Group III to the Fifth Assessment Report of the Intergovernmental Panel on Climate Change, Cambridge University Press, 2014.

[6] United Nations, Paris Agreement, https://unfccc.int/sites/default/files/english_paris_agreement.pdf, last accessed on 01/12/18 (2018).

[7] Working Group III of the Intergovernmental Panel on Climate Change, IPCC Special Report on Carbon Dioxide Capture and Storage, Cambridge University Press, 2005.

[8] J. Rogelj, A. Popp, K. V. Calvin, G. Luderer, J. Emmerling, D. Gernaat, S. Fujimori, J. Strefler, T. Hasegawa, G. Marangoni, Scenarios towards limiting global mean temperature increase below 1.5°C, Nature Climate Change 8 (4) (2018) 325–332.

[9] P. M. Mathias, S. Reddy, A. Smith, K. Afshar, A guide to evaluate solvents and processes

for post-combustion CO_2 capture, Energy Procedia 37 (2013) 1863–1870. doi:10.1016/j.egypro.2013.06.066.

[10] Y. Tan, W. Nookuea, H. Li, E. Thorin, J. Yan, Property impacts on carbon capture and storage (CCS) processes: A review, Energy Conversion and Management 118 (2016) 204–222. doi:10.1016/j.enconman.2016.03.079.

[11] E. Braun, A. F. Zurhelle, W. Thijssen, S. K. Schnell, L.-C. Lin, J. Kim, J. A. Thompson, B. Smit, High-throughput computational screening of nanoporous adsorbents for CO_2 capture from natural gas, Mol. Syst. Des. Eng. 1 (2016) 175–188. doi:10.1039/C6ME00043F.

[12] D. Bahamon, L. F. Vega, Systematic evaluation of materials for post-combustion CO_2 capture in a temperature swing adsorption process, Chemical Engineering Journal 284 (2016) 438–447. doi:10.1016/j.cej.2015.08.098.

[13] D. Bahamon, A. Diaz-Marquez, P. Gamallo, L. F. Vega, Energetic evaluation of swing adsorption processes for CO_2 capture in selected mofs and zeolites: Effect of impurities, Chemical Engineering Journal 342 (2018) 458–473. doi:10.1016/j.cej.2018.02.094.

[14] D. Danaci, M. Bui, N. Mac-Dowell, C. Petit, Exploring the limits of adsorption-based CO_2 capture using MOFs with PVSA – from molecular design to process economics, Mol. Syst. Des. Eng. 5 (2020) 212–231. doi:10.1039/C9ME00102F.

[15] A. H. Farmahini, D. Friedrich, S. Brandani, L. Sarkisov, Exploring new sources of efficiency in process-driven materials screening for post-combustion carbon capture, Energy Environ. Sci. 13 (2020) 1018–1037. doi:10.1039/c9ee03977e.

[16] S. Krishnamurthy, J. Boon, C. Grande, A. Lind, R. Blom, R. de Boer, H. Willemsen, G. de Scheemaker, Screening supported amine sorbents in the context of post-combustion carbon capture by vacuum swing adsorption, Chemie Ingenieur Technik 93 (6) (2021) 929–940. doi:10.1002/cite.202000172.

[17] A. Samanta, A. Zhao, G. K. H. Shimizu, P. Sarkar, R. Gupta, Post-combustion CO_2 capture using solid sorbents: A review, Ind. Eng. Chem. Res. 51 (4) (2012) 1438–1463. doi:10.1021/ie200686q.

[18] A. H. Farmahini, S. Krishnamurthy, D. Friedrich, S. Brandani, L. Sarkisov, Performance-

based screening of porous materials for carbon capture, Chemical Reviews 121 (17) (2021) 10666–10741. doi:10.1021/acs.chemrev.0c01266.

[19] C. Halliday, T. A. Hatton, Sorbents for the capture of CO_2 and other acid gases: A review, Industrial & Engineering Chemistry Research 60 (26) (2021) 9313–9346. doi:10.1021/acs.iecr.1c00597.

[20] IPCC, Climate Change 2021: The Physical Science Basis. Contribution of Working Group I to the Sixth Assessment Report of the Intergovernmental Panel on Climate Change, Cambridge University Press, 2021.

[21] UNFCCC, Technical dialogue of the first global stocktake. Synthesis report by the co-facilitators on the technical dialogue, Tech. rep. UN Climate Change Conference-United Arab Emirates Nov/Dec 2023 , 2023.

[22] IEA, World energy outlook 2021doi:https://www.iea.org/reports/world-energy-outlook-2021.

[23] BP, Statistical review of world energydoi:https://www.bp.com/content/dam/bp/business-sites/en/global/corporate/pdfs/energy-economics/statistical-review/bp-stats-review-2021-full-report.pdf.

[24] Emissions Gap Report 2021: The Heat Is On A World of Climate Promises Not Yet Delivered (2021).
URL https://reliefweb.int/sites/reliefweb.int/files/resources/Emissions%20Gap%20Report%202021%20%28Executive%20Summary%29.pdf

[25] R. S. Haszeldine, Carbon capture and storage: How green can black be?, Science 325 (5948) (2009) 1647–1652. doi:10.1126/science.1172246.

[26] C. Bonneuil, P.-L. Choquet, B. Franta, Early warnings and emerging accountability: Total's responses to global warming 1971 - 2021, Global Environmental Change (2021) 102386doi:10.1016/j.gloenvcha.2021.102386.

[27] IEA, Net zero by 2050doi:https://www.iea.org/reports/net-zero-by-2050.

[28] C. F. Heuberger, I. Staffell, N. Shah, N. Mac Dowell, Quantifying the value of CCS for the future electricity system, Energy Environ. Sci. 9 (8) (2016) 2497–2510. doi:10.1039/c6ee01120a.

[29] Royal Society of Chemistry, Royal Academy of Engineering, Greenhouse gas removal, Tech. rep. (2018).

[30] S. E. Baker, J. K. Stolaroff, G. Peridas, S. H. Pang, H. M. Goldstein, F. R. Lucci, W. Li, E. W. Slessarev, J. Pett-Ridge, F. J. Ryerson, J. L. Wagoner, W. Kirkendall, R. D. Aines, Getting to neutral, Tech. rep. (2020).

[31] C. Hepburn, E. Adlen, J. Beddington, E. Carter, S. Fuss, N. Mac Dowell, J. Minx, P. Smith, C. Williams, The technological and economic prospects for CO_2 utilization and removal, Nature 575 (2019) 87–97. doi:10.1038/s41586-019-1681-6.

[32] J. C. Minx, W. F. Lamb, M. W. Callaghan, S. Fuss, J. Hilaire, F. Creutzig, T. Amann, T. Beringer, W. de Oliveira Garcia, J. Hartmann, T. Khanna, D. Lenzi, G. Luderer, G. F. Nemet, J. Rogelj, P. Smith, J. L. V. Vicente, J. Wilcox, M. del Mar Zamora Dominguez, Negative emissions part 1: Research landscape and synthesis, Environmental Research Letters 13 (6) (2018) 063001. doi:10.1088/1748-9326/aabf9b.

[33] S. Fuss, W. F. Lamb, M. W. Callaghan, J. Hilaire, F. Creutzig, T. Amann, T. Beringer, W. de Oliveira Garcia, J. Hartmann, T. Khanna, G. Luderer, G. F. Nemet, J. Rogelj, P. Smith, J. L. V. Vicente, J. Wilcox, M. del Mar Zamora Dominguez, J. C. Minx, Negative emissions Part 2: Costs, potentials and side effects, Environmental Research Letters 13 (6) (2018) 063002. doi:10.1088/1748-9326/aabf9f.

[34] G. F. Nemet, M. W. Callaghan, F. Creutzig, S. Fuss, J. Hartmann, J. Hilaire, W. F. Lamb, J. C. Minx, S. Rogers, P. Smith, Negative emissions part 3: Innovation and upscaling, Environmental Research Letters 13 (6) (2018) 063003. doi:10.1088/1748-9326/aabff4.

[35] National Academies of Sciences, Engineering, and Medicine, Negative Emissions Technologies and Reliable Sequestration: A Research Agenda, The National Academies Press, Washington, DC, 2019. doi:10.17226/25259.

[36] J. Wilcox, P. C. Psarras, S. Liguori, Assessment of reasonable opportunities for direct air capture, Environ. Res. Lett. 12 (6) (2017) 065001.

[37] S. Deutz, A. Bardow, Life-cycle assessment of an industrial direct air capture process based on temperature–vacuum swing adsorption, Nature Energy 6 (2) (2021) 203–213.

[38] A. Kiani, K. Jiang, P. Feron, Techno-economic assessment for CO_2 capture from air using a conventional liquid-based absorption process, Frontiers in Energy Research 8 (2020) 92. doi:10.3389/fenrg.2020.00092.

[39] R. S. Haszeldine, S. Flude, G. Johnson, V. Scott, Negative emissions technologies and carbon capture and storage to achieve the paris agreement commitments, Philosophical Transactions of the Royal Society A: Mathematical, Physical and Engineering Sciences 376 (2119) (2018) 20160447. doi:10.1098/rsta.2016.0447.

[40] V. Scott, R. S. Haszeldine, S. F. Tett, A. Oschlies, Fossil fuels in a trillion tonne world, Nature Climate Change 5 (5) (2015) 419–423.

[41] N. Mac Dowell, P. S. Fennell, N. Shah, G. C. Maitland, The role of CO_2 capture and utilization in mitigating climate change, Nature Climate Change 7 (4) (2017) 243–249.

[42] R. Meys, A. Kätelhön, M. Bachmann, B. Winter, C. Zibunas, S. Suh, A. Bardow, Achieving net-zero greenhouse gas emission plastics by a circular carbon economy, Science 374 (6563) (2021) 71–76. doi:10.1126/science.abg9853.

[43] C. Marchetti, On geoengineering and the CO_2 problem, Clim. Change 1 (1) (1977) 59–68. doi:10.1007/bf00162777.

[44] D. W. Keith, Geoengineering the climate: History and prospect, Annual Review of Energy and the Environment 25 (1) (2000) 245–284. doi:10.1146/annurev.energy.25.1.245.

[45] W. Nordhaus, Can we control carbon dioxide?, IASA Whitepaper, 1975.

[46] M. Steinberg, H. C. Cheng, Modern and prospective technologies for hydrogen production from fossil fuels, Int. J. Hydrogen Energy 14 (11) (1989) 797–820.

[47] M. Steinberg, A. Albanese, V. Dang, Environmental control technology for atmospheric carbon dioxide. Quarterly progress report No. 1, June 20, 1977–September 30, 1977, Tech. rep., Brookhaven National Lab., Upton, NY (USA) (1977).

[48] A. S. Albanese, M. Steinberg, Environmental control technology for atmospheric carbon dioxide, Energy 5 (7) (1980) 641–664. doi:10.1016/0360-5442(80)90044-4.

[49] M. Steinberg, A. S. Albanese, Environmental control technology for atmospheric carbon dioxide, International Workshop on the Energy/Climate Interactions, March 3-7, 1980,

Munster, Germany.

[50] Interactions of Energy and Climate: Proceedings of an International Workshop held in Munster, Germany, March 3-6, 1980, Reidel, Dordrecht; London, 1980.

[51] M. Steinberg, An analysis of concepts for controlling atmospheric carbon dioxide, United States Department of Energy DOE report, Tech. rep., CH/00016-1, Washington DC (1983).

[52] M. Steinberg, Advanced technologies for the recovery, disposal, and reuse of carbon dioxide for atmospheric control, Tech. rep., Brookhaven National Lab., Upton, NY (USA) (1983).

[53] M. Steinberg, H. C. Cheng, F. Horn, A systems study for the removal, recovery and disposal of carbon dioxide from fossil fuel power plants in the U.S., Brookhaven National Laboratory; Available from National Technical Information Service, Upton, N.Y.; Springfield, Va., 1984.

[54] M. Steinberg, H. Cheng, F. Horn, A system study for the removal, recovery, and disposal of carbon dioxide from fossil fuel power plants in the US BNL35666 informal report, Brookhaven National Laboratory.

[55] M. Steinberg, History of CO_2 greenhouse gas mitigation technologies, Energy Conversion and Management 33 (5) (1992) 311–315. doi:10.1016/0196-8904(92)90025-R.

[56] M. Steinberg, A. Albanese, V. Dang, Environmental control technology for atmospheric carbon dioxide. Quarterly progress report No. 1, June 20, 1977–September 30, 1977doi:10.2172/6791792.

[57] M. Steinberg, A. Albanese, Environmental control technology for atmospheric carbon dioxide. Progress report No. 2 for DOE, October 1, 1977–March 31, 1978doi:10.2172/6589260.

[58] A. S. Albanese, M. Steinberg, Environmental control technology for atmospheric carbon dioxide. Final reportdoi:10.2172/5468101.

[59] A. S. Albanese, M. Steinberg, Environmental control technology for atmospheric carbon dioxide. Final report for DOEdoi:10.2172/5384102.

[60] F. L. Horn, M. Steinberg, Control of carbon dioxide emissions from a power plant (and

use in enhanced oil recovery), Fuel 61 (5) (1982) 415–422. doi:10.1016/0016-2361(82)90064-3.

[61] C. Mustacchi, P. Armenante, V. Cena, Carbon dioxide disposal in the ocean, Carbon Dioxide and Society, Proceedings of a IIASA Workshop, 1978. (1978) 283–289.

[62] E. Martin-Roberts, V. Scott, S. Flude, G. Johnson, R. S. Haszeldine, S. Gilfillan, Carbon capture and storage at the end of a lost decade, One Earthdoi:10.1016/j.oneear.2021.10.002.

[63] The global status of CCS. 2021.
URL www.globalccsinstitute.com/resources/global-status-report/download/

[64] E. Oko, M. Wang, A. S. Joel, Current status and future development of solvent-based carbon capture, International journal of coal science & technology 4 (1) (2017) 5–14.

[65] R. Lund, K. Sanden, A.-H. Haaland, T. A. Rikheim, S. Woodhouse, United States Patent No. US 8361425b2, CO_2 absorption method (2013).

[66] C. Braun, Not in My Backyard: CCS Sites and Public Perception of CCS, Risk Analysis 37 (12) (2017) 2264–2275. doi:10.1111/risa.12793.

[67] B. W. Terwel, D. D. Daamen, E. ter Mors, Not in my back yard (nimby) sentiments and the structure of initial local attitudes toward CO_2 storage plans, Energy Procedia 37 (2013) 7462–7463. doi:10.1016/j.egypro.2013.06.689.

[68] R. M. Krause, S. R. Carley, D. C. Warren, J. A. Rupp, J. D. Graham, "not in (or under) my backyard": Geographic proximity and public acceptance of carbon capture and storage facilities, Risk Analysis 34 (3) (2014) 529–540. doi:10.1111/risa.12119.

[69] K. Arning, J. Offermann-van Heek, A. Linzenich, A. Kaetelhoen, A. Sternberg, A. Bardow, M. Ziefle, Same or different? insights on public perception and acceptance of carbon capture and storage or utilization in germany, Energy Policy 125 (2019) 235–249. doi:10.1016/j.enpol.2018.10.039.

[70] E. Dütschke, K. Wohlfarth, S. Höller, P. Viebahn, D. Schumann, K. Pietzner, Differences in the public perception of CCS in germany depending on CO_2 source, transport option and storage location, International Journal of Greenhouse Gas Control 53 (2016) 149–159. doi:10.1016/j.ijggc.2016.07.043.

[71] L. Wallquist, V. H. M. Visschers, S. Dohle, M. Siegrist, Adapting communication to the public's intuitive understanding of CCS, Greenhouse Gases: Science and Technology 1 (1) (2011) 83–91. doi:10.1002/ghg3.4.

[72] M. Ziegler, S. Forbes, Guidelines for community engagement in carbon dioxide capture, transport, and storage projects.
URL https://www.wri.org/research/guidelines-community-engagement-carbon\-dioxide-capture-transport-and-storage-projects

[73] P. Radgen, R. Irons, H. Schoenmakers, Too early or too late for CCS-what needs to be done to overcome the valley of death for carbon capture and storage in europe?, Energy Procedia 37 (2013) 6189–6201.

[74] A. Abdulla, R. Hanna, K. R. Schell, O. Babacan, D. G. Victor, Explaining successful and failed investments in US carbon capture and storage using empirical and expert assessments, Environmental Research Letters 16 (1) (2020) 014036.

[75] R. Gunderson, D. Stuart, B. Petersen, The fossil fuel industrys framing of carbon capture and storage: Faith in innovation, value instrumentalization, and status quo maintenance, Journal of Cleaner Production 252 (2020) 119767. doi:10.1016/j.jclepro.2019.119767.

[76] H. Herzog, Lessons learned from CCS demonstration and large pilot projects, Tech. rep., MIT Energy Initiative, Cambridge, U.S. (2016).

[77] M. Sander, C. Mariz, The Fluor Daniel Econamine FG process: Past experience and present day focus, Energy Conversion and Management 33 (5) (1992) 341–348. doi:10.1016/0196-8904(92)90029-V.

[78] Federal Energy R&D: Carbon Capture, https://www2.itif.org/2019-budget-carbon-capture.pdf, last accessed on 09/11/23.

[79] C. L. Donnison, K. Trdlicova, A. Mohr, G. Taylor, A net-zero storyline for success? News media analysis of the social legitimacy of bioenergy with carbon capture and storage in the United Kingdom, Energy Research & Social Science 102 (2023) 103153. doi:10.1016/j.erss.2023.103153.

[80] M. E. Boot-Handford, J. C. Abanades, E. J. Anthony, M. J. Blunt, S. Brandani, N. Mac

Dowell, J. R. Fernández, M.-C. Ferrari, R. Gross, J. P. Hallett, R. S. Haszeldine, P. Heptonstall, A. Lyngfelt, Z. Makuch, E. Mangano, R. T. J. Porter, M. Pourkashanian, G. T. Rochelle, N. Shah, J. G. Yao, P. S. Fennell, Carbon capture and storage update, Energy Environ. Sci. 7 (2014) 130–189. doi:10.1039/C3EE42350F.
URL http://dx.doi.org/10.1039/C3EE42350F

[81] M. Bui, C. S. Adjiman, A. Bardow, E. J. Anthony, A. Boston, S. Brown, P. S. Fennell, S. Fuss, A. Galindo, L. A. Hackett, J. P. Hallett, H. J. Herzog, G. Jackson, J. Kemper, S. Krevor, G. C. Maitland, M. Matuszewski, I. S. Metcalfe, C. Petit, G. Puxty, J. Reimer, D. M. Reiner, E. S. Rubin, S. A. Scott, N. Shah, B. Smit, J. P. M. Trusler, P. Webley, J. Wilcox, N. Mac Dowell, Carbon capture and storage (CCS): the way forward, Energy Environ. Sci. 11 (5) (2018) 1062–1176. doi:10.1039/c7ee02342a.

[82] W. Gao, S. Liang, R. Wang, Q. Jiang, Y. Zhang, Q. Zheng, B. Xie, C. Y. Toe, X. Zhu, J. Wang, L. Huang, Y. Gao, Z. Wang, C. Jo, Q. Wang, L. Wang, Y. Liu, B. Louis, J. Scott, A.-C. Roger, R. Amal, H. He, S.-E. Park, Industrial carbon dioxide capture and utilization: state of the art and future challenges, Chem. Soc. Rev. 49 (2020) 8584–8686. doi:10.1039/d0cs00025f.

[83] G. Puxty, W. Conway, P. Feron, 4 - liquid absorbent selection criteria and screening procedures, in: P. H. Feron (Ed.), Absorption-Based Post-combustion Capture of Carbon Dioxide, Woodhead Publishing, 2016, pp. 69–100. doi:10.1016/B978-0-08-100514-9.00004-4.

[84] W. Budzianowski, Single solvents, solvent blends, and advanced solvent systems in CO_2 capture by absorption: A review, International Journal of Global Warming 7 (2015) 184–225.

[85] T. Davran-Candan, 2.27 CO_2 capturing materials, in: I. Dincer (Ed.), Comprehensive Energy Systems, Elsevier, Oxford, 2018, pp. 881–912. doi:10.1016/B978-0-12-809597-3.00255-8.

[86] Z. Zhang, T. N. Borhani, A. G. Olabi, Status and perspective of CO_2 absorption process, Energy 205 (2020) 118057. doi:10.1016/j.energy.2020.118057.

[87] D. J. Heldebrant, J. Kothandaraman, Chapter 3 solvent-based absorption, in: Carbon

Capture and Storage, The Royal Society of Chemistry, 2020, pp. 36–68. doi:10.1039/9781788012744-00036.

[88] K. A. Mumford, Y. Wu, K. H. Smith, G. W. Stevens, Review of solvent based carbon-dioxide capture technologies, Frontiers of Chemical Science and Engineering 9 (2) (2015) 125–141.

[89] B. Sreenivasulu, D. V. Gayatri, I. Sreedhar, K. V. Raghavan, A journey into the process and engineering aspects of carbon capture technologies, Renewable and Sustainable Energy Reviews 41 (2015) 1324–1350. doi:10.1016/j.rser.2014.09.029.

[90] T. N.Borhani, M. Wang, Role of solvents in CO_2 capture processes: The review of selection and design methods, Renewable and Sustainable Energy Reviews 114 (2019) 109299. doi:10.1016/j.rser.2019.109299.

[91] Z. H. Liang, W. Rongwong, H. Liu, K. Fu, H. Gao, F. Cao, R. Zhang, T. Sema, A. Henni, K. Sumon, D. Nath, D. Gelowitz, W. Srisang, C. Saiwan, A. Benamor, M. Al-Marri, H. Shi, T. Supap, C. Chan, Q. Zhou, M. Abu-Zahra, M. Wilson, W. Olson, R. Idem, P. Tontiwachwuthikul, Recent progress and new developments in post-combustion carbon-capture technology with amine based solvents, International Journal of Greenhouse Gas Control 40 (2015) 26–54. doi:10.1016/j.ijggc.2015.06.017.

[92] B. Dutcher, M. Fan, A. G. Russell, Amine-based CO_2 capture technology development from the beginning of 2013 – a review, ACS Applied Materials & Interfaces 7 (4) (2015) 2137–2148. doi:10.1021/am507465f.

[93] I. P. Koronaki, L. Prentza, V. Papaefthimiou, Modeling of CO_2 capture via chemical absorption processes - an extensive literature review, Renewable and Sustainable Energy Reviews 50 (2015) 547–566. doi:10.1016/j.rser.2015.04.124.

[94] I. Sreedhar, T. Nahar, A. Venugopal, B. Srinivas, Carbon capture by absorption – path covered and ahead, Renewable and Sustainable Energy Reviews 76 (2017) 1080–1107. doi:10.1016/j.rser.2017.03.109.

[95] M. H. Nematollahi, P. J. Carvalho, Green solvents for CO_2 capture, Current Opinion in Green and Sustainable Chemistry 18 (2019) 25–30. doi:10.1016/j.cogsc.2018.11.012.

[96] B. Adderley, J. Carey, J. Gibbins, M. Lucquiaud, R. Smith, Post-combustion carbon dioxide capture cost reduction to 2030 and beyond, Faraday Discuss. 192 (2016) 27–35. doi:10.1039/c6fd00046k.

[97] G. T. Rochelle, Amine scrubbing for CO_2 capture, Science 325 (5948) (2009) 1652–1654. doi:10.1126/science.1176731.

[98] M. Wang, A. Lawal, P. Stephenson, J. Sidders, C. Ramshaw, Post-combustion CO_2 capture with chemical absorption: A state-of-the-art review, Chem. Eng. Res. Des. 89 (9) (2011) 1609–1624. doi:10.1016/j.cherd.2010.11.005.

[99] F. Vega, F. Baena-Moreno, L. M. Gallego Fernández, E. Portillo, B. Navarrete, Z. Zhang, Current status of CO_2 chemical absorption research applied to CCS: Towards full deployment at industrial scale, Applied Energy 260 (2020) 114313. doi:10.1016/j.apenergy.2019.114313.

[100] F. O. Ochedi, J. Yu, H. Yu, Y. Liu, A. Hussain, Carbon dioxide capture using liquid absorption methods: a review, Environmental Chemistry Letters (2020) 1–33.

[101] R. R. Bottoms, United States Patent No. 1783901, Process for separating acid gases (1930).

[102] A. S. Allen, A. Michalske, United States Patent No. 1934472, Method of separating carbon dioxide from a gas mixture (1933).

[103] L. Knorr, Ueber das diäthanolamin, Berichte der deutschen chemischen Gesellschaft 30 (1) (1897) 915–918. doi:10.1002/cber.189703001179.

[104] A. Wurtz, Ueber die oxyäthylenbasen, Justus Liebigs Annalen der Chemie 121 (2) (1862) 226–232. doi:10.1002/jlac.18621210208.

[105] R. Allam, C. Spilsbury, A study of the extraction of CO_2 from the flue gas of a 500 MW pulverised coal fired boiler, Energy Conversion and Management 33 (5) (1992) 373–378. doi:10.1016/0196-8904(92)90033-S.

[106] C. Hendriks, K. Blok, W. Turkenburg, The recovery of carbon dioxide from power plants, in: Climate and Energy: The Feasibility of Controlling CO_2 Emissions, Springer, 1989, pp. 125–142.

[107] K. Blok, C. A. Hendriks, W. C. Turkenburg, The role of carbon dioxide removal in

the reduction of the greenhouse effect, Department of Science, Technology and Society, University of Utrecht, 1989.

[108] G. Booras, S. Smelser, An engineering and economic evaluation of CO_2 removal from fossil-fuel-fired power plants, Energy 16 (11) (1991) 1295–1305. doi:10.1016/0360-5442(91)90003-5.

[109] H. Herzog, D. Golomb, S. Zemba, Feasibility, modeling and economics of sequestering power plant CO_2 emissions in the deep ocean, Environmental Progress 10 (1) 64–74. doi:10.1002/ep.670100118.

[110] T. Yagi, H. Shibuya, T. Sasaki, Application of chemical absorption process to CO_2 recovery from flue gas generated in power plants, Energy Conversion and Management 33 (5) (1992) 349–355. doi:10.1016/0196-8904(92)90030-Z.

[111] C. Leci, S. Goldthorpe, Assessment of CO_2 removal from power station flue gas, Energy Conversion and Management 33 (5) (1992) 477–485. doi:10.1016/0196-8904(92)90046-Y.

[112] P. Brandl, M. Bui, J. P. Hallett, N. Mac Dowell, Beyond 90% capture: Possible, but at what cost?, International Journal of Greenhouse Gas Control 105 (2021) 103239. doi:10.1016/j.ijggc.2020.103239.

[113] D. Danaci, M. Bui, C. Petit, N. Mac-Dowell, En route to zero emissions for power and industry with amine-based post-combustion capture, Environmental Science & Technology 55 (15) (2021) 10619–10632.

[114] K. Jiang, P. Feron, A. Cousins, R. Zhai, K. Li, Achieving zero/negative-emissions coal-fired power plants using amine-based postcombustion CO_2 capture technology and biomass cocombustion, Environ. Sci. Technol. 54 (4) (2020) 2429–2438. doi:10.1021/acs.est.9b07388.

[115] P. H. Feron, A. Cousins, K. Jiang, R. Zhai, M. Garcia, An update of the benchmark post-combustion CO_2-capture technology, Fuel 273 (2020) 117776. doi:10.1016/j.fuel.2020.117776.

[116] Y. Matsuzaki, H. Yamada, F. A. Chowdhury, T. Higashii, S. Kazama, M. Onoda, Ab initio study of CO_2 capture mechanisms in monoethanolamine aqueous solution: Re-

action pathways from carbamate to bicarbonate, Energy Procedia 37 (2013) 400–406. doi:10.1016/j.egypro.2013.05.124.

[117] M. Caplow, Kinetics of carbamate formation and breakdown, Journal of the American Chemical Society 90 (24) (1968) 6795–6803. doi:10.1021/ja01026a041.

[118] P. Danckwerts, The reaction of CO_2 with ethanolamines, Chemical Engineering Science 34 (4) (1979) 443–446. doi:10.1016/0009-2509(79)85087-3.

[119] N. McCann, D. Phan, X. Wang, W. Conway, R. Burns, M. Attalla, G. Puxty, M. Maeder, Kinetics and mechanism of carbamate formation from CO_2(aq), carbonate species, and monoethanolamine in aqueous solution, The Journal of Physical Chemistry A 113 (17) (2009) 5022–5029. doi:10.1021/jp810564z.

[120] N. McCann, D. Phan, M. Attalla, G. Puxty, D. Fernandes, W. Conway, X. Wang, R. Burns, I. van Altena, G. Lawrance, M. Maeder, Molecular interactions between amine and carbonate species in aqueous solution – kinetics and thermodynamics, Energy Procedia 1 (1) (2009) 995–1002. doi:10.1016/j.egypro.2009.01.132.

[121] T. L. Donaldson, Y. N. Nguyen, Carbon dioxide reaction kinetics and transport in aqueous amine membranes, Industrial & Engineering Chemistry Fundamentals 19 (3) (1980) 260–266. doi:10.1021/i160075a005.

[122] R. J. Littel, W. P. M. van Swaaij, G. F. Versteeg, Kinetics of carbon dioxide with tertiary amines in aqueous solution, AIChE Journal 36 (11) (1990) 1633–1640. doi:10.1002/aic.690361103.

[123] G. Versteeg, W. van Swaaij, On the kinetics between CO_2 and alkanolamines both in aqueous and non-aqueous solutions–II. tertiary amines, Chemical Engineering Science 43 (3) (1988) 587–591. doi:10.1016/0009-2509(88)87018-0.

[124] G. F. Versteeg, L. A. J. Van Dijck, W. P. M. Van Swaaij, On the kinetics between CO_2 and alkanolamines both in aqueous and non-aqueous solutions. an overview, Chemical Engineering Communications 144 (1) (1996) 113–158. doi:10.1080/00986449608936450.

[125] P. M. M. Blauwhoff, G. F. Versteeg, W. P. M. Van Swaaij, A study on the reaction between CO_2 and alkanolamine in aqueous solutions, Chem. Eng. Sci. 39 (1984) 207–225.

[126] D. Fernandes, W. Conway, X. Wang, R. Burns, G. Lawrance, M. Maeder, G. Puxty, Protonation constants and thermodynamic properties of amines for post combustion capture of CO_2, The Journal of Chemical Thermodynamics 51 (2012) 97–102. doi:10.1016/j.jct.2012.02.031.

[127] X. Yang, R. J. Rees, W. Conway, G. Puxty, Q. Yang, D. A. Winkler, Computational modeling and simulation of CO_2 capture by aqueous amines, Chemical Reviews 117 (14) (2017) 9524–9593. doi:10.1021/acs.chemrev.6b00662.

[128] E. Mindrup, W. Schneider, Computational comparison of the reactions of substituted amines with CO_2, ChemSusChem 3 (8) (2010) 931–938. doi:10.1002/cssc.201000060.

[129] A. Chakraborty, G. Astarita, K. Bischoff, CO_2 absorption in aqueous solutions of hindered amines, Chemical Engineering Science 41 (4) (1986) 997–1003. doi:10.1016/0009-2509(86)87185-8.

[130] G. Sartori, D. W. Savage, Sterically hindered amines for carbon dioxide removal from gases, Ind. Eng. Chem. Fundam. 22 (2) (1983) 239–249. doi:10.1021/i100010a016.

[131] G. Sartori, W. S. Ho, D. W. Savage, G. R. Chludzinski, S. Wlechert, Sterically-hindered amines for acid-gas absorption, Separation and Purification Methods 16 (2) (1987) 171–200. doi:10.1080/03602548708058543.

[132] Y. Matsuzaki, H. Yamada, F. A. Chowdhury, S. Yamamoto, K. Goto, Ab initio study of CO_2 capture mechanisms in aqueous 2-amino-2-methyl-1-propanol: Electronic and steric effects of methyl substituents on the stability of carbamate, Industrial & Engineering Chemistry Research 58 (8) (2019) 3549–3554. doi:10.1021/acs.iecr.8b06229.

[133] F. Bougie, M. C. Iliuta, Sterically hindered amine-based absorbents for the removal of CO_2 from gas streams, Journal of Chemical & Engineering Data 57 (3) (2012) 635–669. doi:10.1021/je200731v.

[134] N. McCann, M. Maeder, M. Attalla, Simulation of enthalpy and capacity of CO_2 absorption by aqueous amine systems, Industrial & Engineering Chemistry Research 47 (6) (2008) 2002–2009. doi:10.1021/ie070619a.

[135] E. F. da Silva, H. F. Svendsen, Study of the carbamate stability of amines using ab initio methods and free-energy perturbations, Industrial & Engineering Chemistry Research

45 (8) (2006) 2497–2504. doi:10.1021/ie050501z.

[136] Q. Yang, S. James, M. Ballard, M. Bown, Influence of Amine Chemical Structures to Amine Capacities in CO_2 Capture, 2012, Ch. 2, pp. 29–42. doi:10.1021/bk-2012-1097.ch002.

[137] F. A. Carey, R. J. Sundberg, Advanced organic chemistry: part A: structure and mechanisms, Springer Science & Business Media, 2007.

[138] H. Bosch, G. F. Versteeg, W. P. M. Van Swaaij, Gas–liquid mass transfer with parallel reversible reactions–III. absorption of CO_2 into solutions of blends of amines, Chem. Eng. Sci. 44 (11) (1989) 2745–2750. doi:10.1016/0009-2509(89)85217-0.

[139] D. J. Kubek, D. S. Kovach, European Patent No. EP0331788a1, Tertiary alkanolamine absorbent containing an ethyleneamine promoter and its method of use (1989).

[140] A. Hartono, E. F. da Silva, H. F. Svendsen, Kinetics of carbon dioxide absorption in aqueous solution of diethylenetriamine (DETA), Chemical Engineering Science 64 (14) (2009) 3205–3213. doi:10.1016/j.ces.2009.04.018.

[141] P. Muchan, J. Narku-Tetteh, C. Saiwan, R. Idem, T. Supap, Effect of number of amine groups in aqueous polyamine solution on carbon dioxide CO_2 capture activities, Separation and Purification Technology 184 (2017) 128–134. doi:10.1016/j.seppur.2017.04.031.

[142] T. Sema, A. Naami, Z. Liang, H. Shi, A. V. Rayer, K. Z. Sumon, P. Wattanaphan, A. Henni, R. Idem, C. Saiwan, P. Tontiwachwuthikul, Part 5b: Solvent chemistry: reaction kinetics of CO_2 absorption into reactive amine solutions, Carbon Management 3 (2) (2012) 201–220. doi:10.4155/cmt.12.13.

[143] J. E. Crooks, J. P. Donnellan, Kinetics and mechanism of the reaction between carbon dioxide and amines in aqueous solution, J. Chem. Soc., Perkin Trans. 2 (1989) 331–333doi:10.1039/P29890000331.

[144] P. D. Vaidya, E. Y. Kenig, Termolecular kinetic model for CO_2-alkanolamine reactions: An overview, Chemical Engineering & Technology 33 (10) (2010) 1577–1581. doi:10.1002/ceat.201000050.

[145] E. F. da Silva, H. F. Svendsen, Computational chemistry study of reactions, equilib-

rium and kinetics of chemical CO_2 absorption, International Journal of Greenhouse Gas Control 1 (2) (2007) 151–157. doi:10.1016/S1750-5836(07)00022-9.

[146] J. T. Cullinane, G. T. Rochelle, Kinetics of carbon dioxide absorption into aqueous potassium carbonate and piperazine, Industrial & Engineering Chemistry Research 45 (8) (2006) 2531–2545. doi:10.1021/ie050230s.

[147] G. Puxty, M. Maeder, Using chemometrics tools to gain detailed molecular information on chemical processes, Journal of Chemometrics 34 (7) (2020) e3207. doi:10.1002/cem.3207.

[148] S. Laddha, P. Danckwerts, Reaction of CO_2 with ethanolamines: kinetics from gas-absorption, Chemical Engineering Science 36 (3) (1981) 479–482. doi:10.1016/0009-2509(81)80135-2.

[149] W. Conway, X. Wang, D. Fernandes, R. Burns, G. Lawrance, G. Puxty, M. Maeder, Toward the understanding of chemical absorption processes for post-combustion capture of carbon dioxide: Electronic and steric considerations from the kinetics of reactions of CO_2(aq) with sterically hindered amines, Environmental Science & Technology 47 (2) (2013) 1163–1169. doi:10.1021/es3025885.

[150] X. Han, D. W. Armstrong, Ionic liquids in separations, Accounts of Chemical Research 40 (11) (2007) 1079–1086. doi:10.1021/ar700044y.

[151] B. Arstad, R. Blom, O. Swang, CO_2 absorption in aqueous solutions of alkanolamines: mechanistic insight from quantum chemical calculations, The Journal of Physical Chemistry A 111 (7) (2007) 1222–1228. doi:10.1021/jp065301v.

[152] E. F. da Silva, Theoretical study of the equilibrium constants for solvents for CO_2 capture, Energy Procedia 4 (2011) 164–170. doi:10.1016/j.egypro.2011.01.037.

[153] C. Perinu, B. Arstad, A. M. Bouzga, K.-J. Jens, 13 C and 15 N NMR Characterization of Amine Reactivity and Solvent Effects in CO_2 Capture, The Journal of Physical Chemistry B 118 (34) (2014) 10167–10174. doi:10.1021/jp503421x.

[154] A. Aboudheir, P. Tontiwachwuthikul, A. Chakma, R. Idem, Kinetics of the reactive absorption of carbon dioxide in high CO_2-loaded, concentrated aqueous monoethanolamine solutions, Chemical Engineering Science 58 (23) (2003) 5195–5210.

doi:10.1016/j.ces.2003.08.014.

[155] E. F. da Silva, H. F. Svendsen, Ab initio study of the reaction of carbamate formation from CO_2 and alkanolamines, Industrial & Engineering Chemistry Research 43 (13) (2004) 3413–3418. doi:10.1021/ie030619k.

[156] K. Ohno, Y. Inoue, H. Yoshida, H. Matsuura, Reaction of aqueous 2-(n-methylamino)ethanol solutions with carbon dioxide. chemical species and their conformations studied by vibrational spectroscopy and ab initio theories, The Journal of Physical Chemistry A 103 (21) (1999) 4283–4292. doi:10.1021/jp984821q.

[157] H. Shi, Z. Liang, T. Sema, A. Naami, P. Usubharatana, R. Idem, C. Saiwan, P. Tontiwachwuthikul, Part 5a: Solvent chemistry: NMR analysis and studies for amine–CO_2–H_2O systems with vapor–liquid equilibrium modeling for CO_2 capture processes, Carbon Management 3 (2) (2012) 185–200. doi:10.4155/cmt.12.12.

[158] P. D. Vaidya, E. Y. Kenig, CO_2-alkanolamine reaction kinetics: A review of recent studies, Chemical Engineering & Technology 30 (11) (2007) 1467–1474. doi:10.1002/ceat.200700268.

[159] D. M. Austgen, G. T. Rochelle, X. Peng, C. C. Chen, Model of vapor-liquid equilibria for aqueous acid gas-alkanolamine systems using the electrolyte-nrtl equation, Industrial & Engineering Chemistry Research 28 (7) (1989) 1060–1073. doi:10.1021/ie00091a028.

[160] D. M. Austgen, G. T. Rochelle, C. C. Chen, Model of vapor-liquid equilibria for aqueous acid gas-alkanolamine systems. 2. representation of hydrogen sulfide and carbon dioxide solubility in aqueous MDEA and carbon dioxide solubility in aqueous mixtures of MDEA with MEA or DEA, Industrial & Engineering Chemistry Research 30 (3) (1991) 543–555. doi:10.1021/ie00051a016.

[161] Z. Liang, K. Fu, R. Idem, P. Tontiwachwuthikul, Review on current advances, future challenges and consideration issues for post-combustion CO_2 capture using amine-based absorbents, Chinese Journal of Chemical Engineering 24 (2) (2016) 278–288. doi:10.1016/j.cjche.2015.06.013.

[162] T. N. Borhani, S. A. Nabavi, D. P. Hanak, V. Manovic, Thermodynamic models applied to CO_2 absorption modelling, Reviews in Chemical Engineeringdoi:10.1515/

revce-2019-0058.

[163] H. Suleman, A. S. Maulud, Z. Man, Review and selection criteria of classical thermodynamic models for acid gas absorption in aqueous alkanolamines:, Reviews in Chemical Engineering 31 (6) (2015) 599–639. doi:10.1515/revce-2015-0030.

[164] R. L. Kent, B. Eisenberg, Better data for amine treating, Hydrocarbon Processing 55 (2) (1976) 87–90.

[165] C.-C. Chen, L. B. Evans, A local composition model for the excess gibbs energy of aqueous electrolyte systems, AIChE Journal 32 (3) (1986) 444–454. doi:10.1002/aic.690320311.

[166] R. Deshmukh, A. Mather, A mathematical model for equilibrium solubility of hydrogen sulfide and carbon dioxide in aqueous alkanolamine solutions, Chemical Engineering Science 36 (2) (1981) 355–362. doi:10.1016/0009-2509(81)85015-4.

[167] A. V. Rayer, K. Z. Sumon, T. Sema, A. Henni, R. O. Idem, P. Tontiwachwuthikul, Part 5c: Solvent chemistry: solubility of CO_2 in reactive solvents for post-combustion, Carbon Management 3 (5) (2012) 467–484. doi:10.4155/cmt.12.47.

[168] S. Kumar, J. H. Cho, I. Moon, Ionic liquid-amine blends and CO_2BOLs: Prospective solvents for natural gas sweetening and CO_2 capture technology–a review, International Journal of Greenhouse Gas Control 20 (2014) 87–116. doi:10.1016/j.ijggc.2013.10.019.

[169] T. Sema, A. Naami, R. Idem, P. Tontiwachwuthikul, Correlations for equilibrium solubility of carbon dioxide in aqueous 4-(diethylamino)-2-butanol solutions, Industrial & Engineering Chemistry Research 50 (24) (2011) 14008–14015. doi:10.1021/ie2008345.

[170] M. Afkhamipour, M. Mofarahi, A modeling-optimization framework for assessment of CO_2 absorption capacity by novel amine solutions: 1DMA2P, 1DEA2P, DEEA, and DEAB, Journal of Cleaner Production 171 (2018) 234–249. doi:10.1016/j.jclepro.2017.09.285.

[171] N. McCann, M. Maeder, H. Hasse, Prediction of the overall enthalpy of CO_2 absorption in aqueous amine systems from experimentally determined reaction enthalpies, Energy Procedia 4 (2011) 1542–1549. doi:10.1016/j.egypro.2011.02.023.

[172] P. M. Mathias, J. P. O'Connell, The Gibbs–Helmholtz equation and the thermodynamic consistency of chemical absorption data, Industrial & Engineering Chemistry Research 51 (13) (2012) 5090–5097. doi:10.1021/ie202668k.

[173] H. F. Svendsen, E. T. Hessen, T. Mejdell, Carbon dioxide capture by absorption, challenges and possibilities, Chem. Eng. J. 171 (3) (2011) 718–724. doi:10.1016/j.cej.2011.01.014.

[174] J. Oexmann, A. Kather, Minimising the regeneration heat duty of post-combustion CO_2 capture by wet chemical absorption: The misguided focus on low heat of absorption solvents, International Journal of Greenhouse Gas Control 4 (1) (2010) 36–43. doi:10.1016/j.ijggc.2009.09.010.

[175] C. Mathonat, V. Majer, A. E. Mather, J.-P. E. Grolier, Use of flow calorimetry for determining enthalpies of absorption and the solubility of CO_2 in aqueous monoethanolamine solutions, Industrial & Engineering Chemistry Research 37 (10) (1998) 4136–4141. doi:10.1021/ie9707679.

[176] I. Kim, H. F. Svendsen, Comparative study of the heats of absorption of post-combustion CO_2 absorbents, International Journal of Greenhouse Gas Control 5 (3) (2011) 390–395. doi:10.1016/j.ijggc.2010.05.003.

[177] I. Kim, H. F. Svendsen, Heat of Absorption of Carbon Dioxide (CO_2) in Monoethanolamine (MEA) and 2-(Aminoethyl)ethanolamine (AEEA) Solutions, Industrial & Engineering Chemistry Research 46 (17) (2007) 5803–5809. doi:10.1021/ie0616489.

[178] H. H. Meyer, Zur Theorie der Alkoholnarkose: 3. Mittheilung; der Einfluss wechselnder Temperatur auf Wirkungsstärke und Theilungscoefficient der Narcotica, Pharmakologisches Institut, 1899.

[179] M. A. Kuenemann, D. Fourches, Cheminformatics modeling of amine solutions for assessing their CO_2 absorption properties, Molecular Informatics 36 (7) (2017) 1600143. doi:10.1002/minf.201600143.

[180] A. Chakraborty, K. Bischoff, G. Astarita, J. Damewood, Molecular orbital approach to substituent effects in amine-CO_2 interactions, Journal of the American Chemical Society 110 (21) (1988) 6947–6954.

[181] J.-H. Yoon, J.-I. Baek, Y. Yamamoto, T. Komai, T. Kawamura, Kinetics of removal of carbon dioxide by aqueous 2-amino-2-methyl-1,3-propanediol, Chemical Engineering Science 58 (23) (2003) 5229–5237. doi:10.1016/j.ces.2003.08.019.

[182] R. J. Hook, An investigation of some sterically hindered amines as potential carbon dioxide scrubbing compounds, Industrial & Engineering Chemistry Research 36 (5) (1997) 1779–1790. doi:10.1021/ie9605589.

[183] H.-B. Xie, J. K. Johnson, R. J. Perry, S. Genovese, B. R. Wood, A computational study of the heats of reaction of substituted monoethanolamine with CO_2, The Journal of Physical Chemistry A 115 (3) (2011) 342–350. doi:10.1021/jp1081627.

[184] A. S. Lee, J. C. Eslick, D. C. Miller, J. R. Kitchin, Comparisons of amine solvents for post-combustion CO_2 capture: A multi-objective analysis approach, International Journal of Greenhouse Gas Control 18 (2013) 68–74. doi:10.1016/j.ijggc.2013.06.020.

[185] A. S. Lee, J. R. Kitchin, Chemical and molecular descriptors for the reactivity of amines with CO_2, Industrial & Engineering Chemistry Research 51 (42) (2012) 13609–13618. doi:10.1021/ie301419q.

[186] X. Rozanska, E. Wimmer, F. de Meyer, Quantitative kinetic model of CO_2 absorption in aqueous tertiary amine solvents, Journal of Chemical Information and Modeling 0 (0) (2021) null. doi:10.1021/acs.jcim.0c01386.

[187] Z. Wu, S. Liu, H. Gao, Q. Yin, Z. Liang, A study of structure-activity relationships of aqueous diamine solutions with low heat of regeneration for post-combustion CO_2 capture, Energy 167 (2019) 359–368. doi:10.1016/j.energy.2018.10.194.

[188] C. Perinu, I. M. Bernhardsen, D. Pinto, H. K. Knuutila, K.-J. Jens, NMR Speciation of Aqueous MAPA, Tertiary Amines, and Their Blends in the Presence of CO_2: Influence of pK_a and Reaction Mechanisms, Industrial & Engineering Chemistry Research 57 (5) (2018) 1337–1349. doi:10.1021/acs.iecr.7b03795.

[189] P. M. Mathias, S. Reddy, A. Smith, K. Afshar, Thermodynamic analysis of CO_2 capture solvents, International Journal of Greenhouse Gas Control 19 (7) (2013) 262–270. doi:10.1016/j.ijggc.2013.09.001.

[190] P. M. Mathias, Some examples of the contribution of applied thermodynamics to post-combustion CO_2-capture technology, Fluid Phase Equilibria 362 (2014) 102–107. doi:10.1016/j.fluid.2013.09.016.

[191] P. M. Mathias, J. P. Gilmartin, Quantitative evaluation of the effect of uncertainty in property models on the simulated performance of solvent-based CO_2-capture, Energy Procedia 63 (2014) 1171–1185. doi:10.1016/j.egypro.2014.11.127.

[192] D. J. Heldebrant, P. K. Koech, V.-A. Glezakou, R. Rousseau, D. Malhotra, D. C. Cantu, Water-lean solvents for post-combustion CO_2 capture: Fundamentals, uncertainties, opportunities, and outlook, Chemical Reviews 117 (14) (2017) 9594–9624. doi:10.1021/acs.chemrev.6b00768.

[193] B. A. Oyenekan, G. T. Rochelle, Energy performance of stripper configurations for CO_2 capture by aqueous amines, Industrial & Engineering Chemistry Research 45 (8) (2006) 2457–2464. doi:10.1021/ie050548k.

[194] Y.-J. Lin, G. T. Rochelle, Optimum heat of absorption for CO_2 capture using the advanced flash stripper, International Journal of Greenhouse Gas Control 53 (2016) 169–177. doi:10.1016/j.ijggc.2016.08.002.

[195] H. Kim, K. S. Lee, Design guidance for an energy-thrift absorption process for carbon capture: Analysis of thermal energy consumption for a conventional process configuration, International Journal of Greenhouse Gas Control 47 (2016) 291–302. doi:10.1016/j.ijggc.2016.02.003.

[196] S. Ekins, J. Mestres, B. Testa, In silico pharmacology for drug discovery: methods for virtual ligand screening and profiling, British journal of pharmacology 152 (1) (2007) 9–20.

[197] N. El Hadri, D. V. Quang, E. L. Goetheer, M. R. A. Zahra, Aqueous amine solution characterization for post-combustion CO_2 capture process, Applied Energy 185 (2017) 1433–1449. doi:10.1016/j.apenergy.2016.03.043.

[198] I. M. Bernhardsen, H. K. Knuutila, A review of potential amine solvents for CO_2 absorption process: Absorption capacity, cyclic capacity and pk_a, International Journal of Greenhouse Gas Control 61 (2017) 27–48. doi:10.1016/j.ijggc.2017.03.021.

[199] D. Bonenfant, M. Mimeault, R. Hausler, Determination of the structural features of distinct amines important for the absorption of CO_2 and regeneration in aqueous solution, Ind. Eng. Chem. Res. 42 (14) (2003) 3179–3184. doi:10.1021/ie020738k.

[200] A. I. Papadopoulos, S. Badr, A. Chremos, E. Forte, T. Zarogiannis, P. Seferlis, S. Papadokonstantakis, A. Galindo, G. Jackson, C. S. Adjiman, Computer-aided molecular design and selection of CO_2 capture solvents based on thermodynamics, reactivity and sustainability, Mol. Syst. Des. Eng. 3 (2016) 1645–1669. doi:10.1039/c6me00049e.

[201] N. D. Austin, N. V. Sahinidis, D. W. Trahan, Computer-aided molecular design: An introduction and review of tools, applications, and solution techniques, Chemical Engineering Research and Design 116 (2016) 2–26. doi:10.1016/j.cherd.2016.10.014.

[202] Y. S. Lee, E. J. Graham, A. Galindo, G. Jackson, C. S. Adjiman, A comparative study of multi-objective optimization methodologies for molecular and process design, Computers & Chemical Engineering 136 (2020) 106802. doi:10.1016/j.compchemeng.2020.106802.

[203] E. Grant, Y. Pan, J. Richardson, J. R. Martinelli, A. Armstrong, A. Galindo, C. S. Adjiman, Multi-objective computer-aided solvent design for selectivity and rate in reactions, in: M. R. Eden, M. G. Ierapetritou, G. P. Towler (Eds.), 13th International Symposium on Process Systems Engineering (PSE 2018), Vol. 44 of Computer Aided Chemical Engineering, Elsevier, 2018, pp. 2437–2442. doi:10.1016/B978-0-444-64241-7.50401-8.

[204] C. S. Adjiman, N. V. Sahinidis, D. G. Vlachos, B. Bakshi, C. T. Maravelias, C. Georgakis, Process systems engineering perspective on the design of materials and molecules, Industrial & Engineering Chemistry Research 60 (14) (2021) 5194–5206. doi:10.1021/acs.iecr.0c05399.

[205] L. Fleitmann, J. Kleinekorte, K. Leonhard, A. Bardow, COSMO-susCAMPD: Sustainable solvents from combining computer-aided molecular and process design with predictive life cycle assessment, Chemical Engineering Science 245 (2021) 116863. doi:10.1016/j.ces.2021.116863.

[206] S. Papadokonstantakis, S. Badr, K. Hungerbühler, A. I. Papadopoulos, T. Damartzis, P. Seferlis, E. Forte, A. Chremos, A. Galindo, G. Jackson, C. S. Adjiman, Chapter

11 - toward sustainable solvent-based postcombustion CO_2 capture: From molecules to conceptual flowsheet design, in: F. You (Ed.), Sustainability of Products, Processes and Supply Chains, Vol. 36 of Computer Aided Chemical Engineering, Elsevier, 2015, pp. 279–310. doi:10.1016/B978-0-444-63472-6.00011-2.

[207] A. I. Papadopoulos, G. Shavalieva, S. Papadokonstantakis, P. Seferlis, F. A. Perdomo, A. Galindo, G. Jackson, C. S. Adjiman, An approach for simultaneous computer-aided molecular design with holistic sustainability assessment: Application to phase-change CO_2 capture solvents, Computers& Chemical Engineering 135 (2020) 106769. doi:10.1016/j.compchemeng.2020.106769.

[208] A. I. Papadopoulos, F. A. Perdomo, F. Tzirakis, G. Shavalieva, I. Tsivintzelis, P. Kazepidis, E. Nessi, S. Papadokonstantakis, P. Seferlis, A. Galindo, G. Jackson, C. S. Adjiman, Molecular engineering of sustainable phase-change solvents: From digital design to scaling-up for CO_2 capture, Chemical Engineering Journal 420 (2021) 127624. doi:10.1016/j.cej.2020.127624.

[209] V. Venkatraman, M. Gupta, M. Foscato, H. F. Svendsen, V. R. Jensen, B. K. Alsberg, Computer-aided molecular design of imidazole-based absorbents for CO_2 capture, International Journal of Greenhouse Gas Control 49 (2016) 55–63. doi:10.1016/j.ijggc.2016.02.023.

[210] T. Zarogiannis, A. I. Papadopoulos, P. Seferlis, Off-design operation of conventional and phase-change CO_2 capture solvents and mixtures: A systematic assessment approach, Applied Sciences 10 (15). doi:10.3390/app10155316.

[211] W. Chapman, K. Gubbins, G. Jackson, M. Radosz, SAFT: Equation-of-state solution model for associating fluids, Fluid Phase Equilibria 52 (1989) 31–38. doi:10.1016/0378-3812(89)80308-5.

[212] W. G. Chapman, K. E. Gubbins, G. Jackson, M. Radosz, New reference equation of state for associating liquids, Industrial & Engineering Chemistry Research 29 (8) (1990) 1709–1721. doi:10.1021/ie00104a021.

[213] M. Wertheim, Fluids with highly directional attractive forces. I. statistical thermodynamics, Journal of statistical physics 35 (1) (1984) 19–34.

[214] M. Wertheim, Fluids with highly directional attractive forces. II. thermodynamic perturbation theory and integral equations, Journal of statistical physics 35 (1) (1984) 35–47.

[215] M. Wertheim, Fluids with highly directional attractive forces. III. multiple attraction sites, Journal of statistical physics 42 (3) (1986) 459–476.

[216] M. Wertheim, Fluids with highly directional attractive forces. IV. equilibrium polymerization, Journal of statistical physics 42 (3) (1986) 477–492.

[217] P. Limleamthong, M. González-Miquel, S. Papadokonstantakis, A. Papadopoulos, P. Seferlis, G. Guillén-Gosálbez, Screening of solvents for CO_2 capture considering sustainability criteria via data envelopment analysis, in: 27th European Symposium on Computer Aided Process Engineering, Vol. 40 of Computer Aided Chemical Engineering, Elsevier, 2017, pp. 2011–2016. doi:10.1016/B978-0-444-63965-3.50337-8.

[218] L. Helei, P. Tantikhajorngosol, C. Chan, P. Tontiwachwuthikul, Technology development and applications of artificial intelligence for post-combustion carbon dioxide capture: Critical literature review and perspectives, International Journal of Greenhouse Gas Control 108 (2021) 103307. doi:10.1016/j.ijggc.2021.103307.

[219] H. K. Knuutila, R. Rennemo, A. F. Ciftja, New solvent blends for post-combustion CO_2 capture, Green Energy & Environment 4 (4) (2019) 439–452. doi:10.1016/j.gee.2019.01.007.

[220] Y. Yuan, G. T. Rochelle, Lost work: A comparison of water-lean solvent to a second generation aqueous amine process for CO_2 capture, International Journal of Greenhouse Gas Control 84 (2019) 82–90. doi:10.1016/j.ijggc.2019.03.013.

[221] R. Tennyson, R. Schaaf, Guidelines can help choose proper process for gas-treating plants, Oil and Gas Journal 75 (2) (1977) 78–80, 85–86.

[222] K. A. Hoff, E. F. da Silva, I. Kim, A. Grimstvedt, S. Mamun, Solvent development in post combustion CO_2 capture-selection criteria and optimization of solvent performance, cost and environmental impact, Energy Procedia 37 (2013) 292–299. doi:10.1016/j.egypro.2013.05.114.

[223] F. A. Chowdhury, H. Yamada, T. Higashii, K. Goto, M. Onoda, CO_2 Capture by Ter-

tiary Amine Absorbents: A Performance Comparison Study, Industrial & Engineering Chemistry Research 52 (24) (2013) 8323–8331. doi:10.1021/ie400825u.

[224] N. el Hadri, D. V. Quang, M. R. Abu-Zahra, Study of novel solvent for CO_2 post-combustion capture, Energy Procedia 75 (2015) 2268–2286. doi:10.1016/j.egypro.2015.07.414.

[225] P. Singh, D. W. Brilman, M. J. Groeneveld, Evaluation of CO_2 solubility in potential aqueous amine-based solvents at low CO_2 partial pressure, International Journal of Greenhouse Gas Control 5 (1) (2011) 61–68. doi:10.1016/j.ijggc.2010.06.009.

[226] P. Brúder, A. Grimstvedt, T. Mejdell, H. F. Svendsen, CO_2 capture into aqueous solutions of piperazine activated 2-amino-2-methyl-1-propanol, Chemical Engineering Science 66 (23) (2011) 6193–6198. doi:10.1016/j.ces.2011.08.051.

[227] U. E. Aronu, K. A. Hoff, H. F. Svendsen, CO_2 capture solvent selection by combined absorption–desorption analysis, Chemical Engineering Research and Design 89 (8) (2011) 1197–1203. doi:10.1016/j.cherd.2011.01.007.

[228] A. Hartono, S. Vevelstad, A. Ciftja, H. Knuutila, Screening of strong bicarbonate forming solvents for CO_2 capture, International Journal of Greenhouse Gas Control 58 (2017) 201–211. doi:10.1016/j.ijggc.2016.12.018.

[229] G. Puxty, R. Rowland, A. Allport, Q. Yang, M. Bown, R. Burns, M. Maeder, M. Attalla, Carbon dioxide postcombustion capture: A novel screening study of the carbon dioxide absorption performance of 76 amines, Environ. Sci. Technol. 43 (16) (2009) 6427–6433. doi:10.1021/es901376a.

[230] Y. E. Kim, S. J. Moon, Y. I. Yoon, S. K. Jeong, K. T. Park, S. T. Bae, S. C. Nam, Heat of absorption and absorption capacity of CO_2 in aqueous solutions of amine containing multiple amino groups, Separation and Purification Technology 122 (2014) 112–118. doi:10.1016/j.seppur.2013.10.030.

[231] Y. E. Kim, S. H. Yun, J. H. Choi, S. C. Nam, S. Y. Park, S. K. Jeong, Y. I. Yoon, Comparison of the CO_2 absorption characteristics of aqueous solutions of diamines: Absorption capacity, specific heat capacity, and heat of absorption, Energy & Fuels 29 (4) (2015) 2582–2590. doi:10.1021/ef500561a.

[232] J. K. You, W. Y. Lee, J. Y. Kim, J. Lee, Y. K. Hong, Screening of biphasic solvents for energy efficient CO_2 capture, Energy Procedia 114 (2017) 2096–2102. doi:10.1016/j.egypro.2017.03.1344.

[233] X. Chen, F. Closmann, G. T. Rochelle, Accurate screening of amines by the wetted wall column, Energy Procedia 4 (2011) 101–108. doi:10.1016/j.egypro.2011.01.029.

[234] Q. Ye, X. Wang, Y. Lu, Screening and evaluation of novel biphasic solvents for energy-efficient post-combustion CO_2 capture, International Journal of Greenhouse Gas Control 39 (2015) 205–214. doi:10.1016/j.ijggc.2015.05.025.

[235] L. Zou, H. Gao, Z. Wu, Z. Liang, Fast screening of amine/physical solvent systems and mass transfer studies on efficient aqueous hybrid MEA/Sulfolane solution for postcombustion CO_2 capture, Journal of Chemical Technology & Biotechnology 95 (3) (2020) 649–664. doi:10.1002/jctb.6246.

[236] X. Luo, S. Liu, H. Gao, H. Liao, P. Tontiwachwuthikul, Z. Liang, An improved fast screening method for single and blended amine-based solvents for post-combustion CO_2 capture, Separation and Purification Technology 169 (2016) 279–288. doi:10.1016/j.seppur.2016.06.018.

[237] P. Muchan, C. Saiwan, J. Narku-Tetteh, R. Idem, T. Supap, P. Tontiwachwuthikul, Screening tests of aqueous alkanolamine solutions based on primary, secondary, and tertiary structure for blended aqueous amine solution selection in post combustion CO_2 capture, Chemical Engineering Science 170 (2017) 574–582. doi:10.1016/j.ces.2017.02.031.

[238] C. Nwaoha, T. Supap, R. Idem, C. Saiwan, P. Tontiwachwuthikul, M. J. AL-Marri, A. Benamor, Advancement and new perspectives of using formulated reactive amine blends for post-combustion carbon dioxide CO_2 capture technologies, Petroleum 3 (1) (2017) 10–36. doi:10.1016/j.petlm.2016.11.002.

[239] C. Nwaoha, R. Idem, T. Supap, C. Saiwan, P. Tontiwachwuthikul, W. Rongwong, M. J. Al-Marri, A. Benamor, Heat duty, heat of absorption, sensible heat and heat of vaporization of 2–amino–2–methyl–1–propanol (AMP), piperazine (PZ) and monoethanolamine (MEA) tri–solvent blend for carbon dioxide (CO_2) capture, Chemical Engineering Sci-

ence 170 (2017) 26–35. doi:10.1016/j.ces.2017.03.025.

[240] Scopus: Expertly curated abstract and citation database, www.scopus.com, last accessed on 01/05/20.

[241] R. R. Bottoms, Organic bases for gas purification, Industrial & Engineering Chemistry 23 (5) (1931) 501–504. doi:10.1021/ie50257a007.

[242] F. Porcheron, A. Gibert, P. Mougin, A. Wender, High throughput screening of CO_2 solubility in aqueous monoamine solutions, Environmental Science & Technology 45 (6) (2011) 2486–2492. doi:10.1021/es103453f.

[243] F. Porcheron, A. Gibert, M. Jacquin, P. Mougin, A. Faraj, A. Goulon, P.-A. Bouillon, B. Delfort, D. Le Pennec, L. Raynal, High throughput screening of amine thermodynamic properties applied to post-combustion CO_2 capture process evaluation, Energy Procedia 4 (2011) 15–22. doi:10.1016/j.egypro.2011.01.017.

[244] K. Robinson, A. McCluskey, M. I. Attalla, The Effect Molecular Structural Variations Has on the CO_2 Absorption Characteristics of Heterocyclic Amines, Ch. 1, pp. 1–27. doi:10.1021/bk-2012-1097.ch001.

[245] W. Conway, Q. Yang, S. James, C.-C. Wei, M. Bown, P. Feron, G. Puxty, Designer amines for post combustion CO_2 capture processes, Energy Procedia 63 (2014) 1827–1834. doi:10.1016/j.egypro.2014.11.190.

[246] Q. Yang, G. Puxty, S. James, M. Bown, P. Feron, W. Conway, Toward intelligent CO_2 capture solvent design through experimental solvent development and amine synthesis, Energy & Fuels 30 (9) (2016) 7503–7510. doi:10.1021/acs.energyfuels.6b00875.

[247] W. Conway, Y. Beyad, S. Clifford, M. Maeder, P. Feron, G. Puxty, Parametric investigation of chemical equilibrium in mixed aqueous amine systems for CO_2 capture processes: Impact of amine protonation and reaction enthalpies on CO_2 absorption capacity, cyclic capacity, and absorption enthalpies, Energy Procedia 63 (2014) 1818–1826. doi:10.1016/j.egypro.2014.11.189.

[248] W. Conway, S. Bruggink, Y. Beyad, W. Luo, I. Melián-Cabrera, G. Puxty, P. Feron, CO_2 absorption into aqueous amine blended solutions containing monoethanolamine (MEA), N,N-dimethylethanolamine (DMEA), N,N-diethylethanolamine (DEEA) and 2-amino-2-

methyl-1-propanol (AMP) for post-combustion capture processes, Chemical Engineering Science 126 (2015) 446–454. doi:10.1016/j.ces.2014.12.053.

[249] G. Puxty, W. Conway, H. Botma, P. Feron, D. Maher, L. Wardhaugh, A new CO_2 absorbent developed from addressing benzylamine vapour pressure using co-solvents, Energy Procedia 114 (2017) 1956–1965. doi:10.1016/j.egypro.2017.03.1327.

[250] G. Puxty, W. Conway, Q. Yang, R. Bennett, D. Fernandes, P. Pearson, D. Maher, P. Feron, The evolution of a new class of CO_2 absorbents: Aromatic amines, International Journal of Greenhouse Gas Control 83 (2019) 11–19. doi:10.1016/j.ijggc.2018.12.024.

[251] D. Mackay, W. Y. Shiu, Aqueous solubility of polynuclear aromatic hydrocarbons, Journal of Chemical & Engineering Data 22 (4) (1977) 399–402. doi:10.1021/je60075a012.

[252] N. Brautbar, J. Williams, Industrial solvents and liver toxicity: Risk assessment, risk factors and mechanisms, International Journal of Hygiene and Environmental Health 205 (6) (2002) 479–491. doi:10.1078/1438-4639-00175.

[253] A. Al Hinai, N. El Hadri, M. Abu Zahra, Amine-Blends Screening and Characterization for CO_2 Post-combustion Capture, Springer International Publishing, Cham, 2017, pp. 177–189. doi:10.1007/978-3-319-47262-1_8.

[254] F. J. Blas, L. F. Vega, Thermodynamic behaviour of homonuclear and heteronuclear Lennard-Jones chains with association sites from simulation and theory, Molecular Physics 92 (1) (1997) 135–150. doi:10.1080/00268979709482082.

[255] L. M. Pereira, L. F. Vega, A systematic approach for the thermodynamic modelling of CO_2-amine absorption process using molecular-based models, Applied Energy 232 (2018) 273–291. doi:10.1016/j.apenergy.2018.09.189.

[256] I. Alkhatib, L. M. Pereira, L. F. Vega, 110th anniversary: Accurate modeling of the simultaneous absorption of h2s and CO_2 in aqueous amine solvents, Industrial & Engineering Chemistry Research 58 (16) (2019) 6870–6886. doi:10.1021/acs.iecr.9b00862.

[257] I. I. Alkhatib, L. M. Pereira, A. AlHajaj, L. F. Vega, Performance of non-aqueous amine hybrid solvents mixtures for CO_2 capture: A study using a molecular-based model, Journal of CO_2 Utilization 35 (2020) 126–144. doi:10.1016/j.jcou.2019.09.010.

[258] I. Alkhatib, A. Al-Hajaj, M. Abu Zahra, L. Vega, A Thermodynamic Robust Model to Assess Hybrid Solvents for CO_2 Capture Day 4 Thu, November 12, 2020. doi:10.2118/203020-MS.

[259] I. I. Alkhatib, M. Abu Zahra, L. F. Vega, Screening tool for water-free and water-lean amine-based solvents for CO_2 capture, Available at SSRN 3819211.

[260] I. Alkhatib, C. Alba, D. Bahamon, F. Llovell, L. Vega, Assessing the Feasibility of Deep Eutectic Solvents For CO_2 Capture From Molecular And Process Modeling Day 2 Tue, November 10, 2020. doi:10.2118/202909-MS.

[261] I. I. Alkhatib, D. Bahamon, C. G Albà, F. Llovell Ferret, L. F. Vega, Thermodynamic and process modeling of deep eutectic solvents for CO_2 capture and separation at industrial condition, Carlos and Llovell Ferret, Felix and Vega, Lourdes F.,.

[262] I. I. I. Alkhatib, M. L. Ferreira, C. G. Alba, D. Bahamon, F. Llovell, A. B. Pereiro, J. M. M. Araújo, M. Abu-Zahra, L. F. Vega, Screening of ionic liquids and deep eutectic solvents for physical CO_2 absorption by Soft-SAFT using key performance indicators, Journal of Chemical & Engineering Data 65 (12) (2020) 5844–5861. doi:10.1021/acs.jced.0c00750.

[263] D. Bahamon, I. I. I. Alkhatib, N. Alkhatib, S. Builes, M. Sinnokrot, L. F. Vega, A comparative assessment of emerging solvents and adsorbents for mitigating CO_2 emissions from the industrial sector by using molecular modeling tools, Frontiers in Energy Research 8 (2020) 165. doi:10.3389/fenrg.2020.00165.

[264] H. Kim, S. J. Hwang, K. S. Lee, Novel shortcut estimation method for regeneration energy of amine solvents in an absorption-based carbon capture process, Environmental Science & Technology 49 (3) (2015) 1478–1485. doi:10.1021/es504684x.

[265] H. Yamada, F. A. Chowdhury, K. Goto, T. Higashii, CO_2 solubility and species distribution in aqueous solutions of 2-(isopropylamino)ethanol and its structural isomers, International Journal of Greenhouse Gas Control 17 (2013) 99–105. doi:10.1016/j.ijggc.2013.03.027.

[266] H. Yamada, Y. Matsuzaki, F. Chowdhury, T. Higashii, Computational investigation of carbon dioxide absorption in alkanolamine solutions, Journal of molecular modeling

19 (10) (2013) 4147–4153.

[267] Y. S. Yu, H. F. Lu, G. X. Wang, Z. X. Zhang, V. Rudolph, Characterizing the transport properties of multiamine solutions for CO_2 capture by molecular dynamics simulation, Journal of Chemical & Engineering Data 58 (6) (2013) 1429–1439. doi:10.1021/je3005547.

[268] P. Limleamthong, M. Gonzalez-Miquel, S. Papadokonstantakis, A. I. Papadopoulos, P. Seferlis, G. Guillén-Gosálbez, G. Guillen-Gosalbez, Multi-criteria screening of chemicals considering thermodynamic and life cycle assessment metrics via data envelopment analysis: application to CO_2 capture, Green Chem.doi:10.1039/c6gc01696k.

[269] M. Bortz, J. Burger, N. Asprion, S. Blagov, R. Böttcher, U. Nowak, A. Scheithauer, R. Welke, K.-H. Küfer, H. Hasse, Multi-criteria optimization in chemical process design and decision support by navigation on pareto sets, Computers & Chemical Engineering 60 (2014) 354–363. doi:10.1016/j.compchemeng.2013.09.015.

[270] A. E. P. Popescu, À. González, J. Llorens, J. Bonet, Investigating best available technique for CO_2 chemical absorption: solvent selection based on empirical surrogate model and exergy loss, Clean Technologies and Environmental Policy (2021) 1–18.

[271] L. Faramarzi, D. Thimsen, S. Hume, A. Maxon, G. Watson, S. Pedersen, E. Gjernes, B. F. Fostås, G. Lombardo, T. Cents, A. K. Morken, M. I. Shah, T. de Cazenove, E. S. Hamborg, Results from MEA testing at the CO_2 Technology Centre Mongstad: Verification of baseline results in 2015, Energy Procedia 114 (2017) 1128–1145. doi:10.1016/j.egypro.2017.03.1271.

[272] M. Momeni, S. Riahi, An investigation into the relationship between molecular structure and rich/lean loading of linear amine-based CO_2 absorbents, International Journal of Greenhouse Gas Control 42 (2015) 157–164. doi:10.1016/j.ijggc.2015.07.037.

[273] K. Teranishi, A. Ishikawa, H. Sato, H. Nakai, Systematic investigation of the thermodynamic properties of amine solvents for CO_2 chemical absorption using the cluster-continuum model, Bulletin of the Chemical Society of Japan 90 (4) (2017) 451–460. doi:10.1246/bcsj.20160375.

[274] S. A. Freeman, G. T. Rochelle, Thermal degradation of aqueous piperazine for CO_2

capture. 1. effect of process conditions and comparison of thermal stability of CO_2 capture amines, Industrial & Engineering Chemistry Research 51 (22) (2012) 7719–7725. doi:10.1021/ie201916x.

[275] T. Nguyen, M. Hilliard, G. T. Rochelle, Amine volatility in CO_2 capture, International Journal of Greenhouse Gas Control 4 (5) (2010) 707–715. doi:10.1016/j.ijggc.2010.06.003.

[276] X. Luo, J. Knudsen, D. de Montigny, T. Sanpasertparnich, R. Idem, D. Gelowitz, R. Notz, S. Hoch, H. Hasse, E. Lemaire, P. Alix, F. Tobiesen, O. Juliussen, M. Köpcke, H. Svendsen, Comparison and validation of simulation codes against sixteen sets of data from four different pilot plants, Energy Procedia 1 (1) (2009) 1249–1256. doi:10.1016/j.egypro.2009.01.164.

[277] P. L. Fosbøl, J. Gaspar, S. Ehlers, A. Kather, P. Briot, M. Nienoord, P. Khakharia, Y. Le Moullec, O. T. Berglihn, H. Kvamsdal, Benchmarking and comparing first and second generation post combustion CO_2 capture technologies, Energy Procedia 63 (2014) 27–44. doi:10.1016/j.egypro.2014.11.004.

[278] H. M. Kvamsdal, I. Kim, P. Van Os, C. Pevida, M.-B. Hägg, J. Brown, L. Robinson, P. Feron, HiPerCap: A New FP7 Project for Development and Assessment of Novel and Emerging Post-combustion CO_2 Capture Technologies, Energy Procedia 63 (2014) 6166–6172. doi:10.1016/j.egypro.2014.11.648.

[279] E. O. Agbonghae, K. J. Hughes, D. B. Ingham, L. Ma, M. Pourkashanian, Optimal process design of commercial-scale amine-based CO_2 capture plants, Industrial & Engineering Chemistry Research 53 (38) (2014) 14815–14829. doi:10.1021/ie5023767.

[280] N. Asprion, R. Benfer, S. Blagov, R. Böttcher, M. Bortz, M. Berezhnyi, J. Burger, E. v. Harbou, K.-H. Küfer, H. Hasse, INES – an interface between experiments and simulation to support the development of robust process designs, Chemie Ingenieur Technik 87 (12) (2015) 1810–1825. doi:10.1002/cite.201500020.

[281] N. Asprion, Non equilibrium rate-based simulation of reactive systems: Simulation model, heat transfer, and influence of film discretization, Ind. Eng. Chem. Res. 45 (2006) 2054–2069.

[282] J. C. Morgan, D. Bhattacharyya, C. Tong, D. C. Miller, Uncertainty quantification of property models: Methodology and its application to CO_2-loaded aqueous MEA solutions, AIChE Journal 61 (6) (2015) 1822–1839. doi:10.1002/aic.14762.

[283] J. C. Morgan, A. S. Chinen, B. Omell, D. Bhattacharyya, C. Tong, D. C. Miller, Thermodynamic modeling and uncertainty quantification of CO_2-loaded aqueous MEA solutions, Chemical Engineering Science 168 (2017) 309–324. doi:10.1016/j.ces.2017.04.049.

[284] J. C. Morgan, A. Soares Chinen, B. Omell, D. Bhattacharyya, C. Tong, D. C. Miller, B. Buschle, M. Lucquiaud, Development of a rigorous modeling framework for solvent-based CO_2 capture. part 2: Steady-state validation and uncertainty quantification with pilot plant data, Industrial & Engineering Chemistry Research 57 (31) (2018) 10464–10481. doi:10.1021/acs.iecr.8b01472.

[285] A. Chinen, J. C. Morgan, B. Omell, D. Bhattacharyya, C. Tong, D. C. Miller, Development of a rigorous modeling framework for solvent-based CO_2 capture. 1. hydraulic and mass transfer models and their uncertainty quantification, Industrial & Engineering Chemistry Research 57 (31) (2018) 10448–10463. doi:10.1021/acs.iecr.8b01471.

[286] A. Chinen, J. C. Morgan, B. Omell, D. Bhattacharyya, D. C. Miller, Dynamic data reconciliation and validation of a dynamic model for solvent-based CO_2 capture using pilot-plant data, Industrial & Engineering Chemistry Research 58 (5) (2019) 1978–1993. doi:10.1021/acs.iecr.8b04489.

[287] J. M. Plaza, Modeling of carbon dioxide absorption using aqueous monoethanolamine, piperazine and promoted potassium carbonate, Ph.D. thesis, The University of Texas at Austin (2012).

[288] J. Jakobsen, S. Roussanaly, R. Anantharaman, A techno-economic case study of CO_2 capture, transport and storage chain from a cement plant in norway, Journal of Cleaner Production 144 (2017) 523–539. doi:10.1016/j.jclepro.2016.12.120.

[289] J. P. Jakobsen, S. Roussanaly, A. Brunsvold, R. Anantharaman, A tool for integrated multi-criteria assessment of the CCS value chain, Energy Procedia 63 (2014) 7290–7297. doi:10.1016/j.egypro.2014.11.765.

[290] A. Raksajati, M. T. Ho, D. E. Wiley, Comparison of solvent development options for

capture of CO_2 from flue gases, Industrial & Engineering Chemistry Research 57 (19) (2018) 6746–6758. doi:10.1021/acs.iecr.8b00283.

[291] A. Raksajati, M. T. Ho, D. E. Wiley, Reducing the cost of CO_2 capture from flue gases using aqueous chemical absorption, Industrial & Engineering Chemistry Research 52 (47) (2013) 16887–16901. doi:10.1021/ie402185h.

[292] N. Razi, O. Bolland, H. Svendsen, Review of design correlations for CO_2 absorption into MEA using structured packings, International Journal of Greenhouse Gas Control 9 (2012) 193–219. doi:10.1016/j.ijggc.2012.03.003.

[293] N. Razi, H. F. Svendsen, O. Bolland, Validation of mass transfer correlations for CO_2 absorption with MEA using pilot data, International Journal of Greenhouse Gas Control 19. doi:10.1016/j.ijggc.2013.10.006.

[294] K. R. Putta, H. F. Svendsen, H. K. Knuutila, CO_2 absorption into loaded aqueous MEA solutions: Impact of different model parameter correlations and thermodynamic models on the absorption rate model predictions, Chemical Engineering Journal 327 (2017) 868–880. doi:10.1016/j.cej.2017.06.134.

[295] G. Q. Wang, X. G. Yuan, K. T. Yu, Review of mass-transfer correlations for packed columns, Industrial & Engineering Chemistry Research 44 (23) (2005) 8715–8729. doi:10.1021/ie050017w.

[296] S. Mirzaei, A. Shamiri, M. K. Aroua, A review of different solvents, mass transfer, and hydrodynamics for postcombustion CO_2 capture, Reviews in Chemical Engineering 31 (6) (2015) 521–561. doi:10.1515/revce-2014-0045.

[297] B. I. Dvorak, D. F. Lawler, J. R. Fair, N. E. Handler, Evaluation of the onda correlations for mass transfer with large random packings, Environmental Science & Technology 30 (3) (1996) 945–953. doi:10.1021/es950408+.

[298] J. L. Bravo, J. A. Rocha, J. Fair, Mass transfer in gauze packings, Hydrocarbon processing (International ed.) 64 (1) (1985) 91–95.

[299] J. Bravo, J. Rocha, J. Fair, A comprehensive model for the performance of columns containing structured packings, in: Institution of Chemical Engineers Symposium Series, Vol. 128, Hemsphere Publishing Corporation, 1992, pp. A489–A489.

[300] R. Billet, M. Schultes, Predicting mass transfer in packed columns, Chemical Engineering & Technology 16 (1) (1993) 1–9. doi:10.1002/ceat.270160102.

[301] R. Billet, M. Schultes, Prediction of mass transfer columns with dumped and arranged packings, Chem. Eng. Res. Des. 77 (6) (1999) 498–504. doi:10.1205/026387699526520.

[302] J. A. Rocha, J. L. Bravo, J. R. Fair, Distillation Columns Containing Structured Packings: A Comprehensive Model for Their Performance. 2. Mass-Transfer Model, Industrial & Engineering Chemistry Research 35 (5) (1996) 1660–1667. doi:10.1021/ie940406i.

[303] E. Brunazzi, G. Nardini, A. Paglianti, L. Petarca, Interfacial area of mellapak packing: Absorption of 1,1,1-trichloroethane by genosorb 300, Chemical Engineering & Technology 18 (4) (1995) 248–255. doi:10.1002/ceat.270180405.

[304] E. Brunazzi, A. Paglianti, Liquid-film mass-transfer coefficient in a column equipped with structured packings, Industrial & Engineering Chemistry Research 36 (9) (1997) 3792–3799. doi:10.1021/ie970045h.

[305] J. J. Gualito, F. J. Cerino, J. C. Cardenas, J. A. Rocha, Design method for distillation columns filled with metallic, ceramic, or plastic structured packings, Industrial & Engineering Chemistry Research 36 (5) (1997) 1747–1757. doi:10.1021/ie960625z.

[306] Z. Xu, A. Afacan, K. Chuang, Predicting mass transfer in packed columns containing structured packings, Chemical Engineering Research and Design 78 (1) (2000) 91–98. doi:10.1205/026387600526924.

[307] R. E. Tsai, A. F. Seibert, R. B. Eldridge, G. T. Rochelle, A dimensionless model for predicting the mass-transfer area of structured packing, AIChE Journal 57 (5) (2011) 1173–1184. doi:10.1002/aic.12345.

[308] B. Hanley, C.-C. Chen, New mass-transfer correlations for packed towers, AIChE Journal 58 (1) (2012) 132–152. doi:10.1002/aic.12574.

[309] A. Zakeri, A. Einbu, P. O. Wiig, L. E. Øi, H. F. Svendsen, Experimental investigation of pressure drop, liquid hold-up and mass transfer parameters in a 0.5 m diameter absorber column, Energy Procedia 4 (2011) 606–613. doi:10.1016/j.egypro.2011.01.095.

[310] R. E. Dugas, Carbon dioxide absorption, desorption, and diffusion in aqueous piperazine and monoethanolamine, The University of Texas at Austin, 2009.

[311] M. D. Hilliard, A predictive thermodynamic model for an aqueous blend of potassium carbonate, piperazine, and monoethanolamine for carbon dioxide capture from flue gas, Ph.D. thesis, The University of Texas at Austin (2008).

[312] AspenTech, Rate based model of the CO_2 capture process by MEA using aspen plus, Aspen Technology Inc, Cambridge, MA, USA.

[313] H. Hikita, S. Asai, H. Ishikawa, M. Honda, The kinetics of reactions of carbon dioxide with monoethanolamine, diethanolamine and triethanolamine by a rapid mixing method, The Chem. Eng. J. 13 (1) (1977) 7–12. doi:10.1016/0300-9467(77)80002-6.

[314] K. R. Putta, D. D. D. Pinto, H. F. Svendsen, H. K. Knuutila, CO_2 absorption into loaded aqueous MEA solutions: Kinetics assessment using penetration theory, International Journal of Greenhouse Gas Control 53 (2016) 338–353. doi:10.1016/j.ijggc.2016.08.009.

[315] U. E. Aronu, S. Gondal, E. T. Hessen, T. Haug-Warberg, A. Hartono, K. A. Hoff, H. F. Svendsen, Solubility of CO_2 in 15, 30, 45 and 60 mass% MEA from 40 to 120°C and model representation using the extended uniquac framework, Chemical Engineering Science 66 (24) (2011) 6393–6406. doi:10.1016/j.ces.2011.08.042.

[316] E. T. Hessen, T. Haug-Warberg, H. F. Svendsen, The refined e-NRTL model applied to CO_2–H_2O–alkanolamine systems, Chemical Engineering Science 65 (11) (2010) 3638–3648. doi:10.1016/j.ces.2010.03.010.

[317] H. Hikita, S. Asai, Y. Katsu, S. Ikuno, Absorption of carbon dioxide into aqueous monoethanolamine solutions, AIChE Journal 25 (5) (1979) 793–800. doi:10.1002/aic.690250507.

[318] X. Luo, A. Hartono, S. Hussain, H. F. Svendsen, Mass transfer and kinetics of carbon dioxide absorption into loaded aqueous monoethanolamine solutions, Chemical Engineering Science 123 (2015) 57–69. doi:10.1016/j.ces.2014.10.013.

[319] M. Amirkhosrow, J.-F. Pérez-Calvo, M. Gazzani, M. Mazzotti, E. N. Lay, Rigorous rate-based model for CO_2 capture via monoethanolamine-based solutions: effect of kinetic models, mass transfer, and holdup correlations on prediction accuracy, Separation Science and Technology 56 (9) (2021) 1491–1509. doi:10.1080/01496395.2020.1784943.

[320] M. Afkhamipour, M. Mofarahi, Review on the mass transfer performance of CO_2 absorption by amine-based solvents in low- and high-pressure absorption packed columns, RSC Adv. 7 (2017) 17857–17872. doi:10.1039/c7ra01352c.

[321] D. S. Moore, W. Notz, M. A. Fligner, The basic practice of statistics, 6th Edition, W.H. Freeman and Co. New York, 2013. doi:https://worldcat.org/title/733238099.

[322] S. A. Glantz, B. K. Slinker, T. B. Neilands, Primer of applied regression & analysis of variance, ed, Vol. 654, McGraw-Hill, Inc., New York, 2001.

[323] I. E. Grossmann, R. W. H. Sargent, Optimum design of chemical plants with uncertain parameters, AIChE Journal 24 (6) (1978) 1021–1028. doi:10.1002/aic.690240612.

[324] D. Straub, I. Grossmann, Integrated stochastic metric of flexibility for systems with discrete state and continuous parameter uncertainties, Computers & Chemical Engineering 14 (9) (1990) 967–985. doi:10.1016/0098-1354(90)87053-R.

[325] W. B. Whiting, T. M. Tong, M. E. Reed, Effect of uncertainties in thermodynamic data and model parameters on calculated process performance, Industrial & Engineering Chemistry Research 32 (7) (1993) 1367–1371. doi:10.1021/ie00019a011.

[326] M. E. Reed, W. B. Whiting, Sensitivty and uncertainty of process designs to thermodynamic model parameters: A monte carlo approach, Chemical Engineering Communications 124 (1) (1993) 39–48. doi:10.1080/00986449308936176.

[327] W. B. Whiting, Effects of uncertainties in thermodynamic data and models on process calculations, Journal of Chemical & Engineering Data 41 (5) (1996) 935–941. doi:10.1021/je9600764.

[328] W. Whiting, V. Vasquez, M. Meerschaert, Techniques for assessing the effects of uncertainties in thermodynamic models and data, Fluid Phase Equilibria 158-160 (1999) 627–641. doi:10.1016/S0378-3812(99)00054-0.

[329] D. Clarke, V. Vasquez, W. Whiting, M. Greiner, Sensitivity and uncertainty analysis of heat-exchanger designs to physical properties estimation, Applied Thermal Engineering 21 (10) (2001) 993–1017. doi:10.1016/S1359-4311(00)00101-0.

[330] V. R. Vasquez, W. B. Whiting, Incorporating uncertainty in chemical process design for environmental risk assessment, Environmental Progress 23 (4) (2004) 315–328. doi:

10.1002/ep.10050.

[331] S. Macchietto, G. Maduabeuke, R. Szczepanski, Exact determination of process sensitivity to physical properties, Fluid Phase Equilibria 29 (1986) 59–67. doi:10.1016/0378-3812(86)85011-7.

[332] C. D. Maranas, Optimal molecular design under property prediction uncertainty, AIChE Journal 43 (5) (1997) 1250–1264. doi:10.1002/aic.690430514.

[333] M. van der Spek, E. Sanchez Fernandez, N. H. Eldrup, R. Skagestad, A. Ramirez, A. Faaij, Unravelling uncertainty and variability in early stage techno-economic assessments of carbon capture technologies, International Journal of Greenhouse Gas Control 56 (2017) 221–236. doi:10.1016/j.ijggc.2016.11.021.

[334] P. M. Mathias, J. P. Gilmartin, Effect of uncertainty in property models on the simulated performance of solvent-based CO_2-capturestudy of aqueous AMP as solvent, International Journal of Greenhouse Gas Control 109 (2021) 103334. doi:10.1016/j.ijggc.2021.103334.

[335] M. van der Spek, T. Fout, M. Garcia, V. N. Kuncheekanna, M. Matuszewski, S. McCoy, J. Morgan, S. M. Nazir, A. Ramirez, S. Roussanaly, E. S. Rubin, Uncertainty analysis in the techno-economic assessment of CO_2 capture and storage technologies. critical review and guidelines for use, International Journal of Greenhouse Gas Control 100 (2020) 103113. doi:10.1016/j.ijggc.2020.103113.

[336] AACE international recommended practice no. 18r-97, Tech. rep., AACE International, USA (2005).

[337] M. van der Spek, A. Ramirez, A. Faaij, Improving uncertainty evaluation of process models by using pedigree analysis. a case study on CO_2 capture with monoethanolamine, Computers & Chemical Engineering 85 (2016) 1–15. doi:10.1016/j.compchemeng.2015.10.006.

[338] J. P. van der Sluijs, P. H. Janssen, A. C. Petersen, P. Kloprogge, J. S. Risbey, W. Tuinstra, J. R. Ravetz, RIVM/MNP guidance for uncertainty assessment and communication: tool catalogue for uncertainty assessment, Utrecht University.
URL www.nusap.net

[339] J. P. Van Der Sluijs, M. Craye, S. Funtowicz, P. Kloprogge, J. Ravetz, J. Risbey, Combining quantitative and qualitative measures of uncertainty in model-based environmental assessment: The nusap system, Risk Analysis 25 (2) (2005) 481–492. doi:10.1111/j.1539-6924.2005.00604.x.

[340] M. T. Mota-Martinez, J. P. Hallett, N. Mac Dowell, Solvent selection and design for CO_2 capture – how we might have been missing the point, Sustainable Energy & Fuels 1 (10) (2017) 2078–2090. doi:10.1039/c7se00404d.

[341] A. Saltelli, M. Ratto, T. Andres, F. Campolongo, J. Cariboni, D. Gatelli, M. Saisana, S. Tarantola, Global sensitivity analysis: the primer, John Wiley & Sons, 2008.

[342] S. O. Funtowicz, J. R. Ravetz, Uncertainty and quality in science for policy, Vol. 15, Springer Science & Business Media, 1990.

[343] P. M. Mathias, Sensitivity of process design to phase equilibriuma new perturbation method based upon the margules equation, Journal of Chemical & Engineering Data 59 (4) (2014) 1006–1015. doi:10.1021/je400748p.

[344] J. Burger, N. Asprion, S. Blagov, M. Bortz, Simple perturbation scheme to consider uncertainty in equations of state for the use in process simulation, Journal of Chemical & Engineering Data 62 (1) (2017) 268–274. doi:10.1021/acs.jced.6b00633.

[345] P. M. Mathias, Effect of VLE uncertainties on the design of separation sequences by distillation – study of the benzene–chloroform–acetone system, Fluid Phase Equilibria 408 (2016) 265–272. doi:10.1016/j.fluid.2015.09.004.

[346] P. M. Mathias, H. Z. Kister, B. Parker, L. Narvaez, T. Schafer, A. Erickson, Component trapping with vapor–liquid equilibrium uncertainty: Principles, design, and troubleshooting, Industrial & Engineering Chemistry Research 56 (40) (2017) 11593–11602. doi:10.1021/acs.iecr.7b02812.

[347] S. Roussanaly, J. A. Ouassou, R. Anantharaman, M. Haaf, Impact of uncertainties on the design and cost of CCS from a waste-to-energy plant, Frontiers in Energy Research 8 (2020) 17. doi:10.3389/fenrg.2020.00017.

[348] M. van der Spek, A. Ramirez, A. Faaij, Challenges and uncertainties of ex ante techno-economic analysis of low TRL CO_2 capture technology: Lessons from a case study of

an NGCC with exhaust gas recycle and electric swing adsorption, Applied Energy 208 (2017) 920–934. doi:10.1016/j.apenergy.2017.09.058.

[349] K. S. Bhat, D. S. Mebane, P. Mahapatra, C. B. Storlie, Upscaling uncertainty with dynamic discrepancy for a multi-scale carbon capture system, Journal of the American Statistical Association 112 (520) (2017) 1453–1467. doi:10.1080/01621459.2017.1295863.

[350] A. Zoelle, M. J. Turner, V. Chou, Quality guide energy system studies: Performing a techno-economic analysis for power generation plants, Tech. rep., National Energy Technology Laboratory (NETL), Pittsburgh, PA, Morgantown, WV (2015).

[351] U. Alstom, European best practice guidelines for assessment of CO_2 capture technologies, SINTEF: Trondheim, Norway.

[352] N. Ferrari, L. Mancuso, K. Burnard, F. Consonni, Effects of plant location on cost of CO_2 capture, International Journal of Greenhouse Gas Control 90 (2019) 102783.

[353] BASF, Amines washing machine - BASF intermediates.

[354] OriginPro V2018-V2024, https://www.originlab.com/, last accessed on 16/03/24.

[355] J. W. Zwolak, P. T. Boggs, L. T. Watson, Algorithm 869: Odrpack95: A weighted orthogonal distance regression code with bound constraints, ACM Transactions on Mathematical Software (TOMS) 33 (4) (2007) 27–es.

[356] G. W. Snedecor, W. G. Cochran, Statistical Methods. Ames, IA, Iowa state university press, 1967.

[357] P. R. Bevington, D. K. Robinson, Data reduction and error analysis for the physical sciences mcgraw-hill, New York 19692 (1969) 235.

[358] Design Institute for Physical Property Data, DIPPR chemical database (2021).

[359] C. L. Yaws, Yaws' Critical Property Data for Chemical Engineers and Chemists, Knovel, 2012.

[360] Y. A. Anufrikov, G. Kuranov, N. Smirnova, Solubility of CO_2 and H_2Ss in alkanolamine-containing aqueous solutions, Russian Journal of Applied Chemistry 80 (4) (2007) 515–527.

[361] A. Henni, A. V. Rayer, K. Z. Sumon, T. Sema, R. Idem, P. Tontiwachwuthikul, Solubility

of CO_2 in reactive solvents for post-combustion CO_2 capture, pp. 58–77. doi:10.4155/ebo.13.360.

[362] H. Arcis, Y. Coulier, K. Ballerat-Busserolles, L. Rodier, J.-Y. Coxam, Enthalpy of solution of CO_2 in aqueous solutions of primary alkanolamines: A comparative study of hindered and nonhindered amine-based solvents, Industrial & Engineering Chemistry Research 53 (27) (2014) 10876–10885. doi:10.1021/ie501589j.

[363] L. Espinal, D. L. Poster, W. Wong-Ng, A. J. Allen, M. L. Green, Measurement, standards, and data needs for CO_2 capture materials: A critical review, Environmental Science & Technology 47 (21) (2013) 11960–11975. doi:10.1021/es402622q.

[364] W. Elliott, A. Benz, J. Gibbins, S. Michailos, An open-access, detailed description of post-combustion CO_2 capture plant, in: Proceedings of the 15th Greenhouse Gas Control Technologies Conference 15-18 March 2021, 2021. doi:10.2139/ssrn.3814671.

[365] S. Arrhenius, Über die Dissociationswärme und den Einfluss der Temperatur auf den Dissociationsgrad der Elektrolyte, Zeitschrift für Physikalische Chemie 4u (1) (1889) 96–116. doi:10.1515/zpch-1889-0408.

[366] T. Daubert, Physical and thermodynamic properties of pure chemicals: data compilation (1989).

[367] C. C. Li, Critical temperature estimation for simple mixtures, The Canadian Journal of Chemical Engineering 49 (5) (1971) 709–710. doi:10.1002/cjce.5450490529.

[368] H. S. Elbro, A. Fredenslund, P. Rasmussen, Group contribution method for the prediction of liquid densities as a function of temperature for solvents, oligomers, and polymers, Industrial & Engineering Chemistry Research 30 (12) (1991) 2576–2582. doi:10.1021/ie00060a011.

[369] S. Sastri, K. Rao, A new group contribution method for predicting viscosity of organic liquids, The Chemical Engineering Journal 50 (1) (1992) 9–25. doi:10.1016/0300-9467(92)80002-R.

[370] Y. Maham, L. G. Hepler, A. E. Mather, A. W. Hakin, R. A. Marriott, Molar heat capacities of alkanolamines from 299.1 to 397.8K group additivity and molecular connectivity analyses, J. Chem. Soc., Faraday Trans. 93 (1997) 1747–1750. doi:10.1039/a607568a.

[371] N. Asprion, Surface tension models for aqueous amine blends, Industrial & Engineering Chemistry Research 44 (18) (2005) 7270–7278. doi:10.1021/ie0504405.

[372] S. Sastri, K. Rao, A new temperature–thermal conductivity relationship for predicting saturated liquid thermal conductivity, Chemical Engineering Journal 74 (3) (1999) 161–169. doi:10.1016/S1385-8947(99)00046-7.

[373] D. R. Schreiber, K. S. Pitzer, Equation of state in the acentric factor system, Fluid Phase Equilibria 46 (2) (1989) 113–130. doi:10.1016/0378-3812(89)80032-9.

[374] P. Li, P.-S. Ma, S.-Z. Yi, Z.-G. Zhao, L.-Z. Cong, A new corresponding-states group-contribution method (CSGC) for estimating vapor pressures of pure compounds, Fluid Phase Equilibria 101 (1994) 101–119. doi:10.1016/0378-3812(94)02607-6.

[375] J. G.-S. Monteiro, H. F. Svendsen, The N_2O analogy in the CO_2 capture context: Literature review and thermodynamic modelling considerations, Chemical Engineering Science 126 (2015) 455–470. doi:10.1016/j.ces.2014.12.026.

[376] G. Puxty, M. Maeder, A simple chemical model to represent CO_2–amine–H_2O vapour–liquid-equilibria, International Journal of Greenhouse Gas Control 17 (2013) 215–224. doi:10.1016/j.ijggc.2013.05.016.

[377] T. Nguyen, M. Hilliard, G. Rochelle, Volatility of aqueous amines in CO_2 capture, Energy Procedia 4 (2011) 1624–1630. doi:10.1016/j.egypro.2011.02.033.

[378] J. Benitez-Garcia, G. Ruiz-Ibanez, H. A. Al-Ghawas, O. C. Sandall, On the effect of basicity on the kinetics of CO_2 absorption in tertiary amines, Chemical Engineering Science 46 (11) (1991) 2927–2931. doi:10.1016/0009-2509(91)85161-P.

[379] D. E. Penny, T. J. Ritter, Kinetic study of the reaction between carbon dioxide and primary amines, Journal of the Chemical Society, Faraday Transactions 1: Physical Chemistry in Condensed Phases 79 (9) (1983) 2103–2109. doi:10.1039/f19837902103.

[380] S. Liu, H. Gao, X. Luo, Z. Liang, Kinetics and new mechanism study of CO_2 absorption into water and tertiary amine solutions by stopped-flow technique, AIChE Journal 65 (2) (2019) 652–661. doi:10.1002/aic.16469.

[381] S. Liu, H. Ling, H. Gao, P. Tontiwachwuthikul, Z. Liang, H. Zhang, Kinetics and new brønsted correlations study of CO_2 absorption into primary and secondary alkanolamine

with and without steric-hindrance, Separation and Purification Technology 233 (2020) 115998. doi:10.1016/j.seppur.2019.115998.

[382] R. Gani, Group contribution-based property estimation methods: advances and perspectives, Current Opinion in Chemical Engineering 23 (2019) 184–196. doi:10.1016/j.coche.2019.04.007.

[383] A. A. Vasserman, A. Kazavchinskii, V. A. Rabinovich, A. Zhuravlev, Thermophysical properties of air and air components.

[384] S. Òsk Garðarsdòttir, F. Normann, R. Skagestad, F. Johnsson, Investment costs and CO_2 reduction potential of carbon capture from industrial plants – a swedish case study, International Journal of Greenhouse Gas Control 76 (2018) 111–124. doi:10.1016/j.ijggc.2018.06.022.

[385] P. L. Mores, J. I. Manassaldi, N. J. Scenna, J. A. Caballero, M. C. Mussati, S. F. Mussati, Optimization of the design, operating conditions, and coupling configuration of combined cycle power plants and CO_2 capture processes by minimizing the mitigation cost, Chemical Engineering Journal 331 (2018) 870–894. doi:10.1016/j.cej.2017.08.111.

[386] A. Alhajaj, N. Mac Dowell, N. Shah, A techno-economic analysis of post-combustion CO_2 capture and compression applied to a combined cycle gas turbine: Part I. a parametric study of the key technical performance indicators, International Journal of Greenhouse Gas Control 44 (2016) 26–41. doi:10.1016/j.ijggc.2015.10.022.

[387] R. Canepa, M. Wang, Techno-economic analysis of a CO_2 capture plant integrated with a commercial scale combined cycle gas turbine (ccgt) power plant, Applied Thermal Engineering 74 (2015) 10–19, 6th International Conference on Clean Coal Technologies CCT2013. doi:10.1016/j.applthermaleng.2014.01.014.

[388] P. Feron, A. Cousins, K. Jiang, R. Zhai, S. S. Hla, R. Thiruvenkatachari, K. Burnard, Towards zero emissions from fossil fuel power stations, International Journal of Greenhouse Gas Control 87 (2019) 188–202. doi:10.1016/j.ijggc.2019.05.018.

[389] N. I. Diamantonis, G. C. Boulougouris, E. Mansoor, D. M. Tsangaris, I. G. Economou, Evaluation of cubic, SAFT, and PC-SAFT equations of state for the vapor - liquid

equilibrium modeling of CO_2 mixtures with other gases, Ind. Eng. Chem. Res. 52 (2013) 3933–3942. doi:10.1021/ie303248q.

[390] M. Lampe, M. Stavrou, J. Schilling, E. Sauer, J. Gross, A. Bardow, Computer-aided molecular design in the continuous-molecular targeting framework using group-contribution PC-SAFT, Computers & Chemical Engineering 81 (2015) 278–287. doi:10.1016/j.compchemeng.2015.04.008.

[391] I. Polishuk, About the numerical pitfalls characteristic for SAFT EOS models, Fluid Phase Equilib. 298 (1) (2010) 67–74. doi:10.1016/j.fluid.2010.07.003.

[392] J. Gross, G. Sadowski, Perturbed-chain SAFT: An equation of state based on a perturbation theory for chain molecules, Ind. Eng. Chem. Res. 40 (4) (2001) 1244–1260. doi:10.1021/ie0003887.

[393] N. Mac Dowell, F. Llovell, C. S. Adjiman, G. Jackson, A. Galindo, Modeling the fluid phase behavior of carbon dioxide in aqueous solutions of monoethanolamine using transferable parameters with the SAFT-VR approach, Industrial & Engineering Chemistry Research 49 (4) (2010) 1883–1899. doi:10.1021/ie901014t.

[394] F. A. Perdomo, S. H. Khalit, C. S. Adjiman, A. Galindo, G. Jackson, Description of the thermodynamic properties and fluid-phase behavior of aqueous solutions of linear, branched, and cyclic amines, AIChE Journal 67 (3) (2021) e17194. doi:10.1002/aic.17194.

[395] P. Brandl, A. L. Pereira, M. T. Mota-Martinez, N. Mac Dowell, L. F. Vega, Integrated approach to optimise CO_2 capture processes: low pressure CO_2 capture from a sru tail gas treatment recovery unit as a case study, in: 14th International Conference on Greenhouse Gas Control Technologies, GHGT-14, 2018.

[396] K. A. Hoff, I. Kim, A. Grimstvedt, B. Bjørkvik, H. Knuutila, Solubility of hydrocarbons in aqueous piperazine and aqueous piperazine/MDEA systems and associated properties, rr-225, Tech. rep., SINTEF Materials and Chemistry, Trondheim, Norway (2015).

[397] S. Cheng, A. Meisen, A. Chakma, Predict amine solution properties accurately, Hydrocarbon Processing 75 (2).

[398] R. M. DiGuilio, W. L. McGregor, A. S. Teja, Thermal conductivities of the

ethanolamines, Journal of Chemical & Engineering Data 37 (2) (1992) 242–245. doi:10.1021/je00006a029.

[399] R. Yusoff, A. Shamiri, M. Aroua, A. Ahmady, M. Shafeeyan, W. Lee, S. Lim, S. Burhanuddin, Physical properties of aqueous mixtures of N-methyldiethanolamine (MDEA) and ionic liquids, Journal of Industrial and Engineering Chemistry 20 (5) (2014) 3349–3355. doi:10.1016/j.jiec.2013.12.019.

[400] S. H. Park, K. B. Lee, J. C. Hyun, S. H. Kim, Correlation and prediction of the solubility of carbon dioxide in aqueous alkanolamine and mixed alkanolamine solutions, Industrial & Engineering Chemistry Research 41 (6) (2002) 1658–1665. doi:10.1021/ie010252o.

[401] P. Brandl, I. Ali, J. Forsyth, N. Mac Dowell, Techno-economic assessment of new solvents for CCS, in: 14th International Conference on Greenhouse Gas Control Technologies, GHGT-14 (Melbourne, Australia, October 2018), pp. 21–26.

[402] Q. Xu, G. Rochelle, Total pressure and CO_2 solubility at high temperature in aqueous amines, Energy Procedia 4 (2011) 117–124. doi:10.1016/j.egypro.2011.01.031.

[403] J. Gabrielsen, M. L. Michelsen, E. H. Stenby, G. M. Kontogeorgis, A model for estimating CO_2 solubility in aqueous alkanolamines, Ind. Eng. Chem. Res. 44 (9) (2005) 3348–3354. doi:10.1021/ie048857i.

[404] K. Goto, F. A. Chowdhury, H. Yamada, T. Higashii, Potential of amine-based solvents for energy-saving CO_2 capture from a coal-fired power plant, Journal of the Japan Institute of Energy 95 (12) (2016) 1133–1141. doi:10.3775/jie.95.1133.

[405] J. Oexmann, Post-combustion CO_2 capture: Energetic evaluation of chemical absorption processes in coal-fired steam power plants, Ph.D. thesis, Technische Universität Hamburg (2011). doi:10.15480/882.989.

[406] P. Alix, L. Raynal, Pressure drop and mass transfer of a high capacity random packing. application to CO_2 post-combustion capture, Energy Procedia 1 (1) (2009) 845–852. doi:10.1016/j.egypro.2009.01.112.

[407] A. Penttilá, C. Dell'Era, P. Uusi-Kyyny, V. Alopaeus, The henry's law constant of N_2O and CO_2 in aqueous binary and ternary amine solutions (MEA, DEA, DIPA, MDEA, and AMP), Fluid Phase Equilib. 311 (1) (2011) 59–66. doi:10.1016/j.fluid.2011.08.019.

[408] S. Laddha, J. M. Diaz, P. V. Danckwerts, The N_2O analogy : the solubilities of CO_2 and N_2O in aqueous solutions of organic compounds, Chem. Eng. Sci. 36 (1981) 229–230. doi:10.1016/0009-2509(81)80074-7.

[409] Y. Wang, S. Xu, F. Otto, A. Mather, Solubility of N_2O in alkanolamines and in mixed solvents, The Chemical Engineering Journal 48 (1) (1992) 31–40. doi:10.1016/0300-9467(92)85004-S.

[410] Y.-G. Li, A. E. Mather, Correlation and prediction of the solubility of N_2O in mixed solvents, Fluid Phase Equilibria 96 (1994) 119–142. doi:10.1016/0378-3812(94)80090-1.

[411] B. E. Poling, J. M. Prausnitz, J. P. O'Connell., The properties of gases and liquids, 5th Edition, McGraw-Hill„ Boston, 2007.

[412] F. Herning, L. Zipperer, Calculation of the viscosity of technical gas mixtures from the viscosity of the individual gases, Gas u. Wasserfach 79 (1936) 69.

[413] A. E. Sherwood, J. M. Prausnitz, The heat of solution of gases at high pressure, AIChE J. 8 (4) (1962) 519–521. doi:10.1002/aic.690080419.

[414] F. Vega, M. Cano, S. Camino, L. M. G. Fernández, E. Portillo, B. Navarrete, Solvents for carbon dioxide capture, in: I. Karamé, J. Shaya, H. Srour (Eds.), Carbon Dioxide Chemistry, Capture and Oil Recovery, IntechOpen, Rijeka, 2018, Ch. 8. doi:10.5772/intechopen.71443.

[415] H. P. Meissner, A. S. Michaels, Surface tensions of pure liquids and liquid mixtures, Industrial & Engineering Chemistry 41 (12) (1949) 2782–2787. doi:10.1021/ie50480a028.

[416] O. Aschenbrenner, P. Styring, Comparative study of solvent properties for carbon dioxide absorption, Energy Environ. Sci. 3 (2010) 1106–1113. doi:10.1039/C002915G.

[417] gPROMS ModelBuilder V. 6.0.4, https://www.psenterprise.com/products/gproms/modelbuilder, last accessed on 16/02/19.

[418] H. C. Mantripragada, H. Zhai, E. S. Rubin, Boundary Dam or Petra Nova – Which is a better model for CCS energy supply?, International Journal of Greenhouse Gas Control 82 (2019) 59–68. doi:10.1016/j.ijggc.2019.01.004.

[419] D. P. Hanak, C. Biliyok, H. Yeung, R. Białecki, Heat integration and exergy analysis for

a supercritical high-ash coal-fired power plant integrated with a post-combustion carbon capture process, Fuel 134 (2014) 126–139. doi:10.1016/j.fuel.2014.05.036.

[420] S. Giannaris, B. Jacobs, W. Srisang, C. Bruce, D. Janowczyk, Heat integration analysis and optimization for a post combustion CO_2 capture retrofit study of saskpowers shand power station, International Journal of Greenhouse Gas Control 84 (2019) 62–71. doi:10.1016/j.ijggc.2019.02.018.

[421] R. K. Sinnott, Coulson and Richardson's chemical engineering volume 6, chemical engineering design (2005).

[422] D. Q. Kern, Process Heat Transfer, International student edition, McGraw-Hill, New York, 1950.

[423] J. C. Chen, Correlation for boiling heat transfer to saturated fluids in convective flow, Ind. Eng. Chem. Process Des. Dev. 5 (3) (1966) 322–329. doi:10.1021/i260019a023.

[424] R. Lockhart, R. Martinelli, Proposed correlation of data for isothermal two-phase, two-component flow in pipes, Chem. Eng. Prog., Symp. Ser. 45 (1949) 39–48.

[425] H. K. Forster, N. Zuber, Dynamics of vapor bubbles and boiling heat transfer, AIChE J. 1 (4) (1955) 531–535. doi:10.1002/aic.690010425.

[426] S. E. Haaland, Simple and explicit formulas for the friction factor in turbulent pipe flow, Journal of Fluids Engineering 105 (1) (1983) 89–90. doi:10.1115/1.3240948.

[427] K. Héberger, S. Kemény, T. Vidóczy, On the errors of arrhenius parameters and estimated rate constant values, International Journal of Chemical Kinetics 19 (3) (1987) 171–181. doi:10.1002/kin.550190302.

[428] K. Onda, H. Takeuchi, Y. Okumoto, Mass transfer coefficients between gas and liquid phases in packed columns, Journal of Chemical engineering of Japan 1 (1) (1968) 56–62. doi:10.1252/jcej.1.56.

[429] M. G. Shi, Effective interfacial area in packed columns, Ger. Chem. Eng. 8 (1985) 87–96.

[430] K. Onda, E. Sada, H. Takeuchi, Gas absorption with chemical reaction in packed column, Journal of Chemical engineering of Japan (1963) (1967) 62–66. doi:10.1252/jcej.1.62.

[431] R. Taylor, Multicomponent mass transfer, Wiley series in chemical engineering, Wiley,

New York ; Chichester, 1993.

[432] R. M. Wellek, R. J. Brunson, F. H. Law, Enhancement factors for gas-absorption with second-order irreversible chemical reaction, The Canadian Journal of Chemical Engineering 56 (2) (1978) 181–186. doi:10.1002/cjce.5450560205.

[433] G. F. Versteeg, W. Van Swaalj, Solubility and diffusivity of acid gases (carbon dioxide, nitrous oxide) in aqueous alkanolamine solutions, Journal of Chemical & Engineering Data 33 (1) (1988) 29–34. doi:10.1021/je00051a011.

[434] E. N. Fuller, J. C. Giddings, A comparison of methods for predicting gaseous diffusion coefficients, Journal of Chromatographic Science 3 (7) (1965) 222–227. doi:10.1093/chromsci/3.7.222.

[435] E. N. Fuller, P. D. Schettler, J. C. Giddings, New method for prediction of binary gas-phase diffusion coefficients, Industrial & Engineering Chemistry 58 (5) (1966) 18–27. doi:10.1021/ie50677a007.

[436] E. Fuller, P. Scettler, J. Giddings, Errata - "a new method for predicting gas diffusivities", Ind. Eng. Chem. 58 (8) (1966) 83. doi:10.1021/ie50680a601.

[437] E. N. Fuller, K. Ensley, J. C. Giddings, Diffusion of halogenated hydrocarbons in helium. The effect of structure on collision cross sections, The Journal of Physical Chemistry 73 (11) (1969) 3679–3685. doi:10.1021/j100845a020.

[438] C. R. Wilke, P. Chang, Correlation of diffusion coefficients in dilute solutions, AIChE J. 1 (2) (1955) 264–270. doi:10.1002/aic.690010222.

[439] M. Takahashi, Y. Kobayashi, H. Takeuchi, Diffusion coefficients and solubilities of carbon dioxide in binary mixed solvents, Journal of Chemical & Engineering Data 27 (3) (1982) 328–331. doi:10.1021/je00029a029.

[440] L. Perkins, C. Geankoplis, Molecular diffusion in a ternary liquid system with the diffusing component dilute, Chemical Engineering Science 24 (7) (1969) 1035–1042. doi:10.1016/0009-2509(69)80075-8.

[441] W. Hayduk, H. Laudie, Prediction of diffusion coefficients for nonelectrolytes in dilute aqueous solutions, AIChE Journal 20 (3) (1974) 611–615. doi:10.1002/aic.690200329.

[442] R. Billet, M. Schultes, Modelling of pressure drop in packed columns, Chemical Engi-

neering & Technology 14 (2) (1991) 89–95. doi:10.1002/ceat.270140203.

[443] R. H. Perry, D. W. Green, Perry's chemical engineers' handbook, 8th Edition, McGraw Hill professional, McGraw-Hill, New York, 2008.

[444] C. Wang, M. Perry, F. Seibert, G. Rochelle, Packing characterization for post combustion CO_2capture: mass transfer model development, Energy Procedia 63 (2014) 1727–1744.

[445] T. H. Chilton, A. P. Colburn, Mass transfer (absorption) coefficients prediction from data on heat transfer and fluid friction, Industrial & Engineering Chemistry 26 (11) (1934) 1183–1187. doi:10.1021/ie50299a012.

[446] P. Mores, E. Godoy, S. Mussati, N. Scenna, A NGCC power plant with a CO_2 post-combustion capture option. optimal economics for different generation/capture goals, Chemical Engineering Research and Design 92 (7) (2014) 1329–1353. doi:10.1016/j.cherd.2013.11.013.

[447] P. Mores, N. Rodríguez, N. Scenna, S. Mussati, CO_2 capture in power plants: Minimization of the investment and operating cost of the post-combustion process using MEA aqueous solution, International Journal of Greenhouse Gas Control 10 (2012) 148–163. doi:10.1016/j.ijggc.2012.06.002.

[448] N. E. Fløa, H. M. Kvamsdal, M. Hillestad, Dynamic simulation of post-combustion CO_2 capture for flexible operation of the Brindisi pilot plant, International Journal of Greenhouse Gas Control 48 (2016) 204–215. doi:10.1016/j.ijggc.2015.11.006.

[449] N. Fløa, H. Knuutila, H. M. Kvamsdal, M. Hillestad, Dynamic model validation of the post-combustion CO_2 absorption process, International Journal of Greenhouse Gas Control 41 (2015) 127–141. doi:10.1016/j.ijggc.2015.07.003.

[450] M. Wilson, R. Wrubleski, L. Yarborough, Recovery of CO_2 from power plant flue gases using amines, Energy Conversion and Management 33 (5) (1992) 325–331. doi:10.1016/0196-8904(92)90027-T.

[451] C. L. Mariz, Carbon dioxide recovery: Large scale design trends, Journal of Canadian Petroleum Technology 37 (7) (1998) 42–47.

[452] K. V. Kwong, R. E. Meissner, S. Ahmed, C. J. Wendt, Application of amines for treating flue gas from coal-fired power plants, Environmental Progress 10 (3) (1991) 211–215.

doi:10.1002/ep.670100321.

[453] R. Meissner, Process alternatives for removing CO_2 from flue gas, in: Pacific Coast Oil Show, 1982.

[454] C. Pauley, CO_2 recovery from flue gas, Chem. Eng. Prog. 80 (5) (1984) 59–62.

[455] C. R. Pauley, S. Haigh, P. L. Simiskey, N-ren recovers CO_2 from flue gas economically, Oil & Gas Journal; (United States) 82:20.

[456] Nobel Prizes 2018, www.NobelPrize.org, last accessed on 16/02/19.

[457] F. J. Dyson, Can we control the carbon dioxide in the atmosphere?, Energy 2 (3) (1977) 287–291. doi:10.1016/0360-5442(77)90033-0.

[458] C. Baes Jr, H. E. Goeller, J. S. Olson, R. M. Rotty, Carbon dioxide and climate: The uncontrolled experiment, American Scientist 65 (1977) 310–320.

[459] J. St. Clair, W. Simister, Process to recover CO_2 from flue gas gets first large-scale tryout in Texas, Oil & Gas Journal 81 (7).

[460] D. Arnold, D. Barrett, R. Isom, CO_2 can be produced from flue gas, Oil & Gas Journal 80 (1982) 130–136.

[461] R. Barchas, R. Davis, The Kerr-McGee/ABB Lummus Crest technology for the recovery of CO_2 from stack gases, Energy Conversion and Management 33 (5) (1992) 333–340. doi:10.1016/0196-8904(92)90028-U.

[462] D. G. Chapel, C. L. Mariz, J. Ernest, Recovery of CO_2 from flue gases: Commercial trends, Canadian Society of Chemical Engineers Annual Meetingdoi:10.1016/j.apenergy.2013.03.089.

[463] J. Alders, Opening speech on the occasion of the first international conference on carbon dioxide removal, Energy Conversion and Management 33 (5) (1992) 283–286. doi:10.1016/0196-8904(92)90021-N.

[464] J. Williams, Carbon Dioxide, Climate and Society: Proceedings of an IIASA Workshop, February 21-24, 1978, Pergamon Press, Oxford, 1978.

[465] M. Wolsky, C. Brooks, Recovering carbon dioxide from man-made sources: Proceedings of a workshop held in Pacific Grove, California, on February 11-13, 1985, 1985.

[466] H. C. Cheng, M. Steinberg, A study on the systematic control of CO_2 emissions from

fossil-fuel power plants in the US, Environmental Progress 5 (4) (1986) 245–255. doi:10.1002/ep.670050409.

[467] M. Abu-Zahra, L. H. J. Schneiders, J. P. M. Niederer, P. H. M. Feron, G. F. Versteeg, CO_2 capture from power plants: Part I. a parametric study of the technical performance based on monoethanolamine, International Journal of Greenhouse Gas Control 1 (1) (2007) 37–46. doi:10.1016/s1750-5836(06)00007-7.

[468] M. Abu-Zahra, J. P. M. Niederer, P. H. M. Feron, G. F. Versteeg, CO_2 capture from power plants: Part II. a parametric study of the economical performance based on monoethanolamine, International Journal of Greenhouse Gas Control 1 (2) (2007) 135–142. doi:10.1016/S1750-5836(07)00032-1.

[469] T. Hirata, T. Tsujiuchi, T. Kamijo, S. Kishimoto, M. Inui, S. Kawasaki, Y.-J. Lin, Y. Nakagami, T. Nojo, Near-zero emission coal-fired power plant using advanced KM CDR™ process, International Journal of Greenhouse Gas Control 92 (2020) 102847. doi:10.1016/j.ijggc.2019.102847.

[470] R. E. Treybal, Adiabatic gas absorption and stripping in packed towers, Ind. & Eng. Chem. 61 (7) (1969) 36–41. doi:10.1021/ie50715a009.

[471] J. D. Pandya, Adiabatic gas absorption and stripping with chemical reaction in packed towers, Chem. Eng. Commun. 19 (4-6) (1983) 343–361. doi:10.1080/00986448308956351.

[472] S. Hatta, Absorption velocity of gases by liquids. I. absorption of carbon dioxide by potassium hydroxide solution, Technology Reports of the Tohoku Imperial University 8 (1-25).

[473] D. W. van Krevelen, P. J. Hoftijzer, Kinetics of simultaneous absorption and chemical reaction., Chem. Eng. Prog. 44 (1948) 529–536.

[474] D. W. van Krevelen, P. J. Hoftijzer, C. J. van Hooren, Studies of gas absorption. IV. simultaneous gas absorption and chemical reaction (1948). doi:10.1002/recl.19480670207.

[475] D. W. van Krevelen, P. J. Hoftijzer, Kinetics of gas-liquid reactions part I. general theory, Recueil des Travaux Chimiques des Pays-Bas 67 (7) (1948) 563–586. doi:10.

1002/recl.19480670708.

[476] J. Wilcox, Carbon Capture, Springer-Verlag, New York, 2012. doi:10.1007/978-1-4614-2215-0.

[477] I. E. Maloka, Generalized liquid molar volume at the normal boiling point correlation, Petroleum Science and Technology 23 (2) (2005) 133–136. doi:10.1081/LFT-200028058.

[478] E. Masiren, N. Harun, W. Ibrahim, F. Adam, Effect of temperature on diffusivity of monoethanolamine (MEA) on absorption process for CO_2 capture, International Journal of Engineering Technology and Sciences 3 (1) (2016) 43–51.

[479] M.-H. Li, M.-D. Lai, Solubility and diffusivity of N_2O and CO_2 in (monoethanolamine + n-methyldiethanolamine + water) and in (monoethanolamine + 2-amino-2-methyl-1-propanol + water), Journal of Chemical & Engineering Data 40 (2) (1995) 486–492. doi:10.1021/je00018a029.

[480] E. D. Snijder, M. J. M. te Riele, G. F. Versteeg, W. P. M. van Swaaij, Diffusion coefficients of several aqueous alkanolamine solutions, Journal of Chemical & Engineering Data 38 (3) (1993) 475–480. doi:10.1021/je00011a037.

[481] K. Miyabe, R. Isogai, Estimation of molecular diffusivity in liquid phase systems by the wilke–chang equation, Journal of Chromatography A 1218 (38) (2011) 6639–6645. doi:10.1016/j.chroma.2011.07.018.

[482] R. K. Sinnott, Chapter 11 - separation columns (distillation and absorption), in: R. K. Sinnott (Ed.), Coulson and Richardson's Chemical Engineering (Second Edition), Pergamon, Amsterdam, 1993, pp. 439–564. doi:10.1016/B978-0-08-041865-0.50019-2.

[483] W. G. Whitman, The two-film theory of gas absorption, Chem. Metall. Eng. 29 (1923) 146–148.

[484] W. K. Lewis, W. G. Whitman, Principles of gas absorption, Ind. Eng. Chem. 16 (12) (1924) 1215–1220. doi:10.1021/ie50180a002.

[485] M. H. Hutchinson, T. K. Sherwood, Liquid film in gas absorption, Industrial & Engineering Chemistry 29 (7) (1937) 836–840. doi:10.1021/ie50331a023.

[486] W. G. Whitman, The two film theory of gas absorption, International Journal of Heat

and Mass Transfer 5 (5) (1962) 429–433. doi:10.1016/0017-9310(62)90032-7.

[487] C. M. Cooper, T. Drew, W. McAdams, Isothermal flow of liquid layers, Industrial & Engineering Chemistry 26 (4) (1934) 428–431.

[488] R. Higbie, The rate of absorption of a pure gas into a still liquid during short periods of exposure, Trans. AIChE 31 (1935) 365–389.

[489] M. Saimpert, G. Puxty, S. Qureshi, L. Wardhaugh, A. Cousins, A new rate based absorber and desorber modelling tool, Chemical Engineering Science 96 (2013) 10–25. doi:10.1016/j.ces.2013.03.013.

[490] L. Simon, Y. Elias, G. Puxty, Y. Artanto, K. Hungerbuhler, Rate based modeling and validation of a carbon-dioxide pilot plant absorbtion column operating on monoethanolamine, Chem. Eng. Res. Des. 89 (9) (2011) 1684–1692. doi:10.1016/j.cherd.2010.10.024.

[491] C. Lu, M. Chen, X. Luo, Z. Liang, The effects of mass transfer on the determination of gas–liquid reaction kinetics in a stirred cell reactor: In the case of CO_2 absorption by aqueous alkanolamine solution, Energy & Fuels 33 (11) (2019) 11524–11535. doi:10.1021/acs.energyfuels.9b02986.

[492] G. Puxty, R. Rowland, M. Attalla, Describing CO_2 mass transfer in amine/ammonia mixtures – no shuttle mechanism required, Energy Procedia 4 (2011) 1369–1376. doi:10.1016/j.egypro.2011.02.001.

[493] I. Hace, Comparison of concentration profiles for boundary layers in absorption with chemical reaction processes, Chemical Engineering & Technology 29 (5) (2006) 574–582. doi:10.1002/ceat.200500403.

[494] P. Danckwerts, Significance of liquid-film coefficients in gas absorption, Industrial & Engineering Chemistry 43 (6) (1951) 1460–1467.

[495] P. Danckwerts, Gas absorption accompanied by chemical reaction, AIChE Journal 1 (4) (1955) 456–463.

[496] E. J. Henley, J. D. Seader, Separation process principles, 2nd Edition, John Wiley & Sons, Ltd, 2006.

[497] S. R. Piché, F. Larachi, B. P. A. Grandjean, Improving the prediction of irrigated pres-

sure drop in packed absorption towers, The Canadian Journal of Chemical Engineering 79 (4) (2001) 584–594. doi:10.1002/cjce.5450790417.

[498] Sulzer structured packings energy-efficient, innovative and profitable., https://www.sulzer.com/-/media/files/products/separation-technology/distillation-and-absorption/brochures/structured_packings.pdf?sc_lang=en, last accessed on 20/07/22.

[499] C. Wang, A. F. Seibert, G. T. Rochelle, Packing characterization: Absorber economic analysis, International Journal of Greenhouse Gas Control 42 (2015) 124–131. doi:10.1016/j.ijggc.2015.07.027.

[500] A. Zakeri, A. Einbu, H. F. Svendsen, Experimental investigation of pressure drop in structured packings, Chemical Engineering Science 73 (2012) 285–298. doi:10.1016/j.ces.2012.01.025.

[501] E. Madsen, R. Neerup, A. Gladis, J. K. Jorsboe, N. von Solms, P. L. Fosbol, Pressure drop of structured packing in pilot column and comparison to common correlations, Chinese Journal of Chemical Engineering 64 (2023) 281–291. doi:10.1016/j.cjche.2023.06.009.

[502] I. von Harbou, M. Imle, H. Hasse, Modeling and simulation of reactive absorption of $CO_2$with mea: Results for four different packings on two different scales, Chemical Engineering Science 105 (2014) 179–190. doi:10.1016/j.ces.2013.11.005.

[503] R. K. Sinnott, Chapter 13 - mechanical design of process equipment, in: R. K. Sinnott (Ed.), Coulson and Richardson's Chemical Engineering (Second Edition), Pergamon, Amsterdam, 1993, pp. 703–796. doi:10.1016/B978-0-08-041865-0.50021-0.

[504] M. Ramezan, T. J. Skone, N. Nsakala, G. Liljedahl, L. Gearhart, R. Hestermann, B. Rederstorff, Carbon dioxide capture from existing coal-fired power plants, National Energy Technology Laboratory, DOE/NETL Report 401 (2007) 110907.

[505] M. Resetarits, M. Lockett, Distillation, in: R. A. Meyers (Ed.), Encyclopedia of Physical Science and Technology (Third Edition), Academic Press, New York, 2003, pp. 547–559. doi:10.1016/B0-12-227410-5/00182-4.

[506] R. K. Sinnott, Chapter 12 - heat-transfer equipment, in: R. K. Sinnott (Ed.), Coulson

and Richardson's Chemical Engineering (Second Edition), Pergamon, Amsterdam, 1993, pp. 565–702. doi:10.1016/B978-0-08-041865-0.50020-9.

[507] Amine-based carbon capture produces small emissions of amines, https://ccsnorway.com/amine-based-carbon-capture-produces-small-emissions-of-amines/#:~:text=The%20emission%20limit%20is%20related,mg%20amine%2FNm3%20flue%20gas., last accessed on 16/09/22.

[508] A. J. Reynolds, T. V. Verheyen, S. B. Adeloju, E. Meuleman, P. Feron, Towards commercial scale postcombustion capture of CO_2 with monoethanolamine solvent: Key considerations for solvent management and environmental impacts, Environmental Science & Technology 46 (7) (2012) 3643–3654. doi:10.1021/es204051s.

[509] W. ElMoudir, T. Supap, C. Saiwan, R. Idem, P. Tontiwachwuthikul, Part 6: Solvent recycling and reclaiming issues, Carbon Management 3 (5) (2012) 485–509. doi:10.4155/cmt.12.55.

[510] T. Supap, C. Saiwan, R. Idem, P. P. Tontiwachwuthikul, Part 2: Solvent management: solvent stability and amine degradation in CO_2 capture processes, Carbon Management 2 (5) (2011) 551–566. doi:10.4155/cmt.11.55.

[511] P. Moser, G. Wiechers, S. Schmidt, J. G. M.-S. Monteiro, E. Goetheer, C. Charalambous, A. Saleh, M. van der Spek, S. Garcia, ALIGN-CCUS: Results of the 18-month test with aqueous AMP/PZ solvent at the pilot plant at Niederaussem – solvent management, emissions and dynamic behavior, International Journal of Greenhouse Gas Control 109 (2021) 103381. doi:10.1016/j.ijggc.2021.103381.

[512] C. Saiwan, T. Supap, R. O. Idem, P. Tontiwachwuthikul, Part 3: Corrosion and prevention in post-combustion CO_2 capture systems, Carbon Management 2 (6) (2011) 659–675. doi:10.4155/cmt.11.63.

[513] D. Gelowitz, T. Supap, N. Abdulaziz, T. Sema, R. Idem, P. Tontiwachwuthikul, Part 8: Post-combustion CO_2 capture: pilot plant operation issues, Carbon Management 4 (2) (2013) 215–231. doi:10.4155/cmt.13.4.

[514] B. J. Drewry, G. T. Rochelle, Simple model for water wash performance in amine scrubbing for CO_2 capture, Carbon Capture Science & Technology 11 (2024) 100186.

doi:10.1016/j.ccst.2023.100186.

[515] L. Hakka, M. Ouimet, United States Patent No. US 7056482b2, Method for recovery of CO_2 from gas streams (2006).

[516] T. R. Haugan, United States Patent No. US 8454726b2, CO_2 absorbent and method for CO_2 capture (2009).

[517] O. M. Bade, O. Gorset, O. F. Graff, S. Woodhouse, European Patent No. WO 2010102877A1, Method and plant for amine emission control (2009).

[518] H. Majeed, H. F. Svendsen, Effect of water wash on mist and aerosol formation in absorption column, Chemical Engineering Journal 333 (2018) 636–648. doi:10.1016/j.cej.2017.09.124.

[519] K. Akinpelumi, C. Saha, G. T. Rochelle, Piperazine aerosol mitigation for post-combustion carbon capture, International Journal of Greenhouse Gas Control 91 (2019) 102845. doi:10.1016/j.ijggc.2019.102845.

[520] M. Afkhamipour, M. Mofarahi, Comparison of rate-based and equilibrium-stage models of a packed column for post-combustion CO_2 capture using 2-amino-2-methyl-1-propanol (AMP) solution, International Journal of Greenhouse Gas Control 15 (2013) 186–199. doi:0.1016/j.ijggc.2013.02.022.

[521] P. D. Vaidya, V. V. Mahajani, Quickly design CO_2 - amine absorber, Indian Journal of Chemical Technology 13 (2006) 47–52.

[522] W. Paterson, A replacement for the logarithmic mean, Chemical Engineering Science 39 (11) (1984) 1635–1636. doi:10.1016/0009-2509(84)80090-1.

[523] O. Frank, Simplified design procedures for tubular exchangers I. Practical aspects of heat transfer, Chem. Eng. Prog. Tech. Manual (Am. Inst. Chem. Eng.).

[524] Z. Abbas, T. Mezher, M. Abu-Zahra, Evaluation of CO_2 purification requirements and the selection of processes for impurities deep removal from the CO_2 product stream, Energy Procedia 37 (2013) 2389–2396. doi:10.1016/j.egypro.2013.06.120.

[525] I. Kim, K. A. Hoff, T. Mejdell, Heat of Absorption of CO_2 with Aqueous Solutions of MEA: New Experimental Data, Energy Procedia 63 (2014) 1446–1455. doi:0.1016/j.egypro.2014.11.154.

[526] S. Lu, F. Yang, J. Zhang, N. Wang, L. Liu, G. Kang, D. Zhao, X. Yu, Q. Li, Experimental Analysis of Reaction Heat of CO_2 Absorption of Phase Change Absorber AEP-DPA at Low Partial Pressure, Energies 16 (4). doi:10.3390/en16041867.

[527] Y. Artanto, J. Jansen, P. Pearson, T. Do, A. Cottrell, E. Meuleman, P. Feron, Performance of MEA and amine-blends in the CSIRO PCC pilot plant at Loy Yang Power in Australia, Fuel 101 (2012) 264–275. doi:10.1016/j.fuel.2012.02.023.

[528] J. R. Couper, W. R. Penney, J. R. Fair, S. M. Walas, Chemical Process Equipment - Selection and Design (Revised 2nd Edition), Elsevier Science, Burlington, 2009.

[529] Front matter, in: R. K. Sinnott (Ed.), Coulson and Richardson's Chemical Engineering (Second Edition), Pergamon, Amsterdam, 1993, p. iii. doi:10.1016/B978-0-08-041865-0.50002-7.

[530] Y. L. Moullec, T. Neveux, 13 - process modifications for CO_2 capture, in: Absorption-Based Post-combustion Capture of Carbon Dioxide, Woodhead Publishing, 2016, pp. 305–340. doi:10.1016/B978-0-08-100514-9.00013-5.

[531] B. A. Oyenekan, G. T. Rochelle, Alternative stripper configurations for CO_2 capture by aqueous amines, AIChE Journal 53 (12) (2007) 3144–3154. doi:10.1002/aic.11316.

[532] Y. Le Moullec, M. Kanniche, Screening of flowsheet modifications for an efficient monoethanolamine (mea) based post-combustion co2 capture, International Journal of Greenhouse Gas Control 5 (4) (2011) 727–740. doi:10.1016/j.ijggc.2011.03.004.

[533] A. Cousins, L. Wardhaugh, P. Feron, A survey of process flow sheet modifications for energy efficient CO_2 capture from flue gases using chemical absorption, International Journal of Greenhouse Gas Control 5 (4) (2011) 605–619. doi:10.1016/j.ijggc.2011.01.002.

[534] Y. Le Moullec, T. Neveux, A. Al Azki, A. Chikukwa, K. A. Hoff, Process modifications for solvent-based post-combustion CO_2 capture, International Journal of Greenhouse Gas Control 31 (2014) 96–112. doi:10.1016/j.ijggc.2014.09.024.

[535] H. Ahn, M. Luberti, Z. Liu, S. Brandani, Process configuration studies of the amine capture process for coal-fired power plants, International Journal of Greenhouse Gas Control 16 (2013) 29–40. doi:10.1016/j.ijggc.2013.03.002.

[536] F. Rezazadeh, W. F. Gale, G. T. Rochelle, D. Sachde, Effectiveness of absorber intercooling for CO_2 absorption from natural gas fired flue gases using monoethanolamine solvent, International Journal of Greenhouse Gas Control 58 (2017) 246–255. doi:10.1016/j.ijggc.2017.01.016.

[537] J. Knudsen, J. Andersen, J. Jensen, O. Biede, Results from test campaigns at the 1 t/h CO_2 PCC pilot plant in Esbjerg under the EU FP7 CESAR project, in: IEAGHG PCC1 Conference, 2011, pp. 17–19.

[538] IEAGHG, CO_2 capture at gas fired power plants (July) (2012) 294.
URL https://ieaghg.org/docs/General_Docs/Reports/2012-08.pdf

[539] Dow, Press release: Prices of amines (2018).

[540] D. Brennan, K. Golonka, New factors for capital cost estimation in evolving process designs, Chemical Engineering Research and Design 80 (6) (2002) 579–586. doi:10.1205/026387602760312773.

[541] G. D. Ulrich, P. T. Vasudevan, How to estimate utility costs, Chem. Eng 113 (4) (2006) 66–69.

[542] J. R. Couper, Cost of individual equipment, in: J. R. Couper (Ed.), Chemical Process Equipment Selection and Design, 2nd Edition, Butterworth-Heinemann, 1990, Ch. 21 Cost of individual equipment, pp. 663–690. doi:10.1016/b978-0-12-372506-6.00019-8.

[543] The chemical engineering plant cost index - chemical engineering, https://www.chemengonline.com/pci-home, last accessed on 12/03/20.

[544] R. K. Sinnott, Chapter 6 - costing and project evaluation, in: R. K. Sinnott (Ed.), Coulson and Richardson's Chemical Engineering (Second Edition), Pergamon, Amsterdam, 1993, pp. 209–244. doi:10.1016/B978-0-08-041865-0.50014-3.

[545] W. M. Vatavuk, Estimating costs of air pollution control, CRC Press, 1990.

[546] R. Turton, R. C. Bailie, W. B. Whiting, J. A. Shaeiwitz, Analysis, synthesis and design of chemical processes, Pearson Education, 2008.

[547] C. King, Analysis, synthesis, and design of chemical processes., Chemie Ingenieur Technik 71 (11) (1999) 1319–1320.

[548] W. Alkhayat, A. Gerrard, Estimating manning levels for process plants, AACE Transactions 1 (1984) 2–1.

[549] M. Fajardy, N. Mac Dowell, Can BECCS deliver sustainable and resource efficient negative emissions?, Energy Environ. Sci. 10 (2017) 1389–1426. doi:10.1039/c7ee00465f.

[550] E. S. Rubin, Understanding the pitfalls of CCS cost estimates, International Journal of Greenhouse Gas Control 10 (2012) 181–190. doi:10.1016/j.ijggc.2012.06.004.

[551] M. van der Spek, S. Roussanaly, E. S. Rubin, Best practices and recent advances in CCS cost engineering and economic analysis, International Journal of Greenhouse Gas Control 83 (2019) 91–104. doi:10.1016/j.ijggc.2019.02.006.

[552] E. S. Rubin, C. Short, G. Booras, J. Davison, C. Ekstrom, M. Matuszewski, S. McCoy, A proposed methodology for CO_2 capture and storage cost estimates, International Journal of Greenhouse Gas Control 17 (2013) 488–503. doi:10.1016/j.ijggc.2013.06.004.

[553] E. S. Rubin, J. E. Davison, H. J. Herzog, The cost of CO_2 capture and storage, International Journal of Greenhouse Gas Control 40 (2015) 378–400. doi:10.1016/j.ijggc.2015.05.018.

[554] E. S. Rubin, Improving cost estimates for advanced low-carbon power plants, International Journal of Greenhouse Gas Control 88 (2019) 1–9. doi:10.1016/j.ijggc.2019.05.019.

[555] M. van der Spek, S. Roussanaly, E. S. Rubin, Best practices and recent advances in CCS cost engineering and economic analysis, International Journal of Greenhouse Gas Control 83 (2019) 91–104. doi:10.1016/j.ijggc.2019.02.006.

[556] S. Roussanaly, C. Fu, M. Voldsund, R. Anantharaman, M. Spinelli, M. Romano, Techno-economic analysis of MEA CO_2 capture from a cement kiln – impact of steam supply scenario, Energy Procedia 114 (2017) 6229–6239. doi:10.1016/j.egypro.2017.03.1761.

[557] S. Roussanaly, N. Berghout, T. Fout, M. Garcia, S. Gardarsdottir, S. M. Nazir, A. Ramirez, E. S. Rubin, Towards improved cost evaluation of carbon capture and storage from industry, International Journal of Greenhouse Gas Control 106 (2021) 103263. doi:10.1016/j.ijggc.2021.103263.

[558] IECM, Integrated environmental control model (IECM), https://www.uwyo.edu/iecm/, last accessed on 02/06/24.

[559] A. Zoelle, D. Keairns, M. J. Turner, M. Woods, N. Kuehn, V. Shah, V. Chou, L. L. Pinkerton, T. Fout, Cost and performance baseline for fossil energy plants volume 1b: Bituminous coal (IGCC) to electricity revision 2b–year dollar update, Tech. rep., NETL (2015).

[560] G. Manzolini, E. Sanchez Fernandez, S. Rezvani, E. Macchi, E. Goetheer, T. Vlugt, Economic assessment of novel amine based CO_2 capture technologies integrated in power plants based on european benchmarking task force methodology, Applied Energy 138 (2015) 546–558. doi:10.1016/j.apenergy.2014.04.066.

[561] I. M. Cerrillo-Briones, L. A. Ricardez-Sandoval, Robust optimization of a post-combustion CO_2 capture absorber column under process uncertainty, Chemical Engineering Research and Design 144 (2019) 386–396. doi:10.1016/j.cherd.2019.02.020.

[562] J. C. Morgan, A. S. Chinen, C. Anderson-Cook, C. Tong, J. Carroll, C. Saha, B. Omell, D. Bhattacharyya, M. Matuszewski, K. S. Bhat, D. C. Miller, Development of a framework for sequential bayesian design of experiments: Application to a pilot-scale solvent-based CO_2 capture process, Applied Energy 262 (2020) 114533. doi:10.1016/j.apenergy.2020.114533.

[563] S. M. Soltani, P. S. Fennell, N. Mac Dowell, A parametric study of CO_2 capture from gas-fired power plants using monoethanolamine (MEA), International Journal of Greenhouse Gas Control 63 (2017) 321–328. doi:10.1016/j.ijggc.2017.06.001.

[564] S. A. Freeman, R. Dugas, D. H. Van Wagener, T. Nguyen, G. T. Rochelle, Carbon dioxide capture with concentrated, aqueous piperazine, International Journal of Greenhouse Gas Control 4 (2) (2010) 119–124. doi:10.1016/j.ijggc.2009.10.008.

[565] F. I. Chowdhury, S. Akhtar, M. Saleh, M. Khandaker, Y. Amin, A. Arof, Volumetric and viscometric properties of aqueous solutions of some monoalkanolamines, Journal of Molecular Liquids 223 (2016) 299–314. doi:10.1016/j.molliq.2016.08.033.

[566] P. Gunasekaran, A. Veawab, A. Aroonwilas, Corrosivity of amine-based absorbents for co2 capture, Energy Procedia 114 (2017) 2047–2054. doi:10.1016/j.egypro.2017.

03.1339.

[567] K. L. S. Campbell, Y. Zhao, J. J. Hall, D. R. Williams, The effect of CO_2-loaded amine solvents on the corrosion of a carbon steel stripper, International Journal of Greenhouse Gas Control 47 (2016) 376–385. doi:10.1016/j.ijggc.2016.02.011.

[568] G. Fytianos, S. Ucar, A. Grimstvedt, A. Hyldbakk, H. F. Svendsen, H. K. Knuutila, Corrosion and degradation in MEA based post-combustion CO_2 capture, International Journal of Greenhouse Gas Control 46 (2016) 48–56. doi:10.1016/j.ijggc.2015.12.028.

[569] E. S. Hamborg, V. Smith, T. Cents, N. Brigman, O. Falk-Pedersen, T. De Cazenove, M. Chhaganlal, J. K. Feste, O. Ullestad, H. Ulvatn, O. Gorset, I. Askestad, L. K. Gram, B. F. Fostås, M. I. Shah, A. Maxson, D. Thimsen, Results from MEA testing at the CO_2 Technology Centre Mongstad. Part II: Verification of baseline results, Energy Procedia 63 (2014) 5994–6011. doi:10.1016/j.egypro.2014.11.634.

[570] V. Andersson, K. Wittmeyer, O. Gorset, Y. Maree, K. Sanden, Operational experience and initial results from the first test period at CO_2 technology centre mongstad, Energy Procedia 37 (2013) 6348–6356. doi:10.1016/j.egypro.2013.06.564.

[571] G. de Koeijer, Y. Enge, K. Sanden, O. F. Graff, O. Falk-Pedersen, T. Amundsen, S. Overå, CO_2 technology centre mongstad–design, functionality and emissions of the amine plant, Energy Procedia 4 (2011) 1207–1213. doi:10.1016/j.egypro.2011.01.175.

[572] A. Kothandaraman, Carbon dioxide capture by chemical absorption: A solvent comparison study, Ph.D. thesis, Massachusetts Institute of Technology (2010).

[573] GraphPad Prism for Windows 64-bit Version 9.5, www.graphpad.com, last accessed on 19/05/22.

[574] I. Kim, H. F. Svendsen, Heat of absorption of carbon dioxide (CO_2) in monoethanolamine (MEA) and 2-(aminoethyl)ethanolamine (AEEA) solutions, Ind. Eng. Chem. Res. 46 (17) (2007) 5803–5809. doi:10.1021/ie0616489.

[575] Y. S. Kim, J. H. Jang, B. D. Lim, J. W. Kang, C. S. Lee, Solubility of mixed gases containing carbon dioxide in ionic liquids: Measurements and predictions, Fluid Phase

Equilib. 256 (1–2) (2007) 70–74. doi:10.1016/j.fluid.2006.11.019.

[576] I. M. Sobol, On the distribution of points in a cube and the approximate evaluation of integrals, Zhurnal Vychislitel'noi Matematiki i Matematicheskoi Fiziki 7 (4) (1967) 784–802.

[577] S. Kashiwaya, Dynamic process model parameter estimation by global system analysis, in: M. S. F. Nezhad (Ed.), New Insights into Bayesian Inference, IntechOpen, Rijeka, 2018, Ch. 4. doi:10.5772/intechopen.74635.

[578] B. L. Welch, The generalization of student's problem when several different population variances are involved, Biometrika 34 (1-2) (1947) 28–35. doi:10.1093/biomet/34.1-2.28.

[579] B. L. Welch, On the comparison of several mean values: An alternative approach, Biometrika 38 (3/4) (1951) 330–336.

[580] S. Lee, D. K. Lee, What is the proper way to apply the multiple comparison test?, Korean journal of anesthesiology 71 (5) (2018) 353–360.

[581] M. C. Shingala, A. Rajyaguru, Comparison of post hoc tests for unequal variance, International Journal of New Technologies in Science and Engineering 2 (5) (2015) 22–33.

[582] P. A. Games, J. F. Howell, Pairwise Multiple Comparison Procedures with Unequal N's and/or Variances: A Monte Carlo Study, Journal of Educational Statistics 1 (2) (1976) 113–125. doi:10.3102/10769986001002113.

[583] Copyright, in: P. S. Bandyopadhyay, M. R. Forster (Eds.), Philosophy of Statistics, Vol. 7 of Handbook of the Philosophy of Science, North-Holland, Amsterdam, 2011, p. iv. doi:10.1016/B978-0-444-51862-0.50039-3.

[584] C. Wheelan, Naked statistics: Stripping the dread from the data, WW Norton & Company, 2013.

[585] Statistical Quality Standard E1: Analyzing Data, https://www.census.gov/about/policies/quality/standards/standarde1.html, last accessed on 23/10/22.

[586] K. Pearson, On the criterion that a given system of deviations from the probable in the case of a correlated system of variables is such that it can be reasonably supposed to have arisen from random sampling, The London, Edinburgh, and Dublin Philosophical Maga-

zine and Journal of Science 50 (302) (1900) 157–175. doi:10.1080/14786440009463897.

[587] G. D. Ruxton, The unequal variance t-test is an underused alternative to Student's t-test and the MannWhitney U test, Behavioral Ecology 17 (4) (2006) 688–690. doi:10.1093/beheco/ark016.

[588] B. Derrick, P. White, Why Welch's test is Type I error robust, The Quantitative Methods for Psychology 12 (1) (2016) 30–38. doi:10.20982/tqmp.12.1.p030.

[589] O. J. Dunn, Multiple comparisons among means, Journal of the American Statistical Association 56 (293) (1961) 52–64. doi:10.1080/01621459.1961.10482090.

[590] S.-Y. Chen, Z. Feng, X. Yi, A general introduction to adjustment for multiple comparisons, Journal of Thoracic Disease 9 (6).

[591] M. B. Brown, A. B. Forsythe, Robust tests for the equality of variances, Journal of the American Statistical Association 69 (346) (1974) 364–367. doi:10.1080/01621459.1974.10482955.

[592] K. Moder, Alternatives to F-test in one way ANOVA in case of heterogeneity of variances (a simulation study), Psychological Test and Assessment Modeling 52 (4) (2010) 343.

[593] S. E. Maxwell, H. D. Delaney, K. Kelley, Designing experiments and analyzing data: A model comparison perspective, Routledge, 2017.

[594] J. W. Tukey, Comparing individual means in the analysis of variance, Biometrics (1949) 99–114.

[595] G. D. Ruxton, G. Beauchamp, Time for some a priori thinking about post hoc testing, Behavioral ecology 19 (3) (2008) 690–693.

[596] F. E. Satterthwaite, Synthesis of variance, Psychometrika 6 (5) (1941) 309–316.

[597] F. E. Satterthwaite, An approximate distribution of estimates of variance components, Biometrics Bulletin 2 (6) (1946) 110–114.

[598] L. G. Wang, C. Omar, J. Litster, D. Slade, J. Li, A. Salman, S. Bellinghausen, D. Barrasso, N. Mitchell, Model driven design for integrated twin screw granulator and fluid bed dryer via flowsheet modelling, International Journal of Pharmaceutics 628 (2022) 122186. doi:10.1016/j.ijpharm.2022.122186.

[599] L. F. Richardson, J. A. Gaunt, Viii. the deferred approach to the limit, Philosophical

Transactions of the Royal Society of London. Series A, containing papers of a mathematical or physical character 226 (636-646) (1927) 299–361.

[600] A. Aroonwilas, P. Tontiwachwuthikul, Mechanistic model for prediction of structured packing mass transfer performance in CO_2 absorption with chemical reactions, Chem. Eng. Sci. 55 (18) (2000) 3651–3663. doi:10.1016/s0009-2509(00)00035-x.

[601] A. Aroonwilas, A. Chakma, P. Tontiwachwuthikul, A. Veawab, Mathematical modelling of mass-transfer and hydrodynamics in CO_2 absorbers packed with structured packings, Chem. Eng. Sci. 58 (17) (2003) 4037–4053. doi:10.1016/s0009-2509(03)00315-4.

[602] L. F. Vega, D. Bahamon, I. I. I. Alkhatib, W. A. Fouad, F. Llovell, L. M. C. Pereira, O. Vilaseca, How molecular modelling tools can help in mitigating climate change, in: E. J. Maginn, J. Errington (Eds.), Foundations of Molecular Modeling and Simulation, Springer Singapore, Singapore, 2021, pp. 181–220.

[603] F. A. Chowdhury, H. Okabe, S. Shimizu, M. Onoda, Y. Fujioka, Development of novel tertiary amine absorbents for CO_2 capture, Energy Procedia 1 (1) (2009) 1241–1248. doi:10.1016/j.egypro.2009.01.163.

[604] F. A. Chowdhury, H. Yamada, T. Higashii, Y. Matsuzaki, S. Kazama, Synthesis and characterization of new absorbents for CO_2 capture, Energy Procedia 37 (2013) 265–272. doi:10.1016/j.egypro.2013.05.111.

[605] F. A. Chowdhury, H. Yamada, Y. Matsuzaki, K. Goto, T. Higashii, M. Onoda, Development of novel synthetic amine absorbents for CO_2 capture, Energy Procedia 63 (2014) 572–579. doi:10.1016/j.egypro.2014.11.062.

[606] J. Kim, J. Lee, Y. Lee, H. Kim, E. Kim, K. S. Lee, Evaluation of aqueous polyamines as CO_2 capture solvents, Energy 187 (2019) 115908. doi:10.1016/j.energy.2019.115908.

[607] X. Chen, G. T. Rochelle, Aqueous piperazine derivatives for CO_2 capture: Accurate screening by a wetted wall column, Chemical Engineering Research and Design 89 (9) (2011) 1693–1710. doi:10.1016/j.cherd.2011.04.002.

[608] P. Brandl, Impact of CO_2 composition in flue gas on capture cost, https://public.flourish.studio/visualisation/6238085/, first published 24/06/21, last accessed

on 16/04/24 (2021).

[609] M. M. Sharma, Kinetics of reactions of carbonyl sulphide and carbon dioxide with amines and catalysis by brönsted bases of the hydrolysis of cos, Trans. Faraday Soc. 61 (1965) 681–688. doi:10.1039/tf9656100681.

[610] C. Cacela, R. Fausto, M. L. Duarte, A combined matrix-isolation infrared spectroscopy and MO study of 1-amino-2-propanol, Vibrational Spectroscopy 26 (1) (2001) 113–131. doi:10.1016/S0924-2031(01)00112-6.

[611] A. Goldblum, O. Deeb, G. H. Loew, Semiempirical MNDO/H calculations of opiates: Part 1. Building blocks: conformations of piperidine derivatives and the effect of hydrogen bonding, Journal of Molecular Structure: Theochem 207 (1) (1990) 1–14. doi:10.1016/0166-1280(90)85150-L.

[612] M. Przesawska, S. Melikowa, P. Lipkowski, A. Koll, Gas phase FT-IR spectra and structure of aminoalcohols with intramolecular hydrogen bonds: I. The shape of the (OH) vibrational bands in $R_2NC_3H_6OH$, Vibrational Spectroscopy 20 (1) (1999) 69–83. doi:10.1016/S0924-2031(99)00023-5.

[613] M. A. Ribeiro da Silva, J. I. Cabral, Standard molar enthalpies of formation of 1-methyl-2-piperidinemethanol, 1-piperidineethanol, and 2-piperidineethanol, The Journal of Chemical Thermodynamics 38 (11) (2006) 1461–1466. doi:10.1016/j.jct.2006.01.005.

[614] D. C. Cantu, D. Malhotra, P. K. Koech, D. J. Heldebrant, R. F. Zheng, C. J. Freeman, R. Rousseau, V.-A. Glezakou, Integrated solvent design for CO_2 capture and viscosity tuning, Energy Procedia 114 (2017) 726–734. doi:10.1016/j.egypro.2017.03.1215.

[615] D. C. Cantu, D. Malhotra, M.-T. Nguyen, P. K. Koech, D. Zhang, V.-A. Glezakou, R. Rousseau, J. Page, R. Zheng, R. J. Perry, D. J. Heldebrant, Molecular-level overhaul of γ-aminopropyl aminosilicone/triethylene glycol post-combustion CO_2-capture solvents, ChemSusChem 13 (13) (2020) 3429–3438. doi:10.1002/cssc.202000724.

[616] M. Xiao, H. Liu, R. Idem, P. Tontiwachwuthikul, Z. Liang, A study of structure–activity relationships of commercial tertiary amines for post-combustion CO_2 capture, Applied Energy 184 (2016) 219–229. doi:10.1016/j.apenergy.2016.10.006.

[617] R. Zhang, Q. Yang, Z. Liang, G. Puxty, R. J. Mulder, J. E. Cosgriff, H. Yu, X. Yang, Y. Xue, Toward efficient CO_2 capture solvent design by analyzing the effect of chain lengths and amino types to the absorption capacity, bicarbonate/carbamate, and cyclic capacity, Energy & Fuels 31 (10) (2017) 11099–11108. doi:10.1021/acs.energyfuels.7b01951.

[618] R. Zhang, Q. Yang, B. Yu, H. Yu, Z. Liang, Toward to efficient CO_2 capture solvent design by analyzing the effect of substituent type connected to n-atom, Energy 144 (2018) 1064–1072. doi:10.1016/j.energy.2017.12.095.

[619] M. Xiao, D. Cui, Q. Yang, Z. Liang, G. Puxty, H. Yu, L. Li, W. Conway, P. Feron, Role of mono- and diamines as kinetic promoters in mixed aqueous amine solution for CO_2 capture, Chemical Engineering Science 229 (2021) 116009. doi:10.1016/j.ces.2020.116009.

[620] W. A. Henderson, C. J. Schultz, The nucleophilicity of amines, The Journal of Organic Chemistry 27 (12) (1962) 4643–4646. doi:10.1021/jo01059a507.

[621] H. Mayr, A. R. Ofial, Do general nucleophilicity scales exist?, Journal of Physical Organic Chemistry 21 (7-8) (2008) 584–595. doi:10.1002/poc.1325.

[622] H. Mayr, A. R. Ofial, Kinetics of electrophile-nucleophile combinations: A general approach to polar organic reactivity, Pure and Applied Chemistry 77 (11) (2005) 1807–1821. doi:10.1351/pac200577111807.

[623] H. Mayr, Mayr's Database of Reactivity Parameter, https://www.cup.lmu.de/oc/mayr/reaktionsdatenbank2/, last accessed on 29/01/24 (2024).

[624] Y. H. Jhon, J.-G. Shim, J.-H. Kim, J. H. Lee, K.-R. Jang, J. Kim, Nucleophilicity and accessibility calculations of alkanolamines: Applications to carbon dioxide absorption reactions, The Journal of Physical Chemistry A 114 (49) (2010) 12907–12913. doi:10.1021/jp105914c.

[625] F. Brotzel, Nucleophilicities of amines, amino acids and pyridines, Ph.D. thesis, LMU München (2008).

[626] S. J. Hwang, M. Lee, H. Kim, K. S. Lee, Cyclic CO_2 absorption capacity of aqueous single and blended amine solvents, Journal of Industrial and Engineering Chemistry 65

(2018) 95–103. doi:10.1016/j.jiec.2018.04.017.

[627] P. Brandl, M. Bui, J. P. Hallett, N. Mac Dowell, A century of re-exploring CO_2 capture solvents, International Journal of Greenhouse Gas Control 120 (2022) 103771. doi:10.1016/j.ijggc.2022.103771.

[628] H. Li, B. Dong, Z. Yu, J. Yan, K. Zhu, Thermo-physical properties of CO_2 mixtures and their impacts on CO_2 capture, transport and storage: Progress since 2011, Applied Energy 255 (2019) 113789. doi:10.1016/j.apenergy.2019.113789.

[629] F. Zuiderweg, A. Harmens, The influence of surface phenomena on the performance of distillation columns, Chemical Engineering Science 9 (2) (1958) 89–103. doi:10.1016/0009-2509(58)80001-9.

[630] M. Garcia, H. K. Knuutila, U. E. Aronu, S. Gu, Influence of substitution of water by organic solvents in amine solutions on absorption of CO_2, International Journal of Greenhouse Gas Control 78 (2018) 286–305. doi:10.1016/j.ijggc.2018.07.029.

[631] A. Singh, K. Stéphenne, Shell cansolv CO_2 capture technology: Achievement from the first commercial plant, Energy Procedia 63 (2014) 1678–1685. doi:10.1016/j.egypro.2014.11.177.

[632] L. Li, A. K. Voice, H. Li, O. Namjoshi, T. Nguyen, Y. Du, G. T. Rochelle, Amine blends using concentrated piperazine, Energy Procedia 37 (2013) 353–369. doi:10.1016/j.egypro.2013.05.121.

[633] A. Schäffer, K. Brechtel, G. Scheffknecht, Comparative study on differently concentrated aqueous solutions of MEA and TETA for CO_2 capture from flue gases, Fuel 101 (2012) 148–153. doi:10.1016/j.fuel.2011.06.037.

[634] Z. Feng, M. Jing-Wen, Z. Zheng, W. You-Ting, Z. Zhi-Bing, Study on the absorption of carbon dioxide in high concentrated MDEA and ILs solutions, Chem. Eng. J. (0). doi:10.1016/j.cej.2011.11.066.

[635] S. A. Freeman, R. Dugas, D. Van Wagener, T. Nguyen, G. T. Rochelle, Carbon dioxide capture with concentrated, aqueous piperazine, Energy Procedia 1 (1) (2009) 1489–1496. doi:10.1016/j.egypro.2009.01.195.

[636] M. Appl, U. Wagner, H. J. Henrici, K. Kuessner, K. Volkamer, E. Fuerst, Deutsches

Patent DE 2551717A1, Verfahren zur Entfernung von CO_2 und/oder H_2S s und/oder COS aus Gasen, die diese Bestandteile enthalten (1977).

[637] A. Aroonwilas, A. Veawab, Characterization and comparison of the CO_2 absorption performance into single and blended alkanolamines in a packed column, Industrial & Engineering Chemistry Research 43 (9) (2004) 2228–2237. doi:10.1021/ie0306067.

[638] R. Sakwattanapong, A. Aroonwilas, A. Veawab, Behavior of reboiler heat duty for CO_2 capture plants using regenerable single and blended alkanolamines, Industrial & Engineering Chemistry Research 44 (12) (2005) 4465–4473. doi:10.1021/ie050063w.

[639] Q. Zhuang, B. Clements, Synergistic effect on CO_2 capture by binary solvent system, 2017, p. 139.

[640] H. Shi, L. Zheng, M. Huang, Y. Zuo, M. Li, L. Jiang, R. Idem, P. Tontiwachwuthikul, CO_2 desorption tests of blended monoethanolamine–diethanolamine solutions to discover novel energy efficient solvents, Asia-Pacific Journal of Chemical Engineering 13 (3) (2018) e2186. doi:10.1002/apj.2186.

[641] H. Shi, J. Fu, Q. Wu, M. Huang, L. Jiang, M. Cui, R. Idem, P. Tontiwachwuthikul, Studies of the coordination effect of DEA-MEA blended amines under heterogeneous catalysis by means of absorption and desorption parameters, Separation and Purification Technology 236 (2020) 116179. doi:10.1016/j.seppur.2019.116179.

[642] L. F. Chiu, M. H. Li, Heat capacity of alkanolamine aqueous solutions, Journal of Chemical & Engineering Data 44 (6) (1999) 1396–1401. doi:10.1021/je990131j.

[643] L. Kucka, E. Y. Kenig, A. Górak, Kinetics of the gas-liquid reaction between carbon dioxide and hydroxide ions, Industrial & Engineering Chemistry Research 41 (24) (2002) 5952–5957. doi:10.1021/ie020452f.

[644] A. Abdulkadir, A. V. Rayer, D. V. Quang, N. E. Hadri, A. Dindi, P. H. Feron, M. Abu-Zahra, Heat of absorption and specific heat of carbon dioxide in aqueous solutions of monoethanolamine,3-piperidinemethanol and their blends, Energy Procedia 63 (2014) 2070–2081. doi:10.1016/j.egypro.2014.11.223.

[645] T. Ross, H. Mustafa, Absorption of carbon dioxide by sodium phenolic salt solution, The Chemical Engineering Journal 5 (2) (1973) 261–266. doi:10.1016/0300-9467(73)

80016-4.

[646] M. Origlia-Luster, K. Ballerat-Busserolles, E. Merkley, J. Price, B. McRae, E. Woolley, Apparent molar volumes and apparent molar heat capacities of aqueous phenol and sodium phenolate at temperatures from 278.15 to 393.15K and at the pressure 0.35MPa, The Journal of Chemical Thermodynamics 35 (2) (2003) 331–347. doi:10.1016/S0021-9614(02)00373-7.

[647] B. Minofar, P. Jungwirth, M. R. Das, W. Kunz, S. Mahiuddin, Propensity of formate, acetate, benzoate, and phenolate for the aqueous solution/vapor interface: surface tension measurements and molecular dynamics simulations, The Journal of Physical Chemistry C 111 (23) (2007) 8242–8247. doi:10.1021/jp068804+.

[648] E. Sada, H. Kumazawa, T. Amano, I. Kudo, T. Kondo, Absorption of carbon dioxide in aqueous solutions of sodium phenoxide, The Chemical Engineering Journal 13 (1) (1977) 41–44. doi:10.1016/0300-9467(77)80007-5.

[649] D. K. H. Briggs, G. H. Thompson, Absorption of carbon dioxide in carbolates, Journal of Applied Chemistry 11 (12) (1961) 464–468. doi:10.1002/jctb.5010111203.

[650] Y. Kosugi, Y. Imaoka, F. Gotoh, M. A. Rahim, Y. Matsui, K. Sakanishi, Carboxylations of alkali metal phenoxides with carbon dioxide, Org. Biomol. Chem. 1 (2003) 817–821. doi:10.1039/b210793g.

[651] J. E. Wheatley, S. Bala, D. C. Barnes, C. Schoolderman, G. Jakab, G. Raynel, C. M. Rayner, CO_2 capture using phenoxide salts; alternatives to amine-based capture agents, and comparative speciation studies as components in solvent blends, International Journal of Greenhouse Gas Control 88 (2019) 353–360. doi:10.1016/j.ijggc.2019.06.012.

[652] Y. Kosugi, K. Takahashi, Y. Imaoka, Solvent-assisted carboxylation of alkali metal phenoxide with carbon dioxide, J. Chem. Res. (S) (1999) 114–115doi:10.1039/A805032E. URL http://dx.doi.org/10.1039/A805032E

[653] Y. Zhao, Y. Bian, H. Li, H. Guo, S. Shen, J. Han, D. Guo, A comparative study of aqueous potassium lysinate and aqueous monoethanolamine for postcombustion CO_2 capture, Energy & Fuels 31 (12) (2017) 14033–14044. doi:10.1021/acs.energyfuels.

7b02800.

[654] S. Shen, Y.-n. Yang, Y. Bian, Y. Zhao, Kinetics of CO_2 absorption into aqueous basic amino acid salt: Potassium salt of lysine solution, Environmental Science & Technology 50 (4) (2016) 2054–2063. doi:10.1021/acs.est.5b04515.

[655] H.-J. Song, M.-G. Lee, H. Kim, A. Gaur, J.-W. Park, Density, viscosity, heat capacity, surface tension, and solubility of CO_2 in aqueous solutions of potassium serinate, Journal of Chemical & Engineering Data 56 (4) (2011) 1371–1377. doi:10.1021/je101144k.

[656] R. Ramezani, S. Mazinani, R. D. Felice, State-of-the-art of CO_2 capture with amino acid salt solutions, Reviews in Chemical Engineering (2020) 000010151520200012doi:10.1515/revce-2020-0012.

[657] S. Shen, Y. nan Yang, Y. Wang, S. Ren, J. Han, A. Chen, CO_2 absorption into aqueous potassium salts of lysine and proline: Density, viscosity and solubility of CO_2, Fluid Phase Equilibria 399 (2015) 40–49. doi:10.1016/j.fluid.2015.04.021.

[658] Z. Zhang, Y. Li, W. Zhang, J. Wang, M. R. Soltanian, A. G. Olabi, Effectiveness of amino acid salt solutions in capturing CO_2: A review, Renewable and Sustainable Energy Reviews 98 (2018) 179–188. doi:10.1016/j.rser.2018.09.019.

[659] C. Li, Y. Zhao, S. Shen, Aqueous potassium lysinate for CO_2 capture: Evaluating at desorber conditions, Energy & Fuels 33 (10) (2019) 10090–10098. doi:10.1021/acs.energyfuels.9b02659.

[660] M. S. Shaikh, A. M. Shariff, S. Garg, M. A. Bustam, Physical properties of aqueous solutions of potassium l-prolinate from 298.15 to 343.15ăK at atmospheric pressure, Chemical Papers 71 (7) (2017) 1185–1194. doi:10.1007/s11696-016-0111-6.

[661] F. He, T. Wang, M. Fang, Z. Wang, H. Yu, Q. Ma, Screening test of amino acid salts for CO_2 absorption at flue gas temperature in a membrane contactor, Energy & Fuels 31 (1) (2017) 770–777. doi:10.1021/acs.energyfuels.6b02578.

[662] M. Majchrowicz, D. Brilman, Solubility of CO_2 in aqueous potassium l-prolinate solutions–absorber conditions, Chemical Engineering Science 72 (2012) 35–44. doi:10.1016/j.ces.2011.12.014.

[663] E. R. Smith, P. K. Smith, Thermodynamic properties of solutions of amino acids and

related substances: VIII. the ionization of glycylglycien, ε-aminocaproic acid, and aspartic acid in aqueous solution from one to fifty degrees, Journal of Biological Chemistry 146 (1) (1942) 187–195.

[664] J.-a. Lim, D. H. Kim, Y. Yoon, S. K. Jeong, K. T. Park, S. C. Nam, Absorption of CO_2 into aqueous potassium salt solutions of l-alanine and l-proline, Energy & Fuels 26 (6) (2012) 3910–3918. doi:10.1021/ef300453e.

[665] B. Rumpf, J. Xia, G. Maurer, Solubility of carbon dioxide in aqueous solutions containing acetic acid or sodium hydroxide in the temperature range from 313 to 433K and at total pressures up to 10 MPa, Industrial & Engineering Chemistry Research 37 (5) (1998) 2012–2019. doi:10.1021/ie9706626.

[666] J. Kumełan, A. Pérez-Salado Kamps, G. Maurer, Solubility of CO_2 in aqueous solutions of methionine and in aqueous solutions of (K_2CO_3 and methionine), Industrial & Engineering Chemistry Research 49 (8) (2010) 3910–3918. doi:10.1021/ie902032n.

[667] Y. Liu, S. Lin, H. Lu, C. Liu, K. Wu, W. Jiang, B. Liang, Studies on viscosity and conductivity of 1,8-diazabicyclo[5.4.0]undec-7-ene (DBU)-glycerol and CO_2-DBU-glycerol solutions at temperatures from 288.1k to 328.1K, The Journal of Chemical Thermodynamics 136 (2019) 16–27. doi:10.1016/j.jct.2019.04.017.

[668] H. Duan, K. Zhu, H. Lu, C. Liu, K. Wu, Y. Liu, B. Liang, CO_2 absorption performance in a rotating disk reactor using DBU-glycerol as solvent, Chinese Journal of Chemical Engineering 28 (1) (2020) 104–113. doi:10.1016/j.cjche.2019.03.031.

[669] S. Lin, H. Lu, Y. Liu, C. Liu, B. Liang, K. Wu, Density studies of 1,8-diazabicyclo[5.4.0]undec-7-ene (DBU)-glycerol and CO_2-DBU-glycerol solutions at temperatures between 288.15k and 328.15K, The Journal of Chemical Thermodynamics 123 (2018) 8–16. doi:10.1016/j.jct.2018.03.017.

[670] X. Zhu, H. Lu, K. Wu, Y. Zhu, Y. Liu, C. Liu, B. Liang, DBU-glycerol solution: A CO_2 absorbent with high desorption ratio and low regeneration energy, Environmental Science & Technology 54 (12) (2020) 7570–7578. doi:10.1021/acs.est.0c01332.

[671] Z. S. Baird, A. Dahlberg, P. Uusi-Kyyny, N. Osmanbegovic, J. Witos, J. Helminen, D. Cederkrantz, P. Hyväri, V. Alopaeus, I. Kilpeläinen, Physical properties of 7-methyl-

1, 5, 7-triazabicyclo [4.4. 0] dec-5-ene (mtbd), International Journal of Thermophysics 40 (7) (2019) 1–23.

[672] Y. Liu, S. Lin, H. Lu, C. Liu, K. Wu, B. Liang, Studies on surface tension of 1,8-diazabicyclo [5.4.0] undec-7-ene (DBU)-glycerol and CO_2-DBU-glycerol solutions at temperatures from 288.1k to 323.1K, The Journal of Chemical Thermodynamics 125 (2018) 32–40. doi:10.1016/j.jct.2018.05.013.

[673] M. c. Öztürk, C. S. Ume, E. Alper, Reaction mechanism and kinetics of 1,8-diazabicyclo[5.4.0]undec-7-ene and carbon dioxide in alkanol solutions, Chemical Engineering & Technology 35 (12) (2012) 2093–2098. doi:10.1002/ceat.201200341.

[674] A. Ostonen, E. Sapei, P. Uusi-Kyyny, A. Klemelä, V. Alopaeus, Measurements and modeling of CO_2 solubility in 1,8-diazabicyclo-[5.4.0]-undec-7-ene–glycerol solutions, Fluid Phase Equilibria 374 (2014) 25–36. doi:10.1016/j.fluid.2014.04.021.

[675] S. S. Karunarathne, D. A. Eimer, L. E. Øi, Density, viscosity and free energy of activation for viscous flow of monoethanol amine (1) + H_2O (2) + CO_2 (3) mixtures, Fluids 5 (1). doi:10.3390/fluids5010013.

[676] M. Garcia, H. K. Knuutila, S. Gu, Determination of kinetics of CO_2 absorption in unloaded and loaded DEEA+MAPA blend, Energy Procedia 114 (2017) 1772–1784. doi:10.1016/j.egypro.2017.03.1305.

[677] B. P. Soares, V. Štejfa, O. Ferreira, S. Pinho, K. Růžička, M. Fulem, Vapor pressures and thermophysical properties of selected ethanolamines, Fluid Phase Equilibria 473 (2018) 245–254. doi:10.1016/j.fluid.2018.05.032.

[678] P. Zhang, L. Wang, C. Lu, M. Li, S. Yu, D. Fu, Experiment and model for surface tensions of 2diethylaminoethanoln(2aminoethyl)ethanolamine, 2diethylaminoethanolnmethyl1,3propanediamine and 2diethylaminoethanol1,4butanediamine aqueous solutions, Journal of Molecular Liquids 288 (2019) 111031. doi:10.1016/j.molliq.2019.111031.

[679] P. B. Konduru, P. D. Vaidya, E. Y. Kenig, Kinetics of removal of carbon dioxide by aqueous solutions of n,n-diethylethanolamine and piperazine, Environmental Science & Technology 44 (6) (2010) 2138–2143. doi:10.1021/es902805p.

[680] M. Männistö, P. Uusi-Kyyny, D. Richon, V. Alopaeus, Study of CO_2 Absorption into Phase Change Solvents MAPA and DEEA, Journal of Chemical & Engineering Data 62 (8) (2017) 2261–2271. doi:10.1021/acs.jced.6b01038.

[681] H. Kierzkowska-Pawlak, E. Kruszczak, Revised kinetics of CO_2 absorption in aqueous n,n-diethylethanolamine (DEEA) and its blend with n-methyl-1,3-propane-diamine (MAPA), International Journal of Greenhouse Gas Control 57 (2017) 134–142. doi:10.1016/j.ijggc.2016.12.019.

[682] I. M. Bernhardsen, I. R. Krokvik, C. Perinu, D. D. Pinto, K. J. Jens, H. K. Knuutila, Influence of pk_a on solvent performance of MAPA promoted tertiary amines, International Journal of Greenhouse Gas Control 68 (2018) 68–76. doi:10.1016/j.ijggc.2017.11.005.

[683] I. M. Bernhardsen, A. A. Trollebø, C. Perinu, H. K. Knuutila, Vapour-liquid equilibrium study of tertiary amines, single and in blend with 3-(methylamino)propylamine, for post-combustion CO_2 capture, The Journal of Chemical Thermodynamics 138 (2019) 211–228. doi:10.1016/j.jct.2019.06.017.

[684] I. M. Bernhardsen, H. K. Knuutila, Kinetics of CO_2 absorption into aqueous solutions of 3-dimethylamino-1-propanol and 1-(2-hydroxyethyl)pyrrolidine in the blend with 3-(methylamino)propylamine, Chemical Engineering Science: X 3 (2019) 100032. doi:10.1016/j.cesx.2019.100032.

[685] D. D. Pinto, H. Knuutila, G. Fytianos, G. Haugen, T. Mejdell, H. F. Svendsen, CO_2 post combustion capture with a phase change solvent. pilot plant campaign, International Journal of Greenhouse Gas Control 31 (2014) 153–164. doi:10.1016/j.ijggc.2014.10.007.

[686] J. G. M.-S. Monteiro, S. Hussain, H. Majeed, E. O. Mba, A. Hartono, H. Knuutila, H. F. Svendsen, Kinetics of CO_2 absorption by aqueous 3-(methylamino)propylamine solutions: Experimental results and modeling, AIChE Journal 60 (11) (2014) 3792–3803. doi:10.1002/aic.14546.

[687] J. G.-S. Monteiro, D. D. Pinto, S. A. Zaidy, A. Hartono, H. F. Svendsen, VLE data and modelling of aqueous n,n-diethylethanolamine (DEEA) solutions, International Journal

of Greenhouse Gas Control 19 (2013) 432–440. doi:10.1016/j.ijggc.2013.10.001.

[688] J. Monteiro, H. Majeed, H. Knuutila, H. F. Svendsen, Kinetics of CO_2 absorption in aqueous blends of N,N-diethylethanolamine (DEEA) and N-methyl-1,3-propane-diamine (MAPA), Chemical Engineering Science 129 (2015) 145–155. doi:10.1016/j.ces.2015.02.001.

[689] E. B. Joseph, P. D. Vaidya, Kinetics of CO_2 absorption by aqueous mixtures of N,N-diethylethanolamine and polyamines, International Journal of Chemical Kinetics 51 (2) (2019) 131–137. doi:10.1002/kin.21236.

[690] C. Perinu, I. M. Bernhardsen, D. D. D. Pinto, H. K. Knuutila, K. J. Jens, Aqueous MAPA, DEEA, and their blend as CO_2 absorbents: Interrelationship between NMR speciation, ph, and heat of absorption data, Industrial & Engineering Chemistry Research 58 (23) (2019) 9781–9794. doi:10.1021/acs.iecr.9b01437.

[691] L. Wang, S. An, Q. Li, S. Yu, S. Wu, Phase change behavior and kinetics of CO_2 absorption into DMBA/DEEA solution in a wetted-wall column, Chemical Engineering Journal 314 (2017) 681–687. doi:10.1016/j.cej.2016.12.033.

[692] M. Garcia, H. K. Knuutila, S. Gu, Thermodynamic modelling of unloaded and loaded n,n-diethylethanolamine solutions, Green Energy & Environment 1 (3) (2016) 246–257. doi:10.1016/j.gee.2016.11.003.

[693] M. W. Arshad, H. F. Svendsen, P. L. Fosbøl, N. von Solms, K. Thomsen, Equilibrium total pressure and CO_2 solubility in binary and ternary aqueous solutions of 2-(diethylamino)ethanol (deea) and 3-(methylamino)propylamine (MAPA), Journal of Chemical & Engineering Data 59 (3) (2014) 764–774. doi:10.1021/je400886w.

[694] A. Hartono, F. Saleem, M. W. Arshad, M. Usman, H. F. Svendsen, Binary and ternary VLE of the 2-(diethylamino)-ethanol (DEEA)/3-(methylamino)-propylamine (MAPA)/water system, Chemical Engineering Science 101 (2013) 401–411. doi:10.1016/j.ces.2013.06.052.

[695] R. F. Zheng, D. Barpaga, P. M. Mathias, D. Malhotra, P. K. Koech, Y. Jiang, M. Bhakta, M. Lail, A. V. Rayer, G. A. Whyatt, C. J. Freeman, A. J. Zwoster, K. K. Weitz, D. J. Heldebrant, A single-component water-lean post-combustion CO_2 capture solvent

with exceptionally low operational heat and total costs of capture – comprehensive experimental and theoretical evaluation, Energy Environ. Sci. 13 (2020) 4106–4113. doi:10.1039/d0ee02585b.

[696] A. Awtry, N. Fine, J. Atcheson, B. Dinsdale, R. Kupfer, T. Silverman, G. Staab, J. Tomey, E. Meuleman, A. Brown, Design and costing of an ION clean energy CO_2 capture plant retrofitted to a 700 MW coal-fired power station, Available at SSRN 3816716.

[697] P. M. Mathias, K. Afshar, F. Zheng, M. D. Bearden, C. J. Freeman, T. Andrea, P. K. Koech, I. Kutnyakov, A. Zwoster, A. R. Smith, P. G. Jessop, O. G. Nik, D. J. Heldebrant, Improving the regeneration of CO_2-binding organic liquids with a polarity change, Energy Environ. Sci. 6 (2013) 2233–2242. doi:10.1039/c3ee41016a.

[698] D. J. Heldebrant, C. R. Yonker, P. G. Jessop, L. Phan, CO_2-binding organic liquids (CO_2BOLs) for post-combustion CO_2 capture, Energy Procedia 1 (1) (2009) 1187–1195. doi:10.1016/j.egypro.2009.01.156.

[699] A. Hedayati, F. Feyzi, Towards water-insensitive CO_2-binding organic liquids for CO_2 absorption: Effect of amines as promoter, Journal of Molecular Liquids 306 (2020) 112938. doi:10.1016/j.molliq.2020.112938.

[700] A. Widodo, Y. Sujatnika, D. Awali, T. Prakoso, T. P. Adhi, T. H. Soerawidjaja, A. Indarto, Thermal heat-free regeneration process using antisolvent for amine recovery, Chemical Engineering and Processing: Process Intensification 89 (2015) 75–79. doi:10.1016/j.cep.2015.01.007.

[701] N. Daneshvar, M. Zaafarani Moattar, M. Abedinzadegan Abdi, S. Aber, Carbon dioxide equilibrium absorption in the multi-component systems of CO_2+ TIPA + MEA + H_2O, CO_2+ TIPA + Pz + H_2O and CO_2+ TIPA + H_2O at low CO_2 partial pressures: experimental solubility data, corrosion study and modeling with artificial neural network, Separation and Purification Technology 37 (2) (2004) 135–147. doi:10.1016/j.seppur.2003.09.004.

[702] X. Li, P. Pearson, Q. Yang, G. Puxty, P. Feron, D. Xiao, A study of designer amine 4-amino-1-propyl-piperidine against the corrosion of carbon steel for application in CO_2

capture, International Journal of Greenhouse Gas Control 94 (2020) 102929. doi:10.1016/j.ijggc.2019.102929.

[703] B. Zhao, Y. Sun, Y. Yuan, J. Gao, S. Wang, Y. Zhuo, C. Chen, Study on corrosion in CO_2 chemical absorption process using amine solution, Energy Procedia 4 (0) (2011) 93–100. doi:10.1016/j.egypro.2011.01.028.

[704] L. Zheng, N. S. Matin, J. Thompson, J. Landon, N. E. Holubowitch, K. Liu, Understanding the corrosion of CO_2-loaded 2-amino-2-methyl-1-propanol solutions assisted by thermodynamic modeling, International Journal of Greenhouse Gas Control 54 (2016) 211–218. doi:10.1016/j.ijggc.2016.09.005.

[705] M. Wang, H. J. Herzog, T. A. Hatton, CO_2 capture using electrochemically mediated amine regeneration, Industrial & Engineering Chemistry Research 59 (15) (2020) 7087–7096. doi:10.1021/acs.iecr.9b05307.

[706] R. R. Wanderley, H. K. Knuutila, Evaluating the possibility of high-pressure desorption of CO_2 via volatile co-solvent injection, Chemical Engineering Research and Design 169 (2021) 116–134. doi:10.1016/j.cherd.2021.03.011.

[707] R. R. Wanderley, D. D. Pinto, H. K. Knuutila, From hybrid solvents to water-lean solvents – a critical and historical review, Separation and Purification Technology 260 (2021) 118193. doi:10.1016/j.seppur.2020.118193.

[708] U. Lee, A. Mitsos, C. Han, Optimal retrofit of a CO_2 capture pilot plant using superstructure and rate-based models, International Journal of Greenhouse Gas Control 50 (2016) 57–69. doi:10.1016/j.ijggc.2016.03.024.

[709] A. I. Papadopoulos, P. Linke, A unified framework for integrated process and molecular design, Chem. Eng. Res. Des. 83 (6) (2005) 674–678. doi:10.1205/cherd.04349.

[710] A. Bardow, K. Steur, J. Gross, A continuous targeting approach for integrated solvent and process design based on molecular thermodynamic models, in: R. M. de Brito Alves, C. A. O. do Nascimento, E. C. Biscaia (Eds.), 10th International Symposium on Process Systems Engineering: Part A, Vol. 27 of Computer Aided Chemical Engineering, Elsevier, 2009, pp. 813–818. doi:10.1016/S1570-7946(09)70356-6.

[711] M. Stavrou, M. Lampe, A. Bardow, J. Gross, Continuous molecular targeting–computer-

aided molecular design (comt–camd) for simultaneous process and solvent design for CO_2 capture, Industrial & Engineering Chemistry Research 53 (46) (2014) 18029–18041. doi:10.1021/ie502924h.

[712] P. Rehner, J. Schilling, A. Bardow, Molecule superstructures for computer-aided molecular and process design, Mol. Syst. Des. Eng. 8 (2023) 488–499. doi:10.1039/D2ME00230B.

[713] C. Gertig, L. Kröger, L. Fleitmann, J. Scheffczyk, A. Bardow, K. Leonhard, Rx-cosmo-camd: Computer-aided molecular design of reaction solvents based on predictive kinetics from quantum chemistry, Industrial & Engineering Chemistry Research 58 (51) (2019) 22835–22846. doi:10.1021/acs.iecr.9b03232.

[714] C. Gertig, K. Leonhard, A. Bardow, Computer-aided molecular and processes design based on quantum chemistry: current status and future prospects, Current Opinion in Chemical Engineering 27 (2020) 89–97. doi:10.1016/j.coche.2019.11.007.

[715] Net zero tracker, https://eciu.net/netzerotracker, last accessed on 23/10/21.

[716] Putting a price on carbon: The state of internal carbon pricing by corporates globally, Tech. rep., CDP Worldwide (2021).
URL https://www.cdp.net/en/research/global-reports/putting-a-price-on-carbon

[717] District Court of The Hague, Milieudefensie et al v Royal Dutch Shell PLC C/09/571932/HA ZA 19-379, 26 May 2021., https://uitspraken.rechtspraak.nl/inziendocument?id=ECLI:NL:RBDHA:2021:5339, last accessed on 23/10/21 (2021).

[718] M. Fajardy, S. Chiquier, N. Mac Dowell, Investigating the BECCS resource nexus: delivering sustainable negative emissions, Energy Environ. Sci. 11 (2018) 3408–3430. doi:10.1039/c8ee01676c.

[719] M. Fajardy, N. Mac Dowell, The energy return on investment of BECCS: is BECCS a threat to energy security?, Energy Environ. Sci. 11 (2018) 1581–1594. doi:10.1039/c7ee03610h.

[720] P. Psarras, H. Krutka, M. Fajardy, Z. Zhang, S. Liguori, N. Mac Dowell, J. Wilcox, Slicing the pie: how big could carbon dioxide removal be?, WIREs Energy and Environment

6 (5) (2017) e253. doi:10.1002/wene.253.

[721] B. W. Griscom, J. Adams, P. W. Ellis, R. A. Houghton, G. Lomax, D. A. Miteva, W. H. Schlesinger, D. Shoch, J. V. Siikamäki, P. Smith, P. Woodbury, C. Zganjar, A. Blackman, J. Campari, R. T. Conant, C. Delgado, P. Elias, T. Gopalakrishna, M. R. Hamsik, M. Herrero, J. Kiesecker, E. Landis, L. Laestadius, S. M. Leavitt, S. Minnemeyer, S. Polasky, P. Potapov, F. E. Putz, J. Sanderman, M. Silvius, E. Wollenberg, J. Fargione, Natural climate solutions, Proceedings of the National Academy of Sciences 114 (44) (2017) 11645–11650. doi:10.1073/pnas.1710465114.

[722] K. Z. House, A. C. Baclig, M. Ranjan, E. A. van Nierop, J. Wilcox, H. J. Herzog, Economic and energetic analysis of capturing CO_2 from ambient air, Proceedings of the National Academy of Sciences 108 (51) (2011) 20428–20433. doi:10.1073/pnas.1012253108.

[723] M. J. Realff, P. Eisenberger, Flawed analysis of the possibility of air capture, Proceedings of the National Academy of Sciences 109 (25) (2012) 1589–1589. doi:10.1073/pnas.1203618109.

[724] L. Waller, T. Rayner, J. Chilvers, C. A. Gough, I. Lorenzoni, A. Jordan, N. Vaughan, Contested framings of greenhouse gas removal and its feasibility: Social and political dimensions, WIREs Climate Change 11 (4) (2020) e649. doi:10.1002/wcc.649.

[725] S. Fuss, J. G. Canadell, G. P. Peters, M. Tavoni, R. M. Andrew, P. Ciais, R. B. Jackson, C. D. Jones, F. Kraxner, N. Nakicenovic, C. Le Quéré, M. R. Raupach, A. Sharifi, P. Smith, Y. Yamagata, Betting on negative emissions, Nature Climate Change 4 (10) (2014) 850–853. doi:10.1038/nclimate2392.

[726] A. Larkin, J. Kuriakose, M. Sharmina, K. Anderson, What if negative emission technologies fail at scale? Implications of the paris agreement for big emitting nations, Climate Policy 18 (6) (2018) 690–714. doi:10.1080/14693062.2017.1346498.

[727] M. Batres, F. M. Wang, H. Buck, R. Kapila, U. Kosar, R. Licker, D. Nagabhushan, E. Rekhelman, V. Suarez, Environmental and climate justice and technological carbon removal, The Electricity Journal 34 (7) (2021) 107002. doi:10.1016/j.tej.2021.107002.

[728] L. S. Melzer, Carbon dioxide enhanced oil recovery (CO_2 EOR): Factors involved in adding carbon capture, utilization and storage (ccus) to enhanced oil recovery, Center for Climate and Energy Solutions (2012) 1–17.

[729] V. Núñez-López, E. Moskal, Potential of CO_2-EOR for near-term decarbonization, Frontiers in Climate 1 (2019) 5. doi:10.3389/fclim.2019.00005.

[730] C. Kolster, E. Mechleri, S. Krevor, N. Mac Dowell, The role of CO_2 purification and transport networks in carbon capture and storage cost reduction, International Journal of Greenhouse Gas Control 58 (2017) 127–141. doi:10.1016/j.ijggc.2017.01.014.

[731] A. L. Kohl, R. B. Nielsen, Mechanical design and operation of alkanolamine plants, in: A. L. Kohl, R. B. Nielsen (Eds.), Gas Purification (5th Edition), 5th Edition, Gulf Professional Publishing, Houston, 1997, Ch. 3, pp. 187–277.

[732] E. L. Quinn, Carbon dioxide. III. Its commercial manufacture, J. Chem. Educ. 7 (3) (1930) 637–652.

[733] H. Sommers, The manufacture and distribution of carbon dioxide, Chem. Eng. Prog. 49 (7) (1933) 333–339.

[734] H. Anada, M. Fraser, A. King, Economics of by-product CO_2 recovery and transportation for EOR, Energy Prog. 3.

[735] W. M. Rump, M. Hare, R. Porter, Supply of carbon dioxide for enhanced oil recovery. final report, October 15, 1976–September 1, 1977, Tech. rep., Pullman Kellogg, Houston, TX (USA) (1977).

[736] F. T. Sparrow, A. M. Wolsky, G. F. Berry, C. Brooks, T. B. Cobb, E. P. Lynch, D. J. Jankowski, E. W. Walbridge, Carbon dioxide from flue gases for enhanced oil recovery, Argonne National Laboratory, Report ANL/CNSV-65, 1988.

[737] IPCC, Global warming of 1.5℃, Intergovernmental Panel on Climate Change IPCC, 2018.

[738] C. Zahasky, S. Krevor, Global geologic carbon storage requirements of climate change mitigation scenarios, Energy Environ. Sci. 13 (2020) 1561–1567. doi:10.1039/D0EE00674B.

[739] The global status of CCS. 2023.

URL https://www.globalccsinstitute.com/wp-content/uploads/2024/01/Global-Status-of-CCS-Report-1.pdf

[740] A. R. W. Brand, United Kingdom Patent GB190414464, Improvements in and relating to the recovery of carbonic acid from waste gases (1904).

[741] A. R. W. Brand, Kaiserlich Königliches Patentamt Österreich AT000000025024b, Verfahren zur absorption von gasen durch flüssigkeiten. (1904).

[742] R. N. Maddox, J. M. Campbell, Gas conditioning and processing. Vol.4, Gas and liquid sweetening, 3rd Edition, Campbell Petroleum Series, Norman, 1982.

[743] M. Shoeld, United States Patent No. 1971798, Purification and separation of gaseous mixtures (1934).

[744] I. Kim, X. Ma, J.-P. Andreassen, Study of the Solid-liquid Solubility in the Piperazine-H_2O-CO_2 System using FBRM and PVM, Energy Procedia 23 (2012) 72–81. doi:10.1016/j.egypro.2012.06.056.

[745] H. Benson, J. Field, R. Jimeson, CO_2 absorption: Employing hot potassium carbonate solutions, Chem. Eng. Prog.;(United States) 50 (7).

[746] H. Benson, Improved process for CO_2 absorption used hot carbonate solutions, Chem. Eng. Progr. 52 (1956) 433–438.

[747] S. Milidovich, E. Zbacnik, Increasing efficiency of hot potassium carbonate CO_2 removal systems, UOP LLC: Des Plaines, IL, USA (2013) 11–14.

[748] K. Smith, N. Nicholas, G. Stevens, 7 - inorganic salt solutions for post-combustion capture, in: P. H. Feron (Ed.), Absorption-Based Post-combustion Capture of Carbon Dioxide, Woodhead Publishing, 2016, pp. 145–166. doi:10.1016/B978-0-08-100514-9.00007-X.

[749] A. G. Eickmeyer, Eidgenössisches Institut für Geistiges Eigentum Patent No. CH467094a, Verfahren zum Reinigen von Gasen (1965).

[750] A. G. Eickmeyer, United States Patent No. 4271132a, Method and compositions for removing acid gases from gaseous mixtures (1981).

[751] M. Sharma, GB Patent No. 1058304, Process for the purification of fluids (1964).

[752] M. Sharma, Deutsches Patent No. DE1542415, Verfahren zum Entfernen von H_2S

und/oder CO_2 und/oder COS aus Gasen und Flüssigkeiten mittels wässriger Absorptionsflüssigkeiten, welche mindestens eine Sauerstoffhaltige Aminverbindung enthalten (1970).

[753] S. Mokhatab, W. A. Poe, J. Y. Mak, Chapter 7 - natural gas treating, in: S. Mokhatab, W. A. Poe, J. Y. Mak (Eds.), Handbook of Natural Gas Transmission and Processing (Fourth Edition), fourth edition Edition, Gulf Professional Publishing, 2019, pp. 231–269. doi:10.1016/B978-0-12-815817-3.00007-1.

[754] E. Bartholome, J. friebe, H. W. Schmidt, Deutsches Patent DE1903065A1, Verfahren zur Entfernung von Kohlendioxid aus Gasgemischen (1969).

[755] M. Appl, U. Wagner, H. J. Henrici, K. Kuessner, K. Volkamer, E. Fuerst, United States Patent No. 3622267, Process for removing carbon dioxide from gas mixtures (1971).

[756] M. Appl, U. Wagner, H. J. Henrici, K. Kuessner, K. Volkamer, E. Fuerst, United States Patent No. 4336233, Removal of CO_2 and/or H_2S and/or COS from gases containing these constituents (1982).

[757] J. Ying, S. Raets, D. Eimer, The activator mechanism of piperazine in aqueous methyldiethanolamine solutions, Energy Procedia 114 (2017) 2078–2087. doi:10.1016/j.egypro.2017.03.1342.

[758] G. Astarita, D. W. Savage, J. M. Longo, Promotion of CO_2 mass transfer in carbonate solutions, Chemical Engineering Science 36 (3) (1981) 581–588. doi:10.1016/0009-2509(81)80146-7.

[759] R. G. Asperger, L. S. Krawczyk, B. D. Oakes, J. T. Lake, Deutsches Patent No. DE2748216A1, Korrosionsinhibitor für Metall, das in Berührung mit Säuregasen ist (1977).

[760] A. Chakma, Formulated solvents: New opportunities for energy efficient separation of acid gases, Energy Sources 21 (1-2) (1999) 51–62. doi:10.1080/00908319950014957.

[761] G. Sartori, F. Leder, United States Patent No. US 4112050, Process for removing carbon dioxide containing acidic gases from gaseous mixtures using a basic salt activated with a hindered amine (1978).

[762] T. Mimura, T. Suda, I. Iwaki, A. Honda, H. Kumazawa, Kinetics of reaction between

carbon dioxide and sterically hindered amines for carbon dioxide recovery from power plant flue gases, Chemical Engineering Communications 170 (1) (1998) 245–260.

[763] G. Sartori, S. David, United States Patent No. US us4405577, Non-sterically hindered-sterically hindered amine co-promoted acid gas scrubbing solution and process for using same (1983).

[764] T. Mimura, S. Shimojo, T. Suda, M. Iijima, S. Mitsuoka, Research and development on energy saving technology for flue gas carbon dioxide recovery and steam system in power plant, Energy Conversion and Management 36 (6) (1995) 397–400. doi:10.1016/0196-8904(95)00029-D.

[765] T. Mimura, H. Simayoshi, T. Suda, M. Iijima, S. Mitsuoka, Development of energy saving technology for flue gas carbon dioxide recovery in power plant by chemical absorption method and steam system, Energy Conversion and Management 38 (1997) S57 – S62. doi:10.1016/S0196-8904(96)00246-4.

[766] T. Mimura, Y. Yagi, T. Takashina, R. Yoshiyama, A. Honda, Evaluation of alkanolamine chemical absorbents for CO_2 from vapor-liquid equilibrium measurements, Kagaku Kogaku Ronbunshu 31 (4) (2005) 237–242. doi:10.1252/kakoronbunshu.31.237.

[767] K. Yoshida, T. Mimura, S. Shimojo, M. Karasaki, M. Iijima, S. Mitsuoka, Japan Patent No.JPH05237341a, Method for removing carbon dioxide in waste combustion gas (1992).

[768] K. Yoshida, T. Mimura, S. Shimojo, M. Karasaki, M. Iijima, S. Mitsuoka, European Patent No. EP0588178, Process for removing carbon dioxide from combustion gases (1993).

[769] P. Just, Advances in the development of CO_2 capture solvents, Energy Procedia 37 (2013) 314–324. doi:10.1016/j.egypro.2013.05.117.

[770] K. Stéphenne, Start-up of world's first commercial post-combustion coal fired CCS project: Contribution of shell cansolv to saskpower boundary dam iccs project, Energy Procedia 63 (2014) 6106–6110. doi:10.1016/j.egypro.2014.11.642.

[771] J. Gibbins, Published Cansolv / BD3 solvent management information, Tech. rep., UKCCSRC, Sheffield (UK) (2019).

[772] D. Shaw, Cansolv CO_2 capture: The value of integration, Energy Procedia 1 (1) (2009)

237–246. doi:10.1016/j.egypro.2009.01.034.

[773] C. M. Rayner, D. C. Barnes, G. Jakab, C. Schoolderman, European Patent Office No. EP3083012b1, Method for the capture and release of acid gases (2019).

[774] C. M. Rayner, D. C. Barnes, G. Jakab, C. Schoolderman, United States Patent No. US 20200206677a1, C1-C8 carboxylic acid salt solution for the absorption of CO_2 (2020).

[775] A. Guyer, G. Pürner, Über die Absorption von Kohlendioxyd durch wässerige Lösungen organischer Basen und Salze, Helvetica Chimica Acta 21 (1) (1938) 1337–1345. doi:10.1002/hlca.193802101164.

[776] P. Bumb, United States Patent No. US20170274317a1, Carbon capture solvents having alcohols and amines and methods for using such solvents (2017).

[777] P. Bumb, European Patent Office No. EP3183050, Carbon capture solvents having alcohols and amines and methods for using such solvents (2020).

[778] R. A. Frimpong, H. Nikolic, J. Pelgen, M. Ghorbanian, J. D. Figueroa, K. Liu, Evaluation of different solvent performance in a 0.7 MWe pilot scale CO_2 capture unit, Chemical Engineering Research and Design 148 (2019) 11–20. doi:10.1016/j.cherd.2019.05.053.

[779] R. A. Frimpong, H. Nikolic, D. Bahr, G. Kiran, K. Liu, Pilot scale testing of an advanced solvent in a 0.7 MWe post-combustion CO_2 capture unit, International Journal of Greenhouse Gas Control 106 (2021) 103290. doi:10.1016/j.ijggc.2021.103290.

[780] K. Takeshita, A. Kitamoto, Chemical equilibria of absorption of CO_2 into nonaqueous solution of amine, Journal of Chemical Engineering of Japan 21 (4) (1988) 411–417. doi:10.1252/jcej.21.411.

[781] R. Perry, T. Grocela-Rocha, M. O'Brien, S. Genovese, B. Wood, L. Lewis, H. Lam, G. Soloveichik, M. Rubinsztajn, S. Kniajanski, S. Draper, R. Enick, J. Johnson, H.-b. Xie, D. Tapriyal, Aminosilicone solvents for CO_2 capture, ChemSusChem 3 (8) (2010) 919–930. doi:10.1002/cssc.201000077.

[782] F. A. Chowdhury, K. Goto, H. Yamada, Y. Matsuzaki, A screening study of alcohol solvents for alkanolamine-based CO_2 capture, International Journal of Greenhouse Gas Control 99 (2020) 103081. doi:10.1016/j.ijggc.2020.103081.

[783] K. Goto, H. Okabe, F. A. Chowdhury, S. Shimizu, Y. Fujioka, M. Onoda, Development of novel absorbents for CO_2 capture from blast furnace gas, International Journal of Greenhouse Gas Control 5 (5) (2011) 1214–1219. doi:10.1016/j.ijggc.2011.06.006.

[784] N. Brown, G. A. Staab, T. R. Silverman, G. W. Heller, R. Kupfer, C. Panaccione, A. Brown, Protreat simulation accurately represents experimental results for post-combustion carbon dioxide capture with novel mixed amine solvent in real process environment, Energy Procedia 114 (2017) 1380–1387. doi:10.1016/j.egypro.2017.03.1259.

[785] H. Bai, A. C. Yeh, Removal of CO_2 greenhouse gas by ammonia scrubbing, Industrial & Engineering Chemistry Research 36 (6) (1997) 2490–2493. doi:10.1021/ie960748j.

[786] A. C. Yeh, H. Bai, Comparison of ammonia and monoethanolamine solvents to reduce CO_2 greenhouse gas emissions, Science of The Total Environment 228 (2) (1999) 121–133. doi:10.1016/S0048-9697(99)00025-X.

[787] E. Gal, United States Patent No. 7641717, Ultra cleaning of combustion gas including the removal of CO_2 (2010).

[788] D. Sutter, M. Gazzani, M. Mazzotti, A low-energy chilled ammonia process exploiting controlled solid formation for post-combustion CO_2 capture, Faraday Discuss. 192 (2016) 59–83. doi:10.1039/c6fd00044d.

[789] E. Behrens, J. Behrens, Kaiserliches Patentamt No. 226942, Verfahren zur Abscheidung von Kohlensäure aus solche enthaltenden Gasgemischen (1909).

[790] F. Danulat, H.-U. Kohrt, W. Herbert, R. Becker, Deutsches Patentamt No. DE935144, Verfahren zur Reinigung von Gasen, insbesondere von solchen fuer Synthese- und Heizzwecke (1949).

[791] F. Porter, J. C. Eck, United States Patent No. 2649166, Absorption of carbon dioxide from gases containing the same (1953).

[792] G. Hochgesand, H. Heidl, H. Unland, A. Doerges, K. Bratzler, United States Patent No. 3505784, Absorption of carbon dioxide from gases containing the same (1966).

[793] L. Raynal, P. A. Bouillon, A. Gomez, P. Broutin, From MEA to demixing solvents and future steps, a roadmap for lowering the cost of post-combustion carbon capture, Chem.

Eng. J. 171 (3) (2011) 742–752. doi:10.1016/j.cej.2011.01.008.

[794] L. Raynal, P. Alix, P. A. Bouillon, A. Gomez, M. Le Febvre De Nailly, M. Jacquin, J. Kittel, A. Di Lella, P. Mougin, J. Trapy, The DMX process: An original solution for lowering the cost of post-combustion carbon capture, in: Energy Procedia, Vol. 4, Elsevier, 2011, pp. 779–786. doi:10.1016/j.egypro.2011.01.119.

[795] J. Zhang, Y. Qiao, W. Wang, R. Misch, K. Hussain, D. W. Agar, Development of an energy-efficient CO_2 capture process using thermomorphic biphasic solvents, Energy Procedia 37 (2013) 1254–1261. doi:10.1016/j.egypro.2013.05.224.

[796] A. I. Papadopoulos, F. Tzirakis, I. Tsivintzelis, P. Seferlis, Phase-change solvents and processes for postcombustion CO_2 capture: A detailed review, Industrial & Engineering Chemistry Research 58 (13) (2019) 5088–5111. doi:10.1021/acs.iecr.8b06279.

[797] S. Gabriel, J. Weiner, Ueber einige abkoemmlinge des propylamins, Berichte der deutschen chemischen Gesellschaft 21 (2) (1888) 2669–2679. doi:10.1002/cber.18880210288.

[798] P. Walden, Ueber die molekulargrosse und elektrische leitfaähigkeit einiger geschmolzenen salze, Salze Bull. Acad. Imper. Sci. 8 (6) (1914) 405–422.

[799] K. R. Seddon, Ionic liquids for clean technology, Journal of Chemical Technology & Biotechnology 68 (4) (1997) 351–356. doi:10.1002/(sici)1097-4660(199704)68:4<351::aid-jctb613>3.0.co;2-4.

[800] E. D. Bates, R. D. Mayton, I. Ntai, J. H. Davis, CO_2 capture by a task-specific ionic liquid, J. Am. Chem. Soc. 124 (6) (2002) 926–927. doi:10.1021/ja017593d.

[801] R. Quinn, G. P. Pez, United States Patent No. us4973456a, Use of salt hydrates as reversible absorbents of acid gases (1990).

[802] G. P. Pez, R. T. Carlin, D. V. Laciak, J. C. Sorensen, United States Patent No. us4761164a, Method for gas separation (1988).

[803] M. Aghaie, N. Rezaei, S. Zendehboudi, A systematic review on CO_2 capture with ionic liquids: Current status and future prospects, Renewable and Sustainable Energy Reviews 96 (2018) 502–525. doi:10.1016/j.rser.2018.07.004.

[804] M. Mota-Martinez, P. Brandl, J. Hallett, N. Mac Dowell, Challenges and opportunities

for the utilisation of ionic liquids as solvents for CO_2 capture, Mol. Syst. Des. Eng. 3 (3). doi:10.1039/c8me00009c.

[805] V. M. Shama, A. R. Swami, R. Aniruddha, I. Sreedhar, B. M. Reddy, Process and engineering aspects of carbon capture by ionic liquids, Journal of CO_2 Utilization 48 (2021) 101507. doi:10.1016/j.jcou.2021.101507.

[806] T. Aissaoui, I. M. AlNashef, U. A. Qureshi, Y. Benguerba, Potential applications of deep eutectic solvents in natural gas sweetening for CO_2 capture, Reviews in Chemical Engineering 33 (6) (2017) 523–550. doi:10.1515/revce-2016-0013.

[807] S. Sarmad, J.-P. Mikkola, X. Ji, Carbon dioxide capture with ionic liquids and deep eutectic solvents: A new generation of sorbents, ChemSusChem 10 (2) (2017) 324–352. doi:10.1002/cssc.201600987.

[808] C. Florindo, F. Lima, B. D. Ribeiro, I. M. Marrucho, Deep eutectic solvents: overcoming 21st century challenges, Current Opinion in Green and Sustainable Chemistry 18 (2019) 31–36. doi:10.1016/j.cogsc.2018.12.003.

[809] X. Ge, C. Gu, X. Wang, J. Tu, Deep eutectic solvents (DESs)-derived advanced functional materials for energy and environmental applications: challenges, opportunities, and future vision, J. Mater. Chem. A 5 (2017) 8209–8229. doi:10.1039/C7TA01659J.

[810] C. Ma, S. Sarmad, J.-P. Mikkola, X. Ji, Development of low-cost deep eutectic solvents for CO_2 capture, Energy Procedia 142 (2017) 3320–3325. doi:10.1016/j.egypro.2017.12.464.

[811] A. Pereiro, J. Araújo, J. Esperança, I. Marrucho, L. Rebelo, Ionic liquids in separations of azeotropic systems – a review, The Journal of Chemical Thermodynamics 46 (2012) 2–28. doi:10.1016/j.jct.2011.05.026.

[812] Y. Zhang, X. Ji, X. Lu, Choline-based deep eutectic solvents for CO_2 separation: Review and thermodynamic analysis, Renewable and Sustainable Energy Reviews 97 (2018) 436–455. doi:10.1016/j.rser.2018.08.007.

[813] V. Venkatraman, S. Evjen, K. C. Lethesh, J. J. Raj, H. K. Knuutila, A. Fiksdahl, Rapid, comprehensive screening of ionic liquids towards sustainable applications, Sustainable Energy Fuels 3 (2019) 2798–2808. doi:10.1039/C9SE00472F.

[814] B. Li, Y. Duan, D. Luebke, B. Morreale, Advances in CO_2 capture technology: A patent review, Applied Energy 102 (2013) 1439–1447. doi:10.1016/j.apenergy.2012.09.009.

[815] M. Ramdin, T. W. de Loos, T. J. H. Vlugt, State-of-the-art of CO_2 capture with ionic liquids, Ind. Eng. Chem. Res. 51 (24) (2012) 8149–8177. doi:10.1021/ie3003705.

[816] L. F. Vega, O. Vilaseca, F. Llovell, J. S. Andreu, Modeling ionic liquids and the solubility of gases in them: Recent advances and perspectives, Fluid Phase Equilib. 294 (1-2) (2010) 15–30. doi:10.1016/j.fluid.2010.02.006.

[817] I. I. Alkhatib, D. Bahamon, F. Llovell, M. Abu-Zahra, L. F. Vega, Perspectives and guidelines on thermodynamic modelling of deep eutectic solvents, Journal of Molecular Liquids 298 (2020) 112183. doi:10.1016/j.molliq.2019.112183.

[818] J. Potka-Wasylka, M. de la Guardia, V. Andruch, M. Vilková, Deep eutectic solvents vs ionic liquids: Similarities and differences, Microchemical Journal 159 (2020) 105539. doi:10.1016/j.microc.2020.105539.

[819] Y. Wang, S. Ren, Y. Hou, W. Wu, Capture of acidic gases from flue gas by deep eutectic solvents, Processes 9 (8). doi:10.3390/pr9081268.

[820] L. L. Zubeir, Carbon capture with novel low-volatile solvents: experiments and modeling, Ph.D. thesis (2016).

[821] L. F. Zubeir, M. H. M. Lacroix, M. C. Kroon, Low transition temperature mixtures as innovative and sustainable CO_2 capture solvents, J. Phys. Chem. B 118 (49) (2014) 14429–14441. doi:10.1021/jp5089004.

[822] Z. Song, X. Hu, H. Wu, M. Mei, S. Linke, T. Zhou, Z. Qi, K. Sundmacher, Systematic screening of deep eutectic solvents as sustainable separation media exemplified by the CO_2 capture process, ACS Sustainable Chemistry & Engineering 8 (23) (2020) 8741–8751. doi:10.1021/acssuschemeng.0c02490.

[823] T. J. Trivedi, J. H. Lee, H. J. Lee, Y. K. Jeong, J. W. Choi, Deep eutectic solvents as attractive media for CO_2 capture, Green Chem. 18 (2016) 2834–2842. doi:10.1039/C5GC02319J.

[824] Y. Liu, H. Yu, Y. Sun, S. Zeng, X. Zhang, Y. Nie, S. Zhang, X. Ji, Screening deep

eutectic solvents for CO_2 capture with cosmo-rs, Frontiers in Chemistry 8 (2020) 82. doi:10.3389/fchem.2020.00082.

[825] G. García, S. Aparicio, R. Ullah, M. Atilhan, Deep eutectic solvents: Physicochemical properties and gas separation applications, Energy & Fuels 29 (4) (2015) 2616–2644. doi:10.1021/ef5028873.

[826] H. Ghaedi, M. Zhao, P. T. Clough, E. J. Anthony, P. S. Fennell, High CO_2 absorption in new amine based-transition-temperature mixtures (deep eutectic analogues) and reporting thermal stability, viscosity and surface tension: Response surface methodology (RSM), Journal of Molecular Liquids 316 (2020) 113863. doi:10.1016/j.molliq.2020.113863.

[827] F. Luo, X. Liu, S. Chen, Y. Song, X. Yi, C. Xue, L. Sun, J. Li, Comprehensive evaluation of a deep eutectic solvent based CO_2 capture process through experiment and simulation, ACS Sustainable Chemistry & Engineering 9 (30) (2021) 10250–10265. doi:10.1021/acssuschemeng.1c02722.

[828] X. Xu, M. B. Myers, F. G. Versteeg, E. Adam, C. White, E. Crooke, C. D. Wood, Next generation amino acid technology for CO_2 capture, J. Mater. Chem. A 9 (2021) 1692–1704. doi:10.1039/D0TA10583J.

[829] H. Guo, H. Li, S. Shen, CO_2 capture by water-lean amino acid salts: Absorption performance and mechanism, Energy & Fuels 32 (6) (2018) 6943–6954. doi:10.1021/acs.energyfuels.8b01012.

[830] D. Wei, H. Junge, M. Beller, An amino acid based system for CO_2 capture and catalytic utilization to produce formates, Chem. Sci. 12 (2021) 6020–6024. doi:10.1039/D1SC00467K.

[831] J. Salazar, U. Diwekar, K. Joback, A. H. Berger, A. S. Bhown, Solvent selection for post-combustion CO_2 capture, Energy Procedia 37 (2013) 257–264. doi:10.1016/j.egypro.2013.05.110.

[832] P. Singh, G. F. Versteeg, Structure and activity relationships for CO_2 regeneration from aqueous amine-based absorbents, Process Saf. Envion. Prot. 86 (5) (2008) 347–359. doi:10.1016/j.psep.2008.03.005.

[833] P. Singh, J. P. Niederer, G. F. Versteeg, Structure and activity relationships for amine-based CO_2 absorbents-ii, Chemical Engineering Research and Design 87 (2) (2009) 135–144. doi:10.1016/j.cherd.2008.07.014.

[834] T. Zarogiannis, A. I. Papadopoulos, P. Seferlis, Systematic selection of amine mixtures as post-combustion CO_2 capture solvent candidates, Journal of Cleaner Production 136 (2016) 159–175. doi:10.1016/j.jclepro.2016.04.110.

[835] S. Gangarapu, A. T. M. Marcelis, H. Zuilhof, Carbamate stabilities of sterically hindered amines from quantum chemical methods: Relevance for CO_2 capture, ChemPhysChem 14 (17) (2013) 3936–3943. doi:10.1002/cphc.201300820.

[836] R. Notz, N. Asprion, I. Clausen, H. Hasse, Selection and pilot plant tests of new absorbents for post-combustion carbon dioxide capture, Chemical Engineering Research and Design 85 (4) (2007) 510–515. doi:10.1205/cherd06085.

[837] A. Hartono, R. Rennemo, M. Awais, S. Vevelstad, O. Brakstad, I. Kim, H. Knuutila, Characterization of 2-piperidineethanol and 1-(2-hydroxyethyl)pyrrolidine as strong bicarbonate forming solvents for CO_2 capture, International Journal of Greenhouse Gas Control 63 (2017) 260–271. doi:10.1016/j.ijggc.2017.05.021.

[838] P. Singh, J. P. Niederer, G. F. Versteeg, Structure and activity relationships for amine based CO_2 absorbents–i, International Journal of Greenhouse Gas Control 1 (1) (2007) 5–10. doi:10.1016/S1750-5836(07)00015-1.

[839] F. Barzagli, C. Giorgi, F. Mani, M. Peruzzini, Screening study of different amine-based solutions as sorbents for direct CO_2 capture from air, ACS Sustainable Chemistry & Engineering 8 (37) (2020) 14013–14021. doi:10.1021/acssuschemeng.0c03800.

[840] F. A. Chowdhury, H. Okabe, H. Yamada, M. Onoda, Y. Fujioka, Synthesis and selection of hindered new amine absorbents for CO_2 capture, Energy Procedia 4 (2011) 201–208. doi:10.1016/j.egypro.2011.01.042.

[841] S. Park, H.-J. Song, M.-G. Lee, J. Park, Screening test for aqueous solvents used in CO_2 capture: K_2CO_3 used with twelve different rate promoters, Korean Journal of Chemical Engineering 31 (1) (2014) 125–131.

[842] A. Sodiq, N. el Hadri, E. L. V. Goetheer, M. R. M. Abu-Zahra, Chemical reaction

kinetics measurements for single and blended amines for CO_2 postcombustion capture applications, International Journal of Chemical Kinetics 50 (9) (2018) 615–632. doi:10.1002/kin.21187.

[843] X. Zhicheng, W. Shujuan, Z. Bo, C. Changhe, Study on potential biphasic solvents: Absorption capacity, CO_2 loading and reaction rate, Energy Procedia 37 (2013) 494–498. doi:10.1016/j.egypro.2013.05.135.

[844] F. A. Chowdhury, H. Yamada, K. Goto, S. Yamamoto, Y. Matsuzaki, Guide to evaluate low viscous non-aqueous solvent for post-combustion CO_2 capture, Available at SSRN 3811973.

[845] S. Ma'mun, H. F. Svendsen, K. A. Hoff, O. Juliussen, Selection of new absorbents for carbon dioxide capture, Energy Conversion and Management 48 (1) (2007) 251–258. doi:10.1016/j.enconman.2006.04.007.

[846] F. A. Chowdhury, K. Goto, H. Yamada, Y. Matsuzaki, S. Yamamoto, T. Higashii, M. Onoda, Results of RITE's advanced liquid absorbents develop for low temperature CO_2 capture, Energy Procedia 114 (2017) 1716–1720. doi:10.1016/j.egypro.2017.03.1300.

[847] W. Conway, X. Wang, D. Fernandes, R. Burns, G. Lawrance, G. Puxty, M. Maeder, Toward rational design of amine solutions for PCC applications: The kinetics of the reaction of CO_2(aq) with cyclic and secondary amines in aqueous solution, Environmental Science & Technology 46 (13) (2012) 7422–7429. doi:10.1021/es300541t.

[848] L. Dubois, D. Thomas, Screening of aqueous amine-based solvents for postcombustion CO_2 capture by chemical absorption, Chemical Engineering & Technology 35 (3) (2012) 513–524. doi:10.1002/ceat.201100523.

[849] F. Barzagli, F. Mani, M. Peruzzini, A comparative study of the CO_2 absorption in some solvent-free alkanolamines and in aqueous monoethanolamine (MEA), Environmental Science & Technology 50 (13) (2016) 7239–7246. doi:10.1021/acs.est.6b00150.

[850] M. Xiao, D. Cui, Q. Yang, Z. Liang, G. Puxty, W. Conway, P. Feron, Advanced designer amines for CO_2 capture: Interrogating speciation and physical properties, International Journal of Greenhouse Gas Control 82 (2019) 8–18. doi:10.1016/j.ijggc.2018.12.

021.

[851] A. Adeosun, N. El-Hadri, E. Goetheer, M. Abu Zahra, Absorption of CO_2 by amine blends solution: An experimental evaluation, International Journal of Engineering and Science 3 (2013) 12–23.

[852] X. Li, Q. Yang, P. Pearson, B. Yu, G. Puxty, D. Xiao, The application of trans-1,4-diaminocyclohexane as a bicarbonate formation rate promoter in CO_2 capture, Fuel 226 (2018) 479–489. doi:10.1016/j.fuel.2018.04.001.

[853] F. Tzirakis, I. Tsivintzelis, A. I. Papadopoulos, P. Seferlis, Experimental measurement and assessment of equilibrium behaviour for phase change solvents used in CO_2 capture, Chemical Engineering Science 199 (2019) 20–27. doi:10.1016/j.ces.2018.12.045.

[854] H. Yamada, F. A. Chowdhury, Y. Matsuzaki, K. Goto, T. Higashii, S. Kazama, Effect of alcohol chain length on carbon dioxide absorption into aqueous solutions of alkanolamines, Energy Procedia 37 (2013) 499–504. doi:10.1016/j.egypro.2013.05.136.

[855] T. Damartzis, A. I. Papadopoulos, P. Seferlis, Process flowsheet design optimization for various amine-based solvents in post-combustion CO_2 capture plants, Journal of Cleaner Production 111 (2016) 204–216. doi:10.1016/j.jclepro.2015.04.129.

[856] H. P. Mangalapally, R. Notz, N. Asprion, G. Sieder, H. Garcia, H. Hasse, Pilot plant study of four new solvents for post combustion carbon dioxide capture by reactive absorption and comparison to MEA, International Journal of Greenhouse Gas Control 8 (2012) 205–216. doi:10.1016/j.ijggc.2012.02.014.

[857] A. V. Rayer, P. D. Mobley, M. Soukri, T. R. Gohndrone, J. Tanthana, J. Zhou, M. Lail, Absorption rates of carbon dioxide in amines in hydrophilic and hydrophobic solvents, Chemical Engineering Journal 348 (2018) 514–525. doi:10.1016/j.cej.2018.03.193.

[858] Y. E. Kim, J. A. Lim, S. K. Jeong, Y. I. Yoon, S. T. Bae, S. C. Nam, Comparison of carbon dioxide absorption in aqueous MEA, DEA, TEA, and AMP solutions, Bull. Korean Chem. Soc. 34 (3) (2013) 783–787. doi:10.5012/bkcs.2013.34.3.783.

[859] S. Murai, Y. Maezawa, D. Muraoka, T. Muramatsu, S. Saito, Development of new sterically hindered amine for PCC, Energy Procedia 114 (2017) 1904–1909. doi:10.1016/j.egypro.2017.03.1321.

[860] H. P. Mangalapally, H. Hasse, Pilot plant study of two new solvents for post combustion carbon dioxide capture by reactive absorption and comparison to monoethanolamine, Chemical Engineering Science 66 (22) (2011) 5512–5522. doi:10.1016/j.ces.2011.06.054.

[861] H. Liu, G. Chen, Z. Liang, Toward rational selection of amine solutions for PCC applications: CO_2 absorption kinetics and absorption heat in tertiary aqueous solutions, International Journal of Greenhouse Gas Control 50 (2016) 206–217. doi:10.1016/j.ijggc.2016.04.020.

[862] H. Yamada, T. Higashii, F. Chowdhury, K. Goto, S. Kazama, Experimental study into carbon dioxide solubility and species distribution in aqueous alkanolamine solutions, WIT Transactions on Ecology and the Environment 157 (2012) 515–523.

[863] M. Sharifzadeh, P. Bumb, N. Shah, Carbon capture from pulverized coal power plant (pcpp): Solvent performance comparison at an industrial scale, Applied Energy 163 (2016) 423–435. doi:10.1016/j.apenergy.2015.11.017.

[864] M. Sharifzadeh, N. Shah, Comparative studies of CO_2 capture solvents for gas-fired power plants: Integrated modelling and pilot plant assessments, International Journal of Greenhouse Gas Control 43 (2015) 124–132. doi:10.1016/j.ijggc.2015.10.009.

[865] W. Luo, Q. Yang, W. Conway, G. Puxty, P. Feron, J. Chen, Evaluation and modeling of vapor–liquid equilibrium and CO_2 absorption enthalpies of aqueous designer diamines for post combustion capture processes, Environmental Science & Technology 51 (12) (2017) 7169–7177. doi:10.1021/acs.est.7b00379.

[866] J. Urech, L. Tock, T. Harkin, A. Hoadley, F. Maréchal, An assessment of different solvent-based capture technologies within an IGCC–CCS power plant, Energy 64 (2014) 268–276. doi:10.1016/j.energy.2013.10.081.

[867] A. Kothandaraman, L. Nord, O. Bolland, H. J. Herzog, G. J. McRae, Comparison of solvents for post-combustion capture of CO_2 by chemical absorption, Energy Procedia 1 (1) (2009) 1373–1380. doi:10.1016/j.egypro.2009.01.180.

[868] W. P. Jencks, J. Carriuolo, Reactivity of nucleophilic reagents toward esters, Journal of the American Chemical Society 82 (7) (1960) 1778–1786. doi:10.1021/ja01492a058.

[869] E. Buncel, I.-H. Um, The α-effect and its modulation by solvent, Tetrahedron 60 (36) (2004) 7801–7825. doi:10.1016/j.tet.2004.05.006.

[870] V. Gineityte, Interpretation of the inductive effect of heteroatoms in substituted alkanes on the basis of both the one-electron density matrix and localized molecular orbitals, Journal of Molecular Structure: Theochem 364 (1) (1996) 85–96. doi:10.1016/0166-1280(95)04462-0.

[871] S. J. Yoon, H. Lee, Substituent effect in amine-CO_2 interaction investigated by NMR and IR spectroscopies, Chemistry Letters 32 (4) (2003) 344–345. doi:10.1246/cl.2003.344.

[872] R. Zhang, X. Luo, Q. Yang, F. Cao, S. Chen, Z. Liang, Impact of the inter- and intramolecular tertiary amino group on the primary amino group in the CO_2 absorption process, Industrial & Engineering Chemistry Research 55 (26) (2016) 7210–7217. doi:10.1021/acs.iecr.6b01404.

[873] D. Leeson, N. Mac Dowell, N. Shah, C. Petit, P. Fennell, A techno-economic analysis and systematic review of carbon capture and storage (CCS applied to the iron and steel, cement, oil refining and pulp and paper industries, as well as other high purity sources, International Journal of Greenhouse Gas Control 61 (2017) 71–84. doi:10.1016/j.ijggc.2017.03.020.

[874] P. Bains, P. Psarras, J. Wilcox, CO_2 capture from the industry sector, Prog. Energy Combust. Sci. 63 (2017) 146–172. doi:10.1016/j.pecs.2017.07.001.

[875] E. J. Anthony, P. T. Clough, Post-combustion carbon capture and storage in industry – CO_2 separation, purification and conversion to chemicals and fuels, Springer Singapore, Singapore, 2019, pp. 39–53. doi:10.1007/978-981-13-3296-8_4.

[876] P. Derks, T. Kleingeld, C. van Aken, J. Hogendoorn, G. Versteeg, Kinetics of absorption of carbon dioxide in aqueous piperazine solutions, Chemical Engineering Science 61 (20) (2006) 6837–6854. doi:10.1016/j.ces.2006.07.009.

[877] W. DeCoursey, Enhancement factors for gas absorption with reversible reaction, Chem. Eng. Sci. 37 (10) (1982) 1483–1489. doi:10.1016/0009-2509(82)80005-5.

[878] W. J. DeCoursey, R. W. Thring, Effects of unequal diffusivities on enhancement factors

for reversible and irreversible reaction, Chem. Eng. Sci. 44 (8) (1989) 1715–1721. doi:10.1016/0009-2509(89)80013-2.

[879] H. Hikita, Gas absorption with (m, n)-th order irreversible chemical reaction, Int. Chem. Eng. 4 (1964) 332–340.

[880] M. Santiago, I. Farina, Mass transfer with second order reaction. numerical solution, Chemical Engineering Science 25 (4) (1970) 744–747. doi:10.1016/0009-2509(70)85106-5.

[881] G. Porter, B. Stevens, H. Berg, Progress in reaction kinetics vol. 1. (1962).

[882] K. Porter, Effect of contact-time distribution on gas absorption with chemical reaction, Transactions of the Institution of Chemical Engineers and the Chemical Engineer 44 (1) (1966) T25.

[883] A. Yeramian, J. Gottifredi, J. Ronco, Mass transfer with homogeneous second order irreversible reaction a note on an explicit expression for the reaction factor, Chemical Engineering Science 25 (10) (1970) 1622–1625. doi:10.1016/0009-2509(70)85087-4.

[884] V. Stepanek, Z. Palatý, H. Bendová, A critical comparison of approximate solutions for enhancement factor for irreversible second-order reaction, Chemical Engineering Science 191 (2018) 410–419. doi:10.1016/j.ces.2018.07.003.

[885] G. Baldi, S. Sicardi, A model for mass transfer with and without chemical reaction in packed towers, Chemical Engineering Science 30 (5) (1975) 617–624. doi:10.1016/0009-2509(75)80034-0.

[886] J. Gaspar, P. L. Fosbøl, A general enhancement factor model for absorption and desorption systems: A CO_2 capture case-study, Chemical Engineering Science 138 (2015) 203–215. doi:10.1016/j.ces.2015.08.023.

[887] J. Gaspar, P. L. Fosbøl, Practical enhancement factor model based on GM for multiple parallel reactions: Piperazine (pz) CO_2 capture, Chemical Engineering Science 158 (2017) 257–266. doi:10.1016/j.ces.2016.10.033.

[888] D. A. Glasscock, G. T. Rochelle, Numerical simulation of theories for gas absorption with chemical reaction, AIChE Journal 35 (8) (1989) 1271–1281. doi:10.1002/aic.690350806.

[889] H. Karlsson, I. Bjerle, A general explicit enhancement factor for irreversible gas-liquid reactions with gas-side resistance, Chemical Engineering Science 35 (4) (1980) 1005–1007. doi:10.1016/0009-2509(80)85090-1.

[890] A. T. Da Silva, Kinetics of gas absorption: absorption with'instantaneous' reaction, Ph.D. thesis, University of Cambridge (1969).

[891] W. Last, J. Stichlmair, Determination of mass transfer parameters by means of chemical absorption, Chemical Engineering & Technology 25 (4) (2002) 385–391. doi:10.1002/1521-4125(200204)25:4<385::AID-CEAT385>3.0.CO;2-L.

[892] J. Pearson, Diffusion of one substance into a semi-infinite medium containing another with second-order reaction, Applied Scientific Research, Section A 11 (4-6) (1963) 321–340.

[893] R. H. Perry, R. L. Pigford, Kinetics of gas-liquid reactions, Industrial & Engineering Chemistry 45 (6) (1953) 1247–1253.

[894] V. Stepanek, Z. Palatý, H. Bendová, Numerical analysis of dialysis with chemical reaction at steady state. irreversible second-order reaction, Chemical Engineering and Processing: Process Intensification 95 (2015) 362–371. doi:10.1016/j.cep.2015.07.015.

[895] W. P. van Swaaij, G. F. Versteeg, Mass transfer accompanied with complex reversible chemical reactions in gas–liquid systems: an overview, Chem. Eng. Sci. 47 (2) (1992) 3181–3195. doi:10.1016/0009-2509(92)85028-a.

[896] Ömer Yildirim, A. A. Kiss, N. Hüser, K. Lessmann, E. Y. Kenig, Reactive absorption in chemical process industry: A review on current activities, Chemical Engineering Journal 213 (2012) 371–391. doi:10.1016/j.cej.2012.09.121.

[897] P. Brandl, Simplified absorber model in SQUASH, https://public.flourish.studio/visualisation/4224871/, accessed: 2021-06-14.

[898] M.-H. Li, Y.-C. Lie, Densities and viscosities of solutions of monoethanolamine + n-methyldiethanolamine + water and monoethanolamine + 2-amino-2-methyl-1-propanol + water, Journal of Chemical & Engineering Data 39 (3) (1994) 444–447. doi:10.1021/je00015a009.

[899] S. Jayarathna, C. K. Jayarathna, D. Kottage, S. Dayarathna, D. Eimer, M. C.

Melaaen, Density and surface tension measurements of partially carbonated aqueous monoethanolamine solutions, Journal of Chemical & Engineering Data 58 (2) (2013) 343–348. doi:10.1021/je300920t.

[900] M. Pagé, J.-Y. Huot, C. Jolicoeur, A comprehensive thermodynamic investigation of water–ethanolamine mixtures at 10, 25, and 40 °C, Canadian Journal of Chemistry 71 (7) (1993) 1064–1072. doi:10.1139/v93-142.

[901] A. Jamal, A. Meisen, C. Jim Lim, Kinetics of carbon dioxide absorption and desorption in aqueous alkanolamine solutions using a novel hemispherical contactor–II: Experimental results and parameter estimation, Chem. Eng. Sci. 61 (19) (2006) 6590–6603. doi:10.1016/j.ces.2006.04.047.

[902] A. Jamal, A. Meisen, C. Jim Lim, Kinetics of carbon dioxide absorption and desorption in aqueous alkanolamine solutions using a novel hemispherical contactor–I. experimental apparatus and mathematical modeling, Chem. Eng. Sci. 61 (19) (2006) 6571–6589. doi:10.1016/j.ces.2006.04.046.

[903] F.-Y. Jou, A. E. Mather, F. D. Otto, The solubility of CO_2 in 30 mass percent monoethanolamine solution, Can. J. Chem. Eng. 73 (1) (1995) 140–147. doi:10.1002/cjce.5450730116.

[904] D. Tong, J. M. Trusler, G. C. Maitland, J. Gibbins, P. S. Fennell, Solubility of carbon dioxide in aqueous solution of monoethanolamine or 2-amino-2-methyl-1-propanol: Experimental measurements and modelling, International Journal of Greenhouse Gas Control 6 (2012) 37–47. doi:10.1016/j.ijggc.2011.11.005.

[905] J. I. Lee, F. D. Otto, A. E. Mather, Equilibrium between carbon dioxide and aqueous monoethanolamine solutions, Journal of Applied Chemistry and Biotechnology 26 (1) (1976) 541–549. doi:10.1002/jctb.5020260177.

[906] I. Kim, K. A. Hoff, E. T. Hessen, T. Haug-Warberg, H. F. Svendsen, Enthalpy of absorption of CO_2 with alkanolamine solutions predicted from reaction equilibrium constants, Chem. Eng. Sci. 64 (9) (2009) 2027–2038. doi:10.1016/j.ces.2008.12.037.

[907] E. I. Concepción, Á. Gómez-Hernández, M. C. Martín, J. J. Segovia, Density and viscosity measurements of aqueous amines at high pressures: DEA-water, DMAE-water and

TEA-water mixtures, The Journal of Chemical Thermodynamics 112 (2017) 227–239. doi:10.1016/j.jct.2017.05.001.

[908] G. Vázquez, E. Alvarez, R. Rendo, E. Romero, J. M. Navaza, Surface tension of aqueous solutions of diethanolamine and triethanolamine from 25 °C to 50 °C, Journal of Chemical & Engineering Data 41 (4) (1996) 806–808. doi:10.1021/je960012t.

[909] J. I. Lee, F. D. Otto, A. E. Mather, Solubility of carbon dioxide in aqueous diethanolamine solutions at high pressures, Journal of Chemical & Engineering Data 17 (4) (1972) 465–468. doi:10.1021/je60055a015.

[910] M. Z. Haji-Sulaiman, M. K. Aroua, Equilibrium of CO_2 in aqueous diethanolamine (DEA(and amino methyl propanol (AMP) solutions, Chemical Engineering Communications 140 (1) (1995) 157–171. doi:10.1080/00986449608936460.

[911] J. Oscarson, R. V. Dam, J. Christensen, R. Izatt, Enthalpies of absorption of carbon dioxide in aqueous diethanolamine solutions, Thermochimica Acta 146 (1989) 107–114. doi:10.1016/0040-6031(89)87081-9.

[912] A. Kahrim, A. E. Mather, Enthalpy of solution of carbon dioxide in diethanolamine solutions, The Canadian Journal of Chemical Engineering 58 (5) (1980) 660–662. doi:10.1002/cjce.5450580518.

[913] A. Kahrim, Enthalpy of solution of CO_2 and H_2S in diethanolamine solutions, Ph.D. thesis, Thesis (M.Sc.)–University of Alberta (1976).

[914] H. Arcis, L. Rodier, J.-Y. Coxam, Enthalpy of solution of CO_2 in aqueous solutions of 2-amino-2-methyl-1-propanol, The Journal of Chemical Thermodynamics 39 (6) (2007) 878–887. doi:10.1016/j.jct.2006.11.011.

[915] R. Helton, J. J. Christensen, R. M. Izatt, Enthalpies of solution of CO_2 in aqueous diethanolamine solutions, Tech. Rep. Jan (1987).

[916] S. Paul, B. Mandal, Density and viscosity of aqueous solutions of (2-piperidineethanol + piperazine) from (288 to 333)K and surface tension of aqueous solutions of (n-methyldiethanolamine + piperazine), (2-amino-2-methyl-1-propanol + piperazine), and (2-piperidineethanol + piperazine) from (293 to 323)K, Journal of Chemical & Engineering Data 51 (6) (2006) 2242–2245. doi:10.1021/je0603271.

[917] K. Zhang, B. Hawrylak, R. Palepu, P. R. Tremaine, Thermodynamics of aqueous amines: excess molar heat capacities, volumes, and expansibilities of {water+ methyldiethanolamine (MDEA)} and {water + 2-amino-2-methyl-1-propanol (AMP)}, The Journal of Chemical Thermodynamics 34 (5) (2002) 679–710. doi:10.1006/jcht.2002.0937.

[918] E. Alvarez, R. Rendo, B. Sanjurjo, M. Sanchez-Vilas, J. M. Navaza, Surface tension of binary mixtures of water + n-methyldiethanolamine and ternary mixtures of this amine and water with monoethanolamine, diethanolamine, and 2-amino-2-methyl-1-propanol from 25 to 50 °C, Journal of Chemical & Engineering Data 43 (6) (1998) 1027–1029. doi:10.1021/je980106y.

[919] N. Haimour, A. Bidarian, O. C. Sandall, Kinetics of the reaction between carbon dioxide and methyldiethanolamine, Chemical Engineering Science 42 (6) (1987) 1393–1398. doi:10.1016/0009-2509(87)85011-X.

[920] J.-J. Ko, M.-H. Li, Kinetics of absorption of carbon dioxide into solutions of n-methyldiethanolamine+water, Chemical Engineering Science 55 (19) (2000) 4139–4147. doi:10.1016/S0009-2509(00)00079-8.

[921] R. Sidi-Boumedine, S. Horstmann, K. Fischer, E. Provost, W. Fürst, J. Gmehling, Experimental determination of carbon dioxide solubility data in aqueous alkanolamine solutions, Fluid Phase Equilibria 218 (1) (2004) 85–94. doi:10.1016/j.fluid.2003.11.014.

[922] F. Y. Jou, A. E. Mather, F. D. Otto, Solubility of hydrogen sulfide and carbon dioxide in aqueous methyldiethanolamine solutions, Industrial & Engineering Chemistry Process Design and Development 21 (4) (1982) 539–544. doi:10.1021/i200019a001.

[923] G. Kuranov, B. Rumpf, N. A. Smirnova, G. Maurer, Solubility of single gases carbon dioxide and hydrogen sulfide in aqueous solutions of n-methyldiethanolamine in the temperature range 313-413 Kat pressures up to 5 MPa, Industrial & Engineering Chemistry Research 35 (6) (1996) 1959–1966. doi:10.1021/ie950538r.

[924] A. P.-S. Kamps, A. Balaban, M. Jödecke, G. Kuranov, N. A. Smirnova, G. Maurer, Solubility of single gases carbon dioxide and hydrogen sulfide in aqueous solutions of

n-methyldiethanolamine at temperatures from 313 to 393 K and pressures up to 7.6 MPa: New experimental data and model extension, Industrial & Engineering Chemistry Research 40 (2) (2001) 696–706. doi:10.1021/ie000441r.

[925] M. H. Li, K. P. Shen, Densities and solubilities of solutions of carbon dioxide in water + monoethanolamine + n-methyldiethanolamine, Journal of Chemical & Engineering Data 37 (3) (1992) 288–290. doi:10.1021/je00007a002.

[926] V. Ermatchkov, A. Pérez-Salado Kamps, D. Speyer, G. Maurer, Solubility of carbon dioxide in aqueous solutions of piperazine in the low gas loading region, Journal of Chemical & Engineering Data 51 (5) (2006) 1788–1796. doi:10.1021/je0601917.

[927] O. Jonassen, I. Kim, H. F. Svendsen, Heat of absorption of carbon dioxide (CO_2) into aqueous n-methyldiethanolamine (MDEA) and n,n-dimethylmonoethanolamine (dmmea), Energy Procedia 63 (2014) 1890–1902. doi:10.1016/j.egypro.2014.11.198.

[928] G. Vazquez, E. Alvarez, J. M. Navaza, R. Rendo, E. Romero, Surface tension of binary mixtures of water plus monoethanolamine and water plus 2-amino-2-methyl-1-propanol and tertiary mixtures of these amines with water from 25°C to 50 °C, Journal of Chemical & Engineering Data 42 (1) (1997) 57–59. doi:10.1021/je960238w.

[929] F. Camacho, S. Sánchez, R. Pacheco, A. Sánchez, M. D. La Rubia, Thermal effects of CO_2 absorption in aqueous solutions of 2-amino-2-methyl-1-propanol, AIChE Journal 51 (10) (2005) 2769–2777. doi:10.1002/aic.10523.

[930] C. Zheng, B. Zhao, K. Wang, G. Luo, Determination of kinetics of CO_2 absorption in solutions of 2-amino-2-methyl-1-propanol using a microfluidic technique, AIChE Journal 61 (12) (2015) 4358–4366. doi:10.1002/aic.14972.

[931] E. Alper, Reaction mechanism and kinetics of aqueous solutions of 2-amino-2-methyl-1-propanol and carbon dioxide, Industrial & Engineering Chemistry Research 29 (8) (1990) 1725–1728. doi:10.1021/ie00104a023.

[932] M.-H. Li, B.-C. Chang, Solubilities of carbon dioxide in water + monoethanolamine + 2-amino-2-methyl-1-propanol, Journal of Chemical & Engineering Data 39 (3) (1994) 448–452. doi:10.1021/je00015a010.

[933] M. Kundu, B. P. Mandal, S. S. Bandyopadhyay, Vapor-liquid equilibrium of CO_2 in

aqueous solutions of 2-amino-2-methyl-1-propanol, Journal of Chemical & Engineering Data 48 (4) (2003) 789–796. doi:10.1021/je0201626.

[934] D.-J. Seo, W.-H. Hong, Solubilities of carbon dioxide in aqueous mixtures of diethanolamine and 2-amino-2-methyl-1-propanol, Journal of Chemical & Engineering Data 41 (2) (1996) 258–260. doi:10.1021/je950197o.

[935] H. Li, P. T. Frailie, G. T. Rochelle, J. Chen, Thermodynamic modeling of piperazine/2-aminomethylpropanol/CO_2/water, Chemical Engineering Science 117 (2014) 331–341. doi:10.1016/j.ces.2014.06.026.

[936] J. Gabrielsen, M. L. Michelsen, E. H. Stenby, G. M. Kontogeorgis, Modeling of CO_2 absorber using an AMP solution, AIChE Journal 52 (10) (2006) 3443–3451. doi:10.1002/aic.10963.

[937] S. A. Freeman, G. T. Rochelle, Density and viscosity of aqueous (piperazine + carbon dioxide) solutions, Journal of Chemical & Engineering Data 56 (3) (2011) 574–581. doi:10.1021/je1012263.

[938] G. Murshid, A. M. Shariff, L. K. Keong, M. A. Bustam, Physical properties of aqueous solutions of piperazine and (2-amino-2-methyl-1-propanol + piperazine) from (298.15 to 333.15)K, Journal of Chemical & Engineering Data 56 (5) (2011) 2660–2663. doi:10.1021/je1012586.

[939] Y.-R. Chen, A. R. Caparanga, A. N. Soriano, M.-H. Li, Liquid heat capacity of the solvent system (piperazine+n-methyldiethanolamine+water), The Journal of Chemical Thermodynamics 42 (1) (2010) 54–59. doi:10.1016/j.jct.2009.07.005.

[940] A. Muhammad, M. Abdul Mutalib, M. Thanapalan, A. Shafeeq, Thermophysical Properties of Aqueous Piperazine and Aqueous (N-Methyldiethanolamine + Piperazine) Solutions at Temperatures (298.15 to 338.15)K, Vol. 54, 2009. doi:10.1021/je9000069.

[941] S. Bishnoi, G. T. Rochelle, Absorption of carbon dioxide into aqueous piperazine: reaction kinetics, mass transfer and solubility, Chem. Eng. Sci. 55 (22) (2000) 5531–5543. doi:10.1016/S0009-2509(00)00182-2.

[942] R. Dugas, G. Rochelle, Absorption and desorption rates of carbon dioxide with monoethanolamine and piperazine, Energy Procedia 1 (1) (2009) 1163–1169. doi:10.

1016/j.egypro.2009.01.153.

[943] R. E. Dugas, G. T. Rochelle, CO_2 absorption rate into concentrated aqueous monoethanolamine and piperazine, Journal of Chemical & Engineering Data 56 (5) (2011) 2187–2195. doi:10.1021/je101234t.

[944] H. Svensson, C. Hulteberg, H. T. Karlsson, Heat of absorption of CO_2 in aqueous solutions of n-methyldiethanolamine and piperazine, International Journal of Greenhouse Gas Control 17 (2013) 89–98. doi:10.1016/j.ijggc.2013.04.021.

[945] S. Paul, B. Mandal, Density and viscosity of aqueous solutions of (n-methyldiethanolamine + piperazine) and (2-amino-2-methyl-1-propanol + piperazine) from (288 to 333) K, Journal of Chemical & Engineering Data 51 (5) (2006) 1808–1810. doi:10.1021/je060195b.

[946] Z.-Y. Yang, A. N. Soriano, A. R. Caparanga, M.-H. Li, Equilibrium solubility of carbon dioxide in (2-amino-2-methyl-1-propanol+piperazine+water), The Journal of Chemical Thermodynamics 42 (5) (2010) 659–665. doi:10.1016/j.jct.2009.12.006.

[947] D. Tong, G. C. Maitland, M. J. Trusler, P. S. Fennell, Solubility of carbon dioxide in aqueous blends of 2-amino-2-methyl-1-propanol and piperazine, Chemical Engineering Science 101 (2013) 851–864. doi:10.1016/j.ces.2013.05.034.

[948] J. F. Richardson, J. M. Coulson, Preface, in: R. K. Sinnott (Ed.), Coulson and Richardson's Chemical Engineering (Second Edition), Pergamon, Amsterdam, 1993, p. viii. doi:10.1016/B978-0-08-041865-0.50006-4.

[949] W. Lewis, L. Squires, The structure of liquids and the mechanism of viscosity, Refiner Nat. Gasoline Manuf 13 (1934) 448.

[950] J. W. Przedziecki, T. Sridhar, Prediction of liquid viscosities, AIChE Journal 31 (2) (1985) 333–335. doi:10.1002/aic.690310225.

[951] J. Prabhakar, M. Venkateshwara Rao, D. Prasad, A corresponding-states' method for the viscosity of liquids and liquid mixtures.

[952] N. Dutt, D. Prasad, Representation of the temperature dependence of the viscosity of pure liquids, Private Communication, Chemical Engineering Division, Indian Institute of Chemical Technology, Hyderabad.

[953] M. Souders, Viscosity and chemical constitution, Journal of the American Chemical Society 60 (1) (1938) 154–158. doi:10.1021/ja01268a048.

[954] D. S. Viswanath, Viscosity of liquids theory, estimation, experiment, and data. (2007).

[955] L. H. Thomas, H. Smith, G. Davies, The viscosity of liquids at temperatures approaching the freezing point, and molecular association of polyphenyls and related compounds, The Chemical Engineering Journal 16 (3) (1978) 223–232. doi:10.1016/0300-9467(78)85059-X.

[956] D. van Velzen, R. L. Cardozo, H. Langenkamp, A liquid viscosity-temperature-chemical constitution relation for organic compounds, Industrial & Engineering Chemistry Fundamentals 11 (1) (1972) 20–25. doi:10.1021/i160041a004.

[957] J. Homer, S. C. Generalis, J. H. Robson, Artificial neural networks for the prediction of liquid viscosity, density, heat of vaporization, boiling point and pitzer's acentric factor part I. hydrocarbons, Phys. Chem. Chem. Phys. 1 (1999) 4075–4081. doi:10.1039/a904096j.

[958] G. S. Sariyerli, O. Sakarya, U. Y. Akcadag, Comparison tests for the determination of the viscosity values of reference liquids by capillary viscometers and stabinger viscometer svm 3001, Int. J. Metrol. Qual. Eng. 9 (2018) 7. doi:10.1051/ijmqe/2018004.

[959] R. S. Marvin, The accuracy of measurements of viscosity of liquids, Journal of Research of the National Institute of Standards and Technology Section A 75 (6) (1971) 535–540.

[960] S. S. Karunarathne, D. A. Eimer, L. E. Øi, Evaluation of systematic error and uncertainty of viscosity measurements of mixtures of monoethanol amine and water in coaxial cylinder rheometers, International Journal of Modeling and Optimization 8 (5) (2018) 260–265.

[961] A. Hartono, E. O. Mba, H. F. Svendsen, Physical properties of partially CO_2 loaded aqueous monoethanolamine (MEA), Journal of Chemical & Engineering Data 59 (6) (2014) 1808–1816. doi:10.1021/je401081e.

[962] U. Arachchige, N. Aryal, D. A. Eimer, M. C. Melaaen, Viscosities of pure and aqueous solutions of monoethanolamine (MEA), diethanolamine (DEA) and N-methyldiethanolamine (MDEA), Annual Transactions of the Nordic Rheology Society

21 (2013) 299.

[963] M. N. Islam, M. M. Islam, M. N. Yeasmin, Viscosity of aqueous solutions of 2-methoxyethanol, 2-ethoxyethanol, and ethanolamine, The Journal of Chemical Thermodynamics 36 (10) (2004) 889–893. doi:10.1016/j.jct.2004.06.004.

[964] T. G. Amundsen, L. E. Øi, D. A. Eimer, Density and viscosity of monoethanolamine + water + carbon dioxide from (25 to 80) °C, Journal of Chemical & Engineering Data 54 (11) (2009) 3096–3100. doi:10.1021/je900188m.

[965] Y. Maham, T. T. Teng, L. G. Hepler, A. E. Mather, Volumetric properties of aqueous solutions of monoethanolamine, mono- and dimethylethanolamines at temperatures from 5 to 80 °C i, Thermochimica Acta 386 (2) (2002) 111–118. doi:10.1016/s0040-6031(01)00812-7.

[966] R. H. Weiland, J. C. Dingman, D. B. Cronin, Heat capacity of aqueous monoethanolamine, diethanolamine, n-methyldiethanolamine, and n-methyldiethanolamine-based blends with carbon dioxide, Journal of Chemical & Engineering Data 42 (5) (1997) 1004–1006. doi:10.1021/je960314v.

[967] D. Fu, L. Chen, L. Qin, Experiment and model for the viscosity of carbonated MDEA–MEA aqueous solutions, Fluid Phase Equilibria 319 (2012) 42–47. doi:10.1016/j.fluid.2012.01.029.

[968] C. F. Chueh, A. C. Swanson, Estimation of liquid heat capacity, The Canadian Journal of Chemical Engineering 51 (5) (1973) 596–600. doi:10.1002/cjce.5450510511.

[969] C. Chueh, A. Swanson, Estimating liquid heat-capacity, Chemical Engineering Progress 69 (7) (1973) 83–85.

[970] M. Zábranský, Z. Kolská, V. Růžička, E. S. Domalski, Heat capacity of liquids: Critical review and recommended values. supplement ii, Journal of Physical and Chemical Reference Data 39 (1) (2010) 013103. doi:10.1063/1.3182831.

[971] J. S. Chickos, D. G. Hesse, J. F. Liebman, A group additivity approach for the estimation of heat capacities of organic liquids and solids at 298K, Structural Chemistry 4 (4) (1993) 261–269.

[972] C. Huang, A. Johnson, Estimation of heat capacity of organic liquids, Canadian Journal

of Technology 33 (1955) 421.

[973] M. Zábranský, V. Růžička, Estimation of the heat capacities of organic liquids as a function of temperature using group additivity: An amendment, Journal of Physical and Chemical Reference Data 33 (4) (2004) 1071–1081. doi:10.1063/1.1797811.

[974] E. S. Domalski, E. D. Hearing, Heat capacities and entropies of organic compounds in the condensed phase. volume III, Journal of Physical and Chemical Reference Data 25 (1) (1996) 1–525. doi:10.1063/1.555985.

[975] M. Zábranský, V. Růžička, E. S. Domalski, Heat capacity of liquids: Critical review and recommended values. supplement i, Journal of Physical and Chemical Reference Data 30 (5) (2001) 1199–1689. doi:10.1063/1.1407866.

[976] G. Le Bas, The molecular volumes of liquid chemical compounds, from the point of view of Kopp., Longmans Green, London ;New York, 1915.

[977] M. Tyn, W. Calus, Estimating liquid molal volume 21 (1975) 16.

[978] T. Yamada, R. D. Gunn, Saturated liquid molar volumes. rackett equation, Journal of Chemical & Engineering Data 18 (2) (1973) 234–236. doi:10.1021/je60057a006.

[979] R. W. Hankinson, G. H. Thomson, A new correlation for saturated densities of liquids and their mixtures, AIChE Journal 25 (4) (1979) 653–663. doi:10.1002/aic.690250412.

[980] R. H. Weiland, J. C. Dingman, D. B. Cronin, G. J. Browning, Density and viscosity of some partially carbonated aqueous alkanolamine solutions and their blends, Journal of Chemical & Engineering Data 43 (3) (1998) 378–382. doi:10.1021/je9702044.

[981] J. Han, J. Jin, D. A. Eimer, M. C. Melaaen, Density of water (1) + monoethanolamine (2) + CO_2(3) from (298.15 to 413.15) Kand surface tension of water (1) + monoethanolamine (2) from (303.15 to 333.15)K, Journal of Chemical & Engineering Data 57 (4) (2012) 1095–1103. doi:10.1021/je2010038.

[982] E. B. Rinker, D. W. Oelschlager, A. T. Colussi, K. R. Henry, O. C. Sandall, Viscosity, density, and surface tension of binary mixtures of water and n-methyldiethanolamine and water and diethanolamine and tertiary mixtures of these amines with water over the temperature range 20-100.degree.c, Journal of Chemical & Engineering Data 39 (2)

(1994) 392–395. doi:10.1021/je00014a046.

[983] C.-H. Hsu, M.-H. Li, Densities of aqueous blended amines, Journal of Chemical & Engineering Data 42 (3) (1997) 502–507. doi:10.1021/je960356j.

[984] Y.-M. Tseng, A. R. Thompson, Densities and refractive indices of aqueous monoethanolamine, diethanolamine, triethanolamine., Journal of Chemical & Engineering Data 9 (2) (1964) 264–267. doi:10.1021/je60021a043.

[985] F. Yang, X. Wang, Z. Liu, Volumetric properties of binary and ternary mixtures of bis(2-hydroxyethyl)amine with water, methanol, ethanol from (278.15 to 353.15)K, Thermochimica Acta 533 (2012) 1–9. doi:10.1016/j.tca.2012.01.007.

[986] V. D. Spasojević, S. P. Šerbanović, B. D. Djordjević, M. L. Kijevčanin, Densities, viscosities, and refractive indices of aqueous alkanolamine solutions as potential carbon dioxide removal reagents, Journal of Chemical & Engineering Data 58 (1) (2013) 84–92. doi:10.1021/je300938w.

[987] Y. Zhao, X. Zhang, S. Zeng, Q. Zhou, H. Dong, X. Tian, S. Zhang, Density, viscosity, and performances of carbon dioxide capture in 16 absorbents of amine + ionic liquid + H_2O, ionic liquid + H_2O, and amine + H_2O systems, Journal of Chemical & Engineering Data 55 (9) (2010) 3513–3519. doi:10.1021/je100078w.

[988] F.-Q. Zhang, H.-P. Li, M. Dai, J.-P. Zhao, J. Chao, Volumetric properties of binary mixtures of water with ethanolamine alkyl derivatives, Thermochimica Acta 254 (1995) 347–357. doi:10.1016/0040-6031(94)02127-A.

[989] D. B. Macleod, On a relation between surface tension and density, Trans. Faraday Soc. 19 (1923) 38–41. doi:10.1039/tf9231900038.

[990] S. Sugden, The variation of surface tension with temperature and some related functions, J. Chem. Soc., Trans. 125 (1924) 32–41. doi:10.1039/ct9242500032.

[991] O. R. Quayle, The parachors of organic compounds. an interpretation and catalogue., Chemical Reviews 53 (3) (1953) 439–589. doi:10.1021/cr60166a003.

[992] J. R. Brock, R. B. Bird, Surface tension and the principle of corresponding states, AIChE Journal 1 (2) (1955) 174–177. doi:10.1002/aic.690010208.

[993] R. F. Curl, K. Pitzer, Volumetric and thermodynamic properties of fluids–enthalpy,

free energy, and entropy, Industrial & Engineering Chemistry 50 (2) (1958) 265–274. doi:10.1021/ie50578a047.

[994] Y.-X. Zuo, E. H. Stenby, Corresponding-states and parachor models for the calculation of interfacial tensions, The Canadian Journal of Chemical Engineering 75 (6) (1997) 1130–1137. doi:10.1002/cjce.5450750617.

[995] S. Sastri, K. Rao, A simple method to predict surface tension of organic liquids, The Chemical Engineering Journal and the Biochemical Engineering Journal 59 (2) (1995) 181–186. doi:10.1016/0923-0467(94)02946-6.

[996] P. Rice, A. S. Teja, A generalized corresponding-states method for the prediction of surface tension of pure liquids and liquid mixtures, Journal of Colloid and Interface Science 86 (1) (1982) 158–163. doi:10.1016/0021-9797(82)90051-0.

[997] J. T. Suarez, C. Torres-Marchal, P. Rasmussen, Prediction of surface tensions of nonelectrolyte solutions, Chemical Engineering Science 44 (3) (1989) 782–785. doi:10.1016/0009-2509(89)85055-9.

[998] M. Tamura, M. Kurata, H. Odani, Practical method for estimating surface tensions of solutions, Bulletin of the Chemical Society of Japan 28 (1) (1955) 83–88. doi:10.1246/bcsj.28.83.

[999] L. Chunxi, W. Wenchuan, W. Zihao, A surface tension model for liquid mixtures based on the Wilson equation, Fluid Phase Equilibria 175 (1) (2000) 185–196. doi:10.1016/S0378-3812(00)00447-7.

[1000] E. Álvarez, A. Cancela, R. Maceiras, J. M. Navaza, R. Táboas, Surface tension of aqueous binary mixtures of 1-amino-2-propanol and 3-amino-1-propanol, and aqueous ternary mixtures of these amines with diethanolamine, triethanolamine, and 2-amino-2-methyl-1-propanol from (298.15 to 323.15)K, Journal of Chemical & Engineering Data 48 (1) (2003) 32–35. doi:10.1021/je020048n.

[1001] E. Alvarez, D. Gomez-Diaz, M. D. La Rubia, J. M. Navaza, Surface tension of aqueous binary mixtures of 2-(methylamino)ethanol and 2-(ethylamino)ethanol and aqueous ternary mixtures of these amines with triethanolamine or n-methyldiethanolamine from (293.15 to 323.15)K, Journal of Chemical & Engineering Data 53 (1) (2008) 318–321.

doi:10.1021/je700536m.

[1002] P. W. Derks, K. J. Hogendoorn, G. F. Versteeg, Solubility of N_2O in and density, viscosity, and surface tension of aqueous piperazine solutions, Journal of Chemical & Engineering Data 50 (6) (2005) 1947–1950. doi:10.1021/je050202g.

[1003] J. Aguila-Hernández, A. Trejo, J. Gracia-Fadrique, Surface tension of aqueous solutions of alkanolamines: single amines, blended amines and systems with nonionic surfactants, Fluid Phase Equilibria 185 (1) (2001) 165–175. doi:10.1016/S0378-3812(01)00467-8.

[1004] A. Venkat, G. Kumar, M. Kundu, Density and surface tension of aqueous solutions of (2-(methylamino)-ethanol +2-amino-2-methyl-1-propanol) and (2-(methylamino)-ethanol + n-methyl-diethanolamine) from (298.15 to 323.15)K, Journal of Chemical & Engineering Data 55 (11) (2010) 4580–4585. doi:10.1021/je1002626.

[1005] Y. Maham, A. Mather, Surface thermodynamics of aqueous solutions of alkylethanolamines, Fluid Phase Equilibria 182 (1) (2001) 325–336. doi:10.1016/S0378-3812(01)00391-0.

[1006] A. Shojaeian, New experimental and modeling based on the N-Wilson-NRF equation for surface tension of aqueous alkanolamine binary mixtures, Journal of Molecular Liquids 254 (2018) 26–33. doi:10.1016/j.molliq.2018.01.077.

[1007] D. Fu, L. Wang, X. Tian, Experiments and model for the surface tension of DEAE-PZ and DEAE-MEA aqueous solutions, The Journal of Chemical Thermodynamics 105 (2017) 71–75. doi:10.1016/j.jct.2016.10.007.

[1008] S. A. Kelayeh, A. H. Jalili, C. Ghotbi, M. Hosseini-Jenab, V. Taghikhani, Densities, viscosities, and surface tensions of aqueous mixtures of sulfolane + triethanolamine and sulfolane + diisopropanolamine, Journal of Chemical & Engineering Data 56 (12) (2011) 4317–4324. doi:10.1021/je200124h.

[1009] G. Latini, M. Pacetti, The Thermal Conductivity of Liquids: A Critical Survey, Springer US, Boston, MA, 1978, pp. 245–253. doi:10.1007/978-1-4615-9083-5_31.

[1010] T. H. Chung, L. L. Lee, K. E. Starling, Applications of kinetic gas theories and multiparameter correlation for prediction of dilute gas viscosity and thermal conductivity, Industrial & Engineering Chemistry Fundamentals 23 (1) (1984) 8–13. doi:

10.1021/i100013a002.

[1011] M. Arikol, H. Gürbüz, A new method for predicting thermal conductivity of pure organic liquids and their mixtures, The Canadian Journal of Chemical Engineering 70 (6) (1992) 1157–1163. doi:10.1002/cjce.5450700616.

[1012] J. Lenoir, Effect of pressure on thermal conductivity of liquids, Petroleum Refiner 36 (8) (1957) 62–4.

[1013] R. DiGuilio, A. S. Teja, Thermal conductivity of poly(ethylene glycols) and their binary mixtures, Journal of Chemical & Engineering Data 35 (2) (1990) 117–121. doi:10.1021/je00060a005.

[1014] M. Shokouhi, A. Jalili, M. Hosseini-Jenab, Thermo physical properties of some physical and chemical solvents at atmospheric pressure, Iranian Journal of Chemical Engineering(IJChE) 10 (4) (2013) 43–54. doi:www.ijche.com/article_11673.html.

[1015] R. J. Littel, G. F. Versteeg, W. P. M. van Swaaij, Solubility and diffusivity data for the absorption of carbonyl sulfide, carbon dioxide, and nitrous oxide in amine solutions, Journal of Chemical & Engineering Data 37 (1) (1992) 49–55. doi:10.1021/je00005a017.

[1016] J. Li, A. Henni, P. Tontiwachwuthikul, Reaction kinetics of CO_2 in aqueous ethylenediamine, ethyl ethanolamine, and diethyl monoethanolamine solutions in the temperature range of 298-313 K, using the stopped-flow technique, Industrial & Engineering Chemistry Research 46 (13) (2007) 4426–4434. doi:10.1021/ie0614982.

[1017] M. H. Oyevaar, H. J. Fontein, K. R. Westerterp, Equilibria of carbon dioxide in solutions of diethanolamine in aqueous ethylene glycol at 298K, Journal of Chemical & Engineering Data 34 (4) (1989) 405–408. doi:10.1021/je00058a010.

[1018] G. F. F. Versteeg, M. H. H. Oyevaar, The reaction between CO_2 and diethanolamine at 298K, Chem. Eng. Sci. 44 (5) (1989) 1264–1268. doi:10.1016/0009-2509(89)87026-5.

[1019] M. Haji-Sulaiman, M. Aroua, A. Benamor, Analysis of Equilibrium Data of CO_2 in Aqueous Solutions of Diethanolamine (DEA), Methyldiethanolamine (MDEA) and Their Mixtures Using the Modified Kent Eisenberg Model, Chemical Engineering Research and Design 76 (8) (1998) 961–968. doi:10.1205/026387698525603.

[1020] H. Arcis, K. Ballerat-Busserolles, L. Rodier, J.-Y. Coxam, Measurement and modeling of enthalpy of solution of carbon dioxide in aqueous solutions of diethanolamine at temperatures of (322.5 and 372.9)K and pressures up to 3 MPa, Journal of Chemical & Engineering Data 57 (3) (2012) 840–855. doi:10.1021/je201012e.

[1021] M. L. Kennard, A. Meisen, Solubility of carbon dioxide in aqueous diethanolamine solutions at elevated temperatures and pressures, Journal of Chemical & Engineering Data 29 (3) (1984) 309–312. doi:10.1021/je00037a025.

[1022] O. F. Dawodu, A. Meisen, Solubility of carbon dioxide in aqueous mixtures of alkanolamines, Journal of Chemical & Engineering Data 39 (3) (1994) 548–552. doi:10.1021/je00015a034.

[1023] D. Lal, F. D. Otto, A. E. Mather, The solubility of H_2S and CO_2 in a diethanolamine solution at low partial pressures, The Canadian Journal of Chemical Engineering 63 (4) (1985) 681–685. doi:10.1002/cjce.5450630423.

[1024] J. D. Lawson, A. W. Garst, Gas sweetening data: equilibrium solubility of hydrogen sulfide and carbon dioxide in aqueous monoethanolamine and aqueous diethanolamine solutions, Journal of Chemical & Engineering Data 21 (1) (1976) 20–30. doi:10.1021/je60068a010.

[1025] J. W. Mason, B. F. Dodge, Equilibrium absorption of carbon dioxide by solutions of the ethanolamines, Ph.D. thesis (1936).

[1026] A. Benamor, M. Aroua, Modeling of CO_2 solubility and carbamate concentration in DEA, MDEA and their mixtures using the Deshmukh–Mather model, Fluid Phase Equilibria 231 (2) (2005) 150–162. doi:10.1016/j.fluid.2005.02.005.

[1027] L. Li, Carbon dioxide solubility and mass transfer in aqueous amines for carbon capture, Ph.D. thesis, The University of Texas at Austin (2015).

[1028] X. Chen, Carbon dioxide thermodynamics, kinetics, and mass transfer in aqueous piperazine derivatives and other amines, Ph.D. thesis, The University of Texas at Austin (2011).

[1029] J. K. Carson, K. N. Marsh, A. E. Mather, Enthalpy of solution of carbon dioxide in (water + monoethanolamine, or diethanolamine, or n-methyldiethanolamine) and (water

+ monoethanolamine + n-methyldiethanolamine) at 298.15K, The Journal of Chemical Thermodynamics 32 (9) (2000) 1285–1296. doi:10.1006/jcht.2000.0680.

[1030] A. Samanta, S. Roy, S. S. Bandyopadhyay, Physical solubility and diffusivity of N_2O and CO_2 in aqueous solutions of piperazine and (n-methyldiethanolamine + piperazine), Journal of Chemical & Engineering Data 52 (4) (2007) 1381–1385. doi:10.1021/je700083b.

[1031] A. K. Saha, S. S. Bandyopadhyay, A. K. Biswas, Kinetics of absorption of CO_2 into aqueous solutions of 2-amino-2-methyl-1-propanol, Chemical Engineering Science 50 (22) (1995) 3587–3598. doi:10.1016/0009-2509(95)00187-A.

A. Additional Scientific Background

A.1 Net-zero World

While the individual definitions of net-zero vary, it generally means that the sum of residual anthropogenic greenhouse gas (GHG) emissions (*e.g.* CO_2, CH_4, N_2O) and GHG sinks is zero. This implies that residual GHG emissions are compensated by GHG removal from the environment. The term carbon negative means that more emissions are removed from the carbon cycle than are emitted. For example, forests and oceans could potentially absorb more than the combined residual carbon emissions from transport and agriculture. At the time of writing, 137 countries announced carbon-neutral targets [22, 715], however, these targets differ in definition, scope, time, legal status (legally binding, policy document, announcements), and associated measures. Legally binding net-zero targets are set by Germany and Sweden (both by 2045), as well as Japan, United Kingdom, France, Canada, South Korea, Spain, Denmark, New Zealand, and Hungary (all by 2050). Finland declared to reach their net-zero target by 2035, which is the earliest of all developed countries[1]. The world's biggest economies/emitters also announced/proposed/debated targets including the USA (by 2050), China, India, Russia and Saudi Arabia (all by 2060).

Assuming a median internal carbon price of $\$25/t_{CO_2e}$, sustainability reached top priority for over 2000 companies [716]. This included fossil fuel processing companies such as Royal Dutch Shell, Total, Equinor, Occidental, Repsol, and BP, who all made announcements to transform their businesses to meet net-zero targets by 2050. This, however, excludes the life cycle emissions of their products [2]. The following companies from different sectors have also announced net-zero targets and several other major organisations are expected to follow: Nestlé (Switzerland, consumer products), Qantas (Australia, airline), Duke Energy (USA, utilities and power), ThyssenKrupp (Germany, steel), HeidelbergCement (Germany, cement), Vale (Brazil, mining

[1] Suriname and Bhutan are reported to be already carbon neutral/negative

[2] with the exception of Repsol; their plan includes scope three emissions, *i.e.* other indirect emissions that occur in the companys value chain such as use of sold product, business travel or waste disposal.

and metals), Microsoft (USA, software), Delta (USA, airline) [716]. This inflation of sustainability commitments has not come without criticism, and calls for strict measures to monitor progress which has moved into litigation for the company Shell [717].

Alternative capture concepts have been analysed in the 70s *e.g.,* floating coal/gas-power plants with ocean water as CO_2 storage site (dissolved), bubbling flue gas directly through seawater, or two-stage processes utilising various solvents (sodium potassium hydroxide or glycerin triactetate) [61].

Carbon diode removal (CDR), or negative emissions technologies (NETs), are umbrella terms for all natural or engineered solutions that remove CO_2 from the atmosphere. These include land management (afforestation/reforestation), mineral carbonation, Bio-Energy with CCS (BECCS), and DACCS [29–39]. All these technologies remove carbon from the atmosphere and they differ significantly in the way they capture and store CO_2 as well as their potential scale and predicted cost [39].

Afforestation covers activities such as planting trees or facilitating the regeneration of trees. BECCS uses biomass (*e.g.* wood pellets) as feedstock, which has over its lifetime removed carbon from the atmosphere. The emissions arising from converting the biomass into an energy product (*e.g.* electricity, hydrogen) are captured and geologically stored, thereby providing a net removal of CO_2 from the atmosphere [549, 718, 719]. BECCS is considered one of the few potential carbon negative ways of producing electricity. DACCS has notably gained attention and a range of start-up companies are actively working on developing and commercialising this technology. It is widely recognised that technical solutions are capable of accelerating the rate of CO_2 removal, and the potentially available cumulative capacity is estimated to be 35 Gt_{CO_2}/year [720–722]. However, the framing of CDRs is contested in technical, social and political dimensions [33, 36, 38, 723–727].

Utilising and partly storing CO_2 for EOR (The majority of injected CO_2 stays in the subsurface in the case of EOR [728]) is reducing the oil's carbon footprint compared to *e.g.,* nitrogen based injection, however, processing and burning the additional products releases more emissions, *i.e.,* no consensus has been found yet if a full life-cycle assessment (cradle-to-grave) is net-negative

or net-positive [729, 730]. Importantly, most of the CO_2 used for EOR comes from natural subsurface sources, thus only little CO_2 (if at all) is removed from the carbon cycle [62, 728, 729]. The additional revenue associated with EOR supports the business case of CCS, but it does not support sustainably mitigating climate change [729]. In the early 1970s, gaseous CO_2 captured from subsurface sources was injected for enhanced oil recovery (EOR) and capturing CO_2 from anthropogenic sources expanded capacity as demand increased [731–736]. Half a decade later, the vast majority of the approximately 40 $Mtpa_{CO_2}$ installed CCS capacity in the year 2020 is still used for EOR. Only Gorgon in Australia, Quest in Canada, Qatar's LNG plant, Equinor's Sleipner and Snohvit projects, and the BECCS plant in Illinois use a dedicated storage [62, 63].

Both the IPCC and IEA predict the total operating capacity of CCS will be in the low gigatonnes scale in 2050 for virtually all likely scenarios; the IPCC predict 15 $Gtpa_{CO_2}$ while the IEA predict 7.5 $Gtpa_{CO_2}$ [27, 737]. Additionally, 3.5 - 16 $Gtpa_{CO_2}$ (IPCC) or 1.9 $Gtpa_{CO_2}$ (IEA) of CDRs will be required in 2050 [27, 720]. There is theoretically enough CO_2 storage capacity available (16 800 Gt_{CO_2}), however, deployment has been slow, and only 718 $Mtpa_{CO_2}$ of safe geological storage capacity is predicted for 2050, based on historic and planned projects [39, 738]. Regardless of the scenario that will be closest to reality in the future, a substantial increase of CCS activities is required.

There appears to be a momentum for investing in CCS-hubs by clustering multiple point sources in close proximity, profiting off shared transport and storage infrastructure. Examples in advanced stages of development are Porthos in the Netherlands, Longship CCS/Northern Lights in Norway, CarboNet in Australia, HyNet Cluster as well as the East Coast Cluster in UK, and the recently operational ACTL facilities in Canada [739]. They include plants from hard to abate sectors such as iron, steel, and cement [62]. These investments are taken by multiple large international companies with some involvement of governments.

A.2 Commercial Amine-based Capture Solvents

In the following paragraphs a critical review of the key elements of solvent R&D over the past century is presented. It is not intended to associate any specific vendor with any particular

exemplary solvent composition and intellectual property is respected. Physical solvents, ionic liquids, deep eutectic solvents, chilled ammonia, amino acids, and phase-change solvents are discussed in the appendix A.3.

One of the oldest patents claimed for CO_2 capture using solvents dates back to 1904 [740, 741] and was issued for potassium carbonate K_2CO_3, which was widely used in hydrogen, ammonia, natural gas, iron, and ethylene oxide plants [462, 742]. The hot potassium carbonate process resembles the typical amine process but requires much higher partial pressures of CO_2 and the absorber is operated at high temperatures (versus low temperatures for the amine process). The higher temperature increases the solubility of potassium bicarbonate in solution, which enables utilising higher concentrations resulting in improved absorption capacity. The typical amine process differs to this process by 1. the addition of a lean-rich cross heat exchanger between the absorber and stripper, and 2. replacing the flue gas to cleaned gas heat exchanger with a direct contact cooler. Split and multi-stage processes were deployed for the hot potassium carbonate process much before they were discussed for amine-based CO_2 capture plants [731, 742].

Bottoms [101] and Allen and Michalske [102] independently from each other filed for US patents in October 1930 claiming the process of using aqueous (alkanol)amines to separate carbon dioxide out of a gas mixture. At that point alkanolamines, which were discovered in Germany mid-19th century [103, 104], became more available. Allen and Michalske claim triethanolamine (TEA) in addition to sodium carbonate as preferable. Bottoms extended his application to primary, secondary and tertiary amines, diamines and alkanolamines. He included precipitating solvents as found within aliphatic herterocyclic ring structures, *e.g.,* piperazine (PZ). Bottoms explicitly lists hexylamine (HEXA), dipropylamine (DPA), propylene diamine (DAP), trimethylene diamine, triaminopropane, monoethanolamine (MEA), diethanolamine (DEA), triethanolamine (TEA), diisopropanolamine (DIPA), diethylethanolamine (DEEA), benzylamine (BZA), phenylethylamine (PEA), piperidyl ethanol (2PPE), and methylphenylmethyl amine. TEA was also claimed by Shoeld in 1934 as part of a multi-stage multi-solvent absorption with sodium phenolate [743]. Amines were widely used in industry *e.g.,* MEA for natural gas sweetening, or DEA or diglycolamine (DGA) in refinery applications [742]. TEA was the first commercially available amine and is one fo the only commodity amines available

at large scale today [742].

Piperazine (PZ) is a white crystal solid at ambient conditions (melting point at 379K) and its solubility in water is low with an eutectic point near 61 wt%. Concentrated PZ solvents (up to 8M [564]) are constrained by their low solubility [744] as precipitation is not desired. PZ is widely used in industry (manufacture of plastics, resins, pesticides, brake fluid, and others) and was even distributed as anthelmintic in the early 20^{th} century. PZ is a heterocyclic diamine with each amine group of second order. It's theoretical maximum 2:1 CO_2 to amine ratio (via carbamate and dicarbamate) is decreased by possible side reactions and the stability of intermediates.

The commercial successful BenField process was invented by Benson and Field in 1954 [745, 746] and further developed the basic hot carbonate process by adding DEA as promoter. It is licensed by Universal Oil Products (UOP) [462, 747]. The pressure swing replaced the temperature swing as a means to regenerate the solvent (*i.e.,* absorption and regeneration both happening at higher temperatures) which accelerates the reaction rate and decreases the energy loads [748]. Other commercial successful processes utilising potassium carbonate are CATACARB (with catalyst) [749, 750], ExxonMobil's FLEXSORB SE process (with hindered amine promoter for H_2S removal), or GiammarcoVetrocoke (As_2O_3 and glycine) [748].

"Hybrid solvents" contain a physical and chemical reactant. They are advantageous at high partial pressures and able to capture more than just CO_2. Comprehensive Shell patents published in 1967 [751] and 1970 [752] claim an aqueous solution of, amongst others, methylaminoethanol (MAE), ethylaminoethanol (EAE), isopropanol amines, and morpholines such as morpholine (MOR) and 2,6-dimethylmorpholine (2,6-DMM) for the removal of CO_2, H_2S, OCS. They found MAE, EAE, and 2,6-DMM (or a blend thereof) to be particularly preferable added by glycols *e.g.,* monoethylene glycol (MEG), diethylene glycol (DEG), or triethylene glycol (TEG) for water removal. A modification additionally contains a physical solvent that may be water-free or water-lean (up to 30 wt% water) with sulfone, dimethyl formamide, N-methyl pyrrolidone (NMP), or blend thereof, being preferred. Sulfinol is the tradename of Shell's hybrid solvents which consists of sulfolane, and a chemical reactant such as MDEA, MDEA+PZ, or DIPA and

DOW's hybrid solvents are marketed as Ucarsol [753].

In the 1970s, BASF tried to reduce the cost of producing ammonia by scrubbing CO_2 from the synthetic gas. The solvent was initially only aqueous MDEA (patented in 1969 [754][3]) until PZ was added (German patent in 1977 [636] followed by US patent in 1982 [756]). The blend is sold as "activated MDEA" (aMDEA) which is slightly misleading and in contrast to the strict definition of an activator or (homogeneous) catalyst, because PZ reacts in parallel to MDEA with CO_2 [757], changes the equilibrium (loading), depletes during absorption, and does not decrease the activation energy without changing the transition state. Astarita *et al.* [758] describe PZ as a promoter which binds CO_2 as carbamate, "shuttles" it through the film layer, and shifts to bicarbonate with MDEA in the bulk close to equilibrium. Puxty *et al.,* [492] delivered an alternative explanation, which is more thoroughly backed up by data: Tertiary and sterically hindered amines are in general better bases than PZ and tend to accept the proton from the reacting PZ, thus, increasing the amount of free PZ at the interface compared to without the second amine present. This effect will also occur when their concentration is in excess compared to PZ [376, 492] as commonly found in activated blends. Regardless of the mechanism involved, the key principle is mixing a fast reacting amine with a highly loading amine to create a blend. BASF widely deployed their aMDEA technology after successful tests on one train of Pertamina's LNG site on Kalimantan (Borneo) in 1997 [353]. Union Carbide followed BASF in 1989 and claimed a tertiary amine *e.g.* MDEA (preferred) or TEA preferably promoted by ethylenediamine (EDA), diethylenetriamine (DETA), or tetraethylenepentamine (TEPA) with the promoter again having more than one amine group [139].

DOW Chemical and Union Carbide developed the GAS/SPEC[4] FT-1 technology and FS-1 solvent (originally inhibited [759] 30 wt% MEA) and delivered a 1120 t_{CO_2}/ day plant to Carbon Dioxide Technology Corporation in Lubbock, Texas in 1982 [454]. The process was sold to Fluor in 1989 and renamed Econamine FG[5]. It is now based on aqueous DGA[6] (also known as

[3]Note that the US patent from 1971 [755] additionally includes monomethylmonoethanolamine (MMEA)

[4]trademark now with INEOS and solvent MDEA based

[5]Not to be mistaken for the refrigerated Fluor Solvent process utilising propylene carbonate and regenerating the solvent by multi-stage flashing. It was commercialised in the 1960s with the first plant in Terrell County, Texas built in 1960.

[6]trademark protected by now Huntsman Corporation

amino-di-ethylene-glycol ADEG, or aminoethoxyethanol AEE) which is a primary amine and utilised in Fluor's "Improved Econamine" process. DGA has a lower vapour pressure and lower corrosion tendency than MEA and can be concentrated up to 60 wt%. The Econamine FG+ process additionally uses absorber-intercooling and is based on primary amines [462].

"Formulated" (designer) amines cover a broad range of molecules that are designed to do a specific task such as bulk absorption of CO_2 [245, 760]. Examples are commonly found in proprietary capture solvents with increasing molecular complexity. Sterically hindered amines are sometimes seen as separate chemical class but actually are per definition either primary amines attached to a tertiary carbon, or secondary amines attached to at least one secondary or tertiary carbon and were first patented in 1978 [761]. Sartori *et al.* of ExxonMobil define them as any primary or secondary amines with the amino group attached to a secondary or tertiary carbon [130, 131]. The key element is that steric hindrance towards the nitrogen makes the carbamate formation more difficult ("shielding"), or the carbamate less stable, thus shifting the reaction towards bicarbonate and protonated amine which should increase the limiting CO_2 to amine ratio. However, increasing the steric hindrance decreases the reaction rate [762]. Examples are 2-amino-2-methyl-1-propanol (AMP, α-dimethylated derivative of MEA) or DIPA (secondary amine). ExxonMobil added an alkaline promoter and are licensing the process as Flexsorb since 1983 [763]. The patent claims a blend of 1. a basic alkali metal salt or hydroxide, and 2. an activator for said basic salt or alkali metal salt or hydroxide comprising at least one sterically hindered amine. They claim, amongst others, N-cyclohexyl-1,3-propanediamine (sold as Baxxodur by BASF) to be especially preferred.

Kansai Electric Power Company KEPCO and Mitsubishi Heavy Industries Engineering MHIENG developed the KM CDR Process (Kansai Mitsubishi Carbon Dioxide Recovery Process, KP-1 packing, and KS-1[7] solvent, which contains a proprietary alkaline hindered amine that shows similarity to AMP [451, 462, 764–766]. This technology was first commercially deployed in 1999 for Petronas Fertilizer plant in Gurun Kedah (Malaysia) capturing 160 t_{CO_2}/ day and also deployed in Petra Nova in 2016 (coal power plant in Texas, USA) separating 4800 t_{CO_2}/ day. It is difficult to unravel the impact from the process, packing, and solvent as the exact solvent

[7] Other solvents are also branded KS with the latest being KS-21

composition is unknown. Patents mention amongst others EDA, DETA, 2PPE, 1DMA2P, and AMP (as preferable) [767, 768].

Cansolv[8] developed proprietary technology for sequential SO_2 and CO_2 capture, and its process, which includes a lean flash split with mechanical vapour compression, is in use at Boundary Dam's coal unit 3 located in Saskatchewan, Canada [631, 769, 770]. Surprisingly, Cansolv's amine maintenance cost for Boundary Dam were around $15 million per year which sparked far-reaching debates about the feasibility of CCS [771]. Cansolv offers two variants of its second generation CO_2 capture solvent DC-103 favouring minimising operational cost and the other DC-103B minimising capital cost. DC-103 is kinetically slower and has a lower heat of absorption than DC-103B [771]. Cansolv reported a specific reboiler duty of 2.33MJ/kg_{CO_2}, which has been widely shared although their solvent composition is proprietary. The value of 2.33MJ/kg_{CO_2} corresponds to their process with lean flash split and mechanical vapour compression operated at an absorber temperature of 36.5° and being fully integrated with a coal power plant's steam cycle [631, 772]. It is important to unravel and quantify the impact of the process topology, the integration into a coal plant, the operating conditions, and the solvent when comparing the 2.33MJ/kg_{CO_2} value with other studies. The solvent is an aqueous blend of a tertiary (di)amine mixed with a secondary (di)amine promoter, which is also acting as a buffer to stay within a specific pH region, and oxidation inhibitors (mixture of oxygen scavenger *e.g.,* sulfite, and free radical scavenger *e.g.,* thiosulfate). Their original patent filed in 2003 [515] claims a range of amines from simple molecules such as PZ to complex ones such as 4-(2-hydroxyethyl)-1-piperazineethane sulfonic acid (HEPES, tertiary diamine buffer), or N,N,N',N'-tetrakis(2-hydroxypropyl)-1,6-hexanediamine (tertiary diamine). [9] For the purpose and context of this academic analysis, a blend containing N,N'-di-(2-hydroxyethyl)piperazine (BHEPz, "piperazinediethanol" tertiary diamine), N-(2-hydroxyethyl)piperazine (HEPz, "piperazineethanol" secondary and tertiary) and/or piperazine shall suffice. As an example, 30 wt% BHEPz, 15 wt% HEPz, and 5 wt% PZ with the rest being water would classify as preferred under Cansolv's

[8] Cansolv was formed after a management buyout in 1997 from Union Carbide Corporation and is now owned by Shell.

[9] The general description embodies an aqueous solution with 10-50 wt% tertiary amine and 1-40 wt% secondary amine and another embodiment comprises 10-50 wt% of tertiary amine, 0-8 wt% PZ, 1-30 wt% of N-(2-hydroxyethyl)piperazine (HEP) with the remainder being water.

invention. Although this working example contains 50 wt% amine [631], the total effective molar fraction is only 11.1 mol% due to the high molar mass of the amines. Interestingly, this is the same value as for 30 wt% MEA.

Aker Carbon Capture's proprietary process and solvent is patented since 2013 [65] and claims an aqueous blend of DEA, MDEA, aminoethyl ethanolamine (AEEA), 2-(methylamino)ethanol (MMEA), and/or "mono methyl ethanolamine"[10]. They also hold patents on slurry/suspension-based capture with supermagnetic solid sorbents [516].

C-Capture developed a blend of at least one 2-6 molar metal-organic salt (C1-C8 carboxylate or phenolate), at least one water-miscible non-aqueous solvent (*e.g.,* Dimethyl sulfoxide (DMSO), NMP, or ethylene glycol monobutyl ether), at least one protic solvent (*e.g.,* MeOH, EtOH, glycerol, PEG), and/or a promoter (*e.g.,* PZ or 1,8-diazabicyclo[5.4.0]undec-7-ene, DBU) [773, 774]. The key difference to other blends is that the carboxylic acid salt (*e.g.,* tetrabutylammonium acetate, potassium hexanoate, potassium phenolate, potassium pivalate) does not contain an amino group. Phenolates were already patented in the 1930s [743, 775] and C-Capture developed this concept further. They could take advantage of solvent effects to influence the reactant's pK_a , which depends on the stability of its conjugate base, leading to different pK_a values for the same reactant in different solvents. Examples of solvent effects are *e.g.,* intramolecular hydrogen bonding, charge stabilising functional groups, or charge de-localisation which dissipate negative charges of the conjugate base. The blend preferably contains 50 wt% water (at least one mole of water per mole of captured CO_2 [773]), which, again, ends up to be less than 15 mol% total active ingredient. A key feature is the option of regenerating the solvent either by stripping, or, by injecting the solvent with a releasing additive (protic solvent) which creates a bi-phasic liquid that subsequently is regenerated by removing the additive again (*e.g.,* by using a membrane). The latter option resembles the concept of an "anti-solvent" [192, 697].

Carbon Clean's[11] solvent is a single-phase aqueous blend of alkanolamines, more reactive amines, and a carbonate buffer [776, 777]. It combines already discussed elements such as buffering the pH, using PZ (or its derivatives) as promoter, adding formulated sterically hin-

[10]Molecule is insufficiently named and creates ambiguity as it might be an isomer of N-Methylethanolamine.
[11]former Carbon Clean Solutions

dered amines for higher loadings, and reducing the water content. They tested an amine promoted buffer solution APBS-CDRMax at a coal power plant and reached 2.9-3.3 MJ/kg_{CO_2} [778, 779]. While the most preferred embodiment is not obvious, an example for their solvent is 20 wt% 2-amino-2-methylproponol, 2 wt% 2-methylamino-2-methyl-1-propanol, 22 wt% 2-piperazine-1-ethylamine, 0.3 wt% diethylenetriamine, 0.7 wt% potassium carbonate, with the remaining 55 wt% being water. Similar to CANSOLV, the effective mole fraction, *i.e.,* without the buffer, is only 11.8 mol% due to the high molar mass of the individual solutes.

Non-aqueous / water-lean solvents are a range of liquids containing concentrated organic binder without water / at low water contents and are met with scepticism due to the scarce data and often proprietary compositions despite being discussed since the 1980s [168, 263, 780]. Examples for non-aqueous blends are RITE's NAS, ION Engineering's solvent, GE's aminosilicones [781], PNNL's CO_2-Binding Organic Liquids (CO_2BOLs), RILs (non-nucleophilic amidine or guanidine superbase mixed with alcohol that reversibly binds CO_2 as alkylcarbonate salts) [87, 192]. They gained a lot of interest in recent years, yet lack commercial experience compared to aqueous amines. Their non-linear increase in viscosity when CO_2 is absorbed leads to high capture costs (due to equipment size and low lean loadings) and remains a main challenge [782]. Research into the tuning of the viscosity is carried out [168, 614, 615]. Non-aqueous amine solvents require 10-30% less energy for regeneration than their aqueous counterparts at the same total amine weight fraction [263]. RITE A and RITE B are IPAE based (50 wt% and 55 wt% respectively) with additives and measured 3.3 and 3.1 MJ/kg_{CO_2} at a 1 t/d pilot plant [783]. ION modelled their fast reacting ICE-21 solvent with a bespoke/proprietary ProTreat model which yielded a specific reboiler duty of 2.4 MJ/kg_{CO_2} at a 6 130 t/d plant [696, 784] and estimate the capture cost to $\$32.5/t_{CO_2}$. Interestingly, ION found removing the lean solvent cooler and absorber-intercooler reduces the total capture cost because their capital expense outweighs potential savings in operating costs due to cooler temperatures [696].

A.3 Other Capture Solvents

A.3.1 Chilled Ammonia

Ammonia is one of the most produced base chemicals in the world and predominantly used for fertilizers. The chilled ammonia process was proposed by Bai and Yeh [785, 786] in the late 1990s and the process additionally patented by Gal [787] (Alstom's CAP). The reaction route varies between ammonium carbamate (dry and low temperature and pressure), ammonium dicarbonate (moist and low temperature), or urea (high pressure and temperature) and the reaction products are solids [785]. The dry injection route is avoided because large ammonia volumes would be required which leads to HSE concerns (explosive limit for NH_3 gas is 15-28 vol% [785]). Updated chilled ammonia processes shift the solid formation outside the absorber into a dedicated crystallizer [788].

A.3.2 Physical Solvents

Examples of physical solvents are propylene carbonate (PC), dimethyl ether of polyethylene glycol (DEPG), methanol (MeOH), or N-methyl-2-pyrrolidone (NMP). The key differences to chemical solvents are the nearly pure composition (up to 10 wt% water), the absorption at elevated pressures, and the regeneration by multi-stage flashing instead of steam-stripping. Methanol was the first commercial organic physical solvent [753] with the earliest patents dating back to 1895 (as mentioned in German patent from 1909 [789]) and was utilised in ammonia plant, natural gas treating, dehydration units, and hydrocarbon recovery. It can operate at cryogenic temperatures without freezing or viscosity problems. Linde and Lurgi (now Air Liquide) independently developed the Rectisol process utilising MeOH in 1949[790] and now share the rights and patents.

Extensive research was carried out verifying the claim and existence of a 1904 patent for CO_2 capture. A standard textbook [742] mentioned a "German" patent from 1904 without accurately referencing the patent itself. Other literature subsequently adapted the textbook as reference for the claim. In fact, the patent was not issued by the German Empire but by the United

Kingdom [740] (and K.u.K. Austria [741]) and its inventors were based in Charlottenburg, Germany.

DEPG is utilised in DOW's Selexol (patent from 1953 [791] claims dimethoxytetraethylene glycol = tetraethylene glycol dimethyl ether, TEGDME as preferable) as well as Clariant's Genosorb, and the process is licensed by UOP as Selexol process and by Fluor as EconoSolv process. DEPG is limited by its high viscosity at low temperatures and has a higher selectivity towards H_2S than CO_2. It has been used in IGCC and syngas applications due to its high resistance to degradation and oxidation [753]. NMP is utilised in the Purisol process as licensed by Lurgi (now Air Liquide) and patented in 1966 [792]. NMP's vapour pressure is higher than PC or DEPG hence the absorption is operated at temperatures below 0℃.

A.3.3 Phase-Change Solvents

Phase-change solvents undergo a liquid-liquid phase separation upon CO_2 absorption or at increased temperature. The CO_2-lean phase is recycled to the absorber and only the CO_2-rich phase is regenerated. This reduces the solvent flowrate in half of the capture plant and also requires less heat for the regeneration (close to 2 GJ/ton_{CO_2} [793–795]). The blends commonly contain poly-amines. Examples are DEEA+MAPA, DAB+DEEA, DMX (developed by IFP Energies Nouvelles) or TBS = CHxA + DMCA (developed by University of Dortmund) [793, 794]. Reviews of these solvents and their systems are available in [796] .

A.3.4 Ionic Liquids

Ionic Liquids are liquid organic salts and often referred to as "designer molecules" due to their thermo-physical properties being tune-able via their ion-pairs. They date back to the late 19th century [797] / early 20th century [241, 798] and gained a lot of interest for clean technology applications in the late 1990s [799] with the number of publications increasing from hundreds to thousands. Task-specific ionic liquids [800] for CO_2 capture, *e.g.,* tetraethylammonium acetate tetrahydrate (TEAA), tetramethylammonium malonate monohydrate (TMAM), or tetramethylammonium fluoride tetrahydrate (TMAF), were first patented in 1990 by Air

Products researchers [801][12]. Conventional ionic liquids are physical solvents and they become chemical solvents if added by suitable moieties [803]. The low vapour pressure and high solubility make them promising for CO_2 capture, however, their high viscosity leads to low mass transfer rates [804]. Reversible ionic liquids (RILs) are solvents that convert between non-ionic liquid and ionic liquid state upon contact with a trigger *e.g.,* CO_2 and are based on *e.g.,* amidines and guanidines. They are water-lean and highly viscous [192]. Reviews on ionic liquids are available in [168, 805–815] and a collection of 20 studies on ionic liquids and deep eutectic solvents for CO_2 capture using semi-empirical, artificial intelligence, quantum chemistry group contributions, or a mix of these approaches is presented in [262]. Thermodynamic methods for screening ionic liquids and deep eutectic solvents are reviewed in [816, 817].

A.3.5 Deep Eutectic Solvents

Deep eutectic solvents (DESs) are similar to ILs yet they need to be classified separately to them (despite some authors considering them a subclass of ILs) [818]. DESs consist of a hydrogen bond acceptor of halide salts and an organic hydrogen bond donor which leads to strong hydrogen bond networks significantly depressing the freezing point. High thermal and chemical stability, and low solvent volatility make DESs promising candidates, yet data is rather limited [819–821]. Recent reviews on DES are available in [806–813, 819, 822–827].

A.3.6 Amino Acids

Amino acids salts are handled like conventional aqueous solvents, react fast, and have good HSE features [656, 658]. Although they were already analysed by Bottoms in the 1930s, they recently re-gained in attention [828, 829] including DAC(CS) [830]. Despite being already analysed by Bottoms in the 1930s and further developed by Siemens (PostCap), AASs have a low commercial readiness [828].

[12]other patent from 1988 claims a membrane containing ILs, *e.g.,* tetrahexylammonium benzoate, THAB) [802]

A.4 List of Screening Studies

Table A.1: List of experimental and modelling screening studies sorted by number of amines and categorised by approach (experimental vs modelling) and KPIs. Other KPIs include *e.g.,* transport properties, absorption rate, pK_a, or degradation. Short-cut modelling indicated with brackets.

Reference	# Amines	Experimental	Modelling	VLE	Kinetics	ΔH_{Abs}	L/G	$\dot{Q}_{\text{Reb}}$	\$/ton$_{\text{CO}_2}$	other	Comment
[198]	132	✓		✓						✓	y_{CO_2}= 15 mol% and 40℃, some at 30℃ and p_{CO_2} = 10 kPa
[268]	125		✓	✓		✓				✓	focus on ten criteria including HSE and transport-properties
[229]	76	✓		✓						✓	constant 30 wt%
[831]	50		✓					✓			CAMD
[242]	50	✓		✓		✓				✓	30 wt%, p_{CO_2}= 13.5 kPa (rich) and 1.35 kPa (lean) at 40℃
[274]	46		✓							✓	estimated maximum stripper temperature and degradation
[179]	41		✓	✓		✓				✓	Cheminformatics, 41 amines for VLE, 37 for kinetics, 26 for for capacity, 37 for rate, 26 for ΔH_{Abs}
[832, 833]	33	✓		✓							Landmark paper deriving structure-property relationships
[246]	32	✓		✓							Systematically designed of di- and tri-amines. Tested at 40℃ and 90℃, y_{CO_2}= 10 mol%
[197]	30	✓		✓	✓	✓					30 wt%, y_{CO_2} = 15mol% CO2, 40℃

Continued on next page

Table A.1 – *continued from previous page*

Reference	# Amines	Experimental	Modelling	VLE	Kinetics	ΔH_{Abs}	L/G	$\dot{Q}_{\text{Reb}}$	$/ton$_{CO_2}$	other	Comment
[245]	30	✓		✓						✓	piperidine derivatives, constant 2M concentration, y_{CO_2} = 15% CO2, 40℃and 90℃, all 2M conc, most better than MEA
[834]	29		✓							✓	multi criteria decision to find best solvent mixtures. No actual capture plant designed.
[145]	29		✓							✓	reaction rate and carbamate stability is correlated
[602]	28		✓	✓		✓					30 wt%, 40℃, p_{CO_2}= 15kPa,
[225]	27	✓		✓							30℃, p_{CO_2}= 1-40kPa
[603]	26	✓		✓		✓					30 wt%
[234]	26	✓									Phase change solvents, DETA + DEEA best
[223]	24	✓		✓		✓					30 wt%
[186]	24		✓		✓						molecular dynamics with classical force fields to predict kinetics
[604]	21	✓		✓		✓					30 wt%
[167]	20	✓		✓							Summarised rigorous thermodynamic models and lists VLE sources for MEA, DEA, MDEA, AMP and PZ until 2012.

Continued on next page

Table A.1 – *continued from previous page*

Reference	# Amines	Experimental	Modelling	VLE	Kinetics	ΔH_{Abs}	L/G	$\dot{Q}_{\mathrm{Reb}}$	$/ton$_{CO_2}$	other	Comment
[272]	20		✓	✓							density functional theory, develop QSPR for VLE with only four descriptors.
[835]	19		✓							✓	Quantum chemical calculations
[158]	17	✓			✓					✓	reviews kinetics for alkanolamines
[244]	17	✓								✓	40℃, heterocyclic piperidine like molecules, FT-IR analysis
[836]	16	✓		✓			✓				Castor project
[837]	15	✓		✓			✓			✓	optimised concentration, 40℃ and 90℃,
[135]	15		✓							✓	used density functional theory and Monte-Carlo free-energy perturbations and continuum models
[838]	14	✓		✓							
[224]	14	✓		✓	✓	✓					30 wt%
[133]	13	✓		✓	✓	✓				✓	commanding review of properties of sterical hindered amines
[839]	13	✓		✓							conventional amines for DAC
[273]	13		✓							✓	continuum cluster model (condensed-phase quantum computation)

Continued on next page

Table A.1 – *continued from previous page*

Reference	# Amines	Experimental	Modelling	VLE	Kinetics	ΔH_{Abs}	L/G	$\dot{Q}_{\text{Reb}}$	$/ton$_{CO_2}$	other	Comment
[605]	12	✓		✓		✓					30 wt%
[187]	12	✓		✓							11 diamines + MEA, all at constant 2M concentration, 40℃, p_{CO_2}= 15 kPa and 100 kPa
[840]	11	✓		✓		✓					30 wt%
[606]	10	✓		✓		✓	✓	(✓)		✓	30 wt%
[250]	10	✓					✓	✓			only two tested at pilot scale, 10 full study
[227]	10	✓		✓							40℃ and 80℃
[841]	10	✓		✓							five primary amines and five secondary amines always with K_2CO_3, 70℃ and 90℃
[253]	10	✓		✓		✓					30 wt% (single amines and blends), 40℃, p_{CO_2}= 15 kPa
[149]	10	✓			✓						
[616]	10	✓		✓		✓					tertiary amines, kinetics and loading loading relationships at 25-40℃
[128]	10		✓							✓	DFT-B3LYP simulations

Continued on next page

Table A.1 – *continued from previous page*

Reference	# Amines	Experimental	Modelling	VLE	Kinetics	ΔH_{Abs}	L/G	$\dot{Q}_{\text{Reb}}$	$/ton$_{CO_2}$	other	Comment
[783]	9	✓		✓		✓		✓			30 wt%, 40℃, y_{CO_2}= 20 mol% (steel blast furnance). Lab scale and 1t/d pilot plant (only three tested at pilot plant).
[263]	9		✓	✓			✓	✓			soft-SAFT and Grand Canonical Monte-Carlo simulations, short cut modelling and compares to adsorbents
[699]	9	✓		✓	✓						CO_2BOL ternary mix: DBU (superbase) + alcohol + amine as promoter, statistical mixture design, 35℃, 25 bar
[237]	9	✓		✓		✓					
[824]	9	✓			✓						established pK_a Brønsted correlations based on only nine solvents
[842]	9	✓			✓						
[270]	9		✓	✓		✓					Created surrogate model, find MEA to be best available technology
[188]	9	✓								✓	identified pKa and carbamate concentration
[182]	8	✓		✓							cocentration constant at 2.5M, y_{CO_2}= 4.7 and 1.1 mol%, includes five carboxylate salts

Continued on next page

Table A.1 – *continued from previous page*

Reference	# Amines	Experimental	Modelling	VLE	Kinetics	ΔH_{Abs}	L/G	$\dot{Q}_{\text{Reb}}$	$/ton_{CO_2}$	other	Comment
[843]	8	✓		✓							bi-phasic solvents at different concentrations, found 1,2-DMBA + DEEA as best solvent
[153]	8	✓								✓	pKb as KPI
[617]	8	✓		✓							6 diamines, 40℃
[844]	8	✓		✓						✓	non-aqueous
[845]	8	✓		✓							40℃, single amines and blends
[199]	8	✓		✓						✓	5 wt%, 23℃ and 100℃,
[132]	8		✓							✓	initio quantum chemical calculations, combined with the SMD solvation model
[846]	7	✓		✓		✓					30 wt% and some > 30 wt%
[189]	7		✓	✓		✓	✓				Created artificial solvents to observe impact of VLE via Gibbs–Helmholtz
[847]	7	✓			✓						
[360]	7	✓		✓							constant mass fraction, historic overview
[219]	6	✓		✓				(✓)		✓	

Continued on next page

Table A.1 – *continued from previous page*

Reference	# Amines	Experimental	Modelling	VLE	Kinetics	ΔH_{Abs}	L/G	$\dot{Q}_{\text{Reb}}$	$/ton$_{CO_2}$	other	Comment
[848]	6	✓		✓	✓					✓	
[780]	6	✓		✓		✓					
[141]	6	✓		✓		✓				✓	impact of amine groups
[849]	6	✓		✓							y_{CO_2} 15% and 40%, 5060℃and 100120℃,
[236]	5	✓		✓			✓	(✓)			30 wt%, absorption-desorption, 40℃, 80℃
[233]	5	✓		✓							varying concentrations
[850]	5	✓		✓							designer cyclic poly-amines
[851]	5	✓		✓							max. 50 wt% amine, blends always 50 wt%
[852]	5	✓		✓						✓	
[853]	5	✓		✓							phase change solvents, 40℃, p_{CO_2}= 10 kPa, DMCA–MCA–AMP highest loading with 44 wt%
[854]	5	✓		✓							30 wt%, y_{CO_2}= 20 mol% CO2, 40℃,
[266]	5		✓	✓						✓	density functional theory with dielectric continuum solvation models (SMD/IEF-PCM and COSMO-RS)
[637]	5	✓					✓				constant amine concentration

Continued on next page

Table A.1 – *continued from previous page*

Reference	# Amines	Experimental	Modelling	VLE	Kinetics	ΔH_{Abs}	L/G	$\dot{Q}_{\text{Reb}}$	\$/ton$_{\text{CO}_2}$	other	Comment
[855]	4		✓				✓	✓	✓		superstructure flowsheeting
[115]	4		✓				✓	✓	✓		ProTreat, integrated for gas and ultra-supercritical coal power
[171]	4		✓			✓		(✓)		✓	
[290]	4		✓				✓	✓	✓		compares aqueous amine, precipitating and encapsulated solvent to 30 wt% MEA
[856]	4	✓					✓	✓			BASF solvents
[236]	4		✓	✓			✓	✓			30 wt%, absorption-desorption, 40℃and 80℃
[836]	4		✓	✓			✓				Castor project
[638]	4	✓		✓				✓			
[782]	4	✓		✓		✓				✓	non-precipitating, single-phase, non-aqueous solvents
[857]	4	✓			✓						Analysed effect of hydrophobic replacements for water
[858]	4	✓		✓		✓					30 wt%
[859]	4	✓		✓		✓					Toshiba commercial solvent
[248]	4	✓		✓						✓	Blending four amines, changes concentration
[232]	4	✓		✓							biphasic solvents, analysed impact of concentration

Continued on next page

Table A.1 – *continued from previous page*

Reference	# Amines	Experimental	Modelling	VLE	Kinetics	ΔH_{Abs}	L/G	$\dot{Q}_{\mathrm{Reb}}$	$/ton$_{CO_2}$	other	Comment
[626]	4		✓	✓						✓	developed Kent-Eisenberg VLE model
[170]	4	✓									
[184]	3		✓				✓	✓	✓		genetic algorithm analysis
[184]	3		✓				✓	✓	✓		Aspen Plus, genetic optimisation, integrated into coal power
[860]	3	✓					✓	✓			tested CESAR1 and CESAR2
[783]	3	✓		✓		✓		✓			30 wt%, 40℃, y_{CO_2}= 20 mol% (steel blast furnance). Lab scale and 1t/d pilot plant (only 3 tested at pilot plant).
[618]	3	✓		✓		✓					three di-amines
[861]	3	✓			✓						
[862]	3	✓		✓							RITE setup
[619]	3	✓								✓	three di-amines investigated as kinetic promoters for tertiary amines
[863]	2		✓				✓	✓	✓		CDRMax (amine-promoted buffer salt) and MEA, SAFT and rate-based modelling, integrated into coal power
[864]	2		✓				✓	✓		✓	SAFT and rate-based modelling, integrated into NGCC power

Continued on next page

Table A.1 – *continued from previous page*

Reference	# Amines	Experimental	Modelling	VLE	Kinetics	ΔH_{Abs}	L/G	$\dot{Q}_{\text{Reb}}$	\$/ton$_{\text{CO}_2}$	other	Comment
[250]	2	✓					✓	✓			only two tested at pilot scale, ten full study
[630]	2	✓			✓					✓	replaced water with organic solvents
[865]	2	✓		✓		✓					15 wt% and 30 wt%, two designer di-amines
[690]	2	✓				✓				✓	impact of pH
[866]	1		✓				✓	✓		✓	integrated with IGCC power plant
[867]	1		✓					✓			Aspen modelling, coal-power
[235]	1	✓		✓						✓	MEA + physical co-solvent, different concentrations of co-solvent
[416]	1	✓								✓	Poly(ethylenimine) largest amine analysed in literature at 10000 g/mol
[249]	1	✓								✓	all solvents are BZA based: 30 wt% BZA + 30 wt% of co-solvent at 40℃
[247]	1		✓								Systematic blending 2.5M MEA + another amine
[262]	1		✓							✓	DES and ILs (physical solvents), p_{CO_2}> 1000 kPa, short-cut modelling

A.5 More Structure Property Relationships

The impact of substituents at α- (carbon adjacent to the amine group) and β-positions of primary or secondary amines is of great interest as this offers the opportunity to tune the basicity through steric and electronic effects and increase the absorption capacity by shifting the equilibrium from carbamate to bicarbonate. These effects are not to be mistaken, although similar in principle, with the α-effect, which describes the impact of an atom's lone electron pair in α-position on the nucleophilicity, because the amino-nitrogen with its own lone electron pair is the main nucleophile [868, 869]. Electron-withdrawing[13] groups (higher electronegativity than carbon, *e.g.,* hydroxyl groups) in close proximities to unhindered primary or secondary alkalinities reduce their charge density and their affinity to act as nucleophile. This reduces the alkalinity's pK_a, loading, and reaction rate. The opposite is true for electron donating substituents (*e.g.,* alkyl chains) that increase the electron density, make the alkalinity a better nucleophile, and thus the loading and rate of unhindered primary and secondary amines increases. However, bulky substituents in close proximity to the nitrogen can also cause steric hindrance to the extent that carbamate formation is completely suppressed [149].

Similar considerations apply to tertiary amines although no direct reaction occurs. Interestingly, the effects of electron donating and withdrawing substituents on the loading of tertiary amines are the opposite of hindered primary and secondary amines. Donating electrons towards the nitrogen will increase its reactivity and loading *e.g.,* an ethyl substituent will increase the reactivity more than an methyl group. Electron withdrawing groups (*e.g.,* hydroxyethyl groups) achieve the opposite effect and reduce both absorption rate and loading [616]. The electron withdrawing effect weakens with distance to the nitrogen and can be neglected if the hydroxyl group is placed more than three carbon atoms away from the nitrogen (*i.e.,* at δ-position) [870]. Intra-molecular bonds in tertiary amines are undesirable because they decrease the charge at the nitrogen and reduce its reactivity [616]. However, these intra-molecular bonds (*e.g.,* hydrogen bonding in alkanolamines leading to ring-structures) will be weaker compared to primary or secondary amines because the other two (non ring-forming) carbon substituents "shield" the

[13] Also known as inductive effect

nitrogen through steric hindrance [616].

Electron-withdrawing groups tend to destabilise the carbamate of hindered amines, because[14] the Π_{Me} and Π^*_{Me} orbitals interact with the lone pair of the nitrogen which reduces its electron density, weakens the N-H bond, and thus makes it a softer base which hydrolyses easier. Electron-donating substituents cause the opposite effect and stabilise the reaction product. However, adding two methyl groups at the α-position creates so much steric hindrance that the equilibrium is fully shifted to bicarbonate [182]. Confusingly, Yoon and Lee [871] found both electron donating and withdrawing groups (methyl and hydroxyl groups) at the β-position act as electron donors that stabilised the resulting carbamate of AMP, AMPD and AEPD.

Singh *et al.,* [225, 833, 838] systematically analysed in total 47 structure derivatives and their impact on loading and absorption rate. Their studies represent the so-far broadest attempt at deriving structure-property relationships as most follow-up studies target a subset of molecular structures. They elegantly emphasize the difference between molar and weight based loadings. No general trends that were valid for all type of amines were observed, but they derived a series of sub-trends valid for a selective few solvents. Changing the carbon chain length of linear and unhindered alkanolamines, alkylamines, and di-amines increased loading and absorption rate for most amines. Interestingly, alkylamines and di-amines with a C_6 chain length had the highest loading and fastest absorption rate appearing to be a sweetspot (local maximum). Introducing steric hindrance at the α-position with one methyl or hydroxyl group affects the loading and rate according to Table 2.2. Alkyl substituents and further alkalinities increase the absorption rate and capacity of amines as long as they do not add any steric hindrance. If these substituents create steric hindrance, then no general prediction is possible. Perinu *et al.,* [153, 188, 690] also used NMR to quantify the impact chain length and number of hydroxyl groups in blends. They found that the amount of carbamate reduced with increasing basicity (lower pK_b) and that tertiary amines blended with MAPA increase the availability of MAPA's alkalinities.

Researchers at CSIRO have analysed relationships between amine structure and reaction path-

[14] simplifying both field effects (through space electrostatic interaction) and resonance effects (through the Π-electrons) into one single causality although these effects are independent from each other.

ways. Fernandes *et al.,* [126] measured the protonation constant and molar enthalpies of formation of 20 amines in the temperature range 288-318 K. They found that adding a OH-group increases the standard molar enthalpy of protonation ΔH_{m} by ≈5 kJ/mol which reduces the exothermicity (assuming constant ΔS_{m}) regardless of the chemical class (primary, secondary, tertiary) *e.g.,* alkylamines more exothermic than trialkanolamines. This disagrees with the findings by Xiao *et al.,* [616] who found that the heat of absorption increased by adding hydroxyl groups to tertiary amines. Fernandes *et al.,* [126] confirmed the general trend that on average primary amines are more exothermic than secondary and then tertiary amines, however, this is merely a rule of thumb and by no means an exclusive criterium. A third study [237] disagrees with both Xiao *et al.,* [616] and Fernandes *et al.,* [126] and found that primary, secondary, or tertiary alkanolamines with one hydroxyl group is only optimal if the OH-group is creating moderate steric hindrance.

Researchers from CSIRO and China (Hunan University and Tsinghua University) [617–619, 865, 872] analysed in total twelve mostly linear diamines with C_2 or C_3 alkyl chains and a constant primary alkalinity, and derivatives of the cyclic[15] designer di-amine 4A1MPD [850]. They found that increasing the number of substitutions on the other alkalinity and increasing the length of the alkyl chain improves the desorption performance (cyclic capacity and faster desorption rate) more than the absorption performance. The chain length (distance) between the amino groups is important as the first protonated alkalinity reduces the pK_a of the second amino group by withdrawing electrons from the second alkalinity. It appears to have a threshold between C_2 and C_3 as the longer distanced di-amines showed higher loadings [187, 850].

Conway *et al.* [149], analysed the effect of steric hindarance and electronic effect of 10 sterically hindered amines. They find that adding a CH_3-group at the β-position relative to the amine nitrogen of branched amines introduces no significant steric hindrance and those amines follow the well known linear Brønsted-relationships of unhindered amines (also confirmed more recently in [132, 381]). Unsurprisingly, they find that increasing the steric hindrance even with just a single CH_3-group at the α-position drastically reduces the kinetic constant. They conclude that

[15]Cyclic features introduce mild steric hindrance which shifts the equilibrium away from carbamate to bicarbonate but also increase the viscosity.

the goal is synthesizing an amine that is strongly basic and sterically hindered but not to the extent that the formation of the fast reacting carbamate is suppressed. In general, Brønsted relationships are more accurate and trustworthy than the rule of thumb between enthalpy and chemical structure identified in [126]. Quantum chemical calculations confirmed these trends by analysing 19 amines and found secondary alkanolamines with moderate sterical hindrance near the alkalinity to be high-potential candidates [835].

Puxty *et al.*, [229] found no correlation between absorption capacity and pK_a for primary or secondary amines because their capacity depends only on the carbamate's stability which differs from amine to amine. They report a "strong" dependence for tertiary amines as the dominating CO_2 hydration reaction strongly depends on the pH/pK_a due to small stability constants for bicarbonate, but the correlation is rather weak compared to the trends identified in [149]. Puxty *et al.*, observed primary and secondary amines that outperformed their pK_a based predictions and explained these with the carbamic acid not being acidic enough (*i.e.,* $pK_a < 7$ not met) due to the Lewis basicity of the nitrogen. This means the carbamic acid would be a weak acid and would not protonate another amine molecule, therefore increasing the CO_2 to amine ratio.

Xie *et al.* [183] and Lee and Kitchin [185] analysed the impact of substituting groups (CH_3, NH_2, OH, OCH_3, and F) at the α- and β-position of MEA on the heat of absorption by using ab initio continuum modelling coupled with geometries generated by density functional theory (DFT). They found that the heats of absorption and the relative basicities correlate linearly for both carbamate and carbamic acid (lower basicity means lower exothermic heat)[16]. Carbamates were much more sensitive to changes in basicity leading to the formation of carbamic acid becoming thermodynamically favoured at the weakest basicities and thus increasing the CO_2 to amine ratio from 1:2 to 1:1. Recent ab-initio quantum chemical calculations confirm that the instability of AMP's carbamate is caused by electric effects from the α-methyl groups [132].

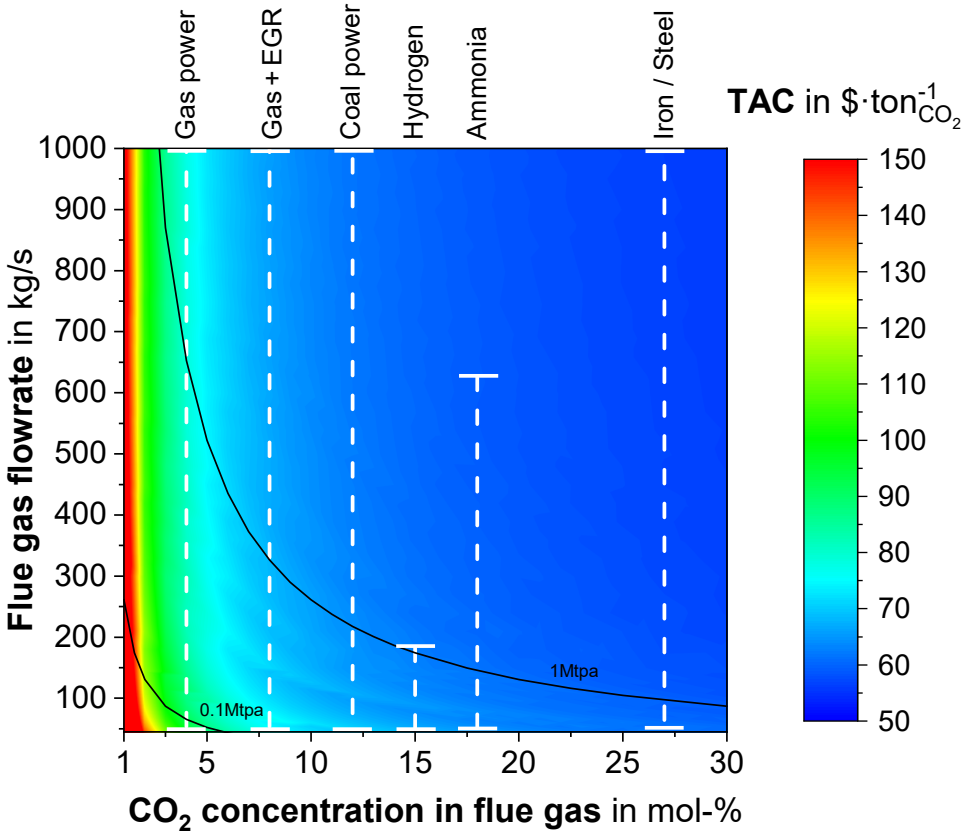


Figure A.1: Impact of flue gas flowrate and CO_2 concentrations on capture cost (TAC) with common flue gas sources at a capture rate of 90%. Black lines indicate annual captured CO_2 at 1 $Mtpa_{CO_2}$ and 0.1 $Mtpa_{CO_2}$ being the minimal threshold to be eligible for the 2021 §45Q tax credit. Solvent is 30 wt% MEA. Adopted from [112].

A.6 Effect of Plant Scale

A range of different flue gas sources has to be decarbonised with a varying impact on sequestered CO_2, *e.g.,* a steel/iron plant will capture seven times more total CO_2 ($Mtpa_{CO_2}$) at the same flue gas flowrate and capture rate than a typical gas-fired power plant. Given that sizes of power and industrial plants significantly vary, it is important to quantify the impact of plant scale on cost as a function of flue gas CO_2 concentration (see Figure A.1). Typical flue gas compositions are indicated with white vertical lines, including gas-power, gas-fired power plant with exhaust gas recycle (EGR) and coal-power, also the maximum $y_{CO_2} = 30\%$ covers common industrial processes such as hydrogen, ammonia and iron/steel [873–875]. These representative concentrations are based on typical processes with exhaust gas at atmospheric pressure, but

[16] meaning $|\Delta H_{Abs}|$ shrinks

the concentration depends on the process conditions and will vary in practice. The upper limit Figure A.1 is set by typical flowrates of power plants, *e.g.,* 914 kg/s for a 528 MW_{net} supercritical coal-fired power plant (650 MW_g), and 905 kg/s for a 506 MW_{net} natural gas-fired combined cycle plant. A large steel plant emits around 500 kg/s accounting for the lime and coke production as well as the hot stoves (excluding the power plant) [873].

The capture cost is relatively constant at high CO_2 concentrations $y_{CO_2} > 10\%$ (blue region) across the range of flue gas flow rates. In general, there is limited evidence of any impact of scale, except in the case of relatively low flow rates and low CO_2 concentrations. Interestingly, a particular tipping point in CO_2 concentration appears at relatively low CO_2 concentrations at which a strong relationship between CO_2 concentration and cost exists. The strength of this relationship declines at CO_2 concentrations beyond approximately 10%. It is therefore unlikely that economy of scale will decrease cost to the extent as it is widely assumed.

A.7 Distributions

The asymmetrical χ^2 distribution depends on the degree of freedom *df* (number of observations minus one). A normal distribution is a good estimation for a χ^2 distribution if $df > 90$ [322]. The mean is equal to *df* and is greater then median and mode. The standard deviation is $\sqrt{2 \cdot df}$. A *t*-distribution is a type of normal distribution with unknown variance and often used to find confidence intervals. As with the χ^2 distribution, the *t*-distribution appropriates a normal distribution with increasing degrees of freedom $df > 30$.

B. Supporting Information for SQUASH

B.1 Database

B.1.1 Solvent Candidates: Amines

Table B.1: List of candidate amines with IUPAC name, abbreviation as used in this thesis, chemical class, CAS number, molecular sum formula, molar mass, and PubChem ID. Some amines do not have a CAS number or abbreviation assigned.

Nr	IUPAC	Abbreviation	Chemical Class	CAS Nr.	Molecular Formula	Molar Mass g/mol	PubChem ID
1	1-(2-Hydroxyethyl)pyrrolidine	1-(2HE)PRLD	c-3	2955-88-6	$C_6H_{13}NO$	115.2	76288
2	1,2-Cyclohexanediamine	1,2-DACH	c-2 + c-2	694-83-7	$C_6H_{14}N_2$	114.2	4610
3	1,3-Dimethylbutylamine	1.3-DMBA	primary	108-09-8	$C_6H_{15}N$	101.2	7908
4	1-amino-butan-2-ol	1A2B	primary	13552-21-1	$C_4H_{11}NO$	89.1	26107
5	1-Dimethylamino-2-propanol	1DMA2P	tertiary	108-16-7	$C_5H_{13}NO$	103.2	37511
6	1-Ethyl-3-hydroxypiperidine	1E3HPP	c-3	13444-24-1	$C_7H_{15}NO$	129.2	114524
7	1-Ethyl-N,N-dimethylbutylamine (3-(Dimethylamino)hexane)	1EDB	tertiary	24552-03-2	$C_8H_{19}N$	129.2	559740
8	1-Methylamino-propan-2-ol	1M2P	secondary	16667-45-1	$C_4H_{11}NO$	89.1	86049

Continued on next page

Table B.1 – *continued from previous page*

Nr	IUPAC	Abbreviation	Chemical Class	CAS Nr.	Molecular Formula	Molar Mass g/mol	Pub-Chem ID
9	1-Methyl-2-piperidineethanol	1M2PPE	c-3	533-15-3	$C_8H_{17}NO$	143.2	98085
10	1-piperidinomethanol	1PPE	c-3	2494-10-2	$C_6H_{13}NO$	115.2	446909
11	1-piperidinepropanol	1PPPr	c-3	104-58-5	$C_8H_{17}NO$	143.2	66032
12	2,5-Dimethylpiperazine	25-t-DMPz	c-2 + c-2	106-55-8	$C_6H_{14}N_2$	114.2	7816
13	2-Amino-1-butanol	2A1B	primary	96-20-8	$C_4H_{11}NO$	89.1	22129
14	2-Amino-1-hexanol	2A1H	primary	5665-74-7	$C_6H_{15}NO$	117.2	249006
15	2-Amino-1-pentanol	2A1PN	primary	4146-04-7	$C_5H_{13}NO$	103.2	249017
16	2-(Amino)-propanol	2AP	primary	6168-72-5	C_3H_9NO	75.1	5126
17	2-Heptylamine	2-HtA	primary	123-82-0	$C_7H_{17}N$	115.2	5603
18	2-Methylimidazole	2MIMI	c-2 + c-2	693-98-1	$C_4H_6N_2$	82.1	12749
19	2-methylpiperazine	2MPZ	c-2 + c-2	109-07-9	$C_5H_{12}N_2$	100.2	66057
20	N,N,N',N',2-Pentamethyl-1,2-propanediamine	2P12P	tertiary + tertiary	68367-53-3	$C_8H_{20}N_2$	144.3	110069

Continued on next page

Table B.1 – *continued from previous page*

Nr	IUPAC	Abbreviation	Chemical Class	CAS Nr.	Molecular Formula	Molar Mass g/mol	Pub-Chem ID
21	2-Piperidineethanol	2PPE	c-2	1484-84-0	$C_7H_{15}NO$	129.2	15144
22	2-piperidinemethanol	2PPM	c-2	3433-37-2	$C_6H_{13}NO$	115.2	94263
23	3-Amino-1-propanol	3AP	primary	156-87-6	C_3H_9NO	75.1	9086
24	3-(Diethylamino)-1-propanol	3DEAP	tertiary	622-93-5	$C_7H_{17}NO$	131.2	12159
25	3,3'-Methyliminobis(N-methylpropylamine)	3-DMAPA	secondary + secondary + tertiary	123-70-6	$C_9H_{23}N_3$	173.3	67161
26	3-Methylpiperidine	3MPD	c-2	626-56-2	$C_6H_{13}N$	99.2	79081
27	3-Piperidinopropylamine	3PDPA	primary + c-3	3529-08-6	$C_8H_{18}N_2$	142.2	19049
28	3-Phenylpropylamine	3PPA	primary	2038-57-5	$C_9H_{13}N$	135.2	16259
29	3-piperidinemethanol	3PPM	c-2	4606-65-9	$C_6H_{13}NO$	115.2	107308
30	4-Amino-1-butanol	4A1B	primary	13325-10-5	$C_4H_{11}NO$	89.1	25868
31	4-Amino-1-methylpiperidine	4A1MPD	primary + c-3	41838-46-4	$C_6H_{14}N_2$	114.2	2737531

Continued on next page

Table B.1 – *continued from previous page*

Nr	IUPAC	Abbreviation	Chemical Class	CAS Nr.	Molecular Formula	Molar Mass g/mol	Pub-Chem ID
32	1-Propylpiperidin-4-amine	4A1PPD	primary + c-3	42389-59-3	$C_8H_{18}N_2$	142.2	541730
33	4-Amino-2-butanol	4A2B	primary	39884-48-5	$C_4H_{11}NO$	89.1	170254
34	4-(Aminomethyl)piperidine	4AMPD	primary + c-2	7144-05-0	$C_6H_{14}N_2$	114.2	23527
35	4-Aminomethyltetrahydropyran	4AMTHP	primary	130290-79-8	$C_6H_{13}NO$	115.2	2773210
36	4-Amino-pentanol	4AP	primary	927-55-9	$C_5H_{13}NO$	103.2	95309
37	4-Aminopiperidine	4APD	primary + c-2	13035-19-3	$C_5H_{12}N_2$	100.2	424361
38	4-(Dimethylamino)butan-2-ol	4DMA2B	tertiary	5867-64-1	$C_6H_{15}NO$	117.2	10855427
39	4-(morpholin-1-yl)butan-2-ol	4M2B	c-3	858440-45-6	$C_8H_{17}NO_2$	159.2	14555601

Continued on next page

Table B.1 – *continued from previous page*

Nr	IUPAC	Abbreviation	Chemical Class	CAS Nr.	Molecular Formula	Molar Mass g/mol	Pub-Chem ID
40	4(5)-Methylimidazole	4MIMI(4M-IMI)	c-2 + c-2	822-36-6	$C_4H_6N_2$	82.1	13195
41	4-Methylpiperidine	4MPD	c-2	626-58-4	$C_6H_{13}N$	99.2	69381
42	4-propylamino-2-butanol	4PA2B	secondary		$C_7H_{17}NO$	131.2	59668597
43	4-(piperidin-1-yl)butan-2-ol	4PP2B	c-3	71648-40-3	$C_9H_{19}NO$	157.3	13155989
44	4-(2-Hydroxyethyl)piperidine	4PPE	c-2	622-26-4	$C_7H_{15}NO$	129.2	73953
45	4-piperidinemethanol	4PPM	c-3	6457-49-4	$C_6H_{13}NO$	115.2	420771
46	5-Amino-pentanol	5AP	primary	2508-29-4	$C_5H_{13}NO$	103.2	75634
47	6-Amino-1-hexanol	6AH	primary	4048-33-3	$C_6H_{15}NO$	117.2	19960
48	2-[(4-Aminocyclohexyl)amino]ethanol	ACHAE	primary + secondary		$C_8H_{18}N_2O$	158.2	84221714
49	N-(2-aminoethyl)ethanolamine	AEEA	primary + secondary	111-41-1	$C_4H_{12}N_2O$	104.2	8112

Continued on next page

Table B.1 – *continued from previous page*

Nr	IUPAC	Abbreviation	Chemical Class	CAS Nr.	Molecular Formula	Molar Mass g/mol	PubChem ID
50	1-[2-Aminoethyl(1-hydroxyethyl)amino]ethanol	AEHEAE	primary + tertiary		$C_6H_{16}N_2O_2$	148.2	21871717
51	4-(2-aminoethyl)morpholine	AEM	primary + c-3	2038-03-1	$C_6H_{14}N_2O$	130.2	408285
52	2-Amino-2-ethyl-1,3-propanediol	AEPD	primary	115-70-8	$C_5H_{13}NO_2$	119.2	8282
53	N3-Amine 3-(2-Aminoethylamino)propylamine	AEPDA	primary + primary + secondary	13531-52-7	$C_5H_{15}N_3$	117.2	26091
54	1-(2-aminoethyl)piperidine	AEPP	primary + c-3	27578-60-5	$C_7H_{16}N_2$	128.2	33944
55	1-(2-aminoethyl)piperazine	AEPz	primary + c-2 + c-3	140-31-8	$C_6H_{15}N_3$	129.2	8795
56	4-amino-1-(2-hydroxyethyl)piperidine	AHEPPD	primary + c-3	89850-72-6	$C_7H_{16}N_2O$	144.2	15733445

Continued on next page

Table B.1 – *continued from previous page*

Nr	IUPAC	Abbreviation	Chemical Class	CAS Nr.	Molecular Formula	Molar Mass g/mol	PubChem ID
57	1-Amino-4-(2-hydroxyethyl)piperazine	AHEPz	primary + c-3 + c-3	3973-70-4	$C_6H_{15}N_3O$	145.2	77597
58	2-amino-2-methyl-1-propanol	AMP	primary	124-68-5	$C_4H_{11}NO$	89.1	11807
59	1-Amino-2-methyl-2-propanol	AMP2	primary	2854-16-2	$C_4H_{11}NO$	89.1	95102
60	2-Amino-2-methyl-1,3-propanediol	AMPD	primary	115-69-5	$C_4H_{11}NO_2$	105.1	1531
61	2-(3-aminopropylamino)ethanol	APAE	primary + secondary	4461-39-6	$C_5H_{14}N_2O$	118.2	78211
62	3-aminopropan-1,2-diol	APD	primary	616-30-8	$C_3H_9NO_2$	91.1	73561
63	1-(3-aminopropyl)imidazole	API	primary + c-2 + c-3	5036-48-6	$C_6H_{11}N_3$	125.2	78736

Continued on next page

Table B.1 – *continued from previous page*

Nr	IUPAC	Abbreviation	Chemical Class	CAS Nr.	Molecular Formula	Molar Mass g/mol	Pub-Chem ID
64	2,2'-[(3-aminopropyl)imino]bis-ethanol	APIBE	primary + tertiary	4985-85-7	$C_7H_{18}N_2O_2$	162.2	21088
65	4-(2-aminopropan-2-yl)-1-methylcyclohexanamine	APMCHA	primary + primary	80-52-4	$C_{10}H_{22}N_2$	170.3	6650
66	N-(3-aminopropyl)-2-pipecoline	APPC	primary + c-3	25560-00-3	$C_9H_{20}N_2$	156.3	520211
67	hexamethylene imine	Azepane	c-3	111-49-9	$C_6H_{13}N$	99.2	8119
68	butylamine	BA	primary	109-73-9	$C_4H_{11}N$	73.1	8007
69	Barton's base	Barton's	tertiary + tertiary + tertiary	29166-72-1	$C_9H_{21}N_3$	171.3	3571581
70	3-(Cyclohexylamino)propylamine	Baxxodur	primary + secondary	3312-60-5	$C_9H_{20}N_2$	156.3	18718
71	N-butyldiethanolamine	BDEA	tertiary	102-79-4	$C_8H_{19}NO_2$	161.2	7620

Continued on next page

Table B.1 – *continued from previous page*

Nr	IUPAC	Abbreviation	Chemical Class	CAS Nr.	Molecular Formula	Molar Mass g/mol	Pub-Chem ID
72	1,4-bis(2-hydroxyethyl)piperazine	BHEPz	c-3 + c-3	122-96-3	$C_8H_{18}N_2O_2$	174.2	67151
73	bis(3-aminopropyl)amine	bis-APA	primary + primary + secondary	56-18-8	$C_6H_{17}N_3$	131.2	5942
74	1,2-bis(3-aminopropylamino)ethane	Bis-APAE	primary (2) + secondary (2)	10563-26-5	$C_8H_{22}N_4$	174.3	25378
75	1,3-Bis(dimethylamino)-2-propanol	Bis-DMA-2P	tertiary + tertiary	5966-51-8	$C_7H_{18}N_2O$	146.2	22263
76	Bis-(dimethylaminopropyl)amine	Bis-DMAPA	secondary + tertiary + tertiary	6711-48-4	$C_{10}H_{25}N_3$	187.3	81207
77	N-Benzylmethylamine	BMA	secondary	103-67-3	$C_8H_{11}N$	121.2	7669
78	2-(Butylamino) ethanol	BMEA	secondary	111-75-1	$C_6H_{15}NO$	117.2	8132
79	Di-(2-methoxyethyl)amine	BMOEA	secondary	111-95-5	$C_6H_{15}NO_2$	133.2	2383

Continued on next page

Table B.1 – *continued from previous page*

Nr	IUPAC	Abbreviation	Chemical Class	CAS Nr.	Molecular Formula	Molar Mass g/mol	Pub-Chem ID
80	N-Butyl triacetone diamine	BuTAD	secondary + c-2	36177-92-1	$C_{13}H_{28}N_2$	212.4	118285
81	Benzylamine	BZA	primary	100-46-9	C_7H_9N	107.2	7504
82	cyclohexylmethyl-dimethylamine	CHDMA	tertiary	16607-80-0	$C_9H_{19}N$	141.3	123363
83	Cycloheptyl-amine	CHtA	primary	5452-35-7	$C_7H_{15}N$	113.2	2899
84	Cyclohexylamine	CHxA	primary	108-91-8	$C_6H_{13}N$	99.2	7965
85	N-Methylcyclohexanamine	CHxMA	secondary	100-60-7	$C_7H_{15}N$	113.2	7514
86	Cyclooctyl-amine	COtA	primary	5452-37-9	$C_8H_{17}N$	127.2	2903
87	diethylamine	DA	secondary	109-89-7	$C_4H_{11}N$	73.1	8021
88	1,3-Diamino-2-propanol	DA2P	primary + primary	616-29-5	$C_3H_{10}N_2O$	90.1	61157
89	1,4-Diazacycloheptane	DAACH	c-2 + c-2	505-66-8	$C_5H_{12}N_2$	100.2	68163

Continued on next page

Table B.1 – *continued from previous page*

Nr	IUPAC	Abbreviation	Chemical Class	CAS Nr.	Molecular Formula	Molar Mass g/mol	PubChem ID
90	1,4-diaminobutane	DAB	primary + primary	110-60-1	$C_4H_{12}N_2$	88.2	1045
91	trans-1,4-Diaminocyclohexane	DACH	primary + primary	2615-25-0	$C_6H_{14}N_2$	114.2	18374
92	1,7-Diaminoheptane	DAHe	primary + primary	646-19-5	$C_7H_{18}N_2$	130.2	69533
93	2,6-diamino-5-hydroxyhexanoicacid	DAHHA	primary + primary	6000-08-4	$C_6H_{14}N_2O_3$	162.2	1029
94	1,5-Diamino-2-methylpentane	DAMP	primary + primary	15520-10-2	$C_6H_{16}N_2$	116.2	85862
95	1,3-diaminopropane	DAP	primary + primary	109-76-2	$C_3H_{10}N_2$	74.1	428
96	1,5-diaminopentane	DAPe	primary + primary	462-94-2	$C_5H_{14}N_2$	102.2	273
97	Di-N-butylamine	DBA	secondary	111-92-2	$C_8H_{19}N$	129.2	8148

Continued on next page

Table B.1 – *continued from previous page*

Nr	IUPAC	Abbreviation	Chemical Class	CAS Nr.	Molecular Formula	Molar Mass g/mol	Pub-Chem ID
98	4-dibutylamino-butan-2-ol	DBAB	tertiary	171908-85-3	$C_{12}H_{27}NO$	201.4	18944395
99	1,8-Diazabicyclo[5.4.0]undec-7-en	DBU	c-2 + c-3	6674-22-2	$C_9H_{16}N_2$	152.2	81184
100	Dicyclohexylamine	DCHxA	secondary	101-83-7	$C_{12}H_{23}N$	181.3	7582
101	diethanolamine	DEA	secondary	111-42-2	$C_4H_{11}NO_2$	105.1	8113
102	1-diethylamino-2-propanol	DEA2P	tertiary	4402-32-8	$C_7H_{17}NO$	131.2	95387
103	4-Diethylamino-2-butanol	DEAB	tertiary	5467-48-1	$C_8H_{19}NO$	145.2	231594
104	2-(Diethylamino)ethylamine	DEAEA	primary + tertiary	100-36-7	$C_6H_{16}N_2$	116.2	60993

Continued on next page

Table B.1 – *continued from previous page*

Nr	IUPAC	Abbreviation	Chemical Class	CAS Nr.	Molecular Formula	Molar Mass g/mol	Pub-Chem ID
105	2-[2-(diethylamino)ethoxy] ethanol	DEAEEO	tertiary	140-82-9	$C_8H_{19}NO_2$	161.2	67327
106	1-diethylamino-2-methyl-3-pentanol	DEAMP	tertiary		$C_{10}H_{23}NO$	173.3	59668598
107	3-(Diethylamino)propylamine	DEAPA	primary + tertiary	104-78-9	$C_7H_{18}N_2$	130.2	61011
108	3-(Diethylamino)-1,2-propanediol	DEAPD	tertiary	621-56-7	$C_7H_{17}NO_2$	147.2	79074
109	N,N-Diethyl-2-aminoethanol	DEEA	tertiary	100-37-8	$C_6H_{15}NO$	117.2	7497
110	N,N'-diethylethylenediamine	DEEDA	secondary + secondary	111-74-0	$C_6H_{16}N_2$	116.2	67105
111	Diethanol Isopropanolamine	DEIPA	tertiary	6712-98-7	$C_7H_{17}NO_3$	163.2	97712

Continued on next page

Table B.1 – *continued from previous page*

Nr	IUPAC	Abbreviation	Chemical Class	CAS Nr.	Molecular Formula	Molar Mass g/mol	PubChem ID
112	4-[Ethyl(methyl)amino]butane-1,3-diol	DEPD	tertiary		$C_7H_{17}NO_2$	147.2	88755594
113	Diethylenetriamine	DETA	primary + primary + secondary	111-40-0	$C_4H_{13}N_3$	103.2	8111
114	Diglycolamine	DGA	primary	929-06-6	$C_4H_{11}NO_2$	105.1	13578
115	Dihexylamine	DHA	secondary	143-16-8	$C_{12}H_{27}N$	185.4	8920
116	1,8-Diamino-3,6-dioxaoctane	DiAEOE	primary + primary	929-59-9	$C_6H_{16}N_2O_2$	148.2	70248
117	Diisobutylamine	DIBA	secondary	110-96-3	$C_8H_{19}N$	129.2	8085
118	1,2-Dimethylimidazole	DIMI	c-2 + c-3	1739-84-0	$C_5H_8N_2$	96.1	15617
119	Diisopropanolamine	DIPA	secondary	110-97-4	$C_6H_{15}NO_2$	133.2	8086
120	2-(diisopropylamino)ethanol	DIPAE	tertiary	96-80-0	$C_8H_{19}NO$	145.2	7313

Continued on next page

Table B.1 – *continued from previous page*

Nr	IUPAC	Abbreviation	Chemical Class	CAS Nr.	Molecular Formula	Molar Mass g/mol	Pub-Chem ID
121	N,N'-Dimethyl-1,3-propanediamine	DM13PDA	secondary + secondary	111-33-1	$C_5H_{14}N_2$	102.2	66978
122	3-Dimethylamino-2,2-dimethyl-1-propanol	DMA22DMP	tertiary	19059-68-8	$C_7H_{17}NO$	131.2	87919
123	2-Dimethylamino-2-methylpropano	DMA2M1P	tertiary	7005-47-2	$C_6H_{15}NO$	117.2	23435
124	4-(Dimethylamino)-1-butanol	DMAB	tertiary	13330-96-6	$C_6H_{15}NO$	117.2	83350
125	1-dimethylamino-4,4-dimethyl-3-pentanol	DMADMP	tertiary	74172-63-7	$C_9H_{21}NO$	159.3	12593007
126	1-O-Dimethylaminoethyl-ethylenglykol	DMAEEO	tertiary	1704-62-7	$C_6H_{15}NO_2$	133.2	74348
127	Bis<2-(N,N-dimethylamino)aethyl>aether	DMAEER	tertiary + tertiary	3033-62-3	$C_8H_{20}N_2O$	160.3	18204

Continued on next page

Table B.1 – *continued from previous page*

Nr	IUPAC	Abbreviation	Chemical Class	CAS Nr.	Molecular Formula	Molar Mass g/mol	PubChem ID
128	2-[[2-[2-(Dimethylamino)ethoxy]ethyl]methylamino]ethanol	DMAEOEMAEO	tertiary + tertiary	83016-70-0	$C_9H_{22}N_2O_2$	190.3	3086157
129	6-(N,N-dimethylamino)-1-hexanol	DMAH	tertiary	1862-07-3	$C_8H_{19}NO$	145.2	74623
130	1-(dimethylamino)-2-methyl-3-pentanol	DMAMP	tertiary		$C_8H_{19}NO$	145.2	23206528
131	3-Dimethylamino-1-propanol	DMAP	tertiary	3179-63-3	$C_5H_{13}NO$	103.2	76646
132	3-Dimethylaminopropylamine	DMAPA	primary + tertiary	109-55-7	$C_5H_{14}N_2$	102.2	7993
133	3-(Dimethylamino)-1,2-propanediol	DMAPD	tertiary	623-57-4	$C_5H_{13}NO_2$	119.2	79078

Continued on next page

Table B.1 – *continued from previous page*

Nr	IUPAC	Abbreviation	Chemical Class	CAS Nr.	Molecular Formula	Molar Mass g/mol	Pub-Chem ID
134	N,N-Dimethylbenzylamine	DMBA	tertiary	103-83-3	$C_9H_{13}N$	135.2	7681
135	N,N-Diethyl-N',N'-dimethylethylenediamine	DMDEEDA	tertiary + tertiary	123-10-4	$C_8H_{20}N_2$	144.3	67153
136	N,N-Dimethylethanolamine	DMEA	tertiary	108-01-0	$C_4H_{11}NO$	89.1	7902
137	N,N'-Dimethylethane-1,2-diamine	DMEDA	secondary + secondary	110-70-3	$C_4H_{12}N_2$	88.2	8070
138	1–2-dimethylamino-aethan	DMEDAEO	tertiary + tertiary	3197-07-7	$C_8H_{20}N_2O_2$	176.3	22056833
139	N,N-Dimethyl-1,6-hexanediamine	DMHDA	secondary + secondary	13093-04-4	$C_8H_{20}N_2$	144.3	83131
140	1,3-Dimethyl-2-imidazolidinone	DMI	c-3 + c-3	80-73-9	$C_5H_{10}N_2O$	114.2	6661

Continued on next page

Table B.1 – *continued from previous page*

Nr	IUPAC	Abbreviation	Chemical Class	CAS Nr.	Molecular Formula	Molar Mass g/mol	PubChem ID
141	2,2-Dimethyl-1,3-propanediamine	DMPDA	primary + primary	7328-91-8	$C_5H_{14}N_2$	102.2	81770
142	N,N'-dimethyl-bis(2-hydroxyethyl)-1,3-propyldiamine	DMPDAEO	tertiary + tertiary	10394-83-9	$C_9H_{22}N_2O_2$	190.3	88210764
143	1,1-Dimethyl-2-pentylhydrazine	DMPH	secondary + tertiary	67398-36-1	$C_7H_{18}N_2$	130.2	547900
144	1,4-dimethylpiperazine	DMPz	c-3 + c-3	106-58-1	$C_6H_{14}N_2$	114.2	7818
145	Dipropylamine	DPA	secondary	142-84-7	$C_6H_{15}N$	101.2	8902
146	4-(dipropylamino)-2-butanol	DPAB	tertiary		$C_{10}H_{23}NO$	173.3	60206798
147	Di-N-Propylethylamine	DPE	tertiary	20634-92-8	$C_8H_{19}N$	129.2	519799
148	1,3-Dimethyl,3,4,5,6-tetrahydro-2-pyrimidinone	DPMU	c-3 + c-3	7226-23-5	$C_6H_{12}N_2O$	128.2	81646

Continued on next page

Table B.1 – *continued from previous page*

Nr	IUPAC	Abbreviation	Chemical Class	CAS Nr.	Molecular Formula	Molar Mass g/mol	Pub-Chem ID
149	Dipentylamine	DPtA	secondary	2050-92-2	$C_{10}H_{23}N$	157.3	16316
150	Di-sec-butylamine	DsBA	secondary	626-23-3	$C_8H_{19}N$	129.2	12277
151	N-Ethyl-Ethanolamine	EAE	secondary	110-73-6	$C_4H_{11}NO$	89.1	8072
152	2-N-ethylamino-2-methyl-1-propanol	EAMP	secondary	82922-13-2	$C_6H_{15}NO$	117.2	15105174
153	4-(2-ethanolamino)piperidine	EAPPD	secondary + c-2	875229-91-7	$C_7H_{16}N_2O$	144.2	61016368
154	Ethylenediamine	EDA	primary + primary	107-15-3	$C_2H_8N_2$	60.1	3301
155	N-ethyldiethanolamine	EDEA	tertiary	139-87-7	$C_6H_{15}NO_2$	133.2	8769
156	N-(2-ethoxyethyl)-3-morpholinopropan-1-amine	EEMPA	secondary + c-3		$C_{11}H_{24}N_2O_2$	216.3	43387925
157	2-Ethylimidazole	EIMI	c-2 + c-2	1072-62-4	$C_5H_8N_2$	96.1	66130

Continued on next page

Table B.1 – *continued from previous page*

Nr	IUPAC	Abbreviation	Chemical Class	CAS Nr.	Molecular Formula	Molar Mass g/mol	Pub-Chem ID
158	4-(ethyl-methyl-amino)-butan-2-ol	EMAB	tertiary		$C_7H_{17}NO$	131.2	23568940
159	2-Ethyl-4-methylimidazole	EMIMI	c-2 + c-2	931-36-2	$C_6H_{10}N_2$	110.2	70262
160	1-Ethylpiperazine	EPZ	c-2 + c-3	5308-25-8	$C_6H_{14}N_2$	114.2	79196
161	3-(2-aminoethyl)pentane-2,4-diol	HEDA	primary		$C_7H_{17}NO_2$	147.2	87126561
162	2-[(3-aminocyclohexyl)amino]ethan-1-ol	HEDACH	primary + secondary	38362-00-4	$C_8H_{18}N_2O$	158.2	79459217
163	4-((2-hydroxyethyl)(ethyl)amino)-2-butanol	HEEAB	tertiary		$C_8H_{19}NO_2$	161.2	104318443

Continued on next page

Table B.1 – *continued from previous page*

Nr	IUPAC	Abbreviation	Chemical Class	CAS Nr.	Molecular Formula	Molar Mass g/mol	Pub-Chem ID
164	N,N-Bis(2-hydroxyethyl)ethylenediamine	HEEDA	primary + tertiary	3197-06-6	$C_6H_{16}N_2O_2$	148.2	98535
165	4,2-hydroxyethylmorpholine	HEM	c-3	622-40-2	$C_6H_{13}NO_2$	131.2	61163
166	4-((2-hydroxyethyl)(methyl)amino)-2-butanol	HEMAB	tertiary		$C_7H_{17}NO_2$	147.2	115674907
167	1-piperidineethanol	HEPP	c-3	3040-44-6	$C_7H_{15}NO$	129.2	18232
168	1-(2-Hydroxyethyl)piperazine	HEPz	c-2 + c-3	103-76-4	$C_6H_{14}N_2O$	130.2	7677
169	Hexanamine	HEXA	primary	111-26-2	$C_6H_{15}N$	101.2	8102
170	Hexamethylenediamine	HMD	primary + primary	124-09-4	$C_6H_{16}N_2$	116.2	16402
171	n-Heptylamine	HtA	primary	111-68-2	$C_7H_{17}N$	115.2	8127
172	Diisopropylethylamine	Hunig's base	tertiary	7087-68-5	$C_8H_{19}N$	129.2	81531

Continued on next page

Table B.1 – *continued from previous page*

Nr	IUPAC	Abbreviation	Chemical Class	CAS Nr.	Molecular Formula	Molar Mass g/mol	Pub-Chem ID
173	isobutylamine	i-BA	primary	78-81-9	$C_4H_{11}N$	73.1	6558
174	2-(Isobutylamino)ethan	IBAE	secondary	17091-40-6	$C_6H_{15}NO$	117.2	28264
175	Imidazole	IMI	c-2 + c-2	288-32-4	$C_3H_4N_2$	68.1	795
176	isopropylamine	IPA	primary	75-31-0	C_3H_9N	59.1	6363
177	4-isopropylamino-2-butanol	IPA2B	secondary	145124-75-0	$C_7H_{17}NO$	131.2	15648977
178	4-(Isopropylamino)butanol	IPAB	secondary	42042-71-7	$C_7H_{17}NO$	131.2	12950986
179	2-(Isopropylamino)-ethanol	IPAE	secondary	109-56-8	$C_5H_{13}NO$	103.2	7994
180	3-(Isopropylamino)propanol	IPAP	secondary	33918-15-9	$C_6H_{15}NO$	117.2	2063457
181	Nisopropy-ldiethanolamine	IPDEA	tertiary	121-93-7	$C_7H_{17}NO_2$	147.2	8498

Continued on next page

Table B.1 – *continued from previous page*

Nr	IUPAC	Abbreviation	Chemical Class	CAS Nr.	Molecular Formula	Molar Mass g/mol	Pub-Chem ID
182	N-isopropyl-1,3-propanediamine	IPPDA	primary + secondary	3360-16-5	$C_6H_{16}N_2$	116.2	76888
183	N,N-Dimethylcyclohexylamine	Lupragen N100	tertiary	98-94-2	$C_8H_{17}N$	127.2	7415
184	Pentamethyldietylenetriamine	Lupragen301	tertiary + tertiary + tertiary	3030-47-5	$C_9H_{23}N_3$	173.3	18196
185	2-N-methylamino-2-methyl-1-propanol	MAMP	secondary	27646-80-6	$C_5H_{13}NO$	103.2	422780
186	N-Methyl-1,3-propanediamine	MAPA	primary + secondary	6291-84-5	$C_4H_{12}N_2$	88.2	80511
187	Methyldiethanolamine	MDEA	tertiary	105-59-9	$C_5H_{13}NO_2$	119.2	7767
188	monoethanolamine	MEA	primary	141-43-5	C_2H_7NO	61.1	700
189	3-methoxypropyldimethylamine	MEPDMA	tertiary		$C_6H_{15}NO$	117.2	547431

Continued on next page

Table B.1 – *continued from previous page*

Nr	IUPAC	Abbreviation	Chemical Class	CAS Nr.	Molecular Formula	Molar Mass g/mol	Pub-Chem ID
190	1-Methylimidazole	MIMI	c-2 + c-3	616-47-7	$C_4H_6N_2$	82.1	1390
191	1-amino-2-propanol	MIPA	primary	78-96-6	C_3H_9NO	75.1	4
192	methylmo-noethanolamine	MMEA	secondary	109-83-1	C_3H_9NO	75.1	8016
193	m-nitroaniline	m-nitroaniline	primary	99-09-2	$C_6H_6N_2O_2$	138.1	7423
194	3-Methoxypropylamine	MOPA	primary	5332-73-0	$C_4H_{11}NO$	89.1	1672
195	1,4-oxazinane	MOR	c-2	110-91-8	C_4H_9NO	87.1	8083
196	3-morpholinopropylamine	MORPA	primary + c-3	123-00-2	$C_7H_{16}N_2O$	144.2	61055
197	1-Methylpiperidin-4-ol	MPDL	c-3	106-52-5	$C_6H_{13}NO$	115.2	66048
198	N-Methyl-3-piperidinol	MPP	c-3	3554-74-3	$C_6H_{13}NO$	115.2	98016
199	1-methylpiperazine	MPz	c-2 + c-3	109-01-3	$C_5H_{12}N_2$	100.2	53167
200	N-Acetyl Morpholine	NAM	c-3	1696-20-4	$C_6H_{11}NO_2$	129.2	15543
201	N-Benzyl Ethanolamine	NBzEA	secondary	104-63-2	$C_9H_{13}NO$	151.2	4348

Continued on next page

Table B.1 – *continued from previous page*

Nr	IUPAC	Abbreviation	Chemical Class	CAS Nr.	Molecular Formula	Molar Mass g/mol	Pub-Chem ID
202	N-cyclohexylethanolamine	n-CHEA	secondary	2842-38-8	$C_8H_{17}NO$	143.2	17827
203	N-cyclopentylethanolamine	n-CPEA	secondary	2842-39-9	$C_7H_{15}NO$	129.2	14187635
204	N-cyclopropylethanolamine	n-CPREA	secondary	35265-06-6	$C_5H_{11}NO$	101.1	19100566
205	N,N-Diethylbutylamine	ND1B	tertiary	4444-68-2	$C_8H_{19}N$	129.2	20513
206	N-ethylethane-1,2-diamine	NEED	primary + secondary	110-72-5	$C_4H_{12}N_2$	88.2	66071
207	N-Ethyl Morpholine	NEM	c-3	100-74-3	$C_6H_{13}NO$	115.2	7525
208	N-Formyl Morpholine	NFM	c-3	4394-85-8	$C_5H_9NO_2$	115.1	20417
209	1-Methyl-2-pyridone	NM2P	tertiary	694-85-9	C_6H_7NO	109.1	12755
210	N-methyl-2-ethanolamine	NMEA	c-2 + tertiary	122321-04-4	$C_8H_{12}N_2O$	152.2	737420

Continued on next page

Table B.1 – *continued from previous page*

Nr	IUPAC	Abbreviation	Chemical Class	CAS Nr.	Molecular Formula	Molar Mass g/mol	PubChem ID
211	N-methyl-1,2-ethanediamine	NMEDA	primary + secondary	109-81-9	$C_3H_{10}N_2$	74.1	8014
212	N-Methyl Morpholine	NMM	c-3	109-02-4	$C_5H_{11}NO$	101.1	7972
213	N-Methyl Morpholine Oxide	NMMO	c-3	7529-22-8	$C_5H_{11}NO_2$	117.1	82029
214	N-Methylpyrrolidone	NMP	c-3	872-50-4	C_5H_9NO	99.1	13387
215	n-Octylamine	OtA	primary	111-86-4	$C_8H_{19}N$	129.2	8143
216	1,8-Diaminooctane	OtDA	primary + primary	373-44-4	$C_8H_{20}N_2$	144.3	24250
217	pentan-1-amine	P1A	primary	110-58-7	$C_5H_{13}N$	87.2	8060
218	2-Propylamino-ethanol	PAE	secondary	16369-21-4	$C_5H_{13}NO$	103.2	85382
219	3-(propylamino)propan-1-ol	PAP	secondary	38825-85-3	$C_6H_{15}NO$	117.2	186621
220	4-Phenylbutylamine	PBA	primary	13214-66-9	$C_{10}H_{15}N$	149.2	83242

Continued on next page

Table B.1 – *continued from previous page*

Nr	IUPAC	Abbreviation	Chemical Class	CAS Nr.	Molecular Formula	Molar Mass g/mol	Pub-Chem ID
221	1,2-Propanediamine	PDA	primary + primary	78-90-0	$C_3H_{10}N_2$	74.1	6567
222	N-propyldiethanolamine	PDEA	tertiary	6735-35-9	$C_7H_{17}NO2$	147.2	42848
223	Phenethylamine	PEA	primary	64-04-0	$C_8H_{11}N$	121.2	1001
224	Pentaethylene-hexamine	PEHA	primary (1) + secondary (4)	4067-16-7	$C_{10}H_{28}N_6$	232.4	19990
225	Piperidine	Piperidine	c-2	110-89-4	$C_5H_{11}N$	85.2	8082
226	2,6,10-Trimethyl-2,6,10-triazaundecane	PMDPTA	tertiary + tertiary + tertiary	3855-32-1	$C_{11}H_{27}N_3$	201.4	77463
227	4-(Propylamino)-1-butanol	PPAB	secondary	42042-70-6	$C_7H_{17}NO$	131.2	12484482
228	3-piperidino-1,2-propanediol	PPPD	c-3	4847-93-2	$C_8H_{17}NO_2$	159.2	97824
229	1-Propylpiperazine	PPz	c-2 + c-3	50733-94-3	$C_7H_{16}N_2$	128.2	415812

Continued on next page

Table B.1 – *continued from previous page*

Nr	IUPAC	Abbreviation	Chemical Class	CAS Nr.	Molecular Formula	Molar Mass g/mol	Pub-Chem ID
230	3-Pyrrolidino-1,2-propanediol	PRLD12PD	c-3	85391-19-1	$C_7H_{15}NO_2$	145.2	174452
231	4-(2-Piperidyl)-1-butanol	PRNB	c-2	90726-50-4	$C_9H_{19}NO$	157.3	69524314
232	Pyridine	Pyridine	c-2	110-86-1	C_5H_5N	79.1	1049
233	pyrrolidine	Pyrrolidine	c-2	123-75-1	C_4H_9N	71.1	31268
234	piperazine	Pz	c-2 + c-2	110-85-0	$C_4H_{10}N_2$	86.1	4837
235	3-quinoclidinol	QCD	c-3	1619-34-7	$C_7H_{13}NO$	127.2	15381
236	sec-butylamine	s-BA	primary	13952-84-6	$C_4H_{11}N$	73.1	24874
237	2-(sec-Butylamino)ethanol	SBAE	secondary	35265-04-4	$C_6H_{15}NO$	117.2	98429
238	(2-aminopropane-1,3-diol)	Serinol	primary	534-03-2	$C_3H_9NO_2$	91.1	68294

Continued on next page

Table B.1 – *continued from previous page*

Nr	IUPAC	Abbreviation	Chemical Class	CAS Nr.	Molecular Formula	Molar Mass g/mol	Pub-Chem ID
239	N1-(3-aminopropyl)butane-1,4-diamine	Spermidine	primary + primary + secondary	124-20-9	$C_7H_{19}N_3$	145.3	1102
240	N1,N1'-(butane-1,4-diyl)dipropane-1,3-diamine	Spermine	primary (2) + secondary (2)	71-44-3	$C_{10}H_{26}N_4$	202.3	1103
241	triacetoneamine	TAA	c-2	826-36-8	$C_9H_{17}NO$	155.2	13220
242	1,4,7-triazacyclononane	TACN	c-2 + c-2 + c-2	4730-54-5	$C_6H_{15}N_3$	129.2	188318
243	2,2',2"-triaminotriethylamine	TAEA	primary (3) + tertiary (1)	4097-89-6	$C_6H_{18}N_4$	146.2	77731
244	1,5,9,13-tetraazatridecane	TATD	primary (2) + secondary (2)	4605-14-5	$C_9H_{24}N_4$	188.3	78350
245	1,4,8,11-tetraazaundecane	TAUD	primary (2) + secondary (2)	4741-99-5	$C_7H_{20}N_4$	160.3	78479
246	tert-butylamine	t-BA	primary	75-64-9	$C_4H_{11}N$	73.1	6385

Continued on next page

Table B.1 – *continued from previous page*

Nr	IUPAC	Abbreviation	Chemical Class	CAS Nr.	Molecular Formula	Molar Mass g/mol	Pub-Chem ID
247	2-(tert-Butylamino)ethanol	t-BAE	secondary	4620-70-6	$C_6H_{15}NO$	117.2	78361
248	Tertiary Butyl Diethanolamine	t-BDEA	tertiary	2160-93-2	$C_8H_{19}NO_2$	161.2	62430
249	2,5-transdimethylpiperazine	t-DMPZ	c-2 + c-2	2815-34-1	$C_6H_{14}N_2$	114.2	220672
250	Triethanolamine	TEA	tertiary	102-71-6	$C_6H_{15}NO_3$	149.2	7618
251	triethylenediamine	TEDA	tertiary + tertiary	280-57-9	$C_6H_{12}N_2$	112.2	9237
252	bis-(diethylamino)methane	TEDAM	tertiary + tertiary	102-53-4	$C_9H_{22}N_2$	158.3	66020
253	N,N,N',N'-Tetraethylethylenediamine	TEEDA	tertiary + tertiary	150-77-6	$C_{10}H_{24}N_2$	172.3	67423
254	Tetraethylenepentamine	TEPA	primary (2) + secondary (3)	112-57-2	$C_8H_{23}N_5$	189.3	8197

Continued on next page

Table B.1 – *continued from previous page*

Nr	IUPAC	Abbreviation	Chemical Class	CAS Nr.	Molecular Formula	Molar Mass g/mol	Pub-Chem ID
255	N,N,N,N-Tetraethyl-1,3-propanediamine	TEPDA	tertiary + tertiary	60558-96-5	$C_{11}H_{26}N_2$	186.3	143710
256	3-aminoproyl triethoxysilane	TESA	primary	919-30-2	$C_9H_{23}NO_3Si$	221.4	13521
257	Triethylenetetramine	TETA	primary (2) + secondary (2)	112-24-3	$C_6H_{18}N_4$	146.2	5565
258	N,N,N,N-Tetrakis(2-hydroxyethyl)ethylenediamine	THEED	tertiary + tertiary	140-07-8	$C_{10}H_{24}N_2O_4$	236.3	67322
259	Triisopropanolamine	TIPA	tertiary	122-20-3	$C_9H_{21}NO_3$	191.3	24730
260	N,N,N',N'-tetramethyl-1,4-butanediamine	TMDAB	tertiary + tertiary	111-51-3	$C_8H_{20}N_2$	144.3	66074
261	N,N,N',N'-Tetramethyl-1,2-ethanediamine	TMEDA	tertiary + tertiary	110-18-9	$C_6H_{16}N_2$	116.2	8037
262	2-[2-(dimethylamino)ethyl]methylaminoethanol	TMEDAEO	tertiary + tertiary	2212-32-0	$C_7H_{18}N_2O$	146.2	75171

Continued on next page

Table B.1 – *continued from previous page*

Nr	IUPAC	Abbreviation	Chemical Class	CAS Nr.	Molecular Formula	Molar Mass g/mol	PubChem ID
263	tris[2-(2-methoxyethoxy)ethyl]amine	TMEEA	tertiary	70384-51-9	$C_{15}H_{33}NO_6$	323.4	112414
264	1,1,3,3-Tetramethylguanidine	TMG	primary + tertiary + tertiary	80-70-6	$C_5H_{13}N_3$	115.2	66460
265	N,N,N,N-Tetramethyl-1,6-hexanediamine	TMHDA	tertiary + tertiary	111-18-2	$C_{10}H_{24}N_2$	172.3	8097
266	2,2,6,6-Tetramethyl-4-piperidinol	TMP	c-2	2403-88-5	$C_9H_{19}NO$	157.3	75471
267	N,N,N'N'-tetramethyl-1,3-propanediamine	TMPDA	tertiary + tertiary	110-95-2	$C_7H_{18}N_2$	130.2	8084
268	2-[3-(dimethylamino)propyl-methylamino]ethanol	TMPDAEO	tertiary + tertiary	82136-26-3	$C_8H_{20}N_2O$	160.3	3086144
269	triethylamine	TREA	tertiary	121-44-8	$C_6H_{15}N$	101.2	8471

Continued on next page

Table B.1 – *continued from previous page*

Nr	IUPAC	Abbreviation	Chemical Class	CAS Nr.	Molecular Formula	Molar Mass g/mol	PubChem ID
270	tris(hydroxymethyl)amino methane	TRIS	primary	77-86-1	$C_4H_{11}NO_3$	121.1	6503
271	8-Methyl-8-azabicyclo[3.2.1]octan-3-ol	Tropine	tertiary	120-29-6	$C_8H_{15}NO$	141.2	8424
272	DL-2-Amino-3-methyl-1-butanol	Valinol	primary	16369-05-4	$C_5H_{13}NO$	103.2	79019
273	Formamide		primary	75-12-7	CH_3NO	45.0	713
274	Dimethylamine anhydrous		secondary	124-40-3	C_2H_7N	45.1	674
275	Ethylamine		primary	75-04-7	C_2H_7N	45.1	6341
276	O-Methylhydroxylamine		primary	67-62-9	CH_5NO	47.1	4113
277	Trimethylamine anhydrous		tertiary	75-50-3	C_3H_9N	59.1	1146
278	Propylamine		primary	107-10-8	C_3H_9N	59.1	7852

Continued on next page

Table B.1 – *continued from previous page*

Nr	IUPAC	Abbreviation	Chemical Class	CAS Nr.	Molecular Formula	Molar Mass g/mol	PubChem ID
279	3-Aminopropanenitrile		primary	151-18-8	$C_3H_6N_2$	70.1	1647
280	Dimethylformamide		tertiary	68-12-2	C_3H_7NO	73.1	6228
281	N-Methylacetamide		secondary	79-16-3	C_3H_7NO	73.1	6582
282	Dimethylethylamine		tertiary	598-56-1	$C_4H_{11}N$	73.1	11723
283	N-Methyl-N-isopropylamine		secondary	4747-21-1	$C_4H_{11}N$	73.1	78485
284	2-Methoxyethylamine		primary	109-85-3	C_3H_9NO	75.1	8018
285	2-Pyrrolidone		c-2	616-45-5	C_4H_7NO	85.1	12025
286	N-Methylpyrrolidine		c-3	120-94-5	$C_5H_{11}N$	85.2	8454
287	N,N-Dimethylacetamide		tertiary	127-19-5	C_4H_9NO	87.1	31374
288	Dimethylpropylamine		tertiary	926-63-6	$C_5H_{13}N$	87.2	61236
289	N,N-Dimethylisopropylamine		tertiary	996-35-0	$C_5H_{13}N$	87.2	70452
290	N-Ethyl-N-propylamine azeotrope		secondary	20193-20-8	$C_5H_{13}N$	87.2	88398

Continued on next page

Table B.1 – *continued from previous page*

Nr	IUPAC	Abbreviation	Chemical Class	CAS Nr.	Molecular Formula	Molar Mass g/mol	Pub-Chem ID
291	N,N-Dimethylethylenediamine		primary + tertiary	108-00-9	$C_4H_{12}N_2$	88.2	66053
292	Butane-1,3-diamine		primary + primary	590-88-5	$C_4H_{12}N_2$	88.2	61136
293	1,2-Propane2-methyl-,Nsc17717		primary + primary	811-93-8	$C_4H_{12}N_2$	88.2	13128
294	Aniline		primary	62-53-3	C_6H_7N	93.1	6115
295	1-Vinylimidazole		c-2 + c-3	1072-63-5	$C_5H_6N_2$	94.1	66171
296	1-Ethylimidazole		c-2 + c-3	7098-07-9	$C_5H_8N_2$	96.1	81540
297	1,4-Dimethylpyrazole		c-2 + c-3	1072-68-0	$C_5H_8N_2$	96.1	136836
298	3-(Dimethylamino)propanenitrile		tertiary	1738-25-6	$C_5H_{10}N_2$	98.2	15615
299	2-Ethyl-2-oxazoline		c-3	10431-98-8	C_5H_9NO	99.1	66412
300	N-Methylpiperidine		c-3	626-67-5	$C_6H_{13}N$	99.2	12291
301	3-Hydroxypiperidine		c-2	6859-99-0	$C_5H_{11}NO$	101.2	23293

Continued on next page

Table B.1 – *continued from previous page*

Nr	IUPAC	Abbreviation	Chemical Class	CAS Nr.	Molecular Formula	Molar Mass g/mol	Pub-Chem ID
302	Piperidin-4-ol		c-2	5382-16-1	$C_5H_{11}NO$	101.2	79341
303	1-amino-2,2-dimethylbutane		primary	41781-17-3	$C_6H_{15}N$	101.2	642325
304	3-amino-3-methylpentane		primary	3495-46-3	$C_6H_{15}N$	101.2	4339626
305	2-Ethylbutylamine		primary	617-79-8	$C_6H_{15}N$	101.2	12049
306	1-amino-3,3-dimethylbutane		primary	15673-00-4	$C_6H_{15}N$	101.2	19709
307	1-amino-2-methylpentane		primary	13364-16-4	$C_6H_{15}N$	101.2	99014
308	2-amino-2,3-dimethylbutane		primary	4358-75-2	$C_6H_{15}N$	101.2	207363
309	1-amino-4-methylpentane		primary	5344-20-7	$C_6H_{15}N$	101.2	219608

Continued on next page

Table B.1 – *continued from previous page*

Nr	IUPAC	Abbreviation	Chemical Class	CAS Nr.	Molecular Formula	Molar Mass g/mol	Pub-Chem ID
310	2-amino-2-methylpentane		primary	53310-02-4	$C_6H_{15}N$	101.2	418247
311	2-amino-3,3-dimethyl butane		primary	3850-30-4	$C_6H_{15}N$	101.2	520907
312	2-amino-3-methylpentane		primary	35399-81-6	$C_6H_{15}N$	101.2	3015773
313	1-amino-3-methylpentane		primary	42245-37-4	$C_6H_{15}N$	101.2	3055957
314	3-amino-2-methylpentane		primary	54287-41-1	$C_6H_{15}N$	101.2	19031167
315	1-amino-2,3-dimethylbutane		primary	66553-05-7	$C_6H_{15}N$	101.2	19822625
316	N2,N2-dimethylpropane-1,2-diamine		primary + tertiary	19764-58-0	$C_5H_{14}N_2$	102.2	89217

Continued on next page

Table B.1 – *continued from previous page*

Nr	IUPAC	Abbreviation	Chemical Class	CAS Nr.	Molecular Formula	Molar Mass g/mol	Pub-Chem ID
317	4-Amino-2-methylbutan-2-ol		primary	26734-08-7	$C_5H_{13}NO$	103.2	15649173
318	1-Amino-2,2-dimethylpropan-1-ol		primary	40898-98-4	$C_5H_{13}NO$	103.2	3016233
319	1-Amino-2-methylbutan-2-ol		primary	51411-49-5	$C_5H_{13}NO$	103.2	3016656
320	2-Hydroxyethyl carbamate		primary	5395-01-7	$C_3H_7NO_3$	105.1	21492
321	3-Methylamino-1,2-propanediol		secondary	40137-22-2	$C_4H_{11}NO_2$	105.1	2734122
322	o-Toluidine		primary	95-53-4	C_7H_9N	107.2	7242
323	p-toluidine		primary	106-49-0	C_7H_9N	107.2	7813
324	m-toluidine		primary	108-44-1	C_7H_9N	107.2	7934
325	N-Vinyl-2-pyrrolidone		c-3	88-12-0	C_6H_9NO	111.1	6917
326	N-Ethylpyrrolidone-2		c-3	2687-91-4	$C_6H_{11}NO$	113.2	17595

Continued on next page

Table B.1 – *continued from previous page*

Nr	IUPAC	Abbreviation	Chemical Class	CAS Nr.	Molecular Formula	Molar Mass g/mol	Pub-Chem ID
327	N-Ethylpiperidine		c-3	766-09-6	$C_7H_{15}N$	113.2	13007
328	trans-4-Aminocyclohexanol		primary	27489-62-9	$C_6H_{13}NO$	115.2	81293
329	2,6-Dimethylmorpholine		c-2	141-91-3	$C_6H_{13}NO$	115.2	110862
330	3-Amino-2,4-dimethylpentane		primary	4083-57-2	$C_7H_{17}N$	115.2	77702
331	N-Isopropylbutylamine		secondary	39099-23-5	$C_7H_{17}N$	115.2	123480
332	1,2-Butane1-(N,N-dimethyl		primary + tertiary	63732-18-3	$C_6H_{16}N_2$	116.2	44652
333	N,N,2-Trimethylpropane-1,3-diamine		primary + tertiary	6105-72-2	$C_6H_{16}N_2$	116.2	110778
334	Methylaminoacetaldehyde dimethyl acetal		secondary	122-07-6	$C_5H_{13}NO_2$	119.2	8503

Continued on next page

Table B.1 – *continued from previous page*

Nr	IUPAC	Abbreviation	Chemical Class	CAS Nr.	Molecular Formula	Molar Mass g/mol	Pub-Chem ID
335	1,1-Dimethoxy-N,N-dimethyl		tertiary	4637-24-5	$C_5H_{13}NO_2$	119.2	78373
336	2,6-Xylidine		primary	87-62-7	$C_8H_{11}N$	121.2	6896
337	toluenediamine		secondary + secondary	95-80-7	$C_7H_{10}N_2$	122.2	7261
338	N-(2-Hydroxyethyl)-2-pyrrolidone		c-3	3445-11-2	$C_6H_{11}NO_2$	129.2	76980
339	1-Methyl-2-piperidinemethanol		c-3	20845-34-5	$C_7H_{15}NO$	129.2	89394
340	isopentyl-propyl-amine		secondary	78579-58-5	$C_8H_{19}N$	129.2	24710094
341	2-Ethylhexylamine		primary	104-75-6	$C_8H_{19}N$	129.2	7719
342	2-amino-1,1-dimethylethylisopropylamine		primary + secondary	5448-29-3	$C_7H_{18}N_2$	130.2	79532
343	N,N,2,2-Tetramethyl-1,3-propanediamine		secondary + tertiary	53369-71-4	$C_7H_{18}N_2$	130.2	104477

Continued on next page

Table B.1 – *continued from previous page*

Nr	IUPAC	Abbreviation	Chemical Class	CAS Nr.	Molecular Formula	Molar Mass g/mol	PubChem ID
344	2-amino-2-methylhexan-3-ol		primary	63765-79-7	$C_7H_{17}NO$	131.2	44673
345	5-Amino-2,2-dimethylpentanol		primary	13532-77-9	$C_7H_{17}NO$	131.2	139489
346	N2-(2-aminoethyl)-N1,N1-dimethylethylenediamine		primary + secondary + tertiary	24229-53-6	$C_6H_{17}N_3$	131.2	90424
347	3-(2-Aminopropylamino)propan-1-ol		primary + secondary	10171-78-5	$C_6H_{16}N_2O$	132.2	112017
348	2-[(3-aminopropyl)methylamino]ethanol		primary + tertiary	41999-70-6	$C_6H_{16}N_2O$	132.2	11434970
349	Anthranilic acid amide		primary + primary	88-68-6	$C_7H_8N_2O$	136.2	6942

Continued on next page

Table B.1 – *continued from previous page*

Nr	IUPAC	Abbreviation	Chemical Class	CAS Nr.	Molecular Formula	Molar Mass g/mol	PubChem ID
350	N-(2-Hydroxyethyl)aniline		secondary	122-98-5	$C_8H_{11}NO$	137.2	31235
351	p-nitroaniline		primary + primary	100-01-6	$C_6H_6N_2O_2$	138.1	7475
352	1-Propyl-4-piperidone		c-3	23133-37-1	$C_8H_{15}NO$	141.2	90006
353	4-(Diethylamino)butan-2-one		tertiary	3299-38-5	$C_8H_{17}NO$	143.2	18694
354	Tripropylamine		tertiary	102-69-2	$C_9H_{21}N$	143.3	7616
355	n-Nonylamine, 1-Aminononane		primary	112-20-9	$C_9H_{21}N$	143.3	16215
356	n-Methyloctylamine		secondary	2439-54-5	$C_9H_{21}N$	143.3	75538
357	N,N,N',N'-TetraMethyl-1,3-diaminobutane		tertiary + tertiary	97-84-7	$C_8H_{20}N_2$	144.3	7350
358	2-(Diisopropylamino)ethylamine		primary + tertiary	121-05-1	$C_8H_{20}N_2$	144.3	8459

Continued on next page

Table B.1 – *continued from previous page*

Nr	IUPAC	Abbreviation	Chemical Class	CAS Nr.	Molecular Formula	Molar Mass g/mol	Pub-Chem ID
359	N,N,N'-Triethylethylenediamine		secondary + tertiary	105-04-4	$C_8H_{20}N_2$	144.3	66040
360	N,N'-Diethyl-N,N'-dimethylethylenediamine		tertiary + tertiary	106-66-1	$C_8H_{20}N_2$	144.3	66942
361	4-(Diethylamino)butylamine		primary + tertiary	27431-62-5	$C_8H_{20}N_2$	144.3	117976
362	2-N-Butyl-2-methylpropane-1,2-diamine		primary + secondary	50540-24-4	$C_8H_{20}N_2$	144.3	3039391
363	6-Amino-2-methyl-2-heptanol		primary	372-66-7	$C_8H_{19}NO$	145.2	3590
364	4-(Diethylamino)butan-1-ol		tertiary	2683-56-9	$C_8H_{19}NO$	145.2	75894
365	N,N-Bis-(3-aminopropyl)methylamine		primary + primary + tertiary	105-83-9	$C_7H_{19}N_3$	145.3	7777

Continued on next page

Table B.1 – *continued from previous page*

Nr	IUPAC	Abbreviation	Chemical Class	CAS Nr.	Molecular Formula	Molar Mass g/mol	Pub-Chem ID
366	1-amino-3-(diethylamino)-2-propanol		primary + tertiary	6322-01-6	$C_7H_{18}N_2O$	146.2	97749
367	2,2'-(methylimino)dipropanol		tertiary	56684-95-8	$C_7H_{17}NO_2$	147.2	92498
368	Methyldiisopropanolamine		tertiary	4402-30-6	$C_7H_{17}NO_2$	147.2	95655
369	N,N-Bis(2-hydroxyethyl)ethylenediamine		secondary + secondary	4439-20-7	$C_6H_{16}N_2O_2$	148.2	78179
370	1-(3-Methoxyphenyl)-ethylamine		primary	62409-13-6	$C_9H_{13}NO$	151.2	4612058
371	n-Decylamine		primary	2016-57-1	$C_{10}H_{23}N$	157.3	8916
372	2,2,4(2,4,4)-Trimethyl-1,6-hexanediamine		primary + primary	25620-58-0	$C_9H_{22}N_2$	158.3	3033875

Continued on next page

Table B.1 – *continued from previous page*

Nr	IUPAC	Abbreviation	Chemical Class	CAS Nr.	Molecular Formula	Molar Mass g/mol	Pub-Chem ID
373	2-Amino-5-diethylaminopentane		primary + tertiary	140-80-7	$C_9H_{22}N_2$	158.3	78953
374	Dimethyldipropylenetriamine		primary + secondary + tertiary	10563-29-8	$C_8H_{21}N_3$	159.3	82728
375	3-Morpholino-1,2-propanediol		c-3	6425-32-7	$C_7H_{15}NO_3$	161.2	110850
376	N-Ethyl-N-(2-hydroxyethyl)aniline		tertiary	92-50-2	$C_{10}H_{15}NO$	165.2	62338
377	3-Pentanamine,N-ethyl-3-methyl-,hydrochloride (1:1)		secondary	1185-93-9	$C_8H_{20}ClN$	165.7	70905
378	Cyclohexylpyrrolidone		c-3	6837-24-7	$C_{10}H_{17}NO$	167.3	81278
379	Isophorone diamine		primary + primary	2855-13-2	$C_{10}H_{22}N_2$	170.3	17857

Continued on next page

Table B.1 – *continued from previous page*

Nr	IUPAC	Abbreviation	Chemical Class	CAS Nr.	Molecular Formula	Molar Mass g/mol	Pub-Chem ID
380	2-Aminoundecane		primary	13205-56-6	$C_{11}H_{25}N$	171.3	114476
381	Dibutylethanolamine		tertiary	102-81-8	$C_{10}H_{23}NO$	173.3	7621
382	2-[(1-methylheptyl)amino]ethanol		secondary	26535-68-2	$C_{10}H_{23}NO$	173.3	98354
383	2-(4-Aminopentyl(ethyl)amino)ethanol		primary + tertiary	69559-11-1	$C_9H_{22}N_2O$	174.3	112288
384	2-((3-(Dimethylamino)-2,2-dimethylpropyl)amino)		secondary + tertiary	84642-65-9	$C_9H_{22}N_2O$	174.3	3020016
385	N,N-Di-(2-hydroxyethyl)aniline		tertiary	120-07-0	$C_{10}H_{15}NO_2$	181.2	8416
386	p-aminodiphenylamine		primary + secondary	101-54-2	$C_{12}H_{12}N_2$	184.2	7564
387	Tributylamine		tertiary	102-82-9	$C_{12}H_{27}N$	185.4	7622
388	Dodecylamine		primary	124-22-1	$C_{12}H_{27}N$	185.4	13583

Continued on next page

Table B.1 – *continued from previous page*

Nr	IUPAC	Abbreviation	Chemical Class	CAS Nr.	Molecular Formula	Molar Mass g/mol	Pub-Chem ID
389	N,N-dimethyldecan-1-amine		primary	1120-24-7	$C_{12}H_{27}N$	185.4	70711
390	3-Aminopropyl(octyl)amine		primary + secondary	7173-57-1	$C_{11}H_{26}N_2$	186.3	81603
391	Diethanol-para-toluidine		tertiary	3077-12-1	$C_{11}H_{17}NO_2$	195.3	76497
392	2-Heptanol,2-methyl-6-(methylamino)-,hydrochloride (1:1)		secondary	17086-16-7	$C_9H_{22}ClNO$	195.7	28254
393	2-Butanol, 3-methyl-3-(N-methyl-Nisopropyl)amino-, hydrochloride		tertiary	64037-42-9	$C_9H_{22}ClNO$	195.7	46415
394	N-Octyl-2-pyrrolidone		c-3	2687-94-7	$C_{12}H_{23}NO$	197.3	3033871

Continued on next page

Table B.1 – *continued from previous page*

Nr	IUPAC	Abbreviation	Chemical Class	CAS Nr.	Molecular Formula	Molar Mass g/mol	PubChem ID
395	4,4'-Diaminodiphenylmethane molten plus		primary + primary	101-77-9	$C_{13}H_{14}N_2$	198.3	7577
396	Tridecylamine		primary	86089-17-0	$C_{13}H_{29}N$	199.4	22833454
397	N,N,N',N',N"-Pentamethyldipropylenetriamine		tertiary + tertiary + tertiary	66537-05-1	$C_{11}H_{27}N_3$	201.4	21884960
398	tert-Butyl (3-amino-2,2-dimethylpropyl)carbamate		primary + secondary	292606-35-0	$C_{10}H_{22}N_2O_2$	202.3	4114359
399	Ethanol,2-[[3-(dimethylamino)propyl](2-methylpropyl)amino]		tertiary + tertiary	78718-56-6	$C_{11}H_{26}N_2O$	202.3	3018790
400	4,9-Dioxadodecane-1,12-diamine		primary + primary	7300-34-7	$C_{10}H_{24}N_2O_2$	204.3	81729
401	4,4'-Diaminodicyclohexylmethane		primary + primary	1761-71-3	$C_{13}H_{26}N_2$	210.4	15660

Continued on next page

Table B.1 – *continued from previous page*

Nr	IUPAC	Abbreviation	Chemical Class	CAS Nr.	Molecular Formula	Molar Mass g/mol	PubChem ID
402	4,7,10-Trioxatridecane-1,13-diamine		primary + primary	4246-51-9	$C_{10}H_{24}N_2O_3$	220.3	20239
403	Diisopropanol-p-toluidine		tertiary	38668-48-3	$C_{13}H_{21}NO_2$	223.3	161976
404	n,n,2,3,3-pentamethylbutan-2-amine hydrobromide(1:1)		tertiary	29773-01-1	$C_9H_{22}BrN$	224.2	122475
405	Tripentylamine		tertiary	621-77-2	$C_{15}H_{33}N$	227.4	12133
406	N,3-diethyl-n-methylpentan-3-amine,hydrobromide		tertiary	33326-98-6	$C_{10}H_{24}BrN$	238.2	118449
407	2-Butylamine, N-ethyl-N,2,3,3-tetramethyl-,hydrobromide		tertiary	33327-00-3	$C_{10}H_{24}BrN$	238.2	118451

Continued on next page

Table B.1 – *continued from previous page*

Nr	IUPAC	Abbreviation	Chemical Class	CAS Nr.	Molecular Formula	Molar Mass g/mol	PubChem ID
408	3,3'-Dimethyl-4,4'-diaminodicyclohexylmethane		primary + primary	6864-37-5	$C_{15}H_{30}N_2$	238.4	91555
409	Di-n-octylamine		tertiary	1120-48-5	$C_{16}H_{35}N$	241.5	3094
410	Di-(2-ethylhexyl)amine		secondary	106-20-7	$C_{16}H_{35}N$	241.5	7791
411	2,2'-Dimorpholinodiethylether		c-3 + c-3	6425-39-4	$C_{12}H_{24}N_2O_3$	244.3	80900
412	N-Dodecyl-2-pyrrolidone		c-3	2687-96-9	$C_{16}H_{31}NO$	253.4	62459
413	N,N,N-Trimethylbis(hexamethylene)triamine		secondary + secondary + tertiary	86018-07-7	$C_{15}H_{35}N_3$	257.5	4357340
414	S-Triazine		tertiary (3) + c-3 (3)	15875-13-5	$C_{18}H_{42}N_6$	342.6	85160
415	Tris-(2-ethylhexyl)amine		tertiary	1860-26-0	$C_{24}H_{51}N$	353.7	102705

B.1.2 Solvent Candidates: Amino Acids

Table B.2: List of candidate amino acids with IUPAC name, abbreviation as used in this thesis, CAS number, molecular sum formula, and molar mass.

Nr	IUPAC	Abbreviation	CAS Nr.	Molecular Formula	Molar Mass g/mol
1	2-Amino-2-phenylpropanoic acid		565-07-1	$C_9H_{11}NO_2$	165.2
2	2-Aminoisobutyric acid		62-57-7	$C_4H_9NO_2$	103.1
3	6-Aminohexanoic acid	Aha	60-32-2	$C_6H_{13}NO_2$	131.2
4	Alanine	Ala	302-72-7	$C_3H_7NO_2$	89.1
5	Arginine	Arg	74-79-3	$C_6H_{14}N_4O_2$	174.2
6	Asparagine	Asn	70-47-3	$C_4H_8N_2O_3$	132.1
7	Aspartic acid	Asp	617-45-8	$C_4H_7NO_4$	133.1
8	Cysteine	Cys	52-90-4	$C_3H_7NO_2S$	121.2
9	Glutamic acid	Glu	617-65-2	$C_5H_9NO_4$	147.1
10	Glutamine	Gln	56-85-9	$C_5H_{10}N_2O_3$	146.1
11	Glycine	Gly	56-40-6	$C_2H_5NO_2$	75.1
12	Glycylglycine		556-50-3	$C_4H_8N_2O_3$	132.1
13	Histidine	His	4998-57-6	$C_6H_9N_3O_2$	155.2
14	Hydroxyproline	Hyp	51-35-4	$C_5H_9NO_3$	131.1

Continued on next page

Table B.2 – *continued from previous page*

Nr	IUPAC	Abbreviation	CAS Nr.	Molecular Formula	Molar Mass g/mol
15	Isoleucine	Ile	2095501-92-9	$C_6H_{13}NO_2$	131.2
16	Leucine	Leu	328-39-2	$C_6H_{13}NO_2$	131.2
17	Lysine	Lys	70-54-2	$C_6H_{14}N_2O_2$	146.2
18	meso-2,3-Diaminosuccinicacid	MDASA	23220-52-2	$C_4H_8N_2O_4$	148.1
19	Methionine	Met	59-51-8	$C_5H_{11}NO_2S$	149.2
20	N-(2-Aminoethyl)glycine	AEGly	24123-14-6	$C_4H_{10}N_2O_2$	118.1
21	Phenylalanine	Phe	150-30-1	$C_9H_{11}NO_2$	165.2
22	Proline	Pro	609-36-9	$C_5H_9NO_2$	115.1
23	Pyroglutamatic	Glp	149-87-1	$C_5H_7NO_3$	129.1
24	Sarcosine	Sar	107-97-1	$C_3H_7NO_2$	89.1
25	Serine	Ser	302-84-1	$C_3H_7NO_3$	105.1
26	Taurine	Tau	107-35-7	$C_2H_7NO_3S$	125.1
27	Threonine	Thr	80-68-2	$C_4H_9NO_3$	119.1
28	Tryptophan	Trp	54-12-6	$C_{11}H_{12}N_2O_2$	204.2
29	Tyrosine	Tyr	60-18-4	$C_9H_{11}NO_3$	181.2
30	Valine	Val	516-06-3	$C_5H_{11}NO_2$	117.1

B.1.3 Solvent Candidates: Carboxylic Acids

Table B.3: List of candidate carboxylic acids with IUPAC name, abbreviation as used in this thesis, CAS number, molecular sum formula, and molar mass.

Nr	IUPAC	Abbreviation	CAS Nr.	Molecular Formula	Molar Mass g/mol
1	2-Ethylhexanoic acid		149-57-5	$C_8H_{16}O_2$	144.2
2	acetic acid		64-19-7	$C_2H_4O_2$	60.1
3	Alginic acid		9005-34-9	$C_{14}H_{22}O_{13}$	398.3
4	butanoic acid		107-92-6	$C_4H_8O_2$	88.1
5	formic acid		64-18-6	CH_2O_2	46.0
6	hydrochloric acid		7647-01-0	ClH	36.5
7	i-Nonanoic acid		3302-10-1	$C_9H_{18}O_2$	158.2
8	nitrous acid		7782-77-6	HNO_2	47.0
9	Oxalic acid		144-62-7	$C_2H_2O_4$	90.0
10	Phenoxide		3229-70-7	$C_6H_5O^-$	93.1
11	phosphoric acid		7664-38-2	H_3O_4P	98.0
12	Phosphorous acid		10294-56-1	H_3O_3P	82.0
13	Pipecolic acid	KPIP	535-75-1	$C_6H_{11}NO_2$	129.2
14	Pivalic acid		75-98-9	$C_5H_{10}O_2$	102.1

Continued on next page

Table B.3 – *continued from previous page*

Nr	IUPAC	Abbreviation	CAS Nr.	Molecular Formula	Molar Mass g/mol
15	propanoic acid		79-09-4	$C_3H_6O_2$	74.1
16	pyrophosphoric acid		2466-09-3	$H_4O_7P_2$	178.0
17	Sarcosine		4316-73-8	$C_3H_6NNaO_2$	111.1
18	Sulfuric acid		7664-93-9	H_2O_4S	98.1
19	Sulfurous acid		7782-99-2	H_2O_3S	82.1
20	Tricine		5704-04-1	$C_6H_{13}NO_5$	179.2

B.2 Database Parameter

Table B.4: Liquid density coefficients of pure amines for Eqn. 3.4 in kmol/m^3.

Solvent	A_{ρ_L}	B_{ρ_L}	C_{ρ_L}	Solvent	A_{ρ_L}	B_{ρ_L}	C_{ρ_L}
1-(2HE)PRLD	9.865	-4.09E-03	-2.54E-06	EAPPD	9.372	-4.10E-03	-2.55E-06
1DMA2P	9.823	-3.91E-03	-6.30E-06	EDA	17.439	-3.57E-03	-1.68E-05
2MPZ	9.442	-4.07E-03	-2.53E-06	EEMPA	6.444	-4.57E-03	-6.71E-06
2PPE	9.282	-4.07E-03	-2.53E-06	EMAB	9.070	-4.13E-03	-1.18E-05
3AP	16.164	-8.21E-03	-8.72E-06	EPZ	9.333	-4.10E-03	-2.55E-06
3PPM	9.848	-4.07E-03	-2.53E-06	HEEAB	9.057	-4.09E-03	-1.16E-05
4A1B	13.367	-5.19E-03	-1.28E-05	HEMAB	10.767	-4.15E-03	-1.18E-05
4PP2B	10.162	-4.11E-03	-2.56E-06	HEPP	9.305	-4.10E-03	-2.55E-06
5AP	11.309	-5.20E-03	-7.14E-06	HEPz	9.542	-4.05E-03	-2.52E-06
AEEA	12.154	-6.36E-03	-4.87E-06	HMD	8.393	-3.28E-03	-4.23E-06
AEPD	11.388	-5.82E-03	-5.10E-06	i-BA	11.559	1.48E-03	-2.28E-05
AEPz	9.070	-3.86E-03	-3.58E-06	IPAE	10.612	-4.56E-03	-6.72E-06
AMP	12.959	-4.77E-03	-1.23E-05	MAPA	11.694	-4.70E-03	-8.25E-06
AMPD	12.117	-5.77E-03	-4.53E-06	MDEA	10.597	-5.17E-03	-4.89E-06
BA	11.994	-6.31E-04	-1.88E-05	MEA	19.242	-4.91E-03	-1.34E-05
BDEA	9.269	-4.10E-03	-1.17E-05	MIPA	15.008	-4.04E-03	-1.19E-05
bis-APA	9.210	-4.04E-03	-2.51E-06	MMEA	15.226	-6.50E-03	-9.36E-06
BMEA	9.196	-4.22E-03	-4.16E-06	MOR	13.665	-4.54E-03	-9.82E-06
BZA	9.905	-1.15E-03	-4.58E-06	MPDL	10.888	-4.11E-03	-2.56E-06
DAMP	8.901	-3.70E-03	-4.49E-06	MPZ	10.082	-4.05E-03	-2.52E-06
DAP	14.838	-6.06E-03	-1.26E-05	NMM	10.591	-4.08E-03	-2.54E-06
DEA	11.745	-2.96E-03	-5.11E-06	PAE	10.662	-4.65E-03	-6.82E-06
DEA2P	8.049	-3.50E-03	-3.06E-06	PZ	12.241	-5.26E-03	-7.25E-06
DEAB	8.795	-4.12E-03	-1.17E-05	Serinol	10.590	-5.19E-03	-7.12E-06

Continued on next page

Table B.4 – *continued from previous page*

Solvent	A_{ρ_L}	B_{ρ_L}	C_{ρ_L}	Solvent	A_{ρ_L}	B_{ρ_L}	C_{ρ_L}
DEEA	9.213	-4.21E-03	-4.14E-06	t-BAE	9.088	-4.11E-03	-4.10E-06
DEPD	9.211	-4.12E-03	-1.17E-05	t-BDEA	8.351	-4.09E-03	-1.16E-05
DETA	11.170	-4.93E-03	-5.26E-06	TEA	8.449	-2.37E-03	-2.60E-06
DGA	12.080	-5.48E-03	-4.93E-06	TEDA	9.185	-3.63E-03	-4.83E-06
DIPA	8.570	-2.54E-03	-4.61E-06	TEPA	6.223	-2.71E-03	-1.77E-06
DMAB	10.605	-4.14E-03	-1.18E-05	TETA	8.004	-3.51E-03	-2.97E-06
DMAEEO	9.173	-4.10E-03	-1.17E-05	TIPA	8.532	-4.14E-03	-1.18E-05
DMAP	10.319	-4.31E-03	-6.57E-06	TMEDA	7.809	-2.78E-03	-3.86E-06
DMAPA	9.503	-3.57E-03	-5.57E-06	TMHDA	7.650	-5.22E-03	-7.16E-06
DMEA	12.162	-4.11E-03	-1.17E-05	TMPDA	7.045	-2.64E-03	-3.04E-06
DMPZ	9.299	-4.10E-03	-2.55E-06	TREA	8.704	-1.66E-03	-1.18E-05
DPAB	6.891	-4.14E-03	-1.18E-05	TRIS	12.458	-5.17E-03	-7.09E-06
EAE	12.619	-4.48E-03	-1.21E-05				

Table B.5: VLE coefficients for semi-empirical correlation Eqn. 3.7.

Solvent	A_{VLE}	B_{VLE}	C_{VLE}	D_{VLE}	E_{VLE}	F_{VLE}
1-(2HE)PRLD	3.28	-21.6	-54.6	0.74	-7.35	-65.3
1DMA2P	5.26	-16.6	-42.8	0.78	-7.49	-47.0
2MPZ	4.82	-22.2	-68.7	1.12	-13.1	-56.0
2PPE	3.33	-24.6	-61.7	0.86	-7.57	-73.0
3AP	11.8	-26.7	-65.9	0.78	-7.50	-79.0
3PPM	4.79	-16.9	-44.2	0.78	-7.45	-47.7
4A1B	13.6	-32.8	-80.3	0.78	-7.51	-99.1
4PP2B	6.41	-21.2	-50.2	0.80	-6.49	-66.4
5AP	54.0	-147	-342	0.78	-7.91	-463
AEEA	10.7	-12.3	-33.1	0.78	-7.49	-33.3

Continued on next page

Table B.5 – *continued from previous page*

Solvent	A_{VLE}	B_{VLE}	C_{VLE}	D_{VLE}	E_{VLE}	F_{VLE}
AEPD	7.72	-25.9	-65.0	0.78	-7.50	-77.8
AEPz	7.20	-26.6	-81.6	0.00	-7.16	-69.3
AMP	6.18	-30.6	-79.5	0.82	-8.07	-90.9
AMPD	6.12	-12.4	-32.0	0.78	-7.48	-32.3
BA	8.69	-23.9	-60.1	0.78	-7.50	-70.8
BDEA	2.09	-30.2	-74.1	0.63	-7.79	-94.5
bis-APA	9.82	-29.7	-80.6	0.79	-8.09	-91.4
BMEA	3.69	-23.2	-59.4	0.78	-7.50	-69.9
BZA	8.12	-16.7	-40.2	0.72	-7.32	-47.1
DAMP	2.90	-11.3	-30.6	0.78	-7.54	-29.9
DAP	9.72	-25.5	-66.8	0.90	-7.73	-77.5
DEA	5.76	-18.7	-44.5	0.85	-6.91	-55.3
DEA2P	8.72	-10.0	-27.9	0.78	-7.55	-25.1
DEAB	13.5	-29.2	-73.1	0.78	-7.50	-89.1
DEEA	4.72	-19.7	-50.8	0.78	-7.48	-58.0
DEPD	11.1	-25.4	-63.4	0.78	-7.50	-75.5
DETA	17.4	-27.8	-75.4	1.03	-7.99	-85.4
DGA	6.72	-24.9	-62.6	0.78	-7.51	-74.5
DIPA	5.67	-9.45	-24.9	0.78	-7.49	-21.9
DMAB	9.21	-42.2	-104	0.78	-7.52	-133
DMAEEO	3.09	-20.7	-52.7	0.78	-7.53	-60.9
DMAP	4.06	-20.8	-52.9	0.78	-7.50	-60.6
DMAPA	11.9	-40.8	-102	0.78	-7.53	-130
DMEA	3.55	-23.3	-59.4	0.78	-7.50	-69.9
DMPZ	4.47	-23.4	-58.8	0.78	-7.50	-69.1
DPAB	3.07	-47.9	-117	0.78	-7.54	-150

Continued on next page

Table B.5 – *continued from previous page*

Solvent	A_{VLE}	B_{VLE}	C_{VLE}	D_{VLE}	E_{VLE}	F_{VLE}
EAE	5.39	-24.8	-63.0	0.78	-7.51	-74.9
EAPPD	5.83	-24.6	-63.3	0.78	-7.50	-75.1
EDA	11.2	-29.9	-74.0	0.78	-7.51	-90.3
EEMPA	1.57	-25.7	-65.3	0.78	-7.45	-77.9
EMAB	6.10	-28.4	-71.2	0.77	-7.50	-87.1
EPZ	6.88	-30.6	-76.4	0.78	-7.51	-93.8
HEEAB	6.09	-32.7	-81.5	0.78	-7.52	-101
HEMAB	4.15	-25.2	-63.2	0.78	-7.49	-75.6
HEPP	6.71	-23.0	-52.7	0.80	-6.92	-74.4
HEPz	4.36	-24.1	-61.1	0.78	-7.49	-72.1
HMD	8.95	-22.7	-58.9	0.99	-7.54	-69.9
i-BA	6.57	-15.6	-40.3	0.78	-7.50	-43.2
IPAE	5.44	-30.9	-77.5	0.78	-7.51	-95.2
MAPA	6.09	-8.88	-18.6	0.68	-5.17	-29.3
MDEA	3.76	-19.3	-46.9	0.48	-7.01	-58.1
MEA	9.18	-26.3	-66.0	0.88	-7.71	-76.9
MIPA	12.0	-26.3	-64.3	0.78	-7.50	-76.8
MMEA	6.33	-18.8	-47.9	0.78	-7.49	-54.1
MOR	4.13	-17.4	-44.6	0.78	-7.50	-49.3
MPDL	5.37	-17.4	-44.9	0.79	-7.52	-49.7
MPZ	3.97	-22.6	-58.0	0.78	-7.50	-68.0
NMM	1.62	-17.9	-45.5	0.78	-7.49	-50.6
PAE	5.46	-25.7	-64.9	0.78	-7.50	-77.5
PZ	6.69	-23.3	-60.1	0.78	-7.52	-70.8
Serinol	4.68	-16.8	-42.8	0.78	-7.49	-46.8
t-BAE	6.53	-34.6	-86.7	0.78	-7.52	-108

Continued on next page

Table B.5 – *continued from previous page*

Solvent	A_{VLE}	B_{VLE}	C_{VLE}	D_{VLE}	E_{VLE}	F_{VLE}
t-BDEA	2.91	-34.3	-85.5	0.78	-7.51	-106
TEA	3.54	-16.1	-41.1	0.78	-7.51	-44.5
TEDA	2.74	-18.2	-46.6	0.79	-7.48	-52.2
TEPA	8.46	-19.2	-50.5	0.88	-7.17	-61.7
TETA	7.36	-18.4	-47.0	0.87	-7.02	-58.0
TIPA	1.65	-14.6	-38.2	0.78	-7.48	-39.7
TMEDA	5.07	-30.6	-77.0	0.79	-7.52	-94.0
TMHDA	7.47	-41.6	-113	1.16	-8.78	-127
TMPDA	4.63	-27.2	-71.1	0.99	-7.87	-82.3
TREA	2.85	-26.3	-65.4	0.78	-7.48	-78.5
TRIS	3.32	-14.4	-37.3	0.78	-7.49	-39.2

Table B.6: Coefficients for Henry's law Eqn. 3.2.

Solvent	He_{A12}	He_{B12}	He_{C12}	$He_{N_2O,A}$	$He_{N_2O,A}$
1-(2HE)PRLD	0	3.13E+02	0	-3.55E+04	132.7
1DMA2P	0	3.11E+02	0	-3.54E+04	132.1
2MPZ	3.88E+06	3.73E+02	10	-6.29E+03	27.2
2PPE	5.15E+06	4.32E+02	12	-6.23E+03	26.9
3AP	0	3.15E+02	0	-3.58E+04	133.7
3PPM	0	3.15E+02	0	-3.59E+04	133.9
4A1B	0	3.11E+02	0	-3.54E+04	132.1
4PP2B	0	3.12E+02	0	-3.54E+04	132.3
5AP	0	3.12E+02	0	-3.55E+04	132.3
AEEA	5.19E+06	3.61E+02	12	-9.22E+03	39.8
AEPD	0	3.15E+02	0	-3.58E+04	133.7
AEPz	0	3.13E+02	0	-3.56E+04	132.8

Continued on next page

Table B.6 – *continued from previous page*

Solvent	He_{A12}	He_{B12}	He_{C12}	$He_{N_2O,A}$	$He_{N_2O,A}$
AMP	4.42E+06	3.21E+02	12	-3.75E+04	161.9
AMPD	6.49E+06	3.53E+02	12	-9.22E+03	39.8
BA	0	3.16E+02	0	-3.59E+04	134.2
BDEA	0	3.15E+02	0	-3.58E+04	133.7
bis-APA	0	3.13E+02	0	-3.57E+04	133.1
BMEA	0	3.11E+02	0	-3.53E+04	131.8
BZA	0	3.11E+02	0	-3.53E+04	131.8
DAMP	0	3.15E+02	0	-3.59E+04	133.9
DAP	4.74E+06	3.55E+02	11	-1.48E+04	64.1
DEA	4.89E+06	3.61E+02	16	-1.19E+04	50.3
DEA2P	0	3.16E+02	0	-3.59E+04	134.1
DEAB	6.45E+06	2.64E+02	13	-3.80E+04	135.7
DEEA	0	3.12E+02	0	-3.55E+04	132.6
DEPD	0	3.16E+02	0	-3.59E+04	134.1
DETA	6.40E+06	3.82E+02	16	-4.26E+03	21.0
DGA	3.70E+06	3.58E+02	7	-2.01E+04	76.5
DIPA	8.73E+06	3.47E+02	17	-7.70E+03	31.8
DMAB	0	3.12E+02	0	-3.54E+04	132.3
DMAEEO	0	3.11E+02	0	-3.54E+04	131.9
DMAP	0	3.11E+02	0	-3.54E+04	132.1
DMAPA	0	3.12E+02	0	-3.54E+04	132.3
DMEA	3.77E+06	3.62E+02	3	-5.31E+04	194.3
DMPZ	0	3.10E+02	0	-3.53E+04	131.7
DPAB	0	3.11E+02	0	-3.54E+04	132.2
EAE	0	3.15E+02	0	-3.59E+04	133.9
EAPPD	1	3.12E+02	0	-3.55E+04	132.6

Continued on next page

Table B.6 – *continued from previous page*

Solvent	He_{A12}	He_{B12}	He_{C12}	$He_{N_2O,A}$	$He_{N_2O,A}$
EDA	2	3.22E+02	17	-1.77E+04	67.8
EEMPA	3	3.11E+02	0	-3.54E+04	132.0
EMAB	4	3.13E+02	0	-3.56E+04	133.0
EPZ	5	3.14E+02	0	-3.58E+04	133.5
HEEAB	6	3.10E+02	0	-3.53E+04	131.8
HEMAB	7	3.15E+02	0	-3.58E+04	133.8
HEPP	8	3.14E+02	0	-3.57E+04	133.4
HEPz	9	3.16E+02	0	-3.59E+04	134.1
HMD	10	3.16E+02	0	-3.59E+04	134.0
i-BA	11	3.13E+02	0	-3.56E+04	132.9
IPAE	12	3.11E+02	0	-3.53E+04	131.9
MAPA	13	3.83E+02	16	-7.73E+03	33.4
MDEA	14	3.39E+02	8	-8.61E+03	34.9
MEA	15	3.23E+02	13	-9.13E+03	39.4
MIPA	16	3.14E+02	0	-3.57E+04	133.4
MMEA	17	3.11E+02	0	-3.54E+04	132.0
MOR	18	3.11E+02	0	-3.54E+04	132.2
MPDL	19	3.16E+02	0	-3.59E+04	134.1
MPZ	20	3.80E+02	12	-1.87E+04	80.8
NMM	21	3.10E+02	0	-3.53E+04	131.7
PAE	22	3.15E+02	0	-3.58E+04	133.6
PZ	23	3.78E+02	13	-4.42E+03	19.1
Serinol	24	3.14E+02	0	-3.58E+04	133.4
t-BAE	25	3.14E+02	0	-3.57E+04	133.2
t-BDEA	26	3.12E+02	0	-3.55E+04	132.6
TEA	27	3.24E+02	12	-1.24E+04	50.3

Continued on next page

Table B.6 – *continued from previous page*

Solvent	He_{A12}	He_{B12}	He_{C12}	$He_{N_2O,A}$	$He_{N_2O,A}$
TEDA	28	3.16E+02	0	-3.59E+04	134.0
TEPA	29	3.10E+02	0	-3.53E+04	131.6
TETA	30	3.12E+02	0	-3.55E+04	132.5
TIPA	31	3.12E+02	0	-3.55E+04	132.6
TMEDA	32	3.15E+02	0	-3.59E+04	133.8
TMHDA	33	3.16E+02	0	-3.60E+04	134.2
TMPDA	34	3.13E+02	0	-3.56E+04	132.8
TREA	35	3.15E+02	0	-3.58E+04	133.8
TRIS	36	3.65E+02	14	-2.93E+04	113.1

Table B.7: Liquid heat capacity coefficients of pure amines for Eqn. 3.4 in J/(mol K).

Solvent	$A_{c_{P,L}}$	$B_{c_{P,L}}$	$C_{c_{P,L}}$	Solvent	$A_{c_{P,L}}$	$B_{c_{P,L}}$	$C_{c_{P,L}}$
1-(2HE)PRLD	136.9	-0.03	7.27E-04	EAPPD	102.6	0.62	4.27E-04
1DMA2P	156.4	0.16	4.45E-04	EDA	170.7	-0.14	4.86E-04
2MPZ	-136.7	1.51	-9.98E-04	EEMPA	388.6	-0.16	1.70E-03
2PPE	29.5	1.12	-6.20E-04	EMAB	265.2	-0.17	1.06E-03
3AP	220.0	-0.10	5.54E-04	EPZ	-198.8	1.92	-1.71E-03
3PPM	259.3	-0.41	1.42E-03	HEEAB	450.1	-0.89	2.17E-03
4A1B	191.3	-0.19	1.02E-03	HEMAB	395.7	-0.71	1.85E-03
4PP2B	319.6	-0.34	1.35E-03	HEPP	227.1	0.02	6.09E-04
5AP	245.7	-0.36	1.33E-03	HEPz	131.1	0.53	-2.36E-18
AEEA	277.6	-0.02	4.97E-04	HMD	253.3	0.03	3.51E-04
AEPD	417.0	-1.04	2.39E-03	i-BA	209.9	-0.40	1.02E-03
AEPz	252.8	-0.02	3.82E-04	IPAE	259.3	-0.40	1.40E-03
AMP	29.2	0.83	-4.26E-04	MAPA	233.2	-0.15	6.45E-04
AMPD	362.6	-0.87	2.08E-03	MDEA	94.6	0.43	4.73E-04

Continued on next page

Table B.7 – *continued from previous page*

Solvent	$A_{c_{P,L}}$	$B_{c_{P,L}}$	$C_{c_{P,L}}$	Solvent	$A_{c_{P,L}}$	$B_{c_{P,L}}$	$C_{c_{P,L}}$
BA	202.1	-0.34	9.07E-04	MEA	30.6	0.59	-4.66E-04
BDEA	350.7	-0.42	1.62E-03	MIPA	225.9	-0.15	5.62E-04
bis-APA	-458.4	3.52	-3.66E-03	MMEA	189.8	-0.11	4.91E-04
BMEA	112.1	0.59	0	MOR	137.3	0.02	2.30E-04
BZA	199.2	-0.03	1.79E-04	MPDL	156.4	0.16	4.48E-04
DAMP	325.0	-0.09	6.30E-04	MPZ	197.1	0.06	0
DAP	250.7	-0.29	9.09E-04	NMM	115.6	0.29	2.21E-04
DEA	68.5	0.61	2.27E-05	PAE	127.1	0.46	0
DEA2P	265.2	-0.17	1.05E-03	PZ	19.0	0.84	-7.81E-04
DEAB	319.6	-0.34	1.36E-03	Serinol	281.0	-0.62	1.63E-03
DEEA	16.5	0.66	3.78E-18	t-BAE	340.9	-0.65	1.85E-03
DEPD	395.7	-0.72	1.88E-03	t-BDEA	-16.2	1.56	-1.02E-03
DETA	230.0	-0.07	4.81E-04	TEA	288.1	0.20	1.52E-04
DGA	168.4	0.22	2.72E-04	TEDA	-268.2	2.18	-2.32E-03
DIPA	69.6	1.08	-4.61E-04	TEPA	386.2	0.11	3.26E-04
DMAB	197.2	0.04	6.75E-04	TETA	313.7	0.07	3.69E-04
DMAEEO	354.9	-0.58	1.62E-03	TIPA	662.2	-1.68	3.44E-03
DMAP	142.8	0.21	3.72E-04	TMEDA	198.8	-0.05	3.52E-04
DMAPA	221.5	-0.11	5.05E-04	TMHDA	-356.1	2.67	-2.98E-03
DMEA	247.8	-0.33	9.44E-04	TMPDA	227.1	-0.02	3.36E-04
DMPZ	137.4	0.27	0	TREA	-64.1	1.40	-1.45E-03
DPAB	428.4	-0.67	1.95E-03	TRIS	50.3	0.26	4.76E-04
EAE	97.4	0.44	0				

Table B.8: Vapour pressure coefficients of pure amines for Antoine equation Eqn. 3.4 in kPa.

Solvent	$A_{p\mathrm{Vap}}$	$B_{p\mathrm{Vap}}$	$C_{p\mathrm{Vap}}$	Solvent	$A_{p\mathrm{Vap}}$	$B_{p\mathrm{Vap}}$	$C_{p\mathrm{Vap}}$
1-(2HE)PRLD	18.6	-5.27E+03	6.49	EAPPD	16.8	-4.73E+03	-58.4
1DMA2P	16.1	-3.95E+03	-51.2	EDA	15.6	-3.65E+03	-54.1
2MPZ	15.5	-4.04E+03	-60.1	EEMPA	16.1	-4.70E+03	-58.1
2PPE	19.6	-6.22E+03	40.0	EMAB	17.1	-4.70E+03	-58.1
3AP	16.6	-4.49E+03	-85.6	EPZ	15.5	-4.05E+03	-60.9
3PPM	14.2	-4.72E+03	-58.4	HEEAB	16.6	-4.74E+03	-58.6
4A1B	16.1	-4.62E+03	-73.7	HEMAB	16.6	-4.70E+03	-58.1
4PP2B	9.9	-4.71E+03	-58.2	HEPP	14.0	-4.69E+03	-57.9
5AP	16.1	-4.79E+03	-78.9	HEPz	23.8	-5.82E+03	-42.2
AEEA	17.5	-5.61E+03	-83.7	HMD	16.2	-5.00E+03	-39.4
AEPD	18.8	-5.37E+03	-65.6	i-BA	14.8	-3.05E+03	-40.5
AEPz	15.4	-4.51E+03	-70.7	IPAE	16.1	-4.37E+03	-65.0
AMP	16.1	-4.34E+03	-63.4	MAPA	15.7	-3.97E+03	-56.4
AMPD	18.3	-6.07E+03	-87.9	MDEA	18.1	-5.77E+03	-93.7
BA	14.6	-3.06E+03	-46.9	MEA	15.1	-3.61E+03	-103
BDEA	10.8	-4.72E+03	-58.3	MIPA	17.8	-5.43E+03	-21.7
bis-APA	12.0	-4.74E+03	-58.6	MMEA	15.7	-4.00E+03	-71.3
BMEA	16.1	-4.62E+03	-72.9	MOR	15.0	-3.65E+03	-48.4
BZA	15.0	-4.19E+03	-57.0	MPDL	15.3	-4.69E+03	-58.0
DAMP	15.7	-4.36E+03	-70.5	MPZ	15.5	-3.85E+03	-55.0
DAP	15.6	-3.95E+03	-56.1	NMM	17.7	-4.50E+03	-29.2
DEA	17.3	-5.77E+03	-84.3	PAE	16.1	-4.45E+03	-67.5
DEA2P	16.1	-4.42E+03	-66.6	PZ	15.0	-3.61E+03	-71.4
DEAB	14.6	-4.75E+03	-58.7	Serinol	10.9	-4.70E+03	-58.1
DEEA	16.1	-4.31E+03	-62.5	t-BAE	16.1	-4.43E+03	-66.5

Continued on next page

Table B.8 – *continued from previous page*

Solvent	$A_{p_{\mathrm{Vap}}}$	$B_{p_{\mathrm{Vap}}}$	$C_{p_{\mathrm{Vap}}}$	Solvent	$A_{p_{\mathrm{Vap}}}$	$B_{p_{\mathrm{Vap}}}$	$C_{p_{\mathrm{Vap}}}$
DEPD	12.6	-4.67E+03	-57.8	t-BDEA	18.5	-5.74E+03	-77.2
DETA	17.1	-5.75E+03	-22.5	TEA	20.3	-9.74E+03	6.74
DGA	16.7	-4.96E+03	-102	TEDA	14.4	-3.45E+03	-95.7
DIPA	18.0	-5.53E+03	-109	TEPA	17.7	-6.70E+03	-93.8
DMAB	15.5	-4.74E+03	-58.6	TETA	16.6	-5.40E+03	-96.2
DMAEEO	18.0	-4.81E+03	-14.3	TIPA	20.4	-9.15E+03	0.01
DMAP	16.1	-4.27E+03	-62.0	TMEDA	15.6	-3.80E+03	-50.9
DMAPA	15.7	-3.89E+03	-54.3	TMHDA	12.1	-4.71E+03	-58.2
DMEA	17.0	-4.79E+03	-20.8	TMPDA	15.7	-4.00E+03	-57.4
DMPZ	15.5	-3.85E+03	-53.8	TREA	13.0	-2.13E+03	-109
DPAB	16.6	-4.74E+03	-58.6	TRIS	5.2	-4.72E+03	-58.4
EAE	16.1	-4.33E+03	-63.9				

Table B.9: Liquid thermal conductivity coefficients of pure amines for Eqn. 3.4 in W/(m·K).

Solvent	$A_{\lambda_{\mathrm{L}}}$	$B_{\lambda_{\mathrm{L}}}$	$C_{\lambda_{\mathrm{L}}}$	Solvent	$A_{\lambda_{\mathrm{L}}}$	$B_{\lambda_{\mathrm{L}}}$	$C_{\lambda_{\mathrm{L}}}$
1-(2HE)PRLD	0.24	-2.06E-04		EAPPD	0.31	-2.06E-04	
1DMA2P	0.19	-2.12E-04		EDA	0.36	-4.45E-04	
2MPZ	0.25	-2.08E-04		EEMPA	0.31	-2.05E-04	
2PPE	0.24	-2.06E-04		EMAB	0.20	-2.05E-04	
3AP	0.31	-3.46E-04		EPZ	0.24	-2.07E-04	
3PPM	0.24	-2.04E-04		HEEAB	0.17	-2.07E-04	
4A1B	0.20	-2.51E-04		HEMAB	0.19	-2.08E-04	
4PP2B	0.28	-2.06E-04		HEPP	0.22	-2.05E-04	
5AP	0.19	-2.13E-04		HEPz	0.24	-2.22E-04	
AEEA	0.27	-2.83E-04		HMD	0.28	-3.00E-04	
AEPD	0.18	-1.88E-04		i-BA	0.26	-3.65E-04	

Continued on next page

Table B.9 – *continued from previous page*

Solvent	A_{λ_L}	B_{λ_L}	C_{λ_L}	Solvent	A_{λ_L}	B_{λ_L}	C_{λ_L}
AEPz	0.23	-1.53E-04		IPAE	0.19	-2.16E-04	
AMP	0.32	-3.81E-04		MAPA	0.20	-2.34E-04	
AMPD	0.19	-1.93E-04		MDEA	0.16	8.06E-05	
BA	0.28	-6.15E-04		MEA	-0.01	1.47E-03	
BDEA	0.23	-2.06E-04		MIPA	0.31	-3.68E-04	
bis-APA	0.31	-2.05E-04		MMEA	0.28	-3.19E-04	
BMEA	0.18	-1.88E-04		MOR	0.25	-2.89E-04	
BZA	0.24	-2.50E-04		MPDL	0.22	-2.06E-04	
DAMP	0.18	-1.93E-04		MPZ	0.24	-2.08E-04	
DAP	0.32	-3.63E-04		NMM	0.22	-2.06E-04	
DEA	0.02	1.04E-03		PAE	0.19	-2.14E-04	
DEA2P	0.17	-1.75E-04		PZ	0.22	-2.53E-04	
DEAB	0.21	-2.05E-04		Serinol	0.23	-2.04E-04	
DEEA	0.20	-2.14E-04		t-BAE	0.18	-1.89E-04	
DEPD	0.17	-2.05E-04		t-BDEA	0.23	-2.04E-04	
DETA	0.31	-3.12E-04		TEA	0.07	7.00E-04	
DGA	0.30	-2.92E-04		TEDA	0.19	-2.13E-04	
DIPA	0.26	-2.84E-04		TEPA	0.22	-2.03E-04	
DMAB	0.21	-2.07E-04		TETA	0.23	-2.35E-04	
DMAEEO	0.22	-2.07E-04		TIPA	0.26	-2.05E-04	
DMAP	0.19	-2.16E-04		TMEDA	0.20	-2.57E-04	
DMAPA	0.26	-3.13E-04		TMHDA	0.26	-2.07E-04	
DMEA	0.26	-3.28E-04		TMPDA	0.17	-1.79E-04	
DMPZ	0.24	-2.06E-04		TREA	0.19	-2.44E-04	
DPAB	0.16	-2.05E-04		TRIS	0.24	-2.04E-04	
EAE	0.20	-2.47E-04					

Table B.10: Surface tension y coefficients of pure amines for Eqn. 3.4 in kg/s^2.

Solvent	A_{σ_L}	B_{σ_L}	C_{σ_L}	Solvent	A_{σ_L}	B_{σ_L}	C_{σ_L}
1-(2HE)PRLD	0.09	-2.11E-04	6.39E-08	EAPPD	0.09	-1.71E-04	4.64E-08
1DMA2P	0.12	-2.44E-04	7.67E-08	EDA	0.10	-2.15E-04	7.44E-08
2MPZ	0.09	-2.11E-04	6.41E-08	EEMPA	0.08	-1.71E-04	4.64E-08
2PPE	0.09	-2.14E-04	6.48E-08	EMAB	0.08	-1.59E-04	3.98E-08
3AP	0.10	-1.88E-04	5.54E-08	EPZ	0.09	-2.13E-04	6.47E-08
3PPM	0.09	-2.12E-04	6.44E-08	HEEAB	0.08	-1.59E-04	3.99E-08
4A1B	0.11	-2.50E-04	9.20E-08	HEMAB	0.09	-1.61E-04	4.02E-08
4PP2B	0.10	-2.14E-04	6.48E-08	HEPP	0.09	-2.14E-04	6.50E-08
5AP	0.09	-1.92E-04	6.01E-08	HEPz	0.08	-1.60E-04	4.00E-08
AEEA	0.08	-1.45E-04	3.13E-08	HMD	0.08	-1.43E-04	4.07E-08
AEPD	0.07	-1.35E-04	3.69E-08	i-BA	0.05	-1.03E-04	3.02E-09
AEPz	0.09	-1.54E-04	3.93E-08	IPAE	0.11	-2.18E-04	6.84E-08
AMP	0.12	-2.78E-04	1.03E-07	MAPA	0.08	-1.58E-04	5.17E-08
AMPD	0.09	-1.62E-04	4.07E-08	MDEA	0.13	-2.44E-04	6.67E-08
BA	0.11	-2.50E-04	9.27E-08	MEA	0.11	-2.13E-04	6.47E-08
BDEA	0.08	-1.61E-04	4.03E-08	MIPA	0.11	-2.33E-04	7.58E-08
bis-APA	0.07	-1.39E-04	3.19E-08	MMEA	0.11	-2.23E-04	6.91E-08
BMEA	0.09	-1.69E-04	4.60E-08	MOR	0.09	-1.82E-04	5.85E-08
BZA	0.08	-1.40E-04	3.22E-08	MPDL	0.09	-2.11E-04	6.41E-08
DAMP	0.07	-1.44E-04	4.09E-08	MPZ	0.09	-2.13E-04	6.47E-08
DAP	0.08	-1.75E-04	6.18E-08	NMM	0.09	-2.10E-04	6.38E-08
DEA	0.11	-1.86E-04	4.67E-08	PAE	0.10	-2.14E-04	6.72E-08
DEA2P	0.09	-1.61E-04	4.03E-08	PZ	0.10	-1.94E-04	5.90E-08
DEAB	0.08	-1.60E-04	3.99E-08	Serinol	0.08	-1.38E-04	3.18E-08
DEEA	0.10	-1.86E-04	5.05E-08	t-BAE	0.10	-1.80E-04	4.88E-08

Continued on next page

Table B.10 – *continued from previous page*

Solvent	A_{σ_L}	B_{σ_L}	C_{σ_L}	Solvent	A_{σ_L}	B_{σ_L}	C_{σ_L}
DEPD	0.09	-1.60E-04	3.99E-08	t-BDEA	0.08	-1.59E-04	3.98E-08
DETA	0.10	-1.87E-04	5.15E-08	TEA	0.09	-1.48E-04	3.20E-08
DGA	0.08	-1.35E-04	3.12E-08	TEDA	0.08	-1.55E-04	4.47E-08
DIPA	0.13	-2.44E-04	6.77E-08	TEPA	0.10	-1.59E-04	3.52E-08
DMAB	0.10	-2.46E-04	6.73E-08	TETA	0.10	-1.72E-04	4.28E-08
DMAEEO	0.08	-1.60E-04	3.99E-08	TIPA	0.08	-1.59E-04	3.97E-08
DMAP	0.11	-2.20E-04	6.90E-08	TMEDA	0.07	-1.26E-04	3.59E-08
DMAPA	0.07	-1.42E-04	4.31E-08	TMHDA	0.07	-1.60E-04	4.00E-08
DMEA	0.13	-2.96E-04	1.10E-07	TMPDA	0.07	-1.23E-04	3.29E-08
DMPZ	0.09	-2.11E-04	6.39E-08	TREA	0.06	-1.36E-04	5.50E-08
DPAB	0.07	-1.61E-04	4.02E-08	TRIS	0.08	-1.40E-04	3.22E-08
EAE	0.12	-2.74E-04	1.02E-07				

Table B.11: Liquid viscosity coefficients of pure amines for Eqn. 3.4 in kg/(m·s).

Solvent	A_{η_L}	B_{η_L}	C_{η_L}	Solvent	A_{η_L}	B_{η_L}	C_{η_L}
1-(2HE)PRLD	-190	1.18E+04	2.54E+01	EAPPD	-190	1.20E+04	2.57E+01
1DMA2P	-192	1.19E+04	2.55E+01	EDA	-53.9	4.07E+03	6.03E+00
2MPZ	-13.0	1.68E+03	2.05E-01	EEMPA	-191	1.19E+04	2.57E+01
2PPE	-292	1.91E+04	3.94E+01	EMAB	-6.45	8.25E+02	6.96E-03
3AP	-16.6	3.67E+03	9.59E-03	EPZ	-192	1.20E+04	2.58E+01
3PPM	-37.2	2.80E+03	4.14E+00	HEEAB	-7.31	8.21E+02	6.93E-03
4A1B	-191	1.19E+04	2.56E+01	HEMAB	-7.63	8.12E+02	6.85E-03
4PP2B	-190	1.19E+04	2.57E+01	HEPP	-191	1.19E+04	2.57E+01
5AP	-191	1.20E+04	2.58E+01	HEPz	-139	1.23E+04	1.70E+01
AEEA	-18.0	4.99E+03	-1.43E-01	HMD	-10.1	1.68E+03	-2.79E-01
AEPD	-190	1.18E+04	2.54E+01	i-BA	-12.1	1.37E+03	0.00E+00

Continued on next page

Table B.11 – *continued from previous page*

Solvent	A_{η_L}	B_{η_L}	C_{η_L}	Solvent	A_{η_L}	B_{η_L}	C_{η_L}
AEPz	-128	8.80E+03	1.65E+01	IPAE	-191	1.18E+04	2.54E+01
AMP	-22.8	6.22E+03	0.00E+00	MAPA	-193	1.20E+04	2.57E+01
AMPD	-189	1.19E+04	2.57E+01	MDEA	-55.6	6.44E+03	5.56E+00
BA	-29.0	1.98E+03	2.56E+00	MEA	-111	8.17E+03	1.40E+01
BDEA	-190	1.19E+04	2.57E+01	MIPA	-19.1	4.52E+03	0.00E+00
bis-APA	-192	1.18E+04	2.54E+01	MMEA	-15.2	3.21E+03	-2.40E-02
BMEA	-191	1.19E+04	2.56E+01	MOR	-50.4	3.62E+03	5.64E+00
BZA	-19.0	1.90E+03	1.11E+00	MPDL	-191	1.19E+04	2.57E+01
DAMP	-192	1.18E+04	2.55E+01	MPZ	-192	1.19E+04	2.57E+01
DAP	-12.3	1.60E+03	1.04E-01	NMM	-193	1.18E+04	2.54E+01
DEA	-161	1.29E+04	2.08E+01	PAE	-191	1.18E+04	2.54E+01
DEA2P	-8.65	8.18E+02	6.90E-03	PZ	-43.7	1.66E+04	2.03E-01
DEAB	-191	1.20E+04	2.57E+01	Serinol	-189	1.20E+04	2.57E+01
DEEA	-84.4	6.07E+03	1.02E+01	t-BAE	-190	1.19E+04	2.56E+01
DEPD	-7.52	8.21E+02	6.93E-03	t-BDEA	-190	1.18E+04	2.54E+01
DETA	-70.1	5.40E+03	8.28E+00	TEA	-77.0	8.30E+03	8.52E+00
DGA	-17.1	4.15E+03	-6.20E-02	TEDA	-18.0	4.80E+03	5.54E-02
DIPA	-584	3.51E+04	8.16E+01	TEPA	-12.7	3.11E+03	-1.03E-02
DMAB	-191	1.18E+04	2.55E+01	TETA	-12.6	2.59E+03	-1.79E-02
DMAEEO	-191	1.19E+04	2.56E+01	TIPA	-189	1.18E+04	2.54E+01
DMAP	-192	1.20E+04	2.57E+01	TMEDA	-12.4	1.82E+03	5.27E-04
DMAPA	-12.3	1.63E+03	0.00E+00	TMHDA	-192	1.18E+04	2.55E+01
DMEA	-17.4	3.39E+03	0.00E+00	TMPDA	-193	1.19E+04	2.56E+01
DMPZ	-193	1.19E+04	2.56E+01	TREA	-6.60	7.51E+02	-6.80E-01
DPAB	-5.70	8.19E+02	6.92E-03	TRIS	-188	1.18E+04	2.53E+01
EAE	-190	1.20E+04	2.58E+01				

Table B.12: Heat of vapourisation coefficients of pure amines for Eqn. 3.4 in kJ/mol.

Solvent	$A_{\Delta H_{Vap}}$	$B_{\Delta H_{Vap}}$	$C_{\Delta H_{Vap}}$	Solvent	$A_{\Delta H_{Vap}}$	$B_{\Delta H_{Vap}}$	$C_{\Delta H_{Vap}}$
1-(2HE)PRLD	40.1	-9.61E-06	-7.36E-08	EAPPD	61.4	-1.76E-05	-4.73E-08
1DMA2P	44.6	-1.04E-05	-5.36E-08	EDA	53.5	-2.87E-06	-8.02E-08
2MPZ	36.9	-2.00E-05	-6.91E-08	EEMPA	54.8	-5.48E-06	-1.25E-07
2PPE	41.5	-1.99E-05	-6.87E-08	EMAB	53.1	-1.37E-05	-8.95E-08
3AP	55.3	-2.47E-05	-8.81E-08	EPZ	37.2	-2.00E-05	-6.91E-08
3PPM	40.8	-1.99E-05	-6.88E-08	HEEAB	59.3	-5.43E-06	-1.24E-07
4A1B	41.8	-1.71E-05	-8.81E-08	HEMAB	57.2	-5.49E-06	-1.25E-07
4PP2B	75.9	-2.27E-06	-1.39E-07	HEPP	41.5	-2.00E-05	-6.91E-08
5AP	74.4	-1.71E-05	-8.79E-08	HEPz	45.8	-1.98E-05	-6.86E-08
AEEA	65.4	-3.78E-05	-8.38E-08	HMD	49.1	-2.42E-05	-7.23E-08
AEPD	59.3	-1.84E-05	-5.09E-08	i-BA	40.6	1.86E-05	-1.39E-07
AEPz	50.1	-2.84E-05	-5.78E-08	IPAE	59.0	-1.36E-05	-6.99E-08
AMP	60.4	-1.80E-06	-1.11E-07	MAPA	59.8	-1.17E-05	-7.86E-08
AMPD	74.7	-2.53E-05	-5.24E-08	MDEA	69.9	-4.01E-05	-1.03E-07
BA	42.0	1.26E-05	-1.16E-07	MEA	70.6	-9.70E-06	-7.43E-08
BDEA	48.6	-5.47E-06	-1.25E-07	MIPA	65.0	-6.16E-06	-8.17E-08
bis-APA	47.9	-2.31E-05	-6.51E-08	MMEA	69.0	-1.76E-05	-8.01E-08
BMEA	69.3	-2.17E-05	-5.83E-08	MOR	53.2	-1.07E-05	-6.70E-08
BZA	64.9	-2.11E-05	-5.45E-08	MPDL	41.3	-1.99E-05	-6.87E-08
DAMP	62.0	-1.84E-05	-5.89E-08	MPZ	35.4	-2.01E-05	-6.93E-08
DAP	52.3	-5.54E-06	-8.41E-08	NMM	33.4	-1.06E-05	-3.39E-08
DEA	64.5	-2.72E-05	-6.82E-08	PAE	61.5	-1.42E-05	-7.32E-08
DEA2P	55.8	-1.88E-05	-3.88E-08	PZ	62.3	-1.99E-05	-6.87E-08
DEAB	52.2	-1.04E-05	-5.34E-08	Serinol	47.6	-5.30E-05	-7.25E-08
DEEA	49.3	-1.55E-05	-4.17E-08	t-BAE	55.7	-1.74E-05	-4.69E-08

Continued on next page

Table B.12 – *continued from previous page*

Solvent	$A_{\Delta H_{\mathrm{Vap}}}$	$B_{\Delta H_{\mathrm{Vap}}}$	$C_{\Delta H_{\mathrm{Vap}}}$	Solvent	$A_{\Delta H_{\mathrm{Vap}}}$	$B_{\Delta H_{\mathrm{Vap}}}$	$C_{\Delta H_{\mathrm{Vap}}}$
DEPD	55.4	-5.40E-06	-1.23E-07	t-BDEA	42.9	-5.45E-06	-1.24E-07
DETA	74.6	-2.32E-05	-6.52E-08	TEA	70.7	-3.83E-05	-5.82E-08
DGA	62.8	-3.43E-05	-7.76E-08	TEDA	65.5	-2.01E-05	-6.49E-08
DIPA	71.1	-3.61E-05	-1.07E-07	TEPA	75.0	-5.30E-05	-7.25E-08
DMAB	46.6	-1.03E-05	-5.31E-08	TETA	63.2	-3.94E-05	-7.44E-08
DMAEEO	41.3	-2.01E-05	-6.94E-08	TIPA	42.3	-3.98E-05	-7.52E-08
DMAP	66.7	-1.54E-05	-7.94E-08	TMEDA	35.9	-1.05E-05	-3.35E-08
DMAPA	47.2	-1.21E-05	-5.23E-08	TMHDA	42.2	-1.06E-05	-3.38E-08
DMEA	67.6	-5.42E-06	-1.24E-07	TMPDA	49.6	-1.59E-05	-3.99E-08
DMPZ	34.8	-1.99E-05	-6.87E-08	TREA	40.5	1.25E-05	-1.08E-07
DPAB	51.6	-1.41E-05	-8.90E-08	TRIS	55.4	-9.67E-06	-7.41E-08
EAE	61.7	-1.86E-06	-1.14E-07				

Table B.13: Pre-exponential factor, activation energy in J/mol, and stoichiometric coefficient, see Eqn. 3.3.

Solvent	$k_{2,\mathrm{PreExp}}$	E_{A}	z	Solvent	$k_{2,\mathrm{PreExp}}$	E_{A}	z
1-(2HE)PRLD	7.61E+08	4.06E+04	1	EAPPD	4.66E+14	5.94E+04	2
1DMA2P	1.36E+15	7.80E+04	1	EDA	8.70E+12	5.07E+04	2
2MPZ	3.19E+12	4.71E+04	2	EEMPA	8.26E+14	5.97E+04	2
2PPE	4.10E+10	4.51E+04	2	EMAB	3.29E+13	6.81E+04	1
3AP	1.26E+12	4.65E+04	2	EPZ	1.34E+07	1.87E+04	1
3PPM	1.17E+17	7.67E+04	2	HEEAB	7.40E+07	2.79E+04	1
4A1B	8.81E+13	5.69E+04	2	HEMAB	1.15E+07	2.28E+04	1
4PP2B	4.04E+13	6.94E+04	1	HEPP	7.22E+09	4.76E+04	1
5AP	9.83E+13	5.70E+04	2	HEPz	1.03E+13	5.05E+04	1
AEEA	5.25E+09	3.19E+04	2	HMD	1.24E+08	2.06E+04	2

Continued on next page

Table B.13 – *continued from previous page*

Solvent	$k_{2,\mathrm{PreExp}}$	E_A	z	Solvent	$k_{2,\mathrm{PreExp}}$	E_A	z
AEPD	6.03E+13	6.48E+04	2	i-BA	1.08E+14	5.70E+04	2
AEPz	4.50E+12	4.72E+04	1	IPAE	3.26E+11	5.10E+04	2
AMP	2.95E+07	2.62E+04	2	MAPA	1.67E+09	2.79E+04	2
AMPD	1.54E+09	3.79E+04	2	MDEA	1.01E+10	4.99E+04	1
BA	1.14E+14	5.72E+04	2	MEA	4.40E+11	4.45E+04	2
BDEA	6.94E+12	6.91E+04	1	MIPA	4.44E+10	3.93E+04	2
bis-APA	5.77E+11	4.16E+04	2	MMEA	9.67E+08	2.95E+04	2
BMEA	6.49E+13	5.69E+04	2	MOR	3.46E+14	5.94E+04	2
BZA	4.57E+10	3.97E+04	2	MPDL	2.34E+07	3.32E+04	1
DAMP	7.56E+13	5.69E+04	2	MPZ	1.29E+07	1.40E+04	1
DAP	8.59E+13	5.71E+04	2	NMM	1.62E+12	6.86E+04	1
DEA	5.70E+11	5.02E+04	2	PAE	4.38E+14	5.92E+04	2
DEA2P	2.81E+18	9.48E+04	1	PZ	4.04E+10	3.33E+04	2
DEAB	7.68E+10	5.26E+04	1	Serinol	9.31E+13	5.71E+04	2
DEEA	9.95E+10	5.22E+04	1	t-BAE	3.82E+12	5.96E+04	2
DEPD	1.17E+10	4.70E+04	1	t-BDEA	1.09E+13	6.92E+04	1
DETA	7.47E+09	3.23E+04	2	TEA	1.30E+07	3.77E+04	1
DGA	2.90E+11	4.46E+04	2	TEDA	3.36E+11	6.19E+04	1
DIPA	1.06E+12	5.86E+04	2	TEPA	2.65E+10	3.69E+04	2
DMAB	7.15E+10	5.50E+04	1	TETA	6.78E+10	4.03E+04	2
DMAEEO	8.43E+12	6.90E+04	1	TIPA	3.44E+12	6.84E+04	1
DMAP	2.14E+14	7.29E+04	1	TMEDA	2.09E+13	6.91E+04	1
DMAPA	5.71E+14	7.63E+04	1	TMHDA	8.44E+13	6.88E+04	1
DMEA	1.92E+11	5.55E+04	1	TMPDA	1.65E+11	5.42E+04	1
DMPZ	1.86E+13	6.91E+04	1	TREA	2.66E+11	5.43E+04	1
DPAB	4.19E+12	6.92E+04	1	TRIS	5.08E+11	5.39E+04	2

Continued on next page

Table B.13 – *continued from previous page*

Solvent	$k_{2,\mathrm{PreExp}}$	E_A	z	Solvent	$k_{2,\mathrm{PreExp}}$	E_A	z
EAE	3.42E+09	3.45E+04	2				

Table B.14: Total heat of absorption ΔH_Abs in kJ/mol, molar volume at normal boiling point V_Mol in cm^3/mol, and atomic diffusion volume AV.

Solvent	ΔH_Abs	V_Mol	AV	Solvent	ΔH_Abs	V_Mol	AV
1-(2HE)PRLD	39.8	1.35E+02	118	EAPPD	83.8	1.59E+02	145
1DMA2P	60.7	1.37E+02	120	EDA	48.6	7.43E+01	59.4
2MPZ	72.8	1.38E+02	98.0	EEMPA	75.0	6.71E+02	233
2PPE	72.3	1.48E+02	138	EMAB	46.3	1.56E+02	161
3AP	62.1	9.49E+01	79.1	EPZ	77.0	1.39E+02	119
3PPM	57.4	1.37E+02	118	HEEAB	69.8	3.00E+02	188
4A1B	72.4	1.22E+02	100	HEMAB	56.2	1.88E+02	167
4PP2B	42.7	1.21E+02	179	HEPP	62.9	1.47E+02	138
5AP	62.1	1.43E+02	120	HEPz	69.0	1.48E+02	125
AEEA	82.5	1.32E+02	107	HMD	98.4	1.71E+02	141
AEPD	53.0	1.44E+02	126	i-BA	97.0	1.06E+02	93.6
AEPz	72.0	1.59E+02	125	IPAE	63.5	1.38E+02	120
AMP	80.9	1.18E+02	100	MAPA	66.0	1.19E+02	100
AMPD	76.2	1.28E+02	106	MDEA	52.5	1.51E+02	126
BA	94.8	1.06E+02	93.6	MEA	85.1	6.93E+01	58.6
BDEA	49.1	2.86E+02	188	MIPA	85.5	9.08E+01	79.1
bis-APA	83.7	1.50E+02	148	MMEA	73.8	9.39E+01	79.1
BMEA	74.4	1.59E+02	141	MOR	67.0	9.75E+01	76.7
BZA	59.5	1.19E+02	137	MPDL	49.1	1.19E+02	118
DAMP	67.3	1.62E+02	141	MPZ	73.0	1.25E+02	98.0
DAP	97.2	9.80E+01	79.9	NMM	59.1	1.16E+02	97.3

Continued on next page

Table B.14 – *continued from previous page*

Solvent	ΔH_{Abs}	V_{Mol}	AV	Solvent	ΔH_{Abs}	V_{Mol}	AV
DEA	74.2	1.16E+02	106	PAE	68.4	1.40E+02	120
DEA2P	43.6	1.72E+02	161	PZ	80.6	1.14E+02	77.5
DEAB	47.5	2.34E+02	182	Serinol	80.1	1.68E+02	85.3
DEEA	73.2	1.52E+02	141	t-BAE	80.6	1.56E+02	141
DEPD	35.8	1.60E+02	167	t-BDEA	64.2	3.36E+02	188
DETA	80.7	1.31E+02	107	TEA	66.6	1.66E+02	153
DGA	50.2	1.23E+02	106	TEDA	51.0	1.52E+02	132
DIPA	47.0	1.67E+02	147	TEPA	85.9	2.58E+02	203
DMAB	61.7	1.55E+02	141	TETA	84.9	1.91E+02	155
DMAEEO	65.2	2.04E+02	147	TIPA	50.8	4.47E+02	214
DMAP	54.6	1.39E+02	120	TMEDA	58.7	1.64E+02	141
DMAPA	91.3	1.40E+02	121	TMHDA	72.1	2.88E+02	224
DMEA	63.3	1.17E+02	100	TMPDA	59.9	1.85E+02	162
DMPZ	62.0	1.38E+02	119	TREA	54.9	1.53E+02	135
DPAB	61.1	3.61E+02	223	TRIS	59.0	1.38E+02	112
EAE	69.0	1.21E+02	100				

B.3 Impact of Logarithmic Mean

All mass transfer rate related KPIs (effective mass transfer area, enhancement factor, diffusivity coefficients, dimensionless numbers such as Hatta, Weber, Reynolds, Froude, Prandtl, concentrations, partial pressures, temperatures) are calculated at the top and bottom of the active absorber section reference. The logarithmic average is the most used averaging method, however, there are two possible ways of calculating an average absorption rate via the logarithmic mean: 1. Calculating the logarithmic mean absorption rate-based on the rate at the top and bottom of the absorber (see Eqn. B.1), or 2. Calculating the ratio of logarithmic mean flux divided by logarithmic mean driving force *i.e.,* the mean logarithmic absorption rate (see Eqn. B.2). The latter method is used most in the literature *e.g.,* Chen *et al.* [14, 233] and in this work. Different approaches and they impact on the height of the absorber column are shown in Fig. B.2)

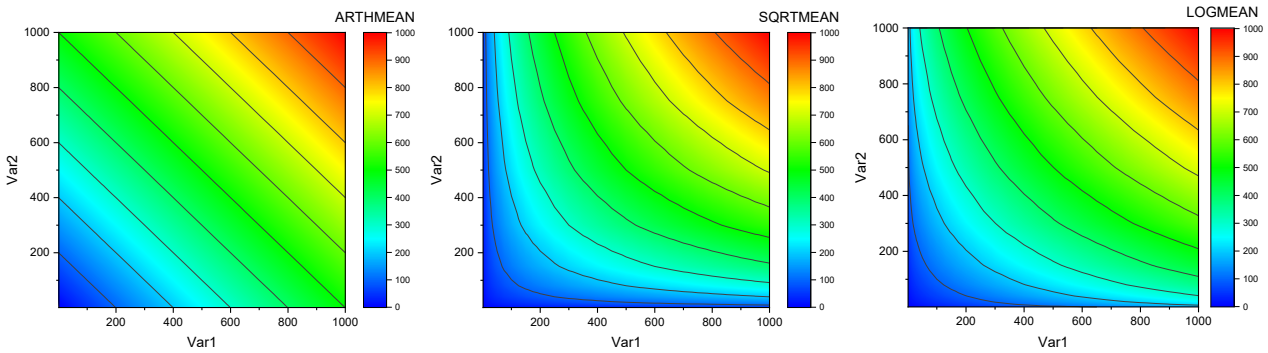
$$\dot{n}_{\mathrm{CO_2}}^{\mathrm{LogMean}} = \frac{\left(\dot{n}_{\mathrm{CO_2}}^{\mathrm{Top}} - \dot{n}_{\mathrm{CO_2}}^{\mathrm{Btm}}\right)}{\ln\left(\dot{n}_{\mathrm{CO_2}}^{\mathrm{Top}} / \dot{n}_{\mathrm{CO_2}}^{\mathrm{Btm}}\right)} \tag{B.1}$$

$$\dot{n}_{\mathrm{CO_2}}^{\mathrm{Mean}} = f\left(k_{\mathrm{L}}^{\mathrm{LogMean}}, E^{\mathrm{LogMean}}, c_{\mathrm{CO_2}}^{\mathrm{IP,LogMean}}, a_{\mathrm{wet}}^{\mathrm{LogMean}}, V_{\mathrm{Abs}}^{\mathrm{LogMean}}\right) \tag{B.2}$$

Calculating the height of the active packing section with properties and KPIs at the top of the column (ZT_{Top}) yields the tallest columns because most of the CO_2 in the flue gas has been already absorbed by the solvent and the remaining driving force is the smallest over the whole column. The highest driving force is found at the bottom of the absorber, thus, the packing height calculated with those properties ZT_{Btm} yield the shortest columns. The real packing height will be between ZT_{Top} and ZT_{Btm}. The logarithmic mean packing height ZT_{LogMean} as presented in Eqn. B.1 yields taller columns compared to using the logarithmic means of the properties and KPIs ZT_{Mean} as presented in Eqn. B.2. The model uses ZT_{LogMean} as an estimate for the packing height. A more accurate estimate can only be achieved by discretizing the liquid film over the packing height, which prohibitively increases the computational effort.

Arithmetic, geometric, and logarithmic means return similar values if two variables that are averaged are of the same order. However, if they are multiple orders apart, then both geo-

metric and logarithmic means weight lower values more than the linear arithmetic mean (see Fig. B.1). For increased numerical stability, all logarithmic means are replaced by Paterson's [522] approach.



(a) Arithmetic Mean (b) Geometric Mean (c) Logarithmic Mean

Figure B.1: Overview of the different means.

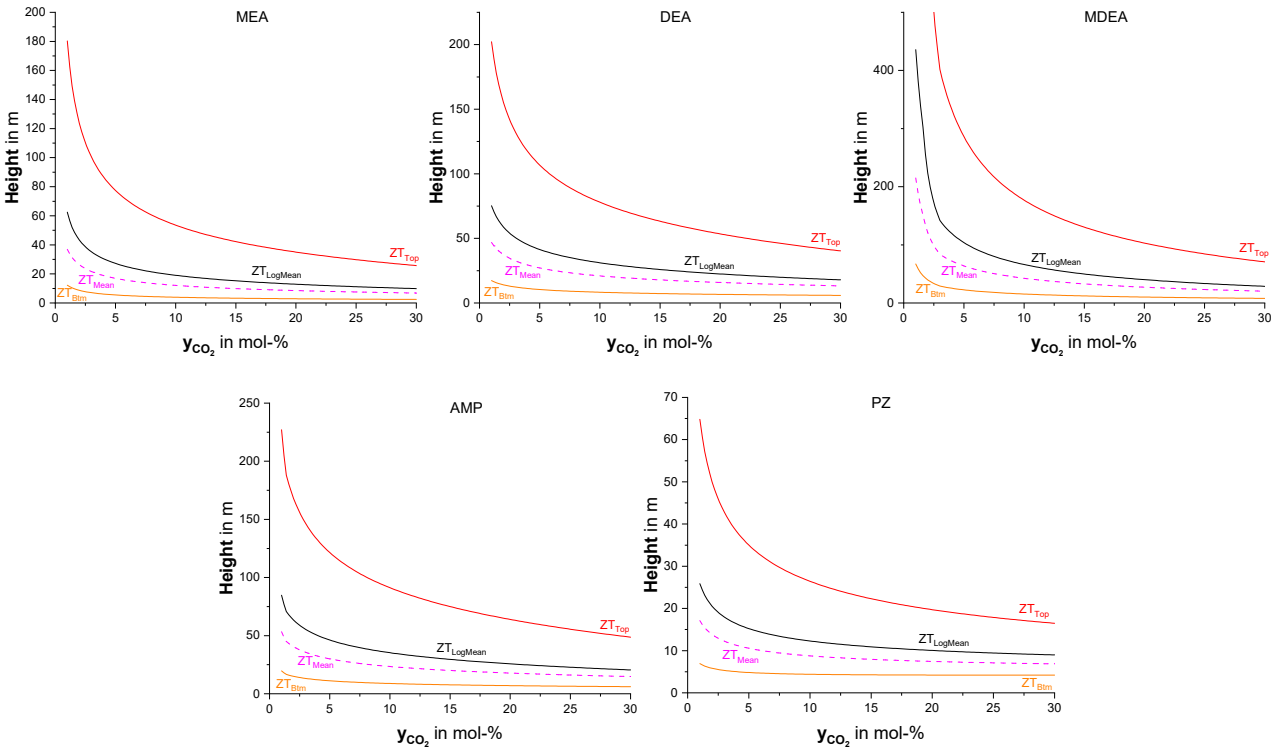


Figure B.2: Impact of different averaging methods on the active absorber packing height for five solvents as a function of CO_2 flue gas concentration. Packing height calculated by KPIs at top (ZT_{Top}, red line), bottom (ZT_{Btm}, orange line), logarithmic average as presented in Eqn. B.1 (ZT_{LogMean}, black line), and logarithmic mean driving force as presented in Eqn. B.2 (ZT_{Mean}, purple dashed line).

B.4 Enhancement Factor

Chemical reactions enhance the mass transfer rate and equations are widely. The enhancement factor varies between one (no/very slow reaction ≈ physical absorption) and the infinite enhancement E_{Inf} factor for an instantaneous reaction.

Van Krevelen [473–475] was the first who derived an enhancement factor to describe the additional driving force for mass transfer caused by an irreversible reaction A + zB → C + F (one kinetically limiting A + B → C + E, and one very fast follow up reaction
E + (z-1) B → F). The stoichiometric coefficient z depends on the reaction and is two for carbamate forming mono-amines and one for bicarbonate forming mono-amines. The exact solution to the differential equation is a lengthy inexplicit expression containing cosh and tanh functions as well as the concentration ratio $\frac{zc_{\mathrm{A}}^{\mathrm{IF}}}{c_{\mathrm{B}}^{\mathrm{Bulk}}}$ and a dimensionless group which is the Hatta number [472]. This expression has been widely reproduced (usually accompanied by a graphical representation), however, the underlying assumption that the concentration of B stays constant during reaction c_{B} = const is often missing. Together with boundary conditions for concentration of A at the interface $c_{\mathrm{A}}^{\mathrm{IP}}$ and bulk liquid $c_{\mathrm{A}}^{\mathrm{Bulk}}$ one can derive an explicit function for the concentration of A. For the case that the concentration of B is changing, van Krevelen introduced the concept of a reaction pane moving through the film layer which integrates the concentration profile for c_{B} = const. The Hatta number depends on the reaction order and describes the ratio of maximum amount of consumed component in the liquid film to the maximum amount of transferred component if no chemical reaction occurs and at zero bulk concentration. It indicates where the reaction pane is located (either in bulk, in film, or at interface). The reaction pane moves closer to the interface with faster kinetics.

Table B.15 list different limiting regimes which can be analytically derived for a second order irreversible reaction CO_2 + z Amine → P assuming $c_{\mathrm{CO_2}} = 0$. For this case, the Hatta number is $\mathrm{Ha} = \frac{\sqrt{k_2 D_{\mathrm{CO_2}} c_{\mathrm{B}}}}{z k_{\mathrm{L}}}$ and the infinite enhancement factor is $E_{\mathrm{Inf}} = 1 + \frac{D_{\mathrm{Amine,L}} c_{\mathrm{Amine}}^{\mathrm{Bulk}}}{z D_{\mathrm{CO_2,L}} c_{\mathrm{CO_2}}^{\mathrm{IP}}}$. Assuming and hard-coding one of these regimes into SQUASH would be a pitfall, because there is no guarantee that all solvents will actually be fast enough to satisfy the conditions. In reality, the reactions

Table B.15: Limiting regimes for analytically derived expressions for the enhancement factor E. These are valid only for a reaction of second order (one in CO_2 and one in Amine) and irreversible reaction
$CO_2 + z$ Amine $\rightarrow$ P, assuming $c_{CO_2} = 0$. Hatta number $\mathrm{Ha} = \frac{\sqrt{k_2 D_{CO_2} c_B}}{z k_L}$. Additionally, Wellek *et al.,* [432] correlation listed.

Regime	Conditions	Equation	Comment
Slow-regime ($\approx$ physical absorption)	$\mathrm{Ha} < 0.3$	$\mathrm{E} = 1$	Reaction is too slow to accelerate mass transfer
Pseudo First Order (PSFO)	$2 < \mathrm{Ha} \leq \frac{E_{Inf}}{10}$ and $\frac{c_{Amine}}{c_{CO_2}} \geq 15$	$E = \frac{\mathrm{Ha}}{\tanh(\mathrm{Ha})}$	Amine must be present in excess to guarantee $c_{Amine} = \text{const}$ [876].
Fast PSFO	$3 < \mathrm{Ha} \leq \frac{E_{Inf}}{10}$ and $\frac{c_{Amine}}{c_{CO_2}} \geq 15$	$E \approx \mathrm{Ha}$	Similar to PSFO but with Ha >3
Instantaneous regime	$2 < E_{Inf} \leq \frac{\mathrm{Ha}}{10}$	$E = E_{Inf}$	Reaction pane and interface are identical.
Wellek *et al.,*	$E = 1 + \frac{1}{\left[(E_{Inf}-1)^{-1.35} + \left(\frac{\mathrm{Ha}}{\tanh \mathrm{Ha}} - 1\right)^{-1.35}\right]^{1/1.35}}$		No depletion of amine, irreversible reaction, film theory holds true.

are not just of second order and reversible. Alternative approaches [432, 731, 758, 877–896] covering the possible range in kinetics ($\mathrm{Ha} \approx 0$ to $\mathrm{Ha} > 3$) and agnostic of reaction order were compared. The Wellek *et al.,* [432] correlation was selected because of its wide application range, and numeric stability. No approach is capable of including reverse reactions (reaction equilibria), which is not a limitation as long as the operating conditions in absorber and stripper lead to a clearly shifted equilibrium.

B.5 Additional Figures and Tables

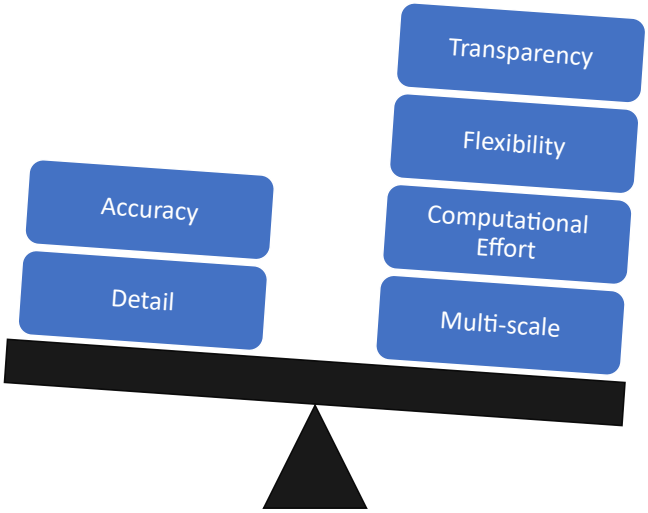


Figure B.3: Design philosophy of SQUASH with clear focus to prioritise the multi-scale and high-throughput screening of a large database of candidate solvents requiring flexibility in thermodynamic and process modelling at short computational times.

Table B.16: Weight-, mole-fractions, molality, and molar mass of amine and solvent of screened amines at constant mole-fraction.

Binder	Weight fraction	Mole fraction	Molality	Molar Mass in $\mathrm{kg\,kmol^{-1}}$	
	$w_{\mathrm{Binder}}\%$	$x_{\mathrm{Binder}}\%$	$\mathrm{mol_{Binder}/kg_{H_2O}}$	Binder	Solvent
MEA	30.0	11.2	7.0	61.1	22.8
DEA	42.5	11.2	7.0	105	27.8
MDEA	45.5	11.2	7.0	119	29.4
AMP	38.5	11.2	7.0	89.1	26.0
PZ	37.7	11.2	7.0	86.1	25.7

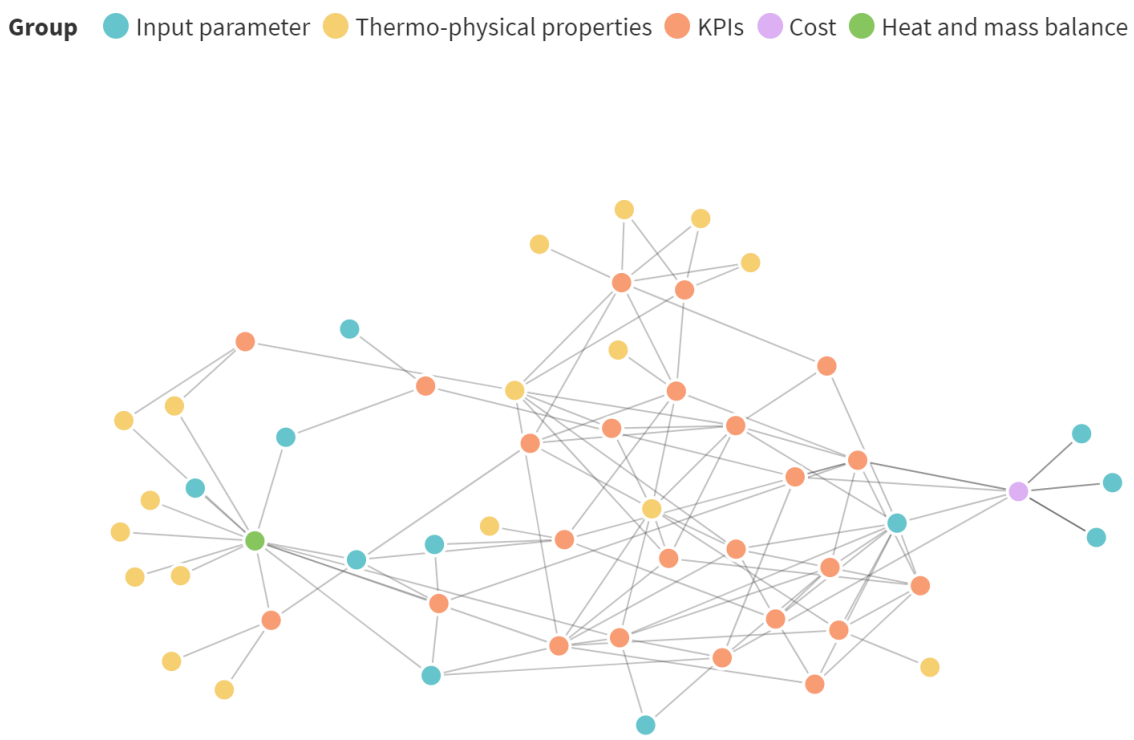


Figure B.4: Example of the relationships and interactions between operating input parameter, thermo-physical solvent properties, key performance indicators (KPIs), and cost for the absorber. Interactive version available online [897].

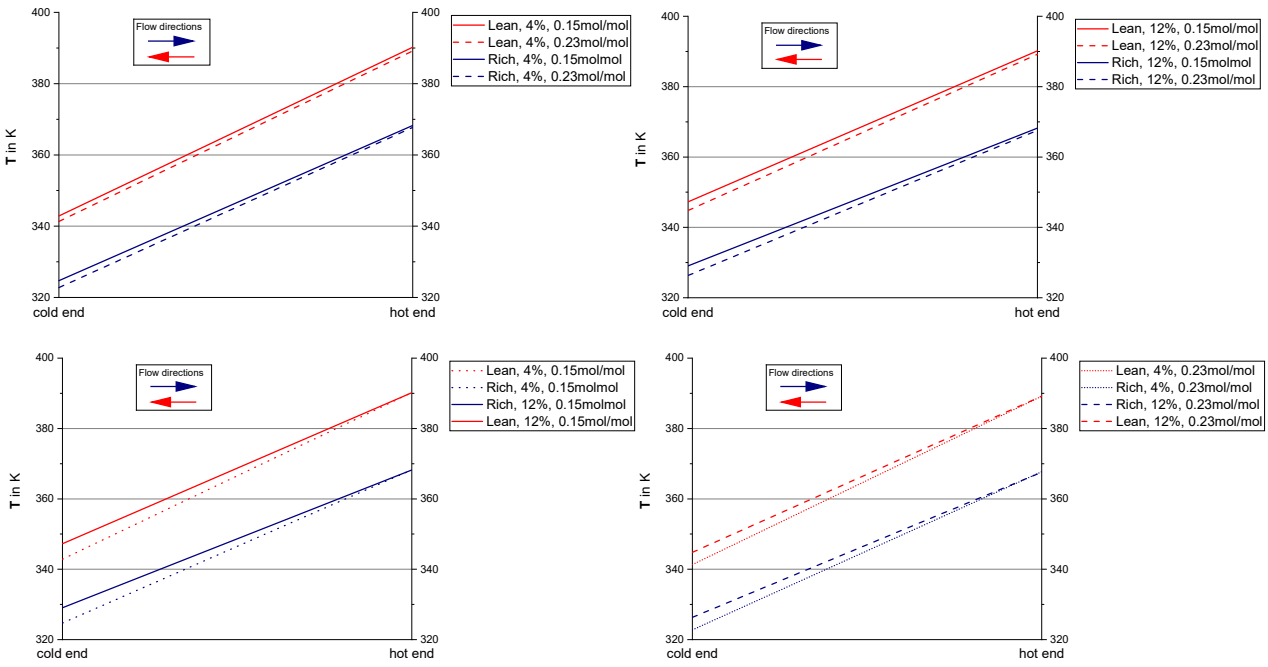


Figure B.5: Comparing simplified linear temperature profiles inside the main heat exchanger for two lean loadings and two flue gas CO_2 concentrations. Solvent is 30 wt% MEA and capture rate is 90%. Hot end temperature difference is not a function of CO_2 concentration but only of lean loading (and solvent).

Table B.17: References for solvent data and their uncertainties. * indicates that referenced data was extrapolated. Heat of absorption includes heat of dissolving CO_2 and heat of reaction (equals overall heat of absorption).

Solvent	Viscosity	Density	Heat Capacity	Thermal Conductivity	Surface Tension	Rate Constant	VLE	Heat of Absorption
MEA	[675, 898]	[675, 899]	[900]	[358]	[899]	[124, 154, 158, 197, 313, 901, 902]	[160, 402, 903–905]	[197, 574, 858, 906]
DEA	[907]	[907]	[642]*	[358]	[908]	[124, 158, 313, 901, 902]	[909, 910]	[197, 858, 911–915]
MDEA	[898]	[916]	[917]	[358]	[918]	[124, 154, 158, 197, 901, 902, 919, 920]	[921–926]	[197, 906, 927]
AMP	[898]	[898]	[917]	[358]	[928]	[124, 158, 901, 902, 929–931]	[233, 904, 932–935]	[176, 197, 858, 936]
PZ	[937, 938]*	[937, 938]*	[939]	[358]	[938, 940]*	[158, 941]	[275, 311, 402, 926, 942, 943]	[197, 783, 944]
CE-SAR1	[938, 945]	[405, 938, 945]	[405]	[358]	[916, 938]	[405]	[226, 405, 946, 947]	[405]

Table B.18: Further amine data including references.

Solvent	Association factor Φ [411, 440, 441]	T_{Vap} in K[359]	Molar volume at T_{Vap}[359] in $\mathrm{cm}^3/\mathrm{mol}$	Molecular diffusion volume Σ_v [411]
MEA	2.26	443.2	69.3	58.62
DEA	2.26	541.5	117.1	105.77
MDEA	2.26	518.0	152.0	126.29
AMP	2.26	438.2	118.5	99.66
PZ	2.26	419.2	113.9	77.48

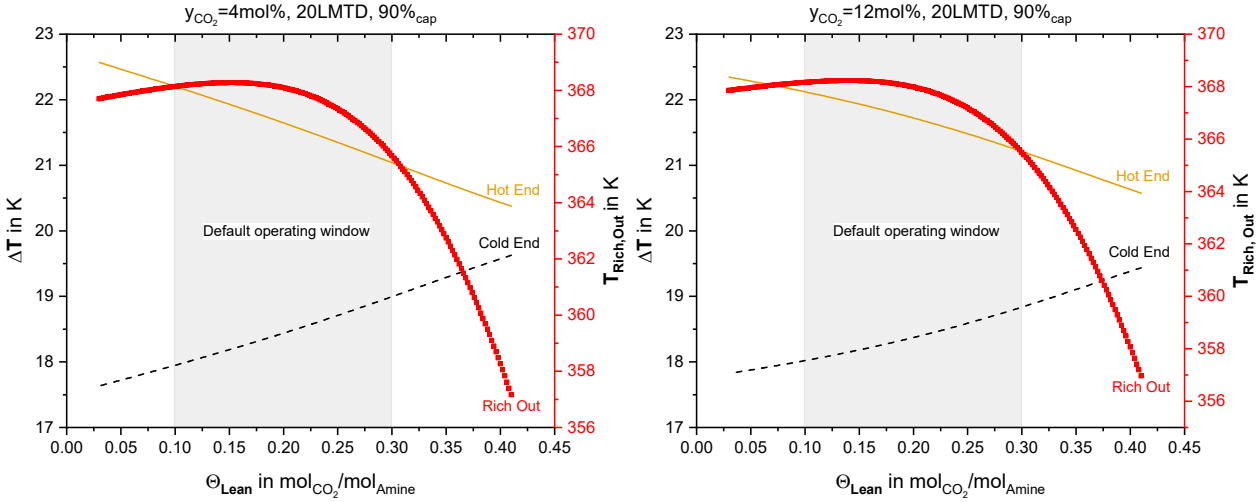


Figure B.6: Hot and cold end temperature differences as a function of lean loading for flue gas CO_2 concentration of 4 mol% (left) and 12 mol% (right) at constant 20 K temperature approach. Solvent is 30 wt% MEA and capture rate is 90%.

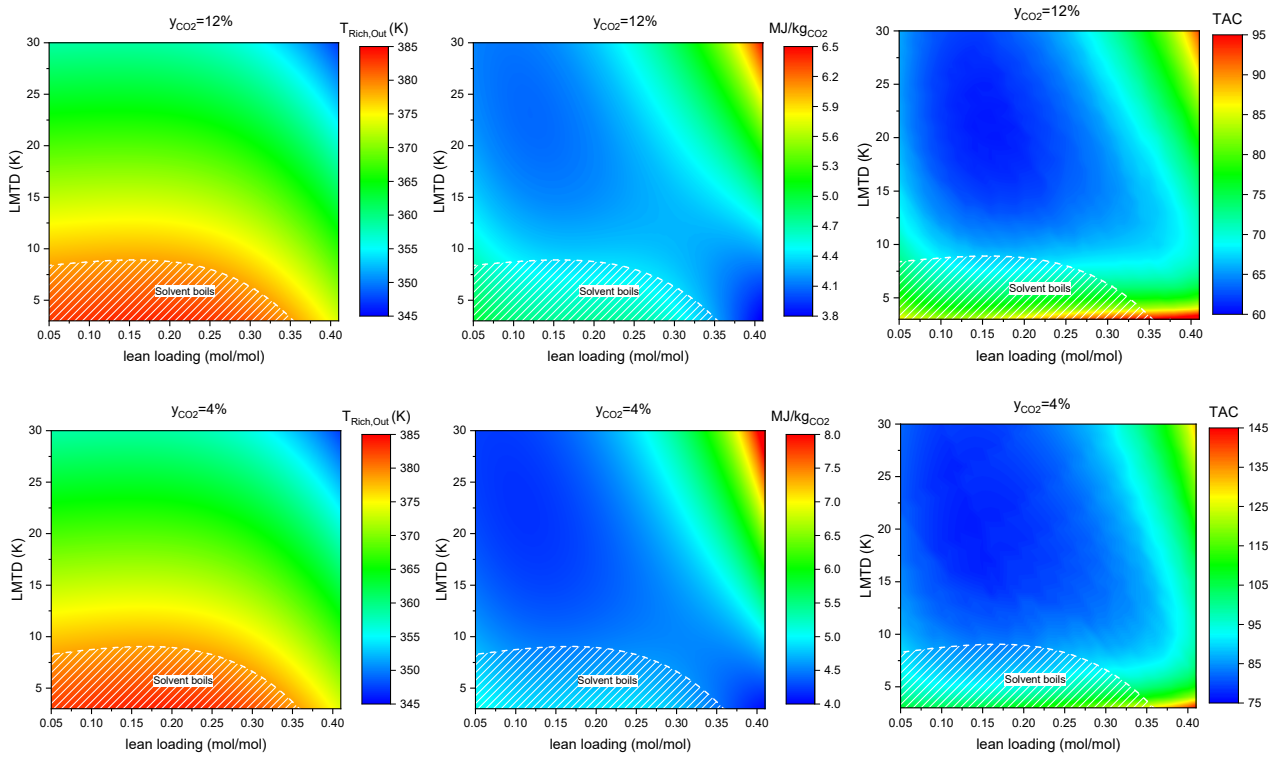


Figure B.7: Impact of lean loading and temperature approach on rich solvent outlet temperature T_{RichSol} (left column), specific reboiler duty (middle column), and capture cost TAC in $\$/\text{ton}_{CO_2}$ (right column) for flue gas CO_2 concentrations of 12 mol% (top row) and 4 mol% (bottom row). Solvent is 30 wt% MEA and capture rate is 90%. Same trends are observed as already discussed in main body.

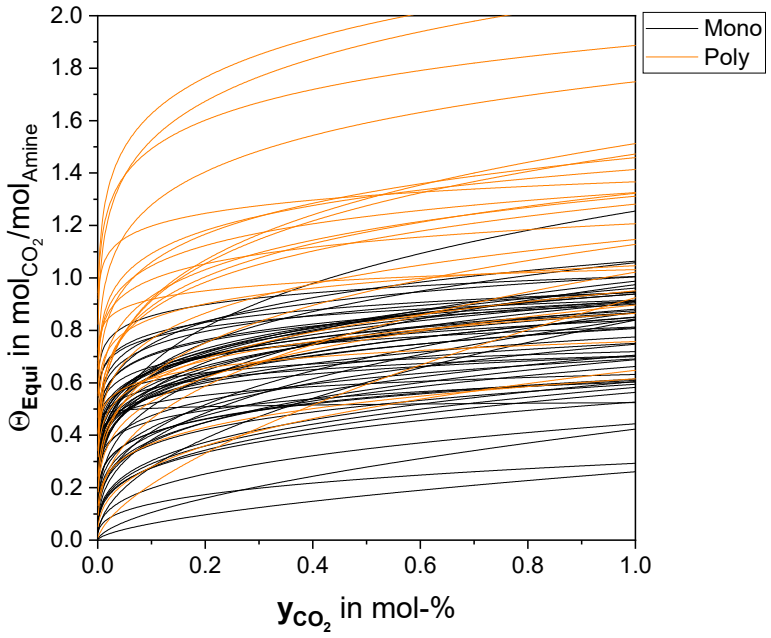


Figure B.8: Equilibrium loading trends of screened amines over flue gas composition at a pressure of 110 kPa and 40°C. Poly-amines (orange) contain more than one alkalinity per amine resulting on average in much higher capacity. Data from SQUASH database.

C. Lower Limit of Heat of Absorption

In the following a thermodynamic view at the misguided focus on low heat of absorption is presented: The Gibbs free energy $\Delta G = \Delta H - T\Delta S$ describes the reaction between amine and CO_2. The absorption of CO_2 reduces the overall entropy $\Delta S < 0$ and is exothermic $\Delta H < 0$. For an exergonic reaction $|\Delta H| > |T \cdot \Delta S|$ must be true. Hence, there is a thermodynamic lower limit to $|\Delta H|$. It is not possible to lower $|\Delta H|$ without also affecting the VLE as described by the Gibbs-Helmholtz[1] equation $\left(\frac{\delta(\Delta G/T)}{\delta T}\right)_p = -\frac{\Delta H}{T^2}$ and $\Delta H_{\text{Abs}} = R \cdot \frac{\delta \ln f_{CO_2}}{\delta(1/T)}\Big|_{\Theta, p_{\text{Tot}}}$. Note the constant total pressure, because it is perfectly possible to increase the loading at constant heat of absorption by simply increasing the (partial) pressure.

[1] Van't Hoff equation can be derived.

Table C.1: List of screened CO_2 capture amines.

Abbreviation	**Name**	**Molecular Formula**	**Molar Mass** g/mol	**CAS Number**
1-(2HE)PRLD	1-(2-Hydroxyethyl)pyrrolidine	C6H13NO	115.2	2955-88-6
1DMA2P	1-Dimethylamino-2-propanol	C5H13NO	103.2	108-16-7
2MPZ	2-Methylpiperazine	C5H12N2	100.2	109-07-9
2PPE	2-Piperidineethanol	C7H15NO	129.2	1484-84-0
3AP	3-Amino-1-propanol	C3H9NO	75.1	156-87-6
3PPM	3-Piperidinemethanol	C6H13NO	115.2	4606-65-9
4A1B	4-Amino-1-butanol	C4H11NO	89.1	13325-10-5
4PP2B	4-(Piperidin-1-yl)butan-2-ol	C9H19NO	157.3	71648-40-3
5AP	5-Amino-pentanol	C5H13NO	103.2	2508-29-4
AEEA	N-(2-Aminoethyl)ethanolamine	C4H12N2O	104.2	111-41-1
AEPD	2-Amino-2-ethyl-1,3-propanediol	C5H13NO2	119.2	115-70-8
AEPZ	1-(2-aminoethyl)piperazine	C6H15N3	129.2	140-31-8
AMP	2-Amino-2-methyl-1-propanol	C4H11NO	89.1	124-68-5
AMPD	2-Amino-2-methyl-1,3-propanediol	C4H11NO2	105.1	115-69-5
BA	Butylamine	C4H11N	73.1	109-73-9
BDEA	N-Butyldiethanolamine	C8H19NO2	161.2	102-79-4

Continued on next page

Table C.1 – *continued from previous page*

Abbreviation	**Name**	**Molecular Formula**	**Molar Mass** g/mol	**CAS Number**
bis-APA	bis(3-aminopropyl)amine	C6H17N3	131.2	56-18-8
BMEA	2-(Butylamino) ethanol	C6H15NO	117.2	111-75-1
BZA	Benzylamine	C7H9N	107.2	100-46-9
DAMP	1,5-Diamino-2-methylpentane	C6H16N2	116.2	15520-10-2
DAP	1,3-Diaminopropane	C3H10N2	74.1	109-76-2
DEA	Diethanolamine	C4H11NO2	105.1	111-42-2
DEA2P	1-Diethylamino-2-propanol	C7H17NO	131.2	4402-32-8
DEAB	4-Diethylamino-2-butanol	C8H19NO	145.2	5467-48-1
DEEA	N,N-Diethyl-2-aminoethanol	C6H15NO	117.2	100-37-8
DEPD	4-[Ethyl(methyl)amino]butane-1,3-diol	C7H17NO2	147.2	NaN
DETA	Diethylenetriamine	C4H13N3	103.2	111-40-0
DGA	Diglycolamine	C4H11NO2	105.1	929-06-6
DIPA	Diisopropanolamine	C6H15NO2	133.2	110-97-4
DMAB	4-(Dimethylamino)-1-butanol	C6H15NO	117.2	13330-96-6
DMAEEO	1-O-Dimethylaminoethyl-ethylenglykol	C6H15NO2	133.2	1704-62-7
DMAP	3-Dimethylamino-1-propanol	C5H13NO	103.2	3179-63-3
DMAPA	3-Dimethylaminopropylamine	C5H14N2	102.2	109-55-7

Continued on next page

Table C.1 – *continued from previous page*

Abbreviation	**Name**	**Molecular Formula**	**Molar Mass** g/mol	**CAS Number**
DMEA	N,N-Dimethylethanolamine	C4H11NO	89.1	108-01-0
DMPZ	1,4-Dimethylpiperazine	C6H14N2	114.2	106-58-1
DPAB	4-(Dipropylamino)-2-butanol	C10H23NO	173.3	NaN
EAE	N-Ethyl-Ethanolamine	C4H11NO	89.1	110-73-6
EAPPD	4-(2-Ethanolamino)piperidine	C7H16N2O	144.2	875229-91-7
EDA	Ethylenediamine	C2H8N2	60.1	107-15-3
EEMPA	N-(2-Ethoxyethyl)-3-morpholinopropan-1-amine	C11H24N2O2	216.3	NaN
EMAB	4-(Ethyl-methyl-amino)-butan-2-ol	C7H17NO	131.2	NaN
EPZ	1-Ethylpiperazine	C6H14N2	114.2	5308-25-8
HEEAB	4-((2-Hydroxyethyl)(ethyl)amino)-2-butanol	C8H19NO2	161.2	NaN
HEMAB	4-((2-Hydroxyethyl)(methyl)amino)-2-butanol	C7H17NO2	147.2	NaN
HEPP	1-Piperidineethanol	C7H15NO	129.2	3040-44-6
HEPZ	1-(2-Hydroxyethyl)piperazine	C6H14N2O	130.2	103-76-4
HMD	Hexamethylenediamine	C6H16N2	116.2	124-09-4
i-BA	Isobutylamine	C4H11N	73.1	78-81-9
IPAE	2-(Isopropylamino)-ethanol	C5H13NO	103.2	109-56-8
MAPA	N-Methyl-1,3-propanediamine	C4H12N2	88.2	6291-84-5

Continued on next page

Table C.1 – *continued from previous page*

Abbreviation	**Name**	**Molecular Formula**	**Molar Mass** g/mol	**CAS Number**
MDEA	Methyldiethanolamine	C5H13NO2	119.2	105-59-9
MEA	Monoethanolamine	C2H7NO	61.1	141-43-5
MIPA	1-Amino-2-propanol	C3H9NO	75.1	78-96-6
MMEA	Methylmonoethanolamine	C3H9NO	75.1	109-83-1
MOR	Morpholine	C4H9NO	87.1	110-91-8
MPDL	1-Methylpiperidin-4-ol	C6H13NO	115.2	106-52-5
MPZ	1-Methylpiperazine	C5H12N2	100.2	109-01-3
NMM	N-Methyl Morpholine	C5H11NO	101.1	109-02-4
PAE	2-Propylamino-ethanol	C5H13NO	103.2	16369-21-4
PZ	Piperazine	C4H10N2	86.1	110-85-0
Serinol	(2-Aminopropane-1,3-diol)	C3H9NO2	91.1	534-03-2
t-BAE	2-(tert-Butylamino)ethanol	C6H15NO	117.2	4620-70-6
t-BDEA	Tertiary Butyl Diethanolamine	C8H19NO2	161.2	2160-93-2
TEA	Triethanolamine	C6H15NO3	149.2	102-71-6
TEDA	Triethylenediamine	C6H12N2	112.2	280-57-9
TEPA	Tetraethylenepentamine	C8H23N5	189.3	112-57-2
TETA	Triethylenetetramine	C6H18N4	146.2	112-24-3

Continued on next page

Table C.1 – *continued from previous page*

Abbreviation	**Name**	**Molecular Formula**	**Molar Mass** g/mol	**CAS Number**
TIPA	Triisopropanolamine	C9H21NO3	191.3	122-20-3
TMEDA	N,N,N',N'-Tetramethyl-1,2-ethanediamine	C6H16N2	116.2	110-18-9
TMHDA	N,N,N,N-Tetramethyl-1,6-hexanediamine	C10H24N2	172.3	111-18-2
TMPDA	N,N,N'N'-Tetramethyl-1,3-propanediamine	C7H18N2	130.2	110-95-2
TREA	Triethylamine	C6H15N	101.2	121-44-8
TRIS	Tris(hydroxymethyl)amino methane	C4H11NO3	121.1	77-86-1

D. Additional Figures and Tables

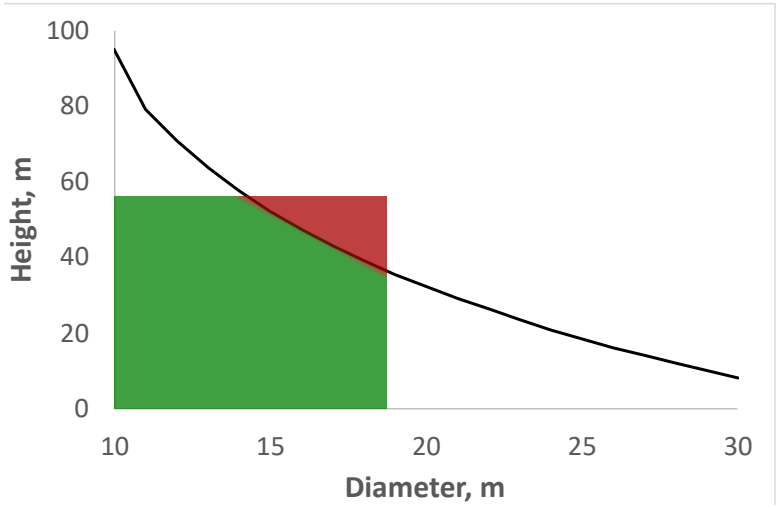


Figure D.1: Weight limitation as a function of diameter and height of the absorber according to [948]. Multiple unites are required if height and diameter are above the line, or the absorber diameter exceeds 18 m. Typical diameter and height range from absorbers highlighted with colour (*i.e.*, red area requires multiple units).

Table D.1: Combined expanded relative uncertainty of measuring (indicated by $\star$) and predicting thermo-physical properties of aqueous amine solvents. Values are rounded and expressed as Average absolute relative deviation (AARD).

Method	AARD
Viscosity, η	
Lewis and Squires [949]	5-15%
Orrick and Erbar [411]	20.1% and 15%
Sastri and Rao [369]	14.8%
Przezdziecki and Sridhar [950]	26.6%
Prabhakar *et al.* [951]	42.9%
Dutt *et al.* [952]	14.6%
Souders [953]	23.7%
Morris [954]	17.1%
Thomas [955]	23.9%
Van Velzen *et al.* [956]	46.9%

To be continued

Table D.1 (continued)

Method	AARD
Artificial Neural Networks *e.g.,* [957]	13.9%
Capilarry and Stabinger viscometers [958]	2%
Systematic error contribution [959]	>0.25%
Karunarathne *et al.* ⋆ [675, 960]	1.4% and 6.2%
Hartono *et al.* [961]⋆	4.2%, 2.4%, and 2%
Arachichge *et al.* [962]⋆	5% and 3.5%
Islam *et al.* [963]⋆	5.1%
Amundsen *et al.* [964]⋆	4.2% and 3%
Maham *et al.* [965]⋆	2.3%
Weiland *et al.* [966]⋆	2.7%
Fu *et al.* [967]⋆	3.2% and 2.3%

To be continued

Table D.1 (continued)

Method	AARD
Heat capacity, c_p	
Domalski and Hearing 1993 [411]	2%
Ruzicka and Domalski [411]	NaN
Chueh and Swanson [968, 969]	5%
Kolska *et al.* [970]	2.5%
Chickos *et al.* [971]	3.9% and 1
Huang and Johnson [972]	10%
Zabransky and Ruzicka [973]	3.0% and 3% deteriorates for alkanolamines
Domalski and Hearing [974]⋆	NaN
Zábransky *et al.*⋆ [975]	0.94% and 1.93%
Page *et al.*⋆[900]	NaN
Chiu *et al.*⋆[642]	2%
Zhang *et al.*⋆[917]	0.42%
Chen *et al.*⋆[939]	4.6%

To be continued

Table D.1 (continued)

Method	AARD
Density, ρ	
Schroeder [411]	3.9% and >10%
Le Bas *et al.* [976]	3.9%
Tyn and Calus [977]	2.8%
Rackett *et al.* [411]	4.1% and 0.8%
Yamada and Gunn [978]	1.8%
Hankinson and Thomson (HBT) [979]	2.6%
Elbro *et al.* [368]	2.8%
Weiland *et al.*⋆ [980]	3.4%
Han *et al.*⋆ [981]	4.0%
Jayarathna *et al.*⋆ [899]	0.2%
Concepcion *et al.*⋆ [907]	2.2% and 0.7%
Rinker *et al.*⋆ [982]	0.1%
Hsu1997 *et al.*⋆ [983]	0.1%
Tseng *et al.*⋆ [984]	0.1%
Yang *et al.*⋆ [985]	0.1%
Spasojevic *et al.*⋆ [986]	1.1%
Zhao *et al.*⋆ [987]	0.3% and 0.2%
Chowdhury *et al.*⋆ [565]	0.2%
Zhang *et al.*⋆ [988]	0.1%
Maham *et al.*⋆ [965]	0.1%
Zhang *et al.*⋆ [988]	0.1%
Karunarathne *et al.*⋆ [675]	0.12%

To be continued

Table D.1 (continued)

Method	AARD
Surface tension, σ	
Macleod-Sugden Corr. [989, 990]	8.6%
Macleod-Sugden Corr. by Quayle [991]	2.4%
Brock and Bird [992]	13.8%
Pitzer *et al.* [993]	17.0%
Zuo and Stenby [994]	13.4%
Sastri and Rao [995]	4.0%
Rice and Teja [996]	5.0%
Suarez (binary organic-liquid mixtures) [997]	3.5%
Tamura *et al.* [998]	<10.0%
Chunxi *et al.* [999]	0.5% and 1.4%
Jayarathna *et al.*⋆ [899]	3.0% and 5.9% and 12.2%
Asprion ⋆ [371]	2.3%
Han *et al.*⋆ [981]	0.7% and 0.2%
Vazquez *et al.*⋆ [908, 928]	0.2% and 0.4% and 0.1%
Alvarez *et al.*⋆ [918, 1000, 1001]	0.1% and 0.05% and 0.4%
Muhammad *et al.*⋆ [940]	0.1%
Derks *et al.*⋆ [1002]	0.1%
Rinker *et al.*⋆ [982]	0.4%
Hernandez *et al.*⋆ [1003]	0.6%
Venkat *et al.*⋆ [1004]	0.1%
Maham and Mather *et al.*⋆ [1005]	2.0%
Shojaeian ⋆ [1006]	0.2%
Zhang *et al.*⋆ [678]	0.1%
Fu *et al.*⋆ [1007]	1.75% and 0.1%
Kelayeh *et al.*⋆ [1008]	0.3%

To be continued

Table D.1 (continued)

Method	AARD
Thermal conductivity, λ	
Latini *et al.* [1009]	$< 10\%$
Sastri *et al.* [411]	8%
Chung *et al.* [1010]	6.5%
Teja and Rice *et al.* [996]	0.2% and 0.2%
Arikol and Gürbüz [1011]	2.0%
Sastri and Rao *et al.* [372]	5.6% and 8.3%
Lenoir [1012]	4.0%
DiGuilio *et al.*$\star$ [398, 1013]	2.0%
Shokouhi *et al.*$\star$ [1014]	0.69%
Rate Constant, k_2	
Jamal *et al.*$\star$ [901, 902]	6.4%
Littel *et al.*$\star$ [1015]	4.0%
Adeosun *et al.*$\star$ [851]	0.1%
Hikita *et al.*$\star$ [313]	5.4%, 3.5%, and 4.3%
Aboudheir *et al.*$\star$ [154]	1.6% and 12.6%
Li *et al.*$\star$ [1016]	5.0%
Haimour 1987 *et al.*$\star$ [919]	1.5% and 8.0%

To be continued

Table D.1 (continued)

Method	AARD
VLE, Θ	
Adeosun *et al.*⋆ [197, 851]	10.0%
Aboudheir *et al.*⋆ [154]	20.0%
Austgen *et al.*⋆ [159, 160]	20.0%
Kim *et al.*⋆ [858]	15.0%
Lee *et al.*⋆ [909]	5.0%
Oyevaar *et al.*⋆ [1017, 1018]	5.0%
Kotto *et al.*⋆ [858]	9.0%
Sidi-Boumedine *et al.*⋆ [921]	2.0%
Haji-Sulaiman *et al.*⋆ [910, 1019]	2.0%, 3.0%, and 12%
Arcis *et al.*⋆ [1020]	2.0%, 5.0%, 1.0% and 3.0
Kennard and Meisen ⋆ [1021]	10.0%
Dawodu and Meisen ⋆ [1022]	13.5%
Lal *et al.*⋆ [1023]	15%
Lawson and Garst ⋆ [1024]	9.0%
Mason and Dodge ⋆ [1025]	2.0%
Benamor and Aroua ⋆ [1026]	2.0%
Tong *et al.*⋆ [947]	6.0%
Gabrielsen *et al.*⋆ [403, 936]	7.5%
Jou *et al.*⋆ [903, 922]	2.0% and 3.0%
Lee *et al.*⋆ [905]	4.0%
Li ⋆ [1027]	5.0% and 3.0%
Kuranov *et al.*⋆ [923]	10.0%
Kamps *et al.*⋆ [924]	0.1% and 4.0%
Ermatchkov *et al.*⋆ [926]	3.9% and 0.1%
Kundu *et al.*⋆ [933]	2.0%

To be continued

Table D.1 (continued)

Method	AARD
Seo and Hong ⋆ [934]	2.0% and 3.0%
Chen *et al.*⋆ [1028]	1.7% and 2.4%
Li *et al.*⋆ [935]	5.0%
Dugas *et al.*⋆ [943]	5.0%
Nguyen *et al.*⋆ [275]	2.0%
Yang *et al.*⋆ [946]	2.0% and 3.0%
Total heat of absorption, ΔH_{Abs}	
Gibbs-Helmholtz equation [411]	20%-30%
ElHadri *et al.*⋆ [197]	2.0%
Kim *et al.*⋆ [176, 574, 575, 858, 906]	2.0% and 2.0%
Oscarson *et al.*⋆ [911]	5.0%
Carson *et al.*⋆ [1029]	2.0%
Helton *et al.*⋆ [1020]	1.0%
Arcis *et al.*⋆ [914]	1.0%, 3.0% and 5.0%
Gabrielsen *et al.*⋆ [936]	7.5%
Svensson *et al.*⋆ [944]	3.2% and 3.4%
Henry's coefficient, He	
Penttilá *et al.*⋆ [407]	6.9%
Wang *et al.*⋆ [409]	2.0%, 2.5%, and 4.3%
Li *et al.*⋆ [479]	2.0%
Li *et al.*⋆ [410, 932]	3.3%
Samanta *et al.*⋆ [1030]	1.3%, 1.5%, and 2.0%
Ko and Li⋆ [920]	2.0% and 3.0
Saha *et al.*⋆ [1031]	2.8%

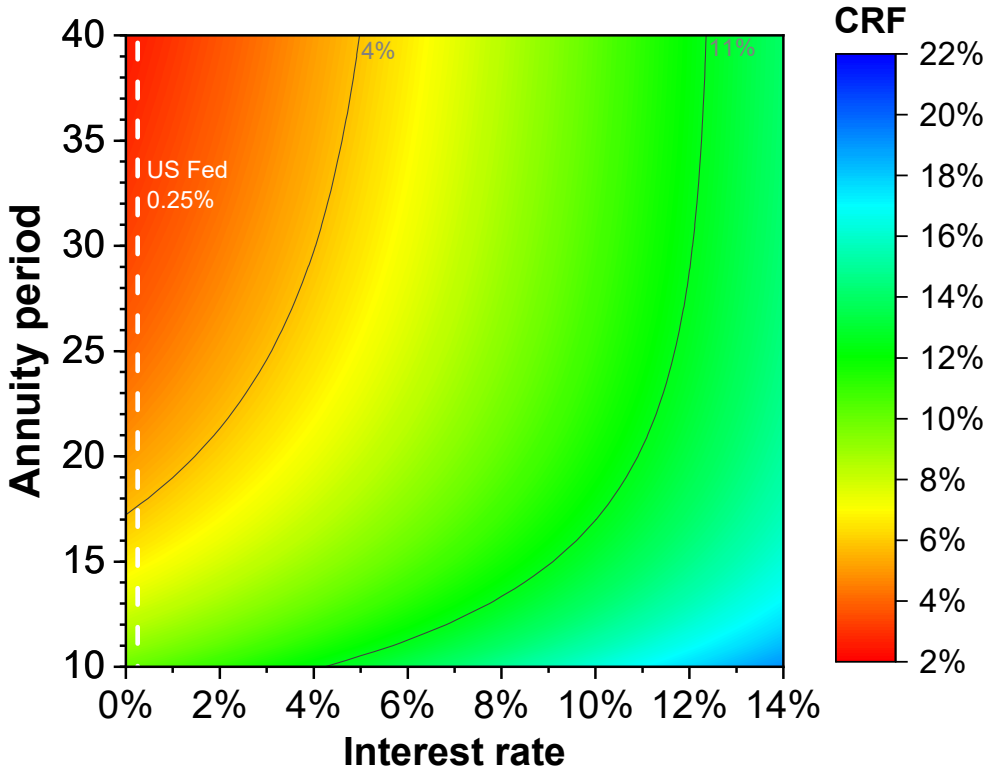


Figure D.2: Capital Recovery Factor CRF as estimated by $CRF = \dfrac{i \cdot (1+i)^n}{(1+i)^n - 1}$ with interest rate i and annuity period n. Common CRF values highlighted at 4% and 11% (grey) as well as US Fed's base rate at 0.25% (white dashed vertical line, January 2022). Adopted from [112].

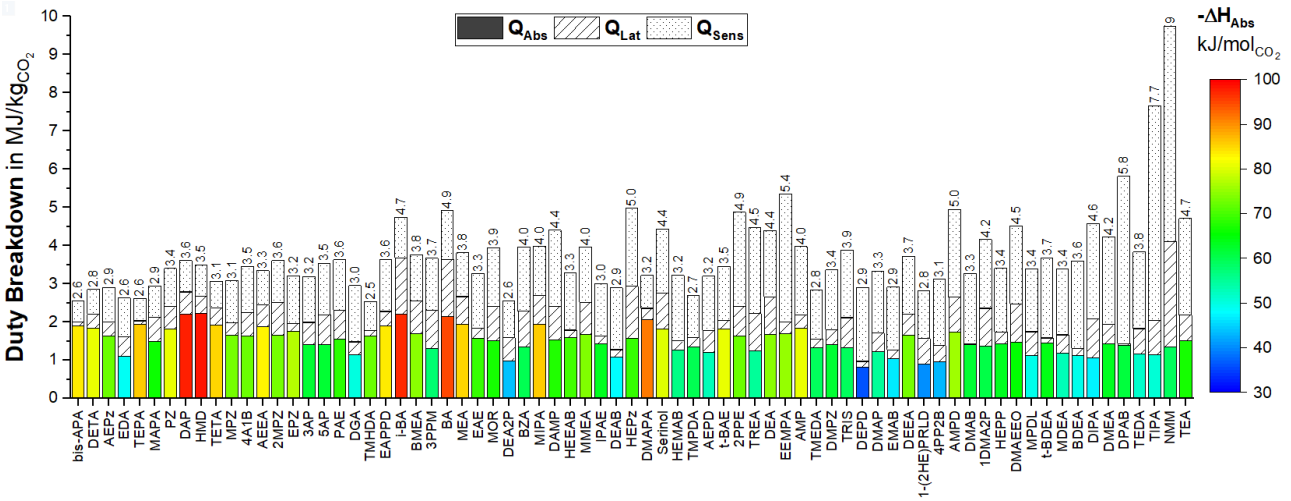


Figure D.3: Breakdown of specific reboiler duty Q_{Reb} into absorption Q_{Abs}, latent Q_{Lat}, and sensible Q_{Sens} duties. Solvents sorted by increasing capture cost from left to right. Negative ΔH_{Abs} is indicated by colour (blue low, red high). Clear trend between heat of absorption and Q_{Abs} but not overall duty.

Table D.2: Comparing calculated (SQUASH) and measured (Exp.) thermo-physical properties of aqueous MEA, DEA, MDEA, AMP, and PZ containing 30 wt% amine at 40 °C and 110 kPa. RD = relative deviation. Note, measured values are reported without their error, and this comparison is no validation.

Property	Unit	MEA			DEA			MDEA			AMP			PZ		
		Exp.	SQUASH	RD	Exp.	SQUASH	RD	Exp.	SQUASH	RD	Exp.	SQUASH	RD	Exp.	SQUASH	RD
Heat Capacity	J/(mol·K)	88.31	85.25	-3%	89.35	88.00	-2%	92.78	87.68	-5%	96.13	88.82	-8%	88.03	89.20	1%
Viscosity	mPa·s	1.616	1.709	6%	1.980	2.276	15%	1.953	1.870	-4%	2.168	2.291	6%	2.852	2.645	-7%
Density	kg/m^3	1003	992	-1%	1026	1018	-1%	1019	998	-2%	988.8	968.4	-2%	1023.2	1154	13%
Thermal Conductivity*	W/(m·K)	0.583	0.507	-13%	0.598	0.475	-20%	0.598	0.472	-21%	0.592	0.472	-20%	0.593	0.516	-13%
Surface Tension	kg/s^2	0.062	0.063	1%	0.058	0.065	12%	0.051	0.064	25%	0.042	0.062	50%	0.065	0.049	-25%

Table D.3: Comparing the capture cost calculated by either a process simulation or the Global System Analysis for five solvents at their individual optimal operating conditions for y_{CO_2} = 4 mol%.

$/t$_{CO_2}$	Converged process simulation	Mean value from GSA	Relative difference
MEA	76.60	76.45	-0.2%
DEA	105.58	105.29	-0.3%
MDEA	197.11	196.54	-0.3%
AMP	109.37	109.7	0.3%
PZ	58.21	58.43	0.4%

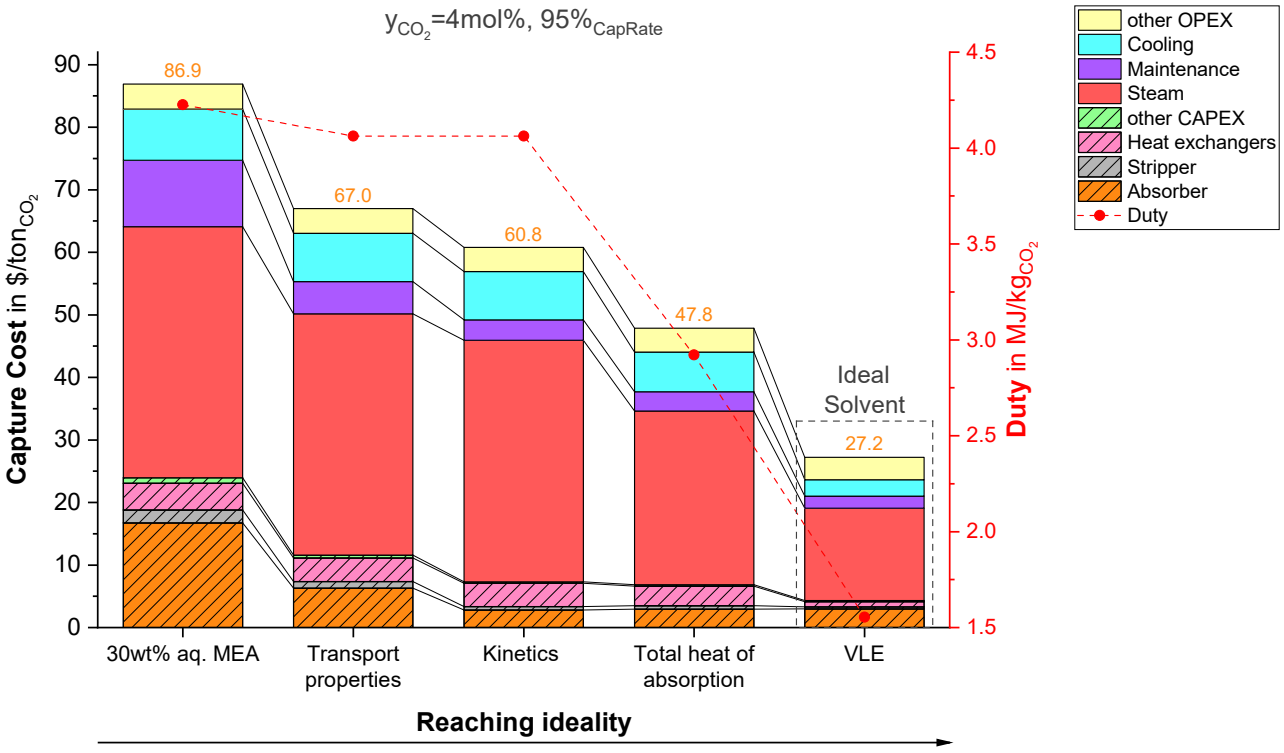


Figure D.4: Deriving the ideal solvent starting from MEA by optimising the solvent properties and its impact on capture cost (colour bar, left scale) and specific reboiler duty (red, right scale) at y_{CO_2} = 4mol% and 90% capture rate.

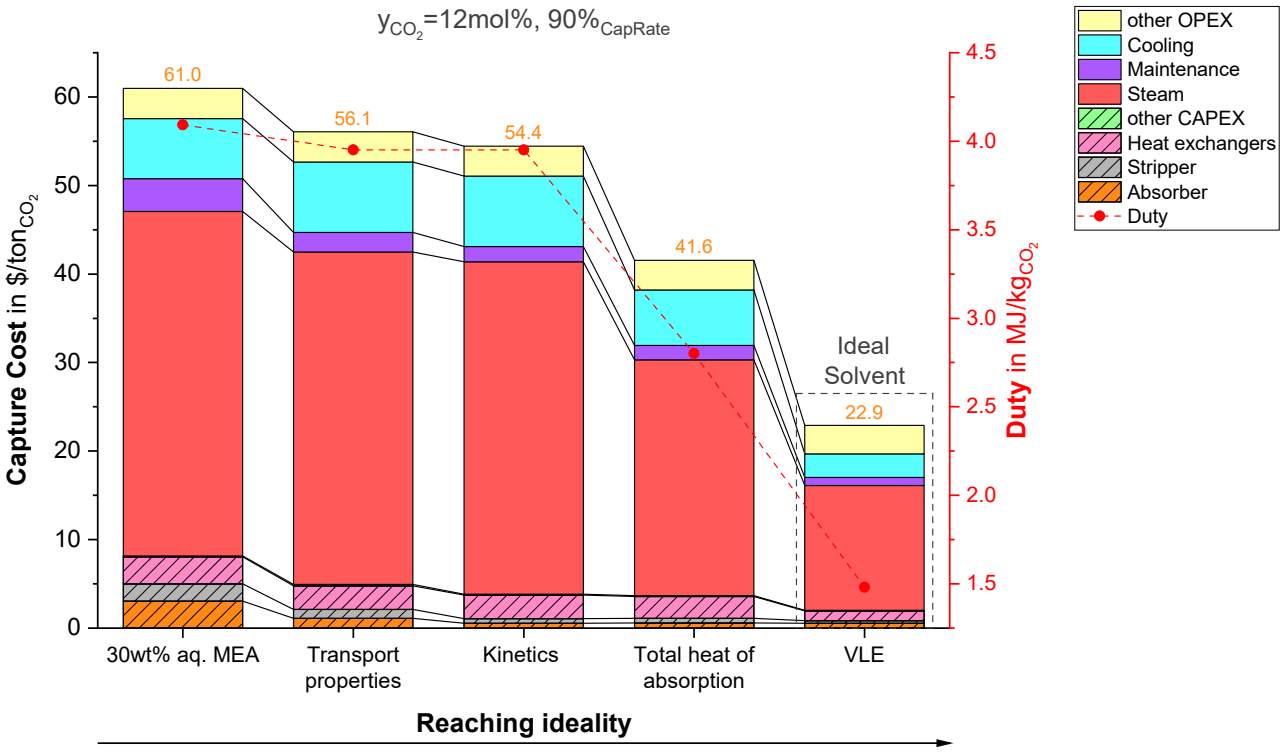


Figure D.5: Deriving the ideal solvent starting from MEA by optimising the solvent properties and its impact on capture cost (colour bar, left scale) and specific reboiler duty (red, right scale) at y_{CO_2}= 12mol% and 90% capture rate.

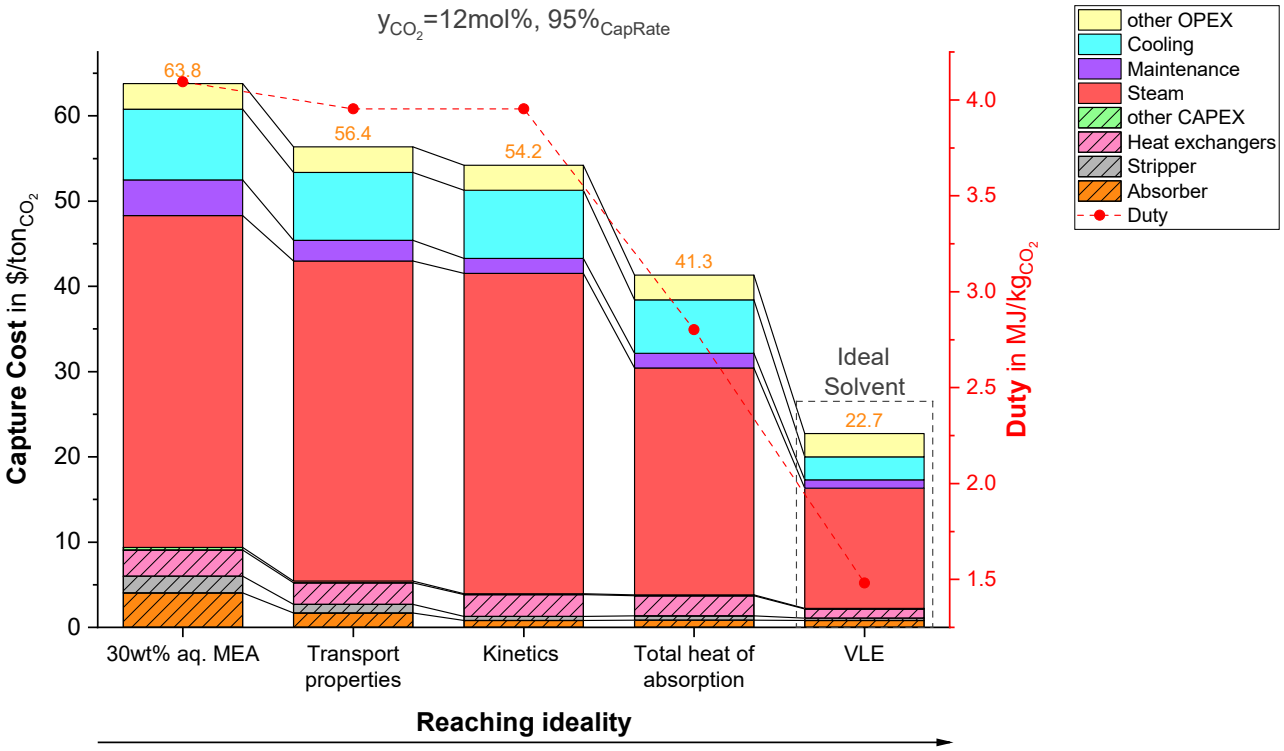


Figure D.6: Deriving the ideal solvent starting from MEA by optimising the solvent properties and its impact on capture cost (colour bar, left scale) and specific reboiler duty (red, right scale) at y_{CO_2}= 12mol% and 95% capture rate.

Table D.4: Excerpt of dimensionless numbers describing the ideal solvent at the top of the absorber for 90% capture and y_{CO_2}= 10 mol%.

Number	Value
Prandtl	0.12
Schmidt	323
Reynold	5.78
$\text{Reynolds}_{\text{Intfac}}$	10.9
Froude	9.95E-6
Weber	1.22E-04
Sherwood	125
Hatta	591
Enhancement factor	591
Nusselt	505